88

INSPECTABILITY OF TENSION LEG PLATFORM TENDONS

PHASE II FINAL REPORT
January 1988

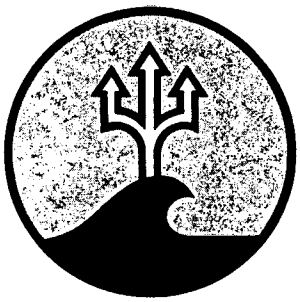

ARCTEC OFFSHORE CORPORATION

TABLE OF CONTENTS

TABLE OF CONTENTS (cont'd.)

1.0 EXECUTIVE SUMMARY

The objectives of Phase II of this study included:

1. Validate the Phase I ultrasonic model, particularly its ability to predict the minimum detectable flaw size as a function of geometry.

2. Evaluate effect on the ultrasonic model of material coatings likely to be used on TLP tendons.

3. Evaluate effect on model of Marine Biofouling.

4. Determine correlation between ultrasonic calibration using EDM notches and actual fatigue cracks.

5. Carry out a suitable 'blind test' to determine typical detection probabilities for actual fatigue cracks in threaded tubulars.

6. Update the Phase I failure analysis model as necessary to incorporate the experimental results of Phase II.

7. Make recommendations for tendon system design and inspection methodologies.

All of these objectives have been met with the exception that the "blind test" (Objective #5) was not carried out. A decision to eliminate this objective was reached after reviewing the data relevant to the sensitivity of thread form inspection. It appeared that the planned tests would not be directly applicable to actual tension leg platform tendon coupling designs.

Eighteen separate test pieces with 81 cracks or notches were used in this study to determine the effect of the various parameters on ultrasonic flaw detection and sizing. The results are summarized below.

1) Validation of Phase I Model

The model proposed in Phase I (Equation 3.1) is conservative for identifying the minimum detectable EOM notch size in a given geometry based on 0.001 echo response. However, it can not be used to accurately size defects much in excess of the minimum detectable size. An improved model is suggested. Attenuation in the materials considered for tension leg platform tendons in this study (i.e., HY-80, 4340, 2 1/4 Cr-Mo) is very low compared to some engineering materials and large grained steel. This means that beam spreading is the largest factor in loss of signal over distance. Inspection over path lengths of 600 mm round trip and greater are possible.

2) Effect of Marine Coatings

Coatings on materials can influence the transmittance and reflection of ultrasonic beams. Epoxy coatings cause about 20% loss in signal strength.

3) Effect of Marine Growth

Marine growth affects inspection significantly when the ultrasonic inspection is performed through the growth. Cleaning methods were tested showing scraping followed by bristle brushing was best. Scraping did not appear to seriously damage aluminum flame spray coatings.

4) Fatigue Cracks Compared to EDM Notches

Fatigue cracks of a given depth, in general, provide a lower reflection than electro-discharge machine (EDM) notches of equivalent depth. The average from the measurements of the response from fatigue cracks was less than 50% of the response from notches. This results in a need for more conservative requirements when setting standards to EDM notch sizes. The amplitude of signals from EDM notches and fatigue crack defects was found to generally increase with size but not proportionally to the defect size. At larger sizes (6 to 8 mm) deep, the amplitude response often saturated or reversed. These results are for fatigue cracks in unstressed specimens. Further tests are recommended with fatigue cracks under tension where ultrasonic response is expected to be greater.

5) Effect of Welds

Weld inspection can be inhibited by root and crown reflections if they are not removed. Allowance for weaker signals from fatigue cracks than notches causes the fatigue crack detectability limits to be even worse in the presence of unprepared welds. Tests with fatigue cracked specimens are recommended to determine crack detectability. Weld defect detection and sizing can be improved by imaging and signal timing methods.

6) Effect of Thread Pattern

The design of the thread pattern can strongly influence the interpretation of signals from thread roots or defects as a function of angle. This implies that optimum beam angles can be selected, and overall connector design should allow for the access of these beam angles to the inspection regions. Sizing of cracks in threaded geometries is expected to be more accurate using a shadowing technique rather than amplitude response. Thread design can be optimized to enhance this sizing method.

These results lead to significant conclusions regarding the design of TLP tendons for inspectibility:

- Thread designs should consider the potential for fatigue cracks in critical areas to be "shadowed". Finer thread forms will generally be more inspectible.

- Weld root and crowns should be removed to increase detectibility limits.

The results contained herein should provide a quantitative basis for evaluating these and other design tradeoffs.

2.0 INTRODUCTION

The 'Inspectability of Tension Leg Platform Tendons' program is a multiphase study to investigate tension leg platform (TLP) designs and how various parameters affect the inspectability. During the Phase I portion of the program, nondestructive evaluation (NDE) methods were evaluated for their applicability to in-service tension leg structure inspection.

Phase I of this study was initiated under the Small Business Innovative Research Program of the U.S. Department of Interior Minerals Management Service. During Phase I, the requirements for in-service inspection for TLP tendons was examined and non-destructive evaluation (NDE) methods were evaluated for their applicability to in-service tendon inspection.

The requirement for inspection was examined from the standpoint of tendon damage tolerance under various loading and other scenarios. The results indicated that in relatively benign fatigue environments and with suitable designs, the frequency of in place inspection could be very low - even beyond the intended service life of the structure. In very severe environments the inspection frequency could be less than the service life, however in any event design specific damage tolerance analysis is required to determine a suitable inspection interval. In any event, the Phase I analysis indicated a desireable threshold for crack detection in the range of 4-8 mm deep.

Ultrasonic NDE was found to be the most viable method for the conditions, designs, and inspection needs. An ultrasonic model was developed for nondestructive evaluation in complex geometries. The model was a mathematical simulation of the ultrasonic inspection, dependent upon the geometry under test for threaded connectors in tension leg platform design. Results of the Phase I investigations have been reported in the final report for Contract 14-12-0001-30204 (May 4, 1985).

The Phase II study has assembled materials and geometries of interest to experimentally test the model for predicting the acoustic response from notch defects. The Phase II program seeks to investigate factors that influence ultrasonic inspection defect detectability and sizing such as the material, coatings, and marine growth. Welded coupling design is also considered. The correlation of notch defect signal response to fatigue crack signal response is also evaluated in the program.

The Phase II program consists of sixteen major tasks. Table 2-1 lists the complete program. During the course of the study additional tests have been added and some tests deleted. Included among the tasks are measurement of the acoustic attenuation in materials of interest, measurement of the acoustic response from notches in coupling geometries without threads, measurement of acoustic response in the presence of threads, measurement of the affects of material coatings on the acoustic response, and measurement of actual fatigue cracks for response comparisons. Both threaded connectors and welded tendon connector geometries and materials were examined. Table 2-2 lists test specimens used in the program.

TABLE 2-1

PHASE II TASKS

Task #	Task Title	Notes
1	Planning	
2	Fabricate test samples	
3	Connector test samples notch response measurements	
	Welded test samples notch response measurement	
4	Fabricate thread samples	
5	Test threaded samples	
6	Correlate model	
7	Marine growth surface effects	
8	Fatigue crack calibrations	
9	Connector acquisition	
10	Connector calibration test	Not completed in program
11	'Blind' test	Deleted from program
12	Connector fatigue cracking	Deleted from program
13	UT of fatigued connector	Not completed in program
14	Joint project participation	
15	Analysis and reporting	
16	Additional tests:	Added to original program
	Image sizing from C-scan of SK001 Transducer spectrum analysis Shear beam spread over long path Off axis response calculations Flame spray surface condition Angle beam on barnacles Repeat fatigue crack measurements Weld defect imaging	

TABLE 2-2

TEST SPECIMENS

Task	Specimen	Purpose	Geometry	Material	Comment
3	1	Attenuation	8 x 4 x 3	2 1/4 Cr-1Mo[1]	
3	2	Attenuation	8 x 4 x 3	HY-80	
3	3	Attenuation	8 x 4 x 3	4340	
3	4	Flaw Size and Location Effects	20 x 6 x 2.5	2 1/4 Cr-1M	Bare Metal
3	5	Flaw Size and Location Effects	20 x 6 x 2.5	2 1/4 Cr-Mo	Epoxy Coated
3	6	Same as 4 and 5	20 x 6 x 1 3/8	2 1/4 Cr-Mo	Tool Joint Dimensions
3		Weld effects	15 x 16 x 1	HY80/WT70 [2]	Chevron
3		Weld effects	15 x 16 x t	X-60	Conoco
5	4A	Thread Effects	20 x 6 x 2.5	2 1/4 Cr-Mo	Buttress Thread
5	6A	Thread Effects	20 x 6 x 1 3/8	2 1/4 Cr-Mo	API V Thread
7	7	Marine Growth	20 x 4 x 2.5	4340 Al Flame Sprayed	Fouled and Water Jet Cleaned
7	8	Marine Growth	20 x 4 x 2.5	4340 Al Flame Sprayed	Fouled and Scraped/ Brushed
8	13	EDM notch versus fatigue crack	20 x 4 x 1	2 1/4 Cr-Mo	EDM Notch
8	14	Same as above	20 x 4 x 1	2 1/4 Cr-Mo	Fatigue cracked
8	15	Same as above	20 x 4 x 1	2 1/4 Cr-Mo	Fatigue cracked
8	16	Same as above	20 x 4 x 1	2 1/4 Cr-Mo	Fatigue cracked
8	5A	Same as above	20 x 6 x 2.5	2 1/4 Cr-Mo	Fatigue crack in thread
8	5AA	Same as above	20 x 6 x 2.5	2 1/4 Cr-Mo	Fatigue crack in thread

Notes:

1. 2 1/4 Cr1Mo is designation for ASME SA 387 Class 1 Steel
2. WT70 is Nippon prioprietary steel similar to HY-80
3. All alloy steel was heat treated to attain a minimum 50 Rc as quenched hardness, and tempered to a maximum 30 Rc.

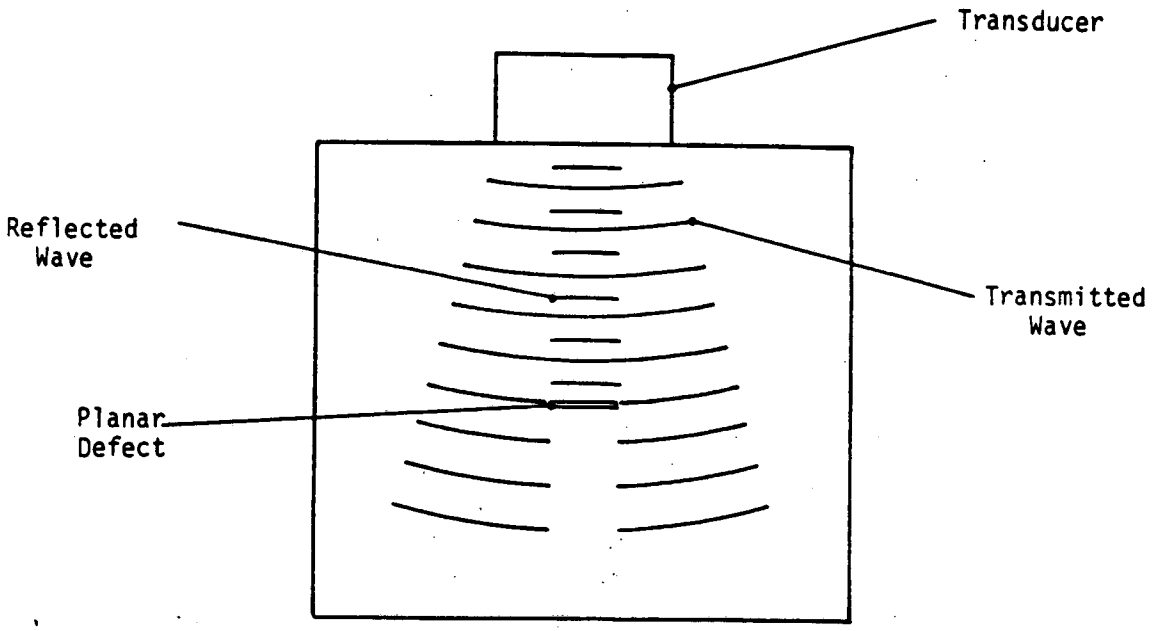

Figure 3-1. Example of ultrasonic reflection from a defect proportional to defect size.

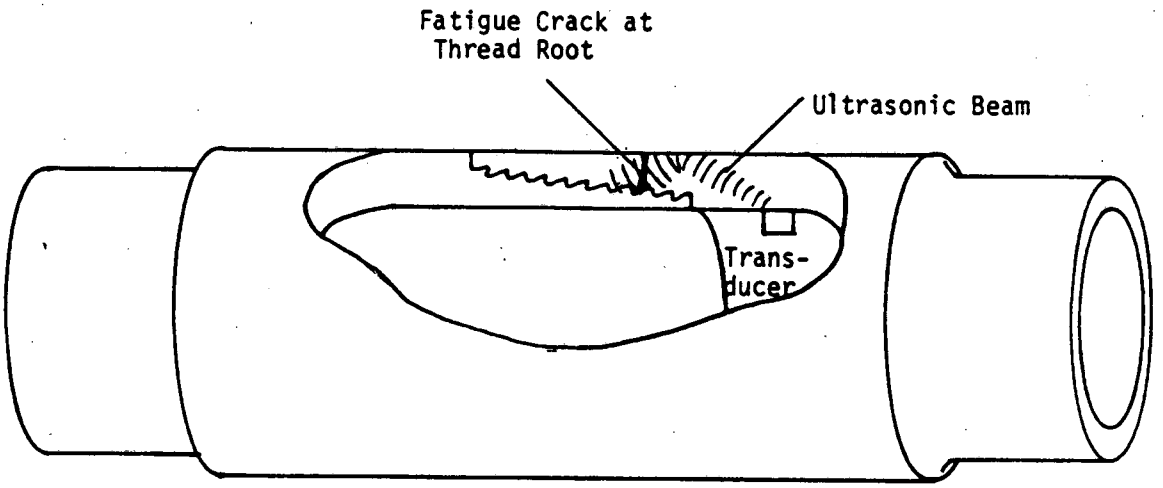

Figure 3-2. Threaded connector example of tension leg tendons with fatigue crack at root of thread.

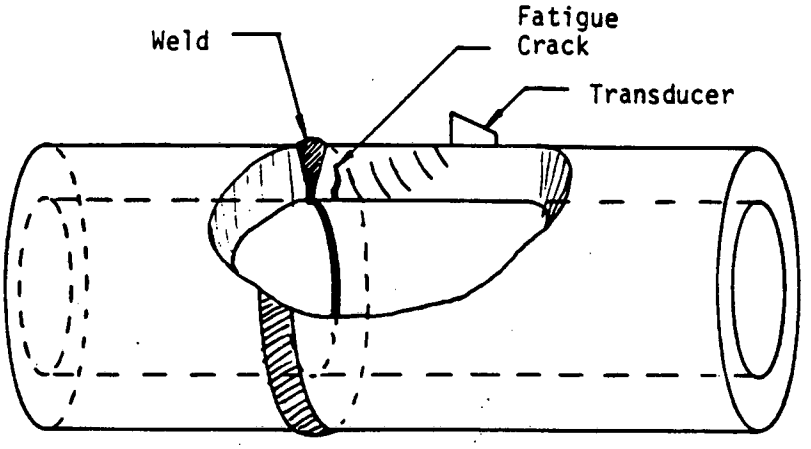

Figure 3-3. Welded connector example of tension leg tendon with fatigue crack in the heat affected zone of weld.

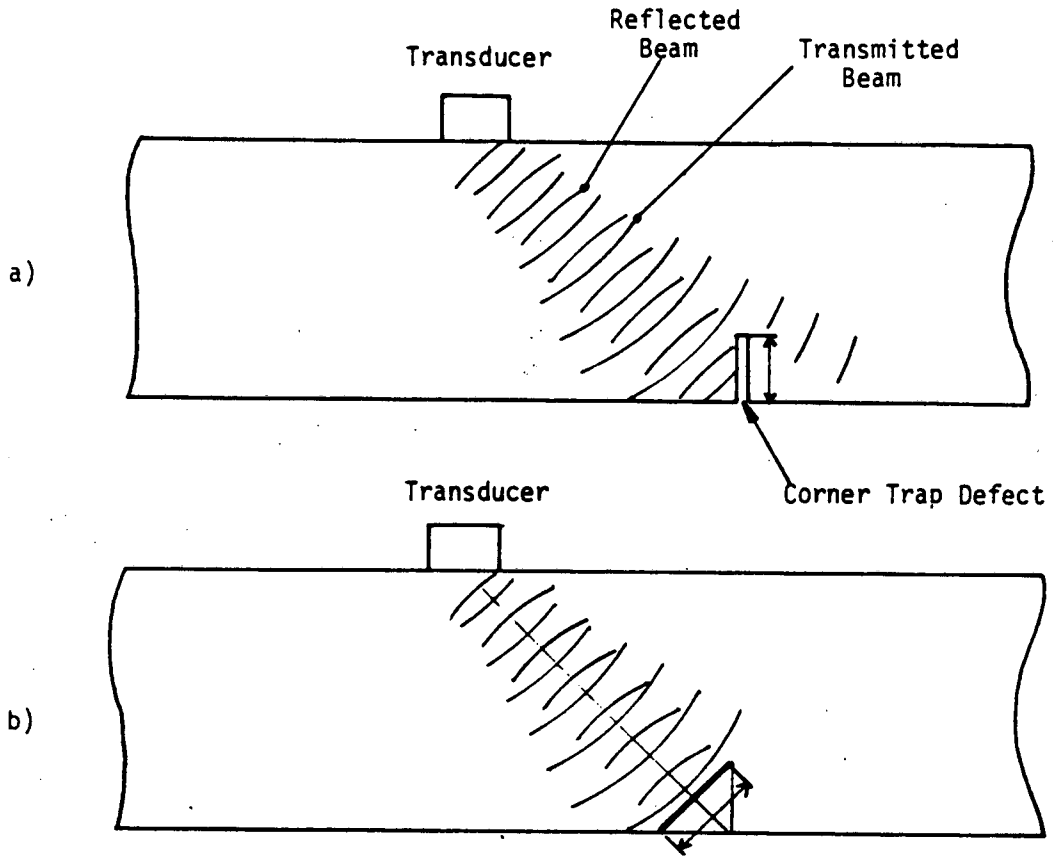

Figure 3-4. Corner trap reflection a) Beam configuration. b) Equivalent sized planar reflector when beam is at 45°.

3.0 BACKGROUND

During Phase I the ultrasonic model was developed from the basic principles of ultrasonic propagation and geometric optics. The equation for the acoustic response from a defect was given by:

$$p/p_0 = C_1 R^2 e^{-\alpha 2d} \frac{S_s S_f}{d^2 \lambda^2} \qquad (3\text{-}1)$$

where

- p = Measured echo response pressure amplitude.
- p_0 = Transmitted pressure pulse amplitude.
- R = Reflection coefficient (=1.0 if beam path does not include reflection from a wall).
- α = Attenuation coefficient.
- d = Nominal distance between source (transducer) and reflection (crack).
- S_s = Area of acoustic source.
- S_f = Area of reflection.
- λ = Acoustic wave length.
- C_1 = Transmisivity coefficient between water and steel.

Equation (3-1) was derived from Kirchhoff diffraction theory considerations. This theoretical model assumes that the defect is planar lying in a plane perpendicular to the ultrasonic beam and that the beam is larger in diameter than the defect. Under these circumstances the energy reflected from the defect will return to the transducer and will be proportional to the defect size. Figure 3-1 demonstrates this condition. The model includes terms for the transmission of ultrasound across a boundary, reflection at a surface, attenuation over a path length and response from a reflector based on source and reflector size and beam spread. Values for the terms in this model can be found in the literature [Krautkramer].

The general geometric configurations of interest for tension leg platform design are shown in Figures 3-2 and 3-3. Figure 3-2 shows the threaded connector and Figure 3-3 the welded connector. The growth of fatigue cracks at roots of threads or in the weld zone will not form the simple geometry of Figure 3-1. Instead, the crack and edge of the part will form a type of corner reflector. It might be expected that the corner trap could be modeled as a planar crack of equivalent size to the shadowing effect of the beam as shown in Figure 3-4. In cases where the beam angle is not 45° and/or the

fatigue crack is not perpendicular to the surface the reflectivity of the corner is altered from that predicted by strict geometric raytracing consideration. A beam will nevertheless be returned to the transmitting transducer. The actual inspection of the tension leg connector therefore differs from the theoretical model in terms of the ultrasonic beam and orientation to the defect.

For actual inspections, transverse waves are preferred. Studies show that longitudinal waves tend to have a lower response from surface breaking cracks than transverse waves [Kapranos]. Also, when longitudinal waves are used in angle beam techniques, transverse waves will also be present which can generate confusing echo responses. In complex geometries, such as connectors, it is preferred to use beam angles of transverse waves such that the longitudinal waves are not present in the initially injected beam. This minimizes the number of confusing signals from multiple modes of ultrasound. Note, both longitudinal and transverse waves can be generated at reflection and refraction interfaces with relative magnitudes dependent upon the incident beam mode and signal. Transverse waves are also preferred because the wavelength is smaller than the longitudinal waves which is important in the detection of small defects.

The model of equation (3-1) is not the only model that could be considered. A more complex model that represents the components realistically can be developed as

$$p/p_0 = C_{21}(\theta,\phi)\, C_{12}(\phi,\theta)\, R_{21}^2(\theta) e^{-2\alpha d} \int_s \frac{R(\beta)}{d^2\lambda^2} e^{j(\omega t - 2kd)} \cos(\beta)\, ds \quad (3\text{-}2)$$

where

- p is the measured response
- p_0 is the amplitude at the first interface.
- $C_{12}(\phi,\theta)$ is the transmission across a boundary at incident angle ϕ in medium 1 and exit angle θ in medium 2.
- $C_{21}(\theta,\phi)$ is the transmission across a boundary at incident angle θ in medium 2 and exit angle ϕ in medium 1.
- $R_{21}(\theta)$ is reflection at an interface of medium 2 and medium 1 with angle θ.
- α is the attenuation coefficient.
- d is the path length to the reflector.
- λ is the wavelength.
- $R(\beta)$ is the reflection coefficient from the reflector as a function of angle β.
- β is the angle between the beam and the reflector.

ω is $2\pi f$ where f is frequency.

k is $2\pi\lambda$,

s is the surface of the reflector.

This model involves parameters that are more accurate than equation (3-1) [Haines]. However, not all the parameters are well understood or readily available. In particular, the parameter $R(\beta)$ must be obtained for every defect type of interest. Other models are under development and measurements are being made of their parameters [Chapman, Coffey, Thompson]. In the future much better predictions than the model of equation (3-1) will be developed. Within the scope of the current program, however, the equation (3-1) model has been used to gain insight into the ultrasonic inspection problem.

The amplitude response from defects, calculated from this theoretical model is useful for predicting conditions which will allow ultrasonic inspections. Other factors which influence inspectability are also important. These include the effects of material selection and coatings on the material and the presence of marine growth and marine growth removal methods. These factors will influence the predicted response from the model. The model predicts the amplitude response as a function of defect size. Defect sizing accuracy is an important element in inspectability. The amplitude response from defects has traditionally been used for crack size estimation in most ultrasonic inspection efforts. It is likewise well recognized that considerable deviations from expected response as a function of size in standards versus real defects exist. Factors such as defect type, shape orientation and surface condition in addition to size will influence the amplitude response [Rogerson].

The Phase II effort involved experimental tests of ultrasonic response from defects to correlate to the model. Although the experimental plan tested the response from geometries of interest it did not experimentally verify every parameter. Terms such as C_1 and R were used as givens from theory, since they are of relatively small overall consequence. Table 3-1 lists values of C_1 (transmission of ultrasound across a boundary) for beam angles utilized in the study and Table 3-2 shows values for the reflection (R) at an interface. Both tables are taken from the literature [Krautkramer]. Attenuation and response from a reflector are evaluated empirically in the tests. Variations from expected trends must be explained in terms of the specific test conditions and the limitations of the theory.

TABLE 3-1

COEFFICIENT FOR ECHO TRANSMISSION
FOR A WATER/STEEL INTERFACE

Incident Angle	Refracted Angle	Coefficient C_1
19.4	45	.17
21	50	.16
24	60	.15
26.1	70	.14
26.9	75	.13
27.2	77.5	.12

TABLE 3-2

REFLECTION COEFFICIENT FOR STEEL/WATER INTERFACE OF TRANSVERSE WAVES

Incident Angle (degrees)	R
45	.91
60	.93
70	.95
75	.96
77.5	.97

4.0 BASIC TEST PROGRAM

A basic test program was developed to investigate parameters that influence inspectability in both threaded and welded tension leg connector geometries. Tasks 1-8 of the Table 2-1 task titles were considered basic tests. The Task 16 additional tests are also part of the basic test program.

The verification of the ultrasonic theoretical model was performed for representative parts of the threaded connector geometry in Task 3. The threads were not included in the Task 3 measurements because there are no factors in the model of Equation (1) to account for threads. Rather, notches of selected sizes at selected locations on the tapered surface were used. Later, Task 5 tests were run on threaded samples to establish how threads affected measurements. Marine growth effects were studied for their effects on the acoustic response in Task 7. Welded samples were also tested for defect detection in the geometries of interest as part of Task 3. Finally, fatigue cracks were generated in samples to compare with notch responses in Task 8.

4.1 Experimental Technique

The experimental technique for the Phase IIA 'Basic Tests' uses conventional ultrasonic equipment. Measurements of ultrasonic response were taken in an immersion tank with a manual, vernier driven scanner. Figure 4.1-1 illustrates the setup used. The pulser/receiver system consists of a Metrotek 215 pulser and 101A receiver. These modules have fairly standard performance for the industry and are used in many modular component systems. The pulser applies a high voltage spike to the transducer. The transducers are common piezoelectric crystal materials. The primary set selected for the study is made of lightly damped lead zirctitanate (PZT). This transducer gives a relatively high response with a moderate bandwidth. Transducers of lead metaniobate, highly damped are also available. These transducers have a broad bandwidth and less noise than the PZT, but have a weaker response. The transducer crystals are cut to have a resonance at a specified frequency; 1 MHz, 2.25 MHz, and 5 MHz primarily. Used with the MP 215 pulser, however, the ultrasonic beam generated will actually be composed of a frequency spectrum about the center frequency. This 'real world' behavior of the transducer/pulser performance differs from the theoretical approach of the model where the calculations are based on specific frequencies values. The measurements are intentionally made using the 'real world' performance characteristics rather than developing specialized ultrasonic systems for theoretical verification measurements. This approach has greater meaning for future implementation of the technique in spite of reduced accuracy from the model representation.

4.2 Transducers

A number of transducers were available for experimentation. Table 4.2-1 lists the transducers. Appendix A includes transducer specifications. Not

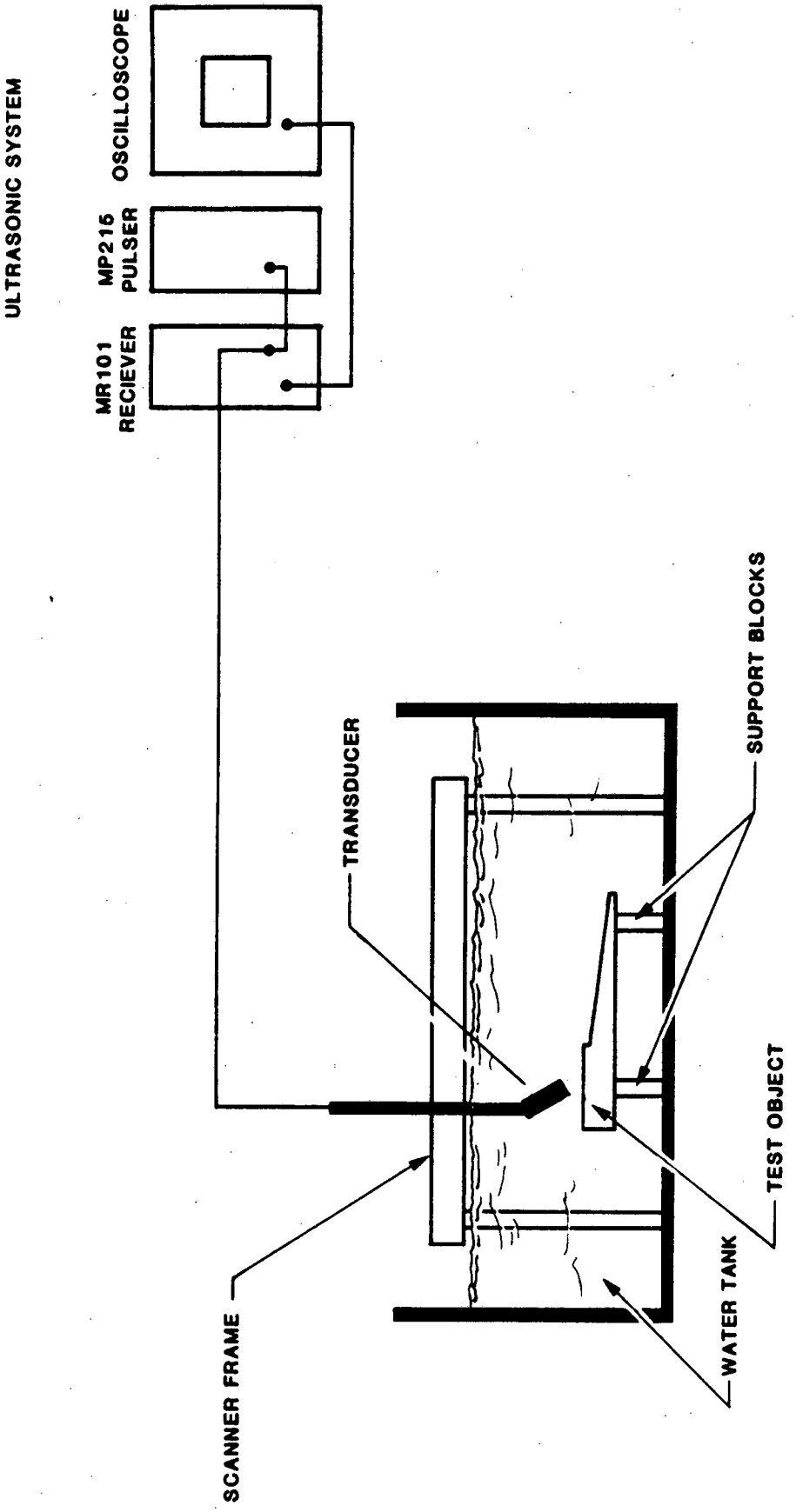

Figure 4.1-1 Experimental Setup

TABLE 4.2-1

TRANSDUCERS

Frequency (MHz)	Diameter (Inch)	Type	Manufacturer
5	1/2	SD-Z	Sigma
2.25	1/2	SD-Z	Sigma
1	1/2	SD-Z	Sigma
5	3/4	SD-Z	Sigma
2.25	3/4	SD-Z	Sigma
1	3/4	SD-Z	Sigma
5	1/2	KS-50	Ultran
2	1/2	KS-50	Ultran
10	1/2	WS-50	Ultran
5	1/2	WS-50	Ultran
2	1/2	WS-50	Ultran

all transducers were used in the experiments because to do so would require excessive testing time. The principal transducers were tested for the spectral characteristics. Appendix A shows the results of the measurements. The data was taken on the spectral content of a longitudinal beam in water and a longitudinal beam that had travelled a large distance (approximately 150 ms) in steel. Also a measurement was made from the echo of a shear beam in steel. The measurements were obtained by digitizing an echo waveform and Fourier transforming to produce the spectra. In many materials the attenuation of the acoustic beam is a function of the frequency. It is expected that over long path lengths, higher frequency contents of the beam will be more attenuated than the lower frequency and the spectral content will be reduced. The spectral tests in 4340 steel did not show significant changes in the spectral contents of the beams. If anything, the measurement shows a sharpening of the beam at 5 MHz for the longitudinal beam over the long steel path length. This indicates that the attenuation is low.

4.3 Attenuation Measurements

The attenuation of ultrasound in a material is composed of absorption and scattering terms. In Phase I, theoretical modeling of these terms were used to establish attenuation coefficients for calculations. The model was based on an assumed attenuation value at one frequency and extrapolating to other frequencies using the theoretical formula and constants for transverse wave scattering [Papadakis]. The attenuation coefficient is estimated as:

$$\alpha = \frac{\pi d^3}{6} f^4 s \text{ for } \lambda > 2\pi d$$

$$\alpha = d f^2 \Sigma \text{ for } \lambda < 2\pi d \qquad (4.3\text{-}1)$$

where

λ = the wave length

d = the average grain diameter

f = frequency

and S and Σ are material parameters. These equations indicate that attenuation is expected to increase with grain size and frequency.

In Phase IIA test samples of the materials were obtained and measurements made to determine values for the attenuation coefficient as a function of the frequency of the test. The measurement technique assumes the return echo from a transverse wave propagated through an isotropic media will be reduced in intensity due to attenuation and beam spread (diffraction). Figure 4.3-1 shows a test object for measurement studies. Two methods of measurement were used. One method sent the UT beam in on the slanting face and reflected off the back walls over short or long paths. Another method sent the beam in on

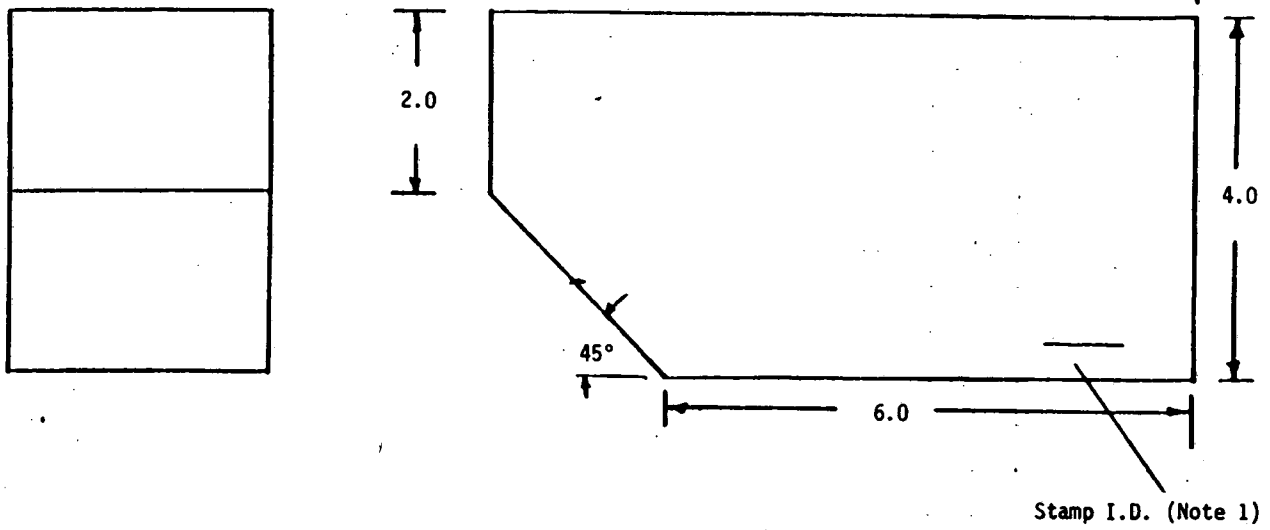

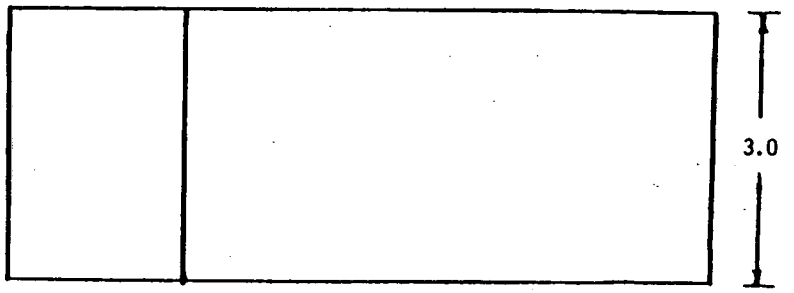

1. I.D. as follows:
   377-1 2 1/4 Cr-Mo
   377-2 HY-80
   377-3 4340

Figure 4.3-1

Acoustic Coupon EE-5			
DR. By	Date	Scale	SK
J.E.H.	11-5-85	1/2	004

the side and reflected off the slanted face. Using a standard diffraction spread that is inversely proportional to distance, the measurements result in no scattering attenuation. This result could be expected if the measurements are performed in test samples of limited size. In this case, the diffracted beam interacts with the side walls of the part and contributes to the measured signal. For the measurement techniques tested with the parts and instruments available, the conclusion is that attenuation is very low.

Longitudinal waves are easier to work with experimentally for attenuation measurements because the transducer is perpendicular to the part surface. Although the part size may also affect the measurements due to sidewall interaction, regimes of useful measurement are possible.

Table 4.3-1 contains a summary of the values obtained from longitudinal wave measurements in samples. There is considerable scatter in the data. Although fairly standard techniques for such measurements were applied [Burkle, Szilard], such variations are not uncommon in these measurements. As one author points out, few reliable absolute measurements of attenuation are reported in the scientific literature [Green, 1984] due to problems which include the coupling media affects which can contribute errors up to 20%, anisotropy in the material under test and diffraction spread of the ultrasonic beam. Also, attenuation measurements are usually performed in highly attenuative material. That is not the case with the materials of this study.

In private communication [Green, 1986] it was also discussed that, depending on grain structure, it is possible for the attenuation to be less at higher frequencies, as indicated by the 5 MHz data in these studies, although general theory predicts increased attenuation.

These attenuation values are useful in that they indicate the generally low attenuation of the sample materials. The values from Table 4.3-1 are in fact close to the values assumed in the Phase I study, except for the 5 MHz reduced values. Table 4.3-1 also includes some values of attenuation for engineering materials obtained from the literature [Papadakis]. The importance of the low attenuation in the materials considered for tension leg platforms is that longer beam paths may be used for inspection. Designing with highly attenuative material could seriously limit the ultrasonic inspection path. In weld zones, where grain sizes are altered, ultrasonic attenuation could be affected. Measurements were made on a Conoco weld sample (20 mm thick) to test for heat affected zone attenuation. However, in this relaitvely thin sample the attenuation difference between zones around the weld and base material could not be qualified. If larger welds are proposed in a design, the affect of heat treatment and grain size should be considered.

These values have therefore been used in calculations of expected response, for comparison to measured response in the next section. No correction of the longitudinal attenuation to equivalent transverse wave attenuation has been made. Transverse wave attenuation is generally greater than longitudinal wave due in part to increased scattering of the shorter wavelengths present. Nevertheless, the effect of the attenuation value over the path lengths in the material is a small effect on the response value. The beam spreading is the factor that contributes most to the loss of signal in the materials tested.

TABLE 4.3-1

EXPERIMENTAL MEASUREMENT OF
THE ATTENUATION COEFFICIENT

Material	Frequency (MHz)	Attenuation Coefficient (Np/mm)	Standard Deviation
2 1/4 Cr-Mo	1	.0012	.001
	2.25	.0024	.001
	5	.0013	.0008
4340	1	.0009	
	2.25	.0023	.001
	5	.00092	.006
HY 80	1	.00092	
	2.25	.0016	.0009
	5	.0014	.001

4.4 Acoustic Response Measurements

Acoustic response measurements from notches have been made on basic test samples. The acoustic response is a measure of the return echo pressure relative to the input wave pressure. The response measured in these sstudies is the ratio of the return echo peak voltage to the peak echo voltage from the front surface of the part. When a shear beam in the material is used, the front surface reference beam must be taken as a normal beam measurement with the same water path distance to the front surface as applied for the shear beam measurement. Prior to testing it was estimated that echo response sensitivities of 0.001 would be detectable. This parameter was used in determining minimum defect sizes to be included in test samples of various path lengths. The response value expected can be estimated by Equation (3-1) for simple geometries.

Measurements were made on specimens 4, 5, and 6 (Table 2.2-1). Figure 4.4-1 shows the configuration for specimens 4 and 5. Specimen 4 was bare while specimen 5 had an epoxy coating. The material is 2 1/4 Cr-Mo in both specimens. Figure 4.4-2 is the configuration for specimen 6 and the material is also 2 1/4 Cr-Mo. The Figure 4.4-1 and 4.4-2 test specimen configuration can represent either box or pin portions of a connector. If the location of the transducer is inside the tension leg the inspection of the threads will involve a bounce path for the box inspection. Figure 4.4-3 shows the assumed ray paths of the beams and Table 4.4-1 lists the general inspection conditions for the response measurements on the two test samples. The pin inspection (assuming an inside location of the transducer) is much simpler because the beam enters the flat surface of connector geometry and has relatively short path lengths to the threads. Angle beams of 45° and 60° were tested in this configuration. For inspections with the transducer on the outside of the tension leg the box and pin geometries are the reverse of those discussed above. The difference on outside and inside inspection with respect to geometry is the curvature of the connector. These tests did not consider curvature. In small diameter legs this would create an additional parameter to be considered by the analysis.

The results of the acoustic response measurements are described in Appendix B. The following conclusions were drawn from these measurements.

- Response sensitivities in the range of 0.0001 are possible.
- Trends of response follow predicted model.
- Sizing of notches based on response using the model is not accurate.

Figures 4.4-4 and 4.4-5 are two representative figures of the acoustic response measurements. The calculated response shows a higher slope than the measured. The measured response shows a leveling off of response with notch size. This effect will appear again in the fatigue crack measurements as well. The conclusion is that the model can be used for order of magnitude estimates of response but not for accurate prediction of notch sizes. The predicted 0.001 sensitivity proved to be conservative. All notches in the test samples were detected. In general, the model is conservative for predicting the minimum notch size, i.e. notches showed a greater response at small sizes than the model predicted. This is helpful, because as later data

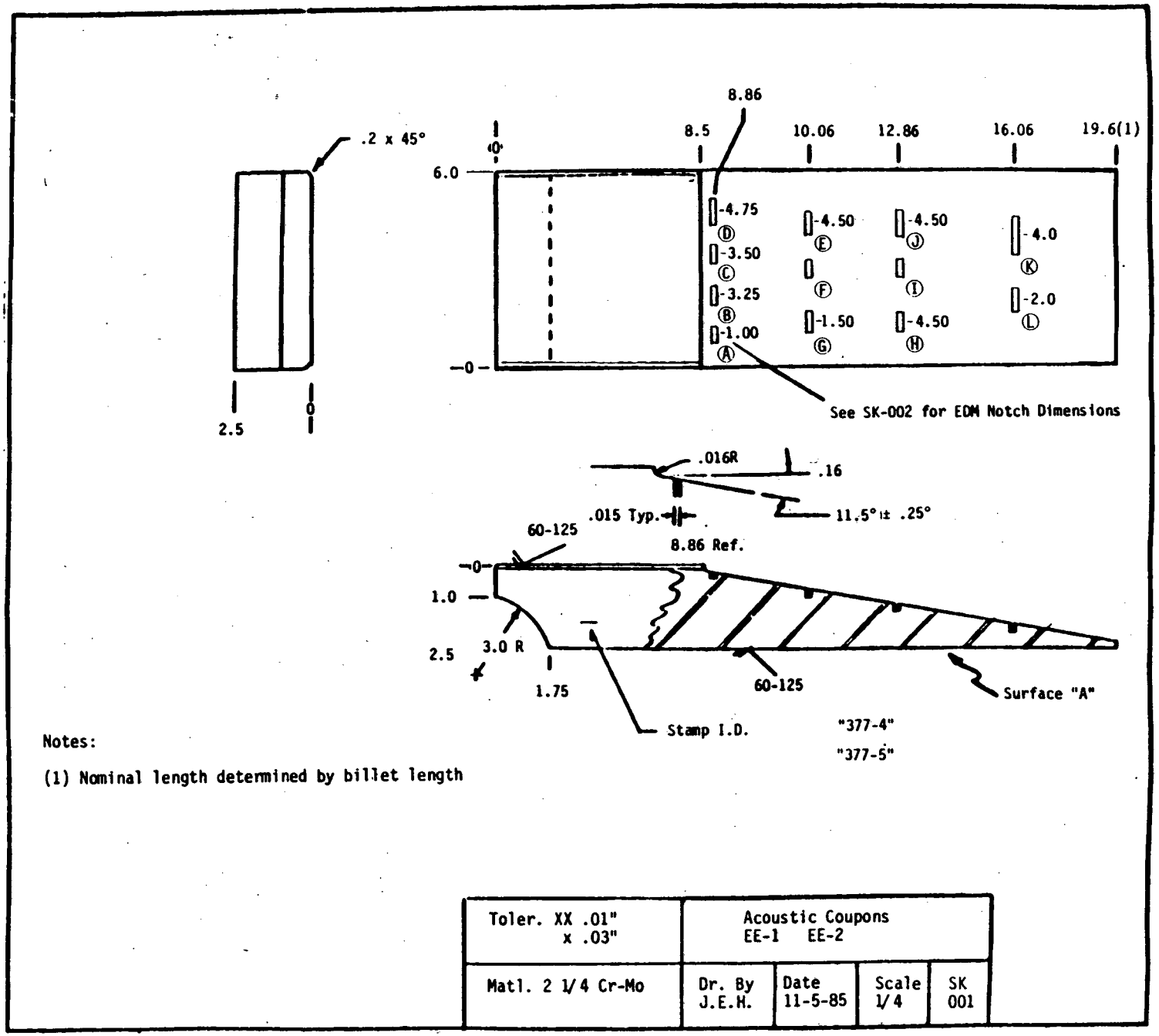

Notes:

(1) Nominal length determined by billet length

Toler. XX .01" x .03"	Acoustic Coupons EE-1 EE-2			
Matl. 2 1/4 Cr-Mo	Dr. By J.E.H.	Date 11-5-85	Scale 1/4	SK 001

Figure 4.4-1a SK 001 Test Sample

Notches	mm			inches			Tolerances (inches)		
	a	c	R	a	c	R	a	c	R
A	2.0	6.0	3.3	.079	.235	.128	.001	.002	.001
B	3.0	9.0	4.9	.118	.354	.192	.001	.004	.002
C	4.0	12.0	6.5	.157	.422	.256	.002	.005	.003
D	6.0	18.0	9.8	.236	.709	.384	.002	.007	.004
E	6.0	19.0	9.6	.236	.709	.384	.002	.007	.004
F	2.0	6.0	3.3	.079	.235	.128	.001	.002	.001
G	4.0	12.0	6.5	.157	.472	.256	.002	.005	.003
H	5.0	15.0	8.1	.197	.591	.320	.002	.006	.003
I	4.0	12.0	6.5	.157	.472	.256	.002	.005	.003
J	6.0	18.0	9.6	.236	.709	.364	.002	.007	.004
K	8.0	24.0	12.0	.315	.945	.512	.003	.009	.005
L	6.0	13.0	9.6	.236	.709	.364	.002	.007	.004
M	1.0	3.0	1.6						

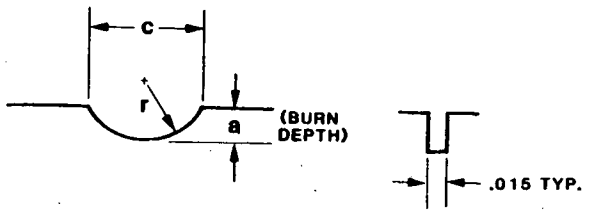

Figure 4.4-1b

$$A = R(\Theta - 1/2 \sin 2\Theta)$$

$$\Theta = \sin^{-1}(c/2R)$$

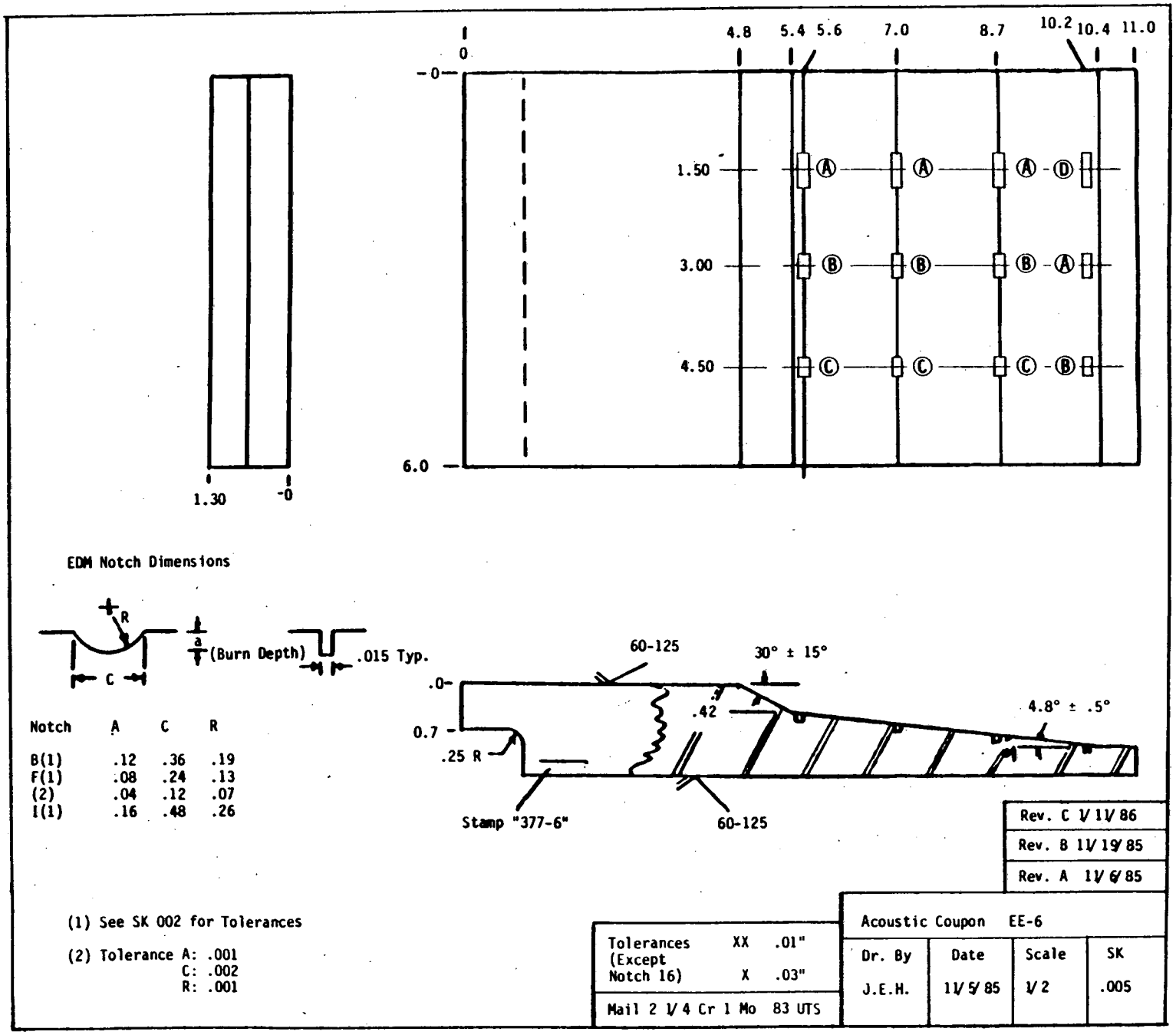

Figure 4.4-2 SK 005 Test Sample

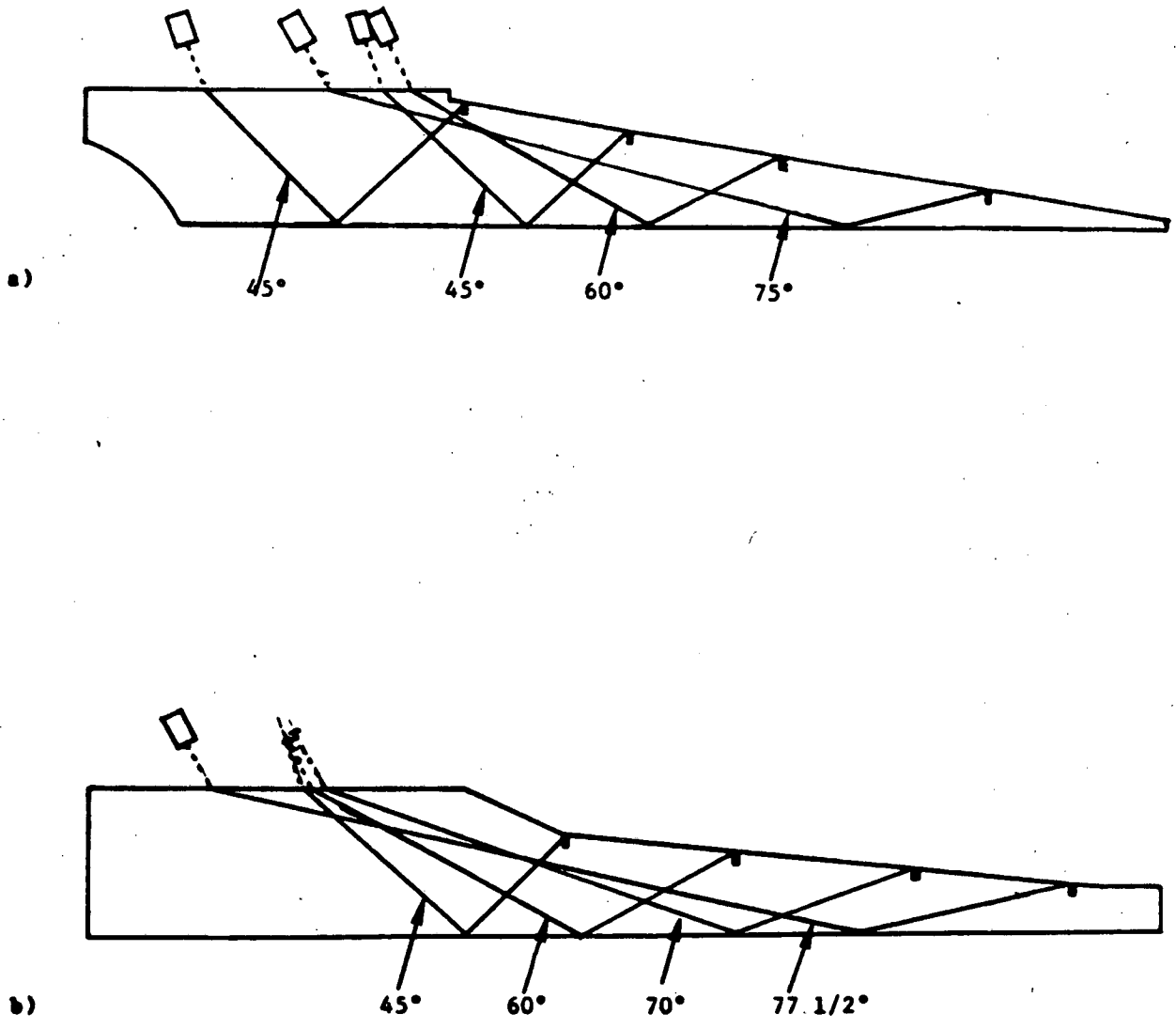

Figure 4.4-3. Ray paths used for box configuration inspection of a) specimens 4 and 5, Figure 5, sk001, and b) specimen 6, Figure 6, sk005.

TABLE 4.4-1

BEAM CONFIGURATION

Specimen	Defect Set	Transducer Angle (degrees)	Shear Beam Angle (degrees)	Path Distance In Part (mm)
4 and 5	A,B,C,D	19.4	45	171
	E,F,G	29.4	45	162
	H,I,J	24	60	201
	K,L	26.9	75	312
6	Row 1	19.4	45	83
	Row 2	24	60	112
	Row 3	26.1	70	153
	Row 4	27.2	75	227

will show (Section 4.10), fatigue cracks have a lower response than EDM notches. By increasing the echo response sensitivity factor for detectability, this can be accounted for. A sensitivity of 0.00-2 is proposed as a possible value for minimlum fatigue crack detection. The model of equation (3.1) can therefore be used in design studies to estimate minimum detectability provided the assumptions of path lengths for far field inspection are correctly applied (see Appendix B). If the minimum defect size predicted by the model is greater than critical size requirements then a more detailed analysis and testing approach would be needed to assure that detectability could be achieved.

4.5 Coating Effect

The effect of coating on the acoustic measurements was tested by the fabrication of specimen 5 with an epoxy coating. The coating was SkotchKote 206N following specifications of the National Association of Pipe Coating Applicators (NAPCO), Bulletin 12-78. The results of Figures 4.4-4 and 4.4-5 show the response when the beam has used the bounce path of Figure 4.4-3 on the uncoated Specimen 4 and epoxy coated Specimen 5 surface. Figure 4.4-5 shows a significant loss due to the coating while 4.4-4 shows little change. Tabulating all measurements, the response shows approximately a 20% loss of signal. Measurement from the pin side configuration where the beam passes through the coating with no bounce path also show the general trend of a reduced signal of 20%.

Measurements were also made at four locations on the coated surface to investigate the coating to metal interface. The following time separations between the front of the coating and the coating/metal interface were found: 220, 340, 480, and 500 ns. If the acoustic velocity in the epoxy coating is known, the thickness can be calculated. The locations were selected to cover the range of thickness found on the sample.

4.6 Thread Effect

Threads were added to the specimens 4 and 5 (SK001 design) and specimen 6 (SK006 design) to test the effect of threads on the acoustic response. Appendix C contains details of the part changes for the thread effects study. The addition of threads into the geometry of Figure 4.4-3 complicates the return echo signal significantly. The echoes from the notches in the threaded geometry can become buried in the periodic spacing of thread echoes. The pattern is a function of the ultrasonic beam angle and the thread pattern design. This results in some important implications for the design of threaded connectors to allow for inspectability.

Tests were performed using the box geometry of Figure 4.4-3 with beam angles between 45° and 60°. Figure 4.6-1 shows a plot of the echo response intensity from the threads as a function of angle for specimen 4A. With this thread shape (EPR modified buttress) there is a strong response from the threads around 45 beam angle in the steel which decreases with increasing angle. Above 53 , the signal from the threads is significantly weaker. Figure 4.6-2 shows the response from notches in specimen 4A as a function of angle. In this case, the notches show a better response around 53 than at 45 . In the

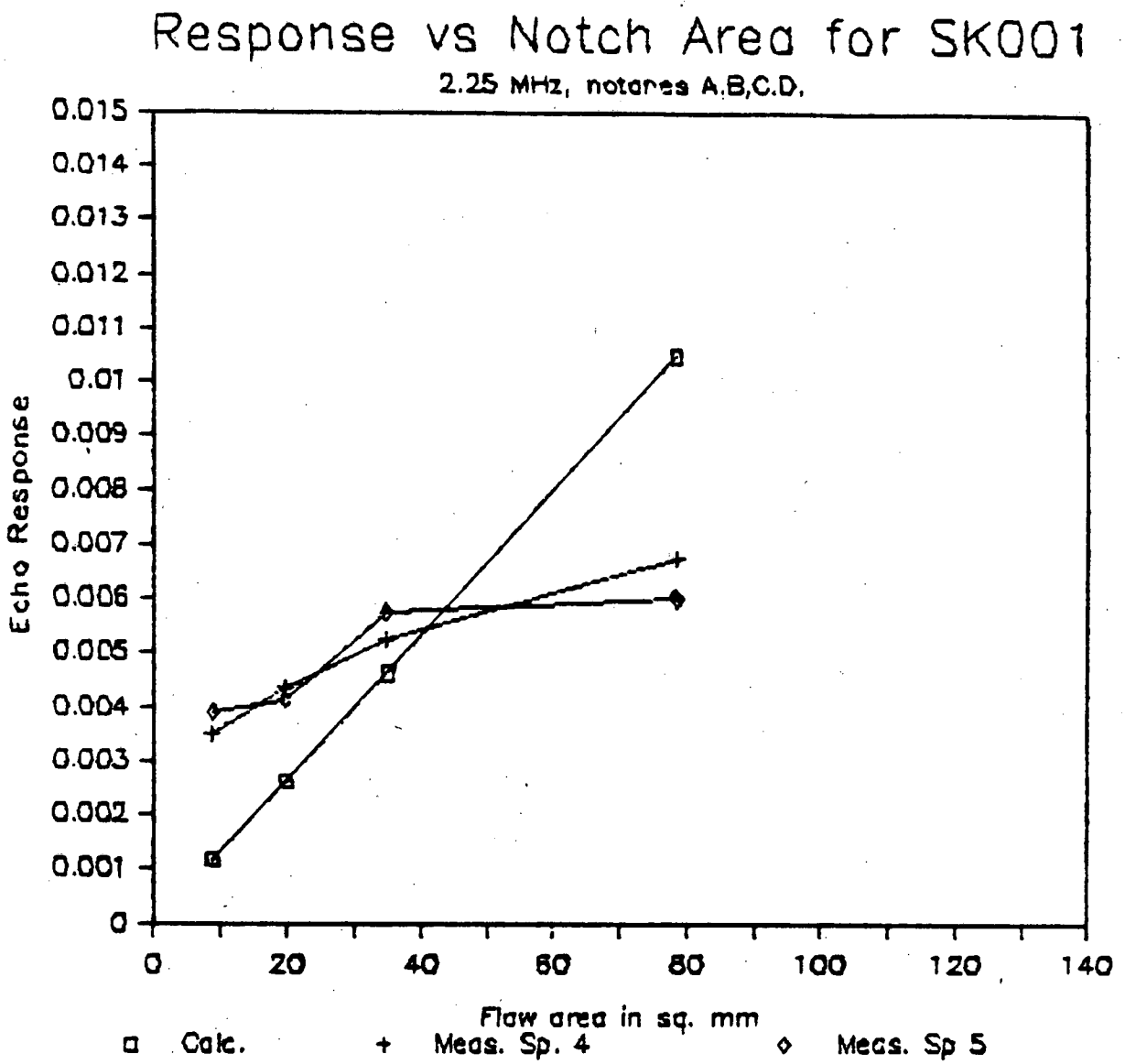
Response vs Notch Area for SK001
2.25 MHz, notches A,B,C,D.
Echo Response
0.015
0.014
0.013
0.012
0.011
0.01
0.009
0.008
0.007
0.006
0.005
0.004
0.003
0.002
0.001
0
0
20
40
60
80
100
120
140
Flaw area in sq. mm
Calc.
Meas. Sp. 4
Meas. Sp 5

Figure 4.4-4

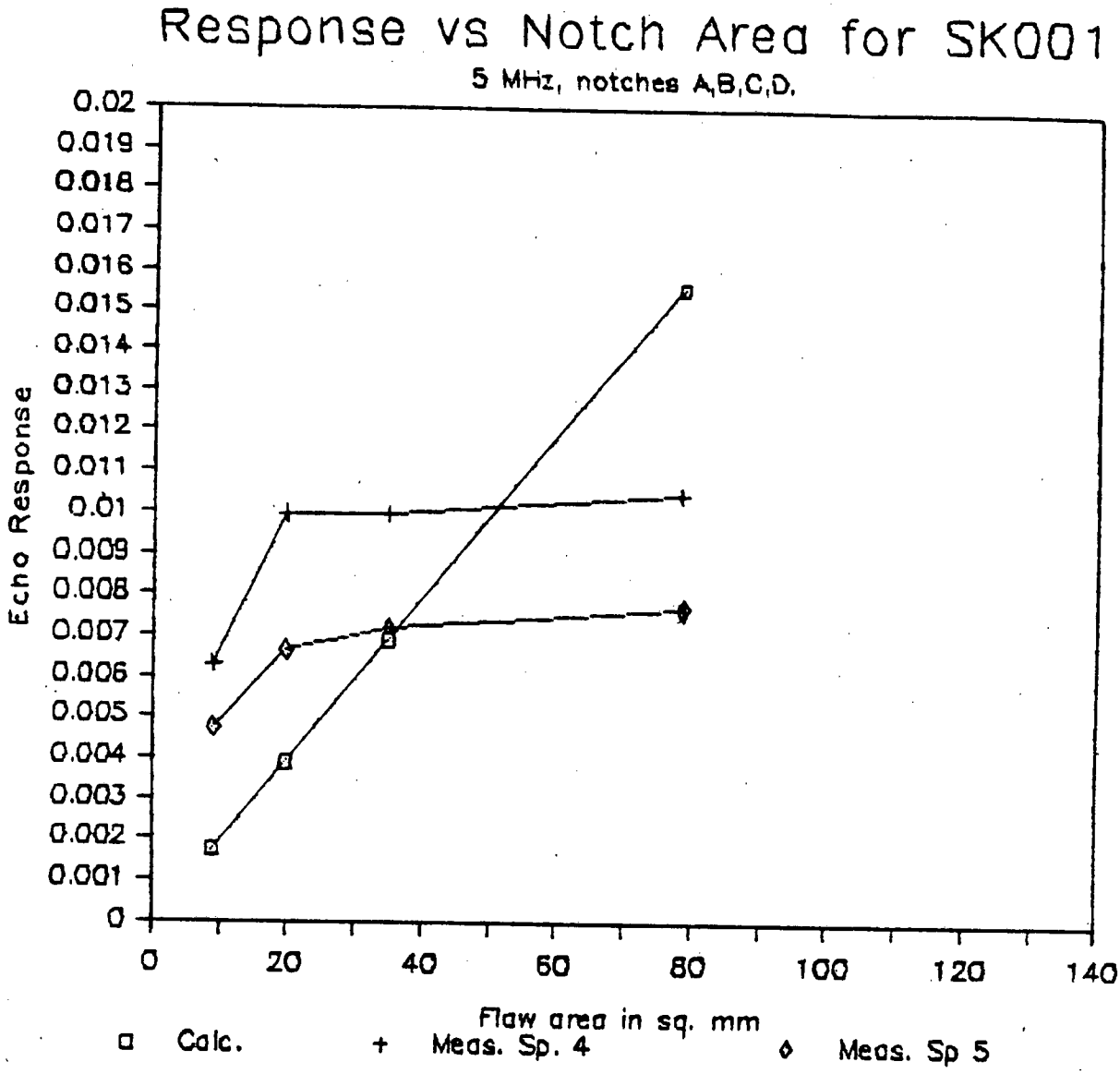
Response vs Notch Area for SK001
5 MHz, notches A,B,C,D.
Echo Response
0.02
0.019
0.018
0.017
0.016
0.015
0.014
0.013
0.012
0.011
0.01
0.009
0.008
0.007
0.006
0.005
0.004
0.003
0.002
0.001
0
0
20
40
60
80
100
120
140
Flaw area in sq. mm
Calc.
Meas. Sp. 4
Meas. Sp 5

Figure 4.4-5

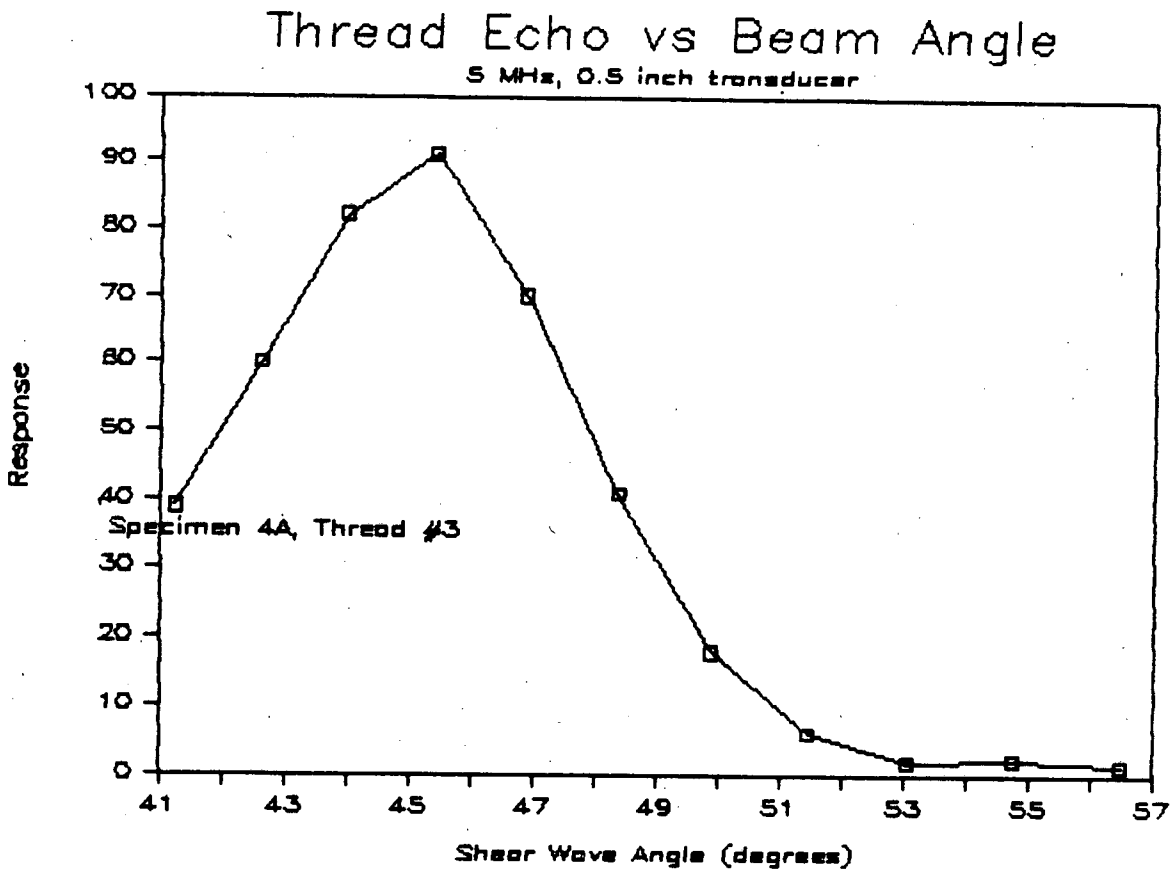
Thread Echo vs Beam Angle
5 MHz, 0.5 inch transducer
Response
100
90
80
70
60
50
40
30
20
10
0
Specimen 4A, Thread #3
41
43
45
47
49
51
53
55
57
Shear Wave Angle (degrees)

Figure 4.6-1

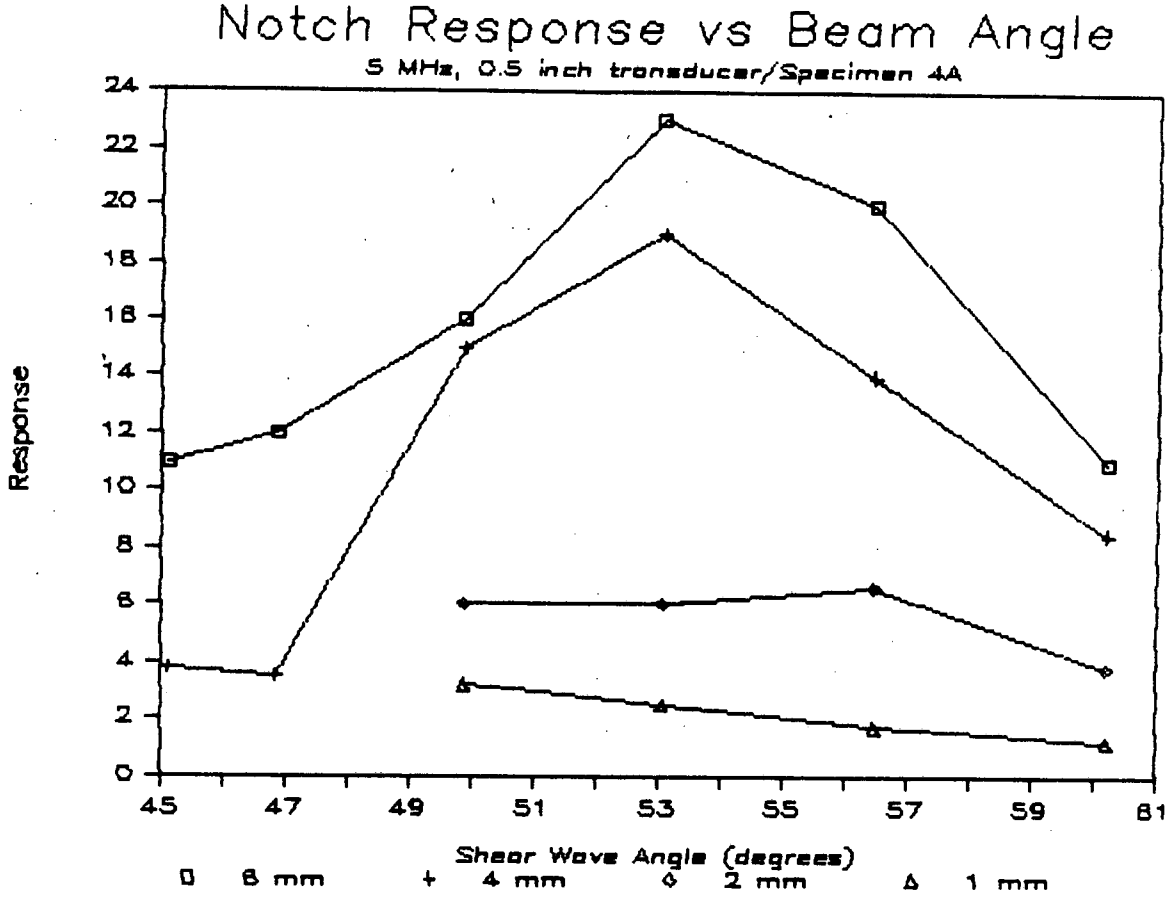
Notch Response vs Beam Angle
5 MHz, 0.5 inch transducer/Specimen 4A
Response
24
22
20
18
16
14
12
10
8
6
4
2
0
45
47
49
51
53
55
57
59
61
Shear Wave Angle (degrees)
□ 6 mm
+ 4 mm
◇ 2 mm
△ 1 mm

Figure 4.6-2

ultrasonic waveform, the timing of the thread and notch signal are a function of the beam angle. Figure 4.6-3 shows the presence of the thread signals with and without a notch at 45° and 53° beam angles. Notice that if conventional ultrasonic gating and amplitude detection is used, the flaw would need to have a response greater than the 2 mm deep notch to be detected above the thread signal in the 53° case and at 45° a 6 mm notch is far too weak relative to the thread. At 60° beam angle the threads are not detectable and so flaw imaging is relatively easy, however the signal strength is not great and background noise can inhibit small defect detection threshold level.

In the specimen 6A geometry case, the threads are smaller than the specimen 4A, such that the ultrasonic beam covers a large number of threads. The thread shape affects the angle at which maximum ultrasonic response is found as shown in figure 4.6-4. These threads in fact look like notches. Figure 4.6-5 shows the threads with and without a notch present. The presence of a notch is not readily detected by its response as shown in this figure because the pattern is only changed slightly. The notch appears at the same time as the thread, however, it shadows succeeding threads. The size of the notch can be predicted from the number of threads shadowed. Figure 4.6-6 is an RF B-scan image showing thread shadowing. Each line of the B scan is a grayscale display of the ultrasonic RF waveform. The 3 mm deep notch casts a significant shadow on a succeeding thread. The 2 mm notch has less effect and the 1 mm notch little or no effect. This technique does not rely on echo response from the defect, it relies on the defect preventing ultrasonic signals from passing through it so that features behind the defect are no longer observed. The comparison of notch and crack in this case should be closer than in the reflection amplitude case. The accuracy of the sizing depends on the thread design.

The thread effects study has shown some truly interesting characteristics in terms of inspectability. Thread design plays a key role in the ultrasonic response. At certain angles and thread designs the thread echo can completely mask the defects making inspection impossible. Other thread designs can be used to enhance the relative response for reference or optimize for shadow imaging of defects. It would appear that these smaller thread sizes are advantageous for aiding inspection.

4.7 Marine Growth Effect

The effect of marine growth on the inspectability was tested by biofouling two test samples. Appendix D discusses the samples and testing.

The samples (labelled A and B) were made of 4340 steel with aluminum flame spray coating on the outside surface. The other surfaces were coated with epoxy to protect them from biofouling. After one year in the Pacific Ocean, they were brought in for testing. The testing involved comparing ultrasonic signal response as a function of cleaning to determine the effect on inspectability. Table 4.7-1 lists the cleaning and the general improvement in straight beam ultrasonic reflection from the cleaned surface. Water jet cleaning (at 5000 psi or greater) or plastic scraping with bristle brushing are good techniques. With plastic scraping it is relatively easy to knock off barnacles, although their residual glue remains on the surface. Following the plastic scraping with a bristle brush is important in order to remove fine

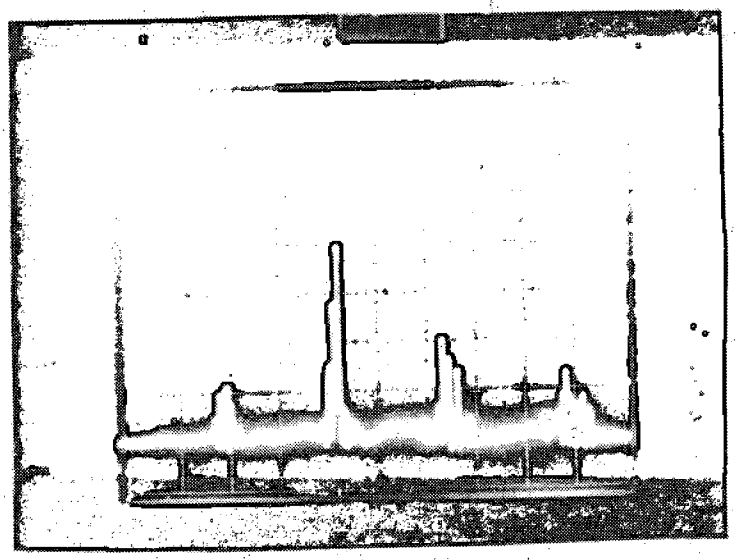

4.6-3a

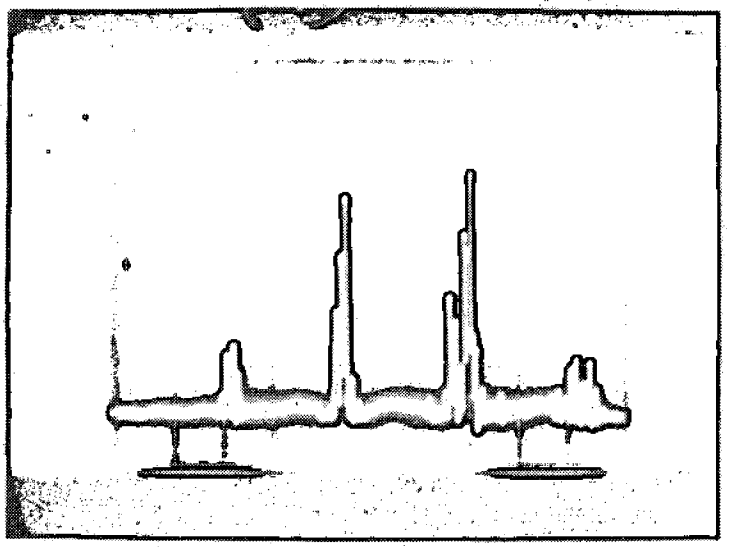

4.6-3b

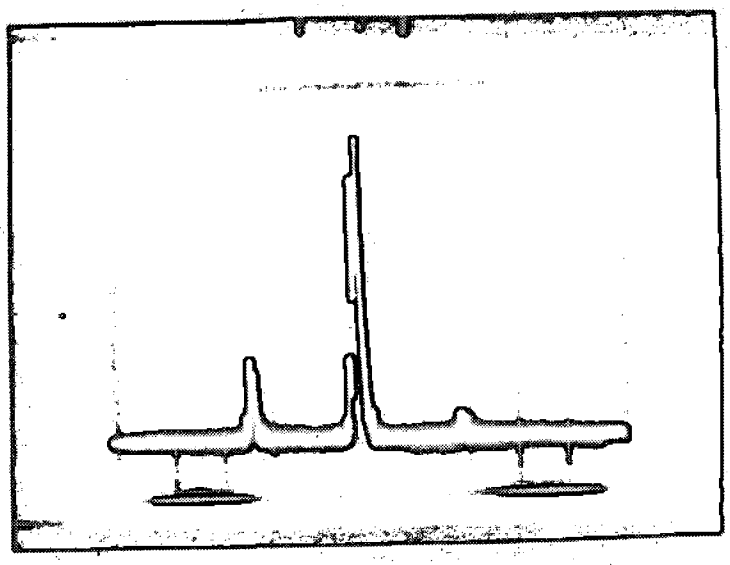

4.6-3c

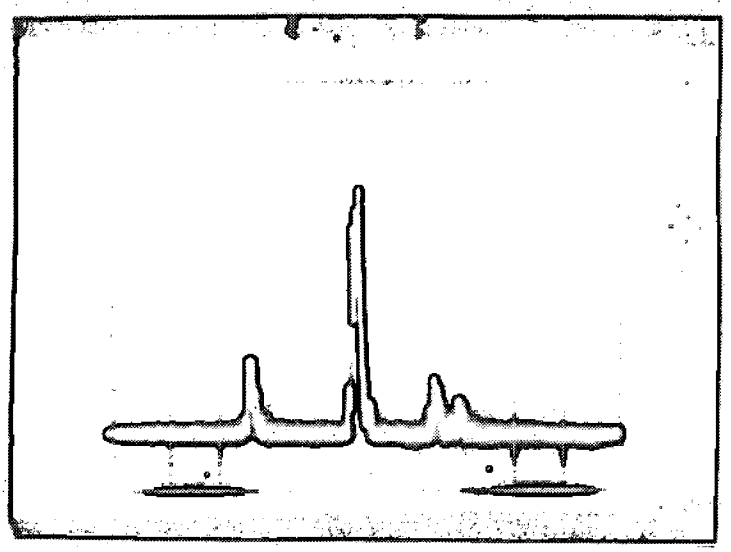

4.6-3d

Figure 4.6-3. Waveforms from specimen 4A using 5 MHz: a) 53° shear with no notch, b) 53° shear with 2 mm deep notch, c) 45° shear with no notch, d) 45° shear with 6 mm deep notch. (time base is 2 s/div, a and b 0.5 V/div at 0 dB attenuation, c and d 2 V/div at 3 dB attenuation.

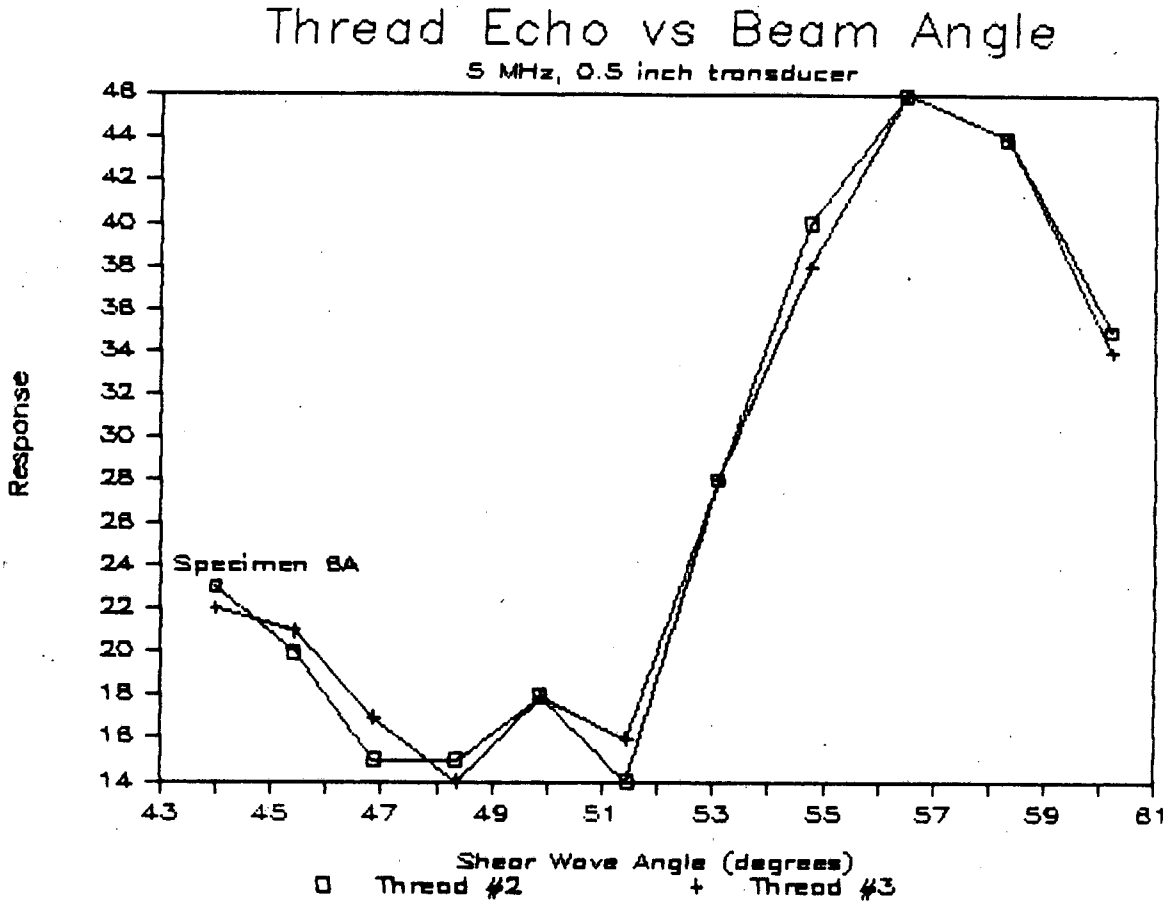
Thread Echo vs Beam Angle
5 MHz, 0.5 inch transducer
Response
48
44
42
40
38
36
34
32
30
28
26
24
22
20
18
16
14
Specimen 8A
43
45
47
49
51
53
55
57
59
61
Shear Wave Angle (degrees)
Thread #2
Thread #3

Figure 4.6-4

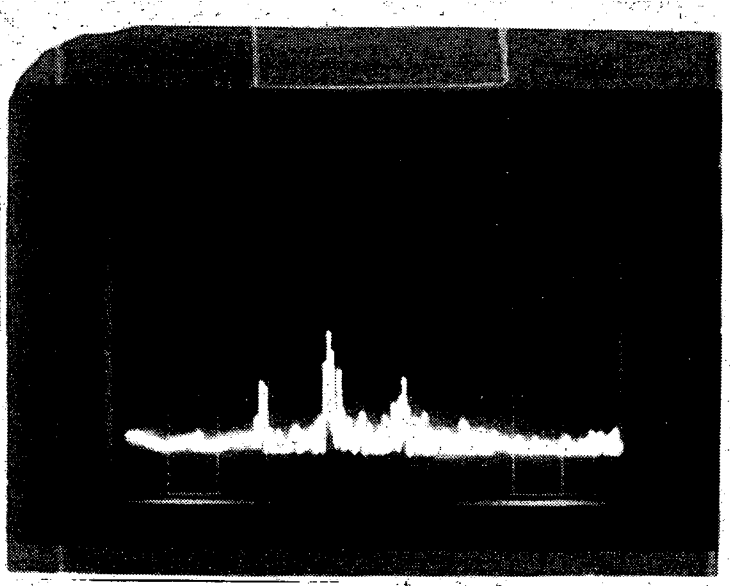

4.6-5a

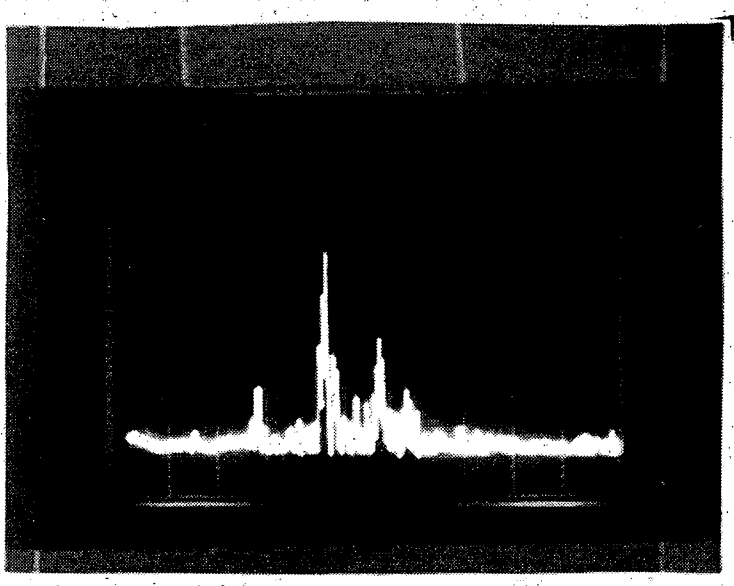

4.6-5b

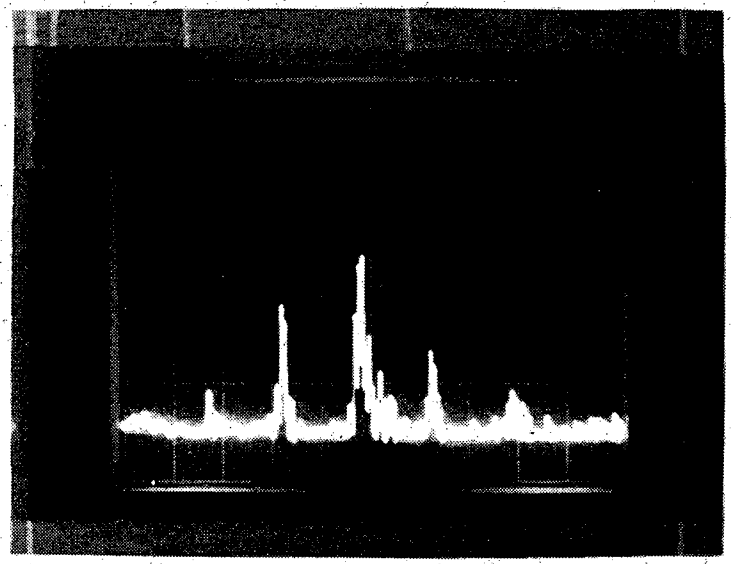

4.6-5c

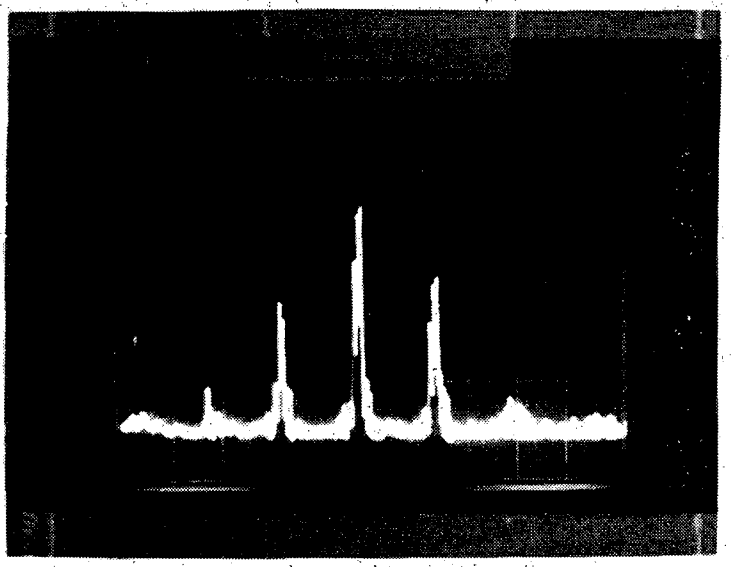

4.6-5d

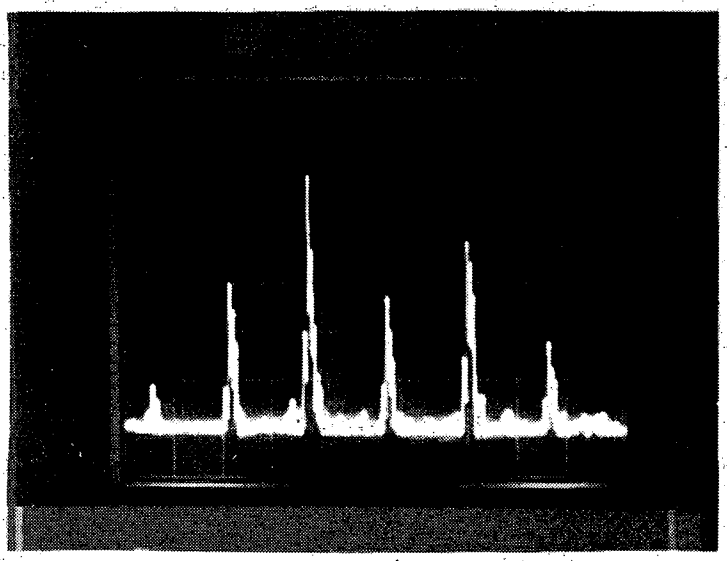

4.6-5e

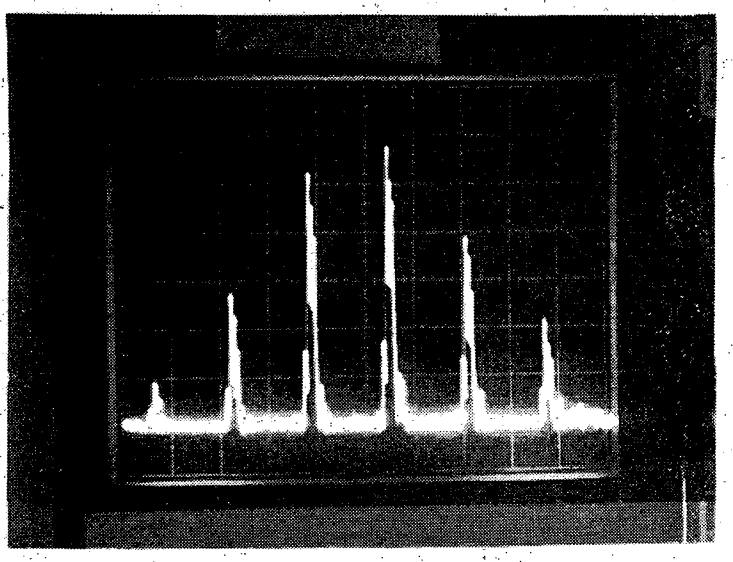

4.6-5f

Figure 4.6-5. Waveforms from specimen 6A using 5 MHz a) 45°, no notch, b) 45°, 3 mm deep notch, c) 53°, no notch, d) 53°, 3 mm deep notch, e) 60°, no notch, f) 60°, 3 mm deep notch. (time base is z s/div, is 1 V/div).

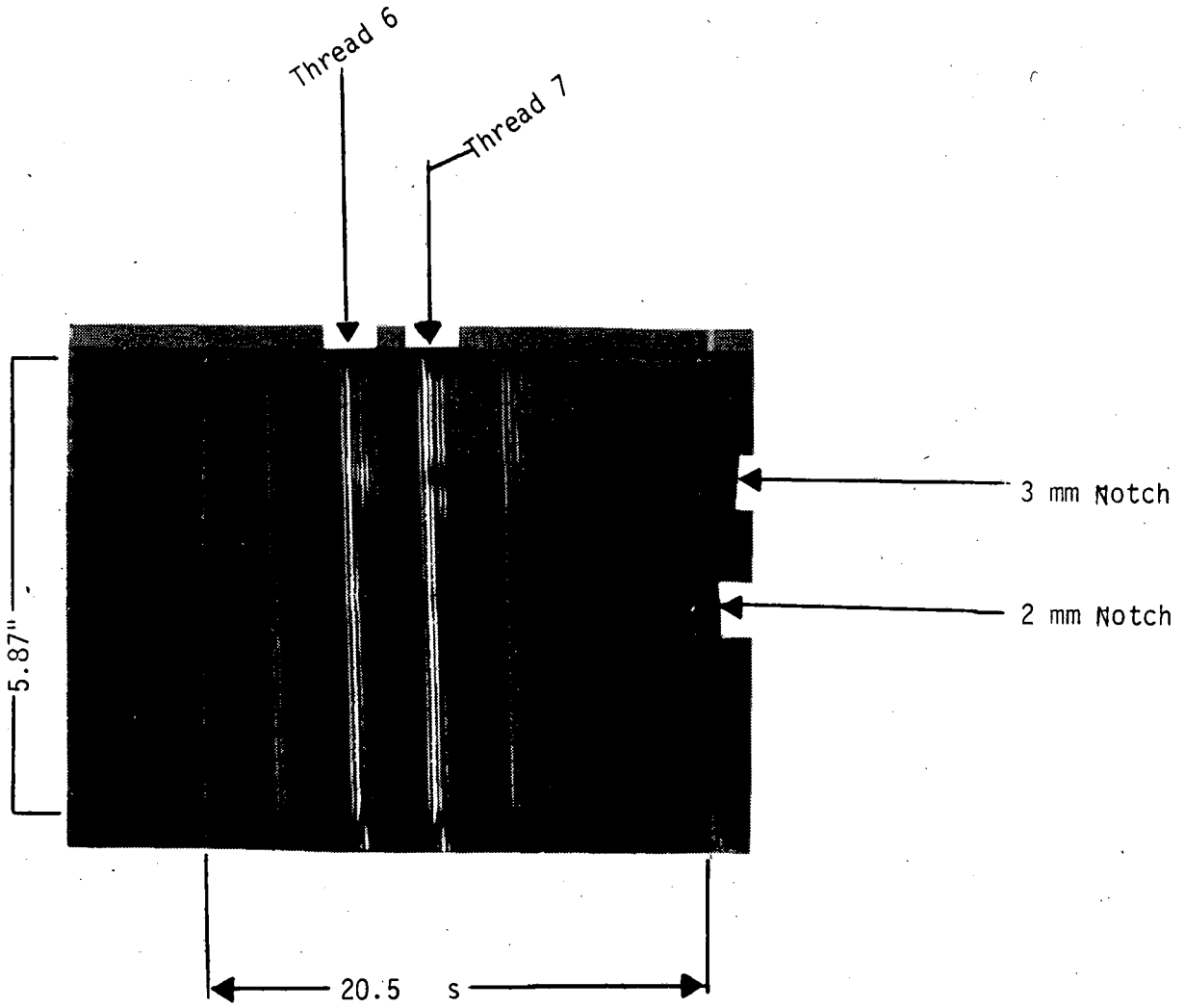

Figure 4.6-6. RF-B-scan of specimen 6A showing thread shadowing by 3 mm and 2 mm deep EDM notches. Image obtained with a 53°, 5 MHz shear wave.

TABLE 4.7-1

EFFECT OF CLEANING ON UT RESPONSE

Cleaning	UT Signal Improvement 2.25	5 MHz
Specimen A		
Water Jet (5000 psi)	2x	10x
Specimen B		
Plastic Scraper	1x	6x
Bristle Brush	2x	1.5x
Wire Brush	1x	1x

growth material. Further cleaning such as sandblasting or wire brushing does not improve response, but rather damages the surface. The flame spray coating was not noticeably damaged by the water jetting or plastic scraping with bristle brushing.

Barnacles, or their residual, cause a significant change in UT amplitude. Inspection over barnacle regions is therefore unreliable if based on UT amplitude. Based on the biofouled specimens, the barnacle residual could result in a 2% loss of inspectable area. When the inspection is performed from a clean inside surface, the biofouling does not appear to influence the response. For most inspections, the use of angle beams is important. The bouncing of angle beams on a biofouled surface is not dependent on biofouling, however there is some evidence that suggest a slight loss of signal if the bounce is at a barnacle location.

Overall, suitable cleaning can be obtained for UT inspection from the growth side. Inspection from the inside does not require external cleaning.

4.8 Imaging

The evaluation of defects by peak ultrasonic amplitude measurement is useful, but can be enhanced by imaging. In the imaging application, the peak amplitude value is plotted as a function of position. This provides the evaluator with a better means of interpretation.

Figure 4.8-1 is an image of the six EDM notches in SK001 (figure 4.4-1). A 60°, 5MHz beam was used. Notch depths are: E - 6 mm, F - 2 mm, G - 4 mm, H - 5 mm, I - 4 mm, and J - 5 mm. Figure 4.8-2 shows plots of the image area, 6dB drop and peak response vs notch depth for the two sets of notches. Each notch set is plotted spearately because the acoustic path length are difference due to the part geometry.

The area imaging results show better correlation to size in the H,I,J, case than the peak response. The 6 dB drop is a method used in defect sizing [Jessop]. The distance between the 6dB drop point from the peak signal is taken in each direction along the defect. The data can be obtained from the image and is plotted on the Figure 4.8-2 graphs on an arbitrary scale. The plot for E, F, G show very poor correlation to depth. The dB drop method often uses a 20dB point instead of six, however, in this data the results are not any more favorable. The area of the imaged defect does appear to be useful for interpretation. This of course, is particularly true for notches with known aspect ratios. Fatigue cracks will also possess an aspect ratio that falls within some prescribed bounds for the known geometry and stress. Imaging is therefore useful to assess not only the extent of the crack, but also estimate the depth. With threads present, however, the gate levels for imaging are restricted by the complicated thread pattern and so the nice image of 4.8-1 is not obtained. In the welded case, as will be shown in section 4.9, this is easier to perform. Images with threads and fatigue cracks are also shown in Section 4.10. Because of the thread problem, the B-scan imaging approach shown in Figure 4.6-6 is useful. Each line in the image is an entire waveform. Many B-scan images must be viewed to make up the area of a typical C-scan. This makes the inspection process much more data intensive.

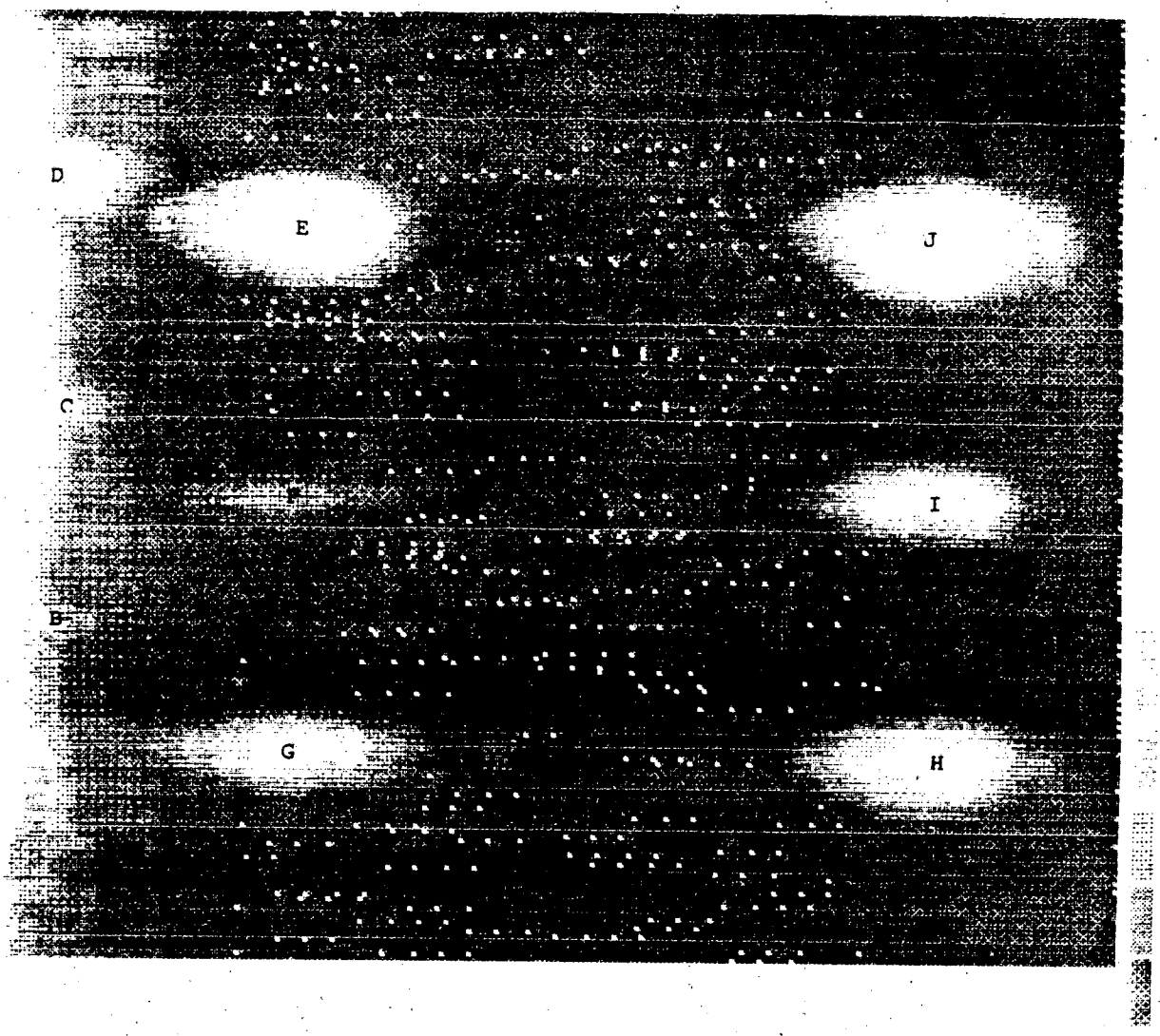

Figure 4.8-1. 60 degree shearwave C-scan of specimen #5 from the uncoated side.

OTC S63

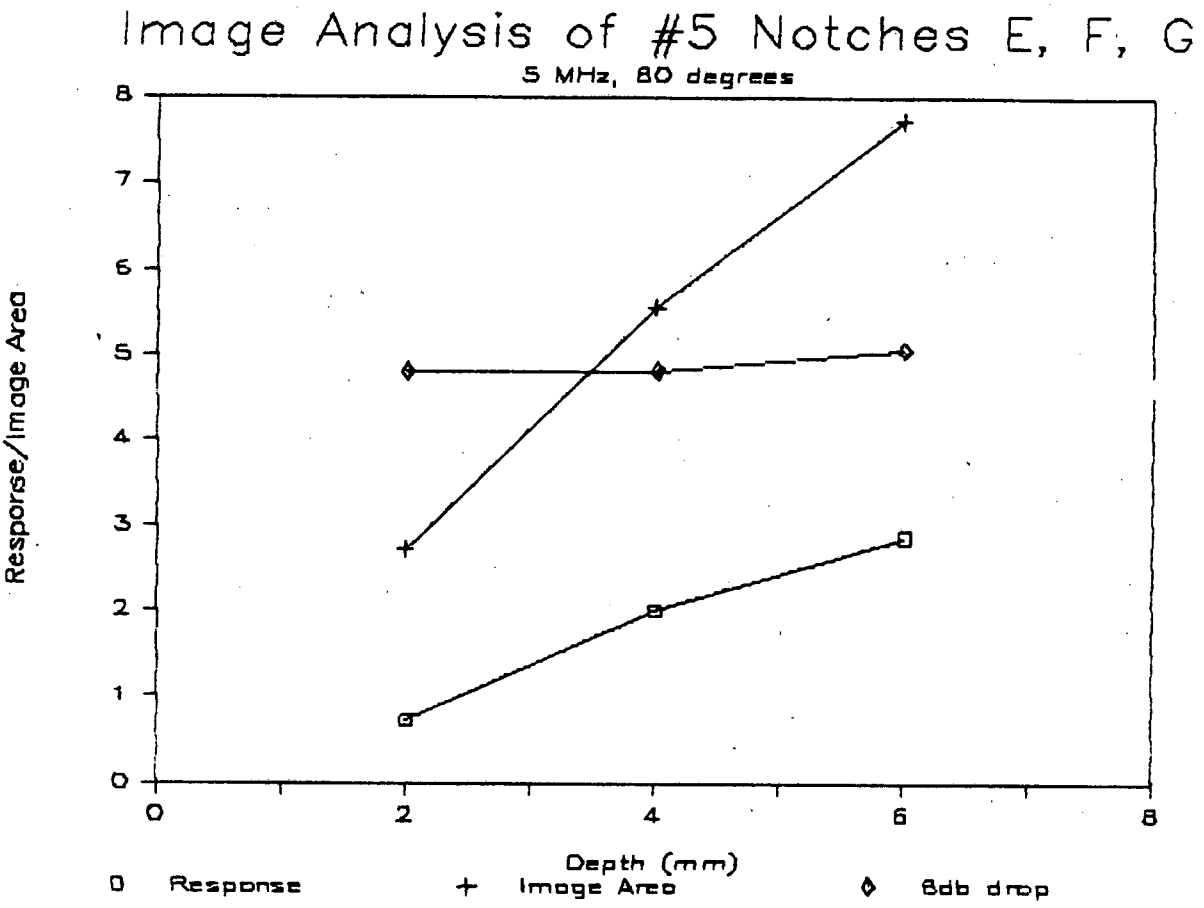

Figure 4.8-2a. Notches E,F,G Values.

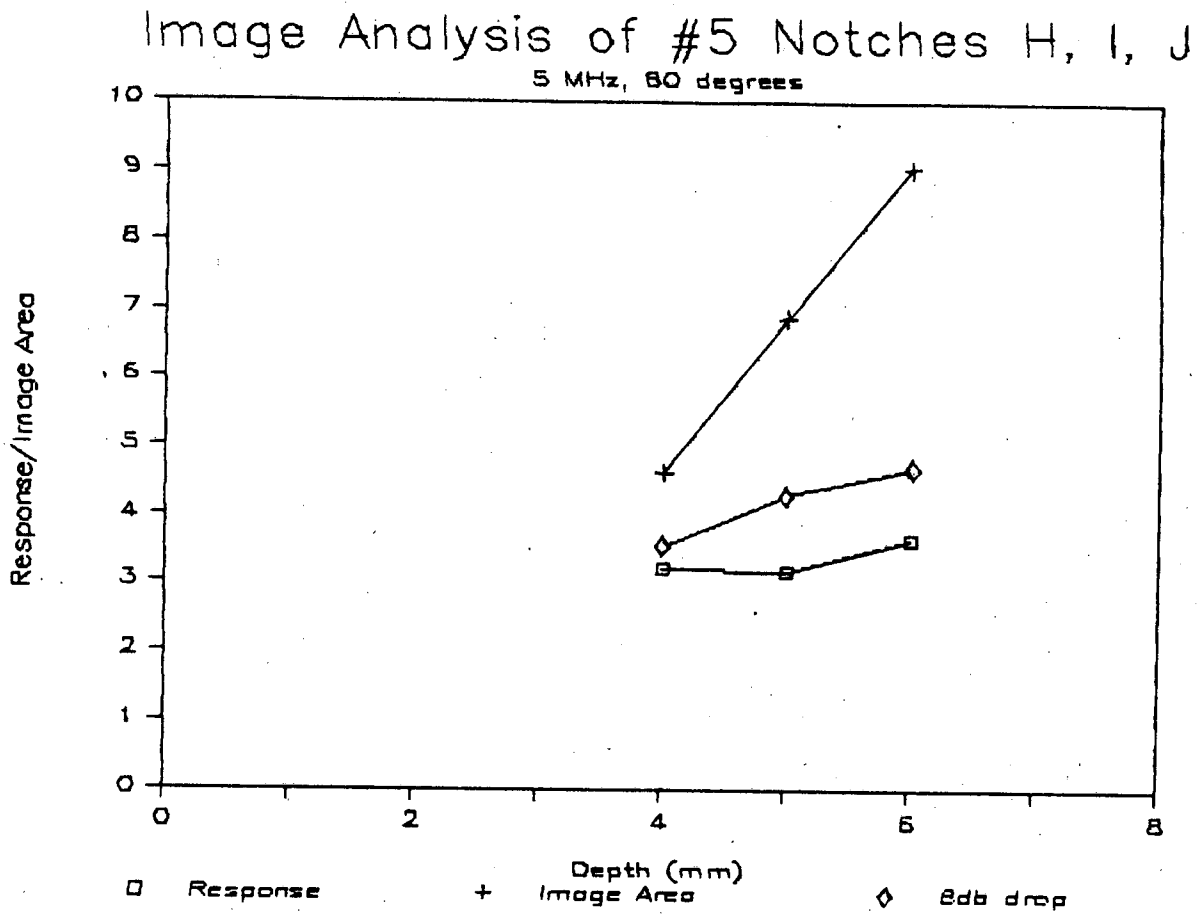

Figure 4.8-2b. Notches H,I,J Image Values.

4.9 Weld Samples

In addition to the threaded connectors, samples of welded specimens were provided by Chevron and Conoco as discussed in Appendix E. The Chevron sample was one inch thick flat plate HY-80 welded to WT70 material, and the weld was ground smooth. The Conoco material was rolled and welded line pipe 20 mm thick. Two samples were coated with epoxy and one was bare. The welds were in the as welded condition with both crown and drop through. The crown was approximately 25 mm wide consisting of about three beads and was 3 mm high. The drop through was approximately 8 mm wide with heights of between 0.9 to 3 mm. EDM notches were placed in the Chevron sample and the coated Conoco sample with notch depths of 5.1, 2.5, 1.3, 0.5, and 0.25 mm all with lengths of 50 mm.

Measurement of the longitudinal beam attenuation in the weld material of the small weld coupons indicated only slightly higher attenuation from the base material. In general, both the Chevron and Conoco samples were relatively clean acoustically. Because the samples are thin (20 to 25 mm), the attenuation is not a concern for inspection.

Ultrasonic C-scan images were taken using the Sigma Research UT2000 ultrasonic scanning system. A 5 MHz 0.5 inch diameter, six inch ground focal length transducer was used. The scanning was performed using a 1/2 V path as if inspection was to be performed from the outside of the tendon. Figure 4.9-1 shows the C-scan image of the flat Chevron piece at both 45 and 60 degrees with the scanning performed from the HY-80 and WT70 side. All notches are clearly detected by the scanning technique (reproduction images seriously degrades the intensity pattern in the images). The notch images appear proportional to their respective sizes. These prepared welds yield good sensitivity to small defects.

The Conoco specimen was scanned from the coated and uncoated sides simulating outside or inside inspection respectively. The curvature of the specimen prevented a single scan over the entire piece. Rather, small sections, where notches were present, were individually scanned. Figure 4.9-2 shows a sectioned layout for scanning. Figure 4.9-4 shows the scan images for notches A through E for the outside inspection using a 45 beam. All the notches are detected. The smallest notch (E) is even seen through the weld. However, the weld root is also imaged, and, in the case of an unknown inspection, the root signal could provide a 'false call'. Table 4.9-1 lists the relative strengths of the signals from the notches and the root for the outside inspection. The root signals in the images are indicated to be on the order of a 1 mm deep notch equivalent. Table 4.9-2 lists the relative response from the notches, root and crown from inside inspection measurements at 2.25 MHz and 5 MHz.

The notches have been shown to be inspectable by immersion, ultrasonic C-scanning, however, the unprepared welds also generate signals that may be misinterpreted as notch equivalent signals based on intensity. Imaging is helpful in discerning the source of the imaged signal, however, fatigue cracks will not necessarily have as distinct a geometry as notches. The signals from the crown and root can generate responses in the range of 1 mm deep notches.

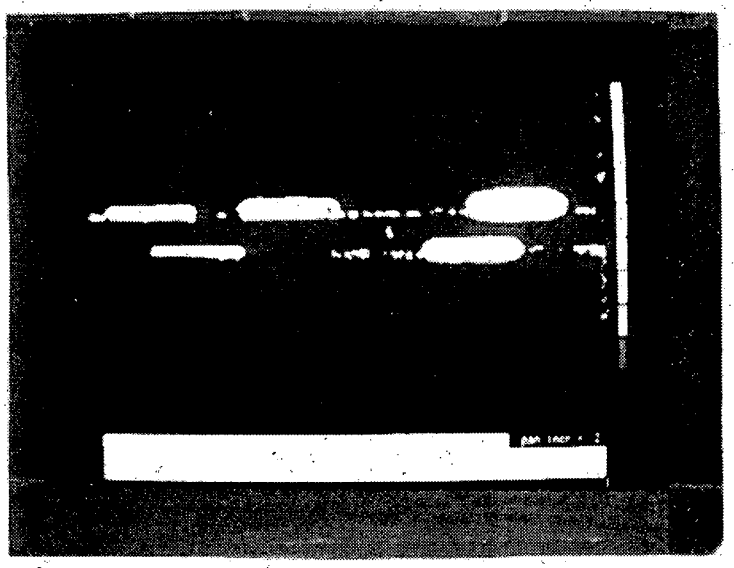

4.9-1a

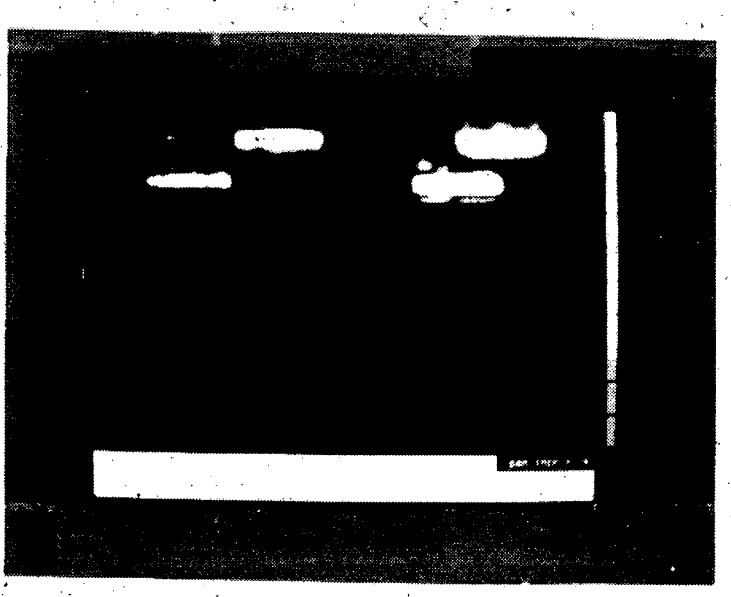

4.9-1b

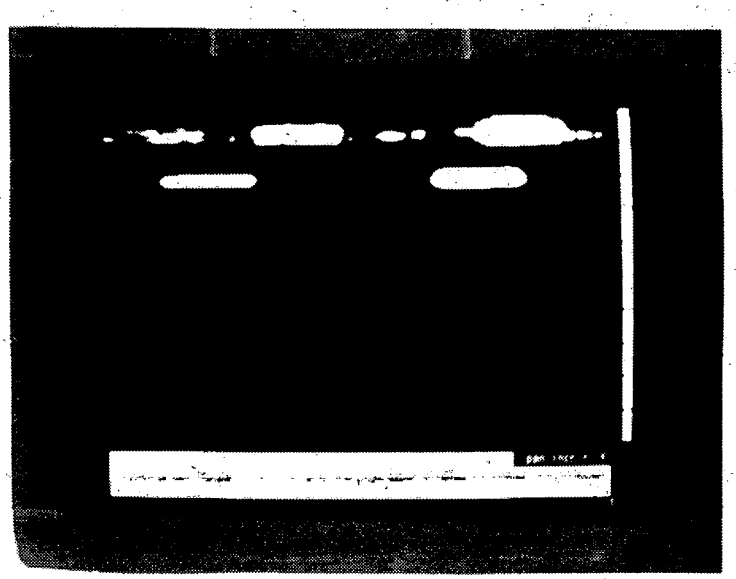

4.9-1c

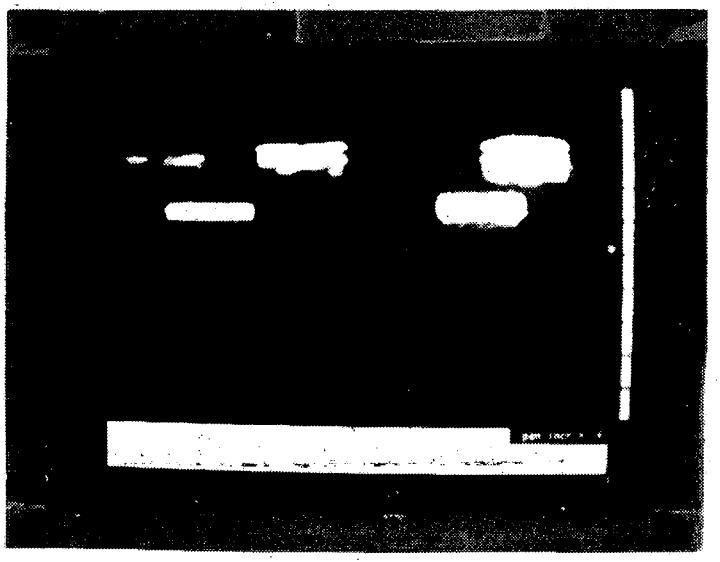

4.9-1d

Figure 4.9-1. Ultrasonic C-scan images of notches in Chevron test plate: a) HY-80, 45° shear, b) HY-80, 60° shear, c) WT70, 45° shear, d) WT70, 60° shear.

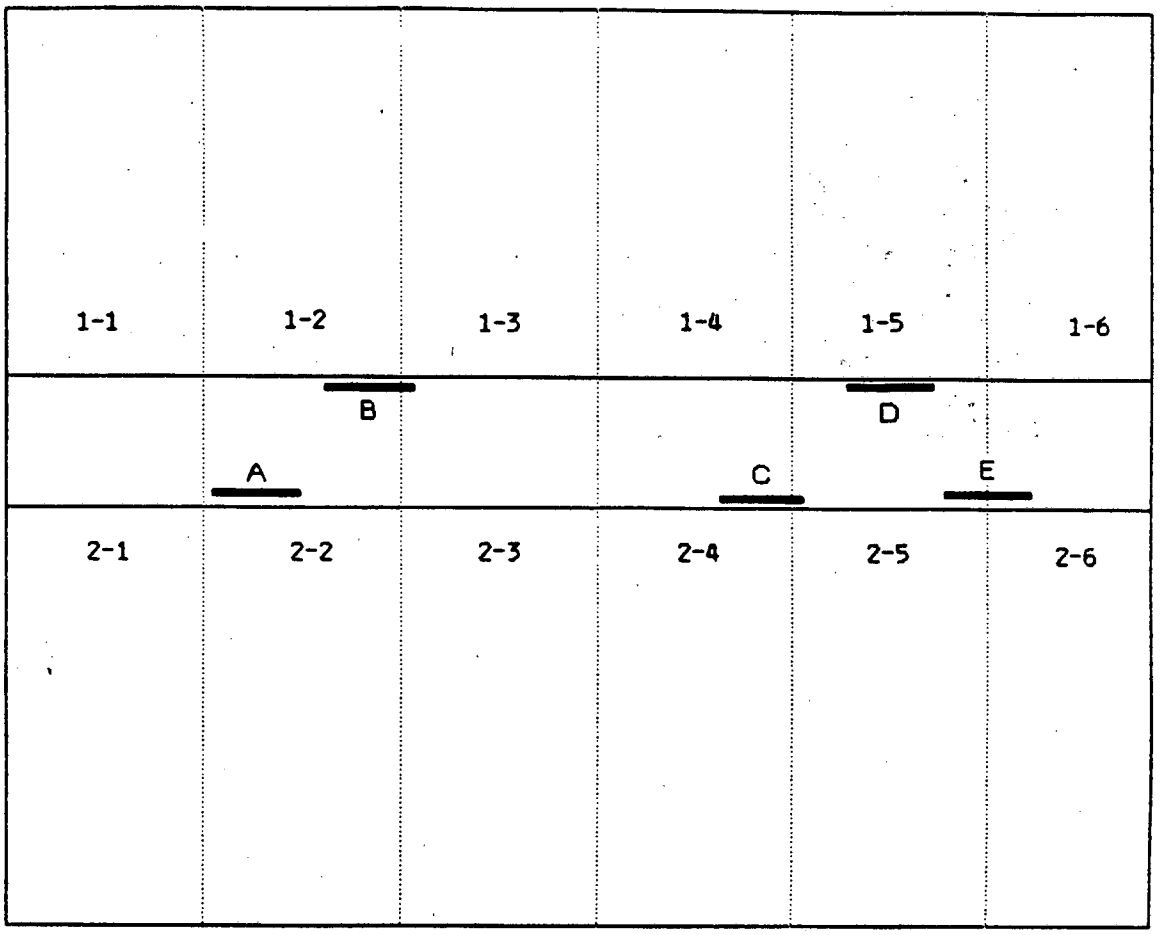

Figure 4.9-2 Section Layout for Scanning of Conoco Test Sample from Outside

68

INSPECTABILITY OF TENSION LEG PLATFORM TENDONS

PHASE II FINAL REPORT
January 1988

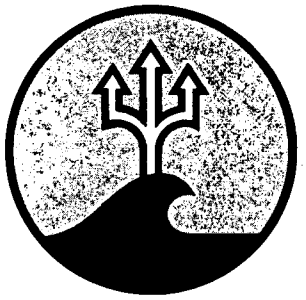

ARCTEC OFFSHORE CORPORATION

TABLE OF CONTENTS

TABLE OF CONTENTS (cont'd.)

1.0 EXECUTIVE SUMMARY

The objectives of Phase II of this study included:

1. Validate the Phase I ultrasonic model, particularly its ability to predict the minimum detectable flaw size as a function of geometry.

2. Evaluate effect on the ultrasonic model of material coatings likely to be used on TLP tendons.

3. Evaluate effect on model of Marine Biofouling.

4. Determine correlation between ultrasonic calibration using EDM notches and actual fatigue cracks.

5. Carry out a suitable 'blind test' to determine typical detection probabilities for actual fatigue cracks in threaded tubulars.

6. Update the Phase I failure analysis model as necessary to incorporate the experimental results of Phase II.

7. Make recommendations for tendon system design and inspection methodologies.

All of these objectives have been met with the exception that the "blind test" (Objective #5) was not carried out. A decision to eliminate this objective was reached after reviewing the data relevant to the sensitivity of thread form inspection. It appeared that the planned tests would not be directly applicable to actual tension leg platform tendon coupling designs.

Eighteen separate test pieces with 81 cracks or notches were used in this study to determine the effect of the various parameters on ultrasonic flaw detection and sizing. The results are summarized below.

1) Validation of Phase I Model

The model proposed in Phase I (Equation 3.1) is conservative for identifying the minimum detectable EOM notch size in a given geometry based on 0.001 echo response. However, it can not be used to accurately size defects much in excess of the minimum detectable size. An improved model is suggested. Attenuation in the materials considered for tension leg platform tendons in this study (i.e., HY-80, 4340, 2 1/4 Cr-Mo) is very low compared to some engineering materials and large grained steel. This means that beam spreading is the largest factor in loss of signal over distance. Inspection over path lengths of 600 mm round trip and greater are possible.

2) Effect of Marine Coatings

Coatings on materials can influence the transmittance and reflection of ultrasonic beams. Epoxy coatings cause about 20% loss in signal strength.

3) Effect of Marine Growth

Marine growth affects inspection significantly when the ultrasonic inspection is performed through the growth. Cleaning methods were tested showing scraping followed by bristle brushing was best. Scraping did not appear to seriously damage aluminum flame spray coatings.

4) Fatigue Cracks Compared to EDM Notches

Fatigue cracks of a given depth, in general, provide a lower reflection than electro-discharge machine (EDM) notches of equivalent depth. The average from the measurements of the response from fatigue cracks was less than 50% of the response from notches. This results in a need for more conservative requirements when setting standards to EDM notch sizes. The amplitude of signals from EDM notches and fatigue crack defects was found to generally increase with size but not proportionally to the defect size. At larger sizes (6 to 8 mm) deep, the amplitude response often saturated or reversed. These results are for fatigue cracks in unstressed specimens. Further tests are recommended with fatigue cracks under tension where ultrasonic response is expected to be greater.

5) Effect of Welds

Weld inspection can be inhibited by root and crown reflections if they are not removed. Allowance for weaker signals from fatigue cracks than notches causes the fatigue crack detectability limits to be even worse in the presence of unprepared welds. Tests with fatigue cracked specimens are recommended to determine crack detectability. Weld defect detection and sizing can be improved by imaging and signal timing methods.

6) Effect of Thread Pattern

The design of the thread pattern can strongly influence the interpretation of signals from thread roots or defects as a function of angle. This implies that optimum beam angles can be selected, and overall connector design should allow for the access of these beam angles to the inspection regions. Sizing of cracks in threaded geometries is expected to be more accurate using a shadowing technique rather than amplitude response. Thread design can be optimized to enhance this sizing method.

These results lead to significant conclusions regarding the design of TLP tendons for inspectibility:

- Thread designs should consider the potential for fatigue cracks in critical areas to be "shadowed". Finer thread forms will generally be more inspectible.

- Weld root and crowns should be removed to increase detectibility limits.

The results contained herein should provide a quantitative basis for evaluating these and other design tradeoffs.

2.0 INTRODUCTION

The 'Inspectability of Tension Leg Platform Tendons' program is a multiphase study to investigate tension leg platform (TLP) designs and how various parameters affect the inspectability. During the Phase I portion of the program, nondestructive evaluation (NDE) methods were evaluated for their applicability to in-service tension leg structure inspection.

Phase I of this study was initiated under the Small Business Innovative Research Program of the U.S. Department of Interior Minerals Management Service. During Phase I, the requirements for in-service inspection for TLP tendons was examined and non-destructive evaluation (NDE) methods were evaluated for their applicability to in-service tendon inspection.

The requirement for inspection was examined from the standpoint of tendon damage tolerance under various loading and other scenarios. The results indicated that in relatively benign fatigue environments and with suitable designs, the frequency of in place inspection could be very low - even beyond the intended service life of the structure. In very severe environments the inspection frequency could be less than the service life, however in any event design specific damage tolerance analysis is required to determine a suitable inspection interval. In any event, the Phase I analysis indicated a desireable threshold for crack detection in the range of 4-8 mm deep.

Ultrasonic NDE was found to be the most viable method for the conditions, designs, and inspection needs. An ultrasonic model was developed for nondestructive evaluation in complex geometries. The model was a mathematical simulation of the ultrasonic inspection, dependent upon the geometry under test for threaded connectors in tension leg platform design. Results of the Phase I investigations have been reported in the final report for Contract 14-12-0001-30204 (May 4, 1985).

The Phase II study has assembled materials and geometries of interest to experimentally test the model for predicting the acoustic response from notch defects. The Phase II program seeks to investigate factors that influence ultrasonic inspection defect detectability and sizing such as the material, coatings, and marine growth. Welded coupling design is also considered. The correlation of notch defect signal response to fatigue crack signal response is also evaluated in the program.

The Phase II program consists of sixteen major tasks. Table 2-1 lists the complete program. During the course of the study additional tests have been added and some tests deleted. Included among the tasks are measurement of the acoustic attenuation in materials of interest, measurement of the acoustic response from notches in coupling geometries without threads, measurement of acoustic response in the presence of threads, measurement of the affects of material coatings on the acoustic response, and measurement of actual fatigue cracks for response comparisons. Both threaded connectors and welded tendon connector geometries and materials were examined. Table 2-2 lists test specimens used in the program.

TABLE 2-1

PHASE II TASKS

Task #	Task Title	Notes
1	Planning	
2	Fabricate test samples	
3	Connector test samples notch response measurements	
	Welded test samples notch response measurement	
4	Fabricate thread samples	
5	Test threaded samples	
6	Correlate model	
7	Marine growth surface effects	
8	Fatigue crack calibrations	
9	Connector acquisition	
10	Connector calibration test	Not completed in program
11	'Blind' test	Deleted from program
12	Connector fatigue cracking	Deleted from program
13	UT of fatigued connector	Not completed in program
14	Joint project participation	
15	Analysis and reporting	
16	Additional tests:	Added to original program
	Image sizing from C-scan of SK001 Transducer spectrum analysis Shear beam spread over long path Off axis response calculations Flame spray surface condition Angle beam on barnacles Repeat fatigue crack measurements Weld defect imaging	

TABLE 2-2

TEST SPECIMENS

Task	Specimen	Purpose	Geometry	Material	Comment
3	1	Attenuation	8 x 4 x 3	2 1/4 Cr-1Mo[1]	
3	2	Attenuation	8 x 4 x 3	HY-80	
3	3	Attenuation	8 x 4 x 3	4340	
3	4	Flaw Size and Location Effects	20 x 6 x 2.5	2 1/4 Cr-1M	Bare Metal
3	5	Flaw Size and Location Effects	20 x 6 x 2.5	2 1/4 Cr-Mo	Epoxy Coated
3	6	Same as 4 and 5	20 x 6 x 1 3/8	2 1/4 Cr-Mo	Tool Joint Dimensions
3		Weld effects	15 x 16 x 1	HY80/WT70 [2]	Chevron
3		Weld effects	15 x 16 x t	X-60	Conoco
5	4A	Thread Effects	20 x 6 x 2.5	2 1/4 Cr-Mo	Buttress Thread
5	6A	Thread Effects	20 x 6 x 1 3/8	2 1/4 Cr-Mo	API V Thread
7	7	Marine Growth	20 x 4 x 2.5	4340 Al Flame Sprayed	Fouled and Water Jet Cleaned
7	8	Marine Growth	20 x 4 x 2.5	4340 Al Flame Sprayed	Fouled and Scraped/ Brushed
8	13	EDM notch versus fatigue crack	20 x 4 x 1	2 1/4 Cr-Mo	EDM Notch
8	14	Same as above	20 x 4 x 1	2 1/4 Cr-Mo	Fatigue cracked
8	15	Same as above	20 x 4 x 1	2 1/4 Cr-Mo	Fatigue cracked
8	16	Same as above	20 x 4 x 1	2 1/4 Cr-Mo	Fatigue cracked
8	5A	Same as above	20 x 6 x 2.5	2 1/4 Cr-Mo	Fatigue crack in thread
8	5AA	Same as above	20 x 6 x 2.5	2 1/4 Cr-Mo	Fatigue crack in thread

Notes:

1. 2 1/4 CrlMo is designation for ASME SA 387 Class 1 Steel
2. WT70 is Nippon prioprietary steel similar to HY-80
3. All alloy steel was heat treated to attain a minimum 50 Rc as quenched hardness, and tempered to a maximum 30 Rc.

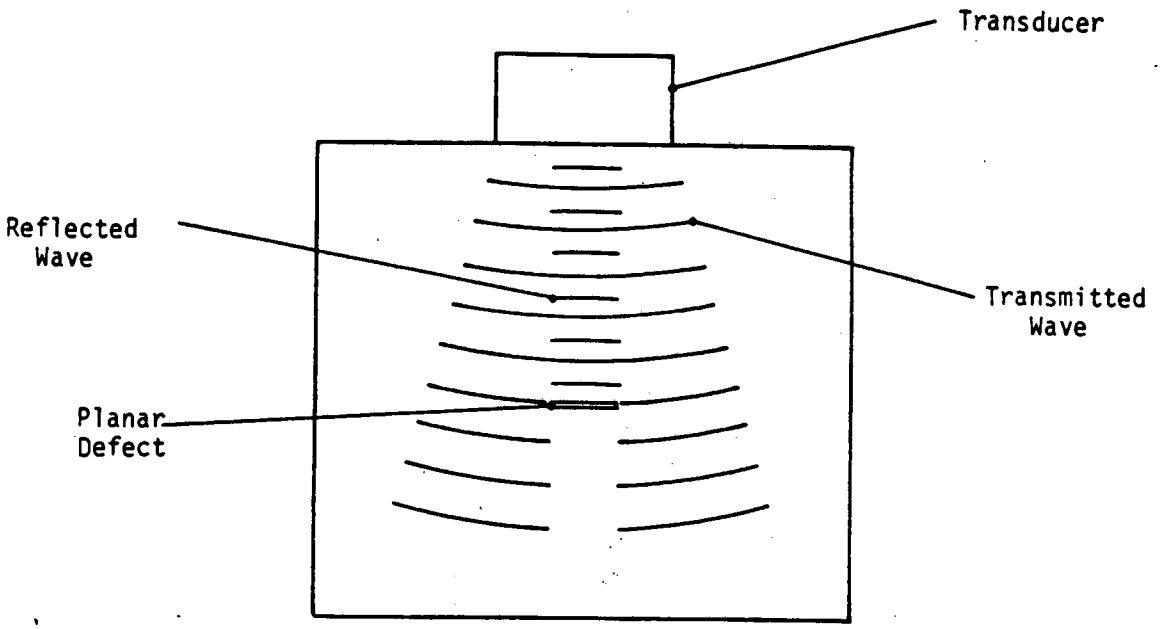

Figure 3-1. Example of ultrasonic reflection from a defect proportional to defect size.

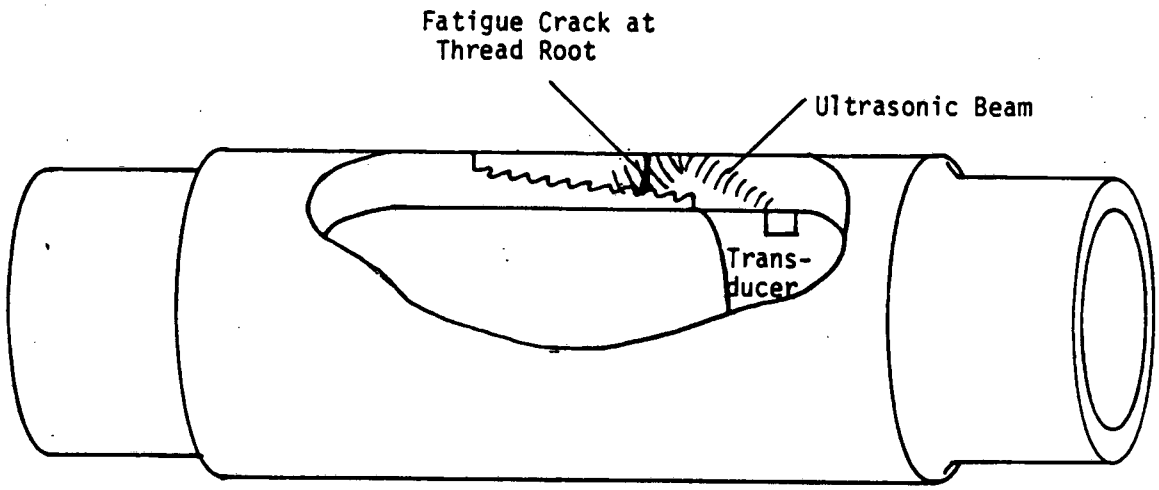

Figure 3-2. Threaded connector example of tension leg tendons with fatigue crack at root of thread.

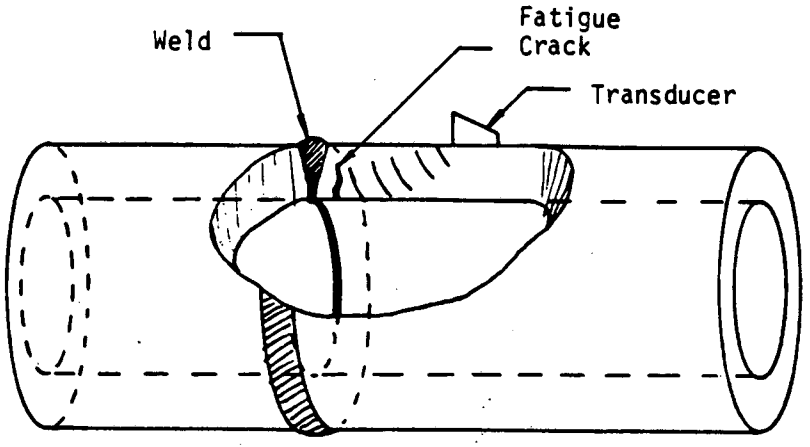

Figure 3-3. Welded connector example of tension leg tendon with fatigue crack in the heat affected zone of weld.

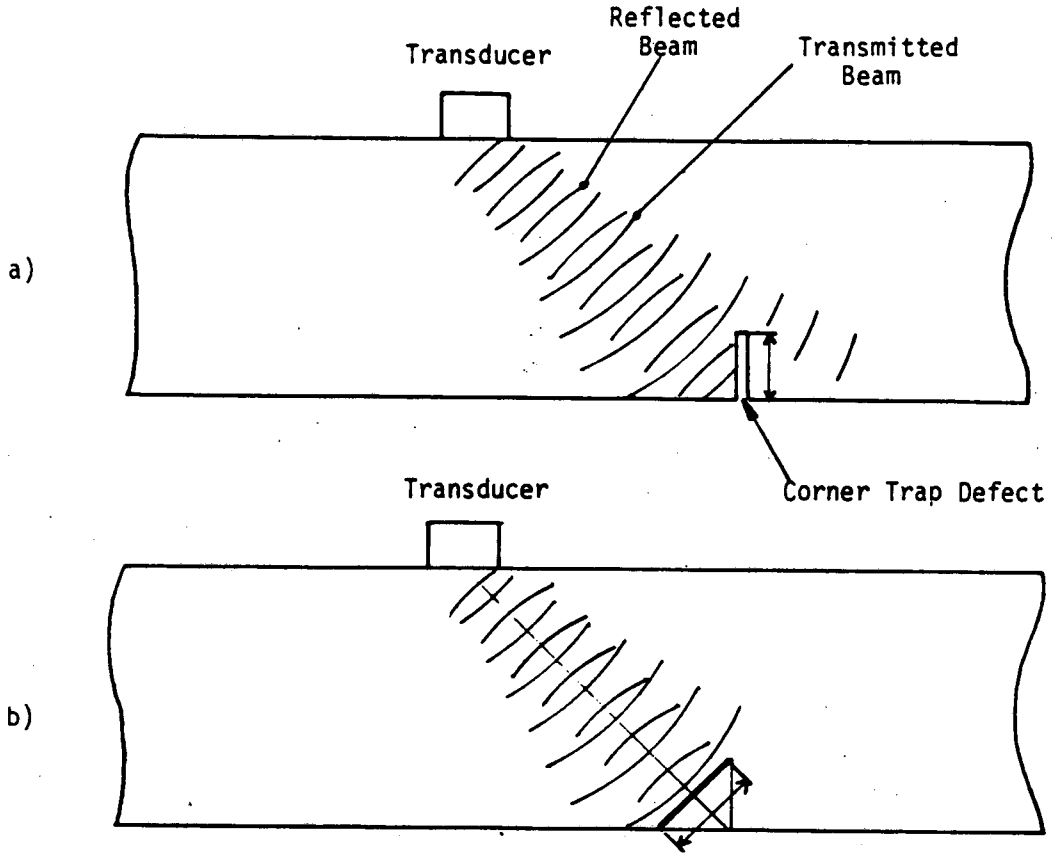

Figure 3-4. Corner trap reflection a) Beam configuration. b) Equivalent sized planar reflector when beam is at 45°.

3.0 BACKGROUND

During Phase I the ultrasonic model was developed from the basic principles of ultrasonic propagation and geometric optics. The equation for the acoustic response from a defect was given by:

$$p/p_0 = C_1 R^2 e^{-\alpha 2d} \frac{S_s S_f}{d^2 \lambda^2} \qquad (3\text{-}1)$$

where

p = Measured echo response pressure amplitude.

p_0 = Transmitted pressure pulse amplitude.

R = Reflection coefficient (=1.0 if beam path does not include reflection from a wall).

α = Attenuation coefficient.

d = Nominal distance between source (transducer) and reflection (crack).

S_s = Area of acoustic source.

S_f = Area of reflection.

λ = Acoustic wave length.

C_1 = Transmisivity coefficient between water and steel.

Equation (3-1) was derived from Kirchhoff diffraction theory considerations. This theoretical model assumes that the defect is planar lying in a plane perpendicular to the ultrasonic beam and that the beam is larger in diameter than the defect. Under these circumstances the energy reflected from the defect will return to the transducer and will be proportional to the defect size. Figure 3-1 demonstrates this condition. The model includes terms for the transmission of ultrasound across a boundary, reflection at a surface, attenuation over a path length and response from a reflector based on source and reflector size and beam spread. Values for the terms in this model can be found in the literature [Krautkramer].

The general geometric configurations of interest for tension leg platform design are shown in Figures 3-2 and 3-3. Figure 3-2 shows the threaded connector and Figure 3-3 the welded connector. The growth of fatigue cracks at roots of threads or in the weld zone will not form the simple geometry of Figure 3-1. Instead, the crack and edge of the part will form a type of corner reflector. It might be expected that the corner trap could be modeled as a planar crack of equivalent size to the shadowing effect of the beam as shown in Figure 3-4. In cases where the beam angle is not 45° and/or the

fatigue crack is not perpendicular to the surface the reflectivity of the corner is altered from that predicted by strict geometric raytracing consideration. A beam will nevertheless be returned to the transmitting transducer. The actual inspection of the tension leg connector therefore differs from the theoretical model in terms of the ultrasonic beam and orientation to the defect.

For actual inspections, transverse waves are preferred. Studies show that longitudinal waves tend to have a lower response from surface breaking cracks than transverse waves [Kapranos]. Also, when longitudinal waves are used in angle beam techniques, transverse waves will also be present which can generate confusing echo responses. In complex geometries, such as connectors, it is preferred to use beam angles of transverse waves such that the longitudinal waves are not present in the initially injected beam. This minimizes the number of confusing signals from multiple modes of ultrasound. Note, both longitudinal and transverse waves can be generated at reflection and refraction interfaces with relative magnitudes dependent upon the incident beam mode and signal. Transverse waves are also preferred because the wavelength is smaller than the longitudinal waves which is important in the detection of small defects.

The model of equation (3-1) is not the only model that could be considered. A more complex model that represents the components realistically can be developed as

$$p/p_0 = C_{21}(\theta,\phi)\, C_{12}(\phi,\theta)\, R_{21}^2(\theta) e^{-2\alpha d} \int_s \frac{R(\beta)}{d^2\lambda^2} e^{j(\omega t - 2kd)} \cos(\beta)\, ds \quad (3\text{-}2)$$

where

- p is the measured response
- p_0 is the amplitude at the first interface.
- $C_{12}(\phi,\theta)$ is the transmission across a boundary at incident angle ϕ in medium 1 and exit angle θ in medium 2.
- $C_{21}(\theta,\phi)$ is the transmission across a boundary at incident angle θ in medium 2 and exit angle ϕ in medium 1.
- $R_{21}(\theta)$ is reflection at an interface of medium 2 and medium 1 with angle θ.
- α is the attenuation coefficient.
- d is the path length to the reflector.
- λ is the wavelength.
- $R(\beta)$ is the reflection coefficient from the reflector as a function of angle β.
- β is the angle between the beam and the reflector.

ω is $2\pi f$ where f is frequency.

k is $2\pi\lambda$,

s is the surface of the reflector.

This model involves parameters that are more accurate than equation (3-1) [Haines]. However, not all the parameters are well understood or readily available. In particular, the parameter $R(\beta)$ must be obtained for every defect type of interest. Other models are under development and measurements are being made of their parameters [Chapman, Coffey, Thompson]. In the future much better predictions than the model of equation (3-1) will be developed. Within the scope of the current program, however, the equation (3-1) model has been used to gain insight into the ultrasonic inspection problem.

The amplitude response from defects, calculated from this theoretical model is useful for predicting conditions which will allow ultrasonic inspections. Other factors which influence inspectability are also important. These include the effects of material selection and coatings on the material and the presence of marine growth and marine growth removal methods. These factors will influence the predicted response from the model. The model predicts the amplitude response as a function of defect size. Defect sizing accuracy is an important element in inspectability. The amplitude response from defects has traditionally been used for crack size estimation in most ultrasonic inspection efforts. It is likewise well recognized that considerable deviations from expected response as a function of size in standards versus real defects exist. Factors such as defect type, shape orientation and surface condition in addition to size will influence the amplitude response [Rogerson].

The Phase II effort involved experimental tests of ultrasonic response from defects to correlate to the model. Although the experimental plan tested the response from geometries of interest it did not experimentally verify every parameter. Terms such as C_1 and R were used as givens from theory, since they are of relatively small overall consequence. Table 3-1 lists values of C_1 (transmission of ultrasound across a boundary) for beam angles utilized in the study and Table 3-2 shows values for the reflection (R) at an interface. Both tables are taken from the literature [Krautkramer]. Attenuation and response from a reflector are evaluated empirically in the tests. Variations from expected trends must be explained in terms of the specific test conditions and the limitations of the theory.

TABLE 3-1

COEFFICIENT FOR ECHO TRANSMISSION
FOR A WATER/STEEL INTERFACE

Incident Angle	Refracted Angle	Coefficient C_1
19.4	45	.17
21	50	.16
24	60	.15
26.1	70	.14
26.9	75	.13
27.2	77.5	.12

TABLE 3-2

REFLECTION COEFFICIENT FOR STEEL/WATER INTERFACE OF TRANSVERSE WAVES

Incident Angle (degrees)	R
45	.91
60	.93
70	.95
75	.96
77.5	.97

4.0 BASIC TEST PROGRAM

A basic test program was developed to investigate parameters that influence inspectability in both threaded and welded tension leg connector geometries. Tasks 1-8 of the Table 2-1 task titles were considered basic tests. The Task 16 additional tests are also part of the basic test program.

The verification of the ultrasonic theoretical model was performed for representative parts of the threaded connector geometry in Task 3. The threads were not included in the Task 3 measurements because there are no factors in the model of Equation (1) to account for threads. Rather, notches of selected sizes at selected locations on the tapered surface were used. Later, Task 5 tests were run on threaded samples to establish how threads affected measurements. Marine growth effects were studied for their effects on the acoustic response in Task 7. Welded samples were also tested for defect detection in the geometries of interest as part of Task 3. Finally, fatigue cracks were generated in samples to compare with notch responses in Task 8.

4.1 Experimental Technique

The experimental technique for the Phase IIA 'Basic Tests' uses conventional ultrasonic equipment. Measurements of ultrasonic response were taken in an immersion tank with a manual, vernier driven scanner. Figure 4.1-1 illustrates the setup used. The pulser/receiver system consists of a Metrotek 215 pulser and 101A receiver. These modules have fairly standard performance for the industry and are used in many modular component systems. The pulser applies a high voltage spike to the transducer. The transducers are common piezoelectric crystal materials. The primary set selected for the study is made of lightly damped lead zirctitanate (PZT). This transducer gives a relatively high response with a moderate bandwidth. Transducers of lead metaniobate, highly damped are also available. These transducers have a broad bandwidth and less noise than the PZT, but have a weaker response. The transducer crystals are cut to have a resonance at a specified frequency; 1 MHz, 2.25 MHz, and 5 MHz primarily. Used with the MP 215 pulser, however, the ultrasonic beam generated will actually be composed of a frequency spectrum about the center frequency. This 'real world' behavior of the transducer/pulser performance differs from the theoretical approach of the model where the calculations are based on specific frequencies values. The measurements are intentionally made using the 'real world' performance characteristics rather than developing specialized ultrasonic systems for theoretical verification measurements. This approach has greater meaning for future implementation of the technique in spite of reduced accuracy from the model representation.

4.2 Transducers

A number of transducers were available for experimentation. Table 4.2-1 lists the transducers. Appendix A includes transducer specifications. Not

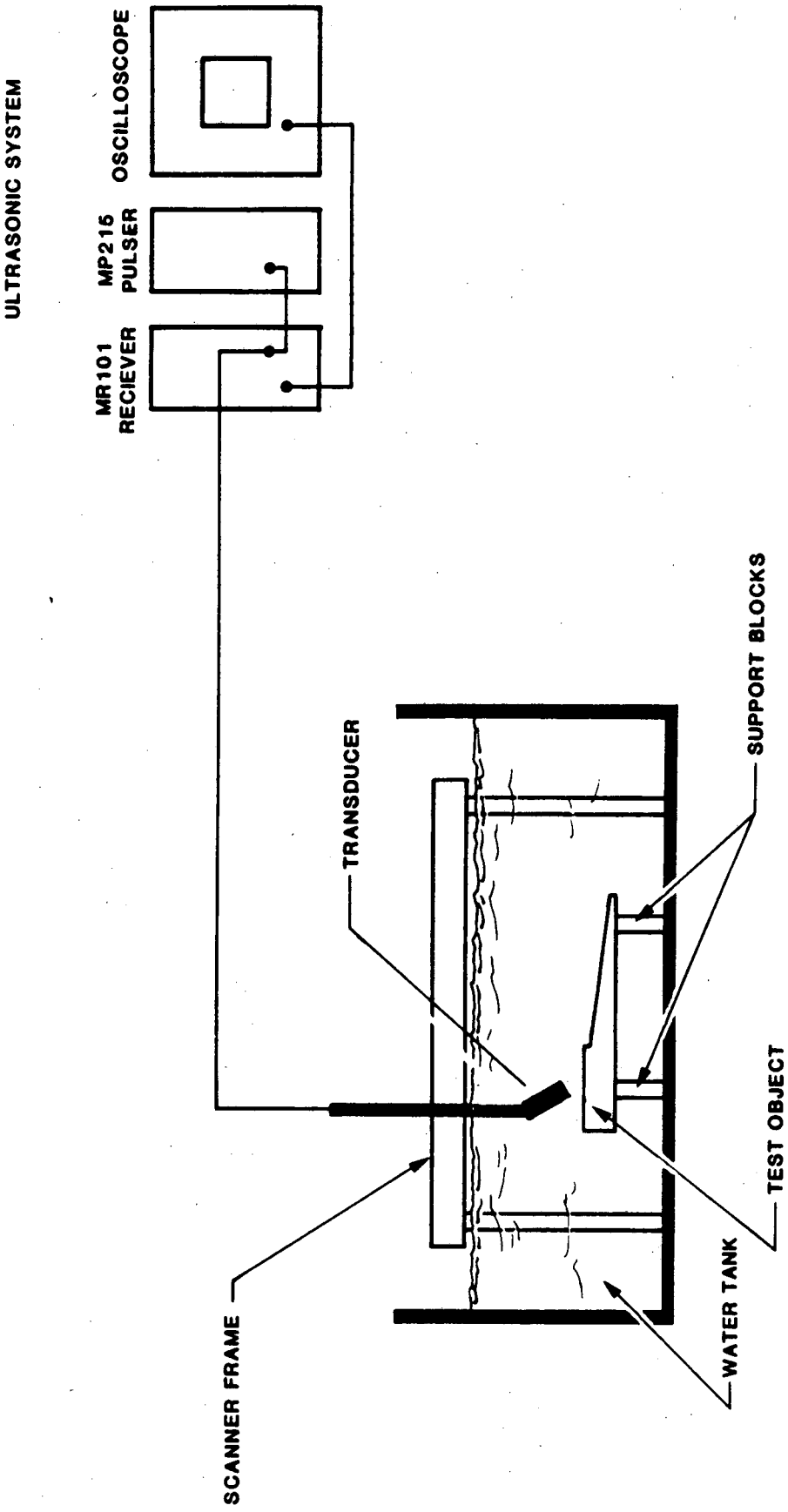

Figure 4.1-1 Experimental Setup

TABLE 4.2-1

TRANSDUCERS

Frequency (MHz)	Diameter (Inch)	Type	Manufacturer
5	1/2	SD-Z	Sigma
2.25	1/2	SD-Z	Sigma
1	1/2	SD-Z	Sigma
5	3/4	SD-Z	Sigma
2.25	3/4	SD-Z	Sigma
1	3/4	SD-Z	Sigma
5	1/2	KS-50	Ultran
2	1/2	KS-50	Ultran
10	1/2	WS-50	Ultran
5	1/2	WS-50	Ultran
2	1/2	WS-50	Ultran

all transducers were used in the experiments because to do so would require excessive testing time. The principal transducers were tested for the spectral characteristics. Appendix A shows the results of the measurements. The data was taken on the spectral content of a longitudinal beam in water and a longitudinal beam that had travelled a large distance (approximately 150 ms) in steel. Also a measurement was made from the echo of a shear beam in steel. The measurements were obtained by digitizing an echo waveform and Fourier transforming to produce the spectra. In many materials the attenuation of the acoustic beam is a function of the frequency. It is expected that over long path lengths, higher frequency contents of the beam will be more attenuated than the lower frequency and the spectral content will be reduced. The spectral tests in 4340 steel did not show significant changes in the spectral contents of the beams. If anything, the measurement shows a sharpening of the beam at 5 MHz for the longitudinal beam over the long steel path length. This indicates that the attenuation is low.

4.3 Attenuation Measurements

The attenuation of ultrasound in a material is composed of absorption and scattering terms. In Phase I, theoretical modeling of these terms were used to establish attenuation coefficients for calculations. The model was based on an assumed attenuation value at one frequency and extrapolating to other frequencies using the theoretical formula and constants for transverse wave scattering [Papadakis]. The attenuation coefficient is estimated as:

$$\alpha = \frac{\pi d^3}{6} f^4 s \text{ for } \lambda > 2\pi d$$

$$\alpha = d f^2 \Sigma \text{ for } \lambda < 2\pi d \qquad (4.3\text{-}1)$$

where

λ = the wave length

d = the average grain diameter

f = frequency

and S and Σ are material parameters. These equations indicate that attenuation is expected to increase with grain size and frequency.

In Phase IIA test samples of the materials were obtained and measurements made to determine values for the attenuation coefficient as a function of the frequency of the test. The measurement technique assumes the return echo from a transverse wave propagated through an isotropic media will be reduced in intensity due to attenuation and beam spread (diffraction). Figure 4.3-1 shows a test object for measurement studies. Two methods of measurement were used. One method sent the UT beam in on the slanting face and reflected off the back walls over short or long paths. Another method sent the beam in on

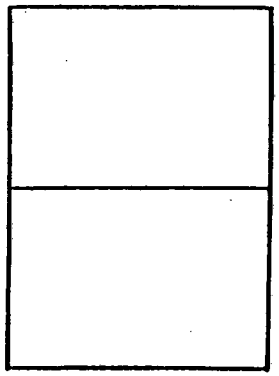

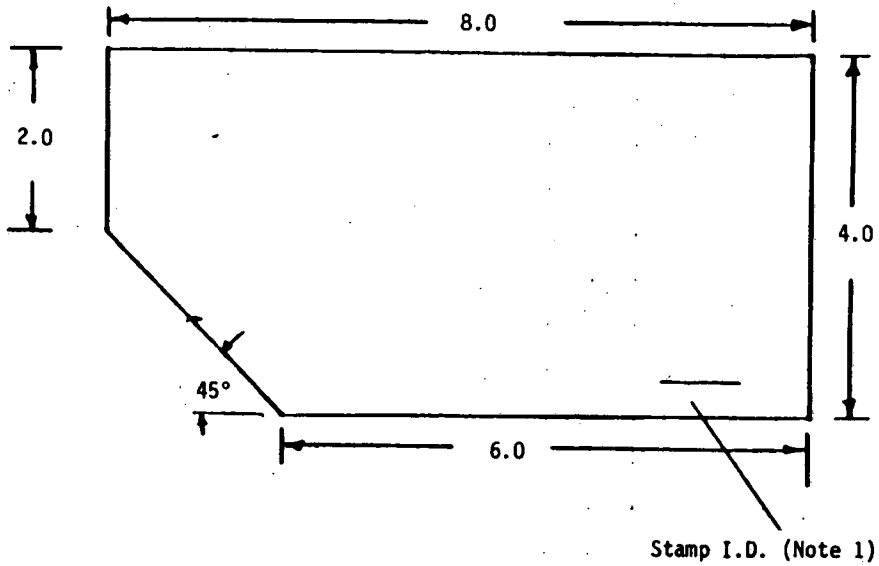

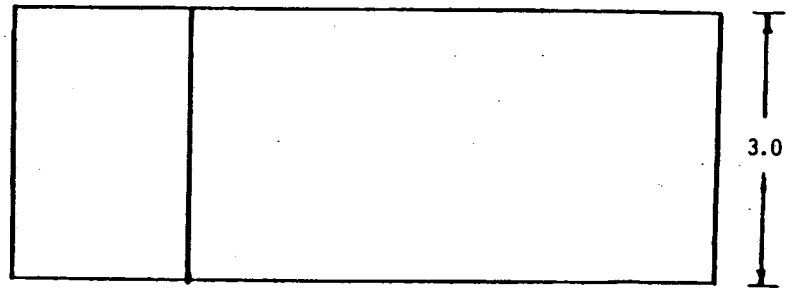

1. I.D. as follows:
   377-1 2 1/4 Cr-Mo
   377-2 HY-80
   377-3 4340

Figure 4.3-1

Acoustic Coupon EE-5			
DR. By	Date	Scale	SK
J.E.H.	11-5-85	1/2	004

the side and reflected off the slanted face. Using a standard diffraction spread that is inversely proportional to distance, the measurements result in no scattering attenuation. This result could be expected if the measurements are performed in test samples of limited size. In this case, the diffracted beam interacts with the side walls of the part and contributes to the measured signal. For the measurement techniques tested with the parts and instruments available, the conclusion is that attenuation is very low.

Longitudinal waves are easier to work with experimentally for attenuation measurements because the transducer is perpendicular to the part surface. Although the part size may also affect the measurements due to sidewall interaction, regimes of useful measurement are possible.

Table 4.3-1 contains a summary of the values obtained from longitudinal wave measurements in samples. There is considerable scatter in the data. Although fairly standard techniques for such measurements were applied [Burkle, Szilard], such variations are not uncommon in these measurements. As one author points out, few reliable absolute measurements of attenuation are reported in the scientific literature [Green, 1984] due to problems which include the coupling media affects which can contribute errors up to 20%, anisotropy in the material under test and diffraction spread of the ultrasonic beam. Also, attenuation measurements are usually performed in highly attenuative material. That is not the case with the materials of this study.

In private communication [Green, 1986] it was also discussed that, depending on grain structure, it is possible for the attenuation to be less at higher frequencies, as indicated by the 5 MHz data in these studies, although general theory predicts increased attenuation.

These attenuation values are useful in that they indicate the generally low attenuation of the sample materials. The values from Table 4.3-1 are in fact close to the values assumed in the Phase I study, except for the 5 MHz reduced values. Table 4.3-1 also includes some values of attenuation for engineering materials obtained from the literature [Papadakis]. The importance of the low attenuation in the materials considered for tension leg platforms is that longer beam paths may be used for inspection. Designing with highly attenuative material could seriously limit the ultrasonic inspection path. In weld zones, where grain sizes are altered, ultrasonic attenuation could be affected. Measurements were made on a Conoco weld sample (20 mm thick) to test for heat affected zone attenuation. However, in this relaitvely thin sample the attenuation difference between zones around the weld and base material could not be qualified. If larger welds are proposed in a design, the affect of heat treatment and grain size should be considered.

These values have therefore been used in calculations of expected response, for comparison to measured response in the next section. No correction of the longitudinal attenuation to equivalent transverse wave attenuation has been made. Transverse wave attenuation is generally greater than longitudinal wave due in part to increased scattering of the shorter wavelengths present. Nevertheless, the effect of the attenuation value over the path lengths in the material is a small effect on the response value. The beam spreading is the factor that contributes most to the loss of signal in the materials tested.

TABLE 4.3-1

EXPERIMENTAL MEASUREMENT OF
THE ATTENUATION COEFFICIENT

Material	Frequency (MHz)	Attenuation Coefficient (Np/mm)	Standard Deviation
2 1/4 Cr-Mo	1	.0012	.001
	2.25	.0024	.001
	5	.0013	.0008
4340	1	.0009	
	2.25	.0023	.001
	5	.00092	.006
HY 80	1	.00092	
	2.25	.0016	.0009
	5	.0014	.001

4.4 Acoustic Response Measurements

Acoustic response measurements from notches have been made on basic test samples. The acoustic response is a measure of the return echo pressure relative to the input wave pressure. The response measured in these sstudies is the ratio of the return echo peak voltage to the peak echo voltage from the front surface of the part. When a shear beam in the material is used, the front surface reference beam must be taken as a normal beam measurement with the same water path distance to the front surface as applied for the shear beam measurement. Prior to testing it was estimated that echo response sensitivities of 0.001 would be detectable. This parameter was used in determining minimum defect sizes to be included in test samples of various path lengths. The response value expected can be estimated by Equation (3-1) for simple geometries.

Measurements were made on specimens 4, 5, and 6 (Table 2.2-1). Figure 4.4-1 shows the configuration for specimens 4 and 5. Specimen 4 was bare while specimen 5 had an epoxy coating. The material is 2 1/4 Cr-Mo in both specimens. Figure 4.4-2 is the configuration for specimen 6 and the material is also 2 1/4 Cr-Mo. The Figure 4.4-1 and 4.4-2 test specimen configuration can represent either box or pin portions of a connector. If the location of the transducer is inside the tension leg the inspection of the threads will involve a bounce path for the box inspection. Figure 4.4-3 shows the assumed ray paths of the beams and Table 4.4-1 lists the general inspection conditions for the response measurements on the two test samples. The pin inspection (assuming an inside location of the transducer) is much simpler because the beam enters the flat surface of connector geometry and has relatively short path lengths to the threads. Angle beams of 45° and 60° were tested in this configuration. For inspections with the transducer on the outside of the tension leg the box and pin geometries are the reverse of those discussed above. The difference on outside and inside inspection with respect to geometry is the curvature of the connector. These tests did not consider curvature. In small diameter legs this would create an additional parameter to be considered by the analysis.

The results of the acoustic response measurements are described in Appendix B. The following conclusions were drawn from these measurements.

- Response sensitivities in the range of 0.0001 are possible.
- Trends of response follow predicted model.
- Sizing of notches based on response using the model is not accurate.

Figures 4.4-4 and 4.4-5 are two representative figures of the acoustic response measurements. The calculated response shows a higher slope than the measured. The measured response shows a leveling off of response with notch size. This effect will appear again in the fatigue crack measurements as well. The conclusion is that the model can be used for order of magnitude estimates of response but not for accurate prediction of notch sizes. The predicted 0.001 sensitivity proved to be conservative. All notches in the test samples were detected. In general, the model is conservative for predicting the minimum notch size, i.e. notches showed a greater response at small sizes than the model predicted. This is helpful, because as later data

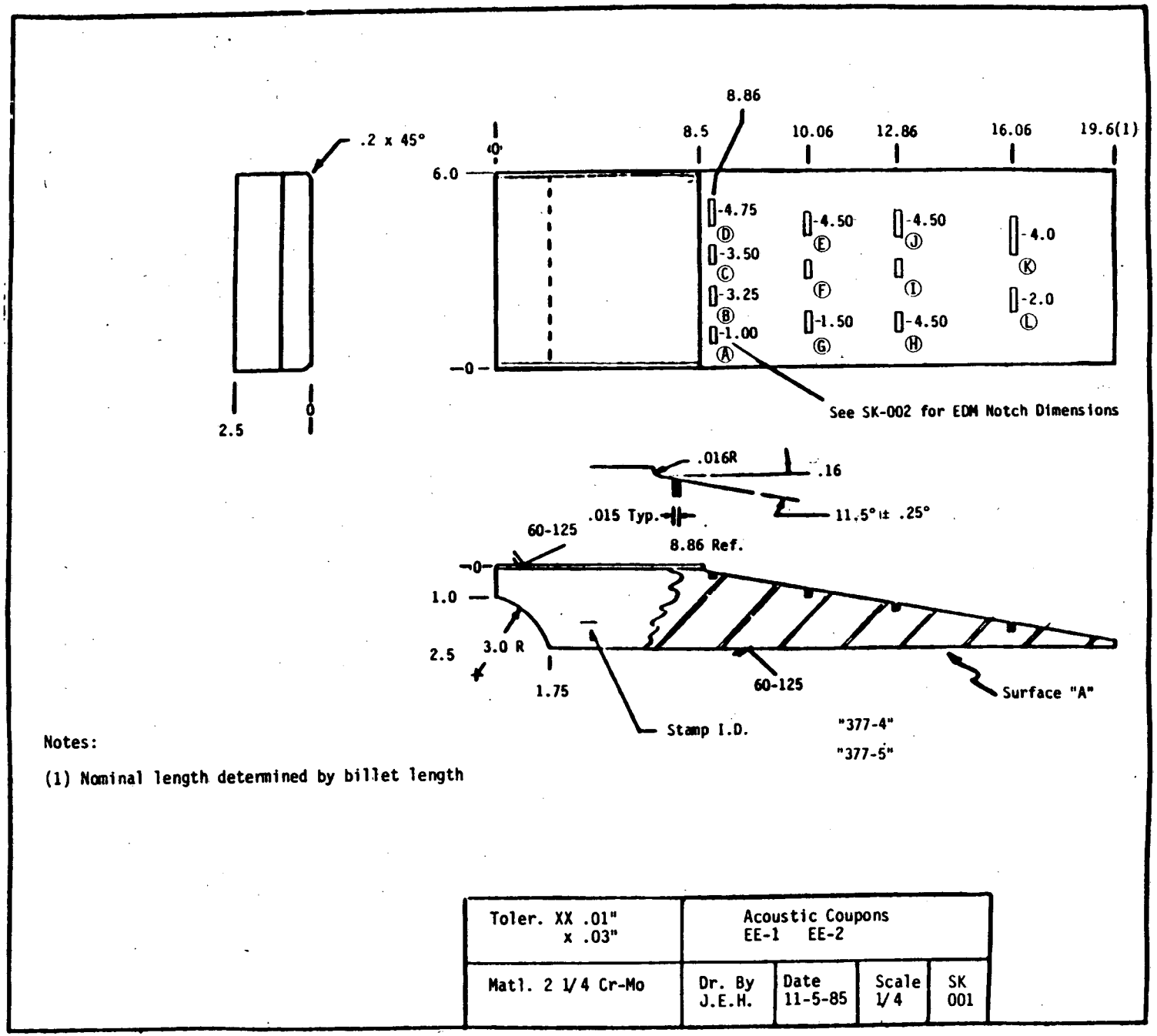

Figure 4.4-1a SK 001 Test Sample

Notches	mm			inches			Tolerances (inches)		
	a	c	R	a	c	R	a	c	R
A	2.0	6.0	3.3	.079	.235	.128	.001	.002	.001
B	3.0	9.0	4.9	.118	.354	.192	.001	.004	.002
C	4.0	12.0	6.5	.157	.422	.256	.002	.005	.003
D	6.0	18.0	9.8	.236	.709	.384	.002	.007	.004
E	6.0	19.0	9.6	.236	.709	.384	.002	.007	.004
F	2.0	6.0	3.3	.079	.235	.128	.001	.002	.001
G	4.0	12.0	6.5	.157	.472	.256	.002	.005	.003
H	5.0	15.0	8.1	.197	.591	.320	.002	.006	.003
I	4.0	12.0	6.5	.157	.472	.256	.002	.005	.003
J	6.0	18.0	9.6	.236	.709	.364	.002	.007	.004
K	8.0	24.0	12.0	.315	.945	.512	.003	.009	.005
L	6.0	13.0	9.6	.236	.709	.364	.002	.007	.004
M	1.0	3.0	1.6						

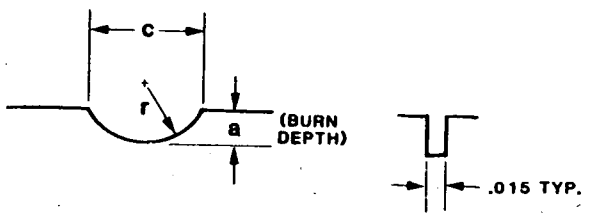

Figure 4.4-1b

$$A = R(\Theta - 1/2 \sin 2\Theta)$$

$$\Theta = \sin^{-1}(c/2R)$$

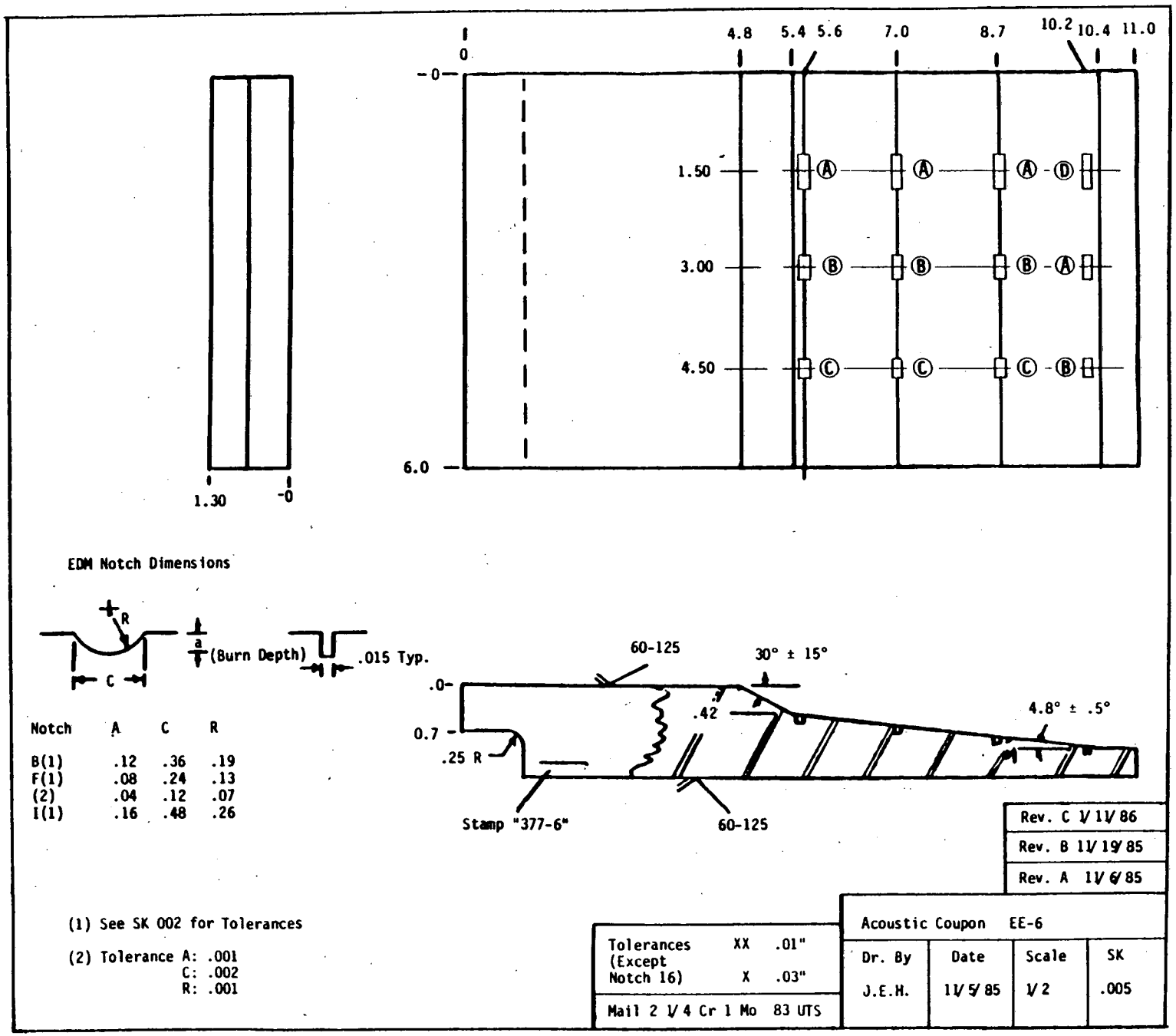

Figure 4.4-2 SK 005 Test Sample

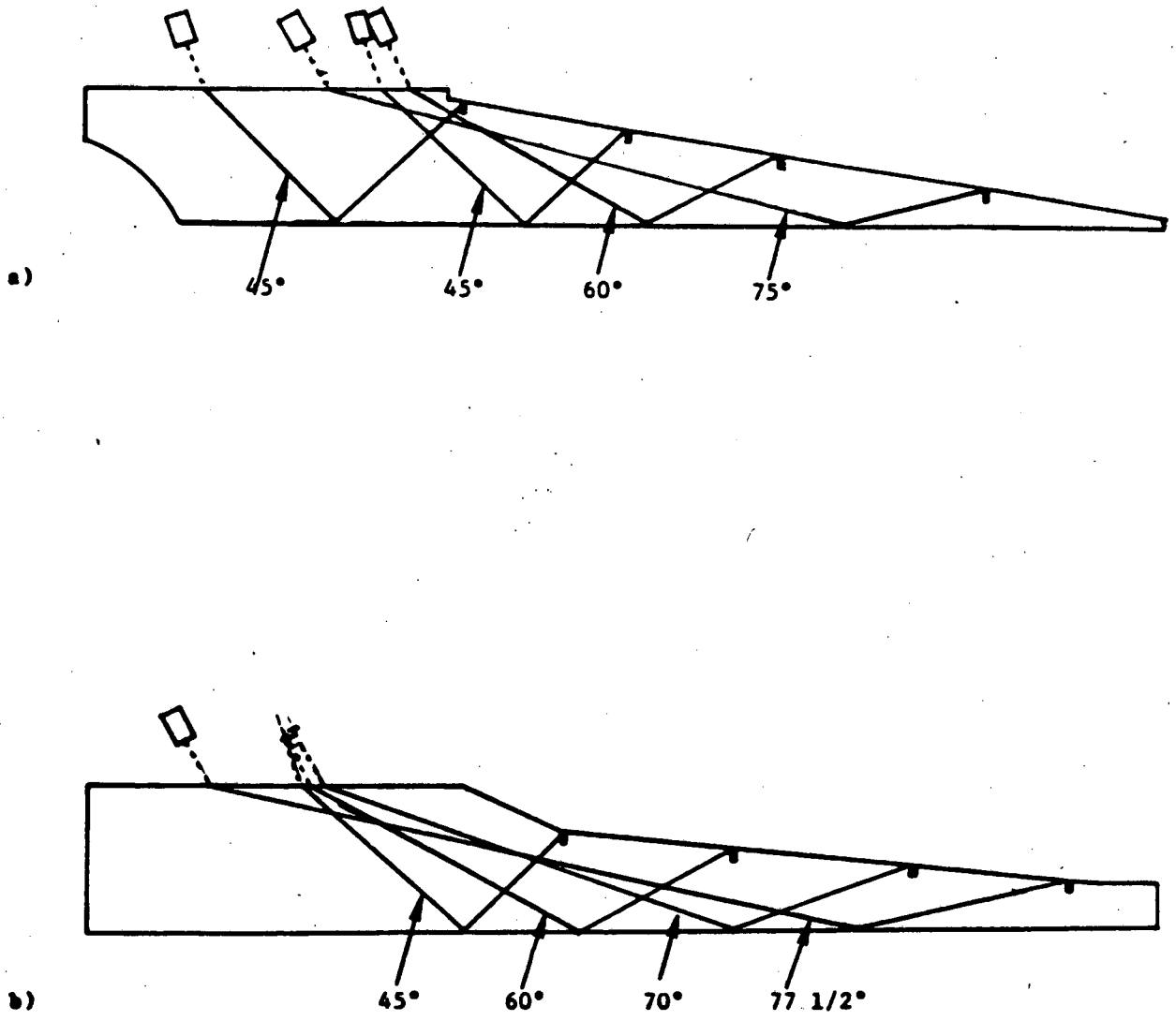

Figure 4.4-3. Ray paths used for box configuration inspection of a) specimens 4 and 5, Figure 5, sk001, and b) specimen 6, Figure 6, sk005.

TABLE 4.4-1

BEAM CONFIGURATION

Specimen	Defect Set	Transducer Angle (degrees)	Shear Beam Angle (degrees)	Path Distance In Part (mm)
4 and 5	A,B,C,D	19.4	45	171
	E,F,G	29.4	45	162
	H,I,J	24	60	201
	K,L	26.9	75	312
6	Row 1	19.4	45	83
	Row 2	24	60	112
	Row 3	26.1	70	153
	Row 4	27.2	75	227

will show (Section 4.10), fatigue cracks have a lower response than EDM notches. By increasing the echo response sensitivity factor for detectability, this can be accounted for. A sensitivity of 0.00-2 is proposed as a possible value for minimlum fatigue crack detection. The model of equation (3.1) can therefore be used in design studies to estimate minimum detectability provided the assumptions of path lengths for far field inspection are correctly applied (see Appendix B). If the minimum defect size predicted by the model is greater than critical size requirements then a more detailed analysis and testing approach would be needed to assure that detectability could be achieved.

4.5 Coating Effect

The effect of coating on the acoustic measurements was tested by the fabrication of specimen 5 with an epoxy coating. The coating was SkotchKote 206N following specifications of the National Association of Pipe Coating Applicators (NAPCO), Bulletin 12-78. The results of Figures 4.4-4 and 4.4-5 show the response when the beam has used the bounce path of Figure 4.4-3 on the uncoated Specimen 4 and epoxy coated Specimen 5 surface. Figure 4.4-5 shows a significant loss due to the coating while 4.4-4 shows little change. Tabulating all measurements, the response shows approximately a 20% loss of signal. Measurement from the pin side configuration where the beam passes through the coating with no bounce path also show the general trend of a reduced signal of 20%.

Measurements were also made at four locations on the coated surface to investigate the coating to metal interface. The following time separations between the front of the coating and the coating/metal interface were found: 220, 340, 480, and 500 ns. If the acoustic velocity in the epoxy coating is known, the thickness can be calculated. The locations were selected to cover the range of thickness found on the sample.

4.6 Thread Effect

Threads were added to the specimens 4 and 5 (SK001 design) and specimen 6 (SK006 design) to test the effect of threads on the acoustic response. Appendix C contains details of the part changes for the thread effects study. The addition of threads into the geometry of Figure 4.4-3 complicates the return echo signal significantly. The echoes from the notches in the threaded geometry can become buried in the periodic spacing of thread echoes. The pattern is a function of the ultrasonic beam angle and the thread pattern design. This results in some important implications for the design of threaded connectors to allow for inspectability.

Tests were performed using the box geometry of Figure 4.4-3 with beam angles between 45° and 60°. Figure 4.6-1 shows a plot of the echo response intensity from the threads as a function of angle for specimen 4A. With this thread shape (EPR modified buttress) there is a strong response from the threads around 45 beam angle in the steel which decreases with increasing angle. Above 53 , the signal from the threads is significantly weaker. Figure 4.6-2 shows the response from notches in specimen 4A as a function of angle. In this case, the notches show a better response around 53 than at 45 . In the

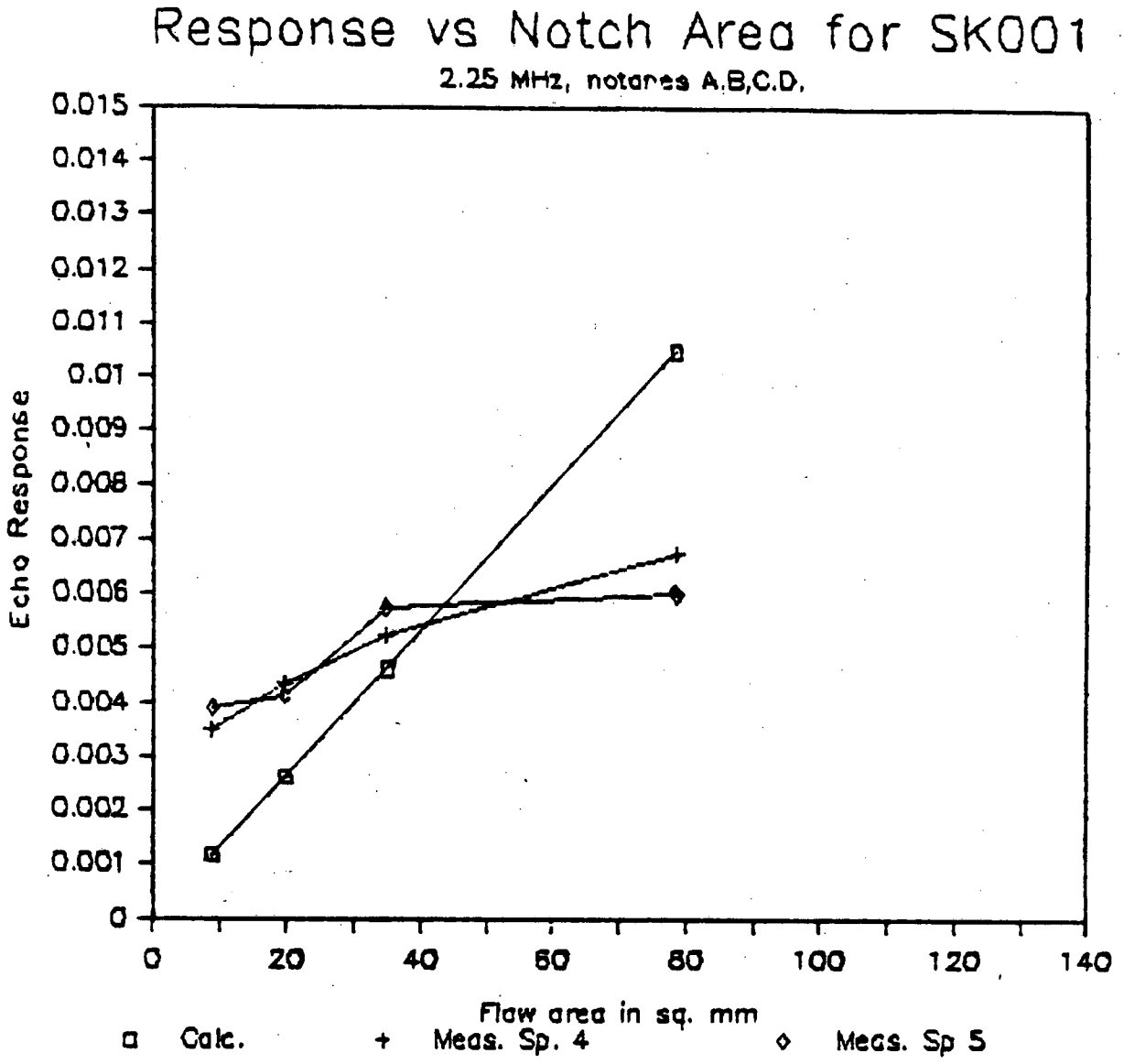
Response vs Notch Area for SK001
2.25 MHz, notches A,B,C,D.
Echo Response
0.015
0.014
0.013
0.012
0.011
0.01
0.009
0.008
0.007
0.006
0.005
0.004
0.003
0.002
0.001
0
0
20
40
60
80
100
120
140
Flaw area in sq. mm
Calc.
Meas. Sp. 4
Meas. Sp 5

Figure 4.4-4

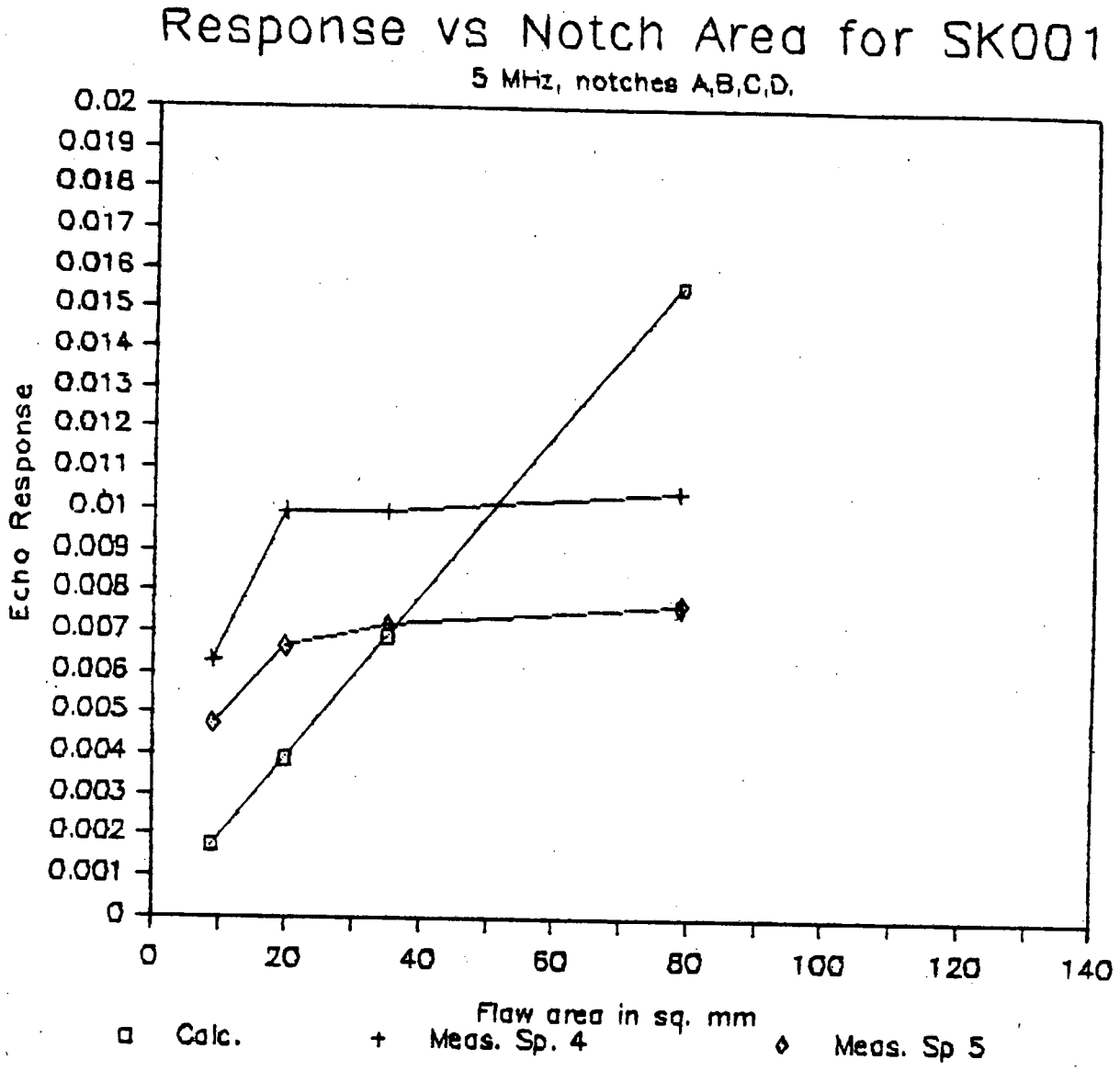
Response vs Notch Area for SK001
5 MHz, notches A,B,C,D.
Echo Response
0.02
0.019
0.018
0.017
0.016
0.015
0.014
0.013
0.012
0.011
0.01
0.009
0.008
0.007
0.006
0.005
0.004
0.003
0.002
0.001
0
0
20
40
60
80
100
120
140
Flaw area in sq. mm
Calc.
Meas. Sp. 4
Meas. Sp 5

Figure 4.4-5

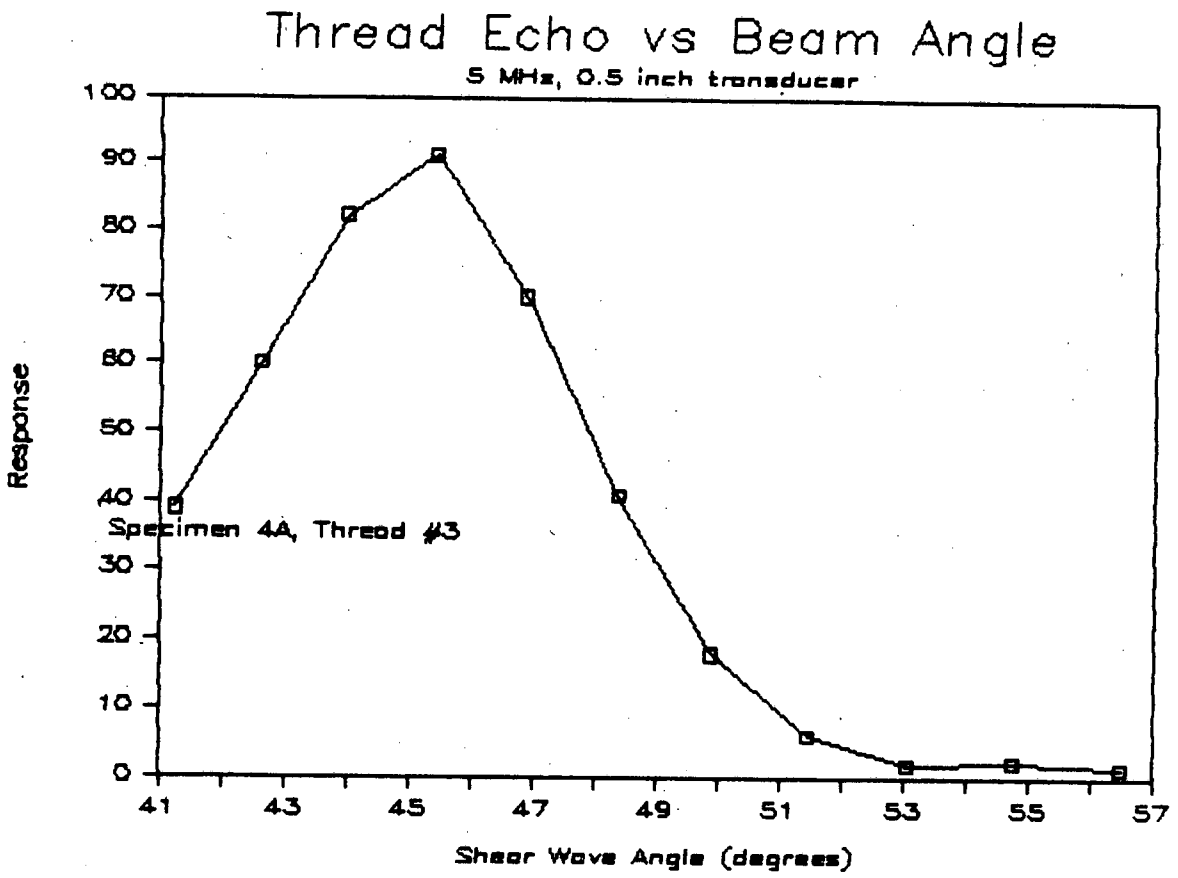
Thread Echo vs Beam Angle
5 MHz, 0.5 inch transducer
Response
100
90
80
70
60
50
40
30
20
10
0
Specimen 4A, Thread #3
41
43
45
47
49
51
53
55
57
Shear Wave Angle (degrees)

Figure 4.6-1

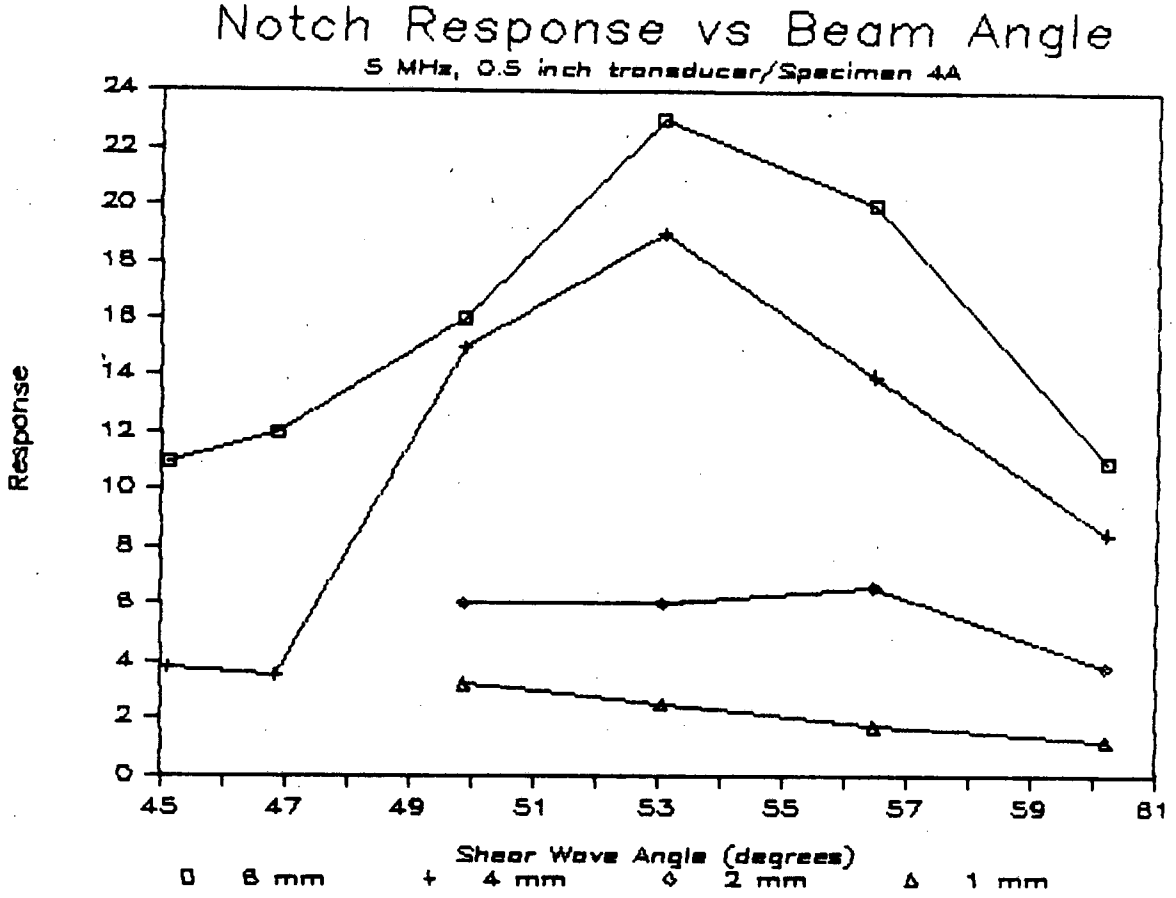
Notch Response vs Beam Angle
5 MHz, 0.5 inch transducer/Specimen 4A
Response
24
22
20
18
16
14
12
10
8
6
4
2
0
45
47
49
51
53
55
57
59
61
Shear Wave Angle (degrees)
□ 6 mm
+ 4 mm
◇ 2 mm
△ 1 mm

Figure 4.6-2

ultrasonic waveform, the timing of the thread and notch signal are a function of the beam angle. Figure 4.6-3 shows the presence of the thread signals with and without a notch at 45° and 53° beam angles. Notice that if conventional ultrasonic gating and amplitude detection is used, the flaw would need to have a response greater than the 2 mm deep notch to be detected above the thread signal in the 53° case and at 45° a 6 mm notch is far too weak relative to the thread. At 60° beam angle the threads are not detectable and so flaw imaging is relatively easy, however the signal strength is not great and background noise can inhibit small defect detection threshold level.

In the specimen 6A geometry case, the threads are smaller than the specimen 4A, such that the ultrasonic beam covers a large number of threads. The thread shape affects the angle at which maximum ultrasonic response is found as shown in figure 4.6-4. These threads in fact look like notches. Figure 4.6-5 shows the threads with and without a notch present. The presence of a notch is not readily detected by its response as shown in this figure because the pattern is only changed slightly. The notch appears at the same time as the thread, however, it shadows succeeding threads. The size of the notch can be predicted from the number of threads shadowed. Figure 4.6-6 is an RF B-scan image showing thread shadowing. Each line of the B scan is a grayscale display of the ultrasonic RF waveform. The 3 mm deep notch casts a significant shadow on a succeeding thread. The 2 mm notch has less effect and the 1 mm notch little or no effect. This technique does not rely on echo response from the defect, it relies on the defect preventing ultrasonic signals from passing through it so that features behind the defect are no longer observed. The comparison of notch and crack in this case should be closer than in the reflection amplitude case. The accuracy of the sizing depends on the thread design.

The thread effects study has shown some truly interesting characteristics in terms of inspectability. Thread design plays a key role in the ultrasonic response. At certain angles and thread designs the thread echo can completely mask the defects making inspection impossible. Other thread designs can be used to enhance the relative response for reference or optimize for shadow imaging of defects. It would appear that these smaller thread sizes are advantageous for aiding inspection.

4.7 Marine Growth Effect

The effect of marine growth on the inspectability was tested by biofouling two test samples. Appendix D discusses the samples and testing.

The samples (labelled A and B) were made of 4340 steel with aluminum flame spray coating on the outside surface. The other surfaces were coated with epoxy to protect them from biofouling. After one year in the Pacific Ocean, they were brought in for testing. The testing involved comparing ultrasonic signal response as a function of cleaning to determine the effect on inspectability. Table 4.7-1 lists the cleaning and the general improvement in straight beam ultrasonic reflection from the cleaned surface. Water jet cleaning (at 5000 psi or greater) or plastic scraping with bristle brushing are good techniques. With plastic scraping it is relatively easy to knock off barnacles, although their residual glue remains on the surface. Following the plastic scraping with a bristle brush is important in order to remove fine

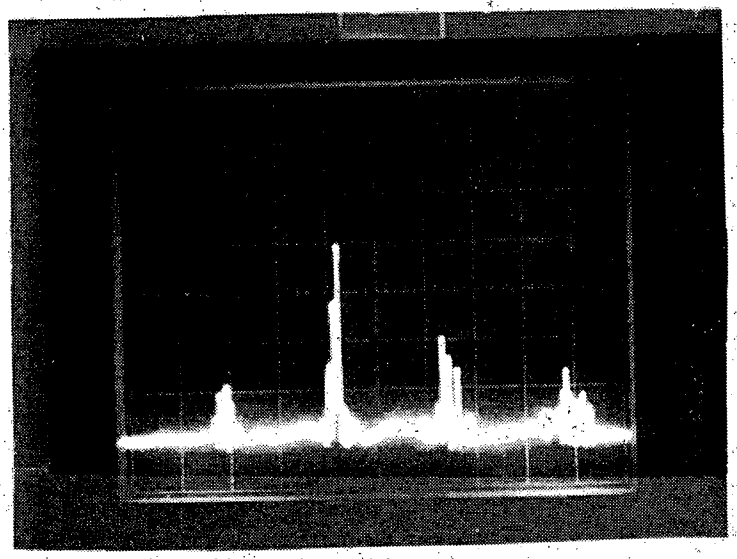

4.6-3a

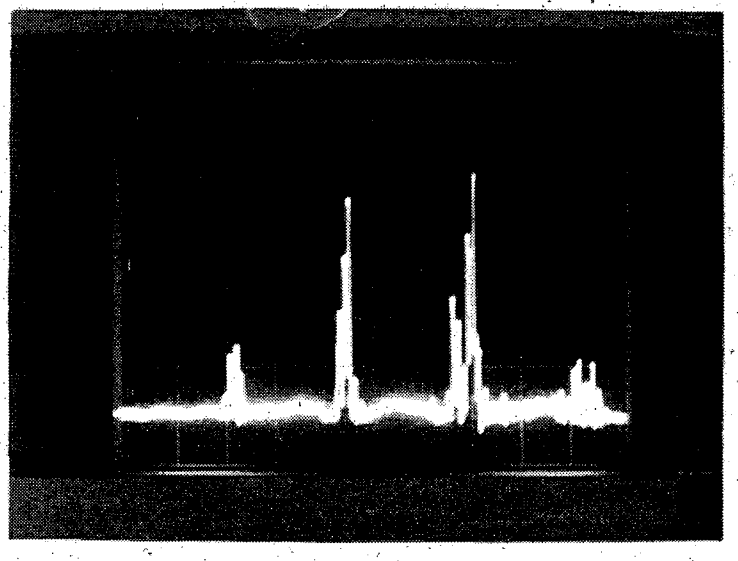

4.6-3b

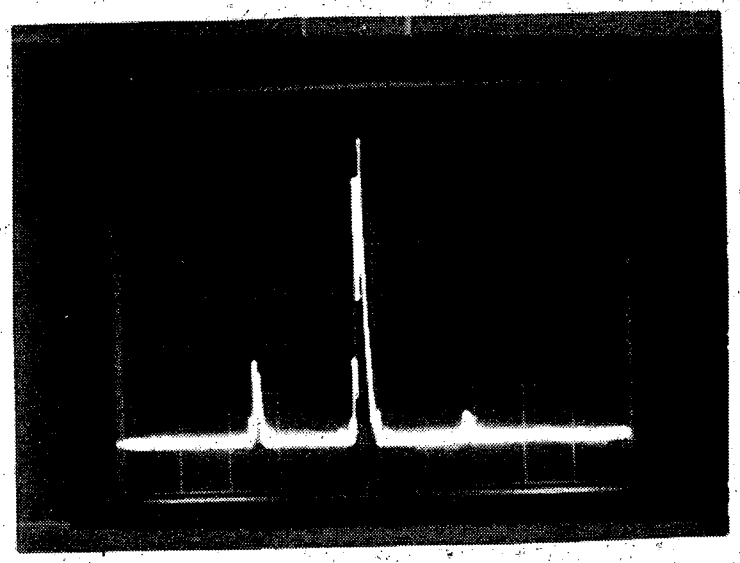

4.6-3c

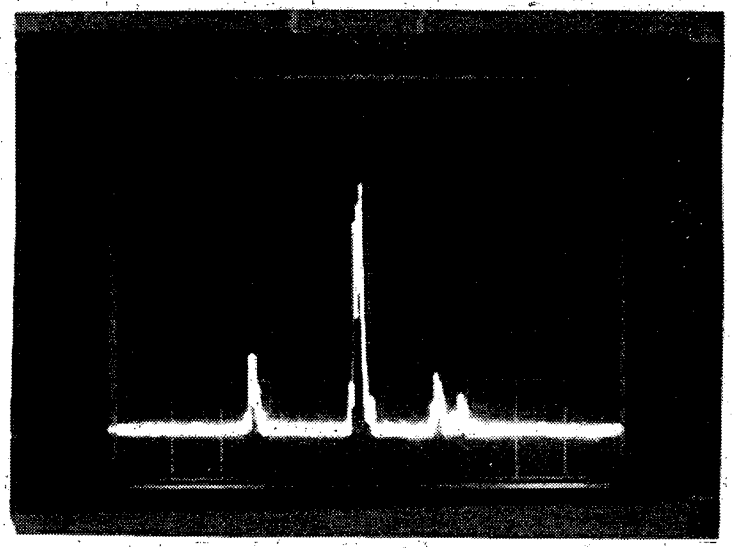

4.6-3d

Figure 4.6-3. Waveforms from specimen 4A using 5 MHz: a) 53° shear with no notch, b) 53° shear with 2 mm deep notch, c) 45° shear with no notch, d) 45° shear with 6 mm deep notch. (time base is 2 s/div, a and b 0.5 V/div at 0 dB attenuation, c and d 2 V/div at 3 dB attenuation.

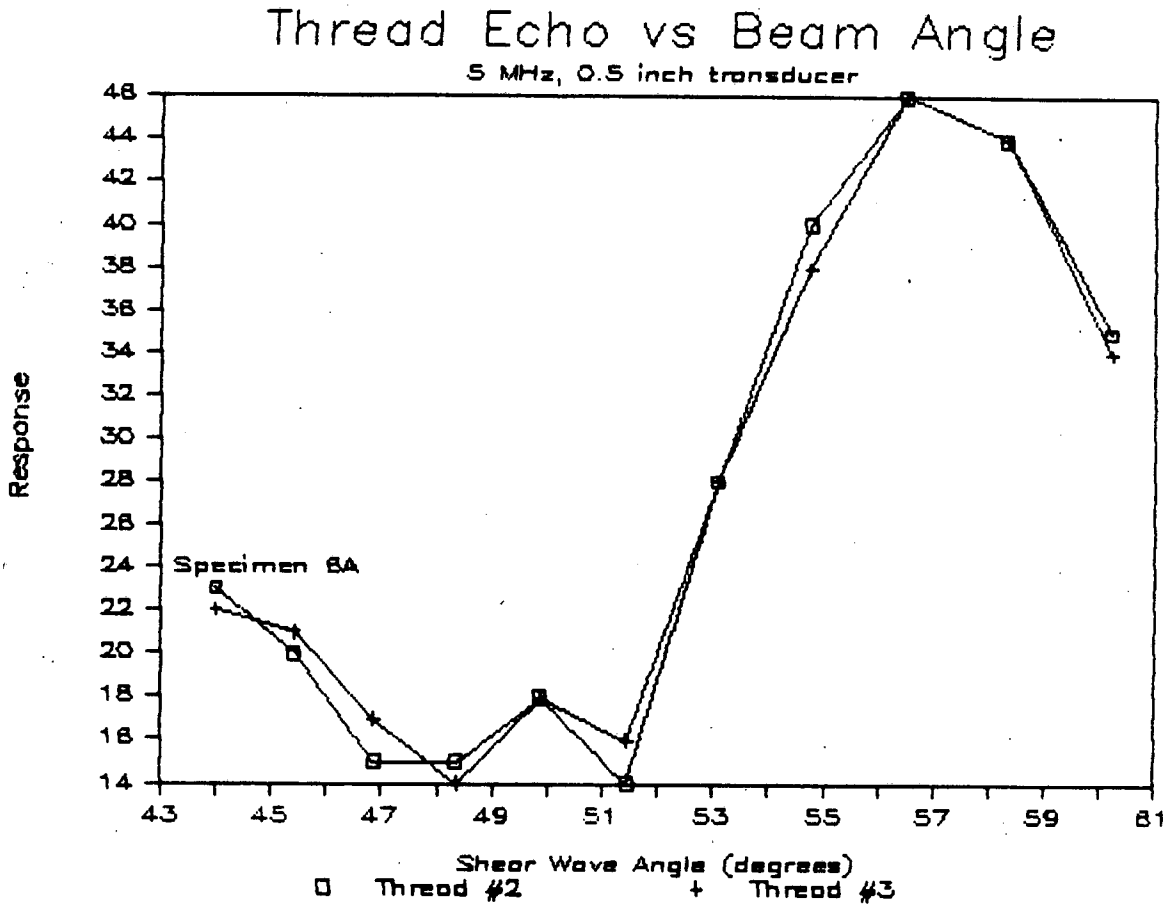

Figure 4.6-4

THRDEFF Graph 2

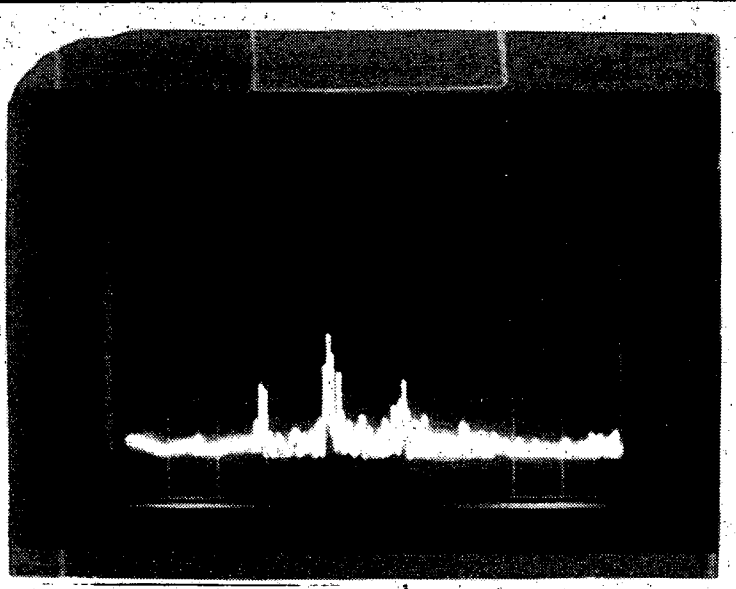

4.6-5a

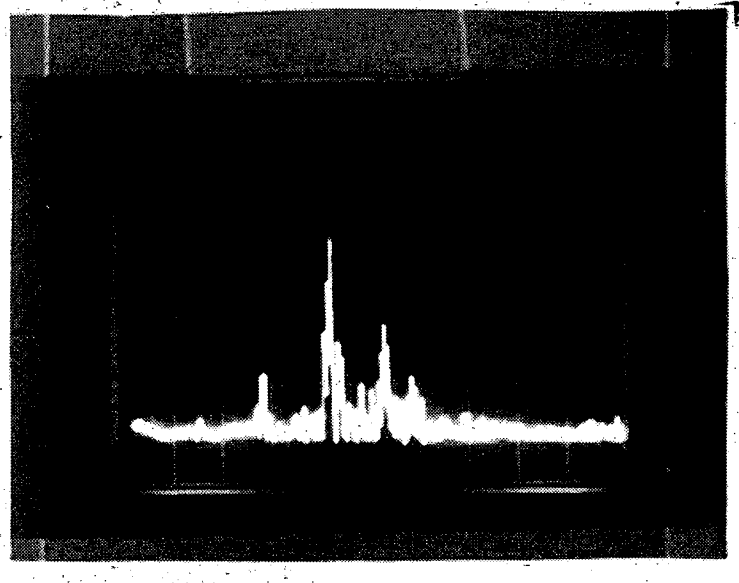

4.6-5b

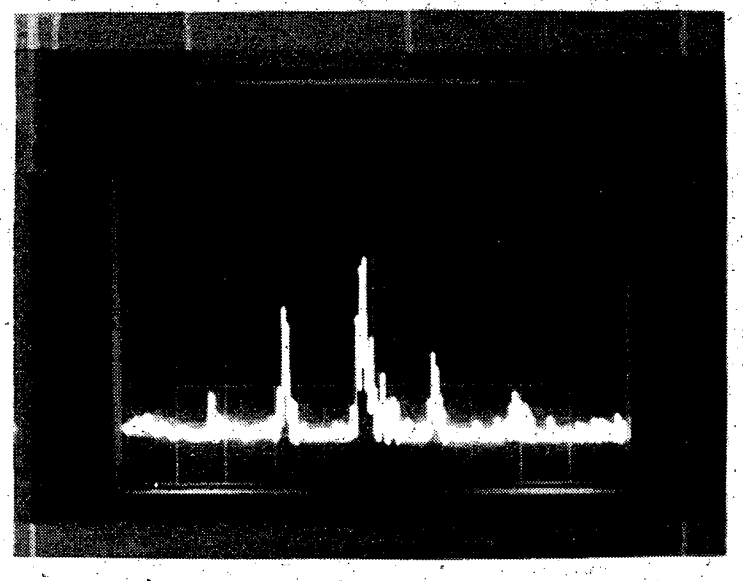

4.6-5c

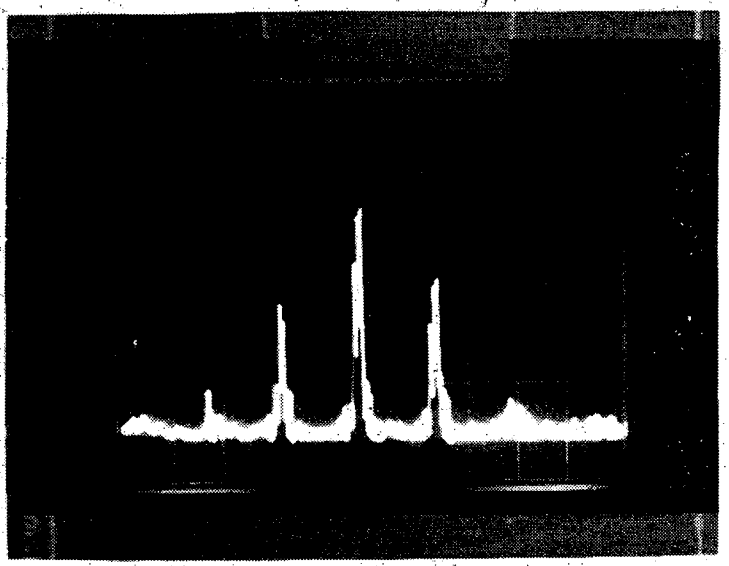

4.6-5d

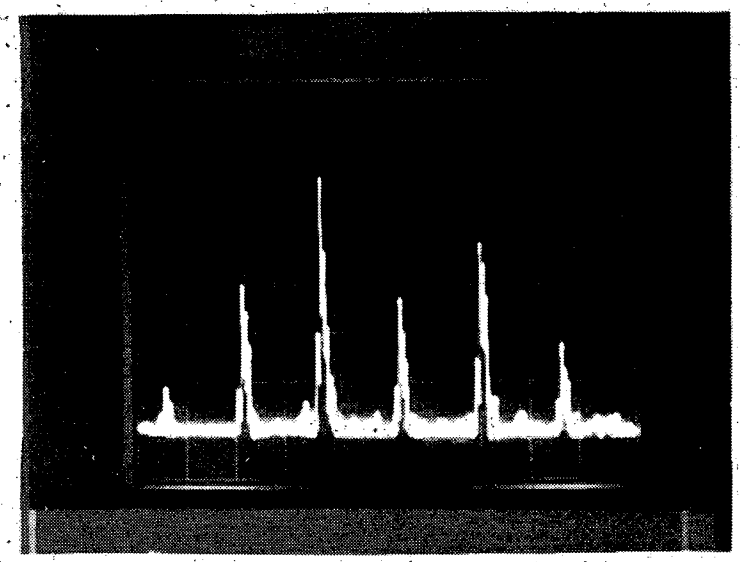

4.6-5e

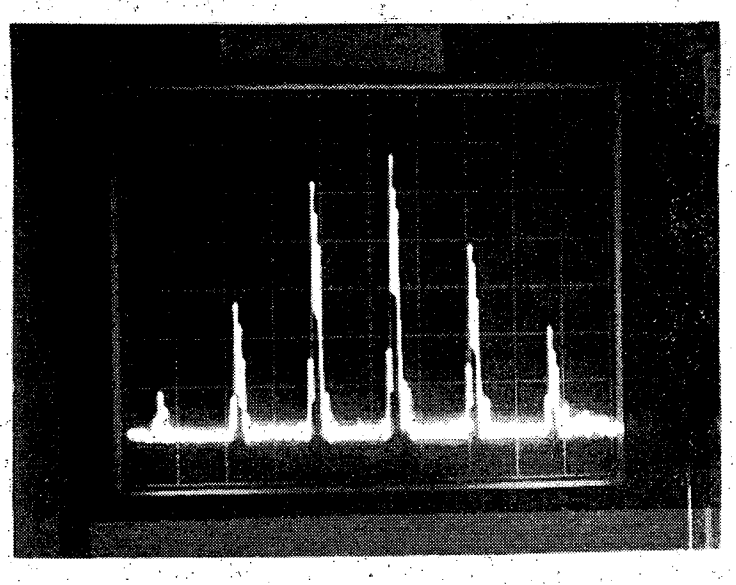

4.6-5f

Figure 4.6-5. Waveforms from specimen 6A using 5 MHz a) 45°, no notch, b) 45°, 3 mm deep notch, c) 53°, no notch, d) 53°, 3 mm deep notch, e) 60°, no notch, f) 60°, 3 mm deep notch. (time base is z s/div, is 1 V/div).

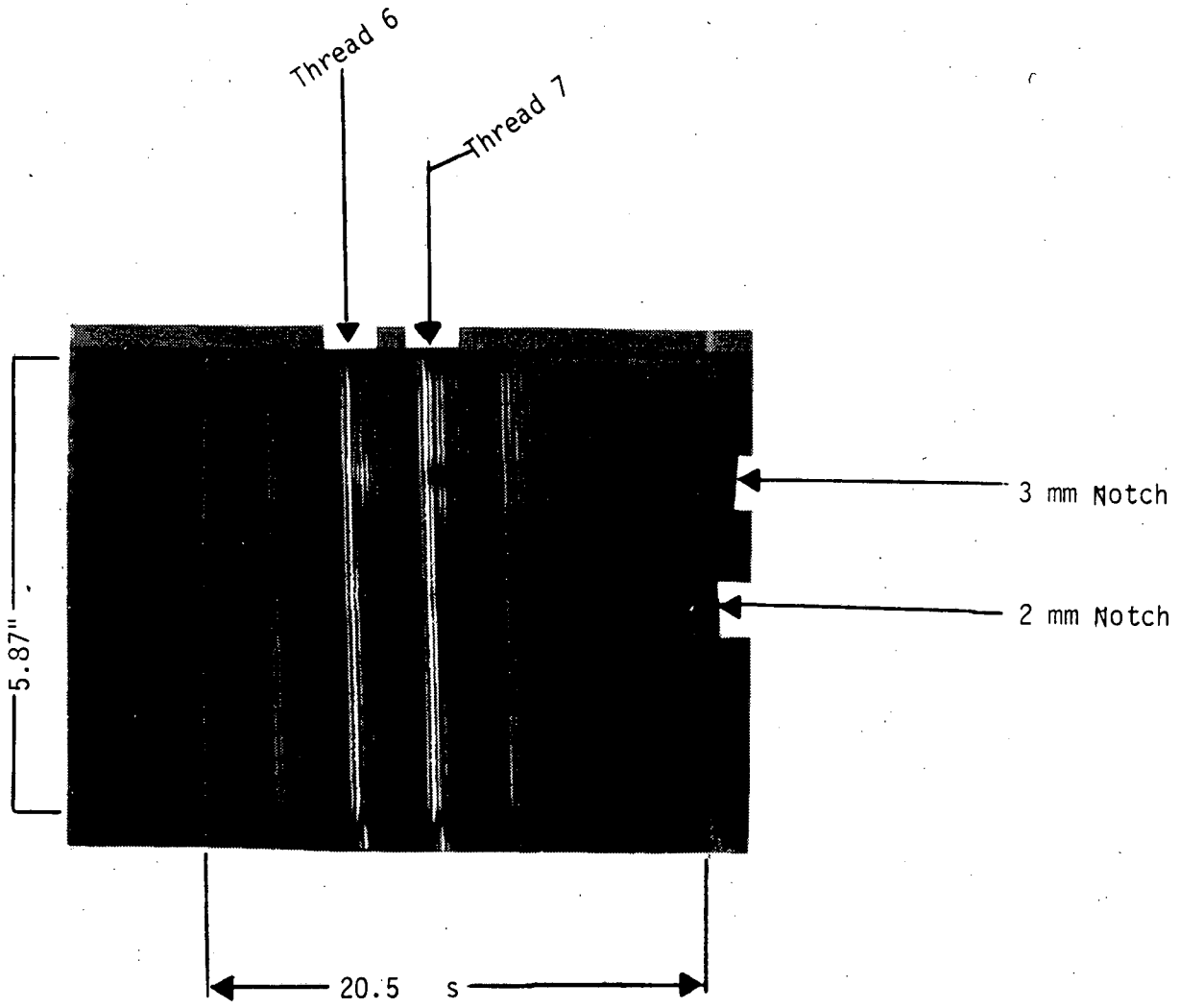

Figure 4.6-6. RF-B-scan of specimen 6A showing thread shadowing by 3 mm and 2 mm deep EDM notches. Image obtained with a 53°, 5 MHz shear wave.

TABLE 4.7-1

EFFECT OF CLEANING ON UT RESPONSE

Cleaning	UT Signal Improvement 2.25	5 MHz
Specimen A		
Water Jet (5000 psi)	2x	10x
Specimen B		
Plastic Scraper	1x	6x
Bristle Brush	2x	1.5x
Wire Brush	1x	1x

growth material. Further cleaning such as sandblasting or wire brushing does not improve response, but rather damages the surface. The flame spray coating was not noticeably damaged by the water jetting or plastic scraping with bristle brushing.

Barnacles, or their residual, cause a significant change in UT amplitude. Inspection over barnacle regions is therefore unreliable if based on UT amplitude. Based on the biofouled specimens, the barnacle residual could result in a 2% loss of inspectable area. When the inspection is performed from a clean inside surface, the biofouling does not appear to influence the response. For most inspections, the use of angle beams is important. The bouncing of angle beams on a biofouled surface is not dependent on biofouling, however there is some evidence that suggest a slight loss of signal if the bounce is at a barnacle location.

Overall, suitable cleaning can be obtained for UT inspection from the growth side. Inspection from the inside does not require external cleaning.

4.8 Imaging

The evaluation of defects by peak ultrasonic amplitude measurement is useful, but can be enhanced by imaging. In the imaging application, the peak amplitude value is plotted as a function of position. This provides the evaluator with a better means of interpretation.

Figure 4.8-1 is an image of the six EDM notches in SK001 (figure 4.4-1). A 60°, 5MHz beam was used. Notch depths are: E - 6 mm, F - 2 mm, G - 4 mm, H - 5 mm, I - 4 mm, and J - 5 mm. Figure 4.8-2 shows plots of the image area, 6dB drop and peak response vs notch depth for the two sets of notches. Each notch set is plotted spearately because the acoustic path length are difference due to the part geometry.

The area imaging results show better correlation to size in the H,I,J, case than the peak response. The 6 dB drop is a method used in defect sizing [Jessop]. The distance between the 6dB drop point from the peak signal is taken in each direction along the defect. The data can be obtained from the image and is plotted on the Figure 4.8-2 graphs on an arbitrary scale. The plot for E, F, G show very poor correlation to depth. The dB drop method often uses a 20dB point instead of six, however, in this data the results are not any more favorable. The area of the imaged defect does appear to be useful for interpretation. This of course, is particularly true for notches with known aspect ratios. Fatigue cracks will also possess an aspect ratio that falls within some prescribed bounds for the known geometry and stress. Imaging is therefore useful to assess not only the extent of the crack, but also estimate the depth. With threads present, however, the gate levels for imaging are restricted by the complicated thread pattern and so the nice image of 4.8-1 is not obtained. In the welded case, as will be shown in section 4.9, this is easier to perform. Images with threads and fatigue cracks are also shown in Section 4.10. Because of the thread problem, the B-scan imaging approach shown in Figure 4.6-6 is useful. Each line in the image is an entire waveform. Many B-scan images must be viewed to make up the area of a typical C-scan. This makes the inspection process much more data intensive.

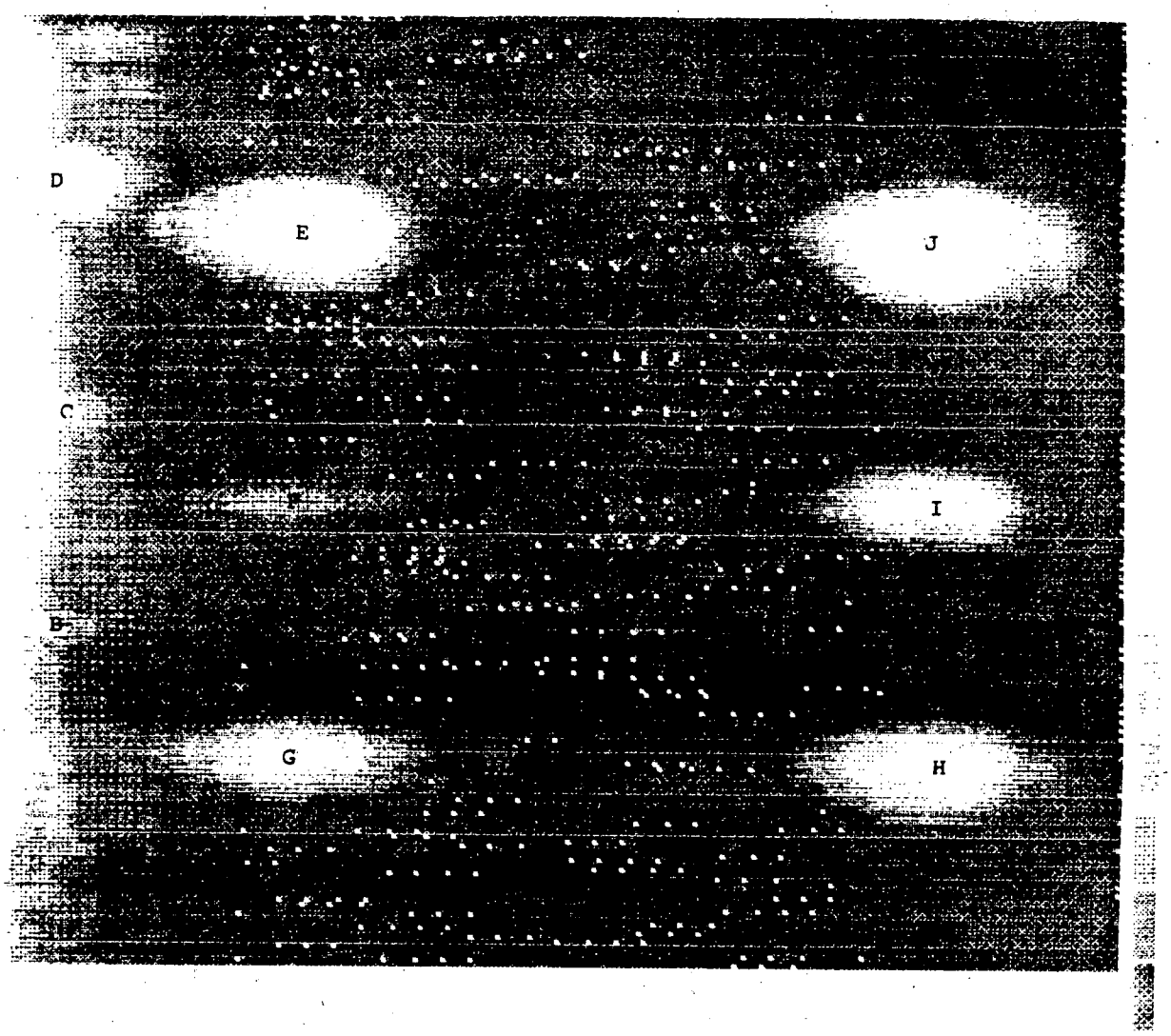

Figure 4.8-1. 60 degree shearwave C-scan of specimen #5 from the uncoated side.

OTC S63

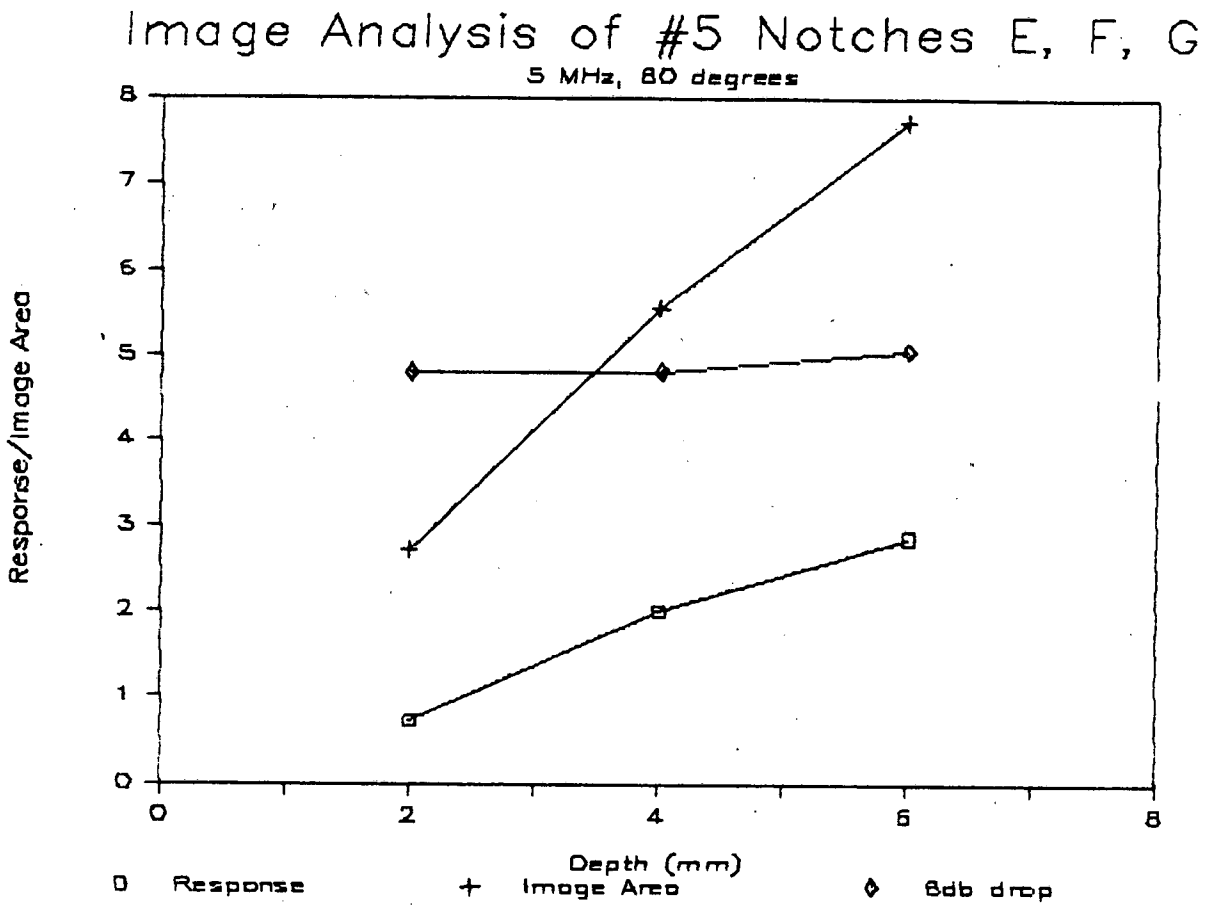

Figure 4.8-2a. Notches E,F,G Values.

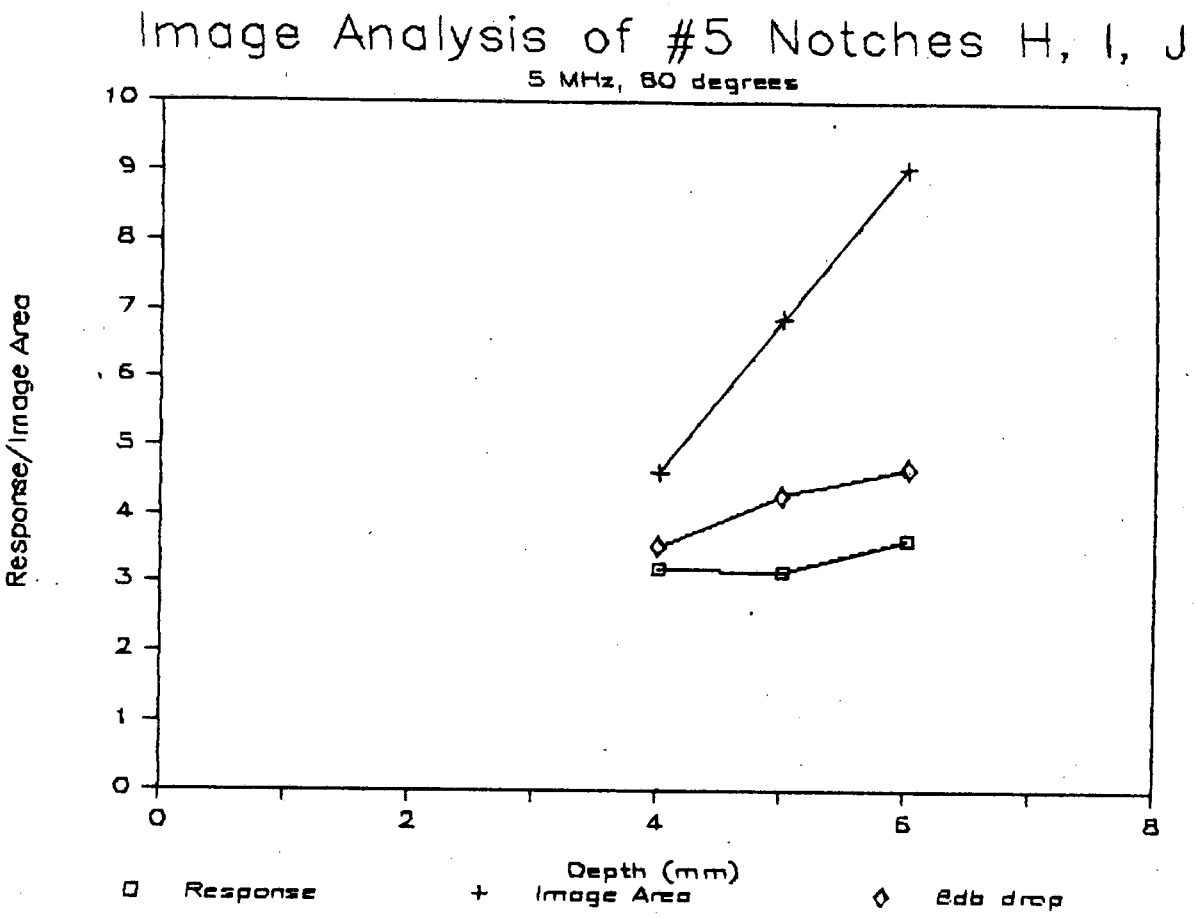

Figure 4.8-2b. Notches H,I,J Image Values.

4.9 Weld Samples

In addition to the threaded connectors, samples of welded specimens were provided by Chevron and Conoco as discussed in Appendix E. The Chevron sample was one inch thick flat plate HY-80 welded to WT70 material, and the weld was ground smooth. The Conoco material was rolled and welded line pipe 20 mm thick. Two samples were coated with epoxy and one was bare. The welds were in the as welded condition with both crown and drop through. The crown was approximately 25 mm wide consisting of about three beads and was 3 mm high. The drop through was approximately 8 mm wide with heights of between 0.9 to 3 mm. EDM notches were placed in the Chevron sample and the coated Conoco sample with notch depths of 5.1, 2.5, 1.3, 0.5, and 0.25 mm all with lengths of 50 mm.

Measurement of the longitudinal beam attenuation in the weld material of the small weld coupons indicated only slightly higher attenuation from the base material. In general, both the Chevron and Conoco samples were relatively clean acoustically. Because the samples are thin (20 to 25 mm), the attenuation is not a concern for inspection.

Ultrasonic C-scan images were taken using the Sigma Research UT2000 ultrasonic scanning system. A 5 MHz 0.5 inch diameter, six inch ground focal length transducer was used. The scanning was performed using a 1/2 V path as if inspection was to be performed from the outside of the tendon. Figure 4.9-1 shows the C-scan image of the flat Chevron piece at both 45 and 60 degrees with the scanning performed from the HY-80 and WT70 side. All notches are clearly detected by the scanning technique (reproduction images seriously degrades the intensity pattern in the images). The notch images appear proportional to their respective sizes. These prepared welds yield good sensitivity to small defects.

The Conoco specimen was scanned from the coated and uncoated sides simulating outside or inside inspection respectively. The curvature of the specimen prevented a single scan over the entire piece. Rather, small sections, where notches were present, were individually scanned. Figure 4.9-2 shows a sectioned layout for scanning. Figure 4.9-4 shows the scan images for notches A through E for the outside inspection using a 45 beam. All the notches are detected. The smallest notch (E) is even seen through the weld. However, the weld root is also imaged, and, in the case of an unknown inspection, the root signal could provide a 'false call'. Table 4.9-1 lists the relative strengths of the signals from the notches and the root for the outside inspection. The root signals in the images are indicated to be on the order of a 1 mm deep notch equivalent. Table 4.9-2 lists the relative response from the notches, root and crown from inside inspection measurements at 2.25 MHz and 5 MHz.

The notches have been shown to be inspectable by immersion, ultrasonic C-scanning, however, the unprepared welds also generate signals that may be misinterpreted as notch equivalent signals based on intensity. Imaging is helpful in discerning the source of the imaged signal, however, fatigue cracks will not necessarily have as distinct a geometry as notches. The signals from the crown and root can generate responses in the range of 1 mm deep notches.

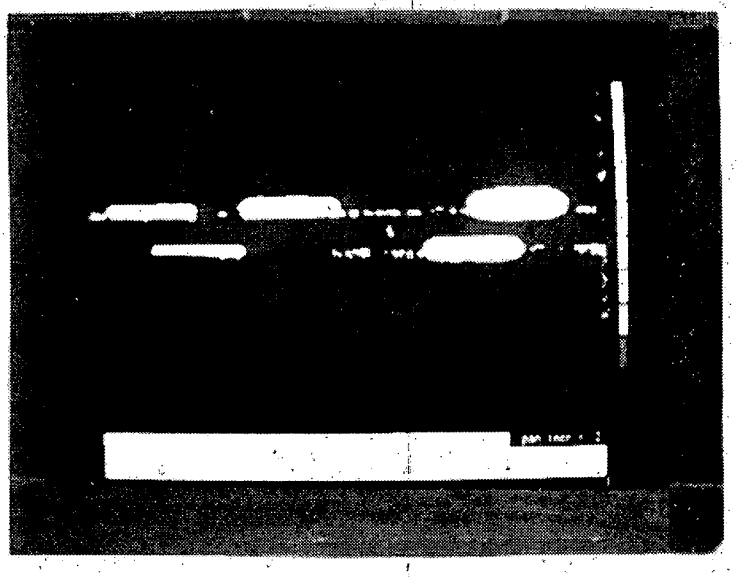

4.9-1a

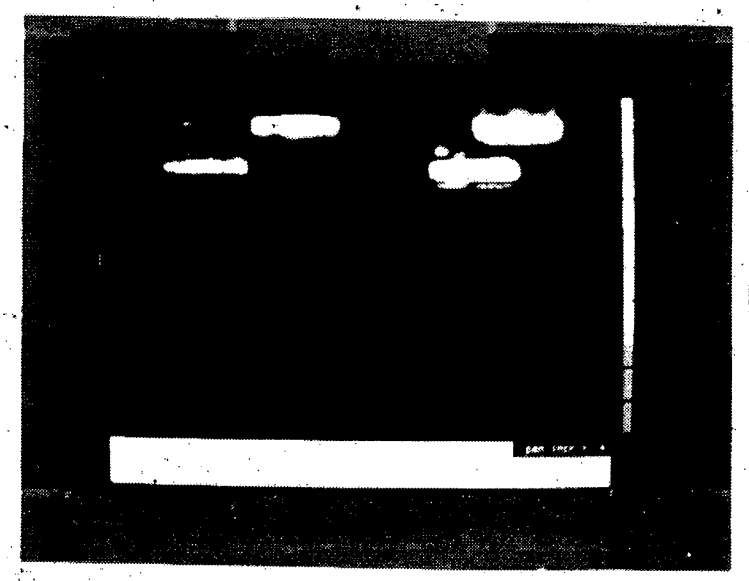

4.9-1b

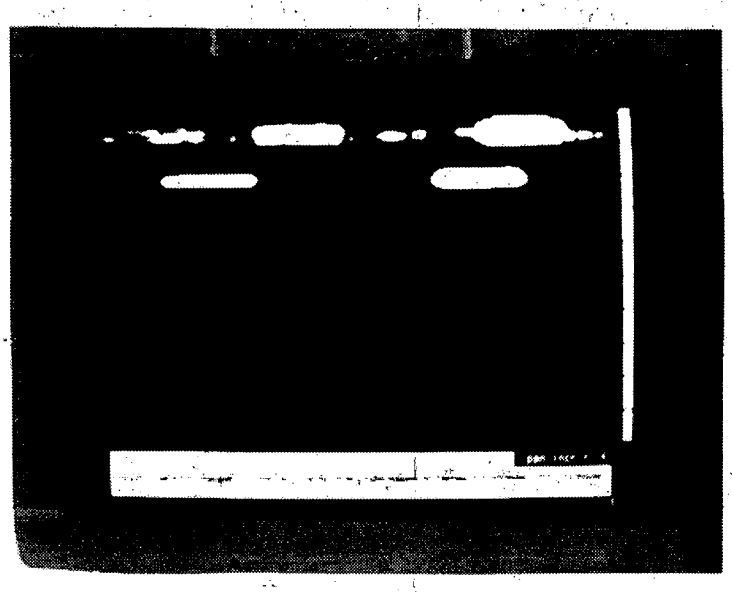

4.9-1c

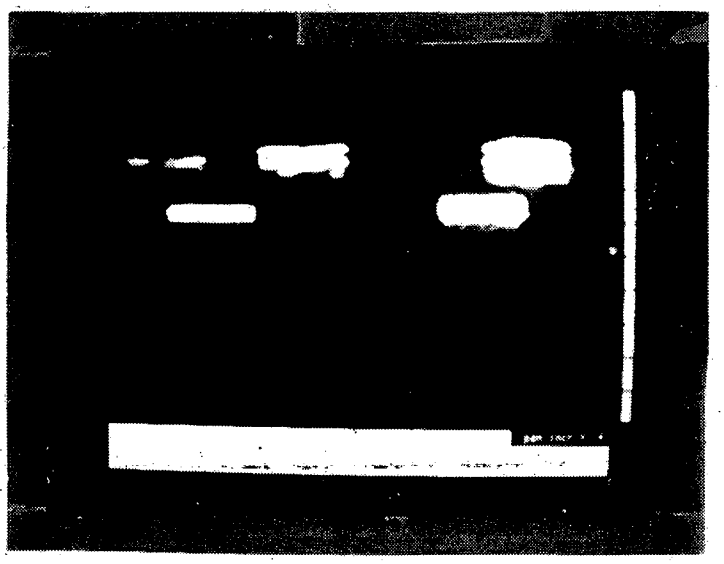

4.9-1d

Figure 4.9-1. Ultrasonic C-scan images of notches in Chevron test plate: a) HY-80, 45° shear, b) HY-80, 60° shear, c) WT70, 45° shear, d) WT70, 60° shear.

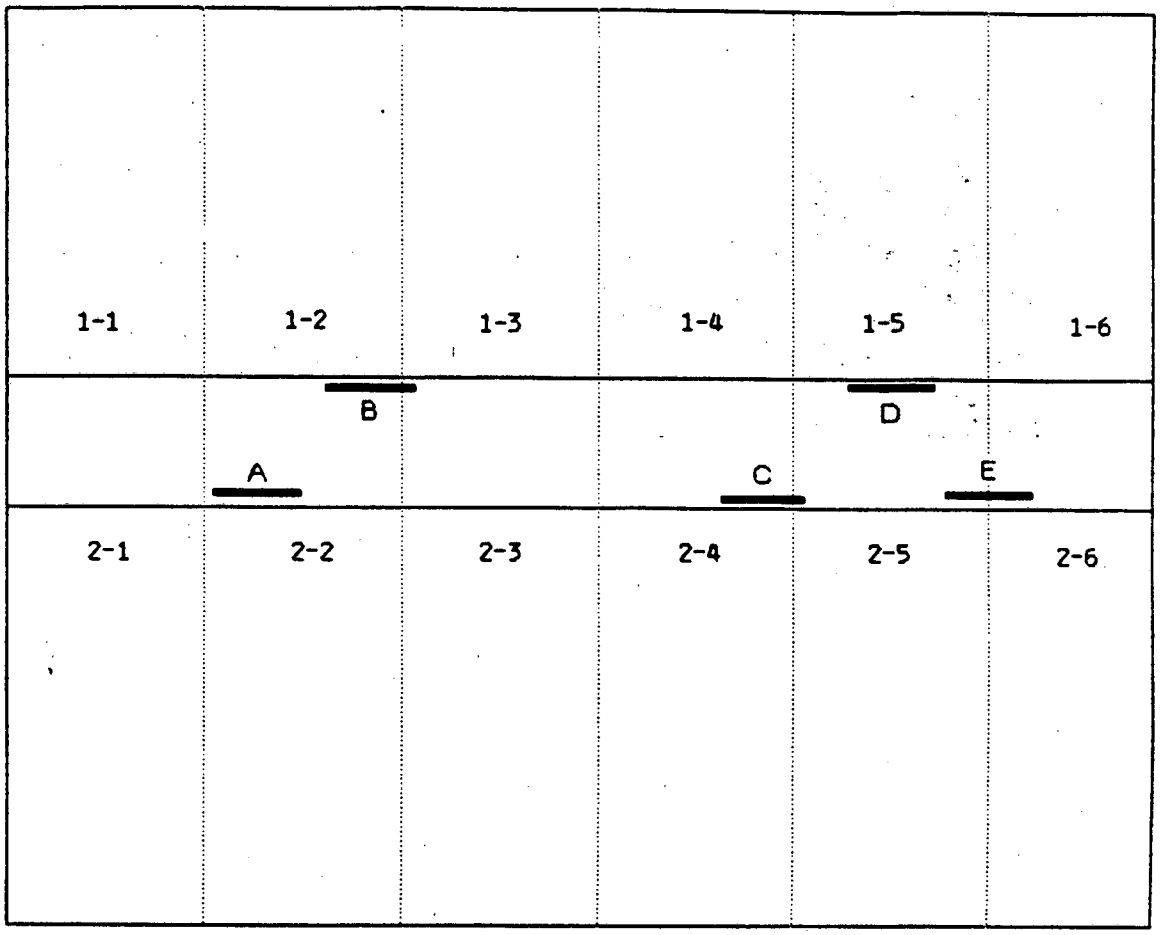

Figure 4.9-2 Section Layout for Scanning of Conoco Test Sample from Outside

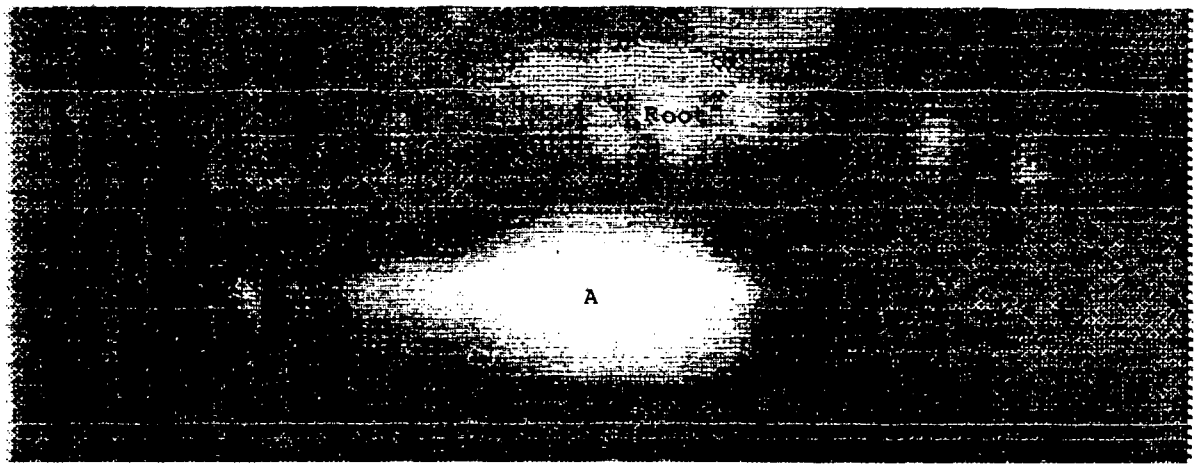

Figure 4.9-4a. C-scan images of notch A in Conoco test sample.

CP22A

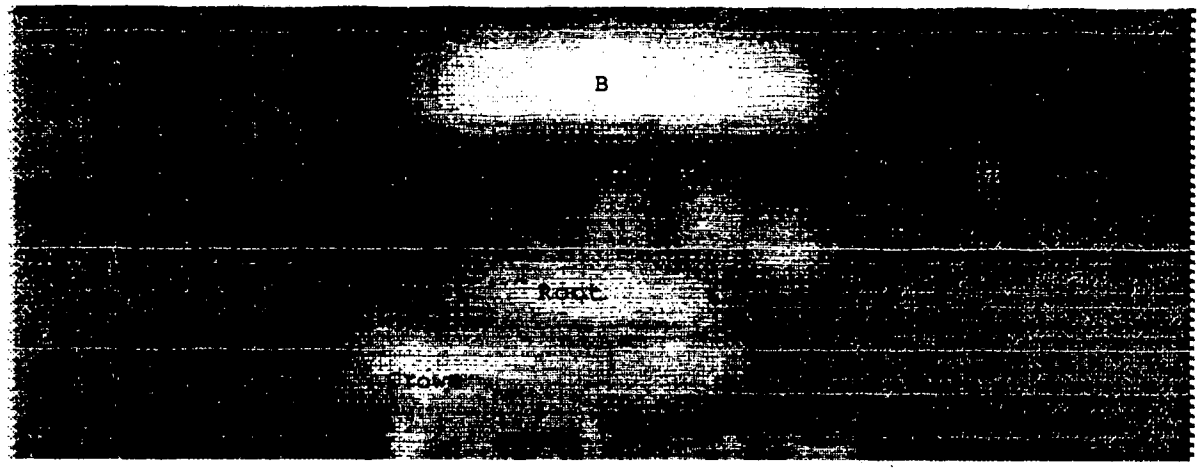

Figure 4.9-4b. C-scan image of notch B in Conoco test sample (section 1-2 scan).

CP12A

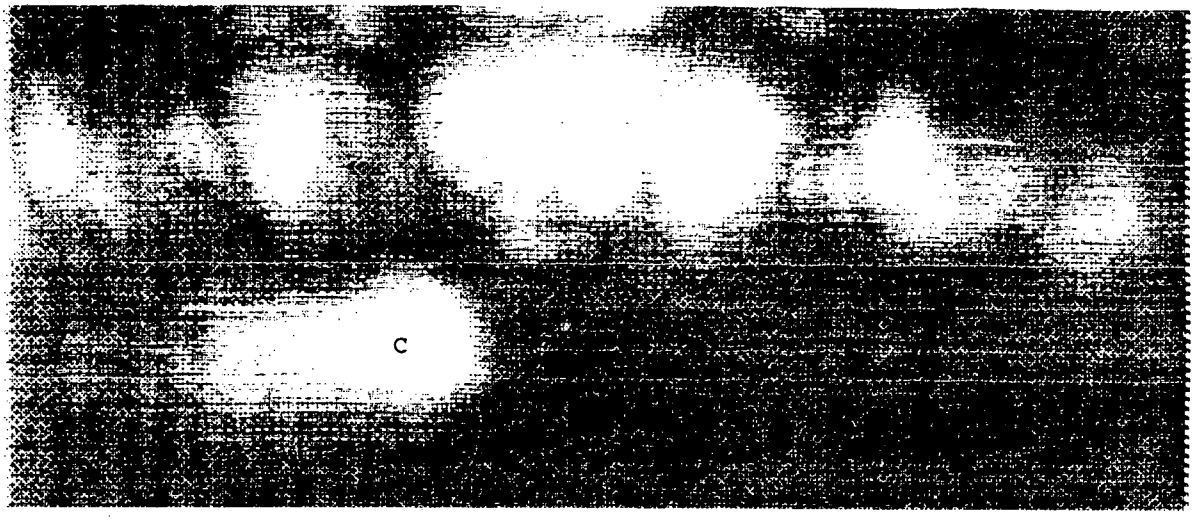

Figure 4.9-4c. C-scan image of notch C in Conoco test sample (section 2-4 scan).

CPNC452

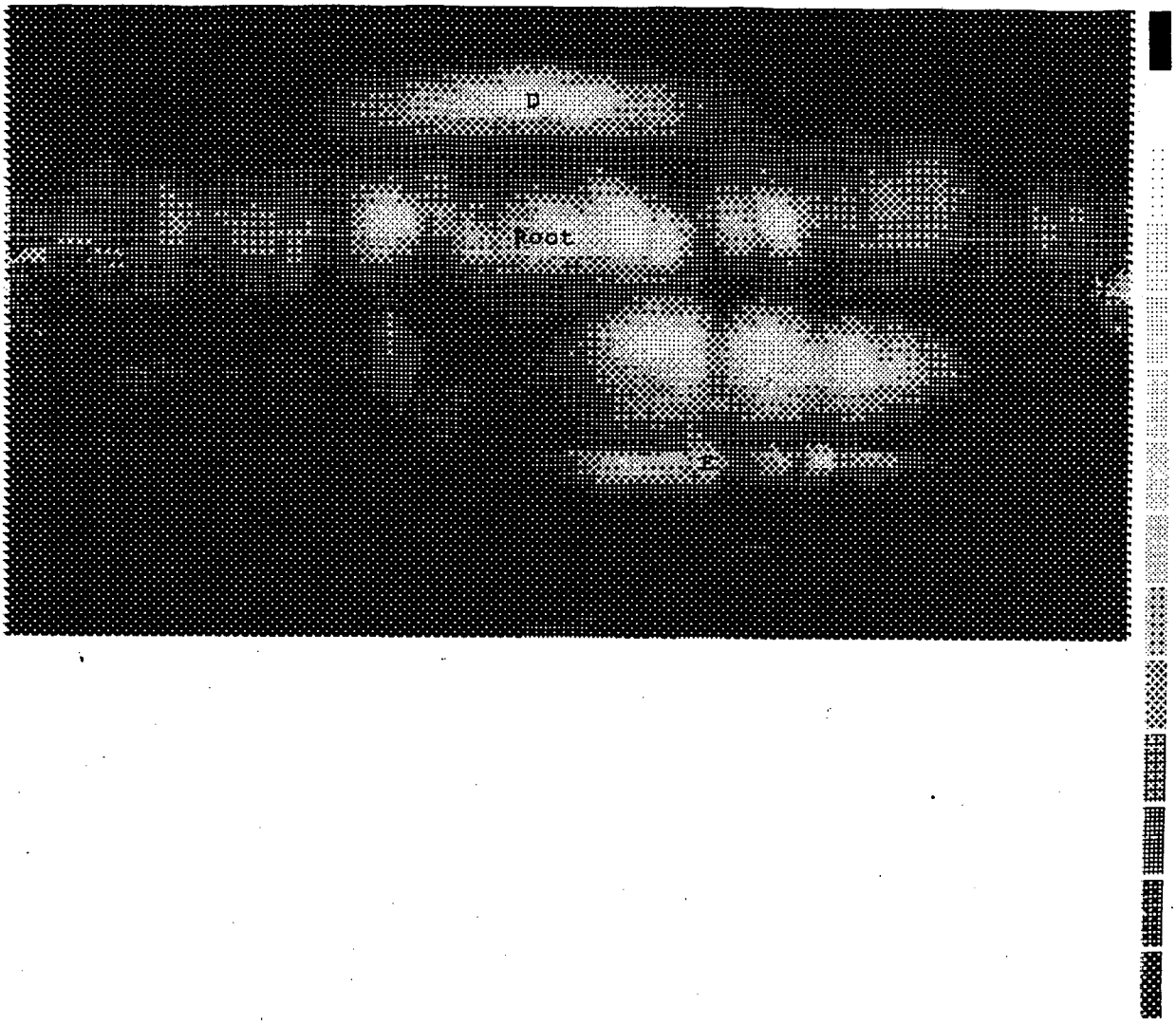

Figure 4.9-4d. C-scan images of notches D and E in Conoco test sample (section 1-5 scan).

CPND451

TABLE 4.9-1

NOTCH TO ROOT SIGNAL RATIOS
FROM OUTSIDE INSPECTION AT 5 MHz

Notch	Depth	Ratio of Notch to Root
A	5.1 mm	3
B	2.5 mm	2
C	1.3 mm	Unmeasured due to saturated signals
D	.5 mm	.95
E	.25 mm	.75

TABLE 4.9-2

CONOCO TEST SAMPLE INSPECTION
FROM INSIDE

Notch	Depth (mm)	Angle (deg)	Direction	Relative Notch Signal	Root Signal	Crown Signal
A	5.1	45	5 MHz notch side	10.6	2.4	1.4
B	2.5	45	5 MHz notch side	9.2	0.32	1.9
C	1.3	45	5 MHz notch side	4	1.12	0.8
A	5.1	45	2.25 MHz notch side	14.94	2.66	1.00
B	2.5	45	2.25 MHz notch side	7.00	2.40	5.40
C	1.3	45	2.25 MHz notch side	6.97	4.48	4.48
D	0.5	45	2.25 MHz notch side	1.10	1.90	
A	5.1	45	2.25 MHz thru weld			
B	2.5	45	2.25 MHz thru weld	3.98	1.99	1.00
C	1.3	45	2.25 MHz thru weld	0.50	3.80	1.10
D	0.5	45	2.25 MHz thru weld			
A	5.1	60	2.25 MHz notch side	2.66	0.50	0.90
B	2.5	60	2.25 MHz notch side	1.20	1.90	
C	1.3	60	2.25 MHz notch side	0.53	0.86	1.99
D	0.5	60	2.25 MHz notch side		1.70	0.60
A	5.1	60	2.25 MHz thru weld	3.10		
B	2.5	60	2.25 MHz thru weld			
C	1.3	60	2.25 MHz thru weld	1.90	1.20	0.50
D	0.5	60	2.25 MHz thru weld			

This creates the problem that a simple thresholding detection scan inspection routine will be limiting. If imaging is used in the inspection plan, then the image pattern of a preservice test can be used to establish the baselilne response. Echo image patterns from roots, crowns or other features would be recorded in a data base. Subsequent inspections with imaging could thne descriminate new defect signals with strengths below the feature signals as differences to the data base pattern.

4.10 Fatigue Crack Calibration

The use of the ultrasonic amplitude response as the measure of defect sizing is routinely applied, in industry by calibrating the response to artificial notches or drilled holes. Figure 4.10-1 shows a plot comparing electro-discharge machined (EDM) notches to bending fatigue cracks [Becker]. The fatigue cracks generally show a lower response than the EDM notches. On average, the difference is about 3-5 db, corresponding to amplitude difference of 56-71 percent. It is well known that a number of factors influence how fatigue cracks may alter the response [Jessop, Posakony]. The primary factors are orientation, size, transparency (crack opening/trans-mittance across crack), and crack roughness. Table 4.10-1 shows some estimates for the variability of fatigue crack sizing due to orientation, roughness and transparency [Rogerson, Silk (1978)]. The total variation due to these factors is estimated at just over 6 dB (50%).

This program has performed experimental investigation into the comparison of peak amplitude response from EDM notches and fatigue cracks in test block samples of 25 mm (1 inch) thickness. Figure 4.10-2 and 4.10-3 show sketches of the four test samples. Test block sample #13 had five EDM notches inserted from one side. The notches were nominally thumbnail in shape on a 3 to 1 aspect ratio (length to depth), however, the 6.0 and 7.2 mm notches had some flattening. Test blocks #14, #15, and #16 had fatigue cracks grown in them at several locations shown in Figure 4.10-3 using a bending technique. Appendix F discusses the generation of fatigue cracks.

The EDM notched block #13 and block #15 were placed in an ultrasonic scanning tank with side A up and scanned using a 45°, 5 MHz shear wave ultrasonic C scan inspection. Figure 4.10-4 shows the image and a flaw map. In this configuration, the five EDM notches and fatigue crack 15-4 were imaged. Additionally, indications of cracks were found on the edges of block #15 at the cross positions of 15-1, 15-3, and 15-4. The edge cracks of 15-1 and 15-3 were visible to the eye as well as a visual crack across face B at the 15-1 position. As discussed in Appendix F, the fatigue cracking clamping technique resulted in crack initiation at the plate edges in many cases on all test fatigue crack test blocks.

Measurement of fatigue crack amplitude response was therefore made by hand positioning of the ultrasonic beam using 45° and 60° shear. Six cracks were used in the evaluation (15-2,15-3,15-4,16-2,16-3, and 16-4) and the five notches. In order to establish an estimate of the true depth of the fatigue cracks, the satellite pulse or tip diffraction method was used [Gruber]. Table 4.10-2 shows the results of measurements for both the notches and cracks. Actual crack depth determined from breaking the test samples (see Appendix F) is also given. Satellite pulse measurements were made with both 5

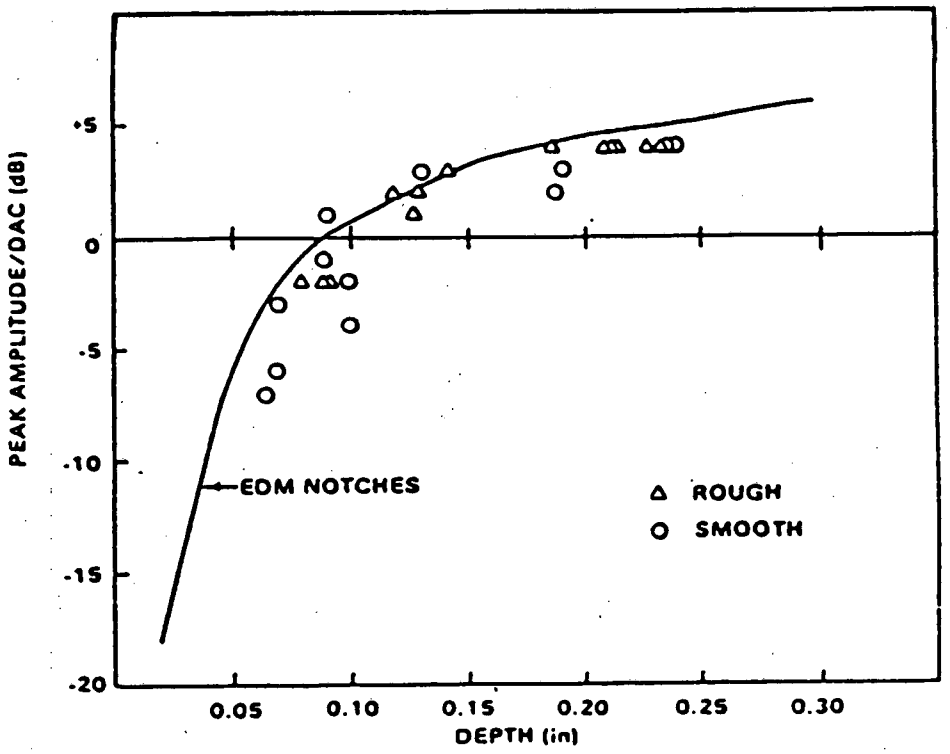

Figure 4.10-1. Ultrasonic response of vertical EDM slits and bending fatigue cracks, 0.5-V path, 45° beam. [Becker]

TABLE 4.10-1

Variation of Ultrasonic
Amplitude Response from Fatigue Cracks [Rogerson]

Orientation	3.5 dB
Roughness	3.0 dB
Transparency	4.0 dB
Combined Total	6.1 dB (50% Response)

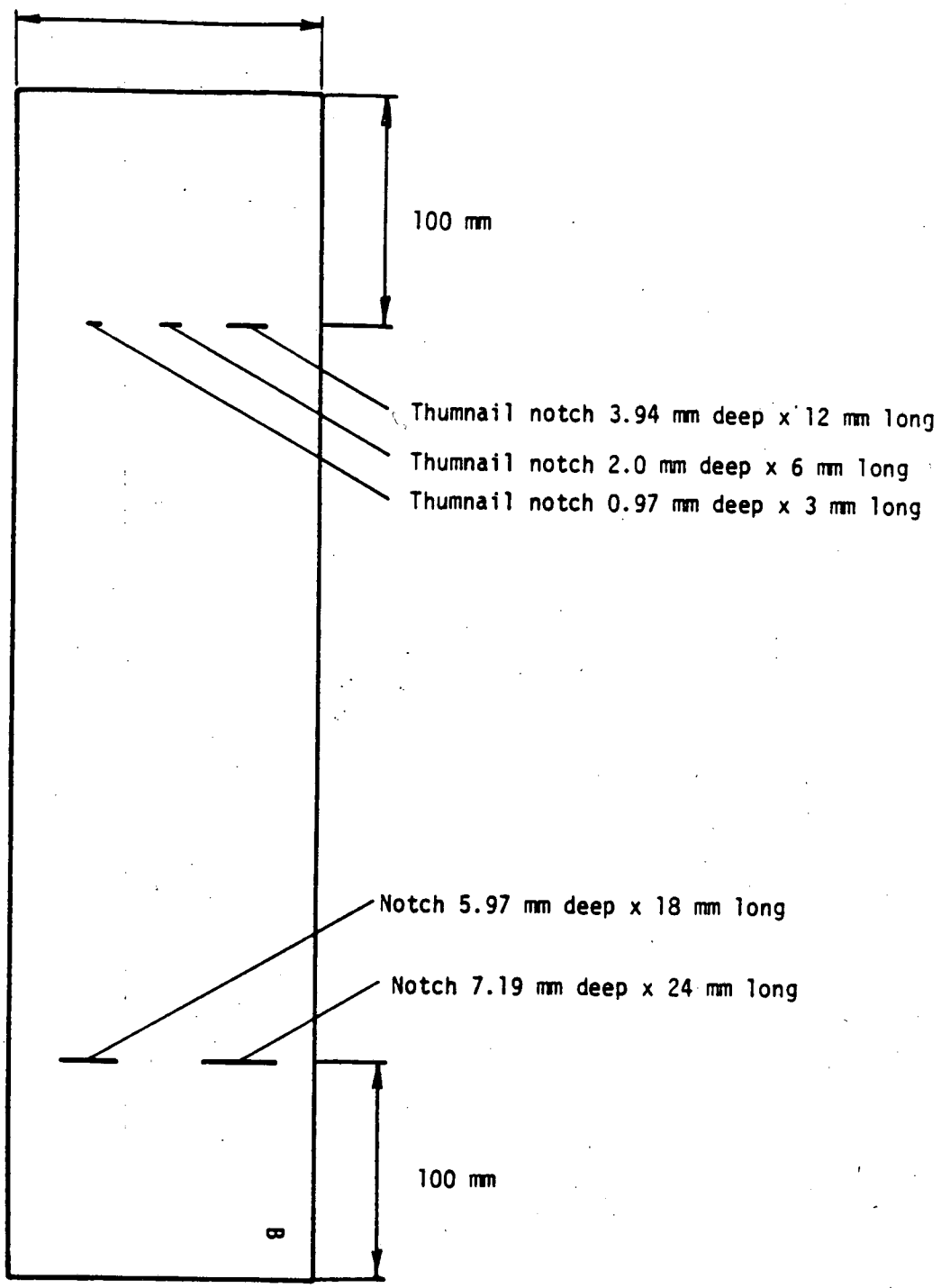

Figure 4.10-2. Steel test block #13. 25 mm thick with EDM notches.

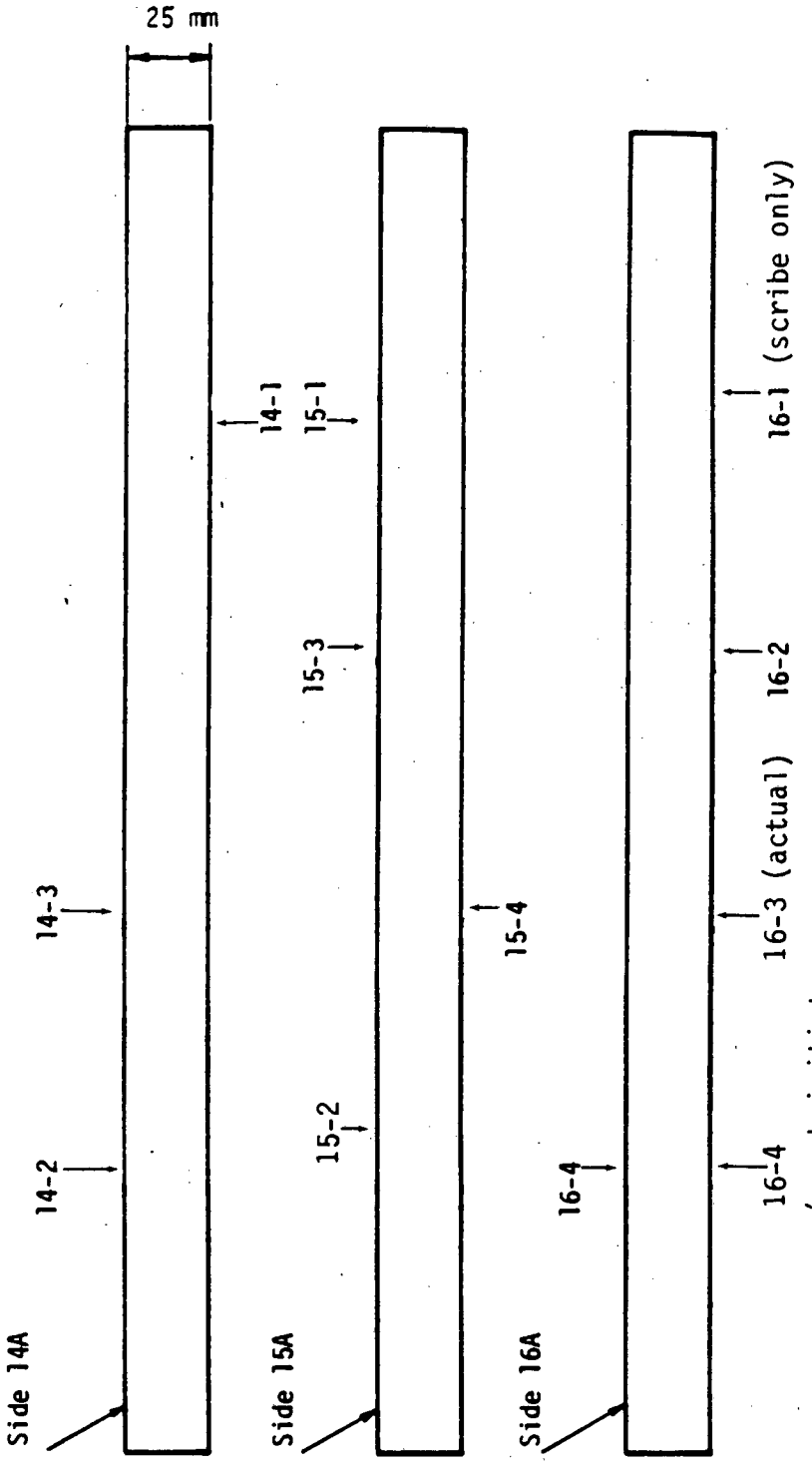

Figure 4.10-3 Steel Test Blocks #14, #15, and #16 With Start Locations for Fatigue Cracks. Plates are 100 mm wide.

TABLE 4.10-2 (A)

TIP/ROOT SEPARATION
MEASUREMENTS FOR NOTCHES

Notch	10MHz 45 deg dir 1	10MHz 45 deg dir 2	5 MHz 45 deg dir 1	5 MHz 45 deg dir 2	Average	Depth
	(μ sec)	(μ sec)	(μ sec)	(μ sec)	(μ sec)	(mm)
1 mm	0.2	0.4	0.4	0.4	0.35	1.0
2 mm	0.7	0.8	0.7	0.8	0.75	2.0
4 mm	1.6	1.5	1.6	1.5	1.55	3.9
6 mm	2.4	2.2	2.2	2.2	2.25	6.0
8 mm	2.8	3.0	2.8	3.0	2.90	7.2

TABLE 4.10-2(B)

TIP/ROOT SEPARATION
MEASUREMENTS FOR FATIGUE CRACKS

Crack	10MHz 45 deg dir 1	10MHz 45 deg dir 2	5 MHz 45 deg dir 1	5 MHz 45 deg dir 2	Average	Estimated Depth	Actual Depth
	(μ sec)	(μ sec)	(μ sec)	(μ sec)	(μ sec)	(mm)	(mm)
15-2	0.8	0.5	0.4	0.5	0.55	1.4	3.9
15-3	2.8	2.0	2.7	2.2	2.43	6.3	8.8
15-4	1.9	2.0	2.4	2.0	2.08	5.4	6.5
16-2	0.4	1.0	1.2	1.0	0.90	2.4	2.1
16-3	1.4	1.4	1.4	1.4	1.40	3.7	6.5
16-4	0.8	1.0	0.5	1.0	0.83	2.2	4.1

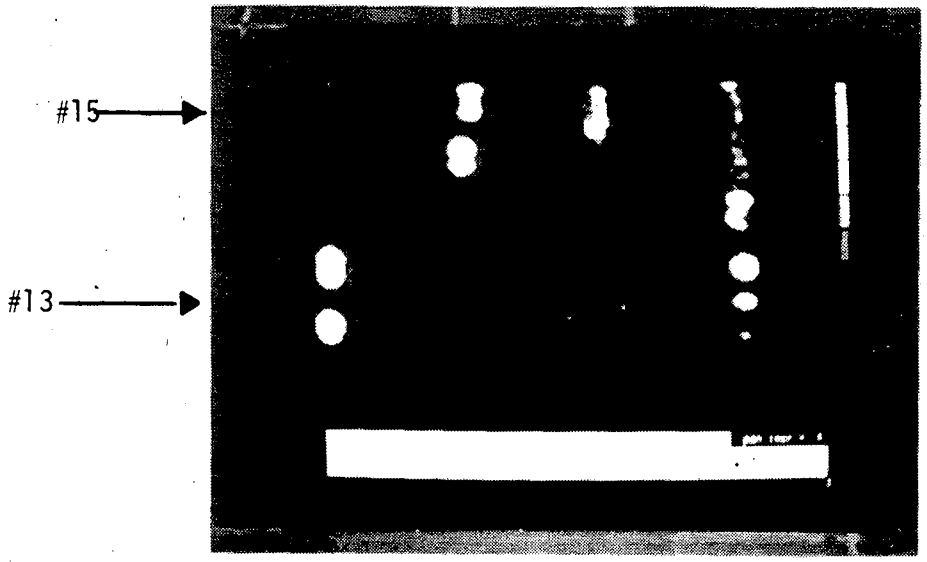

a

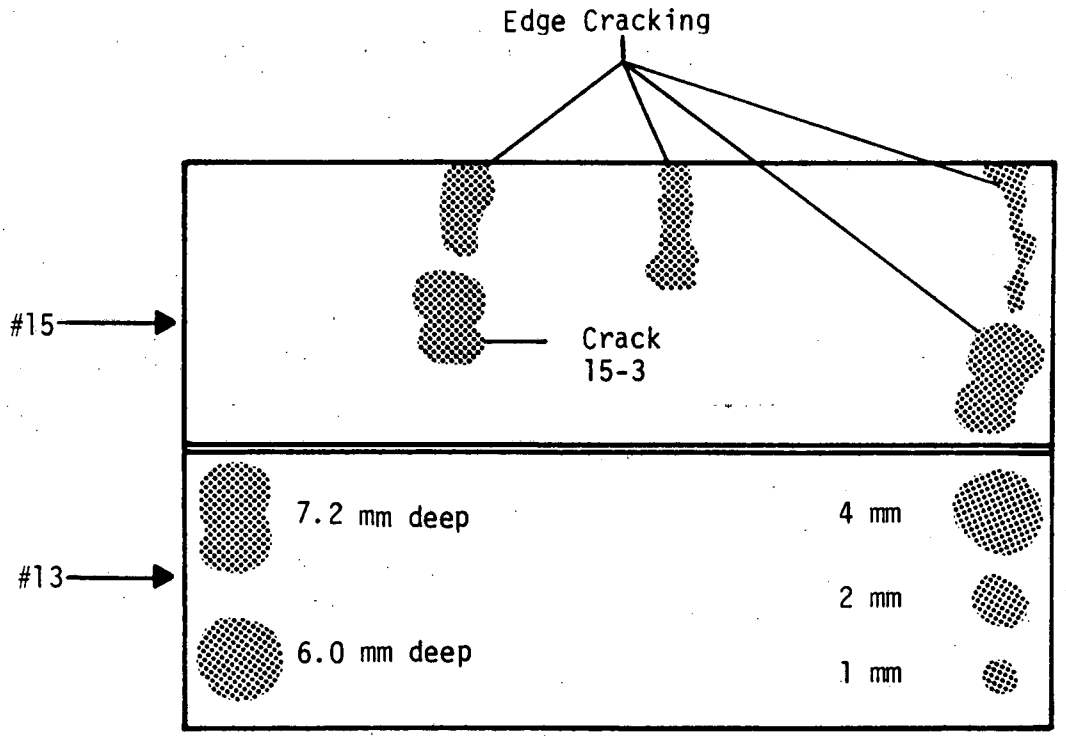

b

Figure 4.10-4. a)C-scan image of test blocks #13 and #15, b) Flaw map drawing.

and 10 MHz transducers of 1/2 inch and 3/4 inch diameter at 45°, and from each side of the notch or crack. In some cases, such as cracks 15-3 and 16-4, the direction indicated different sizing of the crack based on the tip diffraction method. The actual measured depth for the notches can be plotted against the tip/root separation (Figure 4.10-5) and this graph is used to determine the depth of the cracks.

Measurement of the amplitude response from the notches and cracks were made using 2.25 and 5 MHz transducers at 45° and 60° from each direction and using 1/2 V and 3/2 V bounce paths. Data was not obtained for all cracks and notches at all settings due to configuration limitations. Some measurements were also made with 1 MHz transducers. Figure 4.10-6 and 4.10-7 are representative of the results for 5 and 2.25 MHz at 45 . Figure 4.10-8 is 2.25 MHz at 60 . The legend indicates if the response is due to the EDM notches from direction (1) or (2) or fatigue cracks from direction (1) or (2). The fatigue cracks tend to have a lower response than the notches. In many cases the amplitude response is significantly lower. The average response from cracks for all data is 52% of the response from cracks. At 5 MHz the crack average response was 53% with a standard deviation of 16%. Figure 4.10-9 is a c-scan image of fatigue crack 16-3. An image of a 1 mm notch is also shown for comparison. Each scan is 4 cm x 4 cm using a 5 MHz transducer at 45°.

Appendix F contains the results of the fatigue crack study. The fatigue cracks were broken open and measured. The plots in Appendix F use the physical measured sizes rather than the crack tip diffraction estimated size of Table 4.10-2. The difference is significant indicating a need for qreater conservation in fatigue crack sizing interpretation.

The specimen 5A test sample was fatigue loaded and a crack grown. Figure 4.10-10 shows C-scan images at 5 MHz, 60 of the EDM notches in specimen 4A and the crack in specimen 5A. Figure 4.10-11 is a plot of the amplitude response from the C-scan image of the notches vs depth. The maximum amplitude from the crack is indicated on the figure resulting in an equivalent size of 1.7 mm deep. The size of the crack in the image indicates that is in nearly 10 cm across the part.

The specimen 5AA sample was also scanned. The image of Figure 4.10-12 shows both the 5AA sample and a portion of the 4A specimen containing the 1 mm notch. A 53 , 5 MHz beam was used. The thread pattern is detected in this image. The response values are shown in parenthesis. These results indicate that the center crack is less than 1 mm deep and only about 1 cm long whereas the edge cracks are greater than 1 mm deep. Time base measurements of the center crack in Appendix F indicates a depth of 3 mm, while the center crack measured only 1.2 mm after breaking.

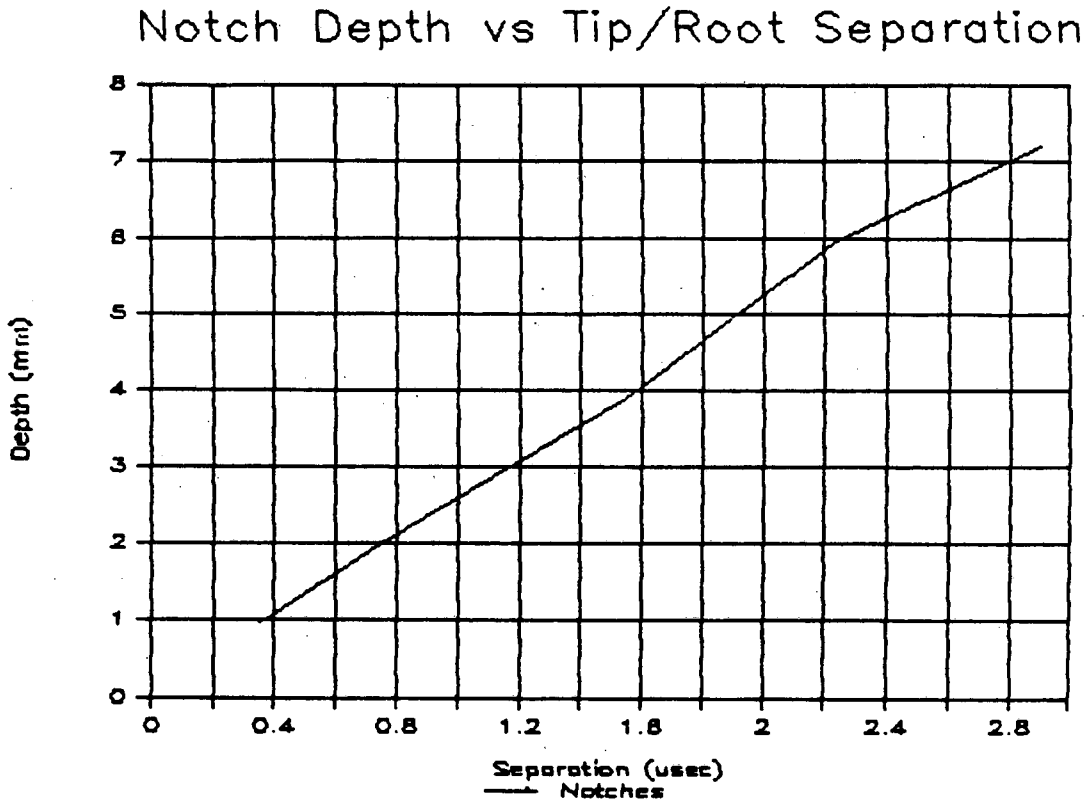

Figure 4.10-5. Plot of notch depth vs average tip/root signal separation for EDM notches in test block #13.

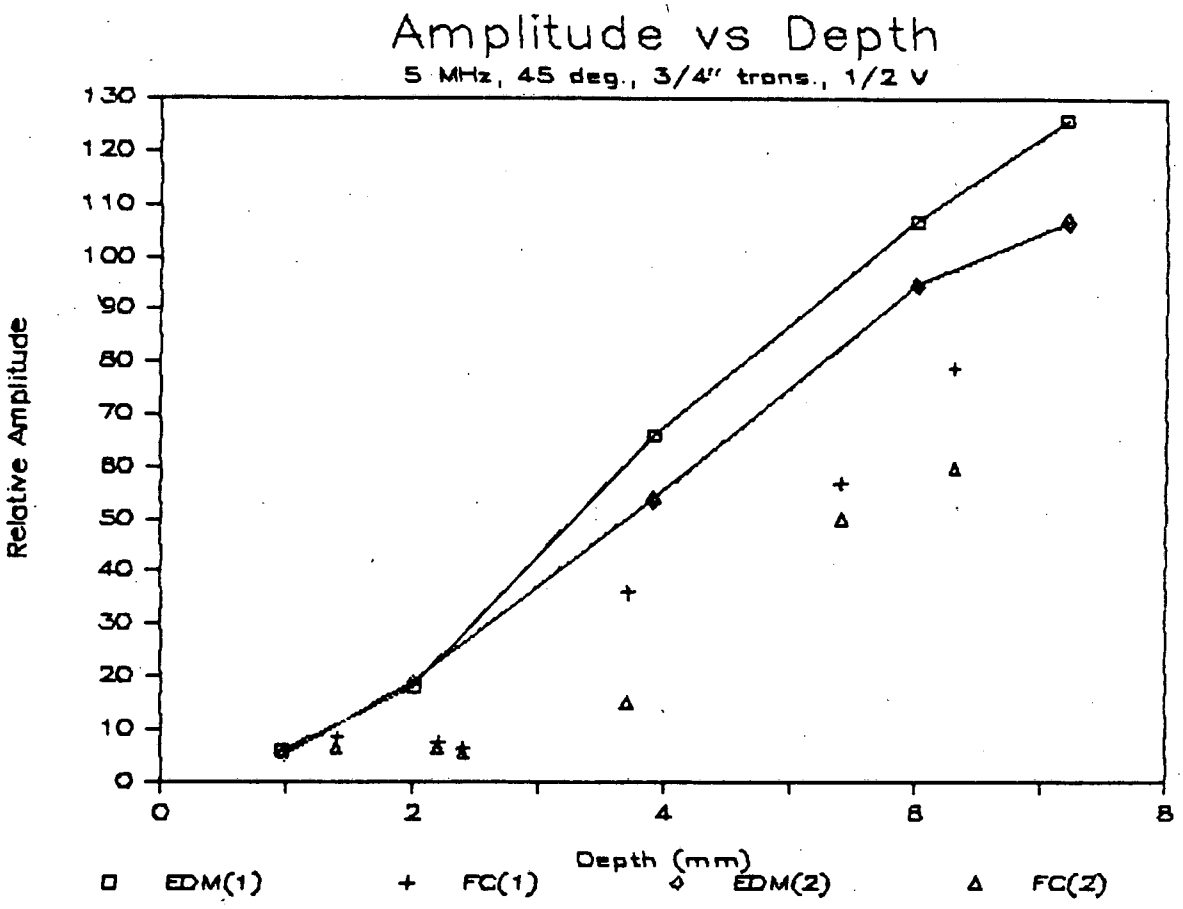

Figure 4.10-6

Plot 10

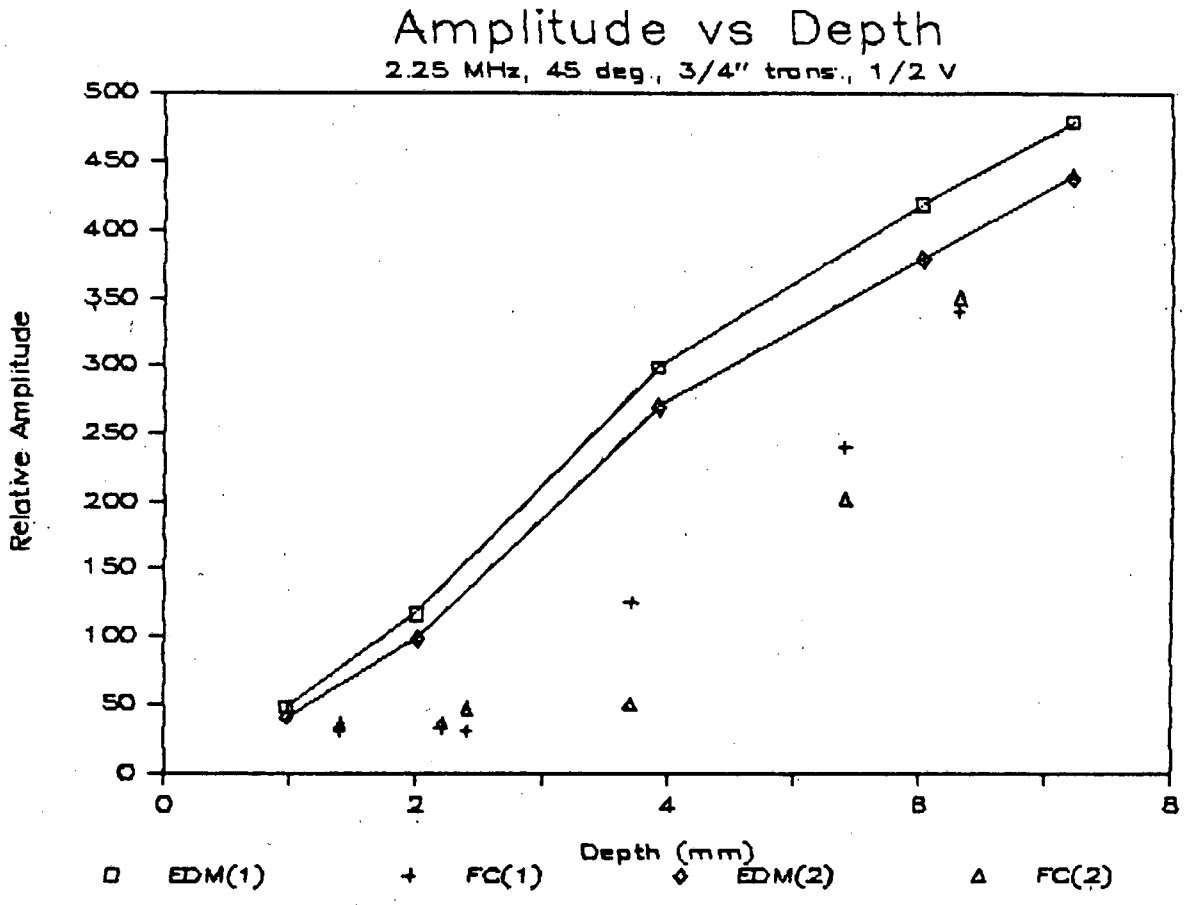

Figure 4.10-7

Plot 13

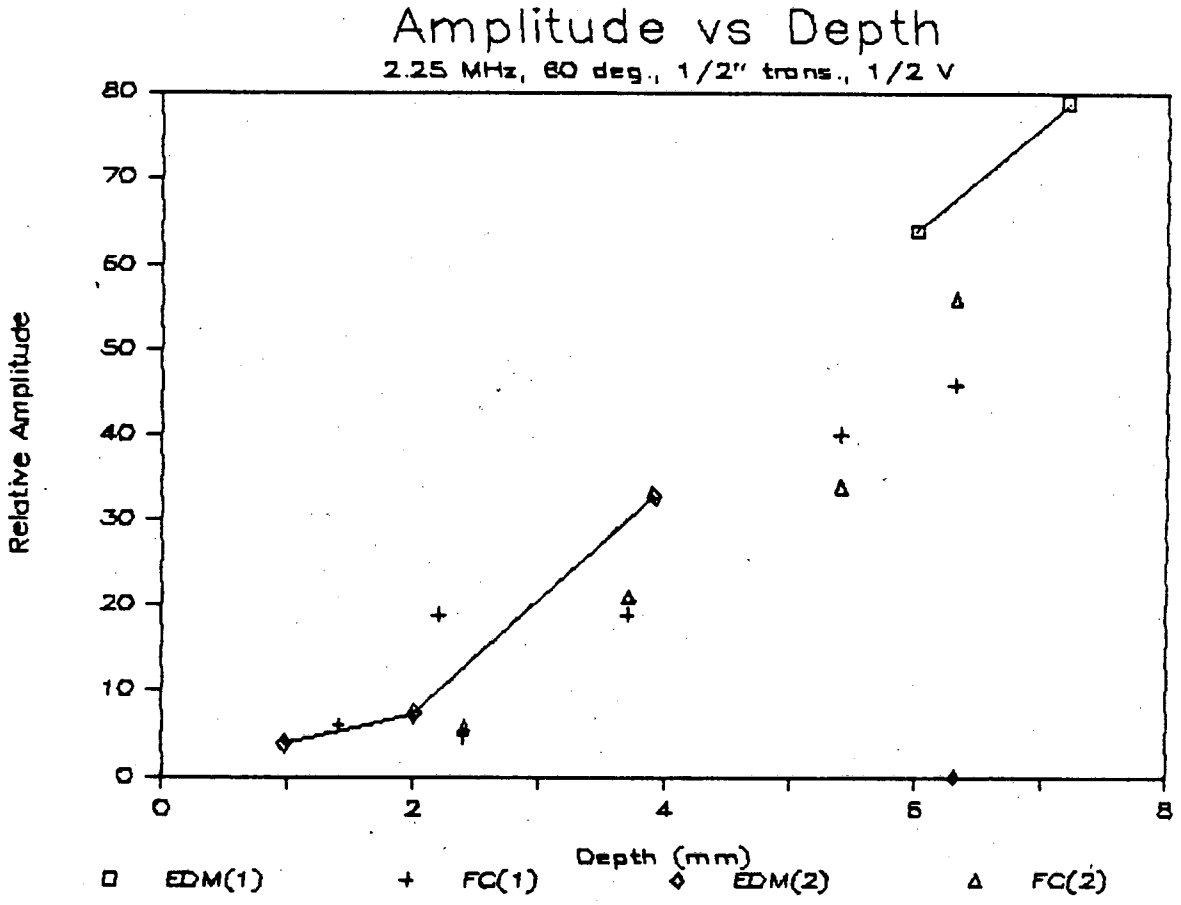
Amplitude vs Depth
2.25 MHz, 60 deg., 1/2" trans., 1/2 V
Relative Amplitude
80
70
60
50
40
30
20
10
0
0
2
4
6
8
Depth (mm)
EDM(1)
FC(1)
EDM(2)
FC(2)

Figure 4.10-8

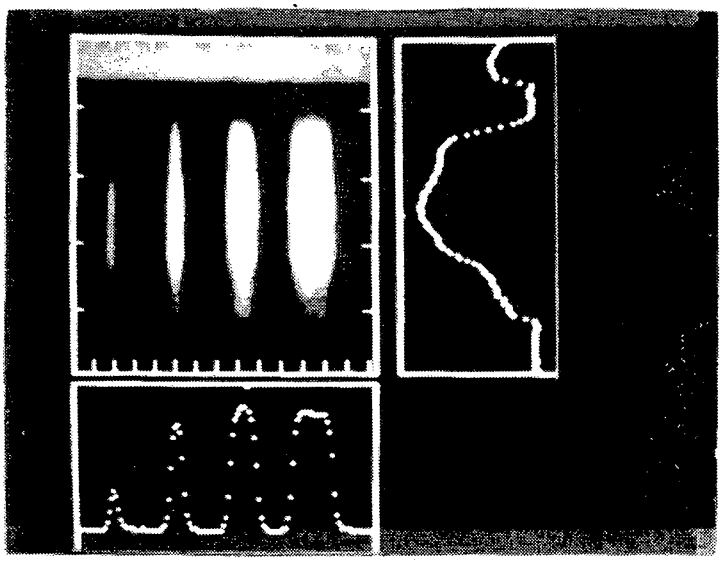

4.10-9a

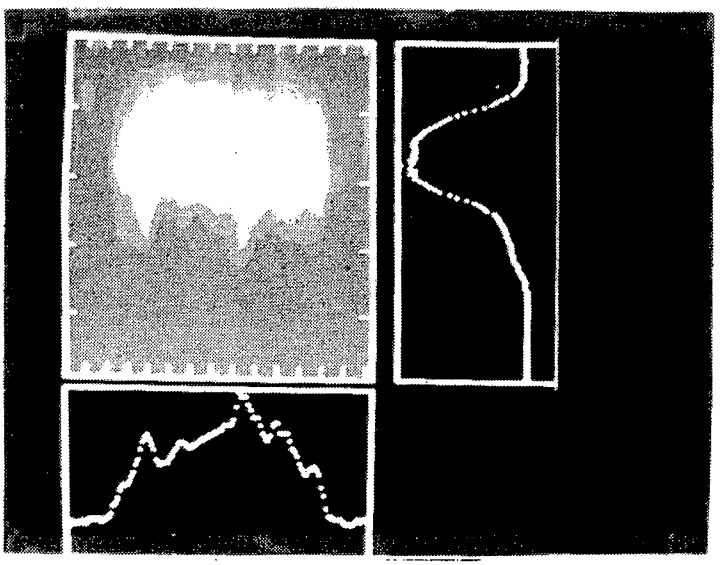

4.10-9b

Figure 4.10-9. C-scan images of a) 1.2.4 and 6 mm notches in specimen 4A b) Fatigue crack in specimen 5A.

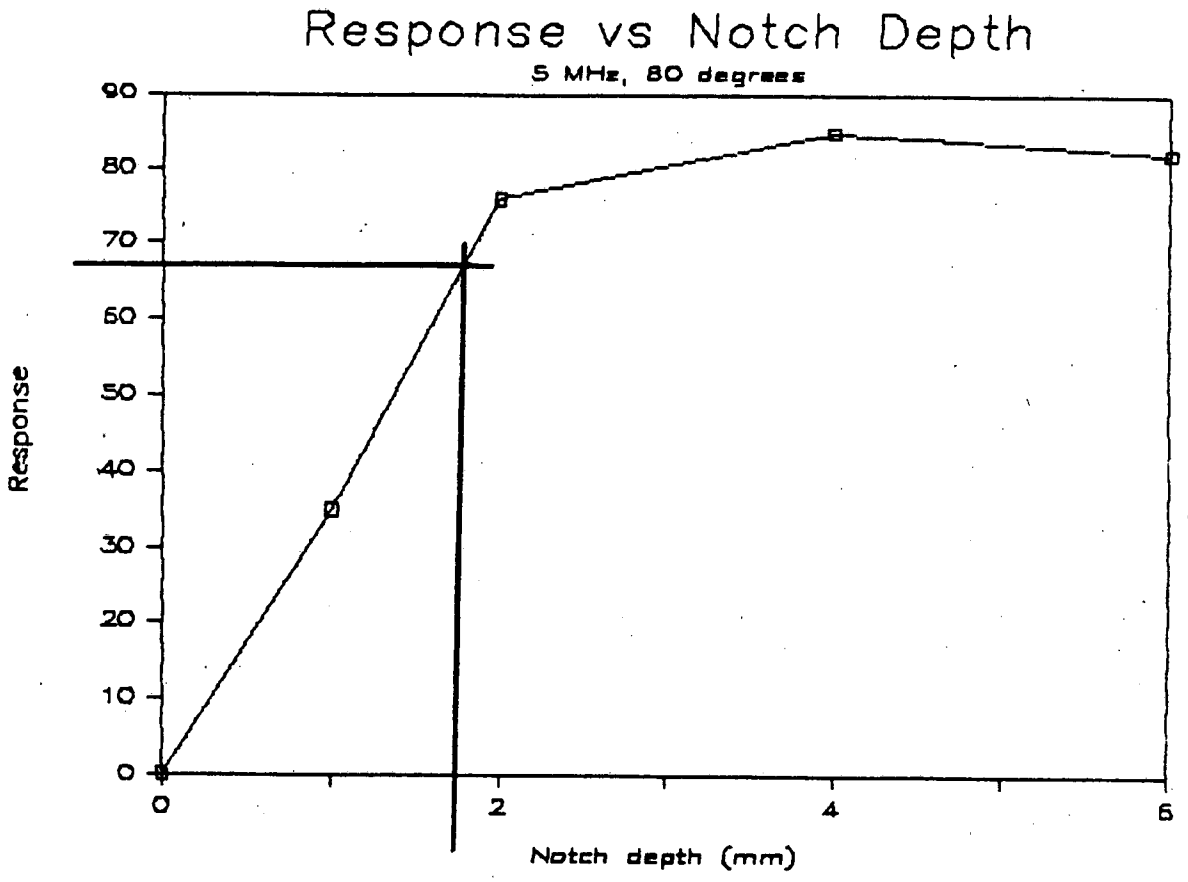

Figure 4.10-10. Plot of peak amplitude in image vs notch depth for specimen 4A from figure 4.10-9a. The fatigue crack peak amplitude response from figure 4.10-9b is indicated.

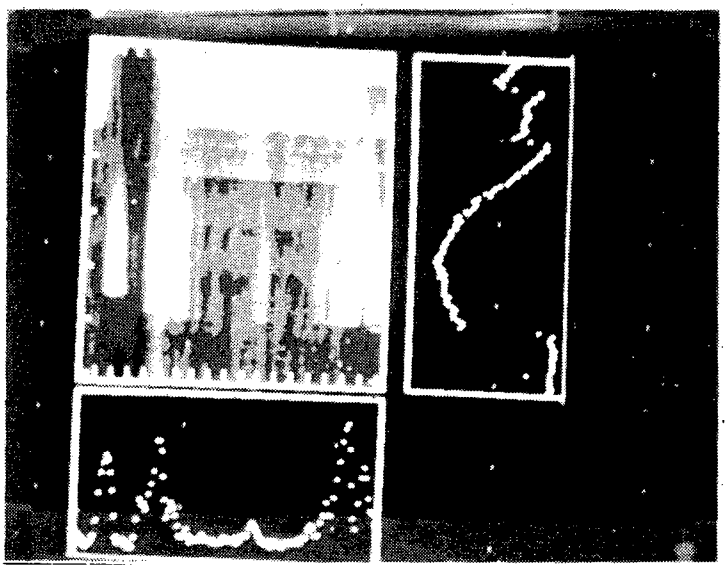

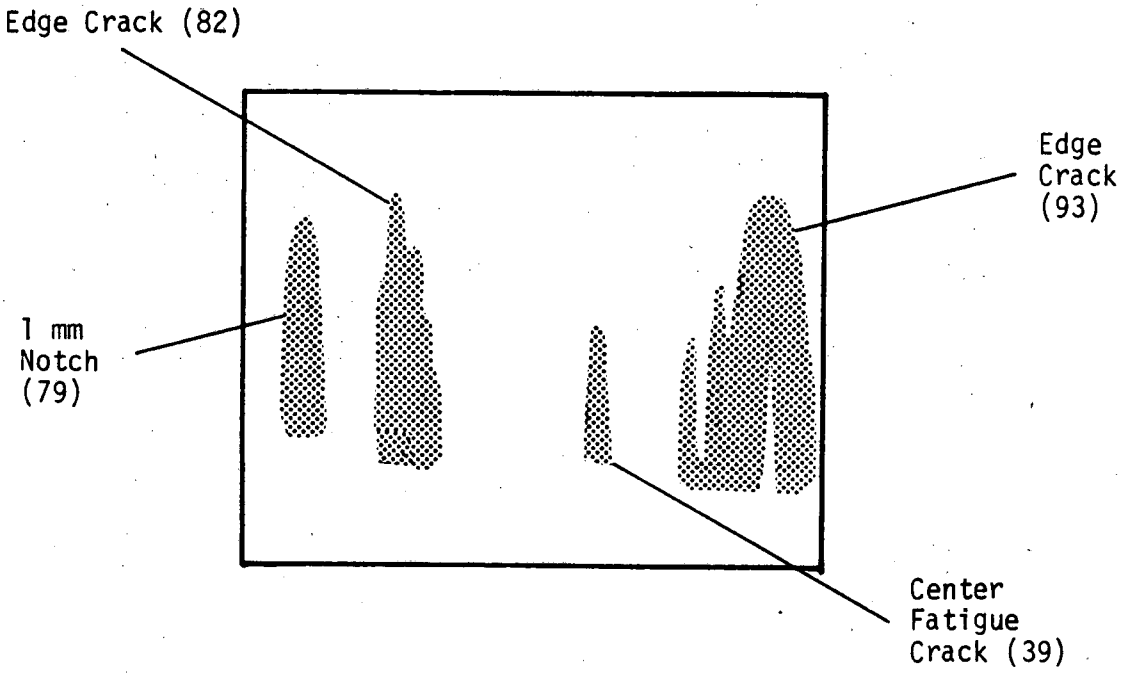

Figure 4.10-11. C-scan of specimen 5AA fatigue cracks and specimen 4A, 1mm notch using a 5 MHz 53° beam.

5.0 CONNECTOR TESTS

In order to test mockup connectors, an equipment configuration was assembled that would allow RF B-scan imaging. Figure 5-1 shows a block diagram of the equipment. The scannner is controlled by the UT 2000 ultrasonic inspection system. The scanner also provides a trigger signal for waveform digitization. The LeCroy digitizer is located in a CAMAC crate. The digitized waveform is sent to a PDP 11/44 computer and stored on disk. Sets of waveforms to create the B-scan image are viewed through a RAMTEK image processing system.

Figure 5-2 shows how the RF-B-scan displays a waveform. Figure 5-3 shows this process for a scan over EDM notches in the #13 test block used in the fatigue crack study. There is no apparent reason for B-scan to be particularly effective in the flat plate inspection. However, as was shown in Figure 4.6-6, which was obtained with this system, the inspection of threaded specimens is aided by the scan imaging.

Connector tests were originally planned. However, that work was deleted from the program. Reasons for deleting these tests included:

- More emphasis was placed on fatigue crack inspection.
- The sensitivity of inspection results to thread form suggested that these tests may not yield representative results, and in any event would not affect the conclusions of this study.

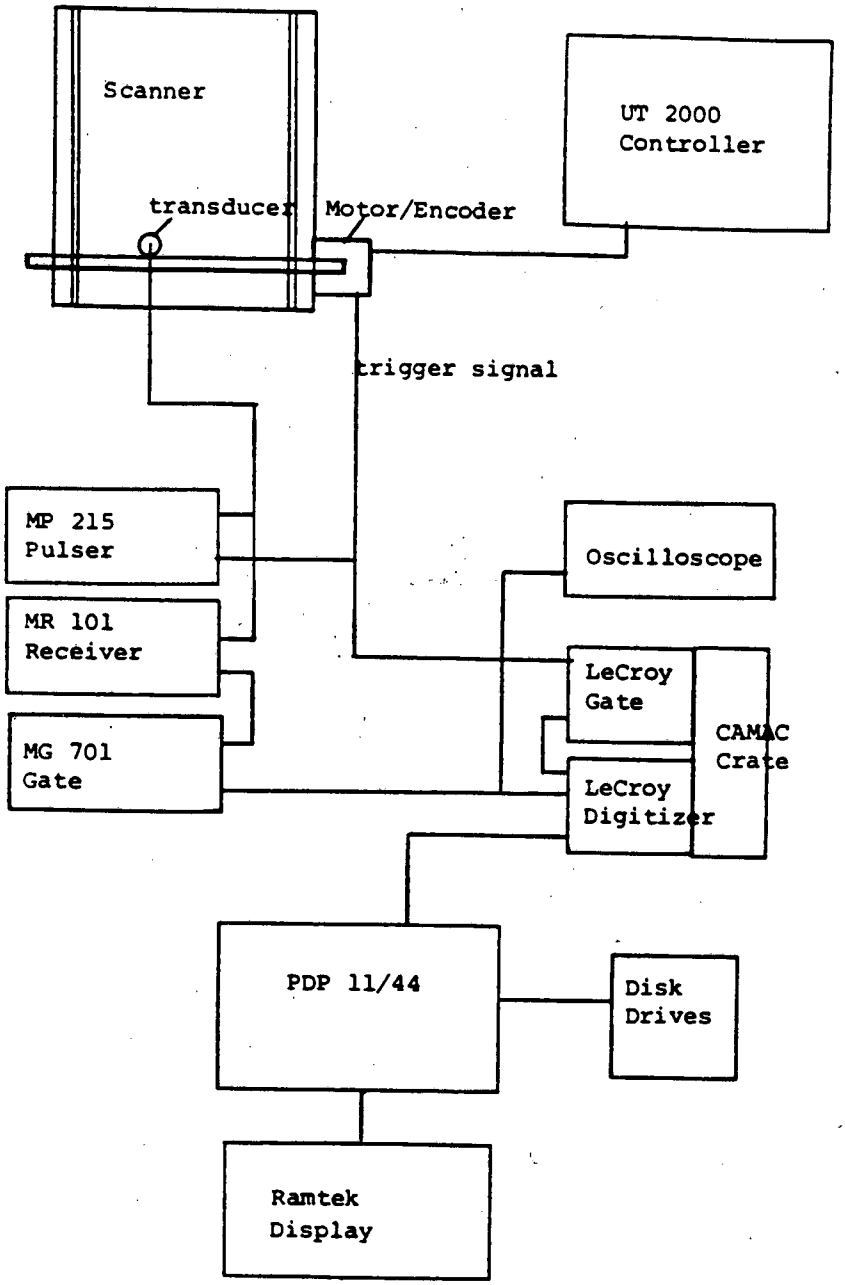

Figure 5-1. Block diagram of FR-B-scan imaging system.

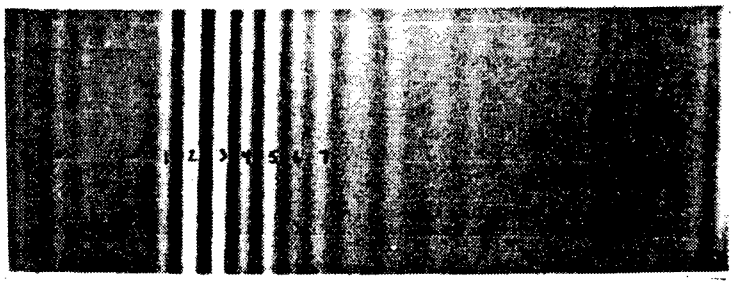

RF B-scan of a single RF wave form repeated approximately 250 times

RF B-scan of the RF signal at right

"Top" View

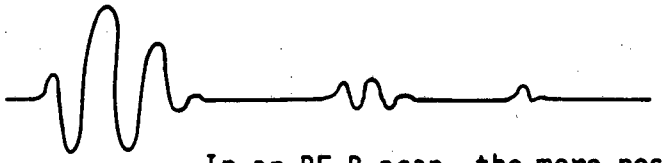

In an RF B-scan, the more positive the signal becomes, the brighter the line is while the more negative the signal, the darker the line becomes.

"Side" View

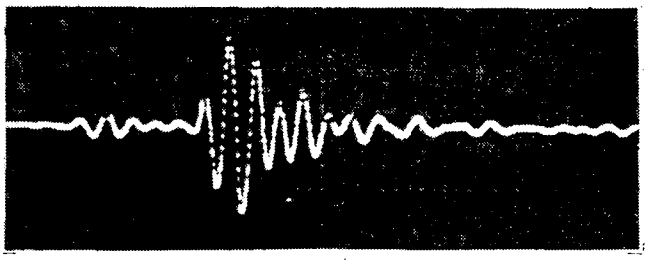

Typical RF Wave Form on a Scope

"Side" View

The positive cycles are numbered

Figure 5-2. RF-13 scan display of a waveform.

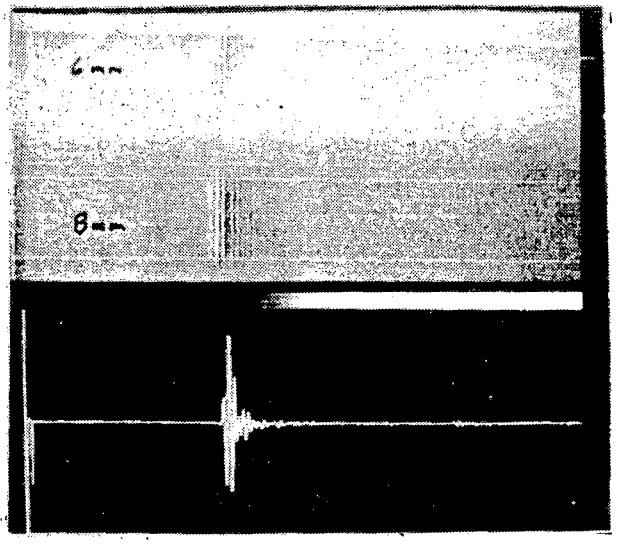

53.3° 1/2 v 5.0 Mhz

Lateral distance = 3.6"

File Name = FC 12A

Raw data

20.5 s time window
window start time (WST) = 47.8 s

RF wave form notch 2 (6mm deep)

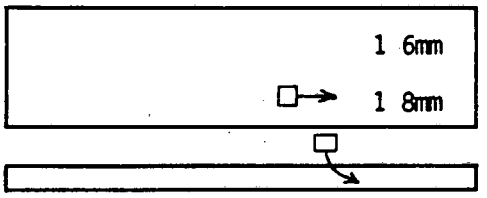

recitified B-scan

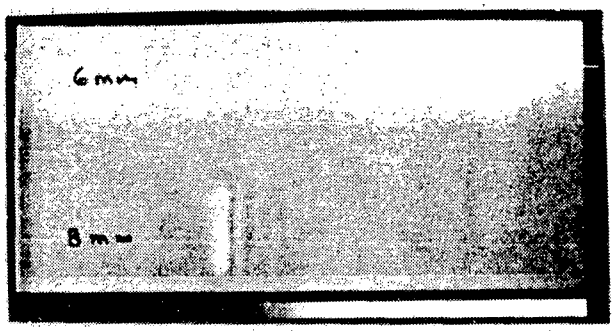

Figure 5-3. B-scan of notches in #13 test sample.

6.0 DEFECT SIZING CONSIDERATIONS

The inspectability of tension leg platform tendon program has resulted in measurements of echo response for a variety of conditions. Generally, the responses have behaved in accordance with expected principles. However, the reliability of the peak amplitude response as an indicator of true depth has not been shown to be particularly accurate. The comparison of fatigue cracks to EDM notches showed that on average the true cracks will return less than half the echo response amplitude of that from a 3 to 1 length to depth ratio notch of equivalent depth. The sensitivity of an ultrasonic inspection system must therefore be such that it will detect notches of at least one half (and in this study approximately one third) the depth of the fatigue crack size that is considered critical at the time of inspection. This critical size would be determined by the fatigue crack growth curve and the inspection interval such that the crack could not grow to failure between inspections. Sufficient sensitivity will be dependent upon the ultrasonic system and the part geometry.

The most common detection method for defects is to perform an ultrasonic scan over a part and look for signals above a threshold level. In objects with clean geometric features, such a technique is entirely appropriate as was shown on the Chevron weld sample. However, in complicated geometries, such as the Conoco weld sample containing root and crown, the ultrasonic return may be large due to the geometric features rather than the defect. In the case of the threaded coupling, the defect may appear behind threads of equal or greater ultrasonic echo strength. Detection in these nine complicated cases often requires comparison to baseline image pattern to observe the difference due to the presence of fatigue cracks.

Once detection has been obtained for a defect, sizing becomes the key issued. Normally, it would be assumed that the detection method could assign a size value to the defect. This is true in the amplitude response measurement however, the accuracy is highly questionable. For cracks in the 1 to 2 mm depth range the amplitude response was pretty good provided the crack orientation was correct. But, as the defect size increases, in the range of 6 to 8 mm deep notches, it was found that the amplitude sizing was not necessarily increasing. The result of these observations for inspection proposes is that the ultrasonic system may well require two modes: a detection technique and sizing technique which may rely on different methodologies.

During this study, it was shown that imaging can play an important role in the detection of defects. In the welded connector case, the image pattern could be used to separate the defects from the crown and root reflection based on the image pattern position. In the case of the threaded connector, the B-scan image allowed the detection of notches, although the peak signal strength was not appreciably higher than the thread signals. Imaging could also be used to apply some conventional depth sizing methods such as the dB drop and of course imaging provided lateral dimensional capability. However, the amplitude and dB drop sizing were not shown to be particularly accurate.

The tip diffraction [Gruber, 84 & Hayman, 85] timing method was used in the fatigue crack studies to establish depth values for notches. This method has been shown to offer good accuracy relative to amplitude measurement, however, they can be difficult to apply. The accuracy found in this study was not particularly good, although it was significantly better than amplitude comparison. In the threaded geometry, timing methods would be very difficult. Thread shadowing would be far superior if optimized by design. In the weld geometry timing would be advantageous, however, in unprepared welds the echo noise can mask the timing method because small diffraction signals must be measured. Section 7 discusses these methods.

In general, if the design can allow for conservatism in detection, then amplitude ultrasonics should be an acceptable methodology. Where the geometry of the object can be assigned to provide clean, interpretable ultrasonic signals from critical inspection regions then the inspection confidence is enhanced. This is true when the stress is understood so that the fatigue crack geometry can be accurately predicted. Imaging of the defects using amplitude and scan approaches can then provide fairly good accuracy for sizing. More sophisticated imaging approaches applied to sizing are discussed in Section 7. In cases where the inspection criteria is not considered, geometric and material problems can seriously hinder suitable sizing.

7.0 ULTRASONIC METHODS FOR SIZING DEFECTS

7.1 Overview of Sizing Methods

Accurate sizing of defects in thin walled material (less than two inches wall thickness) remains more of an art than a science at this time. A high degree of operator skill and training is required, particularly in the case of IGSCC (interganular stress corrosion cracking). Rigorous training courses produce students of whom only 30 to 40 percent pass a detection and sizing test the first time on actual IGSCC samples. Fatigue cracks, on the other hand, result in a better defined, planar type of flaw which is somewhat easier to characterize.

A major consideration in thin walled material is the fact that many flaws are of the surface breaking type, and form a strong corner trap reflector at the point where the surface is broached. Special techniques are required to distinguish the crack tip echo from the much stronger corner trap echo.

There are three basic sizing methods which will be described in this section. These are: amplitude, timing, and imaging.

7.2 Amplitude-based Sizing Methods

Amplitude sizing methods primarily employ angle beam shear waves but can also utilize creeping waves or Lamb waves. A calibration curve of slot depth versus amplitude is first constructed by scanning a specimen having a series of machined notches. Amplitude measurements are then taken on the crack and its depth predicted using the curve. The calibration procedure using a slot as a reference is standard practice in the nuclear industry [ASME] and is widely used as standard practice in non-nuclear industrial plants. The curves, which were developed on notches, generally undersize cracks because a crack reflects less energy than a notch of the same size. To account for undersizing, a compensation factor may be added to the depth predicted by the calibration curve [Singh].

Crack dimensions which appear to be greater than the beam width of the ultrasonic transducer are estimated using a dB drop techniques. The transducer is scanned until endpoints are located for which the amplitude is 6 dB lower than that observed at the center of the indication. The position of these endpoints is then taken as crack dimensions.

Amplitude methods are easy to apply but have several inherent drawbacks. The reflected amplitude depends on several other factors in addition to crack size, including crack tightness, crack orientation, crack shape and crack roughness. Interference between waves, coupling, and surface finish can also contribute error to the method.

An excellent summary of these error-inducing factors is reported by [Birring]. His literature review found that interference effects increased with frequency and, at 5 MHz, could result in an error of up to 0.38 mm (0.015

inches) when sizing cracks in the range from 0.25 mm to 2.5mm (0.010 to 0.100 inches). For fatigue cracks under compressive forces, the reflectivities of both crack face and crack tip can vary as much as 11 dB on the application of a 13,000 psi compressive stress. A crack surface roughness of 500 micrometers was shown to result in a decrease in signal amplitude of 20 dB over that of a smooth surfaced crack. Finally, a flaw tilt angle of 16 degrees off normal resulted in signal losses of up to 18 dB.

In spite of these limitations, amplitude methods are still used extensively for crack sizing, probably because of their relative ease of application. The other two methods, timing and imaging, offer greater degrees of accuracy.

7.3 Timing Methods

Timing methods for sizing flaws rely on detection of signals diffracted from the tips of crack. Two primary schemes have been reported. One is based on pitch-catch transducers located on either side of the weld, and is primarily used for heavy section welds wherein the crack does not break the surface [Curtis]. The difference in arrival times of diffracted signals from the top and bottom of a crack is detected, and can be correlated directly to through-wall dimensions of the crack.

For thin walled materials, pulsed echo or pitch-catch testing is generally performed from the same side of the weld. In the simplest case, an angled shear wave is launced at a backwall crack as shown in Figure 7.3-1, producing an echo from both the crack tip and from the corner trap formed where the flaw breaks the surface. Crack depth can be caluculated using the time difference between the two signals and the reflected angle of the waves. The crack depth (d) is expressed as follows:

$$d = vt/2 \cos R$$

where v is the shear velocity, t is the time difference between pulses, and R is the beam angle.

The technique is quite accurate if the tip signal can be identified in the presense of the much larger corner trap signal. A fair degree of operator training and capability is required to succrssfully employ the test.

The above problem can be overcome to a large extent by using creeping waves with separate transmit and receive transducers [Gruber, EPRI]. Creeping waves are high angle longitudinal waves and are gneerally accompanied by shallow angle shear waves. Under many conditions they provide more equal amplitudes between the tip and corner trap signals.

An example of sizing with creeping wave diffraction methods is shown in Figure 7.3-2. A pair of transducers is used to permit capture of longitudinal wave signals close in time to the transmit pulse. Broad angle, shear and longitudinal waves are launced at approximately 30 + 10 and 70 + 15 degrees respectively to insonify the entire wall.

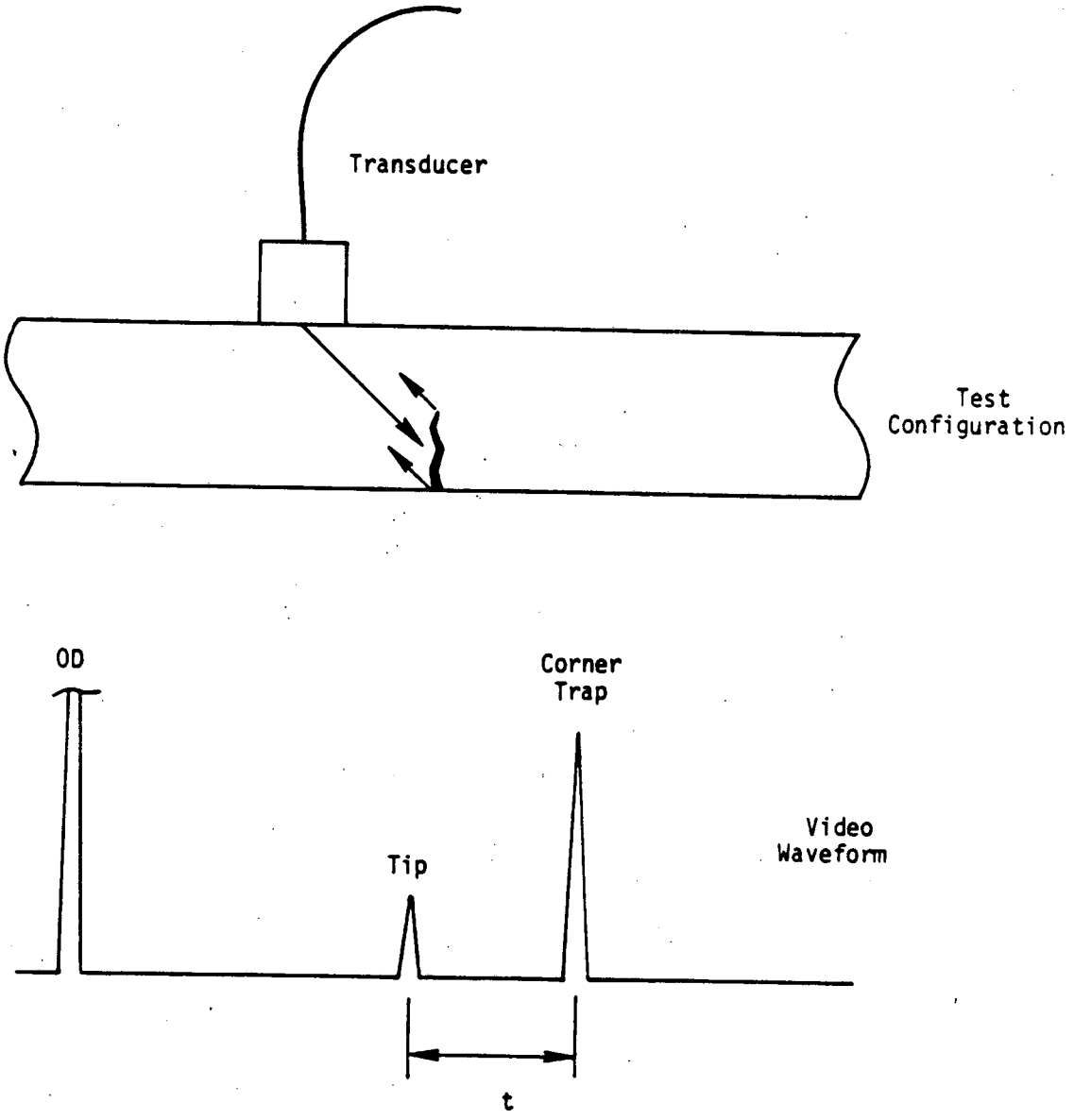

Figure 7.3-1 Crack sizing with tip diffraction methods.

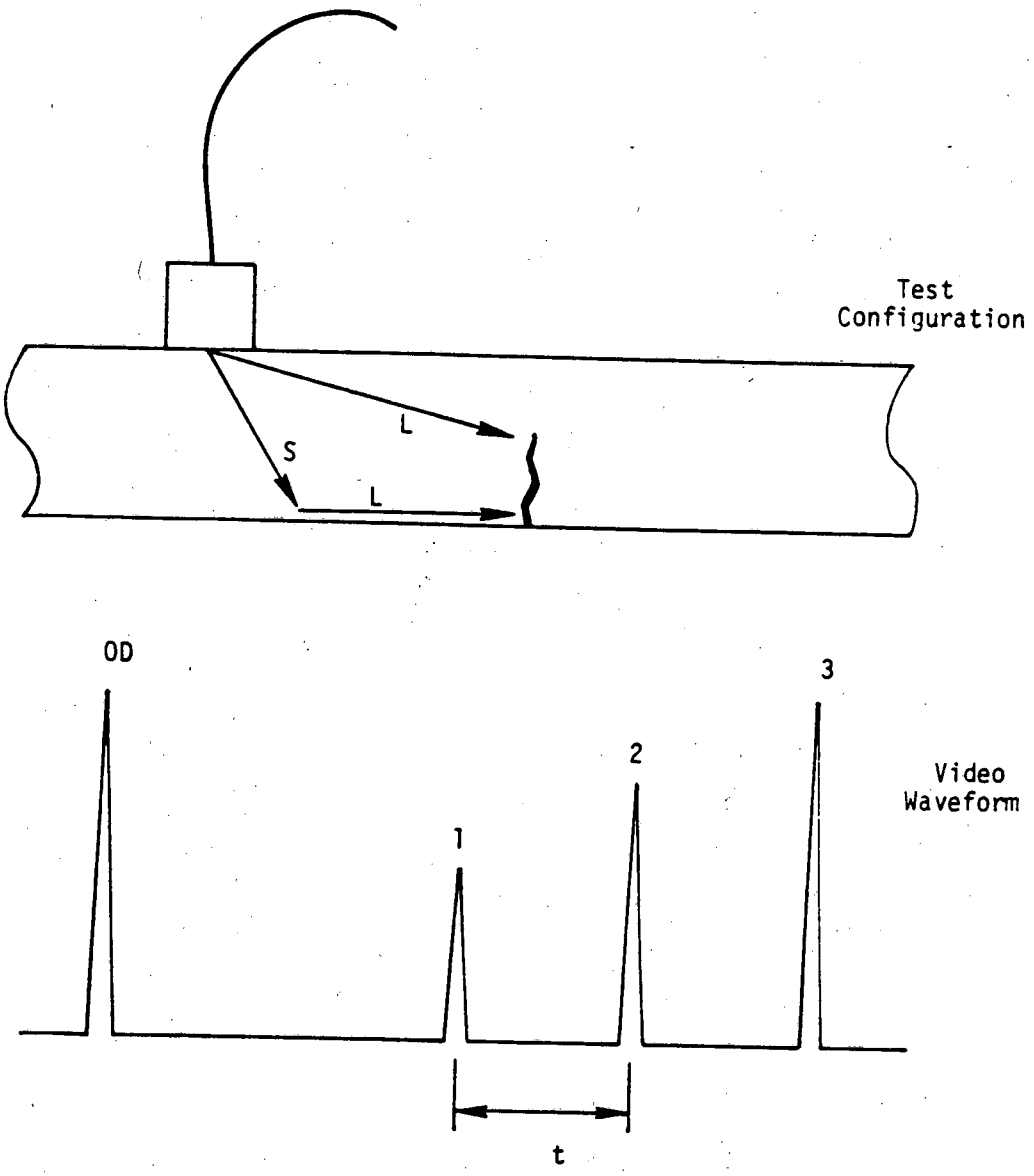

Figure 7.3-2 Tip diffraction sizing with creeping waves.

Two signals are reflected from the crack opening on the far side. These are: 1) shear energy which is mode converted to longitudinal and propagates to the crack opening as a bottom creeping wave, and 2) direct shear insonification of the corner trap. These appear as Pulses 2 and 3 of Figure 7.3-2. A diffracted longitudinal wave from the crack tip (Pulse 1) appears earlier in time. The separation between Pulse 1 and Pulse 2 is a relatively constant function of crack height over a wide range of probe positions.

7.4 Imaging Methods

There are two key imaging methods applicable to flaw sizing, namely holography and synthetic aperture focussing techniques (SAFT). They are able to attain a spatial resolution on the order of 1/2 wavelength of the test frequency, and can thus be used for quite accurate sizing in heavy section materials.

Holography [Hildebrand] uses a single frequency and can reconstruct a C-scan or plan view of the flaw. The method gathers a pair of data points for each discrete location in the scanned aperture. These data are representative of the C-scan actually detected by the transducer. They are back-propagated to the flaw depth via computer and a new C-scan is plotted which is the actual sound field reflected by the flaw. Holography is usually performed using specialized ultrasonic equipment. The equipment uses a "narrow band" approach where a tone burst signal is used. The interference of the defect signal with the tone burst is recorded by in phase and quadrature detection. Using this approach, the data is not particularly useful for anything other than holography (i.e. amplitude C-scan or time-of-flight C-scan analysis) because the tone burst causes the resolution of the timing to be poor. It is possible to perform holography by digitizing A-scans and Fourier transforming for processing. This can be a computer intensive process. Holography also requires that the scanning be performed precisely and the data taken relatively closely. Usually this criteria causes the inspection area to be limited in size due to computational limitations or the size of the arrary that is to be reconstructed. Finally, holography requires that a beam with broad coverage be used. The broad beam is essential so that information is received from a large area in order to get good interference information for accurate reconstruction. This is in conflict with the desires of conventional C-scan imaging where a pencil beam size is desired to get the best discreet data point resolution in an image. For these reasons, holography and conventional scanning are usually performed independently. That is, the conventional scanning system is used to detect defects, then a precision holography sccan using the broader ultrasonic beam and specialized electronics is used for higher resolution imaging.

SAFT performs a similar scan of an aperture about the flaw but stores a waveform for each sample point. The synthetic array formed by scanning may then be focussed on any point in the inspected volume by delay and sum techniques. High resolution C-scans, B-scans or volumetric images may be reconstructed. However, the reconstruction times may be prohibitively long due to the large quantity of data which must be manipulated. SAFT requires that the A-scan be digitized. Similar to holography, it requires a broad ultrasonic beam to cover a large area in the object and a precise physical scan. SAFT and holography are fundamentally the same technique but use different mathematical reconstruction approaches.

These imaging techniques are plagued by the unequal reflections between crack tip and corner trap when applied to thin wall sizing. [Doctor] has reported a SAFT scanning technique for overcoming this problem. A pair of tandem transducers are scanned in opposite directions about the flaw. This tends to maximize sensitivity to the tip signal and permits adequate images to be reconstructed from which crack dimensions may be taken. Resolution of this technique is limited to approximately 1.5 mm.

8.0 CONCLUSIONS AND RECOMMENDATIONS

8.1 Minimum Detectable Flaw Size

The inspectabililty of Tension Leg Platform Tendons depends on several factors including:

a) Geometry
b) Materials
c) Type of inspection tool
d) Method of imaging
e) Inspection criteria

The main objective of this work has been to establish a method for determining a minimum detectable crack size based on a given geometry. The program has considered the theoretical minimum detectable size based on an assumed 100 percent ultrasonic inspection. We have not considered human factors or equipment reliability - except insofar as human factors enter into the operation of laboratory flaw detectors and imaging equipment.

Our main conclusion is that equation 3-1 may be used, with some qualifications, to estimate the minimum detectable flaw in geometries similar to those of TLP threaded connectors. This equation may thus be used in the design phase to evaluate the inspectability of various components, and to prepare a preliminary specification for ultrasonic inspection equipment.

The assumptions and limitations in the use of this equation are as follows:

1. The threshold value of echo response p/po, for a minimum detectable notch is .001 or less. The value for fatigue cracks should tentatively be .002. Since our fatigue crack tests were only conducted on closed (i.e. unstressed) cracks, this conclusion might be altered by further tests on cracks under stress which should show responses closer to those of notches.

2. Experimental verification was limited to the following conditions:

   - Fine grained steels with almost negliglible attenuation were used.
   - 1/2 - 3/4 inch transducers, 1-5 MHz
   - Maximum path length of 312 mm
   - Shear beam of 45-75 degree angles

3. Equation 3-1 does not predict the minimum detectable flaw in thread roots. Thread echoes may hide flaw responses. Flaw detectability is strongly influenced by beam angle and thread form. We recommend tests such as those described in Section 4.6 for specific thread geometries.

8.2 Welded Joints

Equation 3-1 applies only to "far field" acoustic region and should not be applied to thin walled sections (i.e. 30 mm or less). Specific tests on thin walled welded specimens indicated the following:

1. Unless weld root pass through is removed, notches less than approximately 2 mm could not be distinguished from the weld root, even with imaging.

2. Flaws larger than 2 mm generally gave higher responses than the weld root or crown in the samples tested, however their images appeared similar to weld root images. Notches up to 5 mm (the largest tested) could not be easily distinguished from weld root images. Considering the reduced responses from fatigue cracks, even larger fatigue cracks might be indistinguishable from weld root signals.

3. If the weld root is removed, the minimum detectable flaw is below 1 mm.

This suggests that the inspectability of welded joints requires either:

a) Removal of the weld root pass through, or

b) Calibration of initial weld root images for later comparison with inservice imaging.

These conclusions are applicable to butt welds in thin walled pipe (25-30 mm wall thickness).

8.3 Marine Coatings

Studies on fouled specimens suggest that inspection may be carried out from either the inside or outside of a fouled structure provided the fouled surface is suitably cleaned. Scraping followed by bristle brushing provided the best results in these tests. However, all of the cleaning methods attempted left some residual barnacle growth which caused a significant loss of ultrasonic signal when inspecting through the growth. This could affect the reliability of external inspections.

9.0 RECOMMENDATIONS FOR FURTHER RESEARCH

This study has yielded important results about the intrinsic characteristics of the flaw detection and sizing using ultrasonic inspection methods. This is only one component of the broader question of Inspectability of Tension Leg Platform Tendons, or more generally the issue of Inspectability of Offshore Structures.

The broader question which should be addressed is the reliability of practical inspection methods, which would include the intrinsic reliability studied here as well as such factors as equipment reliability, positional accuracy of scanning devices, and interpretive accuracy of human inspectors or flaw detection algorithms.

Aside from this broad area of study, we believe additional studies on the intrinsic reliability of ultrasonic inspection should include the following:

a) UT Response from Fatigue Cracks

Our results indicate that the UT response amplitude from fatigue cracks is less than 50 percent of that from equivalently sized notches. Other data suggests that this result is dependent on the crack face pressure, and that higher response might be expected if the cracks are placed under tension loads. We would suggest further experiments with the cracked specimen using a flaw detector to observe crack responsed while subjecting the specimens to a bending load.

b) Inspectability of Welded Joints

The primary focus of this study has been on threaded joints. The work that was done on welded joints indicates that the minimum detectable flaw might depend on the ability to filter the ultrasonic images due to weld crown and weld root (assuming the weld is not ground smooth, in which case a small flaw is easily detected). This suggests that "blind tests" should be conducted using a number of welded specimens. Images collected before and after the introduction of various size fatigue cracks should be evaluated to determine the smallest crack which can be reliably detected. This evaluation should be made using only the "after" images to evaluate the reliability of detecting cracks without the benefit of a pre-crack image - as for the case of a pre-existing structure.

c) Sizing Considerations

The ability to size cracks which are larger than the minimum detectable flaw size is important for fracture mechanics analysis. This study has shown that amplitude sizing is unreliable. Even the "time of flight" method applied underestimated the size of fatigue cracks under the conditions tested. Further studies aimed at validating crack sizing methods should be carried out using both notched and cracked specimens.

10.0 BIBLIOGRAPHY

American Society of Mechanical Engineers — 'Rules for Inservice Inspection of Nuclear Power Plant Components', Section XI of the ASME Boiler and Pressure Vessel Code. Published every three years.

Anonymous, — 'Handbook on the Ultrasonic Examination of Welds', The Welding Institute, Cambridge, England, 1977.

Becker, F.L., Doctor, S.R., Heasler, P.G., Morris, C.J., Pittman, S.G., Selby, G.P., and Simonen, F.A. — 'Integration of NDE Reliability and Fracture Mechanics', Phase I Report, 'NUREG/CR-1696, PNL-3469, Vol. I, September 1980-March 1981.

Birring, A.S., — 'Ultrasonic Factors for Inspection of Tension Leg Platforms', Final Report to the U.S. Coast Guard Contract No. DTCG 39-85-C-80231., November, 1985.

Bitting, K.R., Allen S.J., and R.T. Walker — 'Tension Leg Platform Tendon and Template Inspection-A Survey of Capabilities', U.S. Coast Guard, Final Report, July 1985.

Bossi, R.H., D. Boyd, O. Oberg, F. Skilback, N. Helm and B. Herd — 'Computer Aided Ultrasonic Inspection of an Offshore Tension Leg Platform', ASME Pressure Vessel and Piping Conference, June 1984, Ts, 84-pvp-125.

Bossi, R.H., Halkyard, J.E., Isaacson, C.A., and B.F. Maki. — "Inspectability of Tension Leg Platform Tendons", Final Report Phase I, U.S. Dept. of Interior Contract 14-12-0001-30204, 4 May 1985

Burkle, W. S., — 'Measurement of Ultrasonic Longitudinal Wave Attenuation', Materials Evaluation, March 1984.

Chapman, R. K. — 'Ultrasonic Reflection from Smooth Flat Cracks: Exact Solution for the Semi-Infinite Crack', CEGB, NW/SSD/RR/145/81, December 1981.

Coffey, J. M., R. K. Chapman — 'Application of Elastic Scattering Theory for Smooth Flat Cracks to the Quantitative Prediction of Ultrasonic Defect Detection and Sizing', Specialist Meeting on Defect Detection and Sizing, Ispra, Italy, May 3-6, 1983.

Curtis, G.J., — 'Crack Sizing by the Time-of-Flight Diffraction Method', Review of Progress in Quantitative Nondestructive Evaluation, Volume 6, 1985.

Doctor, S.R. et. al., — 'Real Time SAFT UT for Nuclear Component Inspections', Proceedings of the 8th International Conference on NDE in the Nuclear Industry., Nov. 1986.

Doyle, P.A., and C. M. Scala	'Crack Depth Measurement by Ultrasonics: A Review', Ultrasonics, July, 1978.
EPRI NDE Center,	'UT Operator Training of Planar Flaw Sizing', EPRI Training Course 3, December, 1984.
Green, Jr., R. E.,	'Ultrasonic Nondestructive Materials Characterization', Proceedings of NASA Conference on Analytical Ultrasonics in Materials Research and Testing, November 1984.
Green, R. E., Jr.,	private communication (1986).
Gruber, G.J., G.J. Hendrix and W.R. Schick	'Characterization of Flaws in Piping Welds Using Satellite Pulses', Materials Evaluation, Vol. 42, No. 4, April 1984.
Haines, N. F.	'A Practical Model of Ultrasonic Reflection from Planar Surfaces', Central Electricity Generating Board, RD/B/N4995, WR/MSG/P(81)114, January 1981.
Hayman, A.J.	'An Improved Ultrasonic Tip-Corner Timing Method for Sizing Shallow Surface Breaking Cracks' British Journal of NDT, September 1985.
Hein, N.W., Skilbeck, F., Herd, B.P., and A.J. DeVries	'Requirements for a Nondestructive Inspection System for the Hutton Tension Leg Platform (TLP) Mooring System', Offshore Mechanics and Arctic Engineering Conference, February 1984, New Orleans, LA.
Hildebrand, B.P., T.J. Davis, A.J. Boland, and R.L. Silta	'A Portable Digital Ultrasonic Holography System for Imaging Flaws in Heavy Section Materials', IEEE Transactions on Sonics and Ultrasonics, July 1984, pp 287-94.
Jessop, J.J., P.J. Mudge, J. D. Harrison.	'Ultransonic Measurement of Weld Flaw Size' National Cooperative Highway Research Program Report 242, Transportation Research Board, 1981.
Kapranos, P. A., V. N. Whittaker	'Ultrasonic Inspection of Corrosion- Fatigue Cracks in Austenitic Stainless Steel Welds', British Journal of NDT, January (1984).
Krautkramer, J.,H. Krautkramer	Ultransonic Testing of Materials, 3rd Edition, Springer-Verlag, New York (1983).

Papadakis, E. P., 'Ultrasonic Attenuation Caused by Scattering in Polycrystalline Media', Physical Acoustics, W. P. Mason, Ed., Vol. IV, Part B 1968.

Posakony, G.J., 'Experimental Analysis of Ultrasonic Responses from Artificial Defects', Materials Evaluation. Vol. 44, No. 12, (December 1987).

Rogerson, A., R. A. Murgatroyd 'Defect Characterization Using Ultrasonic Techniques', Research Techniques in NDT, R. S. Sharpe, Ed., Vol. IV, Academic Press, New York 1980.

Silk, M.G., 'Estimates of the Magnitude of some Basic Sources of Error in Ultrasonic Defect Sizing', AERE - R9023, 1978.

Silk, M.G., 'The Transfer of Ultrasonic Energy in the Diffraction Technique for crack Sizing', Ultrasonics, pages 113-121, May 1979.

Singh, A., & G.P. Singh 'Sizing of Longitudinal Seam Weld Flaws in Thin-Walled Tubes by Ultrasonic Methods', Proceeding of the 13th Symposium on Nondestrucive Evaluation, San Antonio, TX, April, 1981, pp161-172.

Szilard, J., 'Examining the Grain Structure of Metals', Ultrasonic Testing, J. Szilard, Ed., John Wiley, New York (1982).

Thompson, R. B., T. A. Gray 'A Model Relating Ultrasonic Scattering Measurements Through Liquid-Solid Interfaces to Unbounded Medium Scattering Amplitudes', J. Acoust. Soc. Am., 74(4), October 1983.

Thompson, R. B., T. A. Gray 'Analytic Diffraction Corrections to Ultrasonic Scattering Measurements', Review of Progress in Quantitative Nondestructive Evaluation, Vol. 2A, D. Thompson and D. Chimeti, Eds., Plenum Press, 1983.

APPENDIX A

Spectral Analysis of Transducers

APPENDIX A

TRANSDUCER SPECIFICATIONS

The manufacturer specification of the transducers of Table 4.2-1 are given in Figures A-1 through A-10.

A number of transducers were also tested for the spectral content of the beams under similar conditions to those used for measurements. A spike pulse was used to create the ultrasonic beam. The technique digitized a reflection from a surface and Fourier transformed the data. This spectral output was plotted. Three echoes were tested for each transducer:

1. A path of about 120 ms in water to a flat reflector (long. in water).
2. A longitudinal path in steel of approximately 150 ms using a contact method (long. in steel).
3. A shear beam path in steel using an immersion technique (shear).

Figures A-11 through A-22 show the plotted results for four transducer types. In each figure the response is plotted in a linear and a logarithmic scale. The vertical axis values in the linear scale plots are arbitrary units which result from the fast Fourier transform algorithm based on the input intensities. For comparison, the values should be normalized to the peak response in each group. Three of the transducer types were 0.5 inch diameter lead zirctitinate of 5 MHz and 2.25 MHz and a commercial transducer believed to be lead metaniobate. These three are representative of data taken on a number of the table 4.2-1 transducers. In addition to the three transducers of Table 4.2-1, a lithium niobate transducer of the type used in the Hutton TLP inspection system [Hein, Bossi] was also tested.

SIGMA RESEARCH, INC.

TRANSDUCER FREQUENCY ANALYSIS AND BANDWIDTH

Customer

Sigma Project/Contract No.

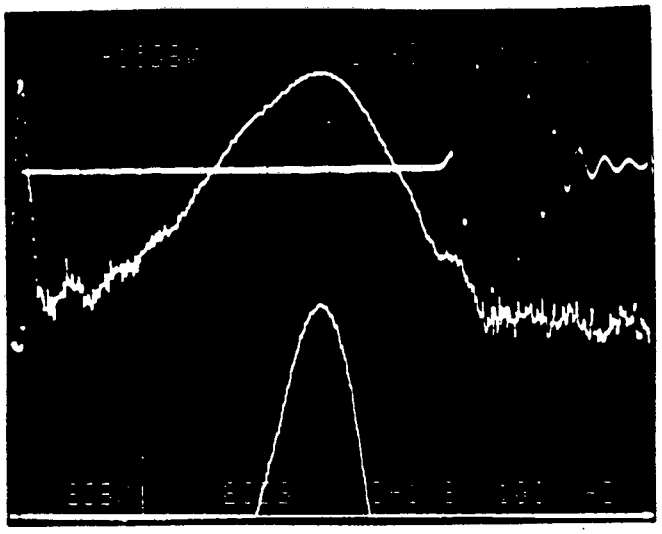

Time Base: .50 usec/div.
Vertical Scale: 200 m volts/div.

TRANSDUCER

Serial No.: 638-1285
Type: SD-Z
½ · 5 MHz

CABLE TYPE: RG 58
Connector: BNC
Length: 20 ft
Couplant: H_2O

PULSER TYPE: MP215
Damping: minimum
Rise Time: 15 ns

RECEIVER TYPE: MR101
Attenuation: 56 dB
Filter: 0.5 MHz MHz

GATE TYPE: MG701
Delay: 199 µs
Width: 2.5 µs

ECHO FROM

- ☐ Radiused Block
- ☐ Cylindrical Hole at Focal Length
- ☐ Flat-Bottom Hole at Focal Length
- ☒ Other (sketch)

Radius = _____

Focal Length = _____

Hole Diameter = _____

SKETCH

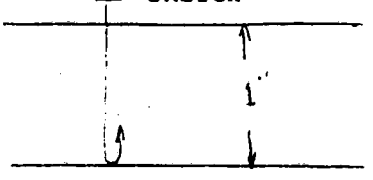

Spectrum Analyzer:
Center Frequency: 4.75 MHz
Bandwidth -3dB: 1.7 MHz

Signature Ken Harmon Title ENG. SPEC. Date 3-JAN-86

Figure A-1

SIGMA RESEARCH, INC.
1200 GEORGE WASHINGTON WAY
RICHLAND, WASHINGTON 99352
(509) 375-0883

SIGMA RESEARCH, INC.

TRANSDUCER FREQUENCY ANALYSIS AND BANDWIDTH

Customer

Sigma Project/Contract No.

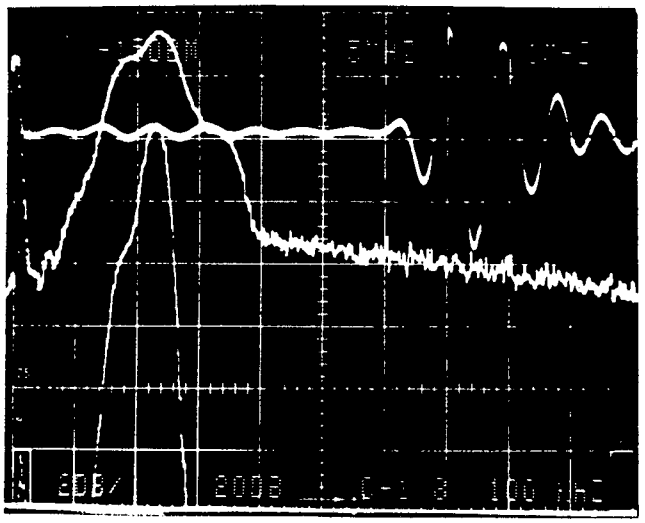

Time Base: .50 usec/div.
Vertical Scale: 200 m volts/div.

TRANSDUCER
Serial No.: 639-1285
Type: Sigma SD-3
½ - 2.25 MHz

CABLE TYPE: RG 58
Connector: BNC
Length: 30 ft
Couplant: H_2O

PULSER TYPE: HP215
Damping: minimum
Rise Time: 15 ns

RECEIVER TYPE: MRI01
Attenuation: 50 dB
Filter: 0.5 MHz

GATE TYPE: MG701
Delay: 199 µs
Width: 3 µs

ECHO FROM

- ☐ Radiused Block
- ☐ Cylindrical Hole at Focal Length
- ☐ Flat-Bottom Hole at Focal Length
- ☒ Other (sketch)

Radius = _____

Focal Length = _____

Hole Diameter = _____

SKETCH

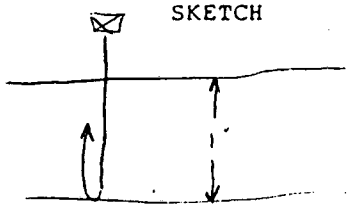

Spectrum Analyzer:
Center Frequency: 2.10 MHz
Bandwidth -3dB: 1.10 MHz

Signature Kim Hansen Title Engineering Specialist Date 12-FEB-86

Figure A-2

SIGMA RESEARCH, INC.

SIGMA RESEARCH, INC.

TRANSDUCER FREQUENCY ANALYSIS AND BANDWIDTH

Customer Seattle Lab (Dick Bossi) Sigma Project/Contract No. 609-2

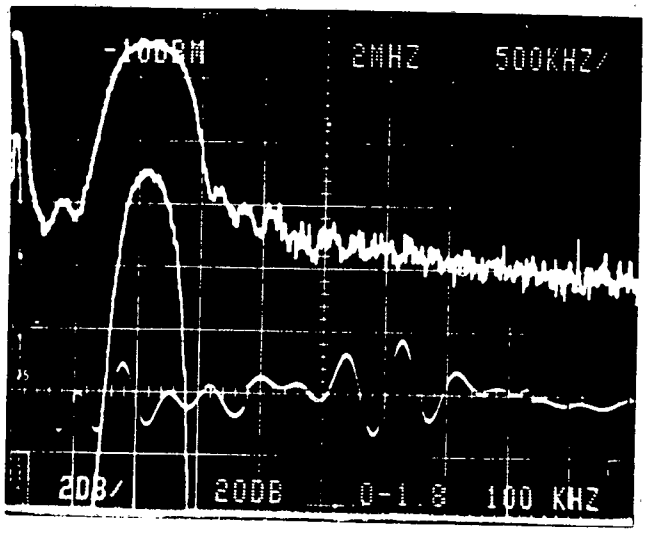

Time Base: 1 usec/div.
Vertical Scale: 500 mvolts/div.

TRANSDUCER
Serial No.: 640-1285
Type: SD-Z
½"Ø - 1MHz

CABLE TYPE: RG 58
Connector: BNC
Length: 20f
Couplant: H₂O

PULSER TYPE: MP215
Damping: minimum
Rise Time: 15 ns

RECEIVER TYPE: MR101
Attenuation: 46 dB
Filter: 0.5 MHz

GATE TYPE: MG701
Delay: 208
Width: 4.6 us

ECHO FROM

- ☐ Radiused Block
- ☐ Cylindrical Hole at Focal Length
- ☐ Flat-Bottom Hole at Focal Length
- ☒ Other (sketch)

Radius =

Focal Length =

Hole Diameter =

SKETCH

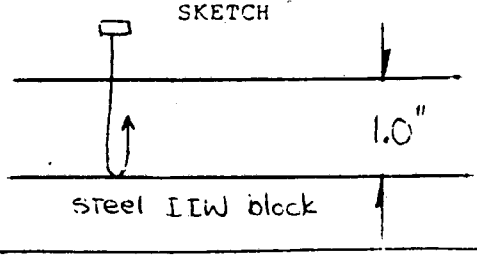

Spectrum Analyzer:
Center Frequency: 1.08 MHz
Bandwidth -3dB: 0.65 MHz

Signature Ken Mazzeo Title Eng. Spec. Date 5-MAR-86

Figure A-3

SIGMA RESEARCH, INC.

SIGMA RESEARCH, INC.

TRANSDUCER FREQUENCY ANALYSIS AND BANDWIDTH

Customer Seattle Lab. Sigma Project/Contract No.

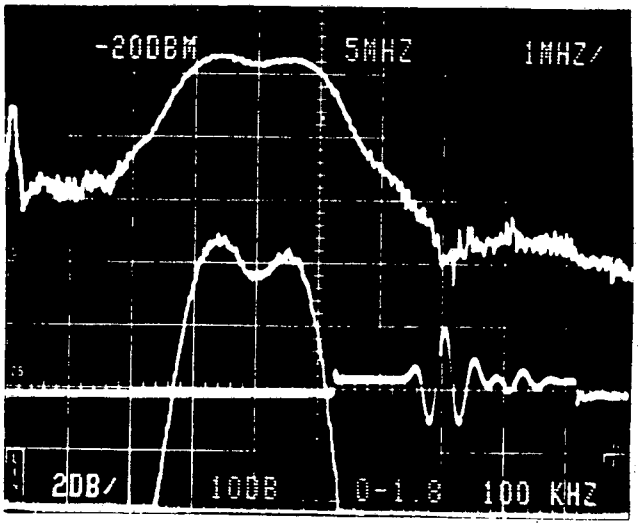

Time Base: .5 usec/div.
Vertical Scale: 500mvolts/div.

Spectrum Analyzer:
Center Frequency: 3.85 MHz
Bandwidth -3dB: 2.5 MHz

TRANSDUCER
Serial No.: 643-1285
Type: SD-2
¾-5MHz

CABLE TYPE: RG58
Connector: BNC
Length: 20ft
Couplant: H_2O

PULSER TYPE: MP21S
Damping: minimum
Rise Time: 15 ns

RECEIVER TYPE: MR101
Attenuation: 49 dB
Filter: 0.5 MHz

GATE TYPE: MG701
Delay: 205 µs
Width: 2 µs

ECHO FROM

- ☐ Radiused Block
- ☐ Cylindrical Hole at Focal Length
- ☐ Flat-Bottom Hole at Focal Length
- ☒ Other (sketch)

Radius =

Focal Length =

Hole Diameter =

SKETCH

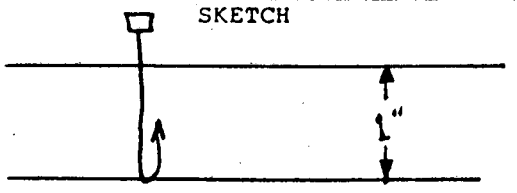

Signature Kenneth L. Harrison Title Eng. Spec. Date 12-MAR-86

Figure A-4

SIGMA RESEARCH, INC.
1700 GEORGE WASHINGTON WAY
RICHLAND, WASHINGTON 99352
509/375-0863

SIGMA RESEARCH, INC.

TRANSDUCER FREQUENCY ANALYSIS AND BANDWIDTH

Customer

Sigma Project/Contract No.

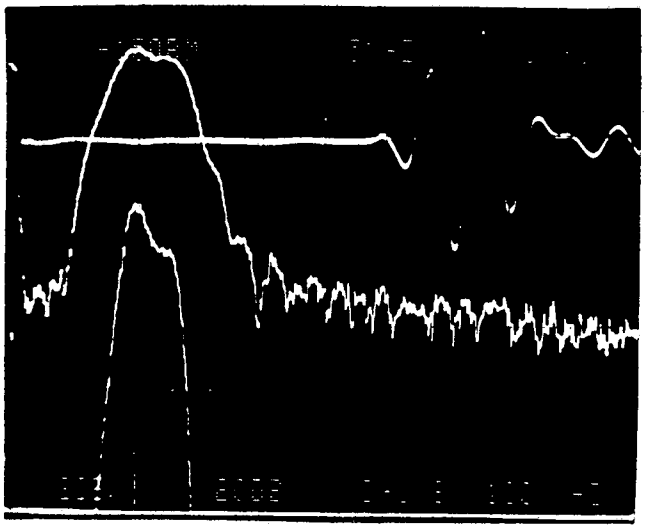

Time Base: .50 usec/div.
Vertical Scale: 200m volts/div.

TRANSDUCER

Serial No.: 642-1255
Type: SD-Z
3/4 - 2.25 MHz

CABLE TYPE: RG 58
Connector: BNC
Length: 20 ft
Couplant: H_2O

PULSER TYPE: MP215
Damping: minimum
Rise Time: 15 ns

RECEIVER TYPE: MR101
Attenuation: 61 dB
Filter: 0.5 MHz

GATE TYPE: MG701
Delay: 199 μs
Width: 3 μs

ECHO FROM

- ☐ Radiused Block
- ☐ Cylindrical Hole at Focal Length
- ☐ Flat-Bottom Hole at Focal Length
- ☒ Other (sketch)

Radius = _____

Focal Length = _____

Hole Diameter = 1

SKETCH

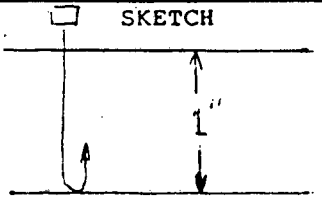

Spectrum Analyzer:
Center Frequency: 2.175 MHz
Bandwidth -3dB: 1.25 MHz

Signature Ken Isaacson Title ENG. SPEC. Date 3-JAN-86

Figure A-5

SIGMA RESEARCH, INC.

SIGMA RESEARCH, INC.

TRANSDUCER FREQUENCY ANALYSIS AND BANDWIDTH

Customer Seattle Labs (Dick Rossi) Sigma Project/Contract No. 609-2

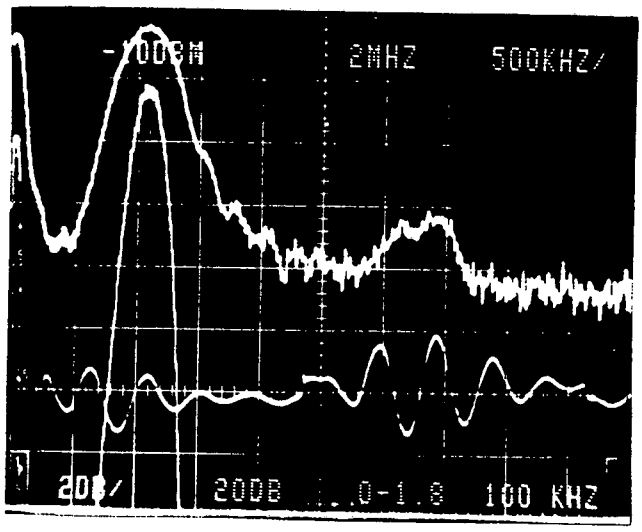

Time Base: 1 usec/div.
Vertical Scale: 500 mvolts/div.

TRANSDUCER
Serial No.: 641-1285
Type: SD-Z
¾"Ø - 1 MHz

CABLE TYPE: RG 58
Connector: BNC
Length: 20 ft
Couplant: H_2O

PULSER TYPE: MP215
Damping: minimum
Rise Time: 15 ns

RECEIVER TYPE: MR101
Attenuation: 49 dB
Filter: 0.5 MHz

GATE TYPE: MG701
Delay: 208 µs
Width: 4.6 µs

ECHO FROM

- ☐ Radiused Block
- ☐ Cylindrical Hole at Focal Length
- ☐ Flat-Bottom Hole at Focal Length
- ☒ Other (sketch)

Radius =

Focal Length =

Hole Diameter =

SKETCH

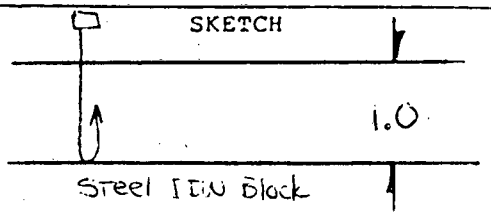

Spectrum Analyzer:
Center Frequency: 1.08 MHz
Bandwidth -3dB: 0.45 MHz

Signature Ken Harrison Title Eng Spec Date 5-MAR-86

Figure A-6

SIGMA RESEARCH, INC.

ultran

redefining the limits of ultrasound

ultran laboratories, inc.
139R north gill street
state college, pa 16801 usa
814·238·9083 *phone*
82·0978 *telex*

ULTRASONIC TRANSDUCER CHARACTERIZATION "A"

ACOUSTICS: REALTIME AND FREQUENCY ANALYSIS

Transducer type KS50-2.2 ; Serial # 82702 ; Customer Sigma Research

Active area 0.75in dia ; Cable RG58/U 6FT ; Other _____

METHOD OF TESTING

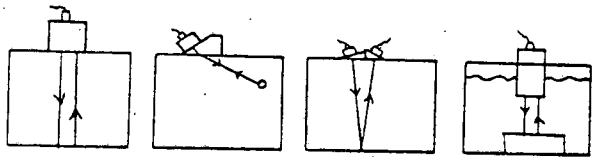

O STRAIGHT CONTACT O ANGLEBEAM/ SHEARWAVE O DUAL ELEMENT X IMMERSION

TARGET MATERIALS:
Material —
Beam Travel —
Water Travel ~2.1in to target
Target in Water Clean Cured Glass

INSTRUMENTS AND THEIR SETTINGS

PULSER	Ultran 5052	RECEIVER	Ultran 5052	OSCILLOSCOPE	Tek Hist 7704A
Voltage	350 V	Attenuation	30dB	50 ohm and 10X attenuator	
Pulse Width	Low ~1	Gain	20dB	Vert. Scale	20mV
Damping	Min	Bandwidth	0.1 - 30MHz	Horiz. Scale	50ns

SPECTRUM ANAL.	Tek Hist 7L14
Vert. Scale	2dB
Horiz. Scale	500KHz

OBSERVATIONS FROM ABOVE TEST METHOD AND TESTING CONDITIONS

PEAK FREQUENCY 2.3MHz ; BANDWIDTH CENTER FREQUENCY 2.3MHz ; BANDWIDTH AT -6dB 700KHz
SENSITIVITY High ; FOCAL LENGTH IN WATER/Y_0^+ Flat 2.1"=Y_0^+ ; OTHER _____
SPECIAL REMARKS _____

1 2 3

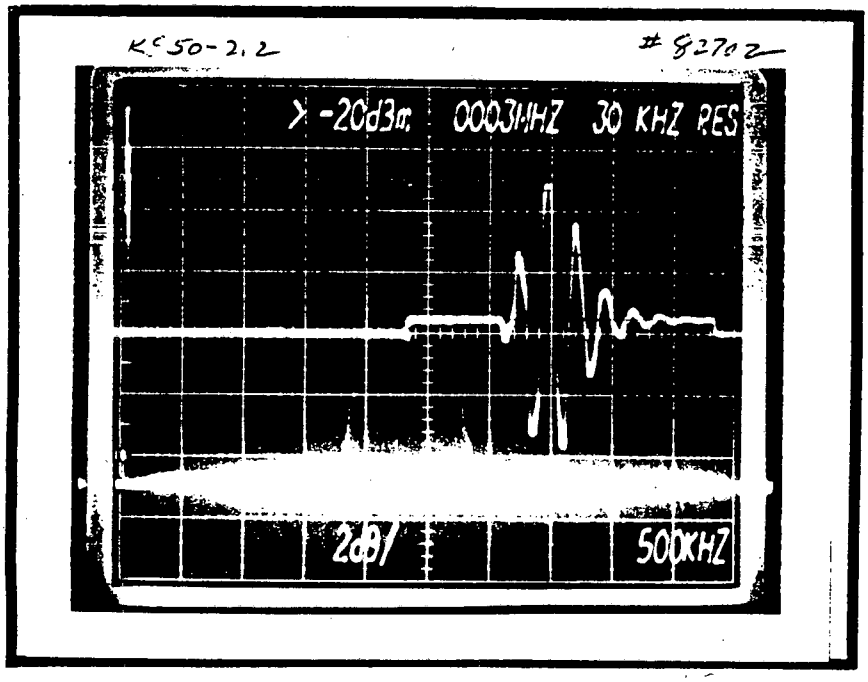

1 4 5 6

Transducer Analyst

April 17, 1986
Date

PHOTOGRAPH EXPLANATION

1. Scope vert. scale/div
2. Spec. anal. vert. scale/div
3. Max. Level at graticule top dBm
4. Spec. anal. resolution
5. Spec. anal. horiz. scale/div
6. Scope horiz. scale/div

For more information on technical terms and their significance, see the back page.

Figure A-7

The data presented in this report was obtained by laboratory analysis of this transducer under the conditions setforth herein. This data is believed to be true and scientific in character. Ultran laboratories, Inc. assumes no responsibility, expilicit or implicit, if these results are found to vary under different sets of test conditions.

ULTRASONIC TRANSDUCER CHARACTERIZATION "A"

redefining the limits of ultrasound

ultran laboratories, inc.
139R north gill street
state college, pa 16801 usa
814·238·9083 *phone*
82·0978 *telex*

ACOUSTICS: REALTIME AND FREQUENCY ANALYSIS

Transducer type KS 50-5 ; Serial # 91301 ; Customer Sigma Research
Active area 0.50 in dia ; Cable RG 58/U 6ft ; Other

METHOD OF TESTING

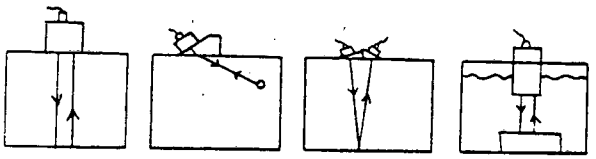

O STRAIGHT CONTACT O ANGLEBEAM/ SHEARWAVE O DUAL ELEMENT X IMMERSION

TARGET MATERIALS:
Material —
Beam Travel —
Water Travel 3 in to target
Target in Water Clear Sweet Orange

INSTRUMENTS AND THEIR SETTINGS

PULSER	Ritec 5052	RECEIVER	Ritec 5052	OSCILLOSCOPE	Tektronix 7704A	SPECTRUM ANAL.	Tektronix 7L14
Voltage	300 V	Attenuation	40dB	50 ohm and 10X attenuator		Vert. Scale	2dB
Pulse Width	400 ns	Gain	20dB	Vert. Scale	20mV	Horiz. Scale	1MHz
Damping	Crystal	Bandwidth	101-30MHz	Horiz. Scale	200ns		

OBSERVATIONS FROM ABOVE TEST METHOD AND TESTING CONDITIONS

PEAK FREQUENCY 4.5MHz ; BANDWIDTH CENTER FREQUENCY 4.5MHz ; BANDWIDTH AT -6dB 2.5MHz
SENSITIVITY High ; FOCAL LENGTH IN WATER/Y_o^+ Flat Y+ 5.3" ; OTHER
SPECIAL REMARKS

1 2 3

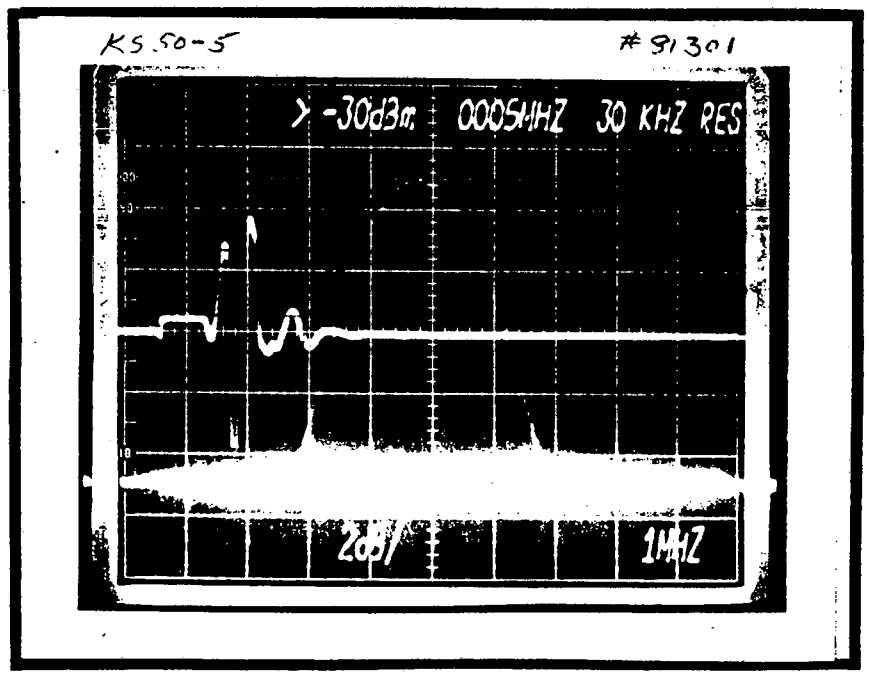

1 4 5 6

Transducer Analyst

April 12, 1984
Date

PHOTOGRAPH EXPLANATION

1. Scope vert. scale/div
2. Spec. anal. vert. scale/div
3. Max. Level at graticule top dBm
4. Spec. anal. resolution
5. Spec. anal. horiz. scale/div
6. Scope horiz. scale/div

For more information on technical terms and their significance, see the back page.

Figure A-8

The data presented in this report was obtained by laboratory analysis of this transducer under the conditions setforth herein. This data is believed to be true and scientific in character. Ultran laboratories, Inc. assumes no responsibility, expilicit or implicit, if these results are found to vary under different sets of

ULTRASONIC TRANSDUCER CHARACTERIZATION "A"

redefining the limits of ultrasound

ultran laboratories, inc.
139R north gill street
state college, pa 16801 usa
814·238·9083 *phone*
82·0978 *telex*

ACOUSTICS: REALTIME AND FREQUENCY ANALYSIS

Transducer type WS50-10-X ; Serial # 93602 ; Customer Ultratechnology

Active area 0.500 dia ; Cable RG58U 6 ft ; Other SI-X Case -X

METHOD OF TESTING

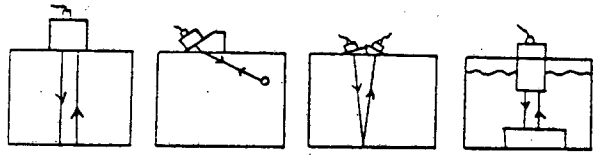

O STRAIGHT CONTACT O ANGLEBEAM/ SHEARWAVE O DUAL ELEMENT X IMMERSION

TARGET MATERIALS:
Material —
Beam Travel —
Water Travel 3" to target
Target in Water Clear face Quartz

INSTRUMENTS AND THEIR SETTINGS

PULSER Panametrics 5052	RECEIVER Panametrics 5052	OSCILLOSCOPE Tektronix 7704A	SPECTRUM ANAL. Tektronix 7L12
Voltage 200	Attenuation 60dB	50 ohm and 10X attenuator	Vert. Scale 2dB
Pulse Width Low #1	Gain 20dB	Vert. Scale 20mV	Horiz. Scale 2MHz
Damping ~50Ω	Bandwidth 10Hz-30MHz	Horiz. Scale 500nS	

OBSERVATIONS FROM ABOVE TEST METHOD AND TESTING CONDITIONS

PEAK FREQUENCY 9MHz ; BANDWIDTH CENTER FREQUENCY 9.9mHz ; BANDWIDTH AT -6dB 8mHz

SENSITIVITY Low-Med ; FOCAL LENGTH IN WATER/Y_o^+ Flat ; OTHER —

SPECIAL REMARKS —

1 2 3

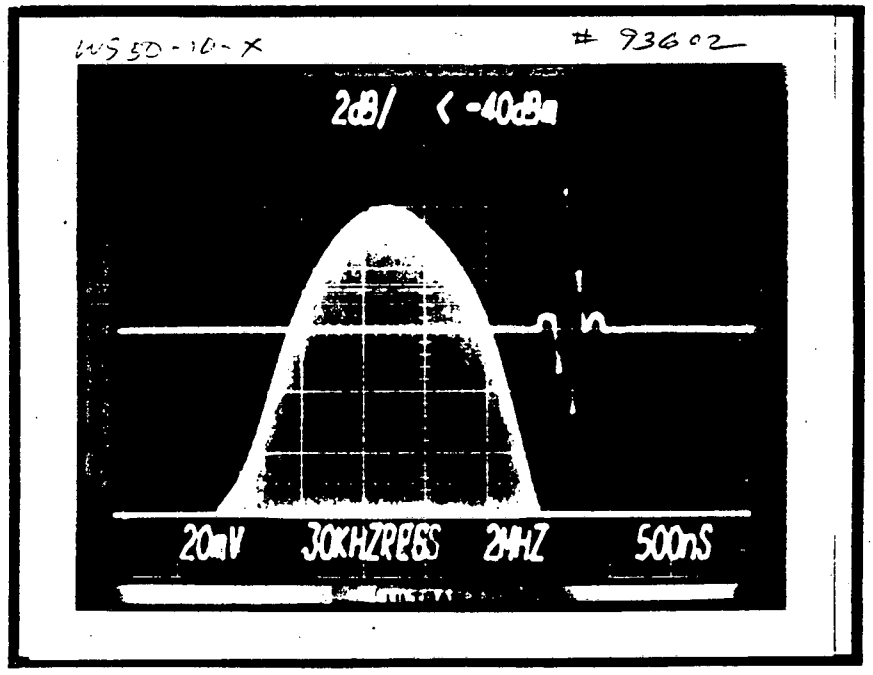

1 4 5 6

Transducer Analyst

September 7, 1984
Date

PHOTOGRAPH EXPLANATION

1. Scope vert. scale/div
2. Spec. anal. vert. scale/div
3. Max. Level at graticule top dBm
4. Spec. anal. resolution
5. Spec. anal. horiz. scale/div
6. Scope horiz. scale/div

For more information on technical terms and their significance, see the back page.

Figure A-9

The data presented in this report was obtained by laboratory analysis of this transducer under the conditions setforth herein. This data is believed to be true and scientific in character. Ultran laboratories, Inc. assumes no responsibility, expilicit or implicit, if these results are found to vary under different sets of test conditions.

ULTRASONIC TRANSDUCER CHARACTERIZATION "A"

redefining the limits of ultrasound

ultran laboratories, inc.
139R north gill street
state college, pa 16801 usa
814·238·9083 *phone*
82·0978 *telex*

ACOUSTICS: REALTIME AND FREQUENCY ANALYSIS

Transducer type WS50-5-X ; Serial # 93601 ; Customer Ultra Technology

Active area 0.50 in. ; Cable RG58/U 4 ft ; Other Short Cable - X

METHOD OF TESTING

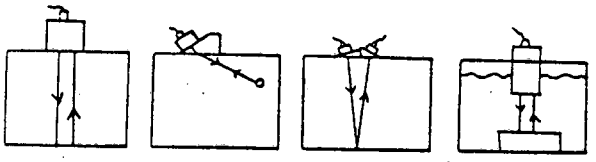

O STRAIGHT CONTACT O ANGLEBEAM/ SHEARWAVE O DUAL ELEMENT O IMMERSION

TARGET MATERIALS:
Material —
Beam Travel —
Water Travel 2 in. to target
Target in Water Clear Fused Quartz

INSTRUMENTS AND THEIR SETTINGS

PULSER Ultran SQ-2
Voltage 150 v
Pulse Width 1 μsec
Damping 50Ω

RECEIVER Ultran RS-2
Attenuation 15 dB
Gain 20 dB
Bandwidth 0.1-3.0 mHz

OSCILLOSCOPE Tektronix 7704A
50 ohm and 10X attenuator
Vert. Scale 20 mV
Horiz. Scale 50 ns

SPECTRUM ANAL. Tektronix 7L13
Vert. Scale 2 dB
Horiz. Scale 1 mHz

OBSERVATIONS FROM ABOVE TEST METHOD AND TESTING CONDITIONS

PEAK FREQUENCY 5.2 mHz ; BANDWIDTH CENTER FREQUENCY 4.8 mHz ; BANDWIDTH AT -6dB 4.5 mHz
SENSITIVITY Adequate ; FOCAL LENGTH IN WATER/Y_o^+ Flat ; OTHER —
SPECIAL REMARKS —

1 2 3

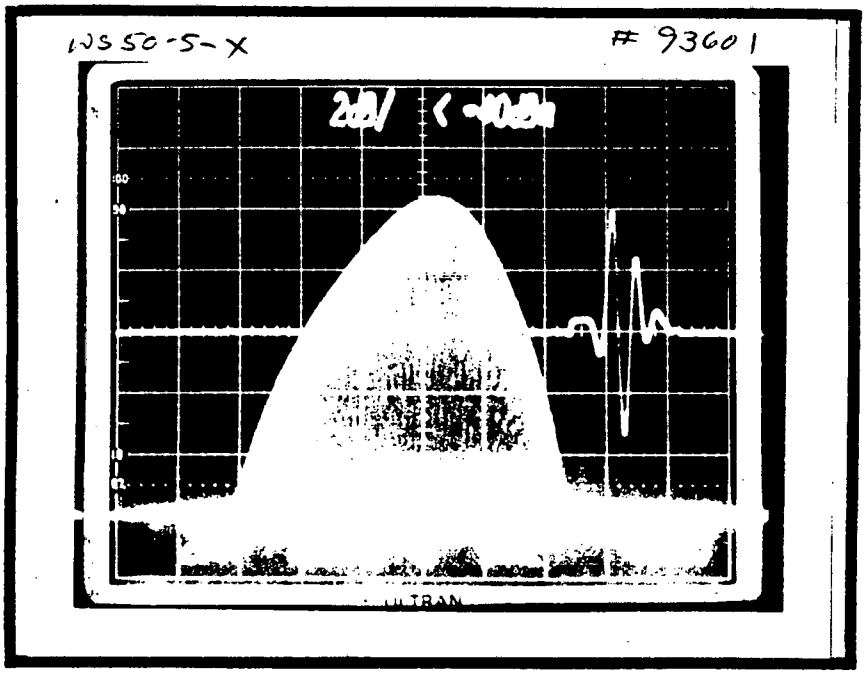

1 4 5 6

Transducer Analyst

September 9, 1982
Date

PHOTOGRAPH EXPLANATION

1. Scope vert. scale/div
2. Spec. anal. vert. scale/div
3. Max. Level at graticule top dBm
4. Spec. anal. resolution
5. Spec. anal. horiz. scale/div
6. Scope horiz. scale/div

For more information on technical terms and their significance, see the back page.

Figure A-10

The data presented in this report was obtained by laboratory analysis of this transducer under the conditions setforth herein. This data is believed to be true and scientific in character. Ultran laboratories, Inc. assumes no responsibility, expilicit or implicit, if these results are found to vary under different sets of test conditions.

APPENDIX B

Acoustic Response Measurements

APPENDIX B

ACOUSTIC RESPONSE MEASUREMENTS

Acoustic response measurements were performed on the test sample configuration of Figure 4.4-3 several times. Repeat measurements were made to correct measurement inconsistencies in earlier tests and improve reliability of readings. These tests included measurements of the linearity of the data acquisition system.

Acoustic Response Calculations

The predicted (calculated) acoustic response for the specimen geometries was obtained by applying equation 3.1 and the parameters of Tables 3-1, 3-2 and 4.3-1. Tables B-1 and B-2 show the parameters used in the calculation for the SK001 and SK005 geometries. The calculation can be applied when the geometry fits the model. This requires that the beam be applied in the far field (N) of the transducer

$$N = S/\pi\lambda$$

where S is the area of the transducer and λ is the wavelength [Bossi et al, 1985]

Acoustic Response Measurements

Measurements of the acoustic response from notches in specimen 4 (SK001), specimen 5 (SK001 with coating), and specimen 6 (SK005) were performed in two series. Table B-3 lists the tests. The measurements were obtained by submerging the sample in a water test tank. The ultrasonic probe was positioned in the water tank, on a scanner frame, above and perpendicular to the part surface with a 30 microsecond delay from the main bang to front surface echo. The echo amplitude at this location was used as the reference strength. Each response measurement, from the notch locations in each test sample, was obtained by:

1. orienting the transducer at the proper angle,
2. adjusting the transducer height above the part to a 30 ms round trip path to the part surface by the central beam,
3. adjusting the horizontal position of the transducer to be at the approximate correct path length for the central beam,
4. peaking the response signal amplitude from the notch by adjustment of the horizontal position,
5. measuring the peak amplitude and normalizing the response to the reference strength.

This procedure was followed for each transducer employed.

TABLE B-1 Calculation of Performance for Test Connector SK 001

Angle	C1	R	f	lambda	alpha	d	a	c	S flaw	trans	S trans	Po/P
45.00	0.17	0.910	1.00	3.20	0.0012	171.0	2.0	6.0	8.8	12.7	127.0	3.47E-04
45.00	0.17	0.910	1.00	3.20	0.0012	171.0	3.0	9.0	19.6	12.7	127.0	7.76E-04
45.00	0.17	0.910	1.00	3.20	0.0012	171.0	4.0	12.0	34.7	12.7	127.0	1.37E-03
45.00	0.17	0.910	1.00	3.20	0.0012	171.0	6.0	18.0	78.3	12.7	127.0	3.10E-03
45.00	0.17	0.910	1.00	3.20	0.0012	171.0	2.0	6.0	8.8	19.0	285.0	7.78E-04
45.00	0.17	0.910	1.00	3.20	0.0012	171.0	3.0	9.0	19.6	19.0	285.0	1.74E-03
45.00	0.17	0.910	1.00	3.20	0.0012	171.0	4.0	12.0	34.7	19.0	285.0	3.08E-03
45.00	0.17	0.910	1.00	3.20	0.0012	171.0	6.0	18.0	78.3	19.0	285.0	6.96E-03
45.00	0.17	0.910	2.25	1.42	0.0024	171.0	2.0	6.0	8.8	12.7	127.0	1.17E-03
45.00	0.17	0.910	2.25	1.42	0.0024	171.0	3.0	9.0	19.6	12.7	127.0	2.62E-03
45.00	0.17	0.910	2.25	1.42	0.0024	171.0	4.0	12.0	34.7	12.7	127.0	4.63E-03
45.00	0.17	0.910	2.25	1.42	0.0024	171.0	6.0	18.0	78.3	12.7	127.0	1.04E-02
45.00	0.17	0.910	2.25	1.42	0.0024	171.0	2.0	6.0	8.8	19.0	285.0	2.62E-03
45.00	0.17	0.910	2.25	1.42	0.0024	171.0	3.0	9.0	19.6	19.0	285.0	5.87E-03
45.00	0.17	0.910	2.25	1.42	0.0024	171.0	4.0	12.0	34.7	19.0	285.0	1.04E-02
45.00	0.17	0.910	2.25	1.42	0.0024	171.0	6.0	18.0	78.3	19.0	285.0	2.34E-02
45.00	0.17	0.910	5.00	0.64	0.0013	171.0	2.0	6.0	8.8	12.7	127.0	8.37E-03
45.00	0.17	0.910	5.00	0.64	0.0013	171.0	3.0	9.0	19.6	12.7	127.0	1.88E-02
45.00	0.17	0.910	5.00	0.64	0.0013	171.0	4.0	12.0	34.7	12.7	127.0	3.32E-02
45.00	0.17	0.910	5.00	0.64	0.0013	171.0	6.0	18.0	78.3	12.7	127.0	7.49E-02
45.00	0.17	0.910	5.00	0.64	0.0013	171.0	2.0	6.0	8.8	19.0	285.0	1.88E-02
45.00	0.17	0.910	5.00	0.64	0.0013	171.0	3.0	9.0	19.6	19.0	285.0	4.21E-02
45.00	0.17	0.910	5.00	0.64	0.0013	171.0	4.0	12.0	34.7	19.0	285.0	7.45E-02
45.00	0.17	0.910	5.00	0.64	0.0013	171.0	6.0	18.0	78.3	19.0	285.0	1.68E-01
45.00	0.17	0.910	1.00	3.20	0.0012	162.0	2.0	6.0	8.8	12.7	127.0	3.95E-04
45.00	0.17	0.910	1.00	3.20	0.0012	162.0	4.0	12.0	34.7	12.7	127.0	1.56E-03
45.00	0.17	0.910	1.00	3.20	0.0012	162.0	6.0	18.0	78.3	12.7	127.0	3.53E-03
45.00	0.17	0.910	1.00	3.20	0.0012	162.0	2.0	6.0	8.8	19.0	285.0	8.86E-04
45.00	0.17	0.910	1.00	3.20	0.0012	162.0	4.0	12.0	34.7	19.0	285.0	3.51E-03
45.00	0.17	0.910	1.00	3.20	0.0012	162.0	6.0	18.0	78.3	19.0	285.0	7.92E-03
45.00	0.17	0.910	2.25	1.42	0.0024	162.0	2.0	6.0	8.8	12.7	127.0	1.36E-03
45.00	0.17	0.910	2.25	1.42	0.0024	162.0	4.0	12.0	34.7	12.7	127.0	5.39E-03
45.00	0.17	0.910	2.25	1.42	0.0024	162.0	6.0	18.0	78.3	12.7	127.0	1.22E-02
45.00	0.17	0.910	2.25	1.42	0.0024	162.0	2.0	6.0	8.8	19.0	285.0	3.05E-03
45.00	0.17	0.910	2.25	1.42	0.0024	162.0	4.0	12.0	34.7	19.0	285.0	1.21E-02
45.00	0.17	0.910	2.25	1.42	0.0024	162.0	6.0	18.0	78.3	19.0	285.0	2.73E-02
45.00	0.17	0.910	5.00	0.64	0.0013	162.0	2.0	6.0	8.8	12.7	127.0	9.55E-03
45.00	0.17	0.910	5.00	0.64	0.0013	162.0	4.0	12.0	34.7	12.7	127.0	3.79E-02
45.00	0.17	0.910	5.00	0.64	0.0013	162.0	6.0	18.0	78.3	12.7	127.0	8.55E-02

TABLE B-1 (cont'd.)
Calculation of Performance for Test Connector SK 001

Angle	C1	R	f	lambda	alpha	d	a	c	S flaw	trans	S trans	Po/P
45.00	0.17	0.910	5.00	0.64	0.0013	162.0	2.0	6.0	8.8	19.0	285.0	2.14E-02
45.00	0.17	0.910	5.00	0.64	0.0013	162.0	4.0	12.0	34.7	19.0	285.0	8.50E-02
45.00	0.17	0.910	5.00	0.64	0.0013	162.0	6.0	18.0	78.3	19.0	285.0	1.92E-01
60.00	0.15	0.930	1.00	3.20	0.0012	201.0	4.0	12.0	34.7	12.7	127.0	8.53E-04
60.00	0.15	0.930	1.00	3.20	0.0012	201.0	5.0	15.0	54.1	12.7	127.0	1.33E-03
60.00	0.15	0.930	1.00	3.20	0.0012	201.0	6.0	18.0	78.3	12.7	127.0	1.92E-03
60.00	0.15	0.930	1.00	3.20	0.0012	201.0	4.0	12.0	34.7	19.0	285.0	1.91E-03
60.00	0.15	0.930	1.00	3.20	0.0012	201.0	5.0	15.0	54.1	19.0	285.0	2.98E-03
60.00	0.15	0.930	1.00	3.20	0.0012	201.0	6.0	18.0	78.3	19.0	285.0	4.32E-03
60.00	0.15	0.930	2.25	1.42	0.0024	201.0	4.0	12.0	34.7	12.7	127.0	2.67E-03
60.00	0.15	0.930	2.25	1.42	0.0024	201.0	5.0	15.0	54.1	12.7	127.0	4.17E-03
60.00	0.15	0.930	2.25	1.42	0.0024	201.0	6.0	18.0	78.3	12.7	127.0	6.03E-03
60.00	0.15	0.930	2.25	1.42	0.0024	201.0	4.0	12.0	34.7	19.0	285.0	6.00E-03
60.00	0.15	0.930	2.25	1.42	0.0024	201.0	5.0	15.0	54.1	19.0	285.0	9.36E-03
60.00	0.15	0.930	2.25	1.42	0.0024	201.0	6.0	18.0	78.3	19.0	285.0	1.35E-02
60.00	0.15	0.930	5.00	0.64	0.0013	201.0	4.0	12.0	34.7	12.7	127.0	2.05E-02
60.00	0.15	0.930	5.00	0.64	0.0013	201.0	5.0	15.0	54.1	12.7	127.0	3.19E-02
60.00	0.15	0.930	5.00	0.64	0.0013	201.0	6.0	18.0	78.3	12.7	127.0	4.62E-02
60.00	0.15	0.930	5.00	0.64	0.0013	201.0	4.0	12.0	34.7	19.0	285.0	4.60E-02
60.00	0.15	0.930	5.00	0.64	0.0013	201.0	5.0	15.0	54.1	19.0	285.0	7.17E-02
60.00	0.15	0.930	5.00	0.64	0.0013	201.0	6.0	18.0	78.3	19.0	285.0	1.04E-01
75.00	0.13	0.950	1.00	3.20	0.0012	312.0	6.0	18.0	78.3	12.7	127.0	5.54E-04
75.00	0.13	0.950	1.00	3.20	0.0012	312.0	8.0	24.0	139.0	12.7	127.0	9.83E-04
75.00	0.13	0.950	1.00	3.20	0.0012	312.0	6.0	18.0	78.3	19.0	285.0	1.24E-03
75.00	0.13	0.950	1.00	3.20	0.0012	312.0	8.0	24.0	139.0	19.0	285.0	2.21E-03
75.00	0.13	0.950	2.25	1.42	0.0024	312.0	6.0	18.0	78.3	12.7	127.0	1.33E-03
75.00	0.13	0.950	2.25	1.42	0.0024	312.0	8.0	24.0	139.0	12.7	127.0	2.36E-03
75.00	0.13	0.950	2.25	1.42	0.0024	312.0	6.0	18.0	78.3	19.0	285.0	2.98E-03
75.00	0.13	0.950	2.25	1.42	0.0024	312.0	8.0	24.0	139.0	19.0	285.0	5.30E-03
75.00	0.13	0.950	5.00	0.64	0.0013	312.0	6.0	18.0	78.3	12.7	127.0	1.30E-02
75.00	0.13	0.950	5.00	0.64	0.0013	312.0	8.0	24.0	139.0	12.7	127.0	2.31E-02
75.00	0.13	0.950	5.00	0.64	0.0013	312.0	6.0	18.0	78.3	19.0	285.0	2.92E-02
75.00	0.13	0.950	5.00	0.64	0.0013	312.0	8.0	24.0	139.0	19.0	285.0	5.18E-02

TABLE B-2

Calculation of Perfomance for Test Connector SK 005

Angle	C1	R	f	lambda	alpha	d	a	c	S fl.	tr.	S tr.	Po/P
45.0	0.17	0.91	1.00	3.20	0.0024	83.0	1.0	3.0	2.2	12.7	127.0	3.74E-04
45.0	0.17	0.91	1.00	3.20	0.0024	83.0	2.0	6.0	8.8	12.7	127.0	1.49E-03
45.0	0.17	0.91	1.00	3.20	0.0024	83.0	3.0	9.0	19.6	12.7	127.0	3.34E-03
45.0	0.17	0.91	1.00	3.20	0.0024	83.0	1.0	3.0	2.2	19.0	285.0	8.40E-04
45.0	0.17	0.91	1.00	3.20	0.0024	83.0	2.0	6.0	8.8	19.0	285.0	3.34E-03
45.0	0.17	0.91	1.00	3.20	0.0024	83.0	3.0	9.0	19.6	19.0	285.0	7.48E-03
45.0	0.17	0.91	2.25	1.42	0.0038	83.0	1.0	3.0	2.2	12.7	127.0	1.51E-03
45.0	0.17	0.91	2.25	1.42	0.0038	83.0	2.0	6.0	8.8	12.7	127.0	5.99E-03
45.0	0.17	0.91	2.25	1.42	0.0038	83.0	3.0	9.0	19.6	12.7	127.0	1.34E-02
45.0	0.17	0.91	2.25	1.42	0.0038	83.0	1.0	3.0	2.2	19.0	285.0	3.38E-03
45.0	0.17	0.91	2.25	1.42	0.0038	83.0	2.0	6.0	8.8	19.0	285.0	1.34E-02
45.0	0.17	0.91	2.25	1.42	0.0038	83.0	3.0	9.0	19.6	19.0	285.0	3.01E-02
45.0	0.17	0.91	5.00	0.64	0.0023	83.0	1.0	3.0	2.2	12.7	127.0	9.52E-03
45.0	0.17	0.91	5.00	0.64	0.0023	83.0	2.0	6.0	8.8	12.7	127.0	3.78E-02
45.0	0.17	0.91	5.00	0.64	0.0023	83.0	3.0	9.0	19.6	12.7	127.0	8.48E-02
45.0	0.17	0.91	5.00	0.64	0.0023	83.0	1.0	3.0	2.2	19.0	285.0	2.14E-02
45.0	0.17	0.91	5.00	0.64	0.0023	83.0	2.0	6.0	8.8	19.0	285.0	8.49E-02
45.0	0.17	0.91	5.00	0.64	0.0023	83.0	3.0	9.0	19.6	19.0	285.0	1.90E-01
60.0	0.15	0.93	1.00	3.20	0.0024	112.0	1.0	3.0	2.2	12.7	127.0	1.65E-04
60.0	0.15	0.93	1.00	3.20	0.0024	112.0	2.0	6.0	8.8	12.7	127.0	6.56E-04
60.0	0.15	0.93	1.00	3.20	0.0024	112.0	3.0	9.0	19.6	12.7	127.0	1.47E-03
60.0	0.15	0.93	1.00	3.20	0.0024	112.0	1.0	3.0	2.2	19.0	285.0	3.70E-04
60.0	0.15	0.93	1.00	3.20	0.0024	112.0	2.0	6.0	8.8	19.0	285.0	1.47E-03
60.0	0.15	0.93	1.00	3.20	0.0024	112.0	3.0	9.0	19.6	19.0	285.0	3.30E-03
60.0	0.15	0.93	2.25	1.42	0.0038	112.0	1.0	3.0	2.2	12.7	127.0	6.12E-04
60.0	0.15	0.93	2.25	1.42	0.0038	112.0	2.0	6.0	8.8	12.7	127.0	2.43E-03
60.0	0.15	0.93	2.25	1.42	0.0038	112.0	3.0	9.0	19.6	12.7	127.0	5.45E-03
60.0	0.15	0.93	2.25	1.42	0.0038	112.0	1.0	3.0	2.2	19.0	285.0	1.37E-03
60.0	0.15	0.93	2.25	1.42	0.0038	112.0	2.0	6.0	8.8	19.0	285.0	5.46E-03
60.0	0.15	0.93	2.25	1.42	0.0038	112.0	3.0	9.0	19.6	19.0	285.0	1.22E-02
60.0	0.15	0.93	5.00	0.64	0.0023	112.0	1.0	3.0	2.2	12.7	127.0	4.21E-03
60.0	0.15	0.93	5.00	0.64	0.0023	112.0	2.0	6.0	8.8	12.7	127.0	1.68E-02
60.0	0.15	0.93	5.00	0.64	0.0023	112.0	3.0	9.0	19.6	12.7	127.0	3.75E-02
60.0	0.15	0.93	5.00	0.64	0.0023	112.0	1.0	3.0	2.2	19.0	285.0	9.46E-03
60.0	0.15	0.93	5.00	0.64	0.0023	112.0	2.0	6.0	8.8	19.0	285.0	3.76E-02
60.0	0.15	0.93	5.00	0.64	0.0023	112.0	3.0	9.0	19.6	19.0	285.0	8.43E-02
70.0	0.14	0.95	1.00	3.20	0.0024	153.0	1.0	3.0	2.2	12.7	127.0	7.07E-05
70.0	0.14	0.95	1.00	3.20	0.0024	153.0	2.0	6.0	8.8	12.7	127.0	2.81E-04

TABLE B-2 (cont'd.)

Calculation of Performance for Test Connector SK 005

Angle	C1	R	f	lambda	alpha	d	a	c	S fl.	tr.	S tr.	Po/P
70.0	0.14	0.95	1.00	3.20	0.0024	153.0	3.0	9.0	19.6	12.7	127.0	6.30E-04
70.0	0.14	0.95	1.00	3.20	0.0024	153.0	1.0	3.0	2.2	19.0	285.0	1.59E-04
70.0	0.14	0.95	1.00	3.20	0.0024	153.0	2.0	6.0	8.8	19.0	285.0	6.31E-04
70.0	0.14	0.95	1.00	3.20	0.0024	153.0	3.0	9.0	19.6	19.0	285.0	1.41E-03
70.0	0.14	0.95	2.25	1.42	0.0038	153.0	1.0	3.0	2.2	12.7	127.0	2.34E-04
70.0	0.14	0.95	2.25	1.42	0.0038	153.0	2.0	6.0	8.8	12.7	127.0	9.30E-04
70.0	0.14	0.95	2.25	1.42	0.0038	153.0	3.0	9.0	19.6	12.7	127.0	2.08E-03
70.0	0.14	0.95	2.25	1.42	0.0038	153.0	1.0	3.0	2.2	19.0	285.0	5.25E-04
70.0	0.14	0.95	2.25	1.42	0.0038	153.0	2.0	6.0	8.8	19.0	285.0	2.09E-03
70.0	0.14	0.95	2.25	1.42	0.0038	153.0	3.0	9.0	19.6	19.0	285.0	4.67E-03
70.0	0.14	0.95	5.00	0.64	0.0023	153.0	1.0	3.0	2.2	12.7	127.0	1.82E-03
70.0	0.14	0.95	5.00	0.64	0.0023	153.0	2.0	6.0	8.8	12.7	127.0	7.24E-03
70.0	0.14	0.95	5.00	0.64	0.0023	153.0	3.0	9.0	19.6	12.7	127.0	1.62E-02
70.0	0.14	0.95	5.00	0.64	0.0023	153.0	1.0	3.0	2.2	19.0	285.0	4.09E-03
70.0	0.14	0.95	5.00	0.64	0.0023	153.0	2.0	6.0	8.8	19.0	285.0	1.63E-02
70.0	0.14	0.95	5.00	0.64	0.0023	153.0	3.0	9.0	19.6	19.0	285.0	3.64E-02
77.5	0.12	0.97	1.00	3.20	0.0024	227.0	2.0	6.0	8.8	12.7	127.0	8.00E-05
77.5	0.12	0.97	1.00	3.20	0.0024	227.0	3.0	9.0	19.6	12.7	127.0	1.79E-04
77.5	0.12	0.97	1.00	3.20	0.0024	227.0	4.0	12.0	34.7	12.7	127.0	3.17E-04
77.5	0.12	0.97	1.00	3.20	0.0024	227.0	2.0	6.0	8.8	19.0	285.0	1.79E-04
77.5	0.12	0.97	1.00	3.20	0.0024	227.0	3.0	9.0	19.6	19.0	285.0	4.02E-04
77.5	0.12	0.97	1.00	3.20	0.0024	227.0	4.0	12.0	34.7	19.0	285.0	7.12E-04
77.5	0.12	0.97	2.25	1.42	0.0038	227.0	2.0	6.0	8.8	12.7	127.0	2.15E-04
77.5	0.12	0.97	2.25	1.42	0.0038	227.0	3.0	9.0	19.6	12.7	127.0	4.82E-04
77.5	0.12	0.97	2.25	1.42	0.0038	227.0	4.0	12.0	34.7	12.7	127.0	8.53E-04
77.5	0.12	0.97	2.25	1.42	0.0038	227.0	2.0	6.0	8.8	19.0	285.0	4.83E-04
77.5	0.12	0.97	2.25	1.42	0.0038	227.0	3.0	9.0	19.6	19.0	285.0	1.08E-03
77.5	0.12	0.97	2.25	1.42	0.0038	227.0	4.0	12.0	34.7	19.0	285.0	1.91E-03
77.5	0.12	0.97	5.00	0.64	0.0023	227.0	2.0	6.0	8.8	12.7	127.0	2.09E-03
77.5	0.12	0.97	5.00	0.64	0.0023	227.0	3.0	9.0	19.6	12.7	127.0	4.69E-03
77.5	0.12	0.97	5.00	0.64	0.0023	227.0	4.0	12.0	34.7	12.7	127.0	8.30E-03
77.5	0.12	0.97	5.00	0.64	0.0023	227.0	2.0	6.0	8.8	19.0	285.0	4.70E-03
77.5	0.12	0.97	5.00	0.64	0.0023	227.0	3.0	9.0	19.6	19.0	285.0	1.05E-02
77.5	0.12	0.97	5.00	0.64	0.0023	227.0	4.0	12.0	34.7	19.0	285.0	1.86E-02

TABLE B-3

MEASUREMENTS TESTS

Early Series:

Code	Object	Transducer Frequency	Transducer Type	Notches
M1	Specimen 4	1 MHz	0.5 in. Sigma	A-J
M1	Specimen 4	2.25 MHz	0.5 in. Sigma	A-L
M1	Specimen 4	5 MHz	0.5 in. Sigma	A-L
M1	Specimen 4	2.25 MHz	0.75 in. Sigma	A-L
M1	Specimen 4	5 MHz	0.75 in. Sigma	A-L
M2	Specimen 4	2.25 MHz	0.5 in. Sigma	A-L
M2	Specimen 4	5 MHz	0.5 in. Sigma	A-L
M2	Specimen 4	2.25 MHz	0.75 in. Sigma	A-L
M2	Specimen 4	5 MHz	0.75 in. Sigma	A-L
M3	Specimen 4	2.25 MHz	0.5 in. Sigma	A-L
M3	Specimen 4	5 MHz	0.5 in. Sigma	A-L
M3	Specimen 4	1 MHz	0.75 in. Sigma	A-L
M3	Specimen 4	2.25 MHz	0.75 in. Sigma	A-L
M3	Specimen 4	5 MHz	0.75 in. Sigma	A-L
M3	Specimen 4	2.25 MHz	0.5 in. Ultran WS	A-L
M3	Specimen 4	5 MHz	0.5 in. Ultran WS	A-L
M4	Specimen 5	2.25 MHz	0.5 in. Sigma	A-L
M4	Specimen 5	5 MHz	0.5 in. Sigma	A-L
M4	Specimen 5	1 MHz	0.75 in. Sigma	A-L
M4	Specimen 5	2.25 MHz	0.75 in. Sigma	A-L
M4	Specimen 5	5 MHz	0.75 in. Sigma	A-K
M1	Specimen 6	2.25 MHz	0.5 in. Sigma	1A-4D
M1	Specimen 6	5 MHz	0.5 in. Sigma	1A-4D
M1	Specimen 6	1 MHz	0.75 in. Sigma	1A-4D
M1	Specimen 6	2.25 MHz	0.75 in. Sigma	1A-4D
M1	Specimen 6	5 MHz	0.75 in. Sigma	1A-4D

Repeat Series:

Object	Transducer Frequency	Transducer Type	Notches
Specimen 4	2.25 MHz	0.5 in. Sigma	A-L
Specimen 4	5 MHz	0.5 in. Sigma	A-L
Specimen 4	5 MHz	0.5 in. Sigma	E,F,G
Specimen 4	2.25 MHz	0.5 in. Sigma	E,F,G
Specimen 4	2.25 MHz	0.5 in. Sigma	A-L
Specimen 4	5 MHz	0.5 in. Sigma	A-L
Specimen 4	5 MHz	0.5 in. Ultran WS	A-J
Specimen 4	5 MHz	0.5 in. Ultran WS	A-L
Specimen 4	2.25 MHz	0.5 in. Ultran WS	A-L
Specimen 4	5 MHz	0.5 in. Ultran KS	E-J
Specimen 4	2.25 MHz	0.5 in. Ultran KS	E-J
Specimen 5	5 MHz	0.5 in. Sigma	A-L
Specimen 5	2.25 MHz	0.5 in. Sigma	A-L

TABLE B-3(cont'd.)

MEASUREMENTS TESTS

Specimen 6	5 MHz	0.5 in. Sigma	1A-4D
Specimen 6	2.25 MHz	0.5 in. Sigma	1A-4D
Specimen 6	2.25 MHz	0.5 in. Sigma	1A-4D
Specimen 6	5 MHz	0.5 in. Sigma	1A-4D
Specimen 4	5 MHz	0.5 in. Sigma	E-J
Specimen 5	5 MHz	0.5 in. Sigma	E-J
Specimen 5	2.25 MHz	0.5 in. Sigma	E-J
Specimen 4	2.25 MHz	0.5 in. Sigma	E-J

Measurements of acoustic response were made and discussed in an interim report on Phase II-A of the Inspectability of Tension Leg Platform Tendons, May 1986 and repeat tests were performed and discussed in Phase II-A Interim Report, Basic Tests Followon, September 1986.

The results of the followon series of measurements are presented in Figures B1-B8 for the acoustic response from specimen 4 (uncoated) and specimen 5 (coated) using 2.25 and 5 MHz, 0.5 inch Sigma transducers. Table B-4 lists the notch sizes. These results show that the trend of the data is in agreement with the calculated response but the accuracy is insufficient for absolute size prediction. The 5 MHz results still show a greater calculated change in signal for a change in notch size than is found in the measurements. The attenuation coefficient used for the 5 MHz calculation was obtained by a best fit to the data. The results indicate that the detectability limit is in the range of $p/p_0 = 0.0001$. The coated and uncoated samples show similar trends in the shape of the response versus notch area curves with an approximately 20% reduction in the coated specimen notch responses.

The repeat measurements of the acoustic response from notches in the connector test specimens indicated that the early series data used saturated signal strength as the reference. This means that the normalizing signal was not correct for the earlier data sets. The shape of the data as a function of notch size is similar in both the early and repeat sets of measurements.

Figures B9-B16 show the average results of two sets of measurements on specimen 6 compared to calculated values. Table B-5 lists the notch conditions. The trends in these results are the same as in previous results, although the magnitudes of the responses are in better agreement with the calculations.

Measurement from the pin side configuration, no bounce path, were also run on the coated and uncoated specimens 4 and 5. The data are plotted in Figures B17-B20 for 2.25 and 5 MHz at 45 and 60 degree beams. The response is not normalized because the normalizing signal from the coated surface varies due to the coating. These results show the general trend of a reduced signal of 20% looking through the coating. The 5 MHz results show considerable variation from expected response. Also, the trend of increasing response with area is not consistently demonstrated.

Linearity Test

A test was run to verify that changes in pulse height would not affect the relative acoustic response measurement. Table B-6 shows the results for measurements from notch I using a 60 degree beam. The relative response values look very good over the full range of the pulser.

Shear Beam Spread Test

An experiment was run to look at the spread of the shear beam in a test block. Figure B21 shows the test configuration. A two transducer pitch/catch method was used. Both 2.25 and 5 MHz, 0.5 inch transducers were used as the source and a very small transducer used to pick up ultrasound near the part surface. The source transducer was fixed to generate a 45° or 60°

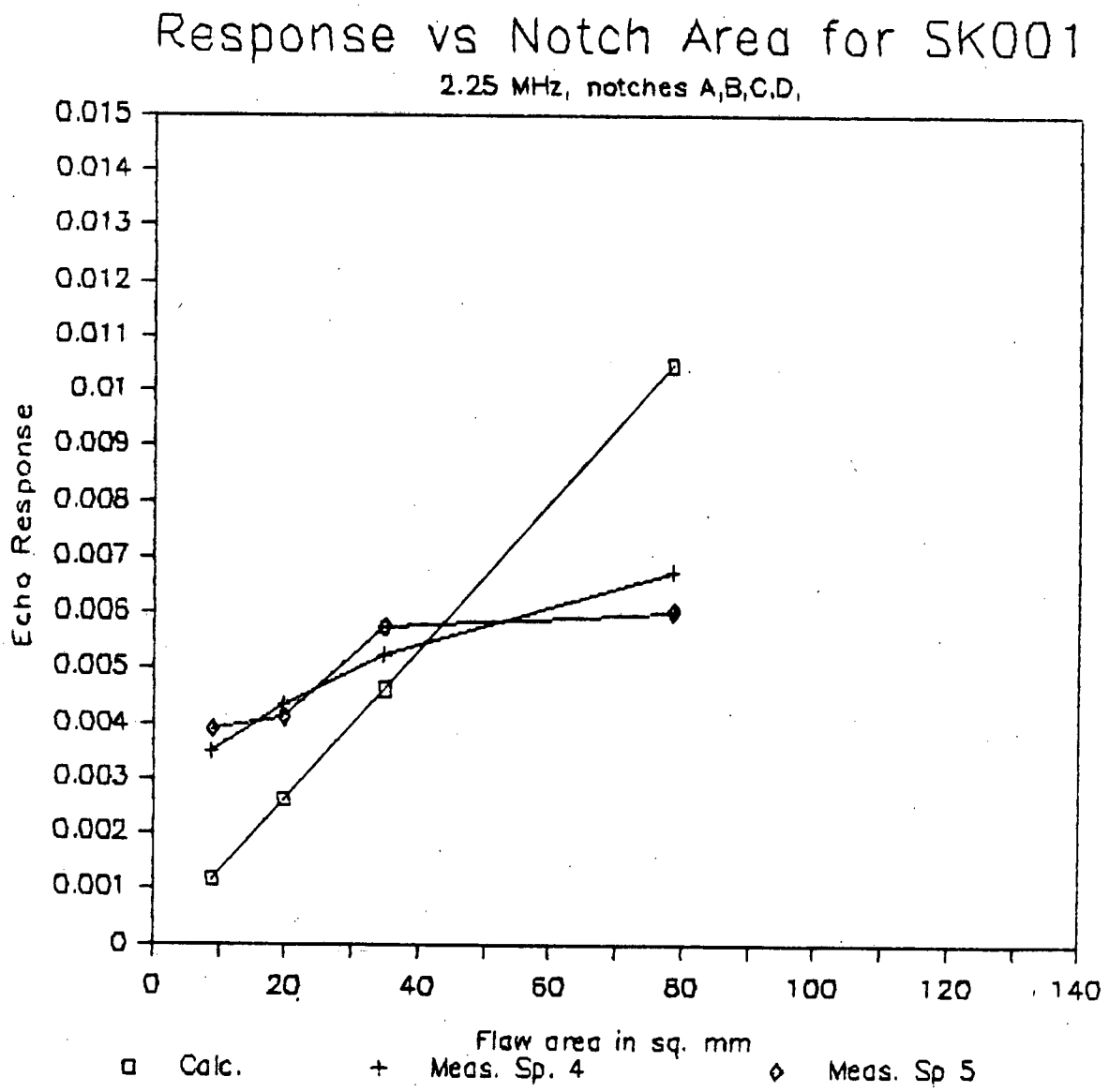
Response vs Notch Area for SK001
2.25 MHz, notches A,B,C,D,
Echo Response
0.015
0.014
0.013
0.012
0.011
0.01
0.009
0.008
0.007
0.006
0.005
0.004
0.003
0.002
0.001
0
0
20
40
60
80
100
120
140
Flaw area in sq. mm
Calc.
Meas. Sp. 4
Meas. Sp 5

Figure B-1

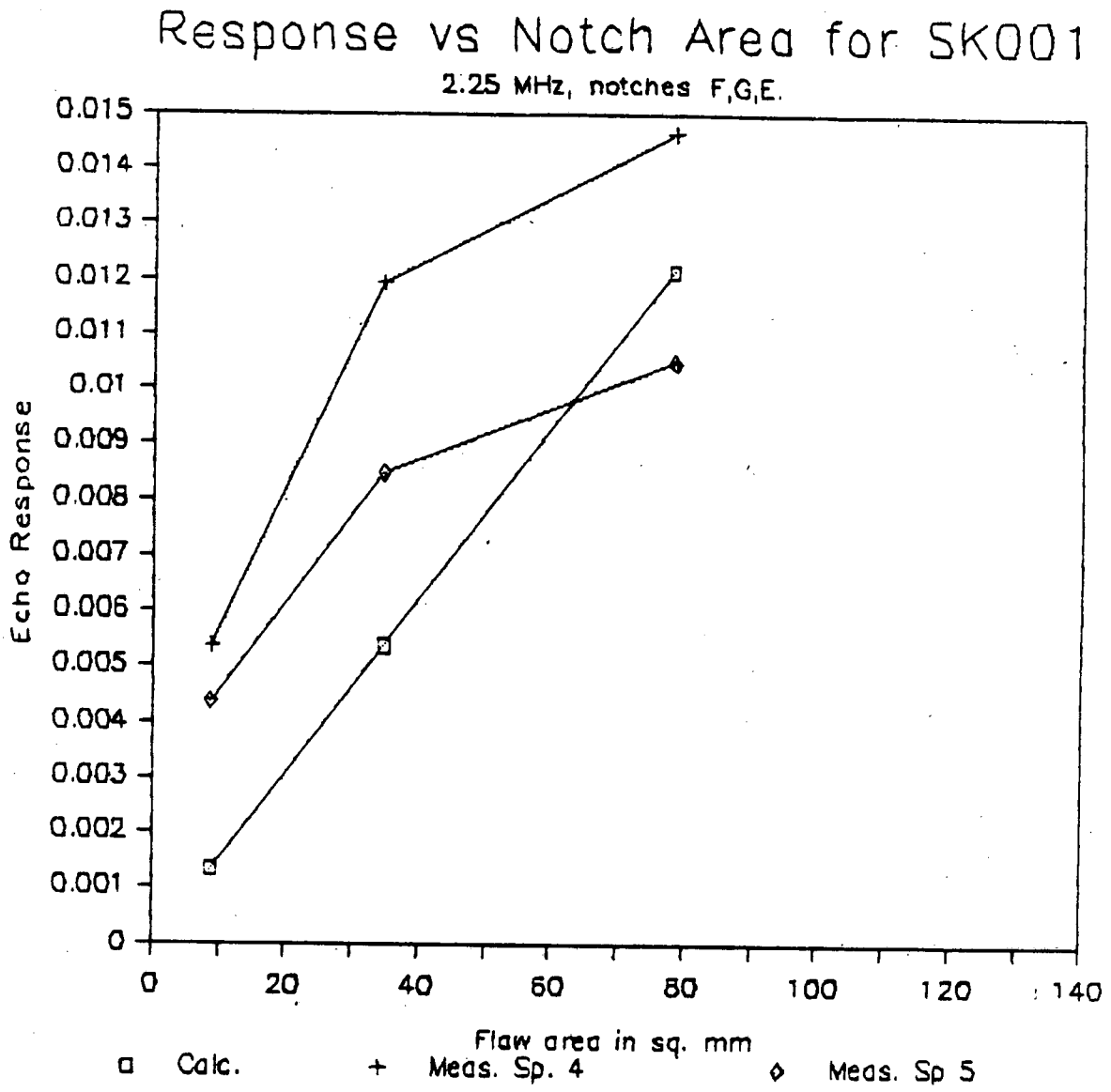
Response vs Notch Area for SK001
2.25 MHz, notches F,G,E.
Echo Response
0.015
0.014
0.013
0.012
0.011
0.01
0.009
0.008
0.007
0.006
0.005
0.004
0.003
0.002
0.001
0
0
20
40
60
80
100
120
140
Flaw area in sq. mm
Calc.
Meas. Sp. 4
Meas. Sp 5

Figure B-2

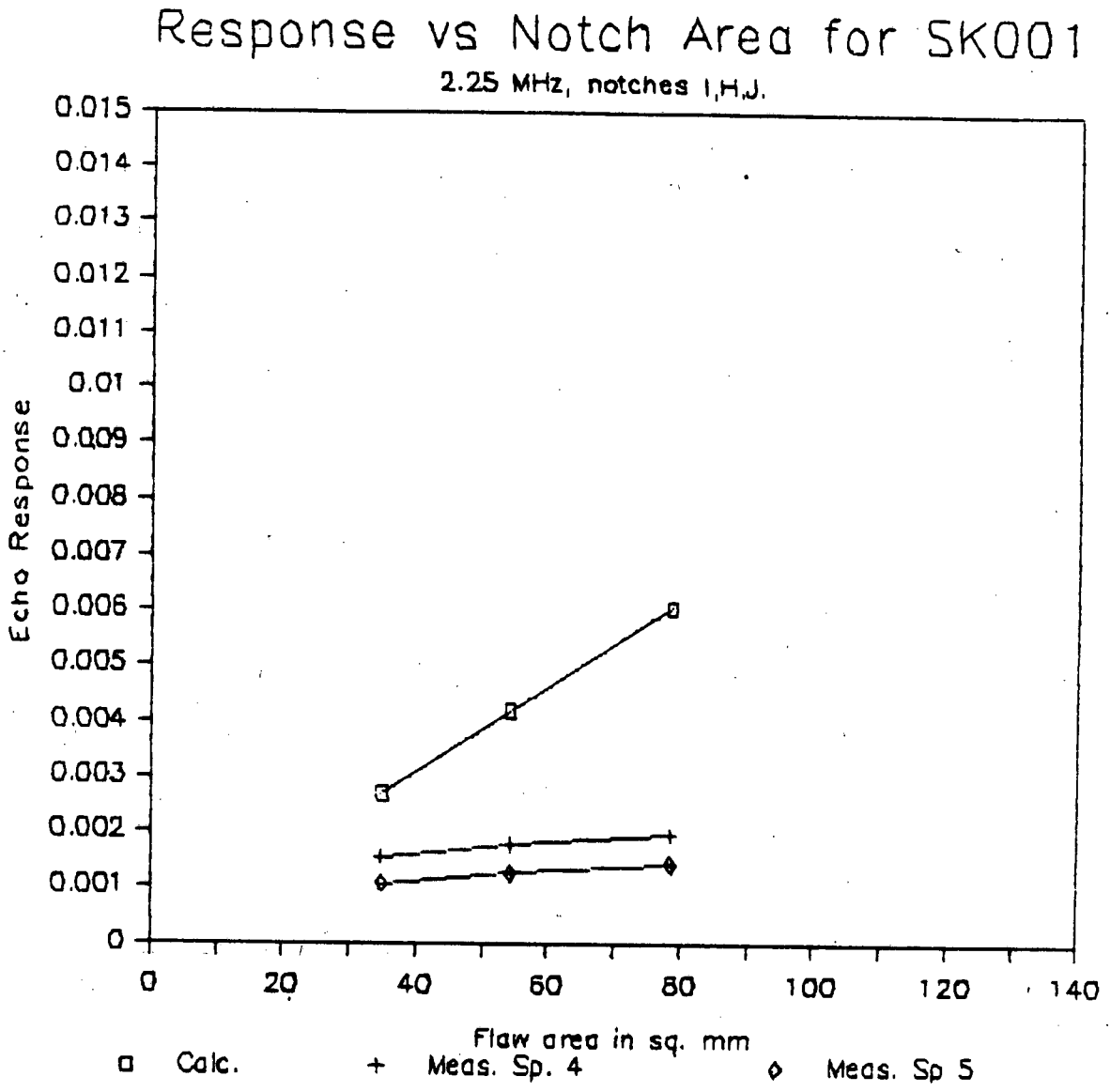
Response vs Notch Area for SK001
2.25 MHz, notches I,H,J.
Echo Response
0.015
0.014
0.013
0.012
0.011
0.01
0.009
0.008
0.007
0.006
0.005
0.004
0.003
0.002
0.001
0
0
20
40
60
80
100
120
140
Flaw area in sq. mm
Calc.
Meas. Sp. 4
Meas. Sp 5

Figure B-3

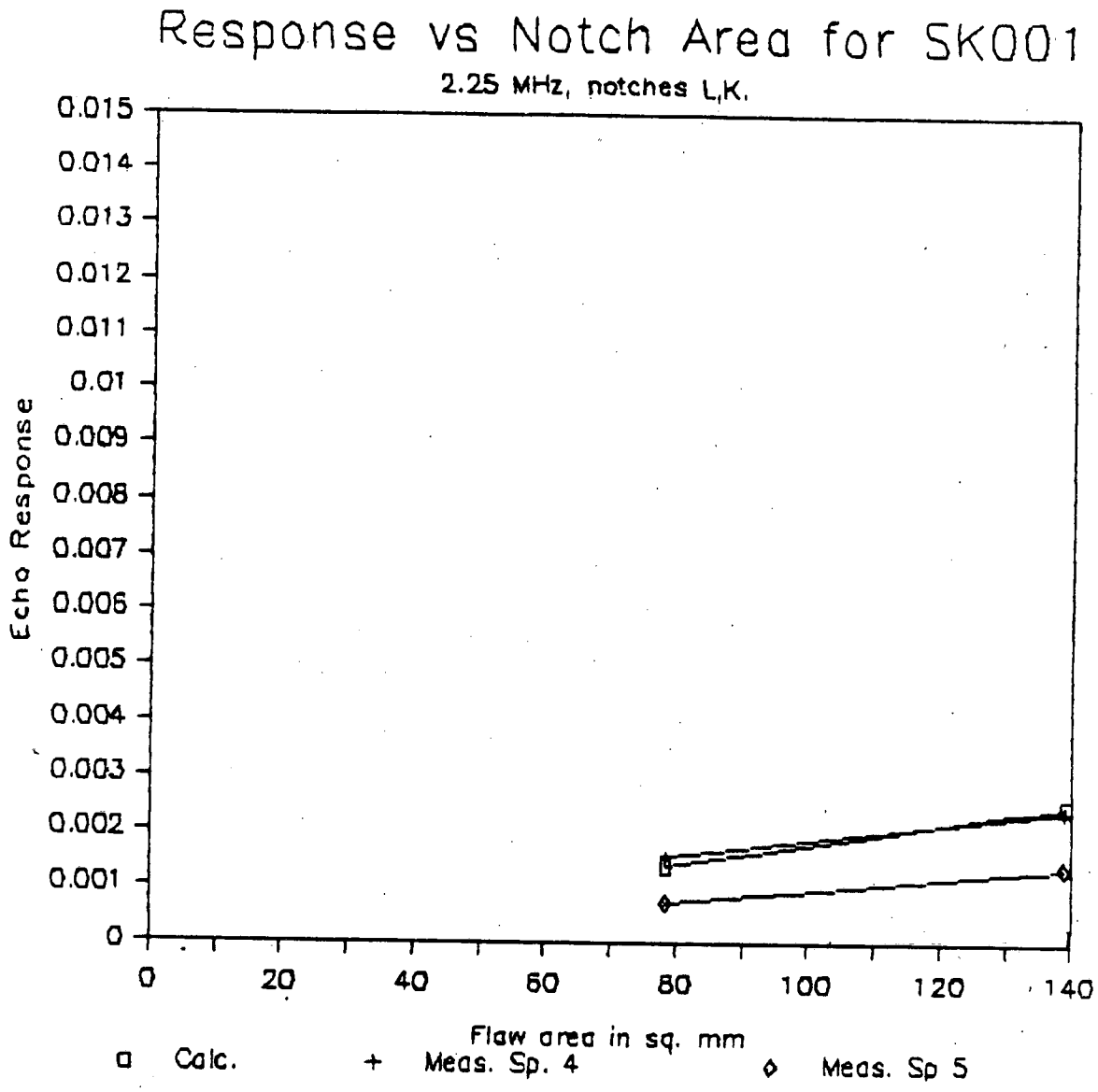
Response vs Notch Area for SK001
2.25 MHz, notches L,K.
Echo Response
0.015
0.014
0.013
0.012
0.011
0.01
0.009
0.008
0.007
0.006
0.005
0.004
0.003
0.002
0.001
0
0
20
40
60
80
100
120
140
Flaw area in sq. mm
Calc.
Meas. Sp. 4
Meas. Sp 5

Figure B-4

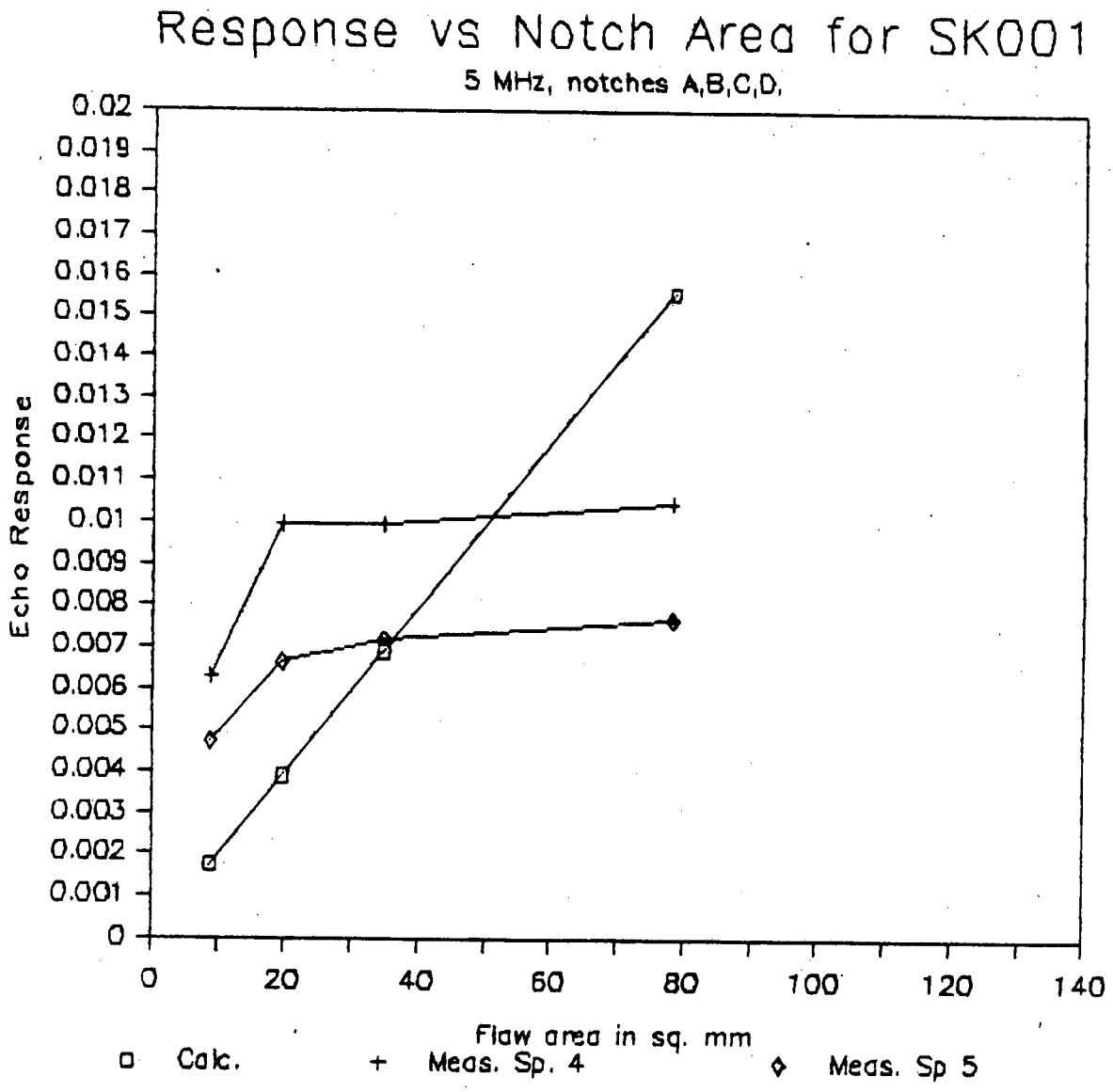
Response vs Notch Area for SK001
5 MHz, notches A,B,C,D,
Echo Response
0.02
0.019
0.018
0.017
0.016
0.015
0.014
0.013
0.012
0.011
0.01
0.009
0.008
0.007
0.006
0.005
0.004
0.003
0.002
0.001
0
0
20
40
60
80
100
120
140
Flaw area in sq. mm
Calc.
Meas. Sp. 4
Meas. Sp 5

Figure B-5

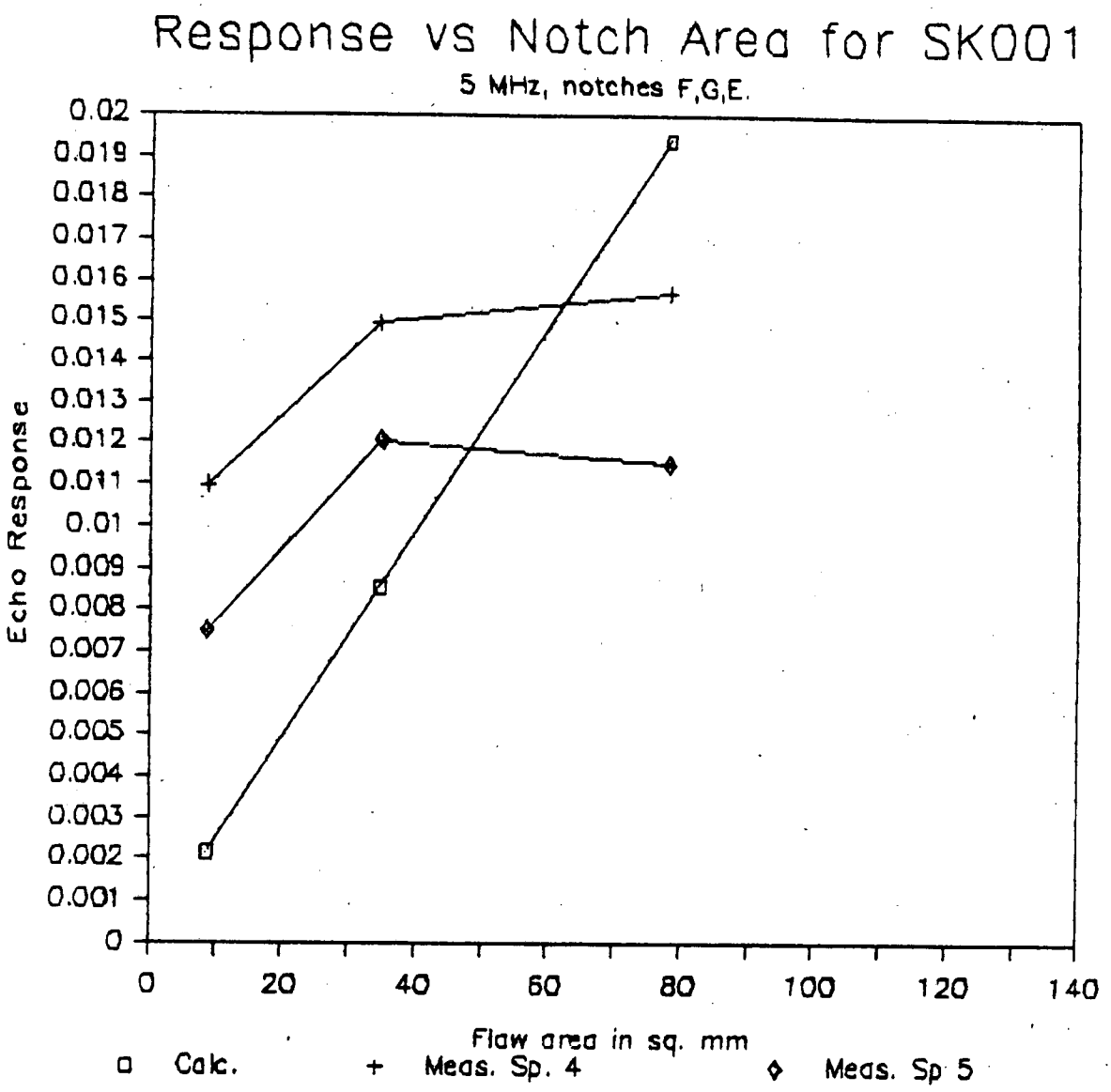
Response vs Notch Area for SK001
5 MHz, notches F,G,E.
Echo Response
0.02
0.019
0.018
0.017
0.016
0.015
0.014
0.013
0.012
0.011
0.01
0.009
0.008
0.007
0.006
0.005
0.004
0.003
0.002
0.001
0
0
20
40
60
80
100
120
140
Flaw area in sq. mm
Calc.
Meas. Sp. 4
Meas. Sp 5

Figure B-6

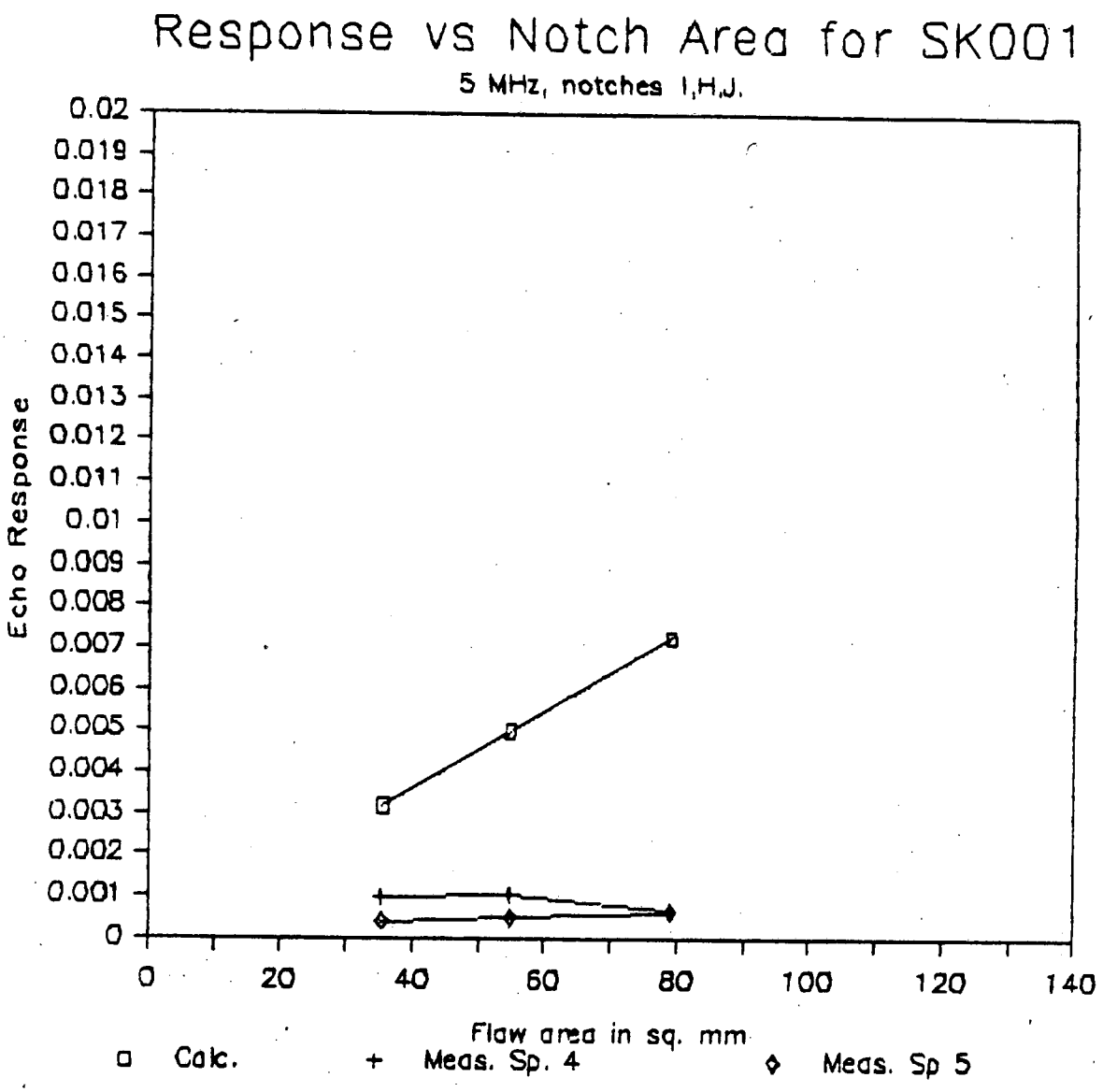
Response vs Notch Area for SK001
5 MHz, notches I,H,J.
Echo Response
0.02
0.019
0.018
0.017
0.016
0.015
0.014
0.013
0.012
0.011
0.01
0.009
0.008
0.007
0.006
0.005
0.004
0.003
0.002
0.001
0
0
20
40
60
80
100
120
140
Flaw area in sq. mm
Calc.
Meas. Sp. 4
Meas. Sp 5

Figure B-7

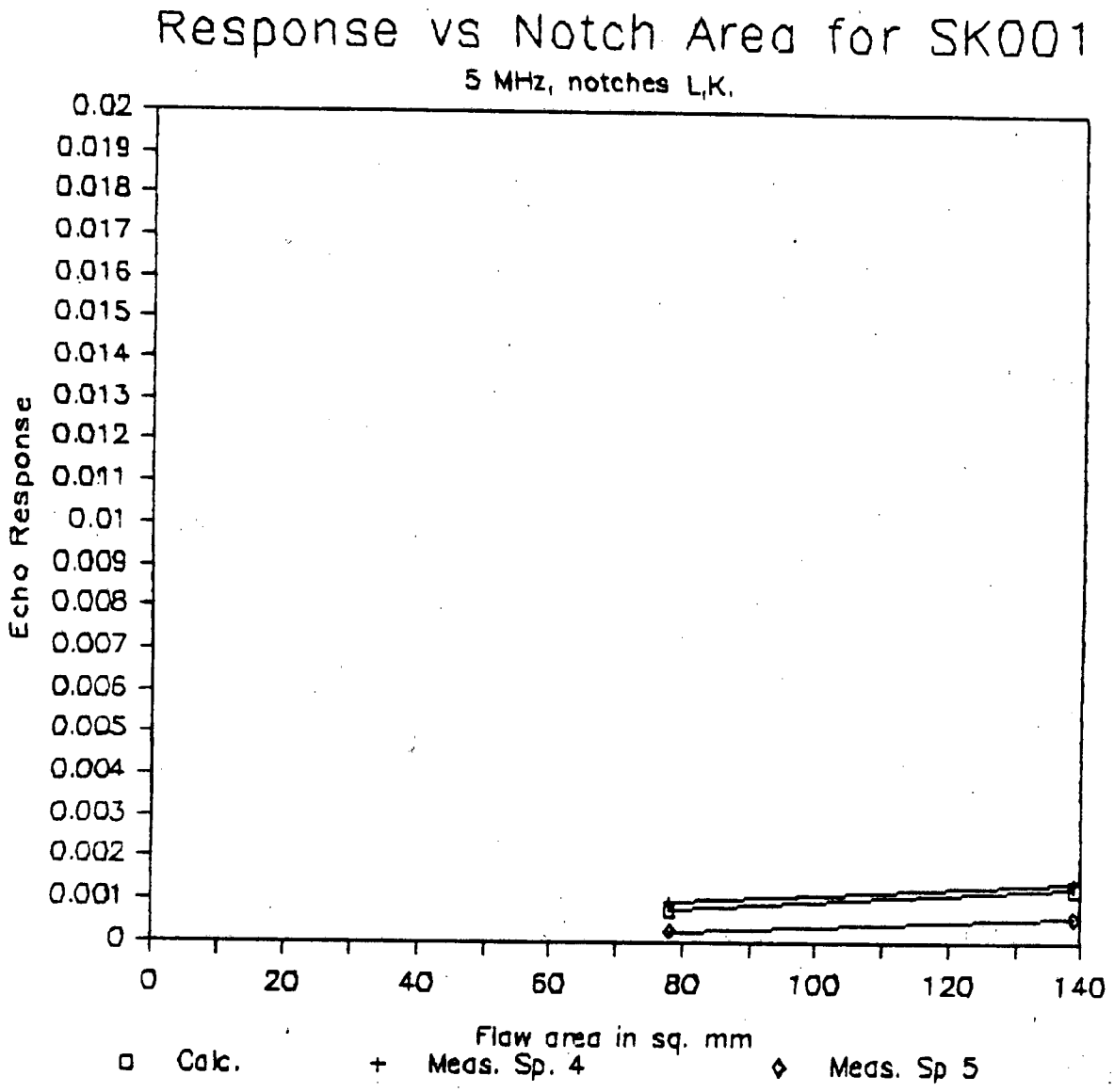
Response vs Notch Area for SK001
5 MHz, notches L,K.
Echo Response
0.02
0.019
0.018
0.017
0.016
0.015
0.014
0.013
0.012
0.011
0.01
0.009
0.008
0.007
0.006
0.005
0.004
0.003
0.002
0.001
0
0
20
40
60
80
100
120
140
Flaw area in sq. mm
Calc.
Meas. Sp. 4
Meas. Sp 5

Figure B-8

TABLE B-4

SPECIMEN 4 AND 5 (SK001) NOTCH SIZES

Notch	Depth (mm)	Length (mm)	Area (mm2)	Beam Angle (degrees)	Beam Path Length (mm)
A	2	6	8.8	45	171
B	3	9	19.6	45	171
C	4	12	34.7	45	171
D	6	18	78.3	45	171
F	2	6	8.8	45	162
G	4	12	34.7	45	162
E	6	18	78.3	45	162
I	4	12	34.7	60	201
H	5	15	54.1	60	201
J	6	18	78.3	60	201
L	6	18	78.3	75	312
K	8	24	139.0	75	312

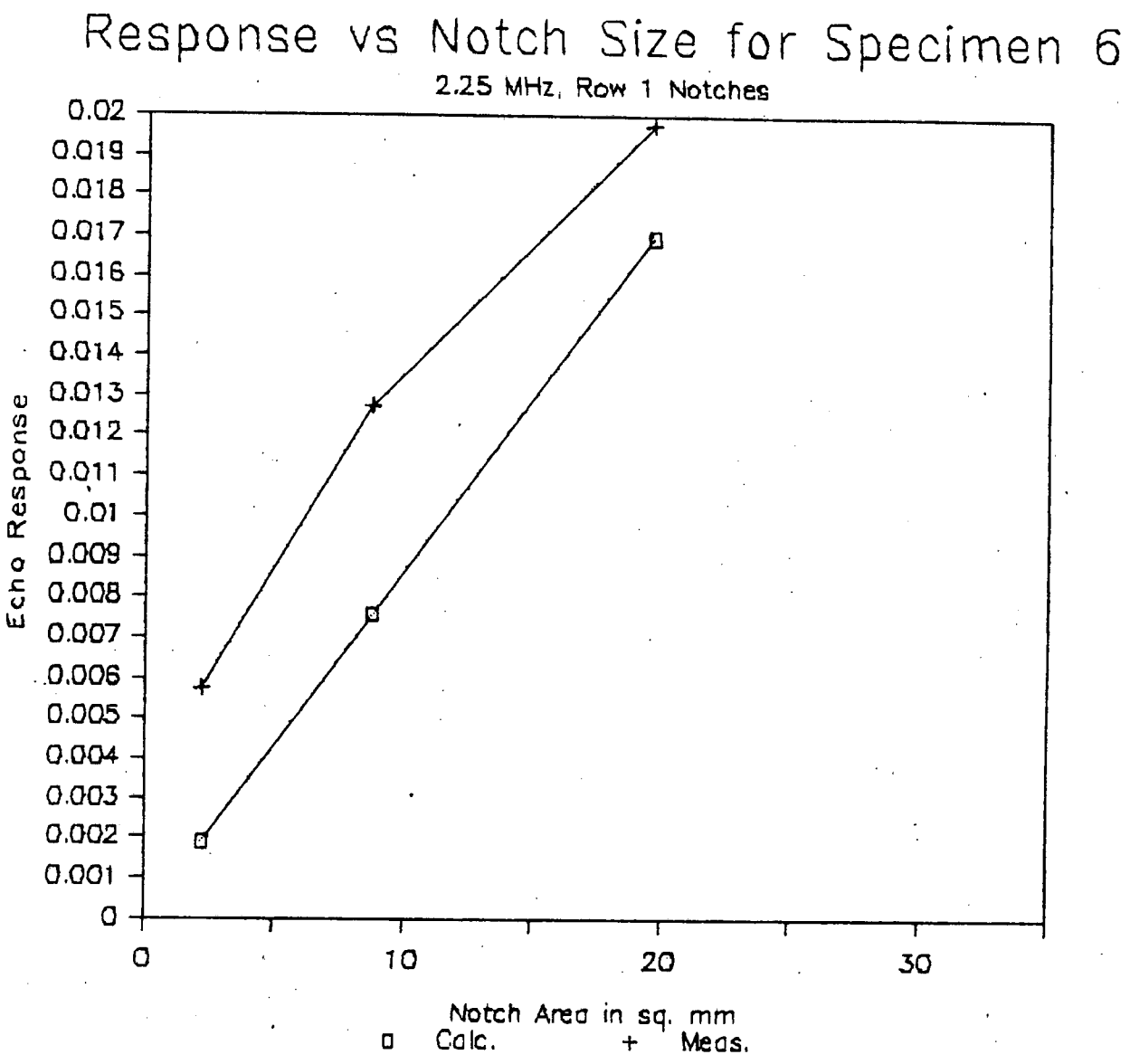
Response vs Notch Size for Specimen 6
2.25 MHz, Row 1 Notches
Echo Response
0.02
0.019
0.018
0.017
0.016
0.015
0.014
0.013
0.012
0.011
0.01
0.009
0.008
0.007
0.006
0.005
0.004
0.003
0.002
0.001
0
0
10
20
30
Notch Area in sq. mm
Calc.
Meas.

Figure B-9

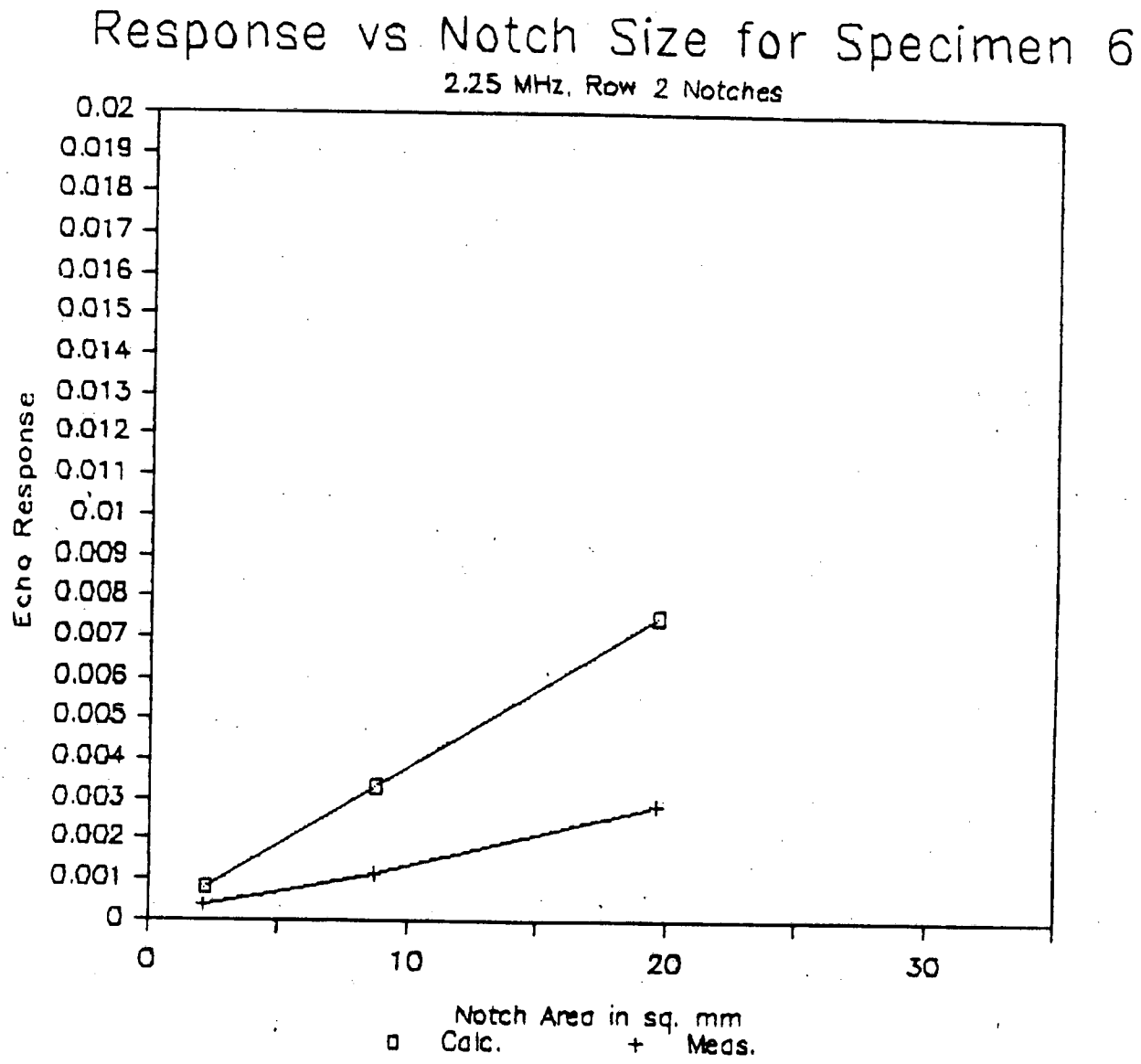
Response vs Notch Size for Specimen 6
2.25 MHz, Row 2 Notches
Echo Response
0.02
0.019
0.018
0.017
0.016
0.015
0.014
0.013
0.012
0.011
0.01
0.009
0.008
0.007
0.006
0.005
0.004
0.003
0.002
0.001
0
0
10
20
30
Notch Area in sq. mm
Calc.
Meas.

Figure B-10

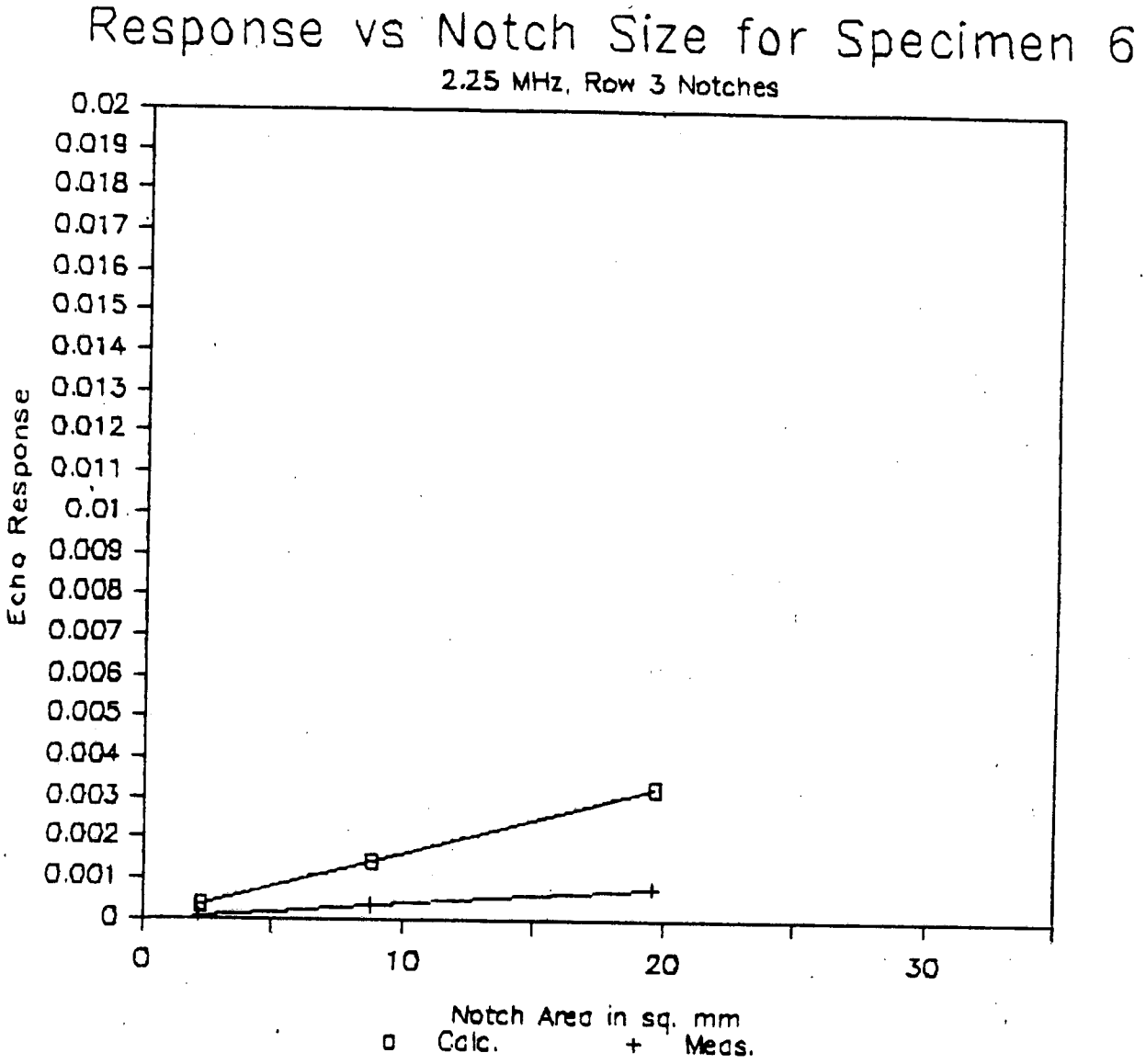
Response vs Notch Size for Specimen 6
2.25 MHz, Row 3 Notches
Echo Response
0.02
0.019
0.018
0.017
0.016
0.015
0.014
0.013
0.012
0.011
0.01
0.009
0.008
0.007
0.006
0.005
0.004
0.003
0.002
0.001
0
0
10
20
30
Notch Area in sq. mm
□ Calc.
+ Meas.

Figure B-11

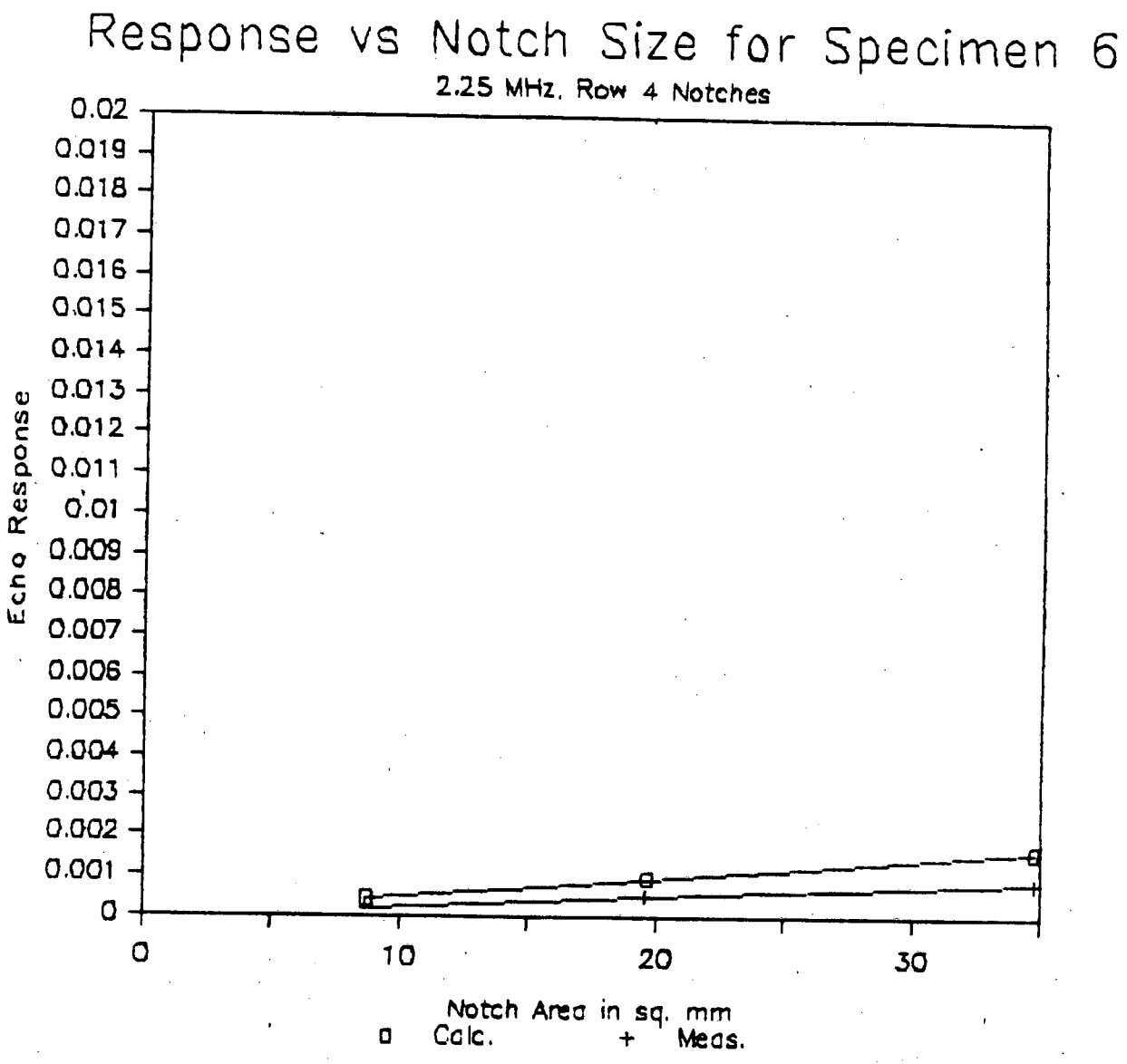
Response vs Notch Size for Specimen 6
2.25 MHz, Row 4 Notches
Echo Response
0.02
0.019
0.018
0.017
0.016
0.015
0.014
0.013
0.012
0.011
0.01
0.009
0.008
0.007
0.006
0.005
0.004
0.003
0.002
0.001
0
0
10
20
30
Notch Area in sq. mm
Calc.
Meas.

Figure B-12

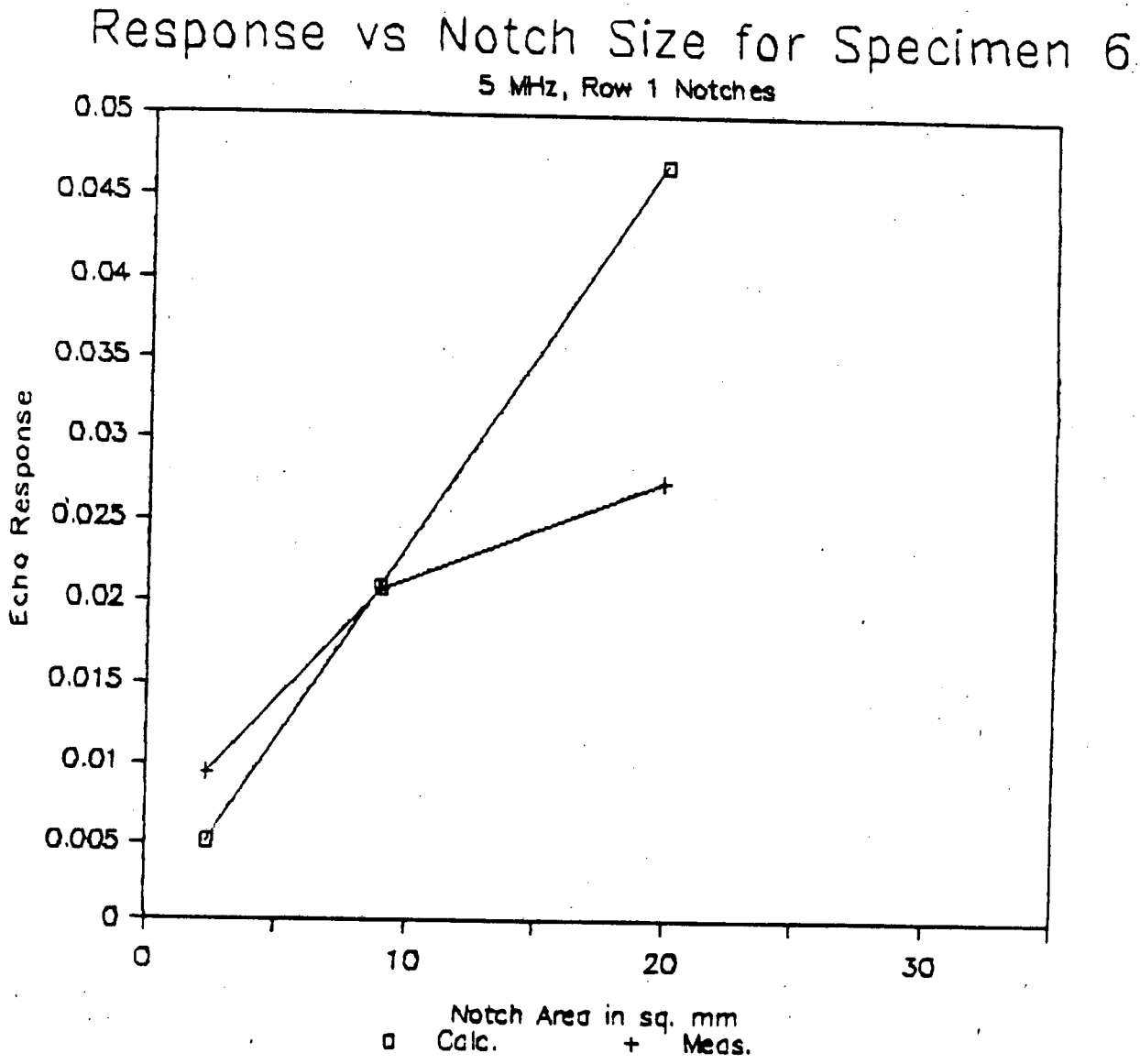
Response vs Notch Size for Specimen 6
5 MHz, Row 1 Notches
Echo Response
0.05
0.045
0.04
0.035
0.03
0.025
0.02
0.015
0.01
0.005
0
0
10
20
30
Notch Area in sq. mm
Calc.
Meas.

Figure B-13

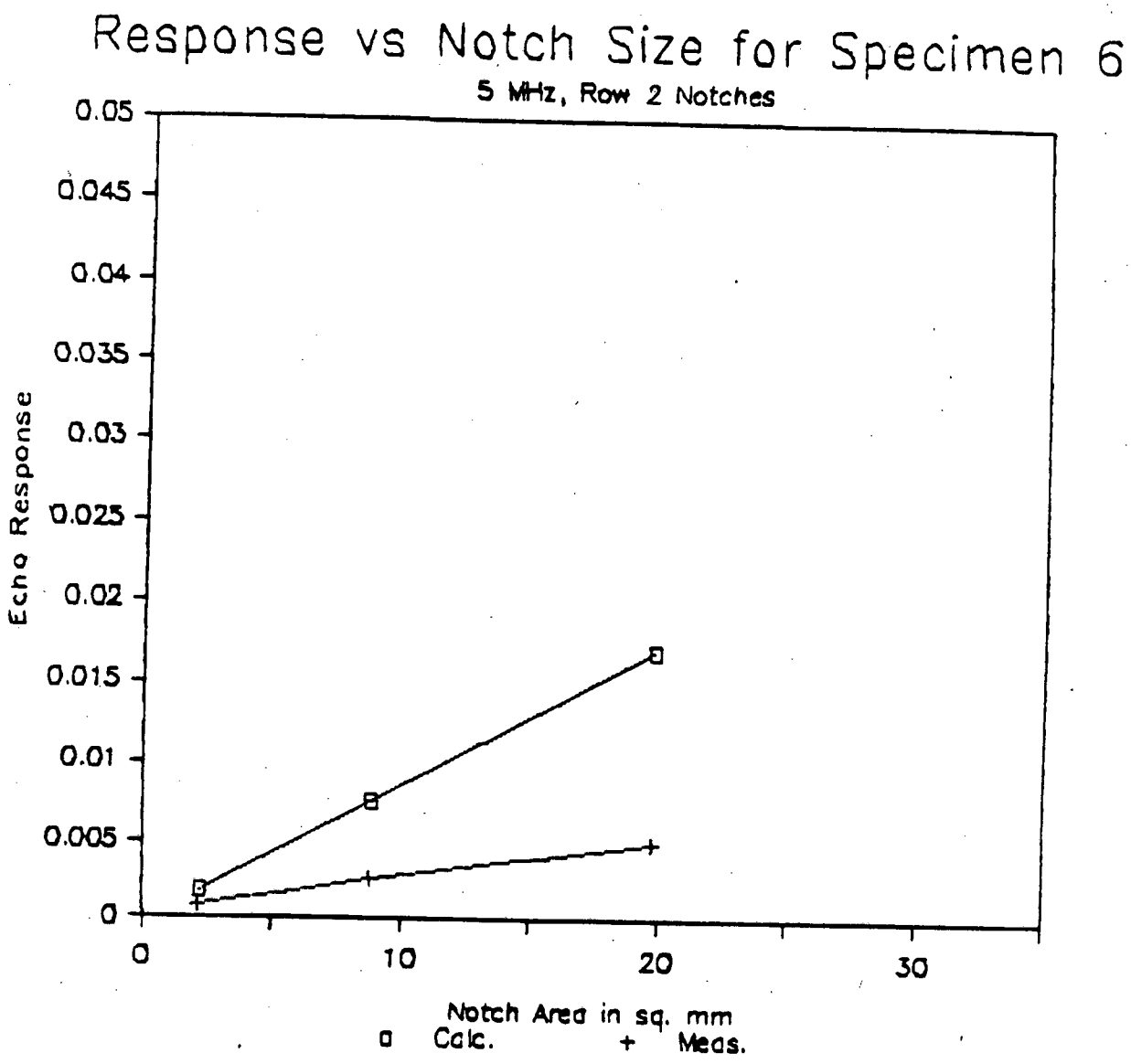
Response vs Notch Size for Specimen 6
5 MHz, Row 2 Notches
Echo Response
0.05
0.045
0.04
0.035
0.03
0.025
0.02
0.015
0.01
0.005
0
0
10
20
30
Notch Area in sq. mm
□ Calc.
+ Meas.

Figure B-14

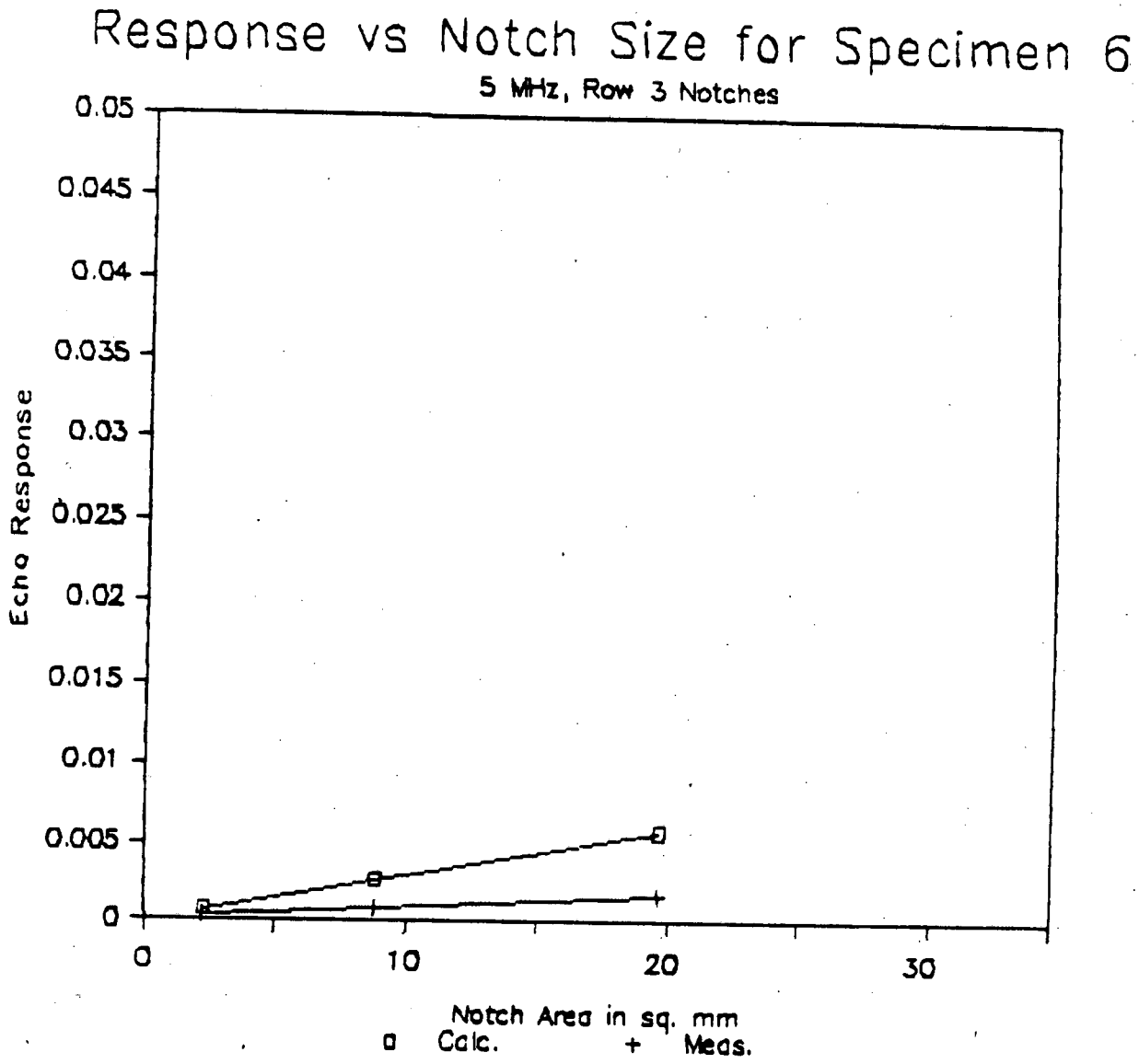
Response vs Notch Size for Specimen 6
5 MHz, Row 3 Notches
Echo Response
0.05
0.045
0.04
0.035
0.03
0.025
0.02
0.015
0.01
0.005
0
0
10
20
30
Notch Area in sq. mm
Calc.
Meas.

Figure B-15

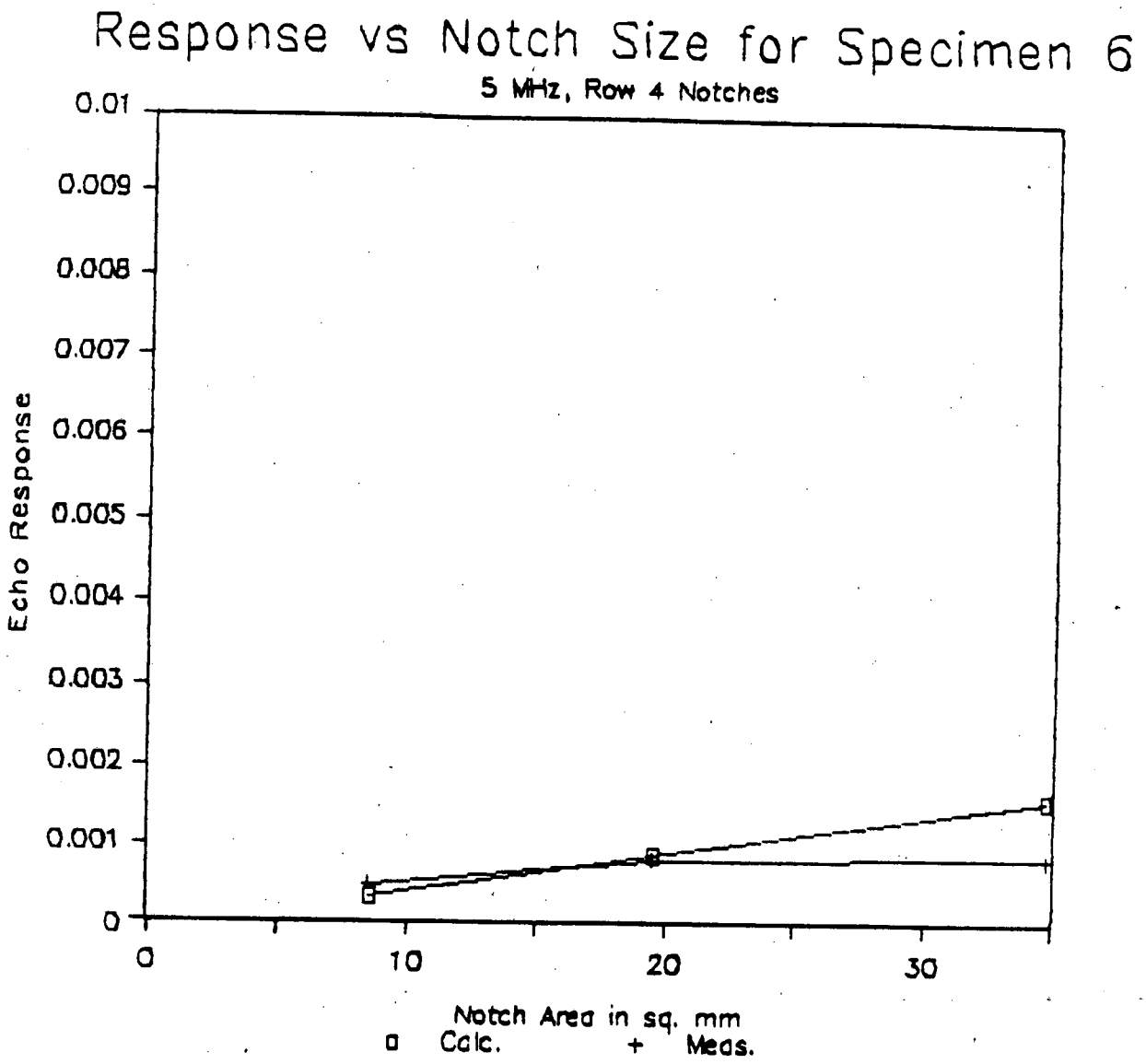
Response vs Notch Size for Specimen 6
5 MHz, Row 4 Notches
Echo Response
0.01
0.009
0.008
0.007
0.006
0.005
0.004
0.003
0.002
0.001
0
0
10
20
30
Notch Area in sq. mm
Calc.
Meas.

Figure B-16

TABLE B-5

SPECIMEN 6, SK005

Row	Notch	Depth (mm)	Length (mm)	Area (mm2)	Beam Angle	Path Length
1	C	1	3	2.2	45	83
1	B	2	6	8.8	45	83
1	A	3	9	19.6	45	83
2	C	1	3	2.2	60	112
2	B	2	6	8.8	60	112
2	A	3	9	19.6	60	112
3	C	1	3	2.2	70	153
3	B	2	6	8.8	70	153
3	A	3	9	19.6	70	153
4	B	2	6	8.8	77.5	227
4	A	3	9	19.6	77.5	227
4	D	4	12	34.7	77.5	227

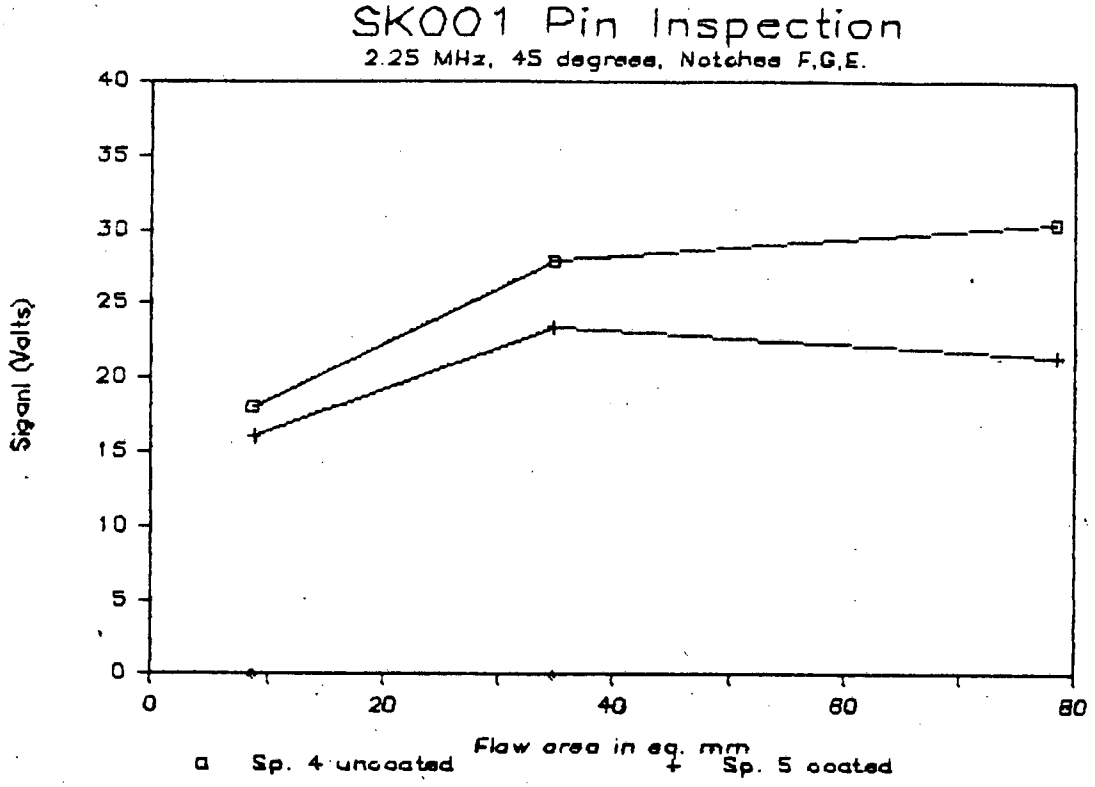
SK001 Pin Inspection
2.25 MHz, 45 degrees, Notches F,G,E.
Signal (Volts)
40
35
30
25
20
15
10
5
0
0
20
40
60
80
Flow area in sq. mm
Sp. 4 uncoated
Sp. 5 coated

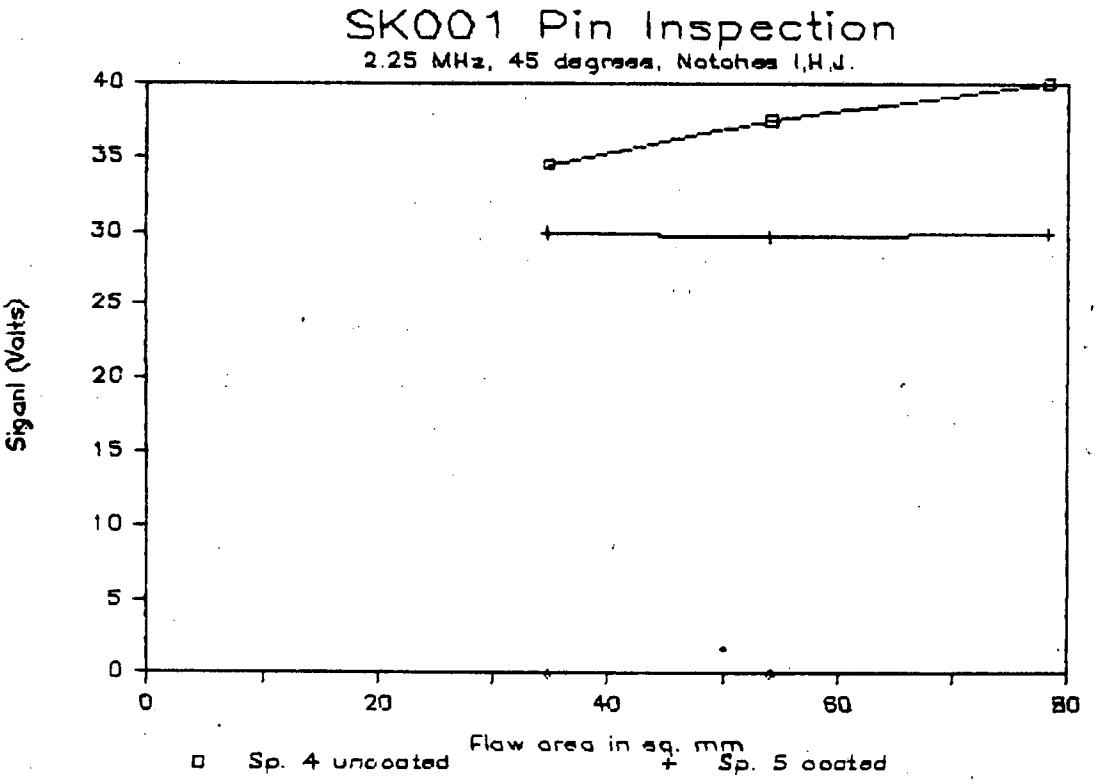
SK001 Pin Inspection
2.25 MHz, 45 degrees, Notches I,H,J.
Signal (Volts)
40
35
30
25
20
15
10
5
0
0
20
40
60
80
Flow area in sq. mm
Sp. 4 uncoated
Sp. 5 coated

Figure B-17

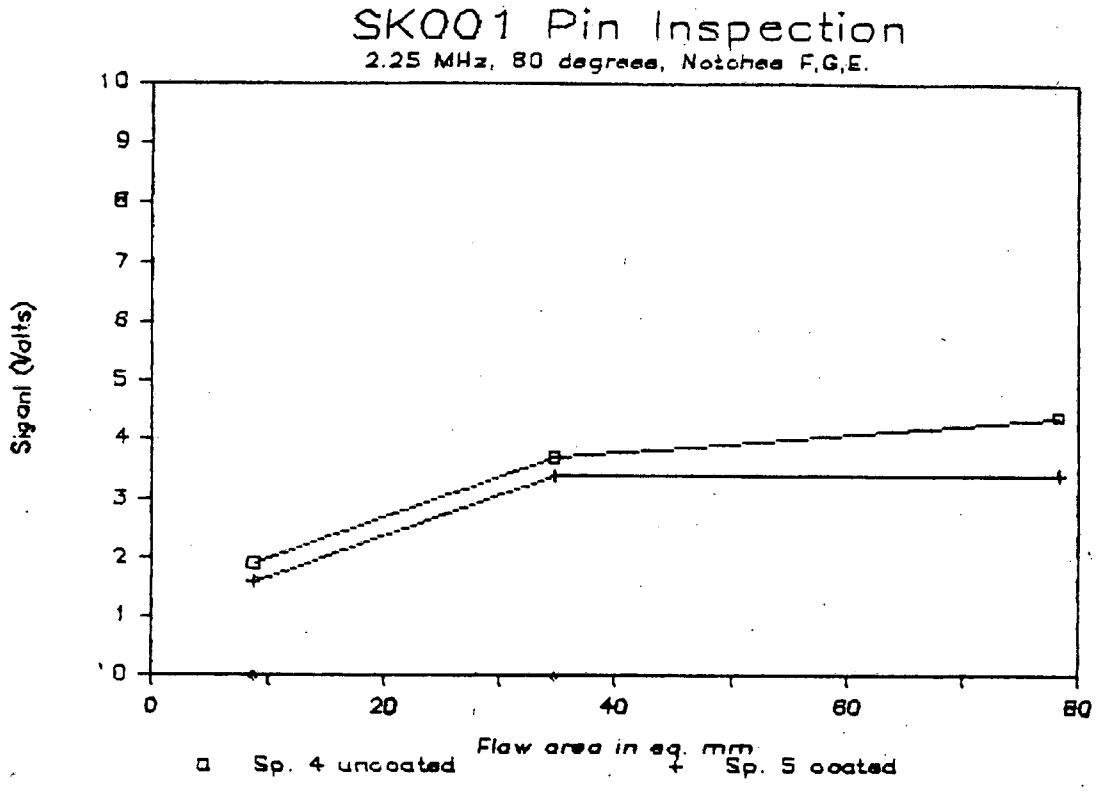
SK001 Pin Inspection
2.25 MHz, 80 degrees, Notches F,G,E.
Signal (Volts)
10
9
8
7
6
5
4
3
2
1
0
0
20
40
60
80
Flow area in sq. mm
Sp. 4 uncoated
Sp. 5 coated

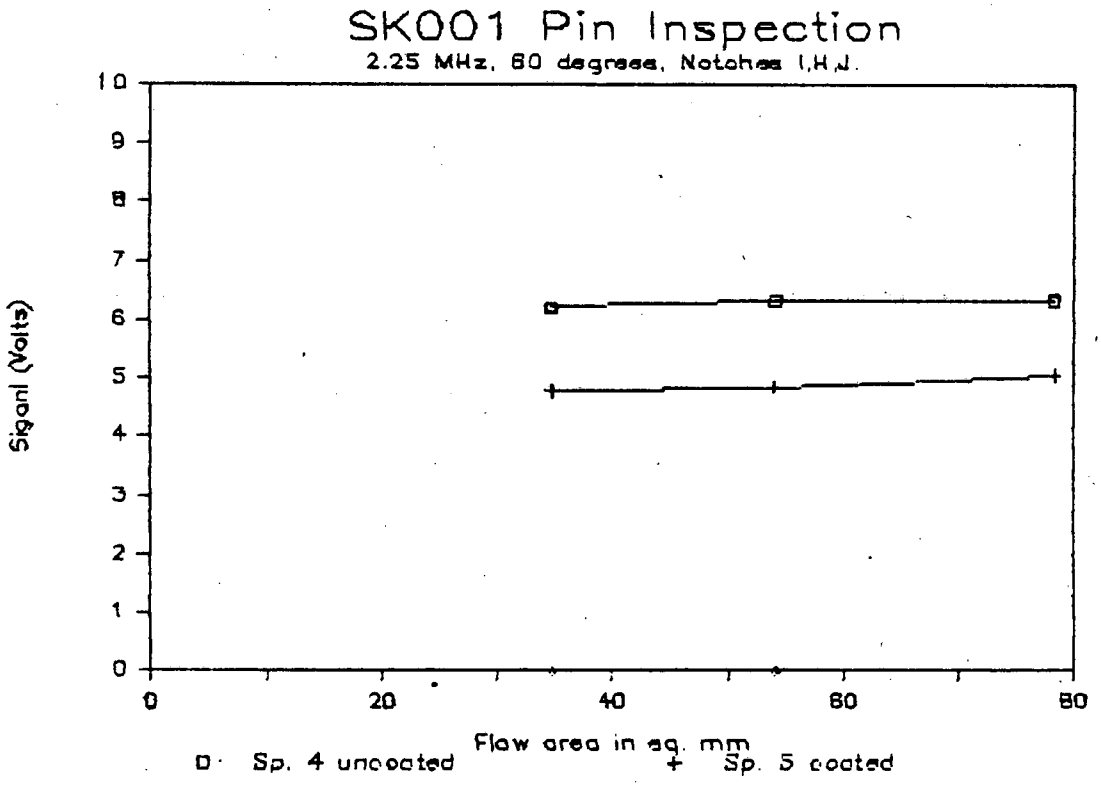
SK001 Pin Inspection
2.25 MHz, 80 degrees, Notches I,H,J.
Signal (Volts)
10
9
8
7
6
5
4
3
2
1
0
0
20
40
60
80
Flow area in sq. mm
Sp. 4 uncoated
Sp. 5 coated

Figure B-18

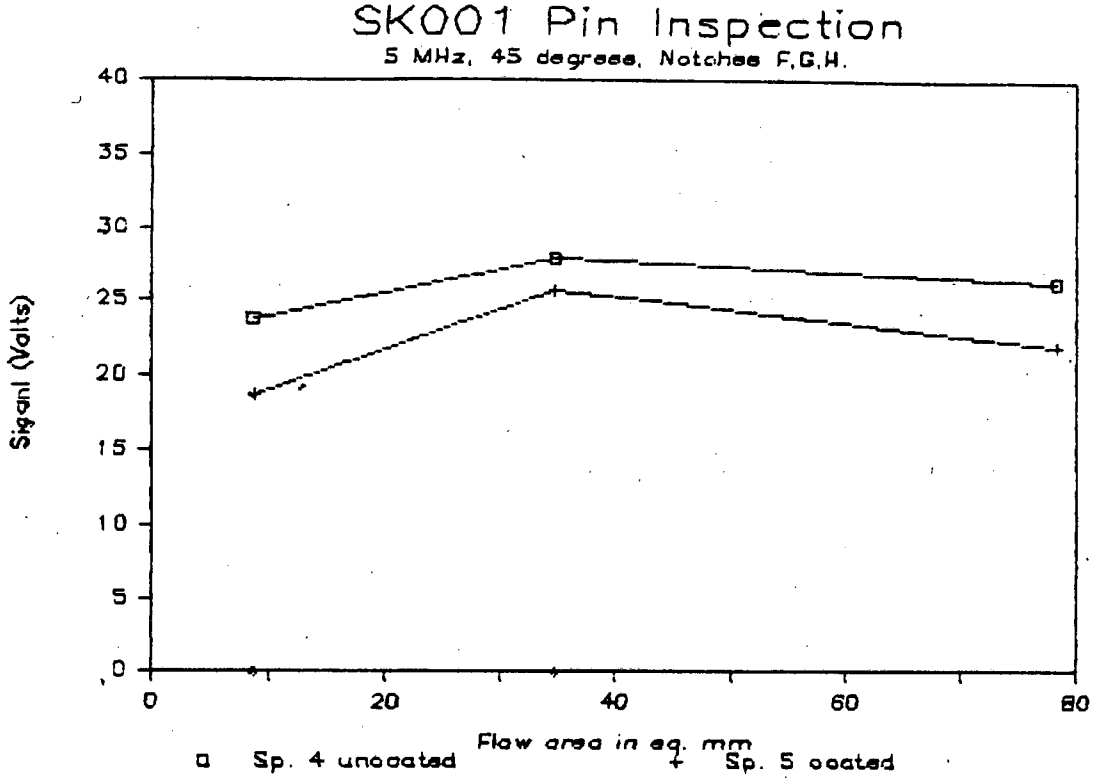
SK001 Pin Inspection
5 MHz, 45 degrees, Notches F,G,H.
Signal (Volts)
40
35
30
25
20
15
10
5
0
0
20
40
60
80
Flaw area in sq. mm
Sp. 4 uncoated
Sp. 5 coated

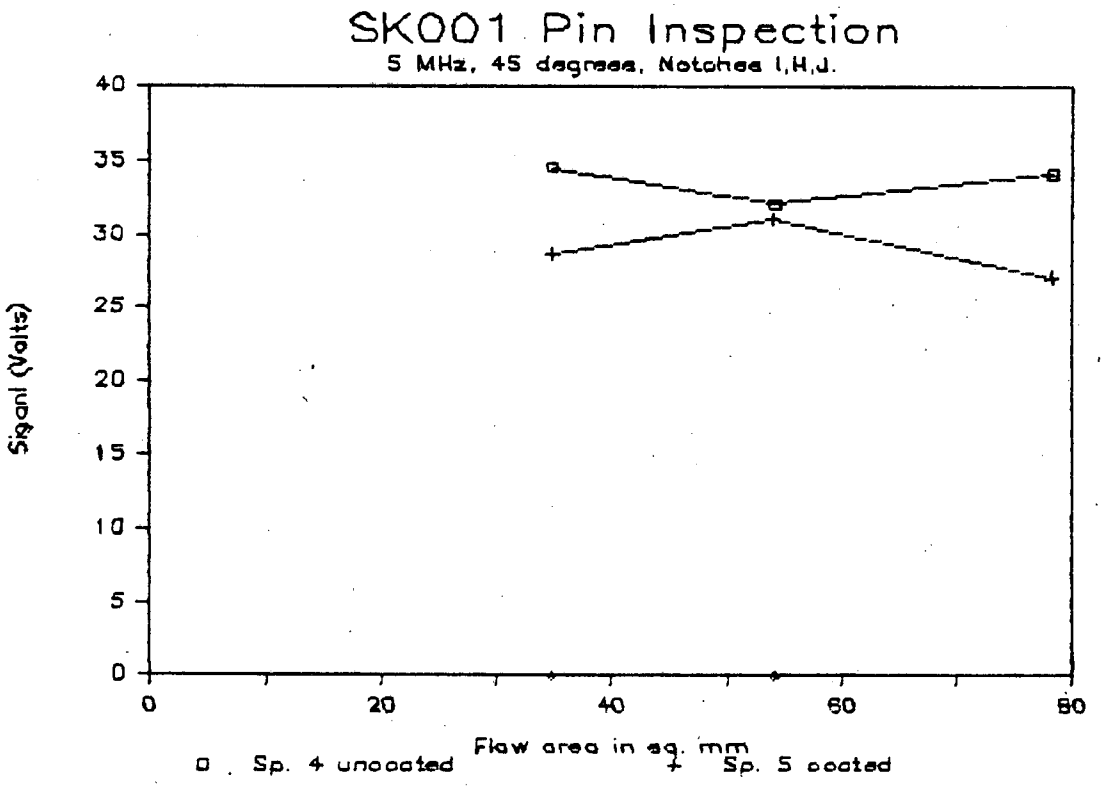
SK001 Pin Inspection
5 MHz, 45 degrees, Notches I,H,J.
Signal (Volts)
40
35
30
25
20
15
10
5
0
0
20
40
60
80
Flaw area in sq. mm
Sp. 4 uncoated
Sp. 5 coated

Figure B-19

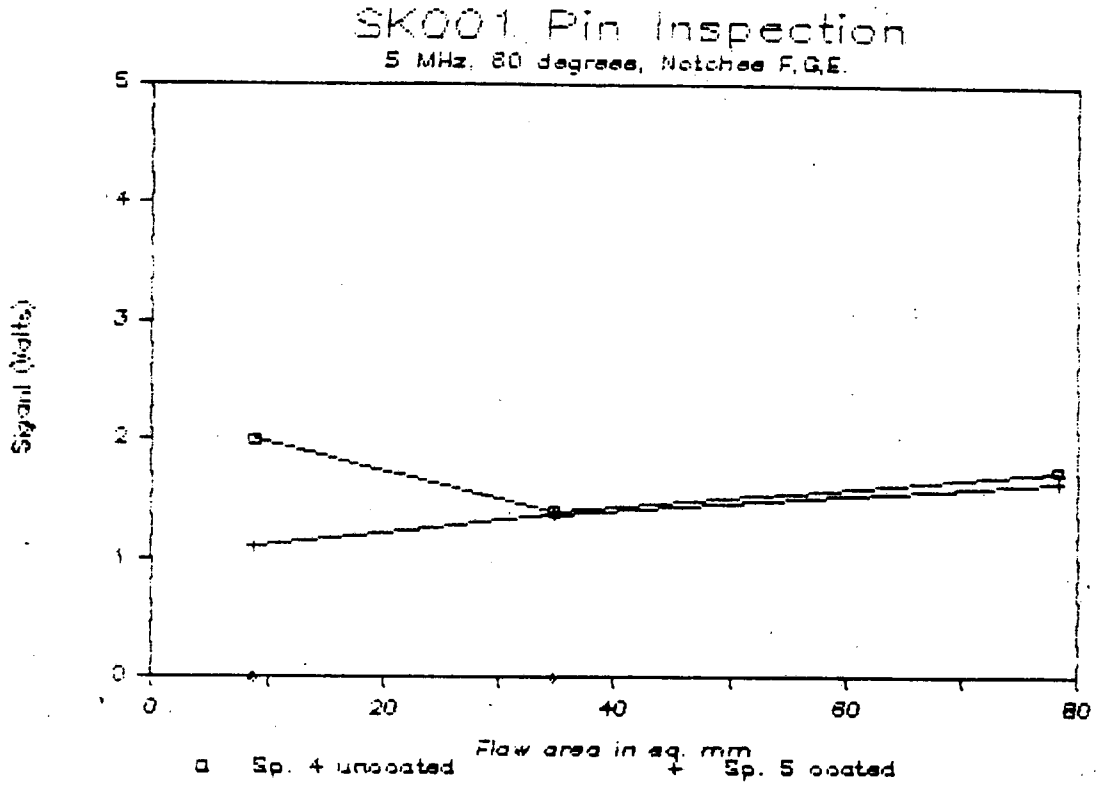
SK001 Pin Inspection
5 MHz, 60 degrees, Notches F,G,E.
Signal (Volts)
0
1
2
3
4
5
0
20
40
60
80
Flaw area in sq. mm
Sp. 4 uncoated
Sp. 5 coated

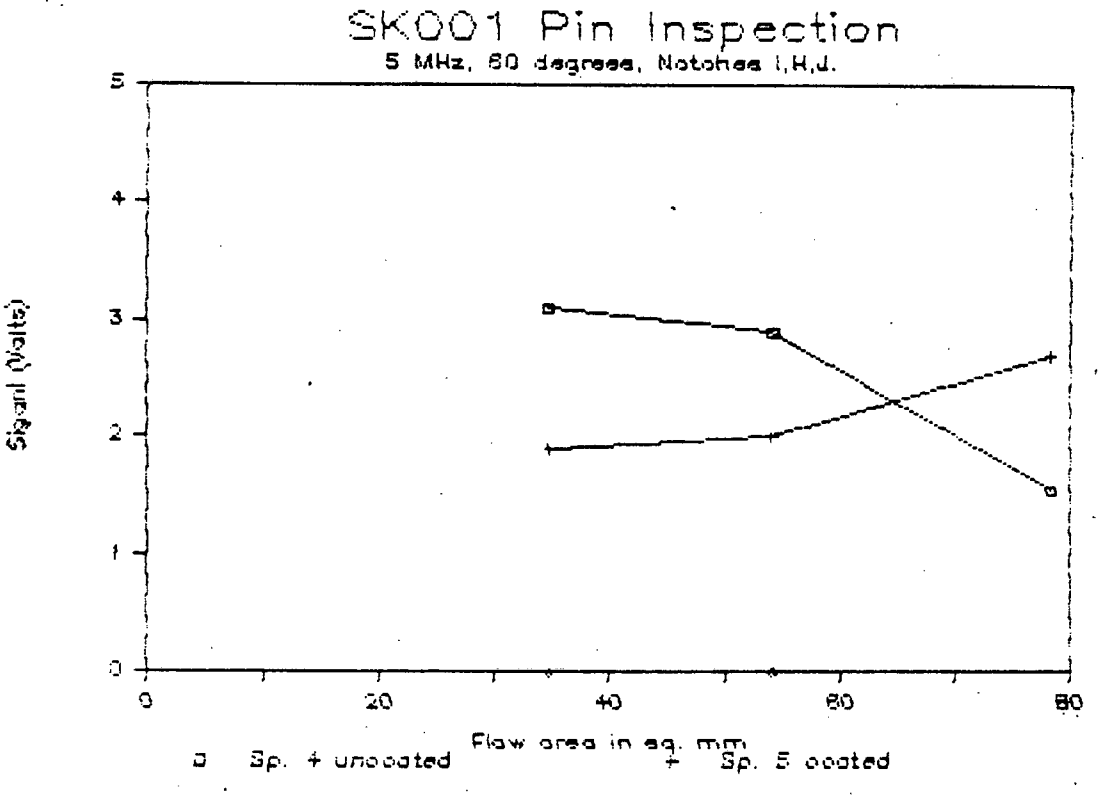
SK001 Pin Inspection
5 MHz, 60 degrees, Notches I,H,J.
Signal (Volts)
0
1
2
3
4
5
0
20
40
60
80
Flaw area in sq. mm
Sp. 4 uncoated
Sp. 5 coated

Figure B-20

TABLE B-6

LINEARITY TEST

Pulse Strength	Front Surface Reference	Notch Response	Relative Response
Max	883V	2.25V	.0025
Mid	555V	1.28V	.0023
Min	148V	.34V	.0023

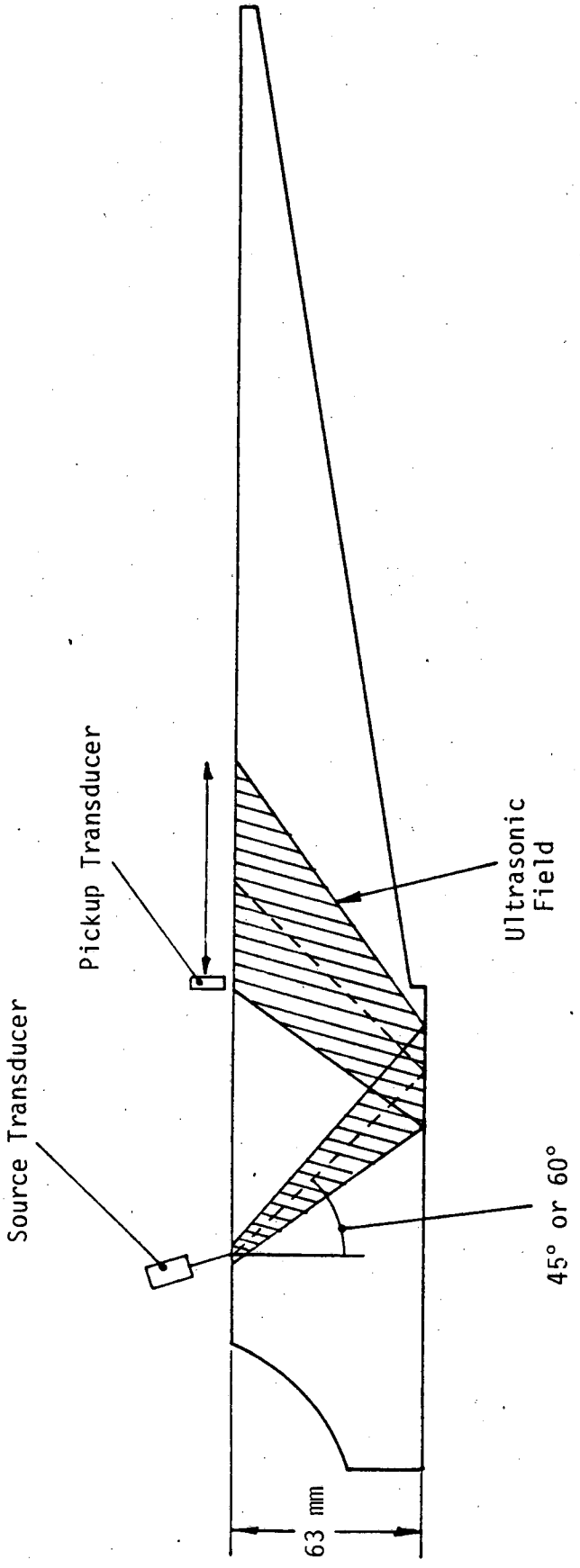

Figure B-21. Test configuration for evaluating beam spread.

shear beam in the part. After the bounce, the ultrasound returns to the entry surface. A C-scan image of the ultrasound field which radiates from that surface was obtained by scanning the small point transducer over the area. Figure B-22 shows the images. Each image is scaled with 1 cm tick marks. The increase in beam size from 5 MHz to 2.25 MHz is dramatic. Also,the beam size increases at 60 over 45 shear. A surprising result is the two lobes of the 60 beam. The lower lobe in the image is at the expected geometric position for the bounce path of the shear wave. The second lobe is apparently due to mode converted waves at a shallower angle on the bounce.

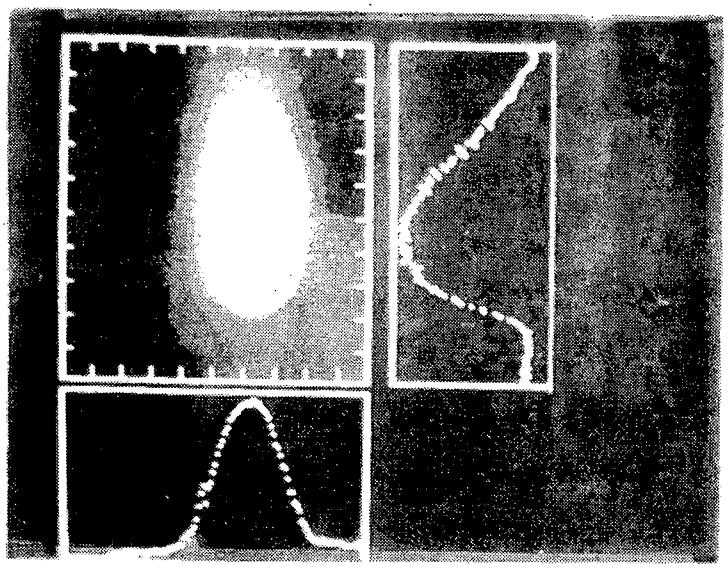

B-22a

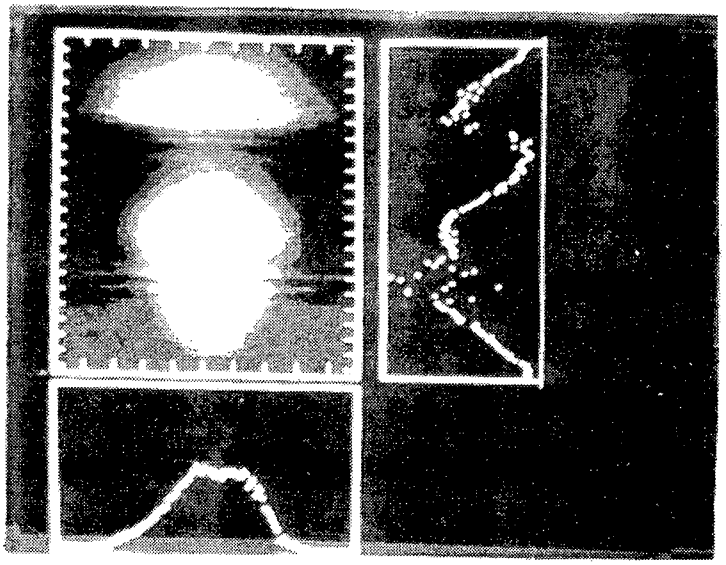

B-22b

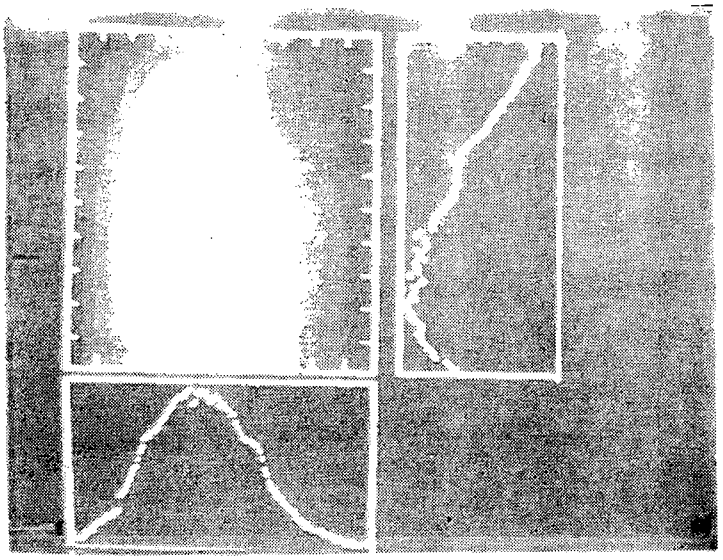

B-22c

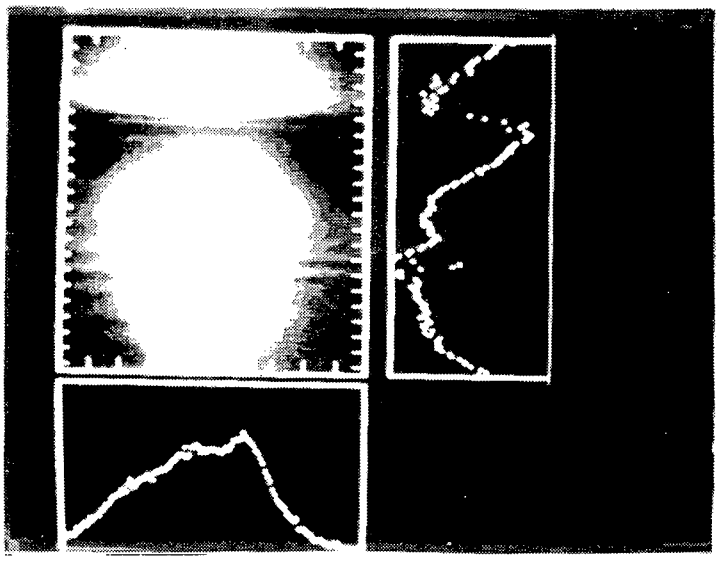

B-22d

Figure B-22.. Shear Wave pattern a) 5 MHz, 45° b) 5MHz, 60° c) 2.25 MHz,45° d) 2.25 MHz, 60°. (Each division along the edge of the images is 1 cm).

APPENDIX C

Thread Effects Study Specimens

APPENDIX C

THREAD EFFECTS STUDY SPECIMENS

The test specimen 4 (SK001, Figure 4.4-1) and specimen 6 (SK005, Figure 4.4-2) were modified to contain representative thread patterns.

Figure C-1 shows the thread pattern for specimen 4 and Figure C-2 shows modified specimen 4A part drawing with EDM notch pattern. The notch size is given in Figure C3. Table C1 summarizes the notch pattern. The specimen 4A thread pattern is an Exxon Production Research (EPR) modified buttress thread.

Figure C4 shows specimen 5A. This is specimen 5 with threads machined and a fatigue crack was grown at the root of the fifth thread. In actual fabrication, however, an error in machining resulted in a different configuration than Figure C4. Therefore, a second specimen 5AA was fabricated and a fatigue crack grown.

Figure C5 shows the thread pattern used on the specimen C6. This is a rotary shoulder connector thread. Figure C6 shows the threaded specimen 6A. Table C1 summarizes the notch pattern.

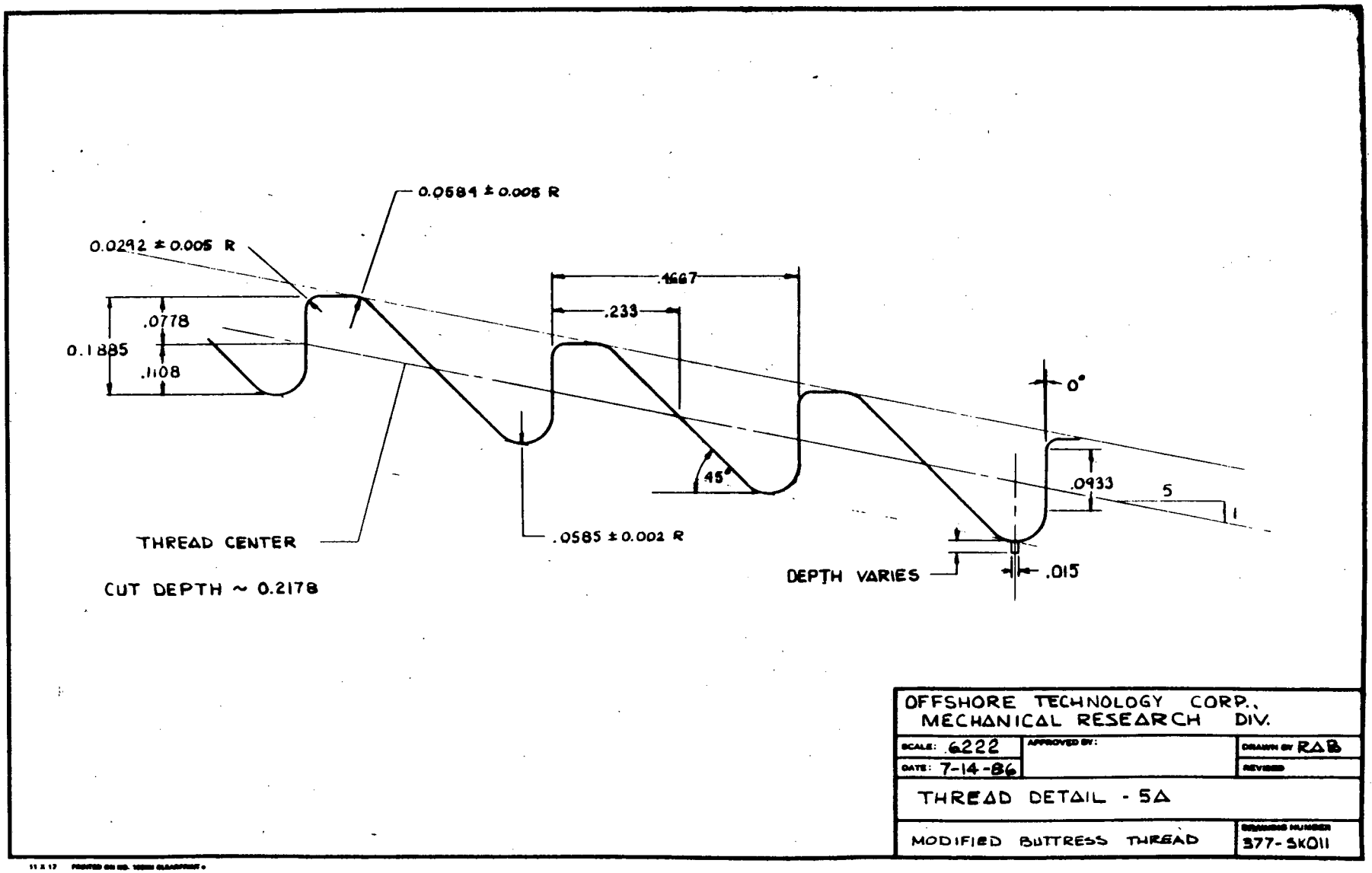
0.0584 ± 0.005 R
0.0292 ± 0.005 R
.1667
.233
.0778
0.1885
.1108
0°
45°
.0933
5
1
THREAD CENTER
CUT DEPTH ~ 0.2178
.0585 ± 0.002 R
DEPTH VARIES
.015
OFFSHORE TECHNOLOGY CORP.,
MECHANICAL RESEARCH DIV.
SCALE: 6222
DATE: 7-14-86
APPROVED BY:
DRAWN BY RAB
REVISED
THREAD DETAIL - 5A
MODIFIED BUTTRESS THREAD
377-SK011

Figure C-1

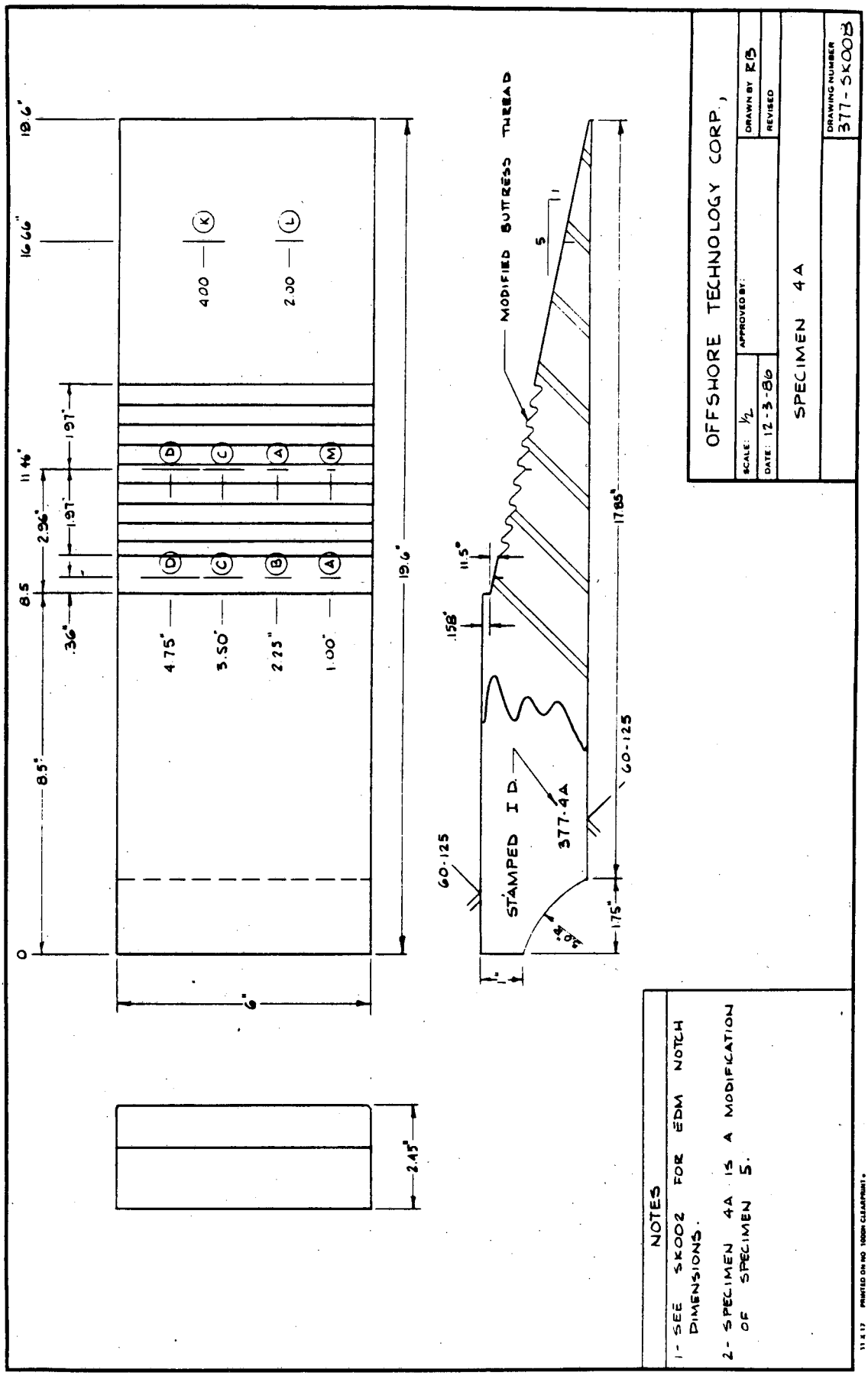
OFFSHORE TECHNOLOGY CORP.
SCALE: 1/2
DATE: 12-3-86
APPROVED BY:
DRAWN BY RS
REVISED
SPECIMEN 4A
DRAWING NUMBER 377-SK002B
MODIFIED BUTRESS THREAD
STAMPED I D
377-4A
60-125
NOTES
1- SEE SK002 FOR EDM NOTCH DIMENSIONS.
2- SPECIMEN 4A IS A MODIFICATION OF SPECIMEN 5.

Figure C-3

Notches	mm			inches			Tolerances (inches)		
	a	c	R	a	c	R	a	c	R
A	2.0	6.0	3.3	.079	.235	.128	.001	.002	.001
B	3.0	9.0	4.9	.118	.354	.192	.001	.004	.002
C	4.0	12.0	6.5	.157	.422	.256	.002	.005	.003
D	6.0	18.0	9.8	.236	.709	.384	.002	.007	.004
E	6.0	19.0	9.6	.236	.709	.384	.002	.007	.004
F	2.0	6.0	3.3	.079	.235	.128	.001	.002	.001
G	4.0	12.0	6.5	.157	.472	.256	.002	.005	.003
H	5.0	15.0	8.1	.197	.591	.320	.002	.006	.003
I	4.0	12.0	6.5	.157	.472	.256	.002	.005	.003
J	6.0	18.0	9.6	.236	.709	.364	.002	.007	.004
K	8.0	24.0	12.0	.315	.945	.512	.003	.009	.005
L	6.0	13.0	9.6	.236	.709	.364	.002	.007	.004
M	1.0	3.0	1.6						

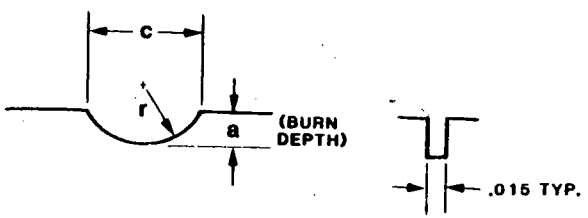

Figure C-3

$A = R(\Theta - 1/2 \sin 2\Theta)$

$\Theta = \sin^{-1}(c/2R)$

TABLE C1

THREADED SPECIMEN NOTCHES

SPECIMEN 4A (SK001):

Notch	Depth (mm)	Length (mm)	Location
D	6	18	Root of thread #5
C	4	12	Root of thread #5
A	2	6	Root of thread #5
M	1	3	Root of thread #5
E (Residual)	approx. 2	approx. 10	Thread 2 but not in root
H (Residual)	approx. 1	approx. 7	Thread 8 but not in root
J (Residual)	approx. 2	approx. 10	Thread 8 but not in root

SPECIMEN 6A (SK005):

Notch	Depth (mm)	Length (mm)	Location
1B	3	9	Root of thread 1
1A	2	6	Root of thread 1
1M	1	3	Root of thread 1
7B	3	9	Root of thread 7
7A	2	6	Root of thread 7
7M	1	3	Root of thread 7

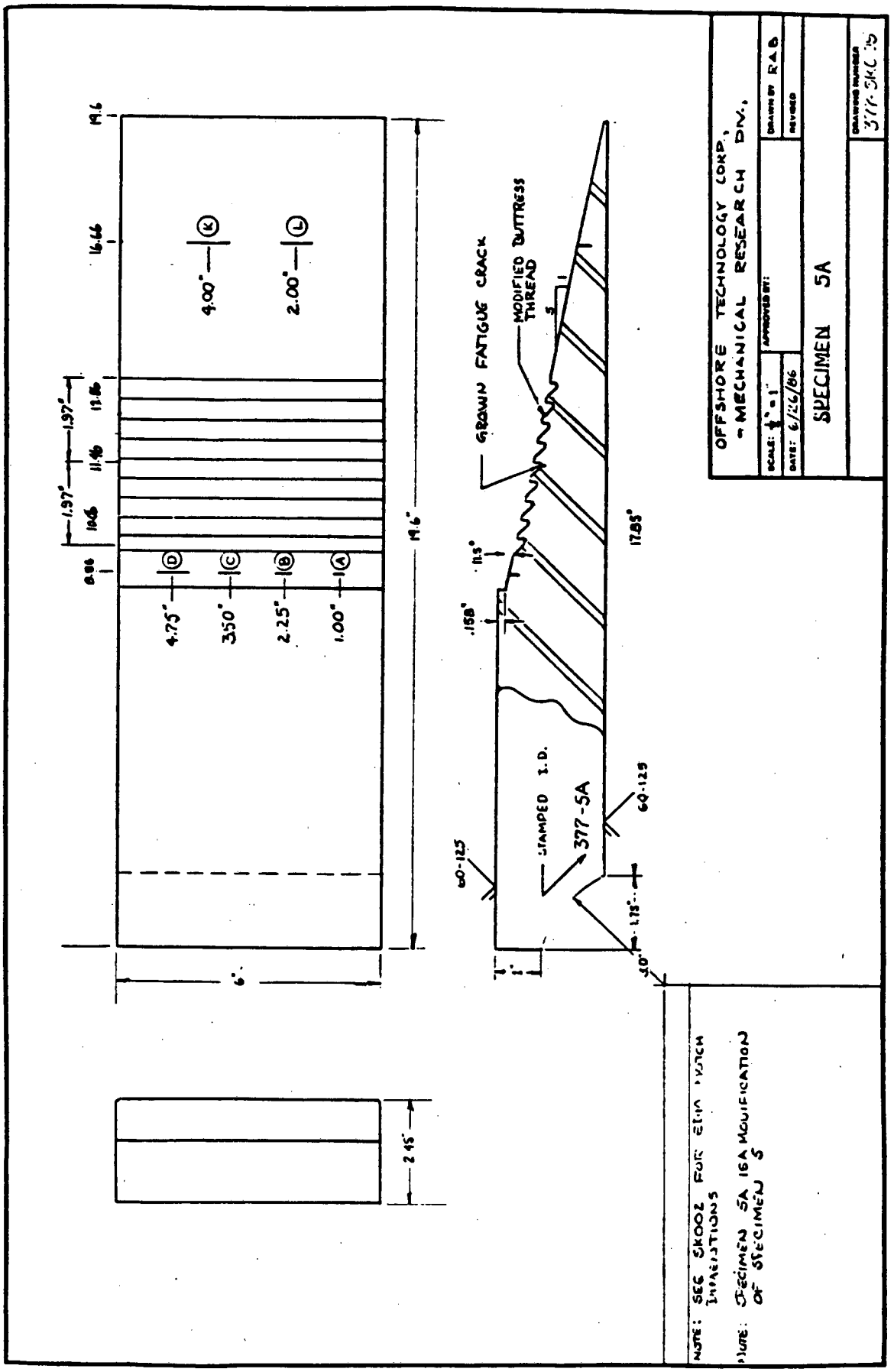
OFFSHORE TECHNOLOGY CORP.
- MECHANICAL RESEARCH DIV.
SPECIMEN 5A
SCALE: 1/2" = 1"
DATE: 6/26/86
DRAWN BY: R.A.B.
REVISED
APPROVED BY:
377-SHC-15
GROWN FATIGUE CRACK
MODIFIED BUTTRESS THREAD
STAMPED I.D.
377-5A
60-125
60-125
4.00"
2.00"
4.75"
3.50"
2.25"
1.00"
19.6"
17.85"
6"
2.15"
NOTE: SEE SHEET FOR EDM WORK INSTRUCTIONS
NOTE: SPECIMEN 5A IS A MODIFICATION OF SPECIMEN 5

Figure C-4

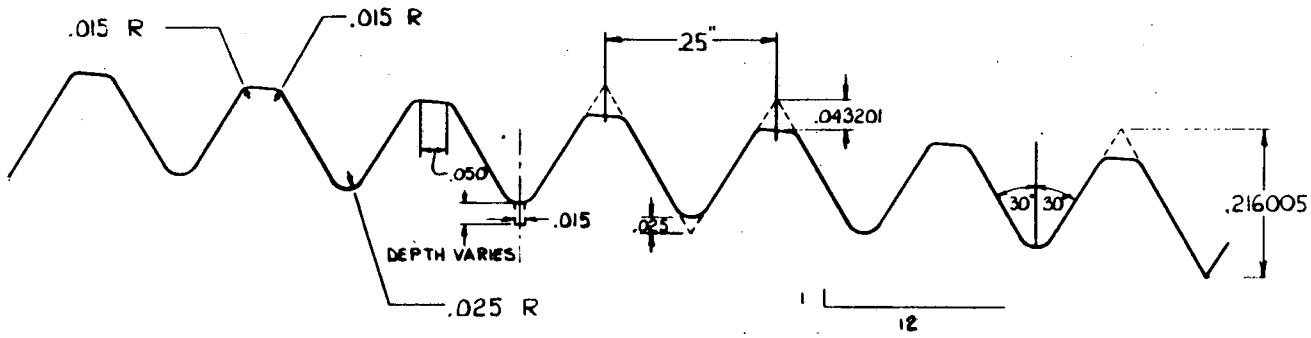

OFFSHORE TECHNOLOGY CORP., MECHANICAL RESEARCH DIV.,		
SCALE: 1 6.22	APPROVED BY:	DRAWN BY RAB
DATE: 7-14-86		REVISED
THREAD DETAIL SPECIMEN 6A		
MODIFIED API THREAD		DRAWING NUMBER 377-5k012

Figure C-5

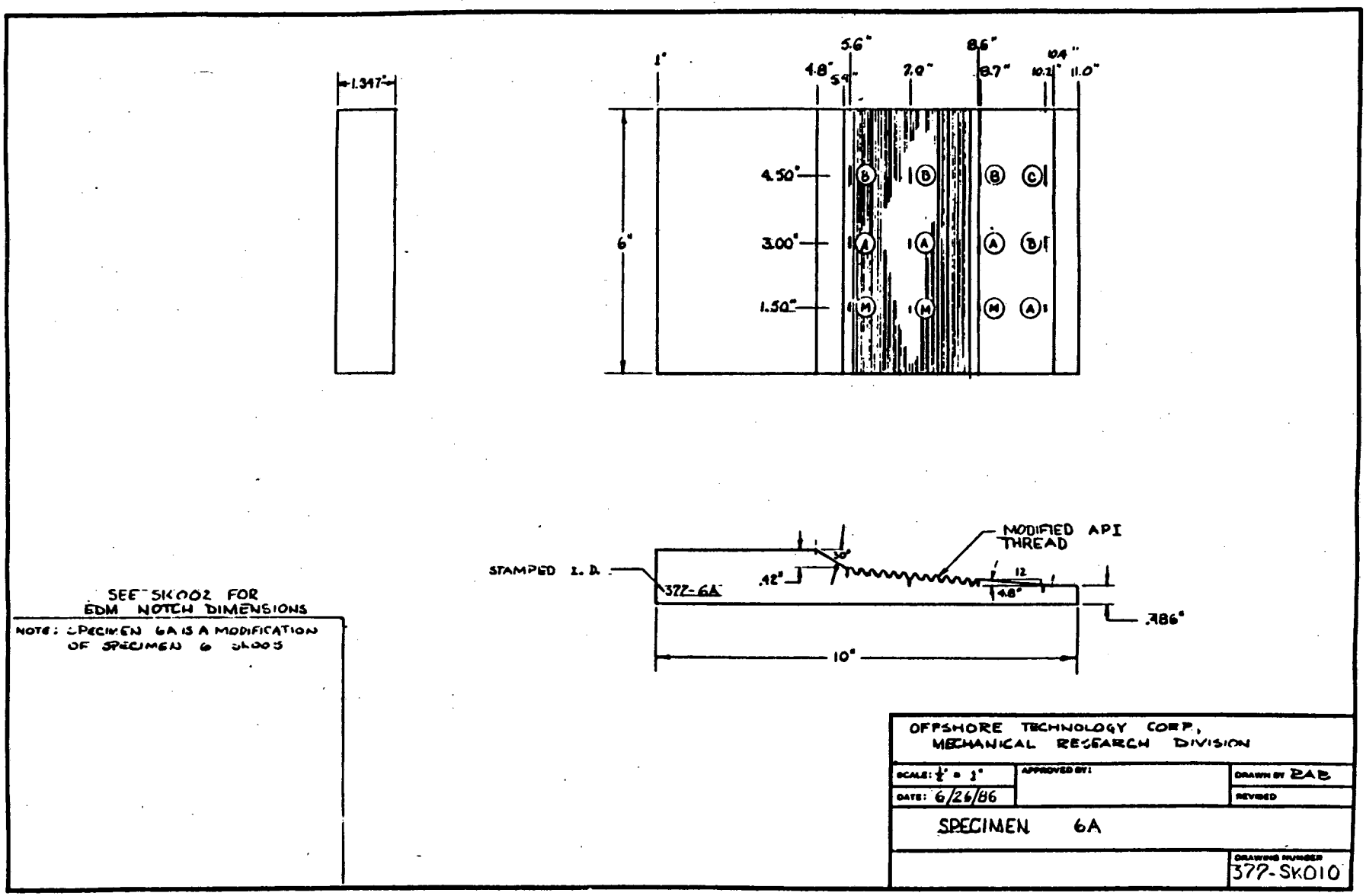
1.347"
1"
4.8"
5.6"
5.9"
7.0"
8.6"
8.7"
10.4"
10.7"
11.0"
6"
4.50"
3.00"
1.50"
B
A
M
C
STAMPED I. D.
377-6A
.42"
30°
MODIFIED API THREAD
12
4.8"
.886"
10"
SEE SK002 FOR EDM NOTCH DIMENSIONS
NOTE: SPECIMEN 6A IS A MODIFICATION OF SPECIMEN 6 SK005
OFFSHORE TECHNOLOGY CORP.
MECHANICAL RESEARCH DIVISION
SCALE: 1/2" = 1"
APPROVED BY:
DRAWN BY EAB
DATE: 6/26/86
REVISED
SPECIMEN 6A
DRAWING NUMBER
377-SK010

Figure C-6

APPENDIX D

Marine Growth Study

APPENDIX D

MARINE GROWTH STUDY

Test Specimens

Two test samples were subjected to biofouling by being submerged for one year on a NOSC test tower one mile offshore from Mission Bay, San Diego, California. The two specimens (later designated A and B) were fabricated from 4340 steel according to Figure D-1 (SK006). The samples were coated with epoxy to protect all but surface A (see Figure D-1) from biofouling. The specimens as they appeared following retrieval from the ocean and delivery for scanning is shown in Figure D-2 and D-3. Figure D-3 shows a grid marker used for locating data acquisition points on the specimens. Figure D-4 is a sketch of the growth on each specimen. Specimen B contained more long, stringy growth than specimen A. Cleaning sequence of the marine biofouled specimens is listed in Table D-1.

Figure D-5 shows plastic scraping of specimen B and the residual. Plastic scraping is not a very difficult task. The main barnacle bodies are removed although their adherent residual remains. Close observations show that some fine grasses remain. Figure D-6 shows bristle brush cleaning of specimen B. The bristle removes much of the fine grass left by the plastic scraper. Figure D-7 shows wire brushing of specimen B. The brushing removes all but the adherent barnacle residual. The wire brushing also scores the surface leaving it rough. Figure D-8 shows water jet cleaning of specimen A. The water jet was 5000 psi. The surface condition is similar to plastic scraping and bristle brushing but the main body of the barnacles are not removed. Figure D-9 shows sandblasting of specimen A. The surface is roughened and, with time, the barnacle bodies are slowly eaten away. The figure shows a barnacle in the lower right being blasted, but removal was very slow.

At each cleaning step measurements were made of the acoustic response in various configurations. Table D-2 lists the experiments performed. The primary experiments measured the effect of the marine growth and the removal method with respect to straight beam transmission into the part and reflection from back surfaces, and with respect to angle beam measurements from notch defects. Measurements were made using 2.25 MHz and 5 MHz, 0.5 inch diameter transducers although experiments 12 through 14 used other transducers to test the ability to penetrate marine growth.

Straight Beam Measurements

Figure D-10 shows the geometry for the straight beam measurements. Figure D-11 shows the test set up. Measurements were taken from the growth side and from the inside (clean surface representing the inside of a possible tension leg configuration). The straight beam measurements looked at the front surface and back surface signal strengths to evaluate the ability to penetrate the biofouling. Table D-3 lists the general behavior of the signal response as a function of cleaning. Table D-4 lists conclusions about the straight beam measurements.

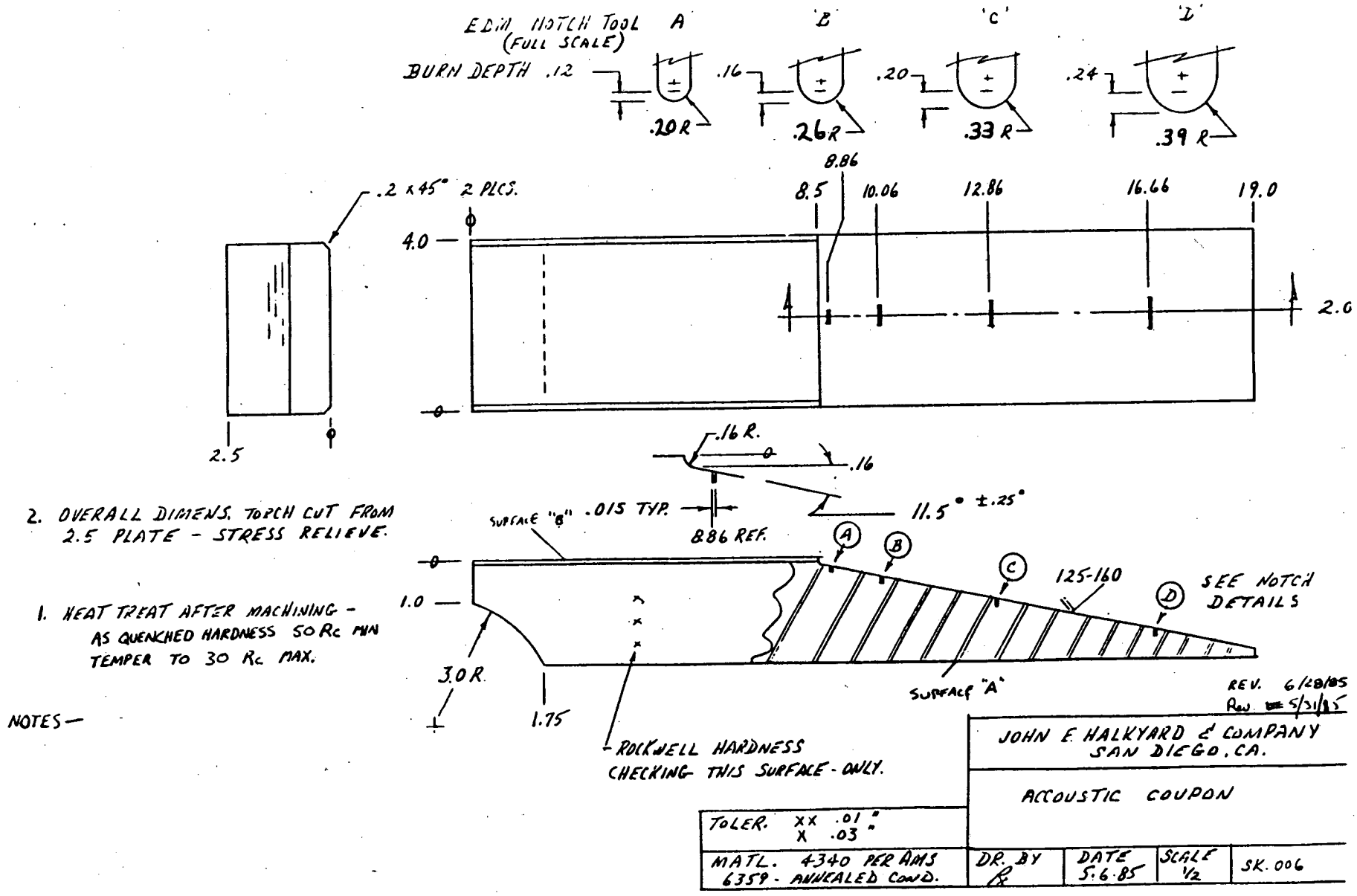

Figure D-1 Marine Growth Test Specimen Drawing

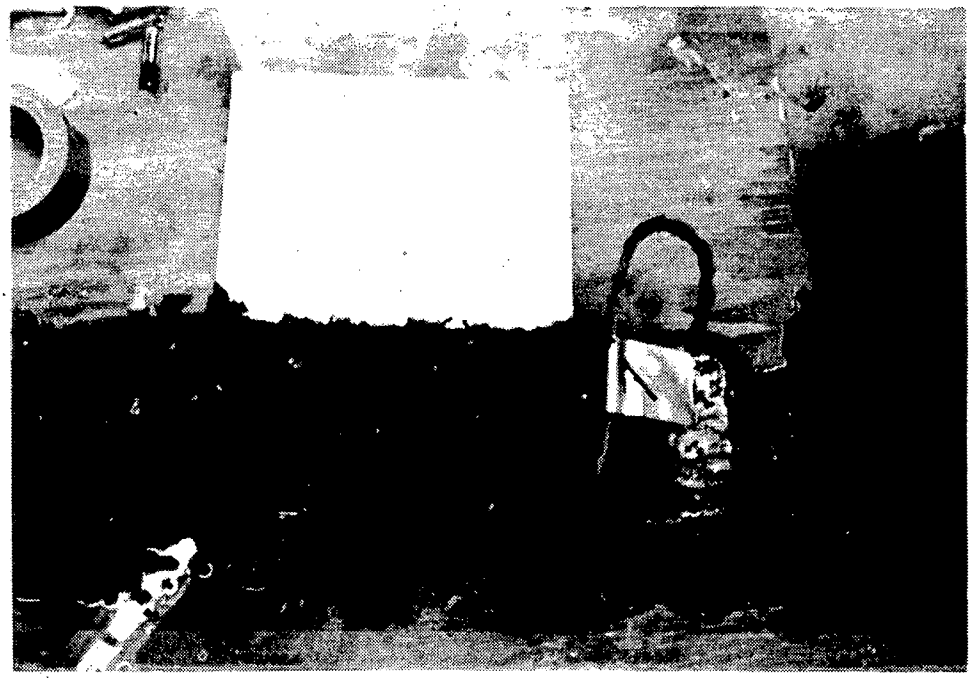

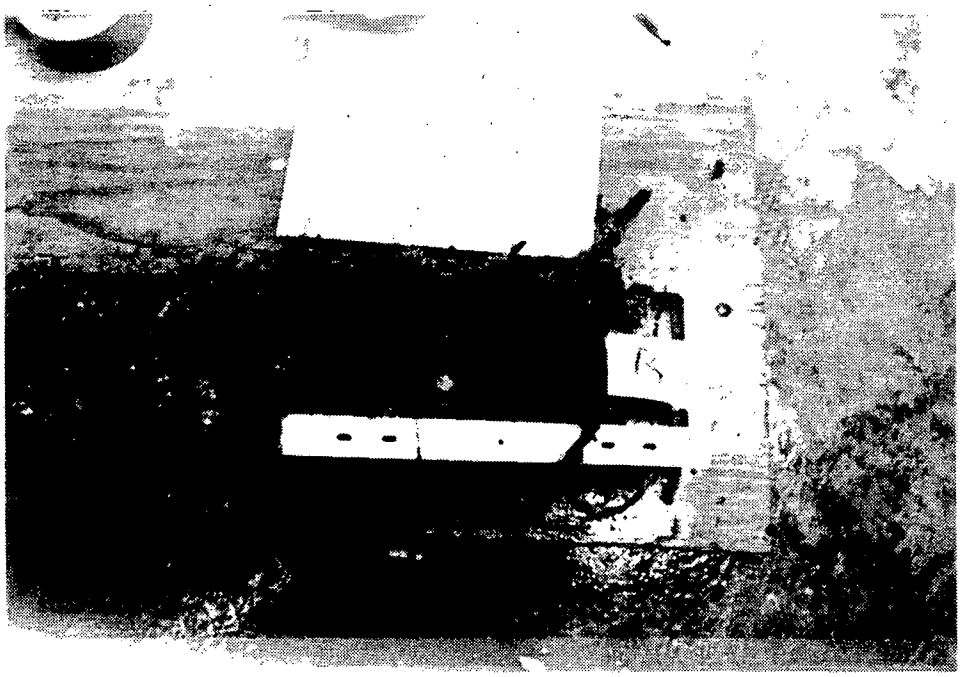

Figure D-2. Marine biofouled test samples A and B as received.

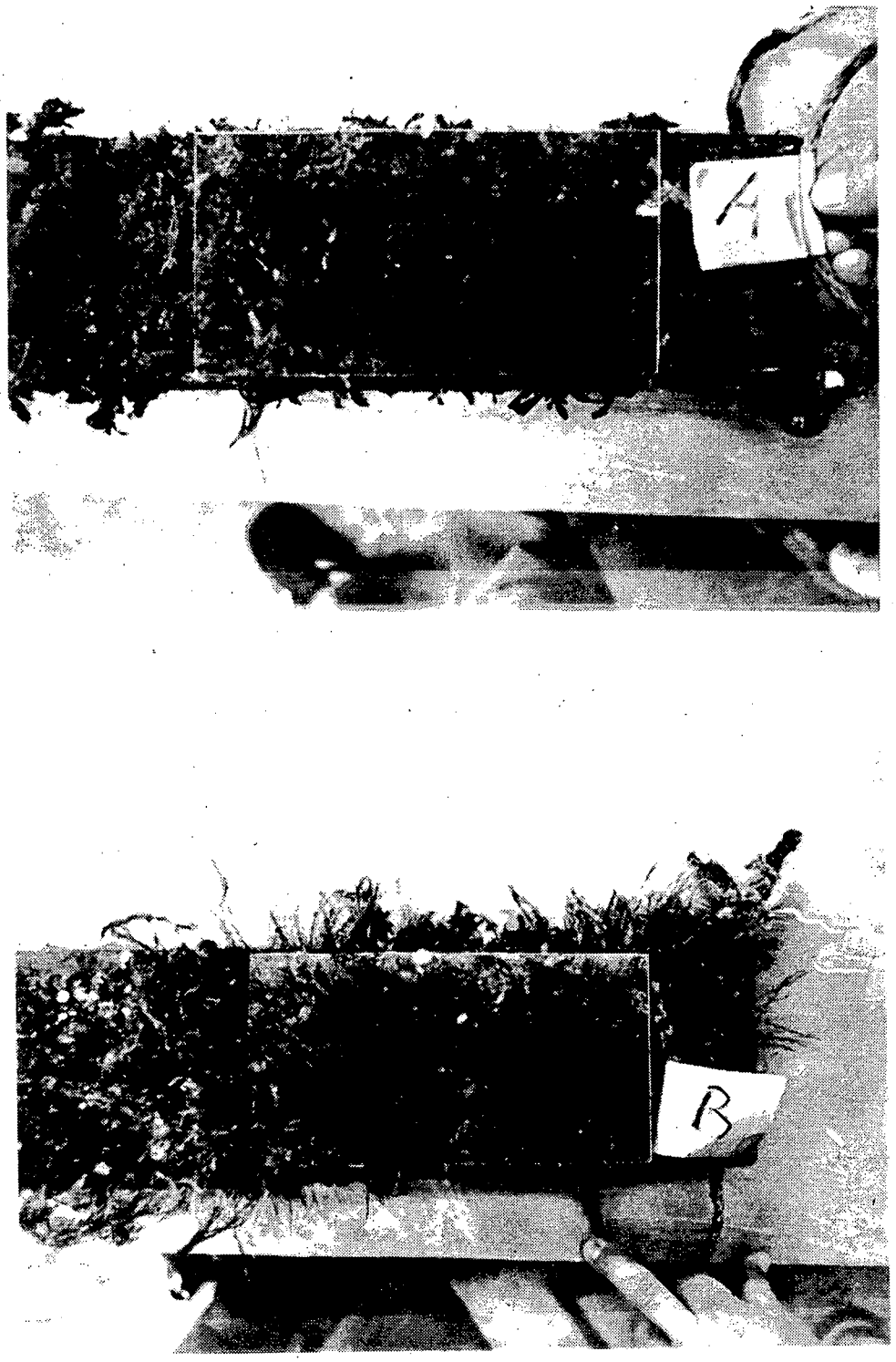

Figure D-3. Test samples with location grid.

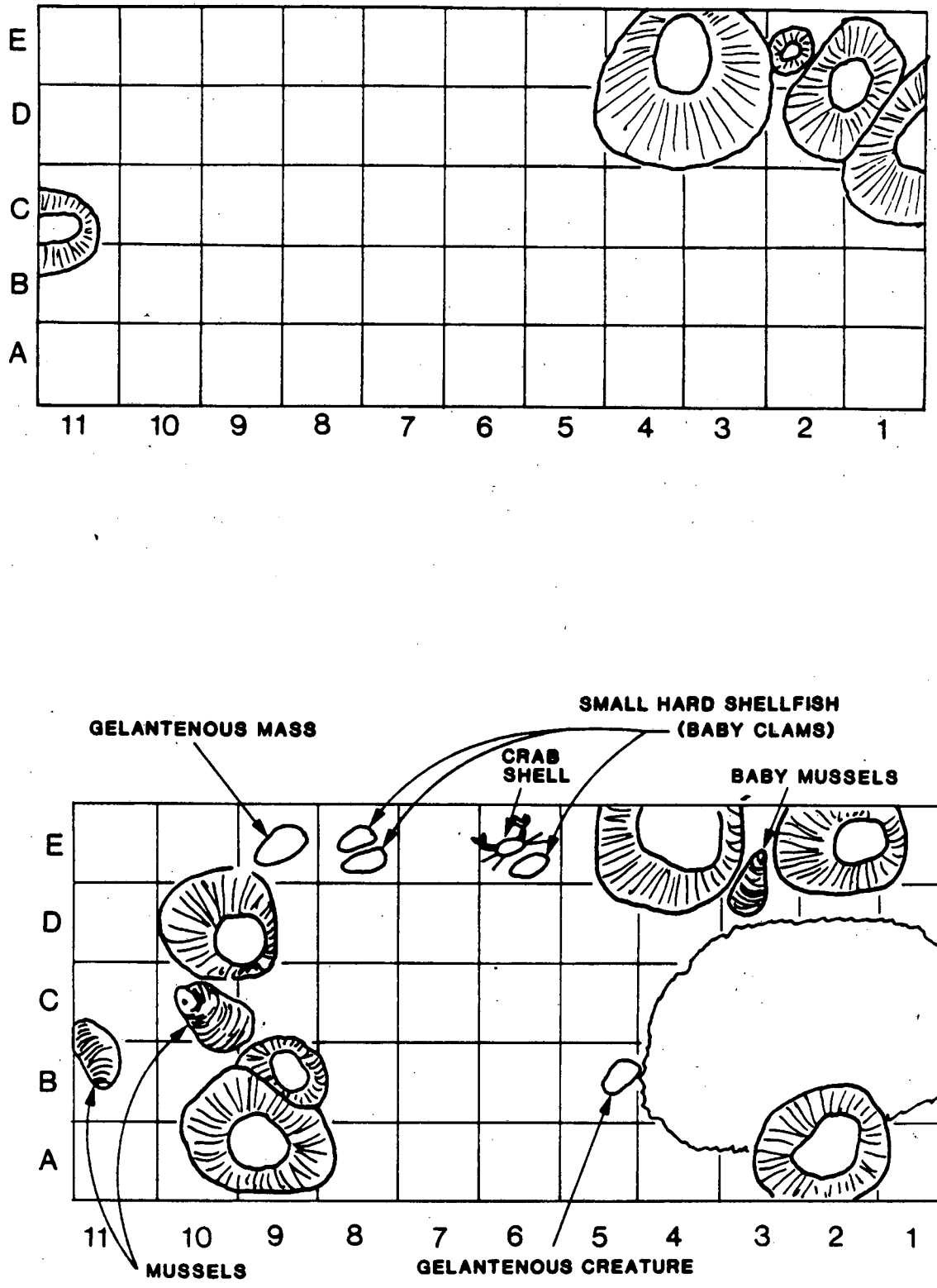

Figure D-4 Sketch of Growth Patterns on Test Specimens

TABLE D-1

CLEANING SEQUENCE FOR SPECIMENS

Steps	Specimen A	Specimen B
1	As received	As received
2	Remove epoxy coating	Remove epoxy coating
3	Use water jet (5000 psi)	Use plastic scraper
4	Use sand blaster	Use bristle brush
5		Use wire brush

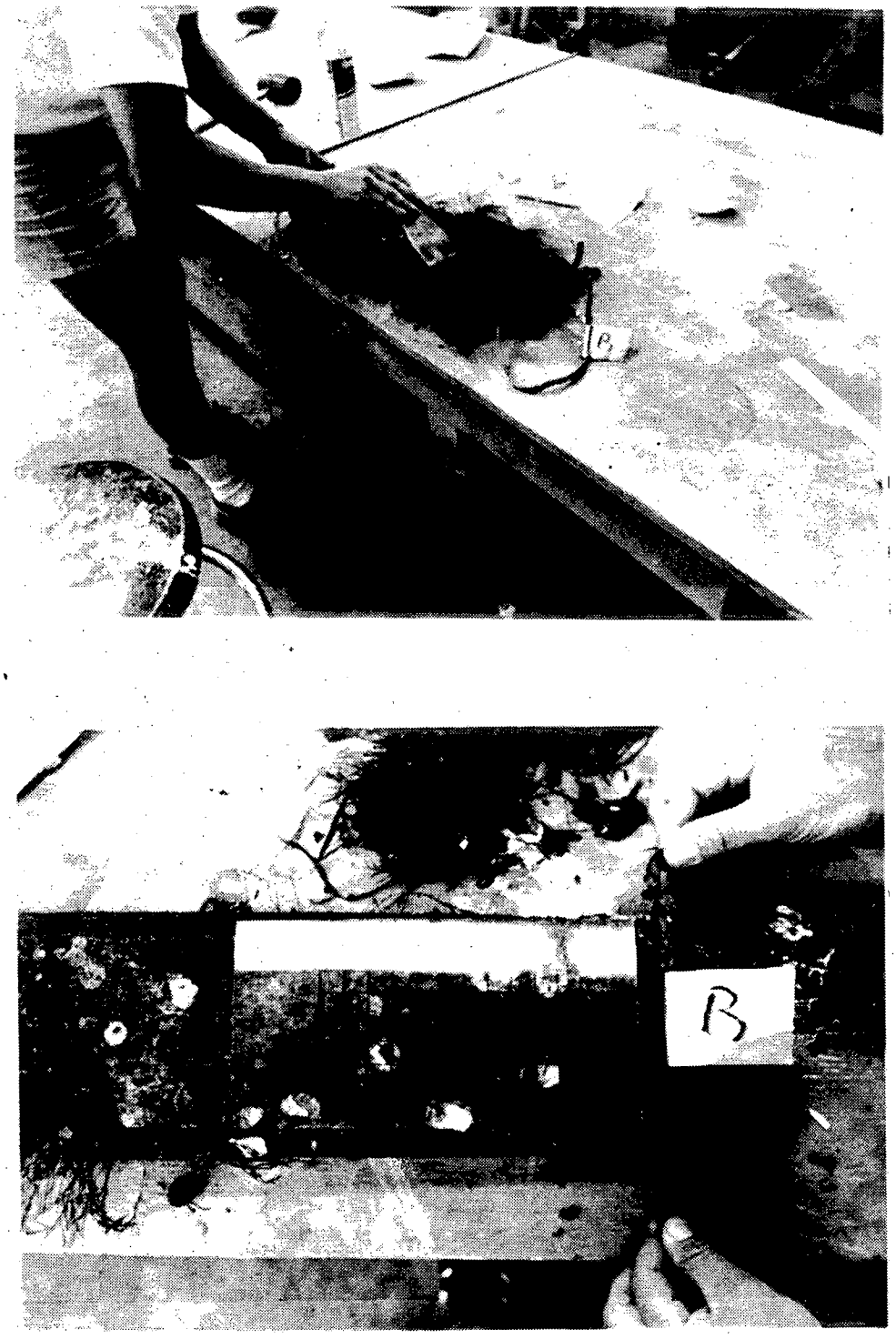

Figure D-5. Plastic scraper cleaning of specimen B.

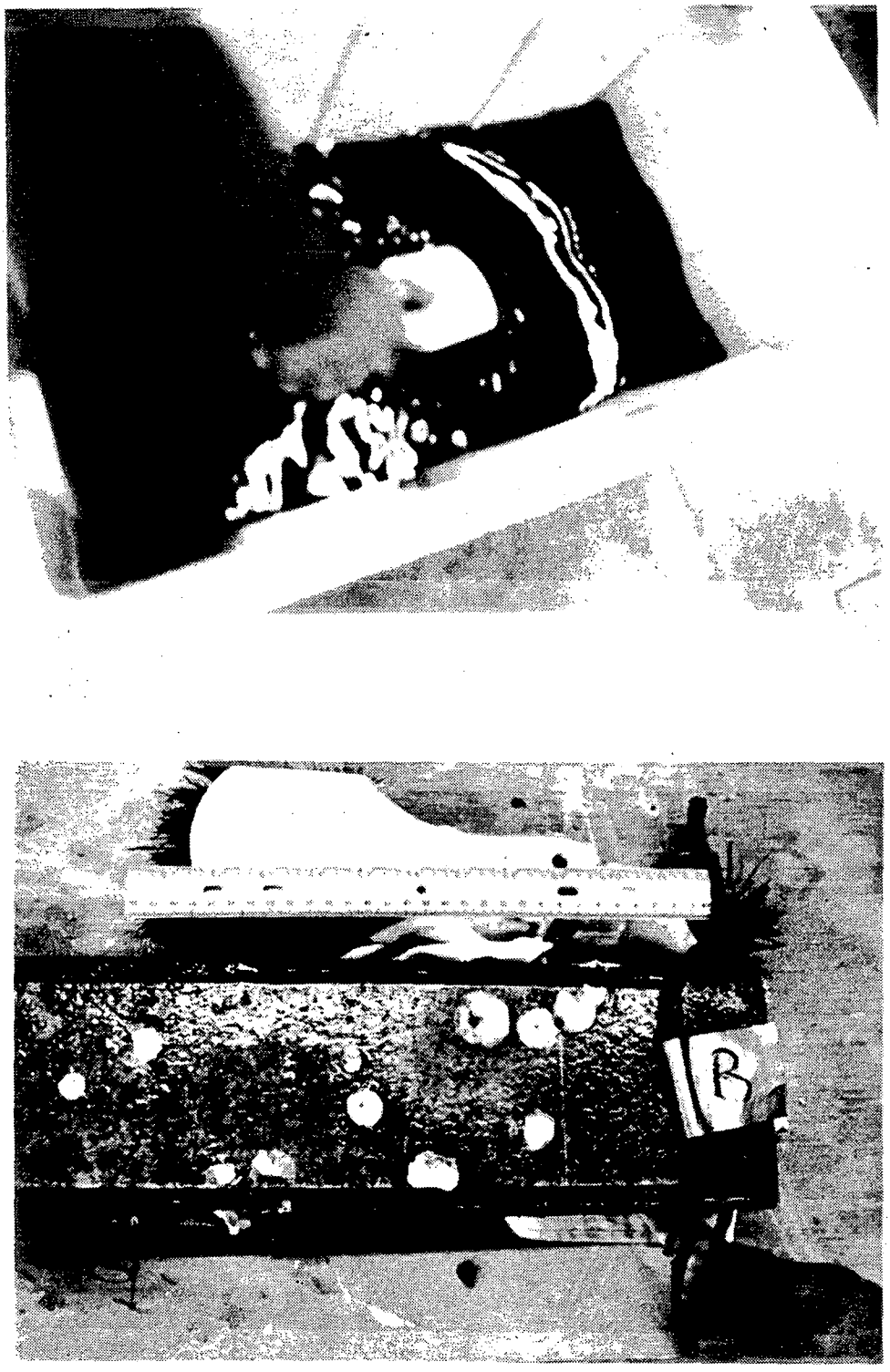

Figure D-6. Bristle brush cleaning of specimen B.

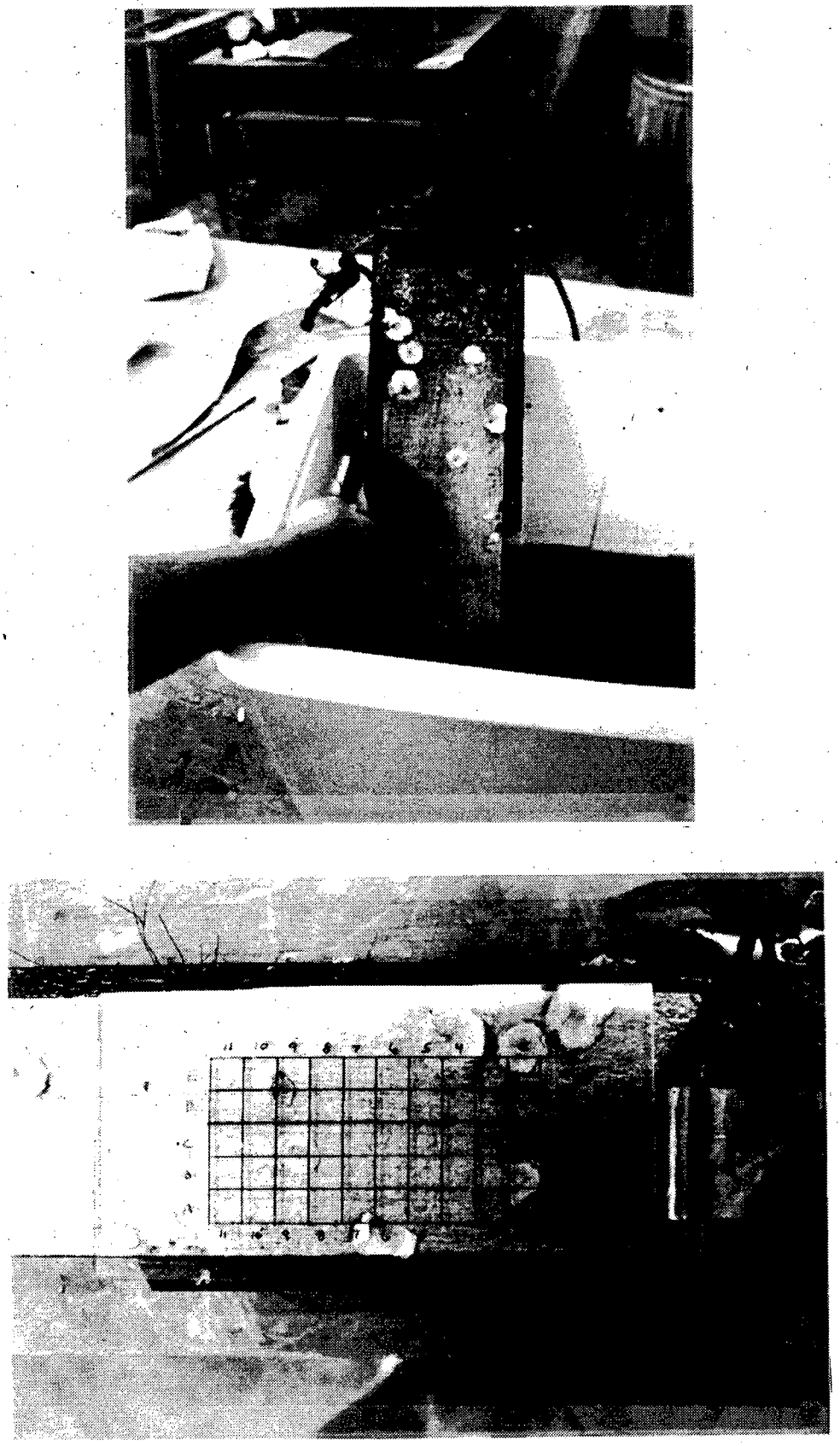

Figure D-7. Wire brush cleaning of specimen B.

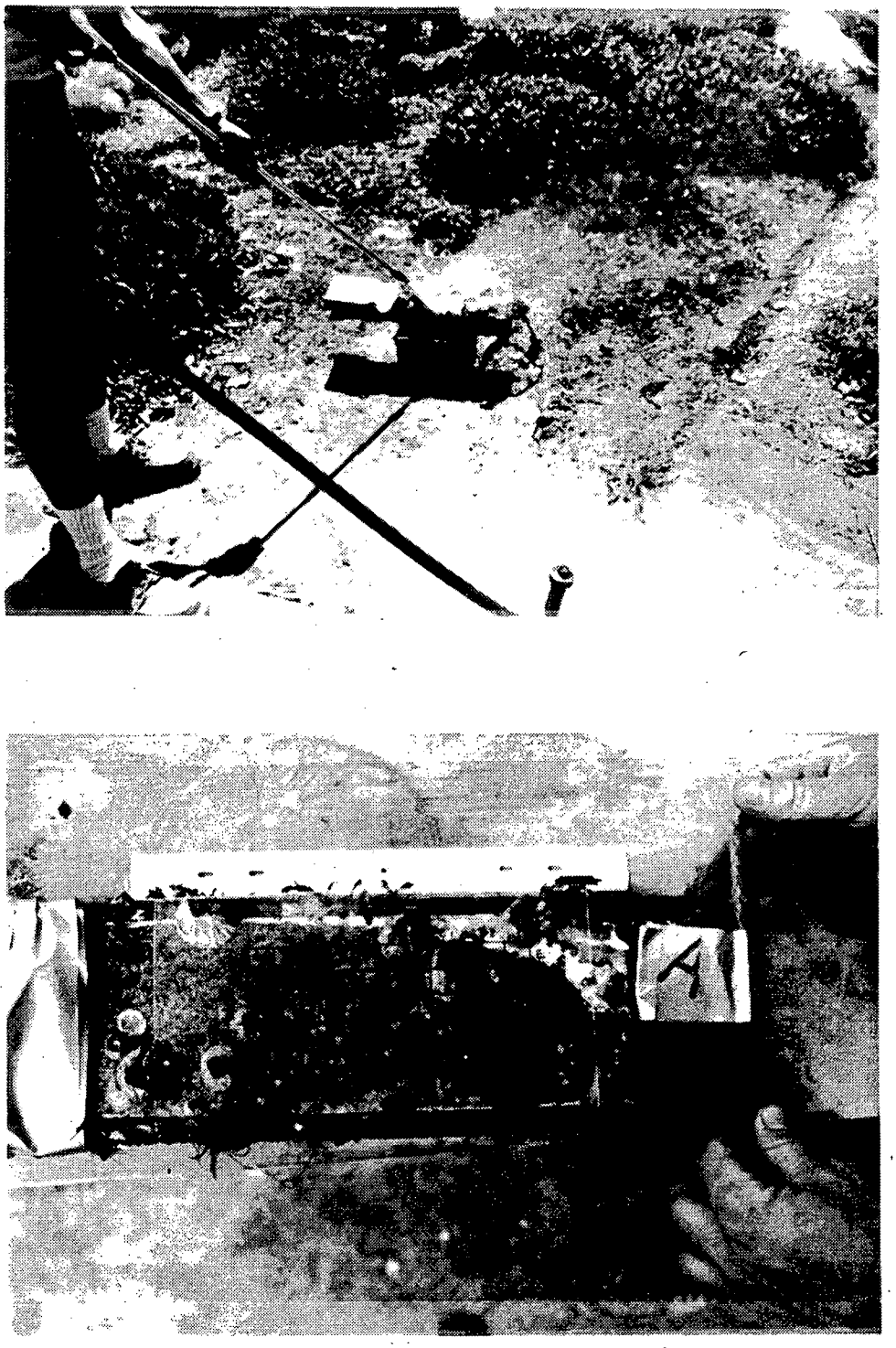

Figure D-8. Water jet cleaning of specimen A.

Figure D-9. Sandblasting of specimen A.

TABLE D-2

Experiment/ Specimen	Ultrasonic Frequency	Beam Orientation to Specimen	Surface Condition	
1A	2.25 MHz - 1/2 in. dia.	Growth side	Undisturbed growth	Straight beam surface and back echo response
2A	5 MHz, 1/2 in. dia.	Growth side	Undisturbed growth	Straight beam
3B	2.25	Growth side	Undisturbed growth	Straight beam
4B	5	Growth side	Undisturbed growth	Straight beam
5A	2.25	Growth side	Epoxy removed	Straight beam
6A	2.25	Inside	Epoxy removed	Straight beam
7A	2.25 and 5	Inside	Epoxy removed	Angle beam on flaws
8A	5	Inside	Epoxy removed	Straight beam
9B	2.25 and 5	Inside	Epoxy removed	Angle beam on flaws
10B	2.25	Inside	Epoxy removed	Straight beam
11B	5	Inside	Epoxy removed	Straight beam
12A	2.25 MHz, 3/4 in. dia.	Growth side	Epoxy removed	Straight beam
13A	1 MHz, 3/4 in dia.	Growth side	Epoxy removed	Straight beam
14A	2.25 MHz, 1 in. dia., 4 in. focal length	Growth side	Epoxy removed	Straight beam
15B	2.25 and 5	Inside	Plastic scraper	Angle beam on flaws
16B	5	Inside	Plastic scraper	Straight beam
17B	2.25	Inside	Plastic scraper	Straight beam
18A	2.25	Inside	Water jet	Straight beam

TABLE D-2 (cont'd.)

19A	2.25 and 5	Inside	Water jet	Angle beam on flaws
20B	2.25	Growth side	Plastic scraper	Straight beam
21B	2.25	Growth side	Plastic scraper	450 shear at edge
22B	5	Growth side	Plastic scraper	Front and back echoes
23B	5	Growth side	Plastic scraper	450 shear at edge
24B	2.25 and 5	Growth side	Plastic scraper	Angle beam at edge
25B	2.25	Growth side	Bristle brush	Straight beam
26B	2.25	Growth side	Bristle brush	450 shear at edge
27B	5	Growth side	Bristle brush	Straight beam
28B	5	Growth side	Bristle brush	450 shear at edge
29B	2.25 and 5	Growth side	Bristle brush	Angle beam on flaws and plot of strength vs. angle at 2.25
30A	2.25	Growth side (inside machined)	Water jet	Straight beam 450 shear at edge
31A	5	Growth side	Water jet	Straight beam Angle beam on flaws
32A	2.25	Growth side	Water jet	Angle beam on flaws
33A	2.25	Inside	Water jet	Straight beam Angle beam on flaws
34A	5	Inside	Water jet	Angle beam on flaws

TABLE D-2 (cont'd.)

35A	2.25 and 5	Inside	Water jet	Response as a function of angle
36B	2.25	Growth side	Wire brush	Straight beam
37B	5	Growth side	Wire brush	Straight beam

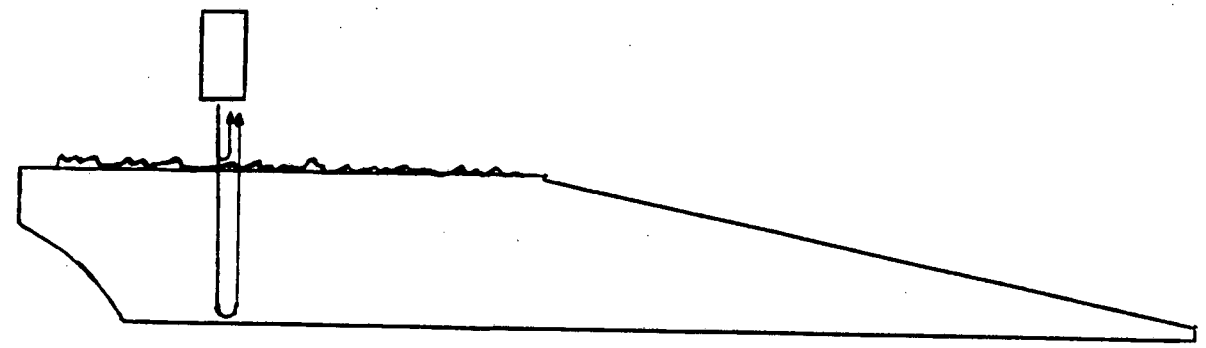

(a)

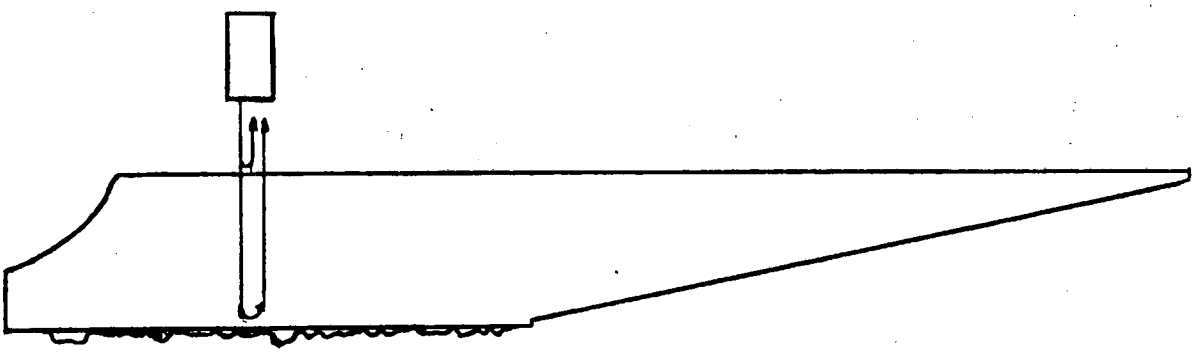

(b)

Figure D-10. Geometry for straight beam measurements; a) growth side, b) inside.

a)

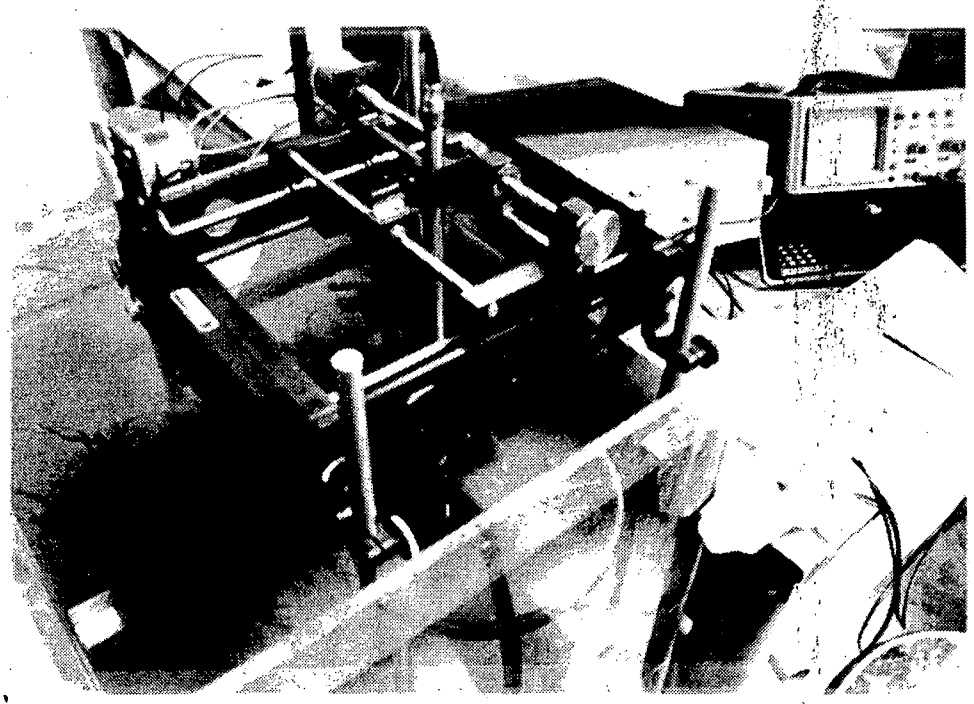

b)

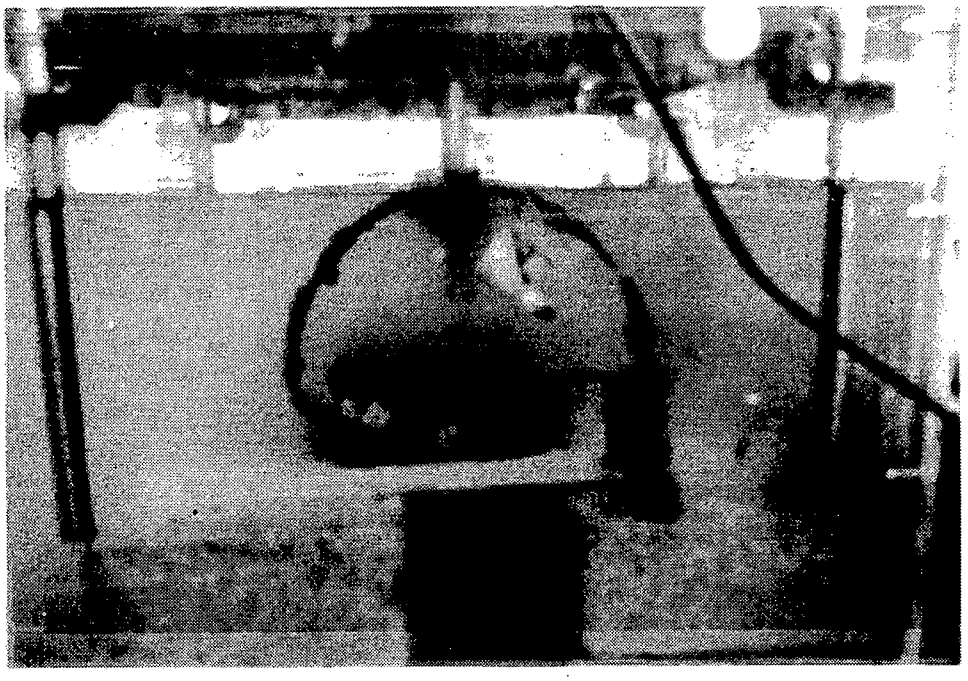

Figure D-11. Test set up for ultrasonic measurements; a) positioning over specimen B on undisturbed growth side, b) positioning over specimen A for inside inspection.

The signals listed in Table D-3 did not include variations due to barnacles. At barnacles the signals could be lost entirely. Figure D-12 shows typical signals and the complete loss of back signal at a barnacle. The readings of Table D-3 indicate that for outside inspection the grassy material should be removed by plastic scraping and bristle brushing, or water jet cleaning. Wire brushing was not deemed to be particularly useful and actually scratched the surface. When a plastic scraper is used, it is important to follow with the bristle brush to remove fine grassy residual which affected the 2.25 MHz signal significantly.

The inside surface condition was also of poorer quality than had been tested in earlier nonfouled specimens. Serious surface marks were present that may have caused problems in obtaining a consistent reference for later angle beam studies. For specimen A the inside surface was later machined to improve the reference.

Barnacles were removed by the plastic scraper, but left adherent residual deposit. The water jet, at 5000 psi, could not remove the barnacles. In the water jet case the barnacle presence naturally severely limited inspection at their locations. In the plastic scraper case, the residual material left a ring which affected the response over that region. Scanning across the barnacle residual caused both the front and back echo signal to fall in strength. The magnitude of the variation is a strong function of position over the barnacle and is not necessarily consistent with frequency. In general, both front and back fall to less than half their values at 2.25 MHz and to less than a quarter of their values at 5 MHz.

An unusual discovery in scanning over the barnacle residual was an increased back signal response over the center of the barnacle while the front surface response is still reduced. This can be understood if the barnacle ring is acting as a lens to focus the acoustic energy. This is an interesting effect but of no obvious value.

The average size of the barnacles was approximately 2 cm diameter, and with significant back surface signal losses occurring over the outer 0.4 cm of the diameter. This is approximately 2 cm^2 of lost inspection region per barnacle. Considering the two samples contained eight barnacles over a combined 850 cm^2 area, this represents about a 2% loss of inspection due to barnacle residual.

Scanning from the inside surface it was found that the back surface reflected signal experienced a reduction in strength at the location of barnacles. The barnacle presence appeared to reduce the echo signal by approximately 30%.

Angle Beam Measurements

Angle beam measurements using shear waves were tested from both the inside and growth side. The inside inspection used a bounce path inspection shown Figure D-13.

The flaws present in the biofouled samples were thumbnail EDM notches of one to three depth to length ratio. The notches labeled in Figure 1 were of depths: A = 3 mm, B = 4 mm, C = 5 mm, and D = 6 mm. The measured response from the notches as a function of cleaning are shown in Figures D- 14 through

TABLE D-3

GENERAL RESPONSE OF STRAIGHT BEAM MEASUREMENTS
AS A FUNCTION OF CLEANING

Specimen	Condition	Orientation	Frequency	Front Surface (relative signal strength)	Back Surface (relative signal strength)
A	Epoxy removed	Growth side	2.25	200-450	15-25
A	Water jet cleaned	Growth side	2.25	500-700	35-45
A	Undisturbed growth	Growth side	5	20-40	1-3
A	Water jet cleaned	Growth side	5	100-300	15-25
A	Undisturbed growth	Inside	2.25	800	25-40
A	Water jet	Inside	2.25	800	24-40
A	Water jet and machined	Inside	2.25	880	38-44
A	Undisturbed growth	Inside	5	500-600	34-40
A	Water jet and machined	Inside	5	730	40-50
B	Undisturbed growth	Growth side	2.25	100-300	5-20
B	Plastic scraper	Growth side	2.25	130-300	13-24
B	Bristle brush	Growth side	2.25	560-720	34-42
B	Wire brush	Growth side	2.25	540-620	32-38
B	Undisturbed growth	Growth side	5	10-80	1-8
B	Plastic scraper	Growth side	5	150-250	10-35
B	Bristle brush	Growth side	5	200-350	25-40
B	Wire brush	Growth side	5	100-300	20-30
B	Undisturbed growth	Inside	2.25	850-880	37-42
B	Plastic scraper	Inside	2.25	790-820	35-40
B	Undisturbed growth	Inside	5	690-740	30-50
B	Plastic scraper	Inside	5	550-700	30-40

TABLE D-4

CONCLUSIONS OF THE STRAIGHT BEAM MEASUREMENT

1. The reflected signal strength from the front and back surface increased significantly with cleaning when inspecting from growth side.

2. Water jet cleaning increased signal strengths when inspecting from growth side, by approximately a factor of 2 at 2.25 MHz and a factor of 10 at 5 MHz.

3 Plastic scraping did not appear to increase the 2.25 MHz response when inspection from the growth side but increased the 5 MHz response by a factor of 5 or 6.

4. Bristle brushing increased the 2.25 MHz response when inspecting from the growth side by a factor of 2 and the 5 MHz response by perhaps a factor of 1.5.

5. Wire brushing did not improve response when inspecting from the growth side and may have damaged surface to slightly decrease response.

6. Water jet cleaning and bristle brush cleaning, when inspecting from the growth side, showed generally equivalent responses.

7. Inspection from the inside did not demonstrate significant changes in response as a function of cleaning.

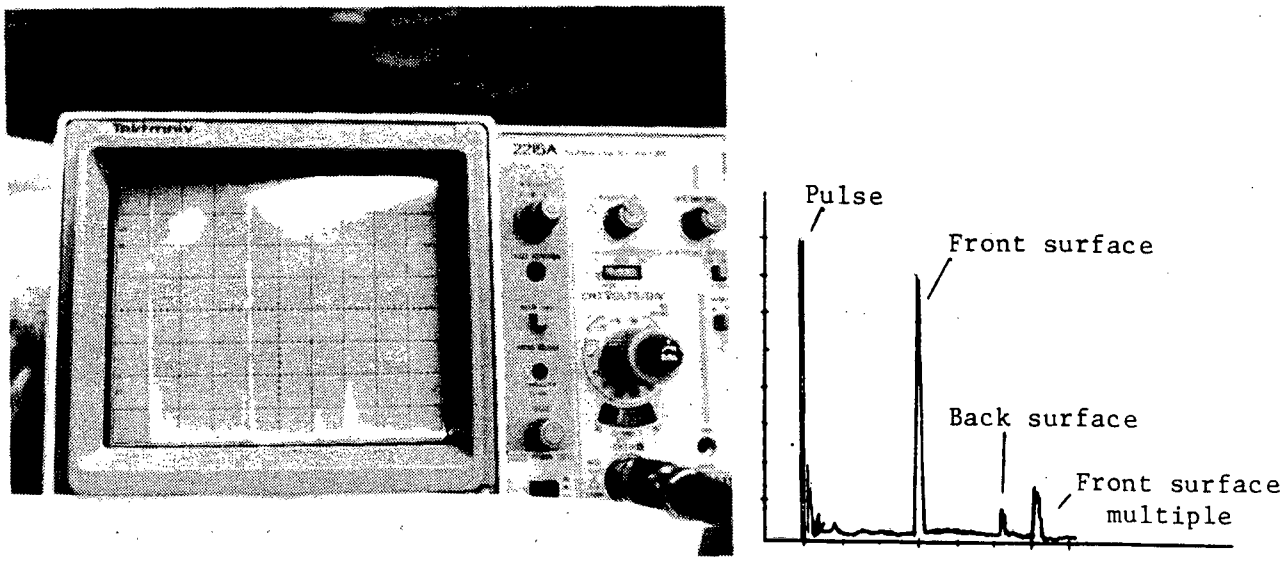

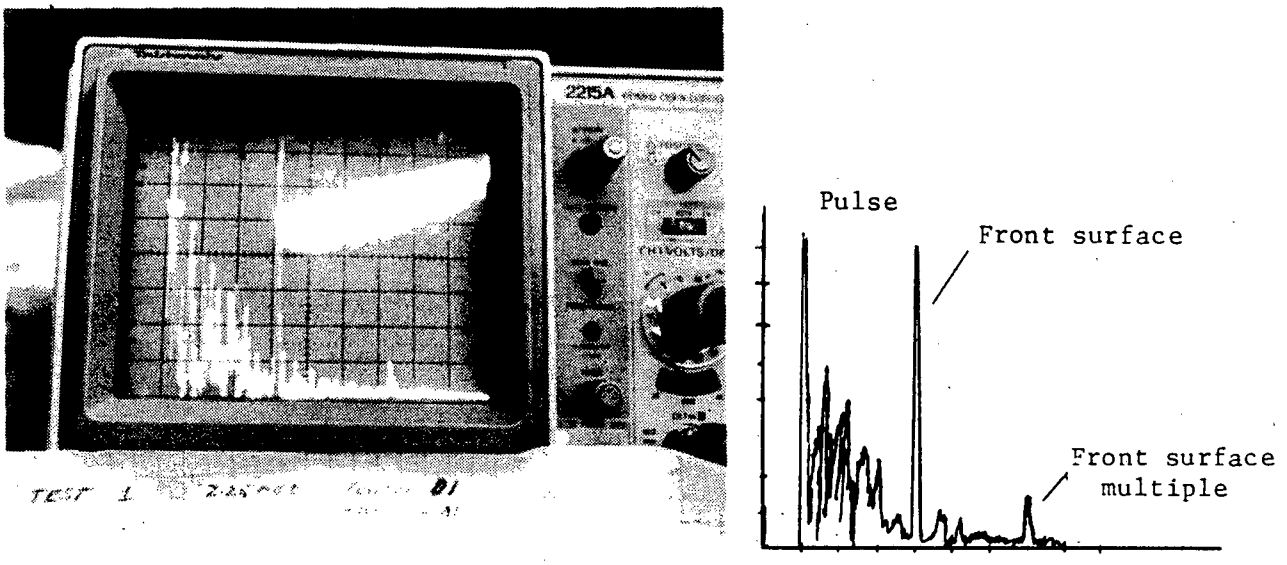

Figure D-12. Typical signals a) over soft marine growth, b) over a barnacle for growth side straight beam inspection. The signal is ten times the level for a), but the back surface signal is lost.

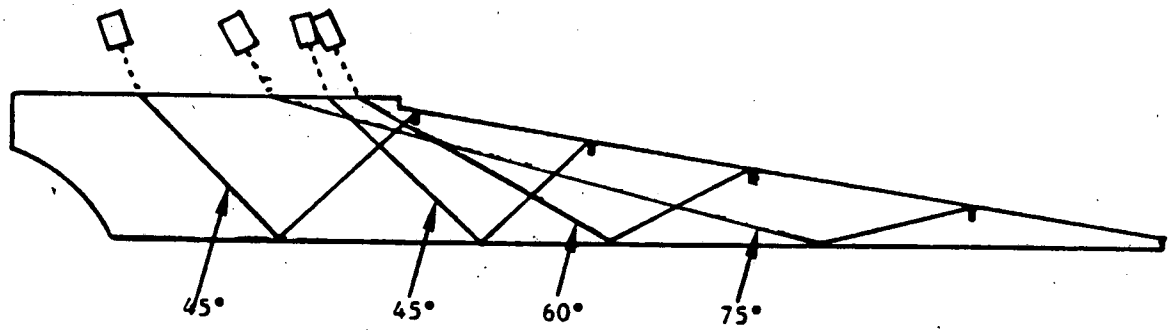

Figure D-13. Inspection configuration for inside angle beam inspection of notches.

D-17 for 2.25 and 5 MHz on specimens A and B for the inside inspection. The data taken on the fouled specimens are plotted as points. The line represent the average reading taken on unfouled specimens. These results show no consistent effect of the biofouling presence and cleaning on the signal. In the specimen A case the response signals increase with water jet cleaning, but a subsequent measurement following machining of the inside surface reduces this effect. Although the values do vary, in most cases they are not significantly different from the average from unfouled samples and are not consistently higher or lower than previous data. These tests did not necessarily involve a bounce at the specific location of a barnacle.

Measurements were taken using angle beams from the growth side to look at notches B and C with 45 degree and 60 degree beams. Notch B is 4 mm deep and notch C is 5 mm deep. The surface condition of the part caused the method of using a front surface reference signal to be inconsistent due to large variations. The amplified signal from the notches is therefore plotted in Figures D-18 and D-19. The 'unfouled' result is data taken from an SK001 sample that was not subjected to marine biofouling. These results indicate water jetting, or plastic scraping and bristle brushing, create a condition suitable for angle beam measurements. Measurements were not made with undisturbed growth because the signals were significantly inhibited in that case.

The angle beam measurement indicates that in this study, variations in response due to all factors appear to be greater than variations due to marine growth biofouling after water jetting or plastic scraping. The total factors involve the beam angle which plays a significant role in the response expected from a notch using shear wave angle beams. Figures D-20 through D-23 show the variation in signal response for inside inspection of notches B and C as a percent of the signal measured at 45 and 60 degrees. Figure D-24 shows a plot of calculated shear wave angle in the material vs. the transducer angle. Small changes in the transducer orientation can cause a much larger change in the shear wave angle in the material. Figure D-25 shows the response from notch C as a function of beam angle for growth side inspection. This was performed on specimen B after bristle brush cleaning at 2.25 MHz. The response is normalized to the response at 45 degrees.

Tests of the effect of the barnacle presence on bounce path measurements were tried. Figure D-26b shows this configuration. These tests were performed approximately eight months after the parts had been removed from sea water. With a 5MHz transducer, there was some evidence that the presence of the barnacle could reduce the return signal. Due to configuration problems, the tests were only run at 45 . The reduction was less than 6 dB (50%) and the signal itself varied by 6 dB over clear (no barnacle) regions. For 2.25 MHz there is less evidence of sensitivity for the barnacle. The conclusion is that the barnacle would not affect bounce path inspection at low energies (2.25 MHz) and may cause a slight loss <3 dB at higher frequency 5MHz. After approximately 15 months, the tests were repeated at 5 MHz on specimen A using C-scan images. Figure D-27 contains the results. In Figure D-27 the signal was gated on an echo after a bounce path skip over an area containing barnacles. No evidence of the barnacle pattern was found. When the gate was reset to the bounce surface, the barnacle pattern of Figure D-27b was imaged. This indicates that the angle beam is scattered in some relation to barnacle residual on the outside. A straight beam C-scan was also made over

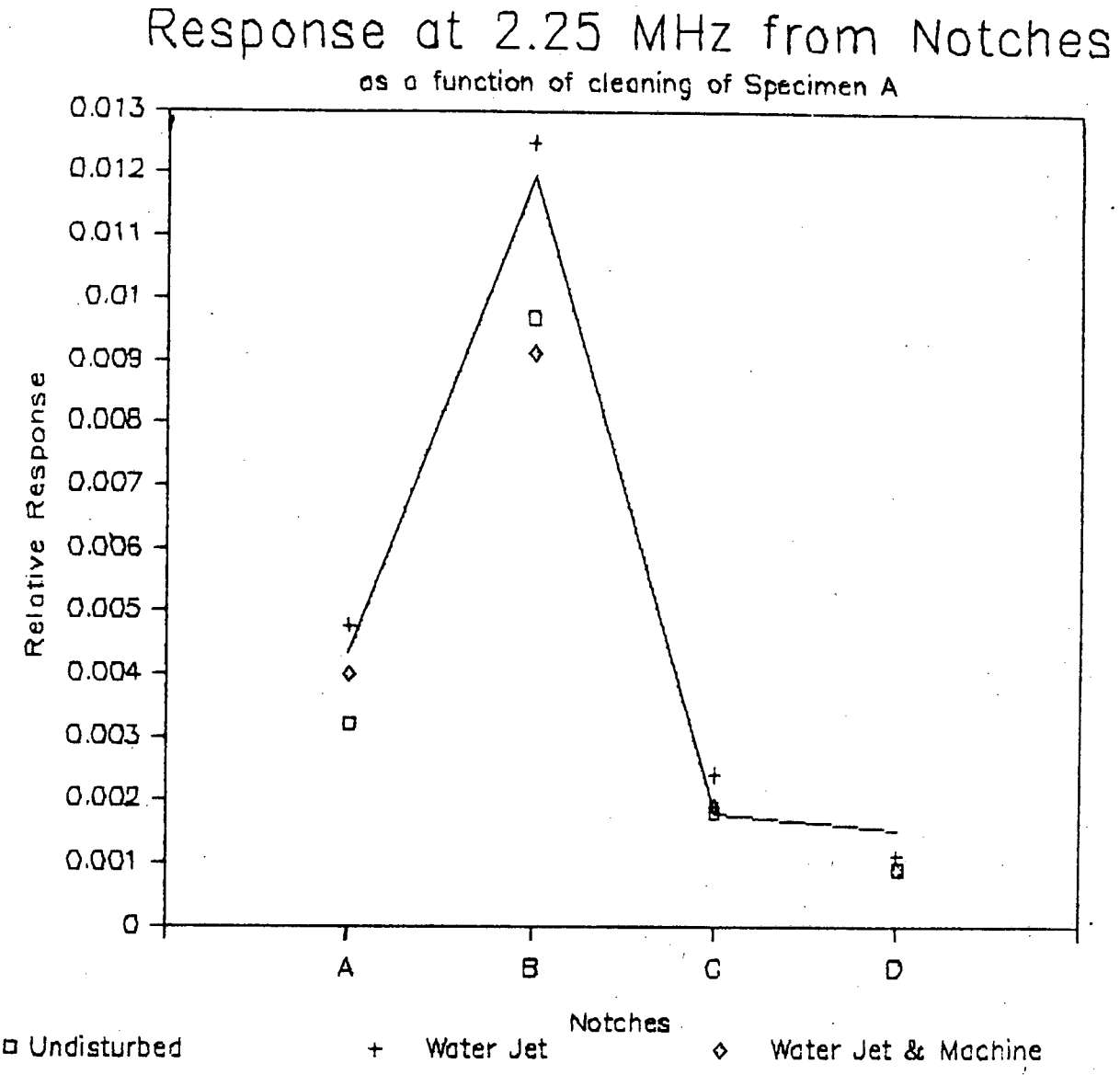

Figure D-14. Response as a function of cleaning. The solid line is the average value of notch response from an unfouled sample.

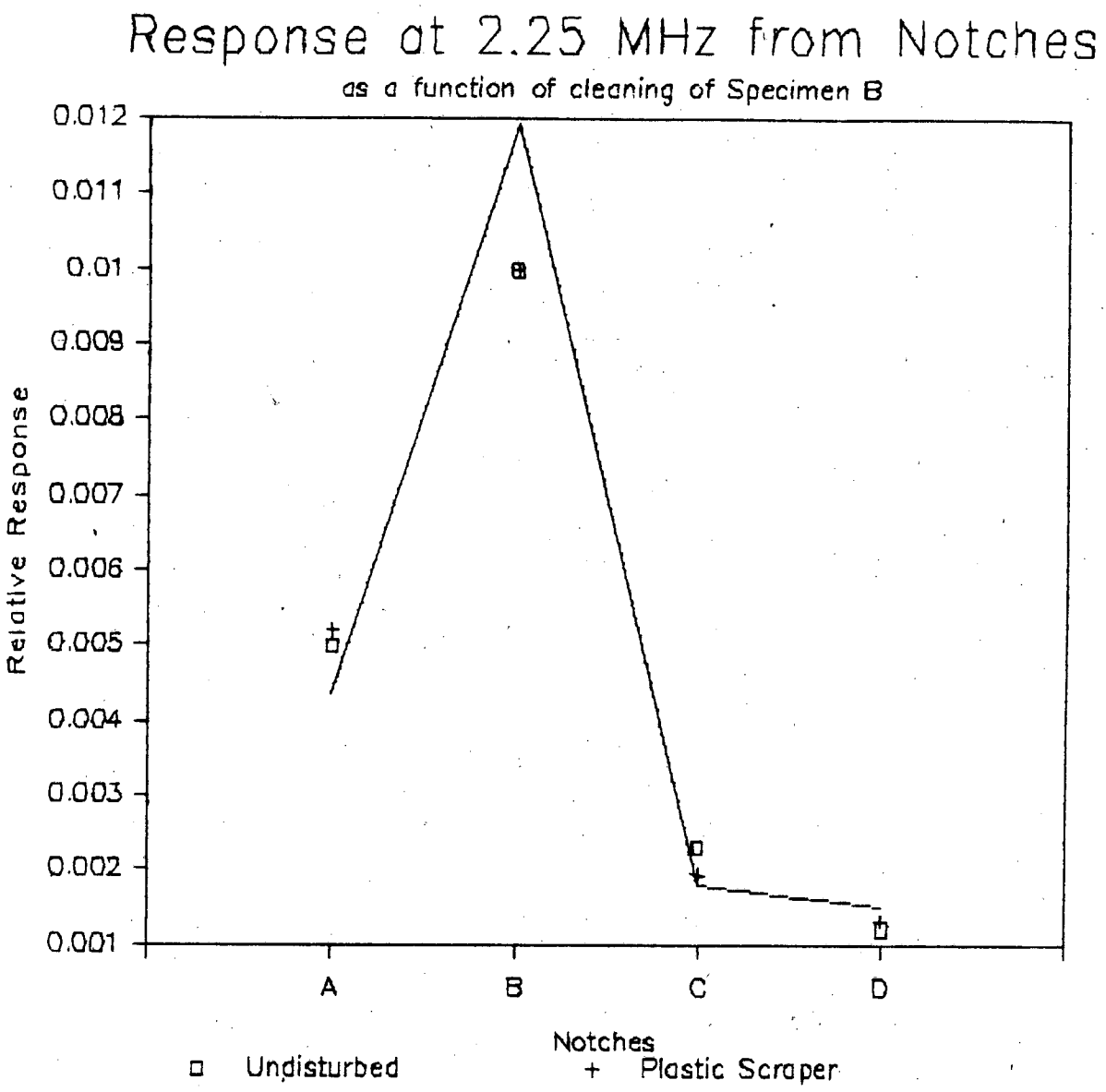

Figure D-15. Response as a function of cleaning. The solid line is the average value of notch response from an unfouled sample.

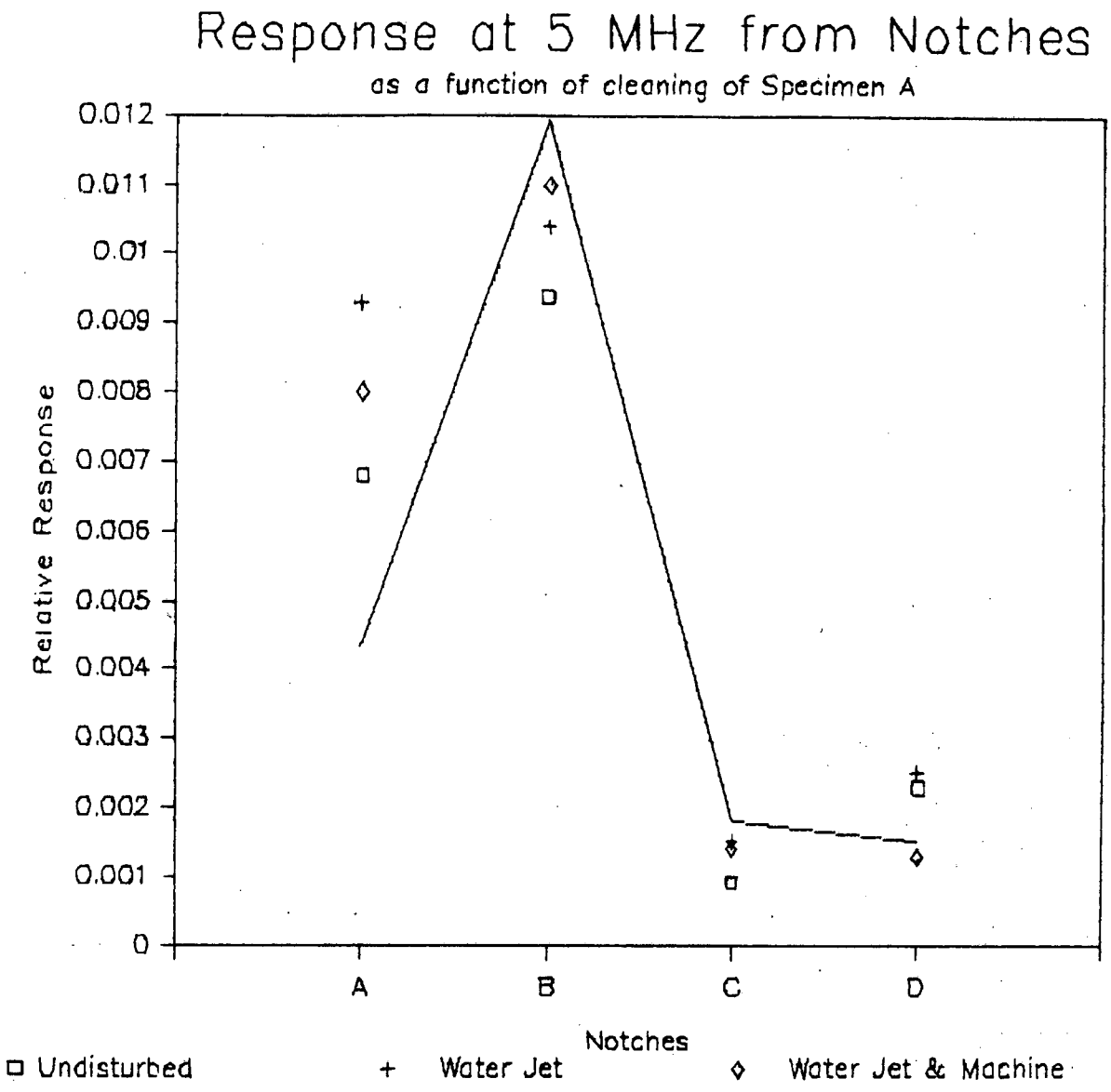

Figure D-16. Response as a function of cleaning. The solid line is the average value of notch response from an unfouled sample.

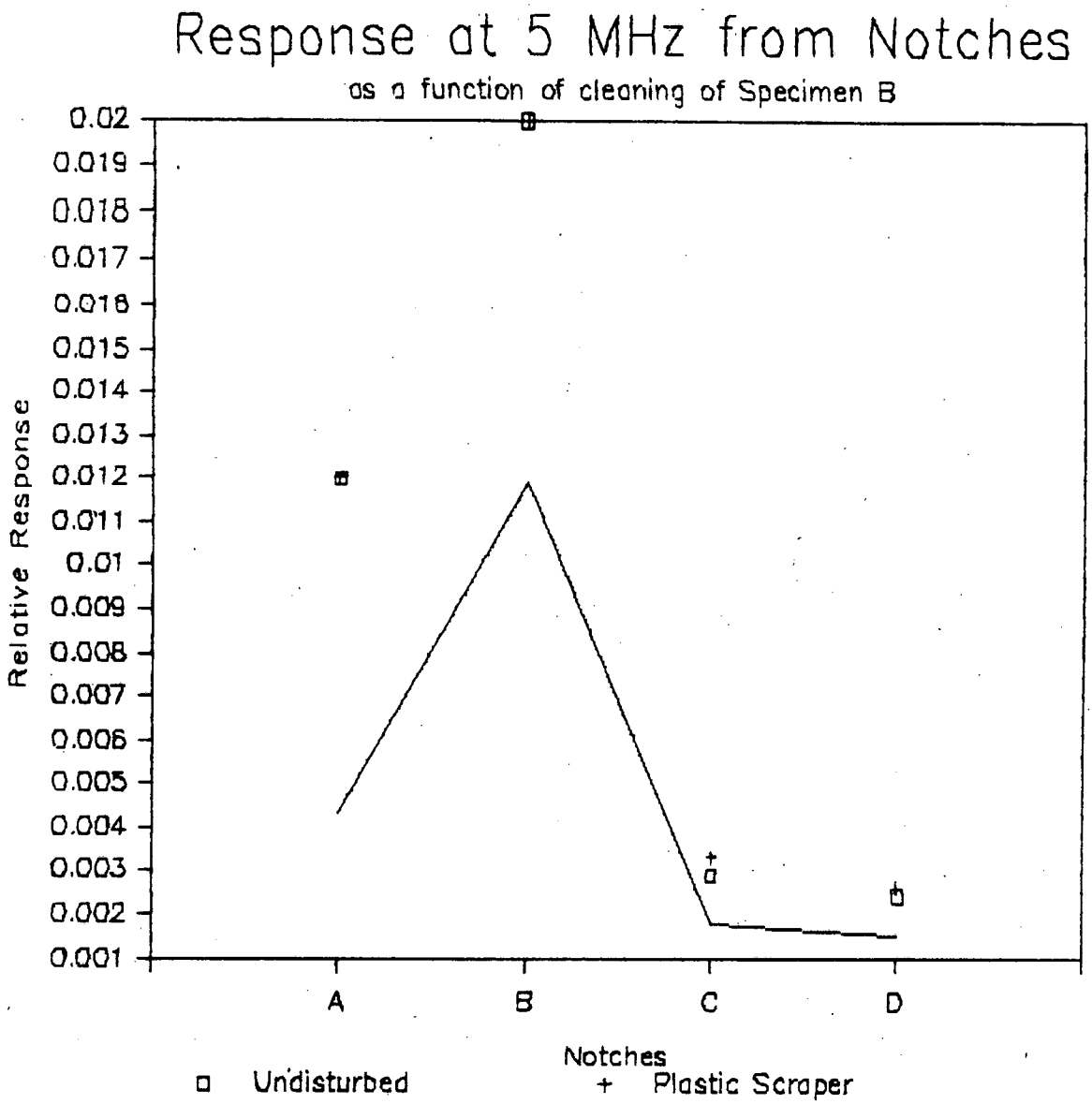

Figure D-17. Response as a function of cleaning. The solid line is the average value of notch response from an unfouled sample.

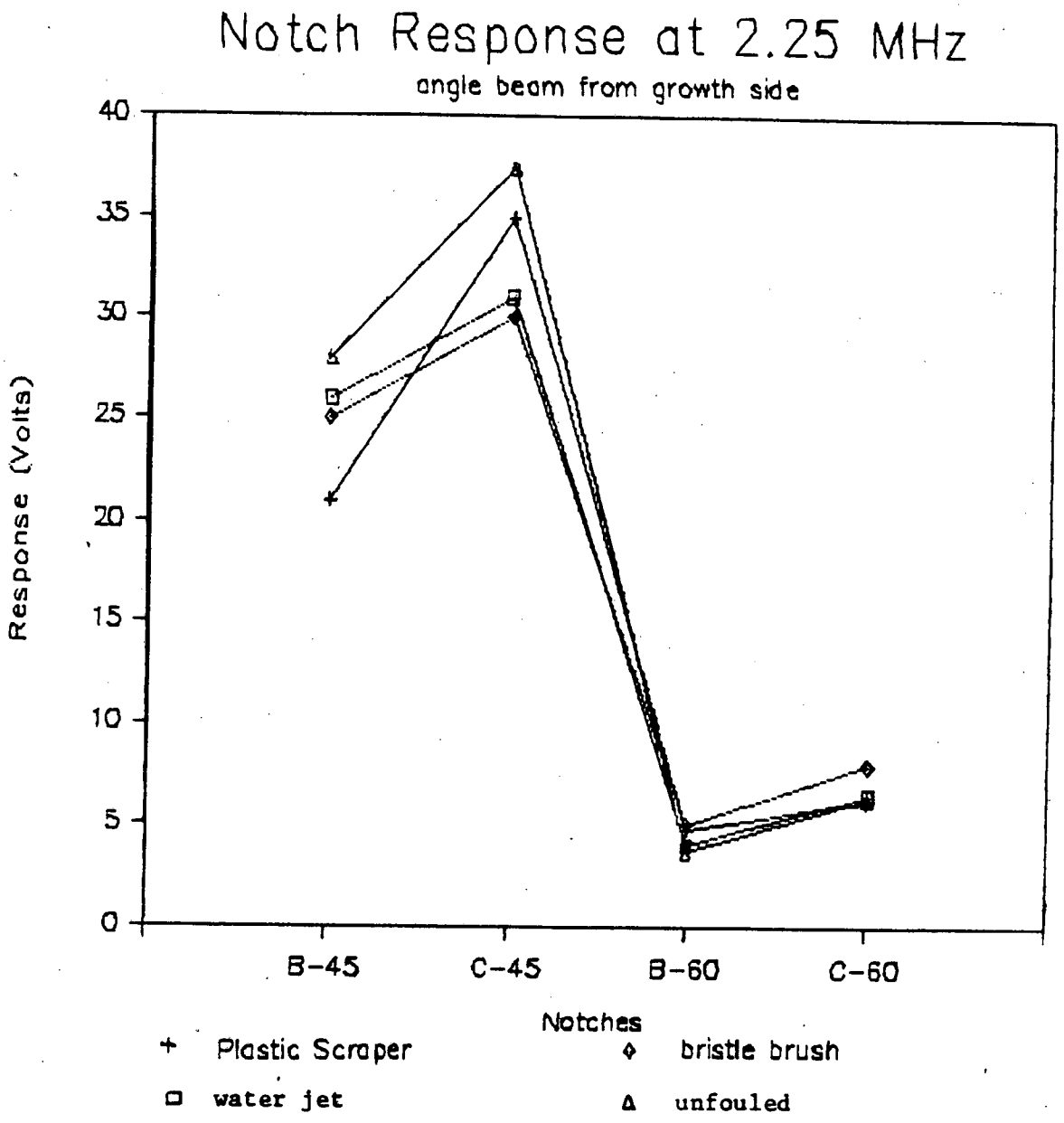
Notch Response at 2.25 MHz
angle beam from growth side
Response (Volts)
40
35
30
25
20
15
10
5
0
B-45
C-45
B-60
C-60
Notches
Plastic Scraper
bristle brush
water jet
unfouled

Figure D-18

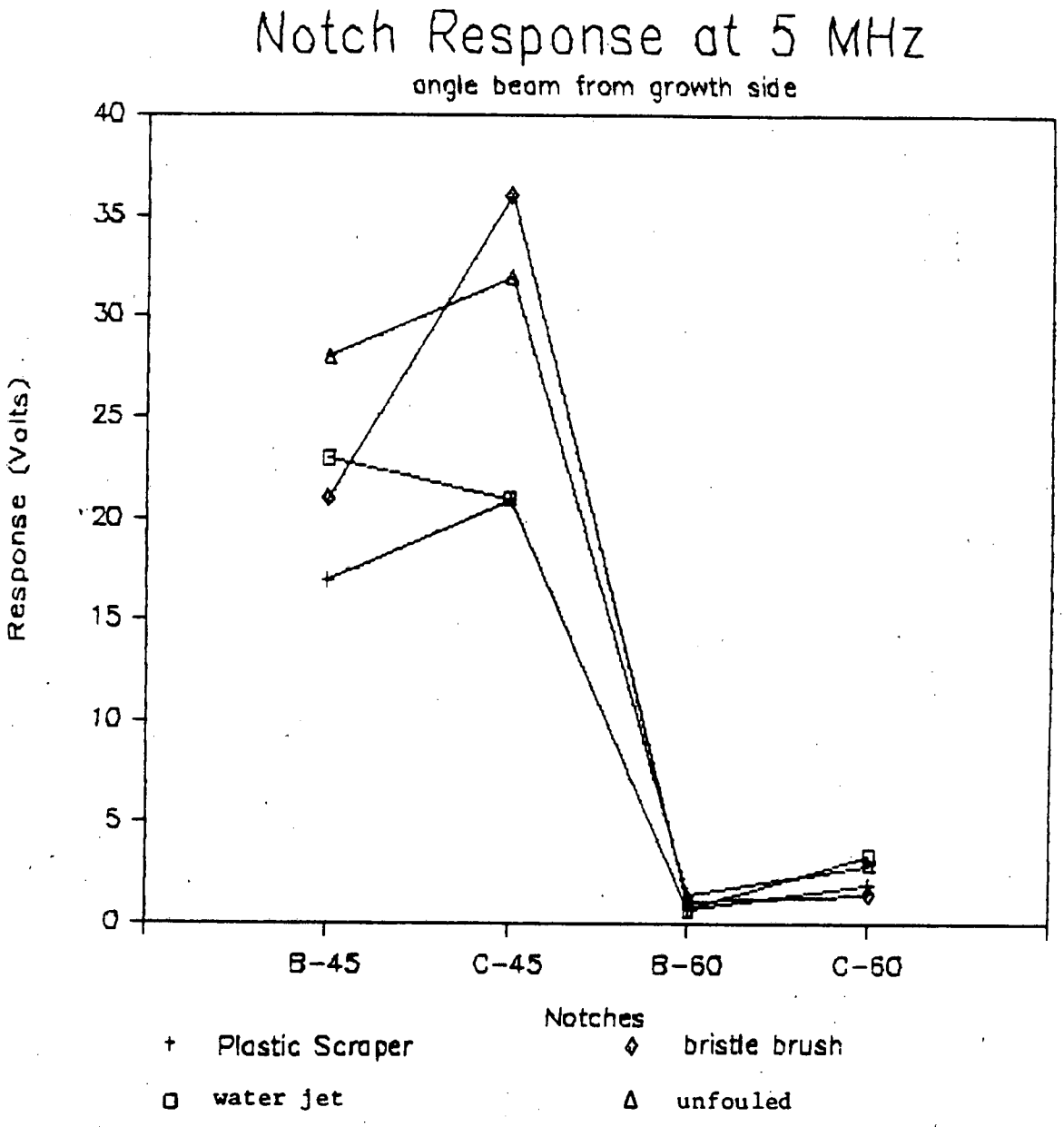
Notch Response at 5 MHz
angle beam from growth side
Response (Volts)
40
35
30
25
20
15
10
5
0
B-45
C-45
B-60
C-60
Notches
+ Plastic Scraper
◊ bristle brush
□ water jet
Δ unfouled

Figure D-19

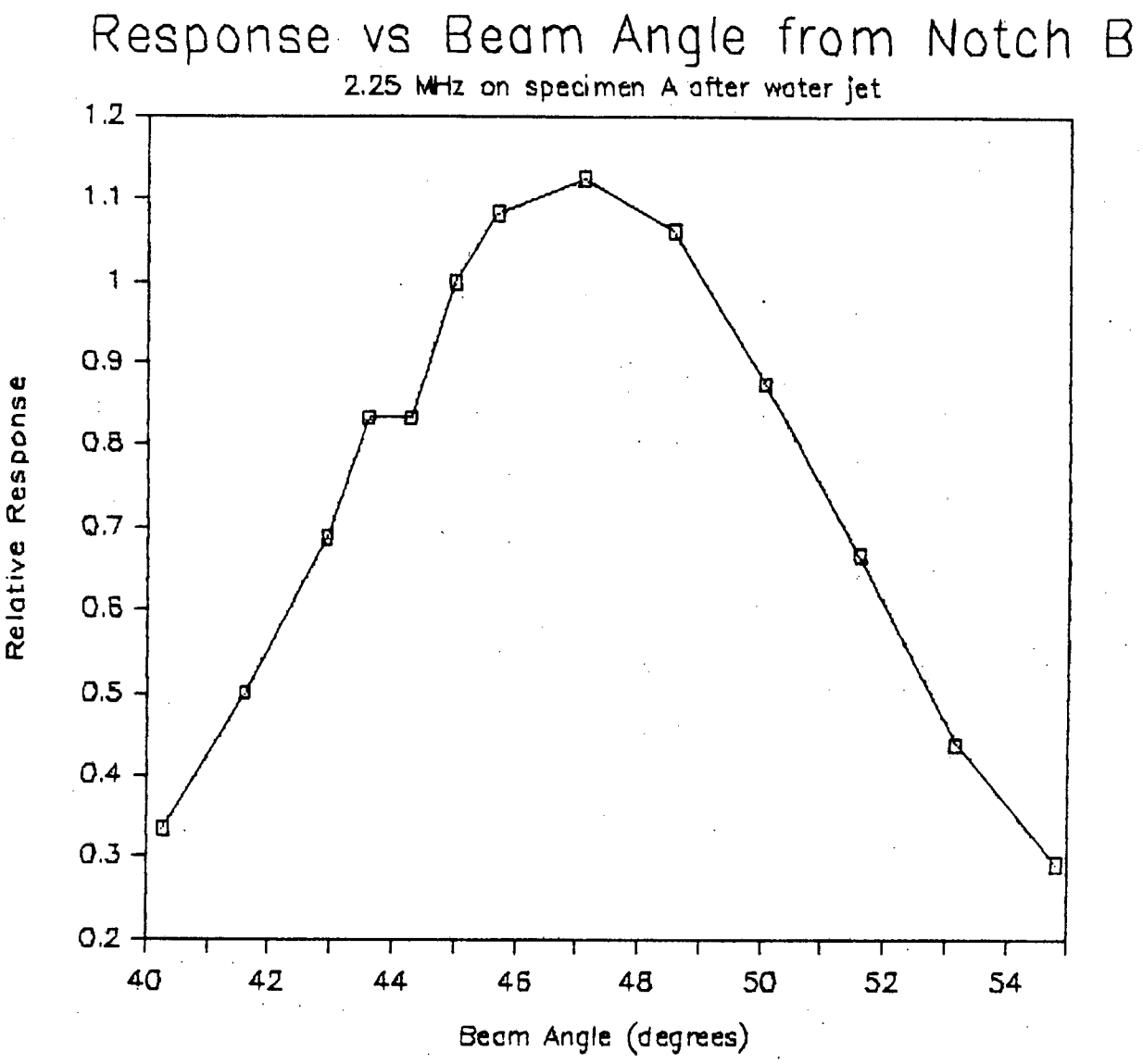
Response vs Beam Angle from Notch B
2.25 MHz on specimen A after water jet
Relative Response
1.2
1.1
1
0.9
0.8
0.7
0.6
0.5
0.4
0.3
0.2
40
42
44
46
48
50
52
54
Beam Angle (degrees)

Figure D-20

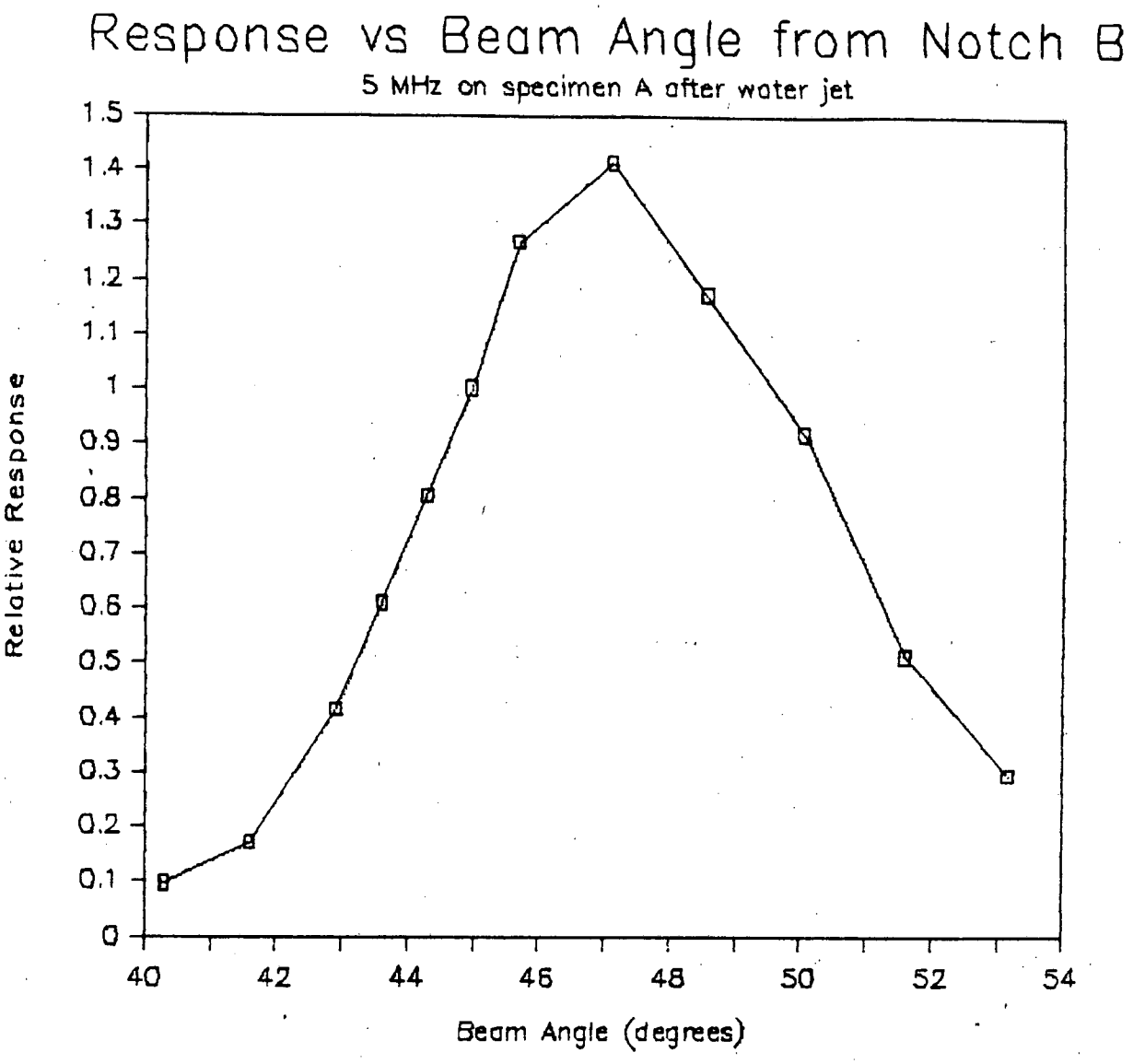
Response vs Beam Angle from Notch B
5 MHz on specimen A after water jet
Relative Response
1.5
1.4
1.3
1.2
1.1
1
0.9
0.8
0.7
0.6
0.5
0.4
0.3
0.2
0.1
0
40
42
44
46
48
50
52
54
Beam Angle (degrees)

Figure D-21

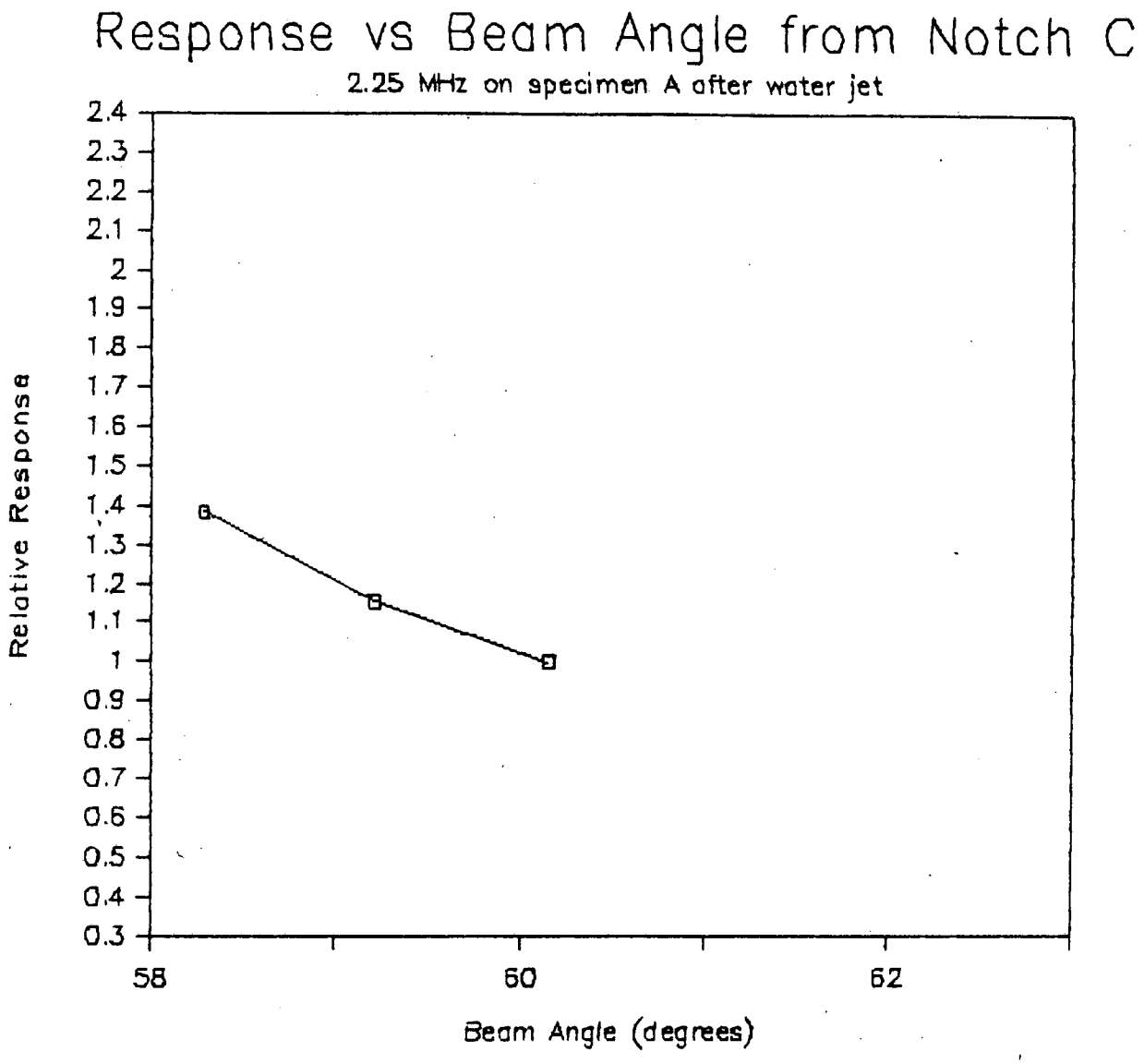
Response vs Beam Angle from Notch C
2.25 MHz on specimen A after water jet
Relative Response
2.4
2.3
2.2
2.1
2
1.9
1.8
1.7
1.6
1.5
1.4
1.3
1.2
1.1
1
0.9
0.8
0.7
0.6
0.5
0.4
0.3
58
60
62
Beam Angle (degrees)

Figure D-22

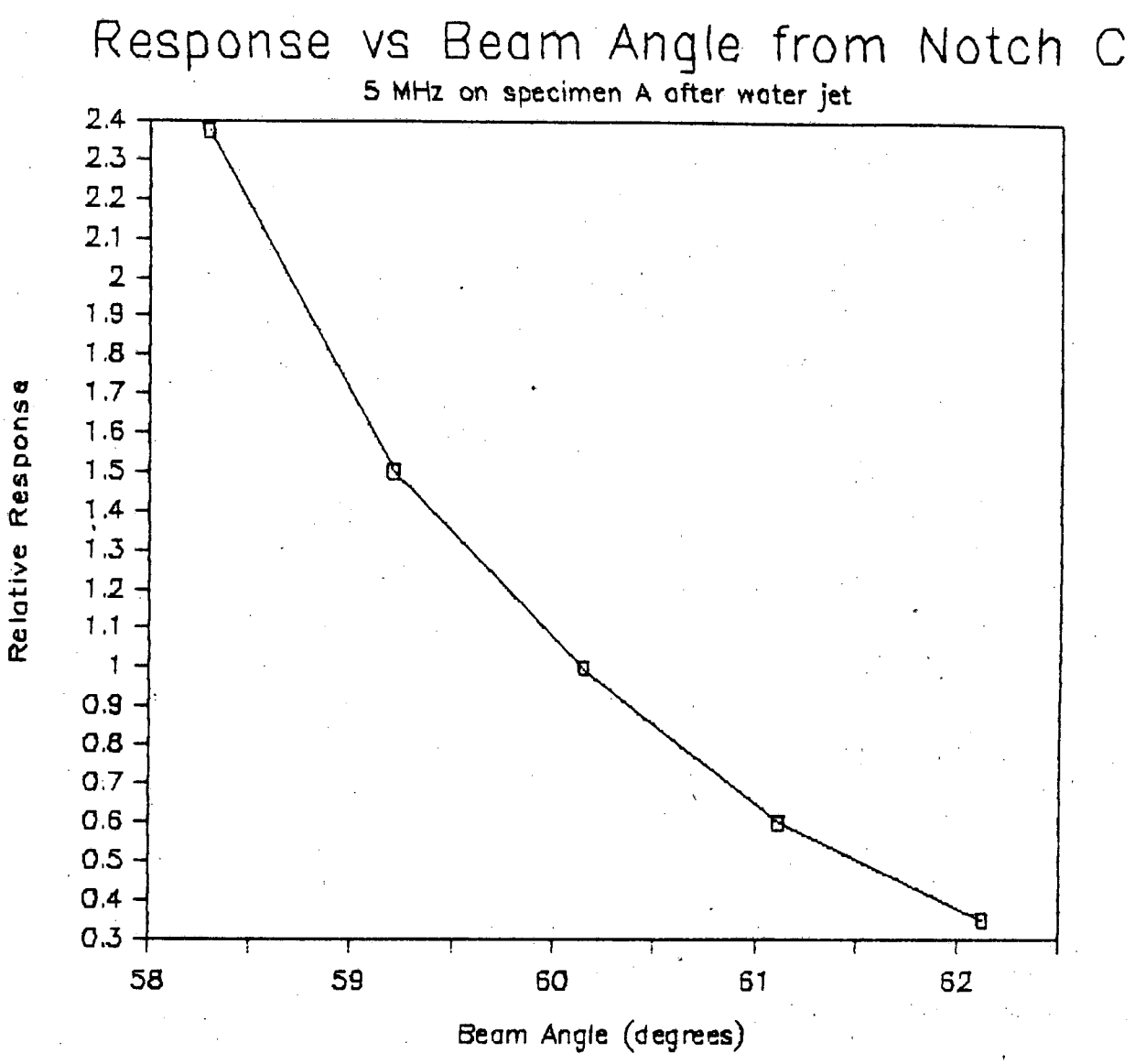
Response vs Beam Angle from Notch C
5 MHz on specimen A after water jet
Relative Response
2.4
2.3
2.2
2.1
2
1.9
1.8
1.7
1.6
1.5
1.4
1.3
1.2
1.1
1
0.9
0.8
0.7
0.6
0.5
0.4
0.3
58
59
60
61
62
Beam Angle (degrees)

Figure D-23

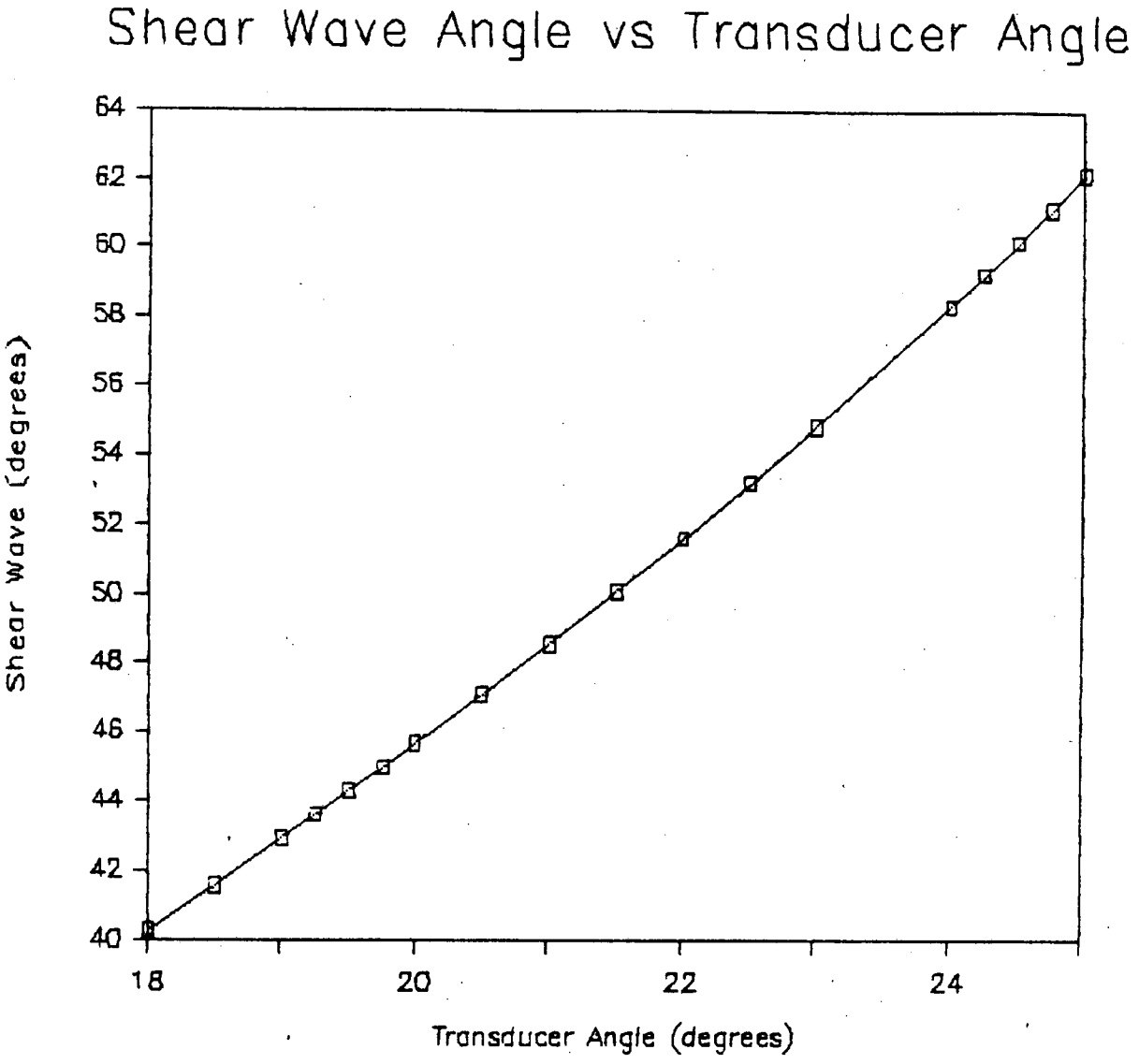
Shear Wave Angle vs Transducer Angle
Shear Wave (degrees)
64
62
60
58
56
54
52
50
48
46
44
42
40
18
20
22
24
Transducer Angle (degrees)

Figure D-24

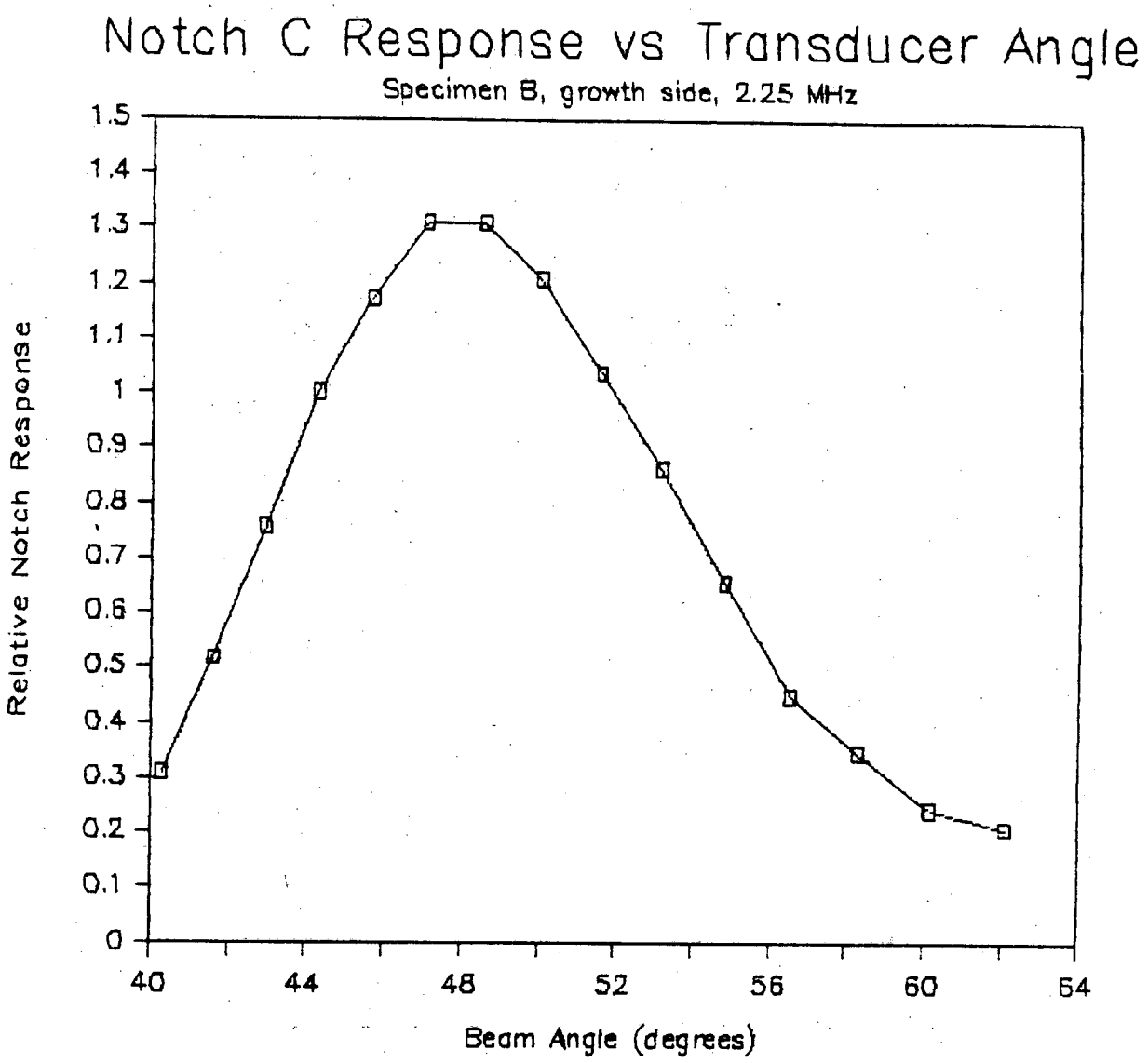
Notch C Response vs Transducer Angle
Specimen B, growth side, 2.25 MHz
Relative Notch Response
1.5
1.4
1.3
1.2
1.1
1
0.9
0.8
0.7
0.6
0.5
0.4
0.3
0.2
0.1
0
40
44
48
52
56
60
64
Beam Angle (degrees)

Figure D-25

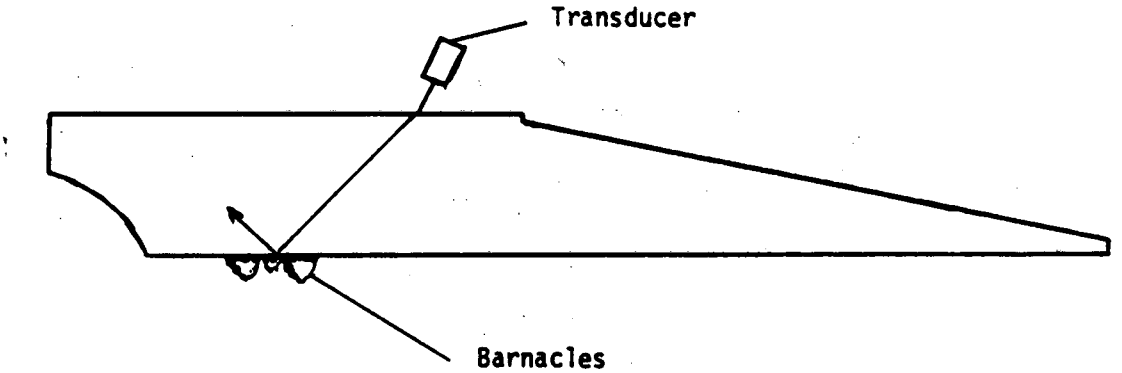

Figure D-26 Configuration for Angle Beam Bounce Off the Barnacle Residual of Specimen A

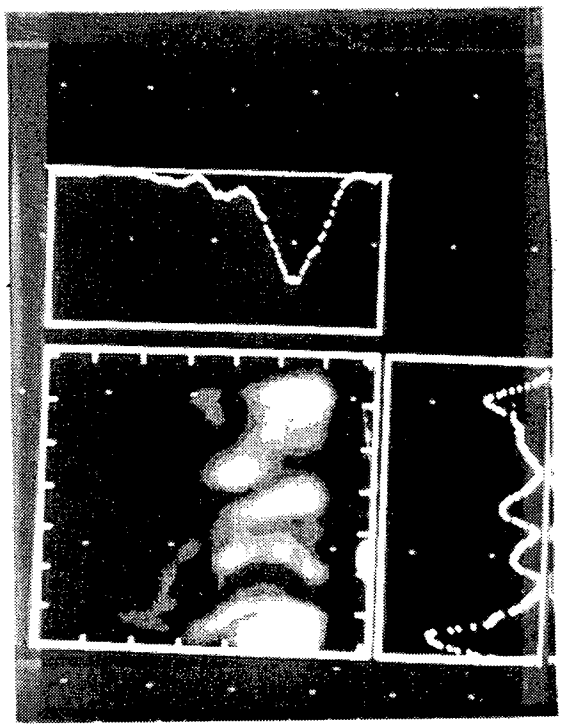

D-27a

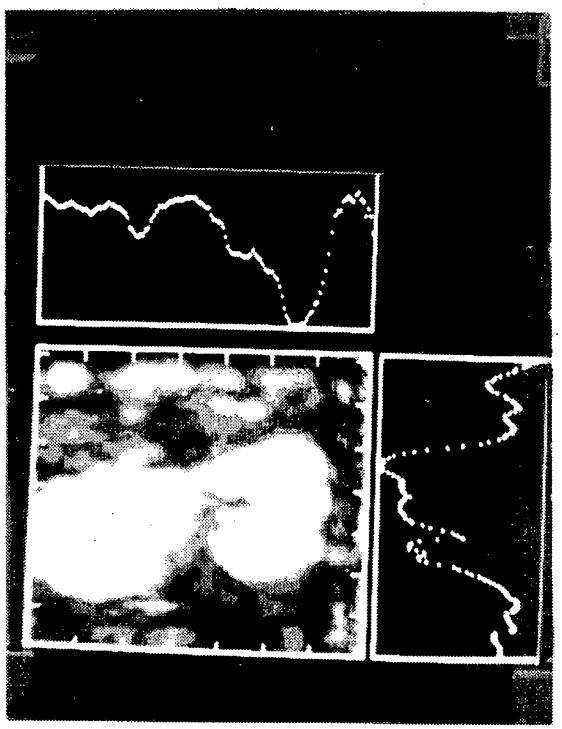

D-27b

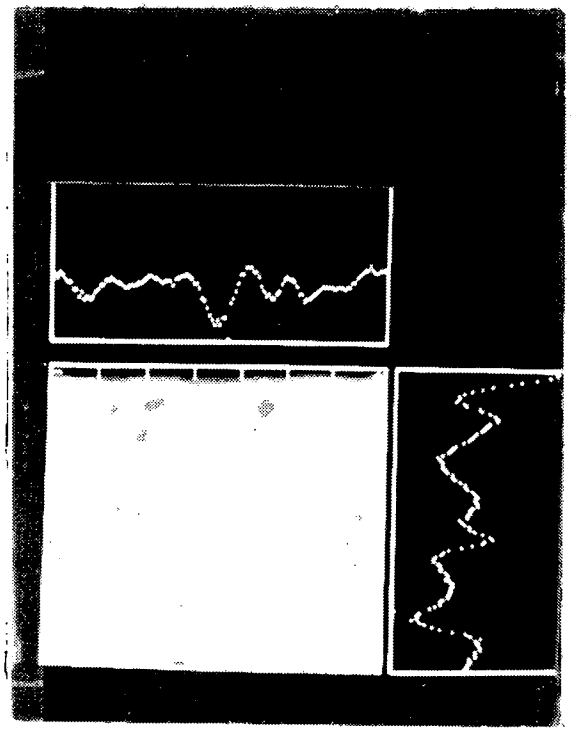

D-27c

Figure D-27. Inspection of specimen A with an inside bounce off barnacle using 5 MHz, 45° beam.
a) Gated beyond bounce surface. b) Gated at bounce surface showing barnacle pattern
c) 0° beam gated at bounce surface.

the same region but the barnacle pattern was not detected, see figure D-28c, probably because the effect is small relative the strong echo of a straight beam inspection.

Other Measurements

Other measurements were made on the biofouled samples using three different transducers (2.25 MHz - 0.75 inch, 1 MHz - 0.75 inch, and a 2.25 MHz - 1 inch focussed transducer) to look through the undisturbed growth. The 0.75 inch, 2.25 MHz transducer did not offer any noticeable improvement over the 0.5 inch diameter transducer used for the bulk of the study. The 1 MHz transducer appeared to have more noise in the signal. The focussed transducer, when used so that the 1 inch diameter beam focussed to about a 0.5 inch beam at the surface appeared to have greater power for inspection in the part. Signals in this case were not lost as easily over barnacles. These few tests were inconclusive that there is or is not a means to improve inspection by lowering frequency or changing beam size.

APPENDIX E

Weld Samples

APPENDIX E

WELD SAMPLES

Samples of welded connector components were provided by Chevron and Conoco. Figure E-1 shows the specimens. The Chevron sample was 25 mm (1 inch) thick flat plate. The weld was HY-80 to WT70 material with the weld ground smooth. The Conoco material was rolled and welded line pipe approximately 20 mm (0.8 inch thick.) Two of the Conoco samples were epoxy coated and one was left bare. The welds were in the as welded condition with both the weld crown and drop through present. The crown was approximately 25 mm wide consisting of about three weld beads and approximately 3 mm high. The drop through was approximately 8 mm wide with heights of between 0.8 to 3 mm.

EDM notches were placed in each sample. Figures E-2 and E-3 show the notch placement and size. Notch depths were nominally 5.1, 2.5, 1.3, 0.5 and 0.25 mm deep with length of approximately 50 mm.

a)

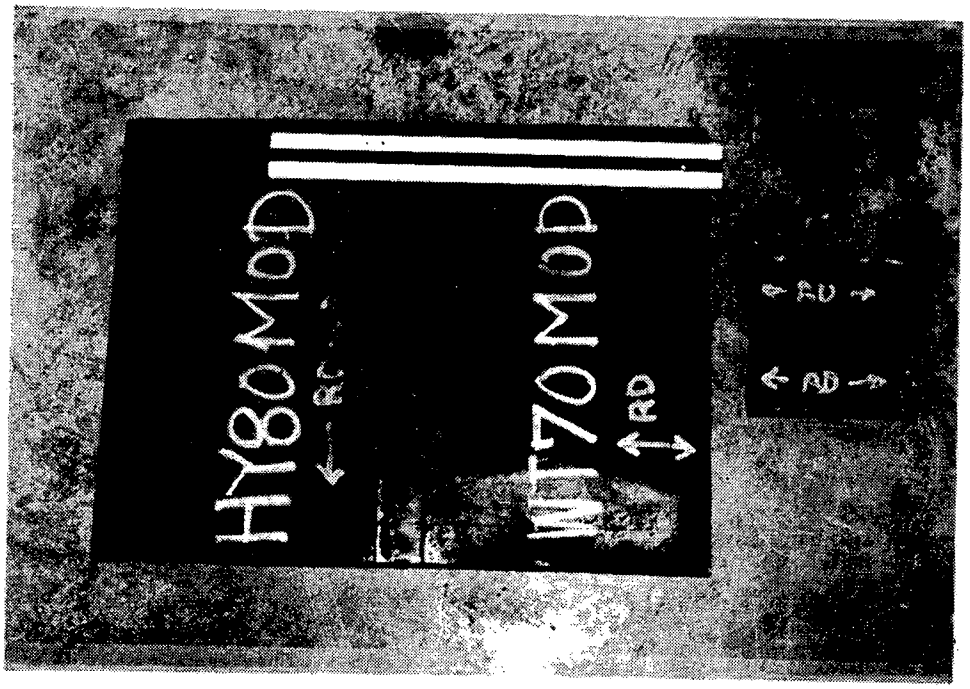

b)

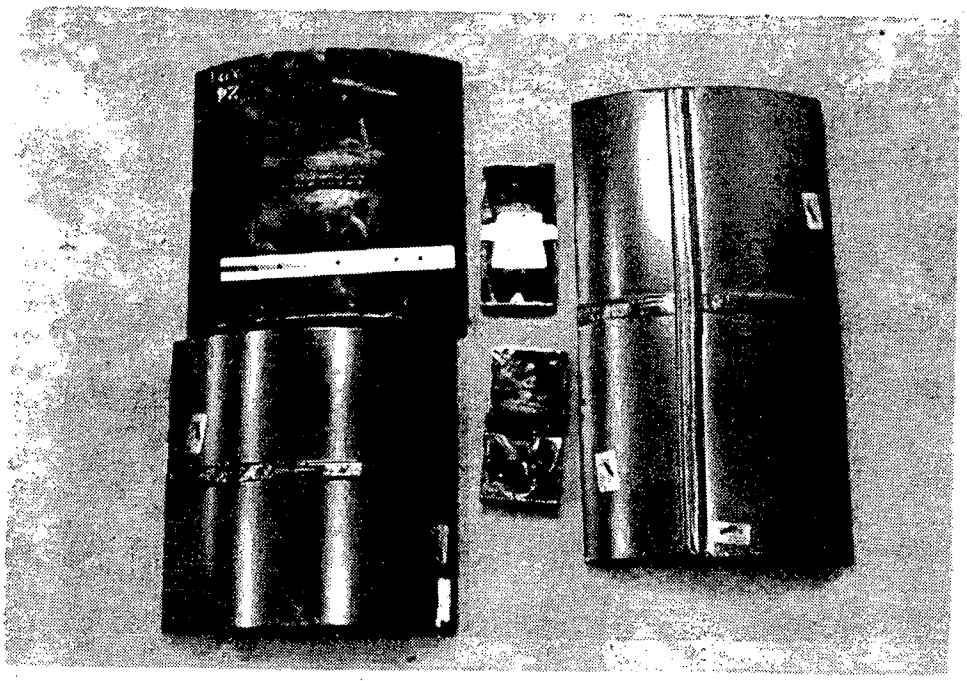

Figure E-1. Test samples for weld tests: a) Chevron, b) Conoco.

Curved Plate With Epoxy Coating

Line Pipe 3/4" Thick
Approximately 1 ft radius Curvature

Place notches at locations shown approximately .250" from center of root of weld.

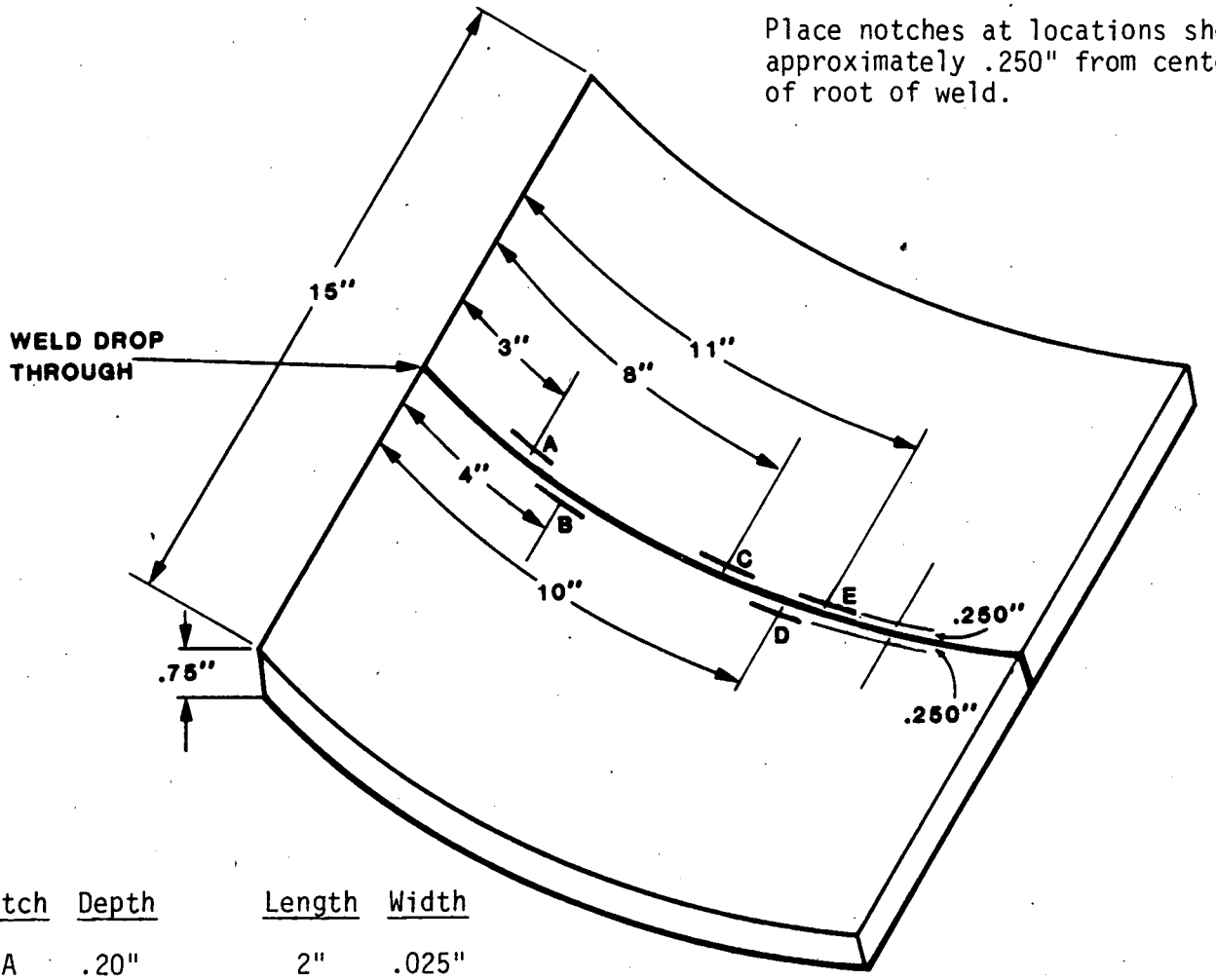

Notch	Depth	Length	Width
A	.20"	2"	.025"
B	.10"	2"	.025"
C	.050"	2"	.025"
D	.020"±.002"	2"	.025"
E	.010"±.002"	2"	.025"

Nominal Tolerances: Depth ±.005"
Length ±.10"
Width ±.005"

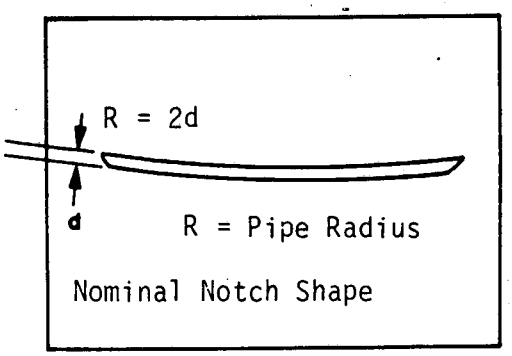

Figure E-2
EDM Notch Placement

Flat Plate

Material: HY 80
Thickness: 1 inch

Scale = 1/4

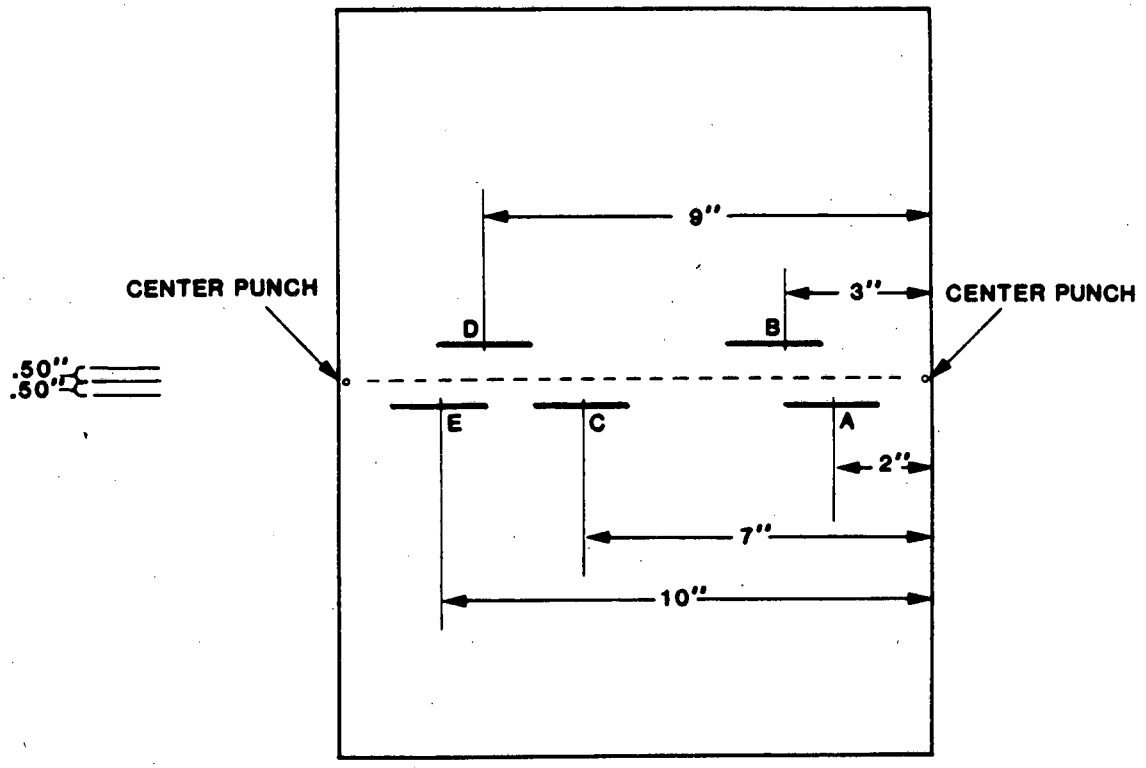

Place Notches 1/2" off Centerline between punch marks at locations shown.

Notch	Depth	Length	Width
A	.20"	2"	.025"
B	.10"	2"	.025"
C	.050"	2"	.025"
D	.020"± .002"	2"	.025"
E	.010"± .002"	2"	.025"

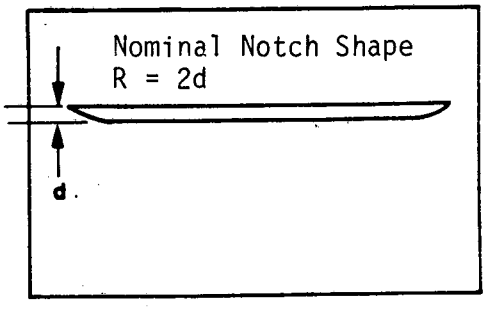

Nominal Tolerances: Depth ± .005"
Length ± .1"
Width ± .005"

Figure E-3 EDM Notch Placement

APPENDIX F

Fatigue Crack Tests

APPENDIX F

FATIGUE CRACK TESTS

Fatigue cracks in specimen 5A, 5AA and specimens 14 through 16 were generated at Arctec Offshore using bending test fixtures. Specimen 5AA is an SK001 connector with threads. Specimens 13 through 16 are 1 inch thick flat plate specimens. Specimen 13 was a calibration piece with EDM notches, specimens 14 through 16 were bending loaded to generate fatique cracks. The fatigue generating equipment is shown in Figures F-1 and F-2 for the fatigue cracking of specimen 5AA and 14-16 respectively. The system uses an off center weight on a rotating wheel at the end of a lever arm from the test part to fatigue load the sample. Cycles are counted by the rotation of the motor.

The test fixture clamps to the part being fatigued and is also clamped to a bench. The clamping caused cracks to initiate and grow not only at the center location where a scribe or notch was placed to start the crack, but also at edges of the fixture. Edge cracking was bad in specimen 5A and therefore a second test was run on specimen 5AA to try to reduce the edge crack effect.

Ultrasonic inspections of the cracks were conducted at Arctec Offshore on the test samples using a 5 MHz contact transducer. Appendix G contains a photo record of these ultrasonic inspections. For specimens 13-16, the ultrasonic inspection schemes are shown in Figure F-3. Calibration results on specimen 13 are shown in figures F-4 and F-5 as a function of the beam orientation. Figure F-4 shows correlation between peak amplitude and notch size. Figure F-5 shows correlation between the time of flight distance for the reflection from the notch tip and the notch root. The amplitude data is consistent with that shown in previous tests: peak amplitude correlates with size for small cracks but not for large cracks. The saturation threshold increases with path length, which supports the theory that beam spreading is the reason for this effect. The tip-root time delay data is much more correlated for all notch sizes. Figure F-5 also shows the tip-root delay results for the fatigue cracks.

Interestingly, the tip root time delay method under predicts crack size. Table F-1 shows the estimated versus actual crack size based on time of flight measurements made at OTC using a contact transducer (see Appendix G) and those made at SIGMA discussed in Section 4.10. In both cases the estimated crack sizes were under estimated by 32-34 percent. Similar results were found by [Hayman] as shown in Figure F-33. One possible explanation for this is that the leading edge of the fatigue crack may not be a reflector of ultrasonic energy, thus making the crack appear smaller than it really is. This would account for the fact that the time delay curve for fatigue cracks in Figure F-5 does not appear to pass through the origin. Repeating those experiments with cracks subject to tensile stress could yield different results, however.

Figure F-6 shows the amplitude results of contact transducer inspection for fatigue cracks in specimens 14 through 16. Interestingly, the comparison of fatigue crack data with EDM data is very good, indicating that fatigue cracks are good reflectors of energy at 5 MHz. These results show better correlation than the immersion ultrasonics discussed below.

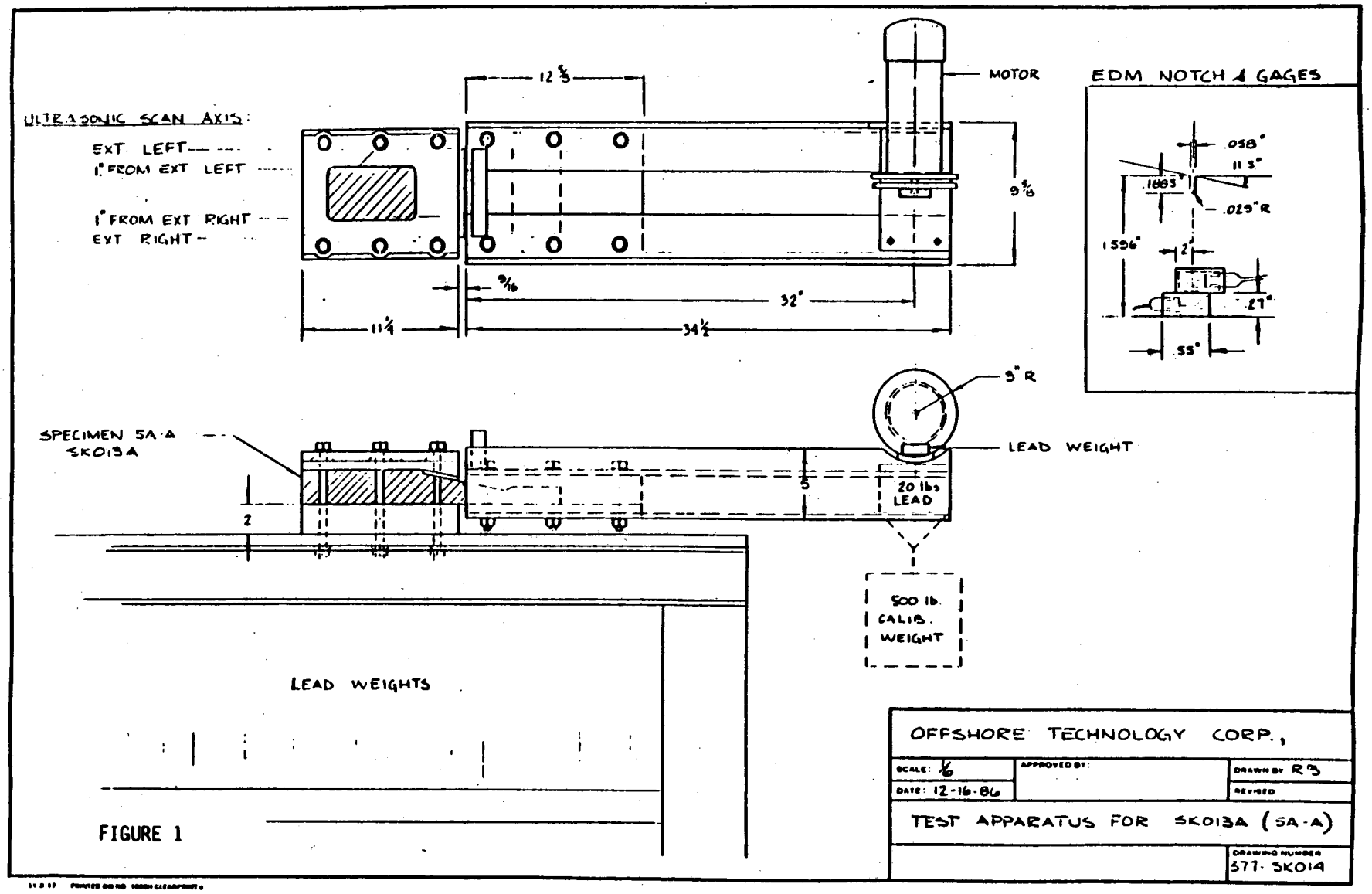

FIGURE 1

Figure F-1

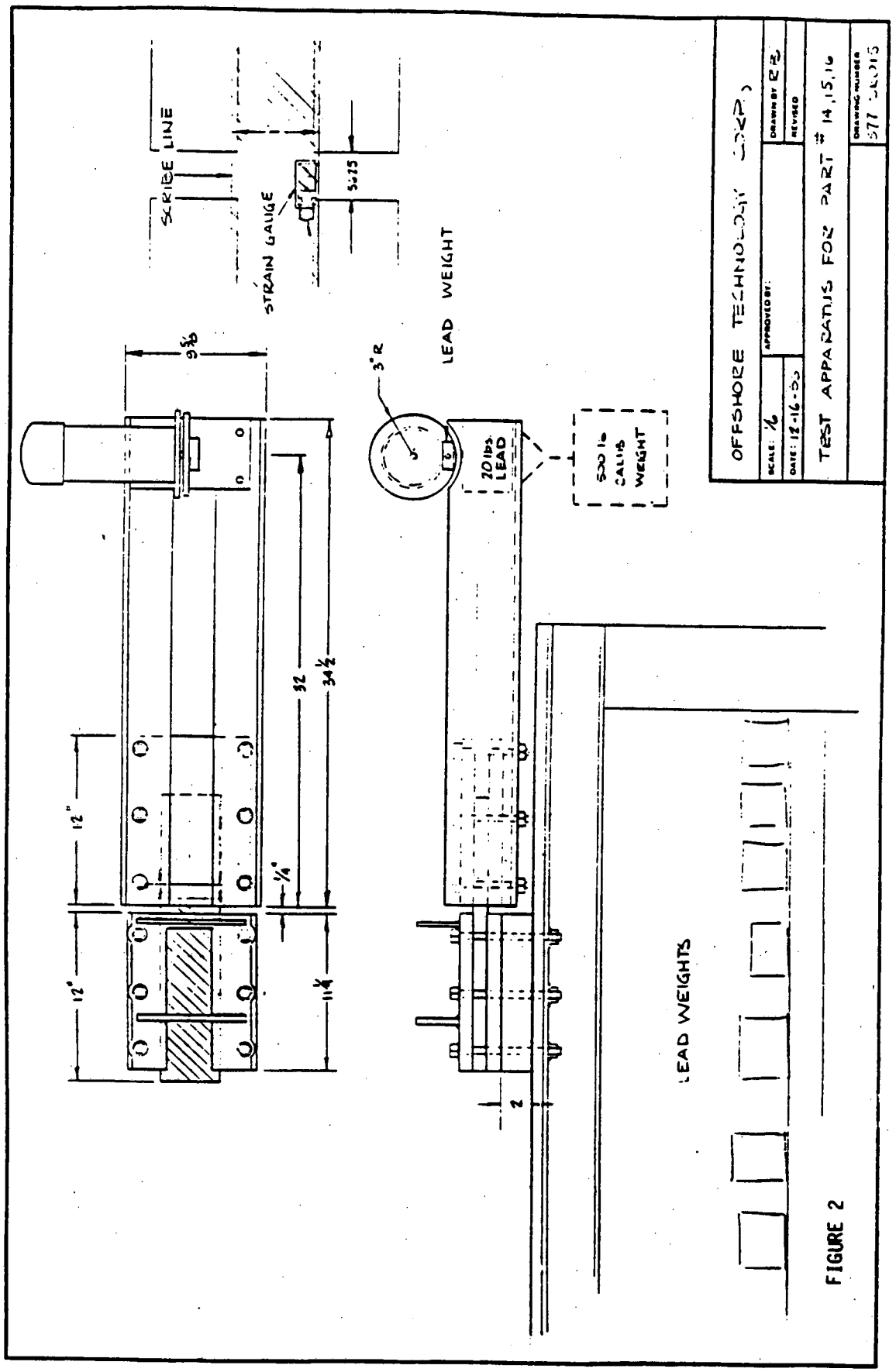
SCRIBE LINE
STRAIN GAUGE
5.375
LEAD WEIGHT
3"R
20 lbs. LEAD
530 lb CALIB WEIGHT
9⅝
12"
32
34½
¼"
12"
11¼
LEAD WEIGHTS
FIGURE 2
OFFSHORE TECHNOLOGY CORP.
TEST APPARATUS FOR PART # 14,15,16

Figure F-2

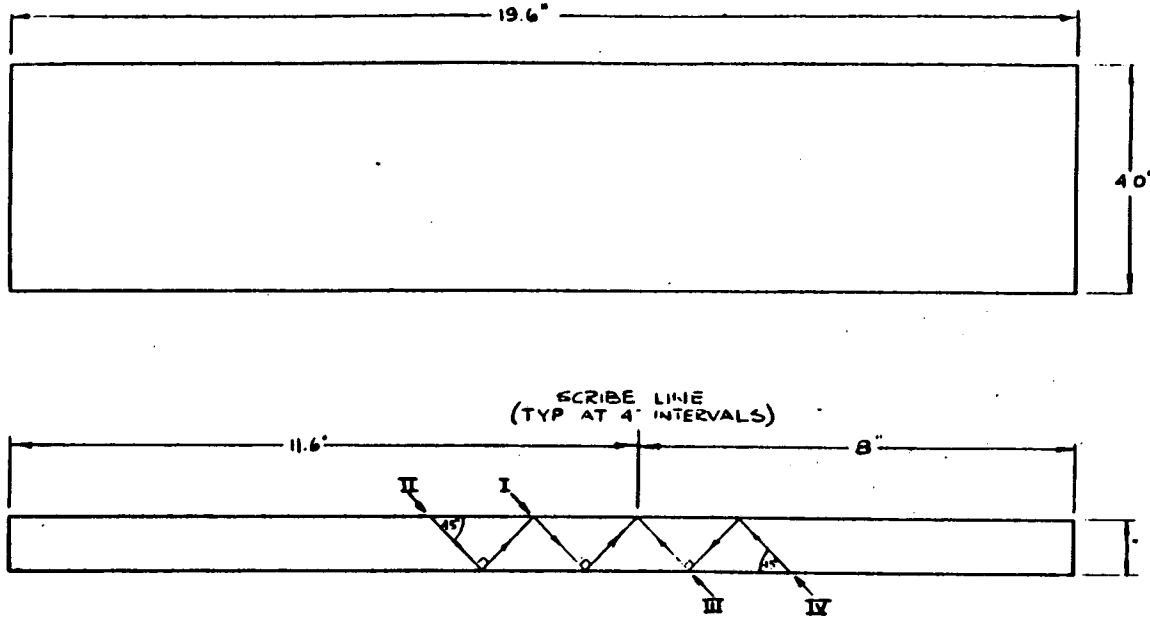

45° BEAM TRAVEL LENGTHS:

I.	2.828"	71.83 mm
II.	5.656"	143.66 mm
III.	1.414"	35.92 mm
IV	4.242"	107.75 mm

OFFSHORE TECHNOLOGY CORP,		
SCALE: ½	APPROVED BY:	DRAWN BY RB
DATE: 12-4-83		REVISED
SPECIMEN 14, 15, 16		
ACCOUSTIC COUPON EE3 & EE4		DRAWING NUMBER 377-SK003

Figure F-3

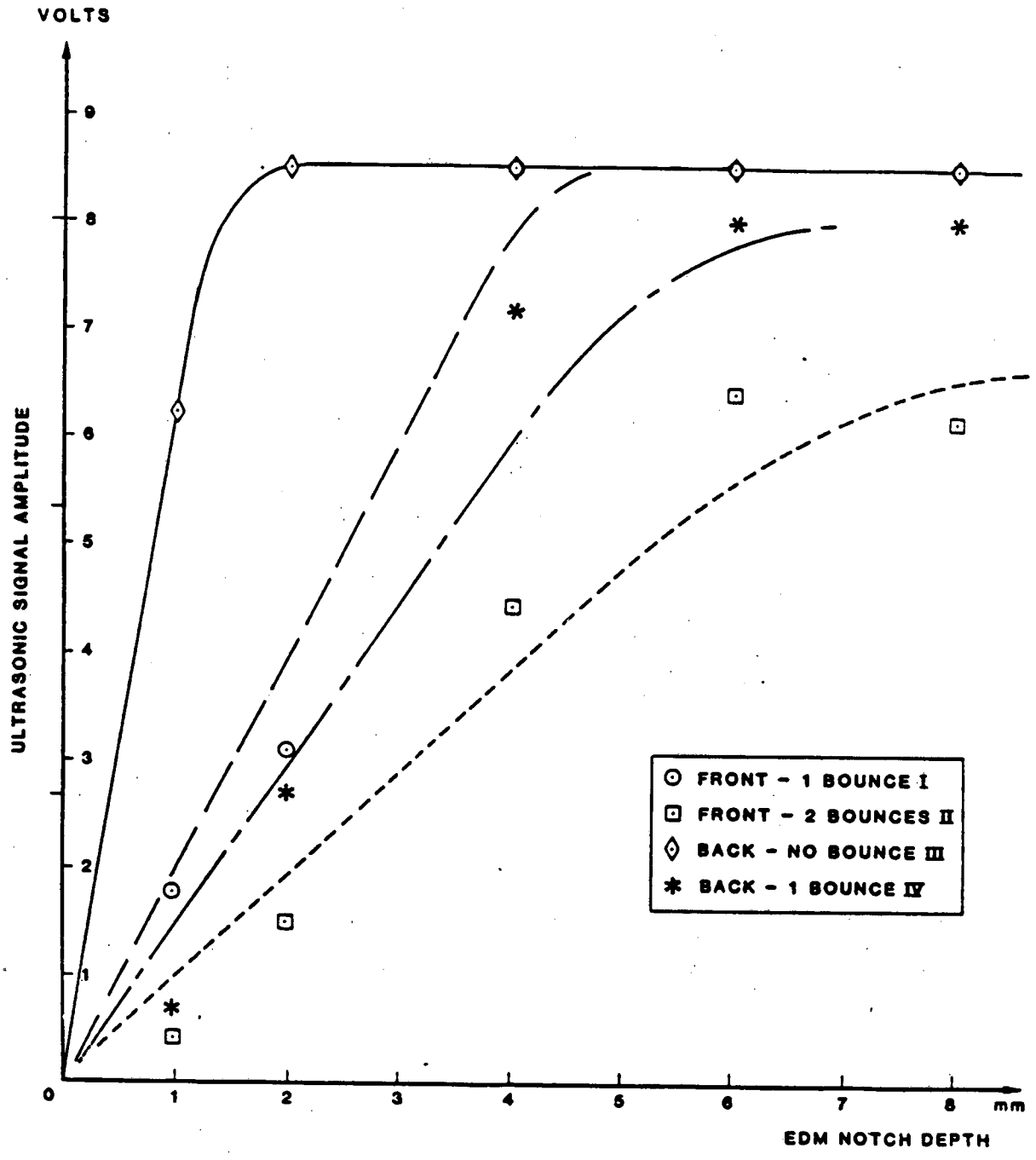

FIGURE F-4. EDM Notch Calibration (Specimen 13)

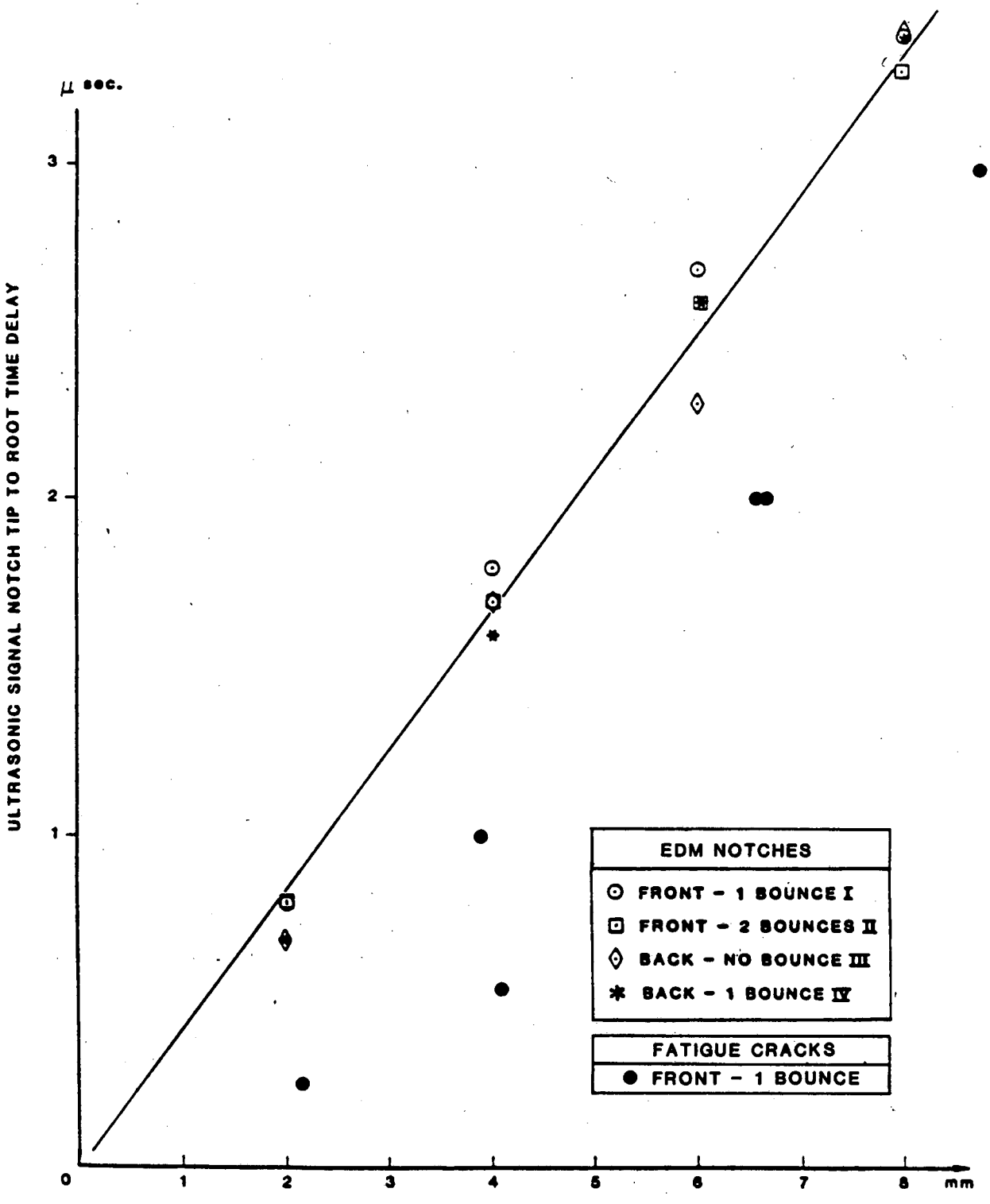

FIGURE F-5. Notch/Crack Depth Comparison of Notch and Fatigue Crack Tip to Root Time Delay

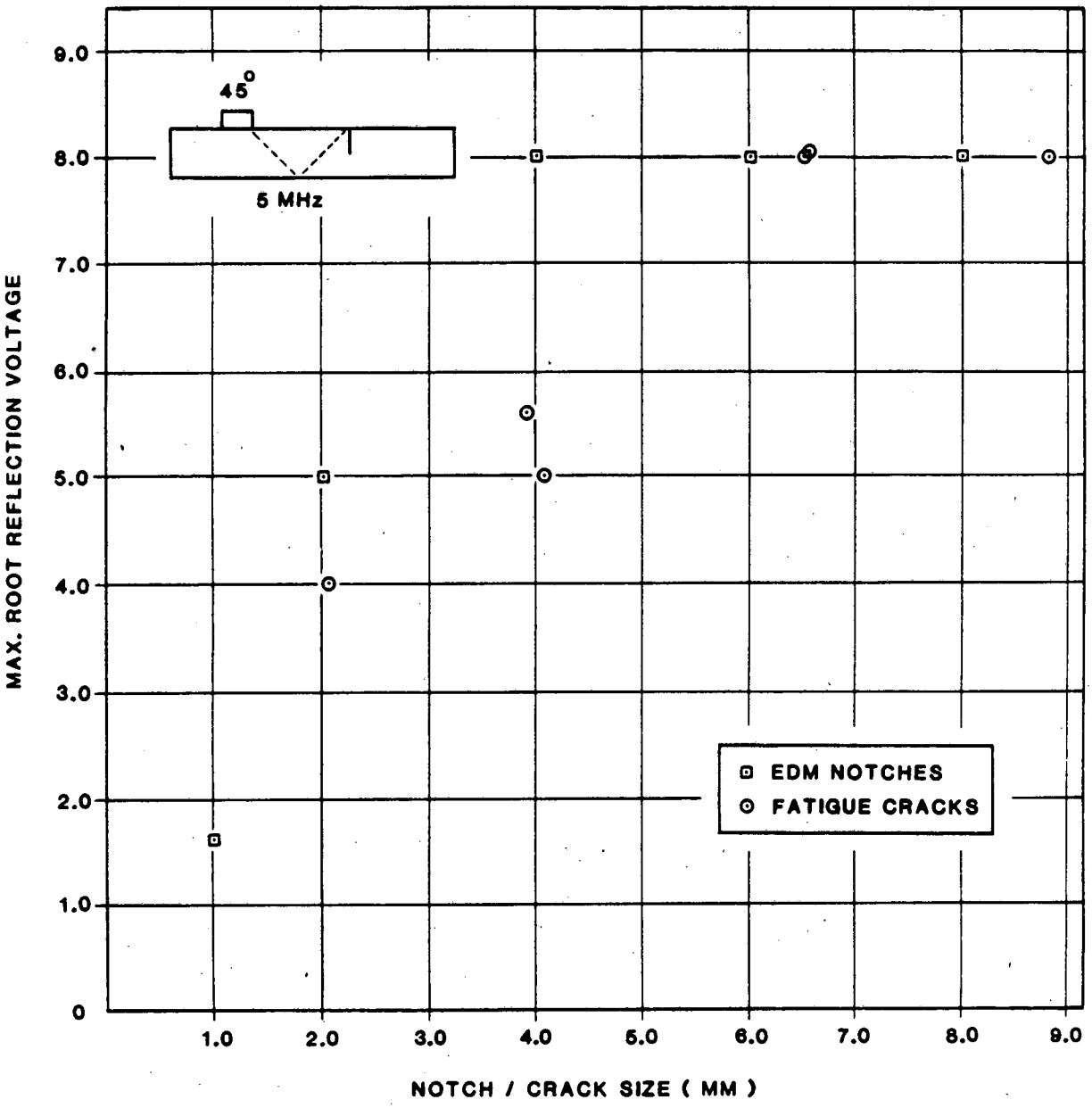

Figure F-6 Comparison of Notch and Fatigue Crack Reflection Amplitude with Contact UT Inspection

TABLE F-1

COMPARISON OF CRACK SIZE ESTIMATES
BASED UPON TIME OF FLIGHT METHODS

	Actual Fatigue Crack Size	Estimated by SIGMA (Immersion Transducers)	Estimated by OTC (Contact Transducers)
15-1	---	---	---
15-2	3.9	1.4	2.4
15-3	8.8	6.3	7.1
15-4	6.5	5.4	4.8
16-2	2.1	2.4	0.6
16-3	6.5	3.7	4.8
16-4	4.1	2.2	1.2
Average	5.3	3.6 (68%)	3.5 (66%)

For specimen 5AA the ultrasonic inspection paths are shown in Figure F-7. Figure F-8 shows the estimated crack size (based on tip root delay) versus fatigue cycles. The initial crack growth occured at the edges. After about 60,000 cycles the clamping mechanism was changed to distribute greater stress to the center of the notched piece. This reduced the edge crack growth and generated a center crack.

Specimens 13-16 were inspected using immersion ultrasonics to determine the amplitude response from fatigue cracks. The tip/root separation method (sattellite pulse) was used to establish crack depth using the notch responses shown in Figure 4.10-5. Six cracks were found to be in a good range of interest, notch 15-2 estimated at 1.4 mm deep, 14-4 estimated at 2.2 mm deep, 16-2 estimated at 2.4 mm deep, 16-3 estimated at 3.7 mm deep, 15-4 estimated at 5.4 mm deep and 15-3 estimated at 6.3 mm deep.

Actual fatigue crack sizes for specimens 15, 16 and 5A-A were determined by breaking the specimens at the crack location. Figures F-22 through F-29 show the fatigue cracks clearly visible because of their darker corroded surfaces. The crack sizes for specimens 15, 16 and 5A-A are shown in Figures F-30, 31 and 32, respectively.

Amplitude responses were measured from these cracks and the specimen 13 notches plotted against depth for 5, 2.25 and 1 MHz, 1/2 inch and 3/4 inch transducers at 15 and 60 degrees from each direction to the crack using 1/2 v or 3/2 v beam paths. Not all configurations were possible for testing. Figures F-9 through F-21b show the plots.

The actual fatigue cracks were larger than the estimated sizes by a factor of greater than 2 (on average). We recommend further analysis of this data to assess the factors which affect the inspectibility of fatigue cracks. Other investigations have shown that these results could be at least partially accounted for by crack shape and/or crack opening. Hayman [1985], Figure F-34, shows defect depth estimates on the order of 50% of true depths. Becker et al [1981] show that crack comparison of 25% of yield results in a reduction in echo response of 5-10 db (32-79%). These results are shown in Figure F-35. Figure F-36, also from Becker et al [Ibid) shows the theoretical reflected amplitude from plane stainless steel plates as a function of separation. Clearly a fatigue crack under tensile stress would be a better ultrasonic reflector than one under no stress, such as those used in this study.

Since fatigue cracks in TLP tendons will likely be under tensile loadings during in place inspections we recommend that the fatigue tests on the plate specimens be repeated with UT measurements being taken under various calibrated stress levels.

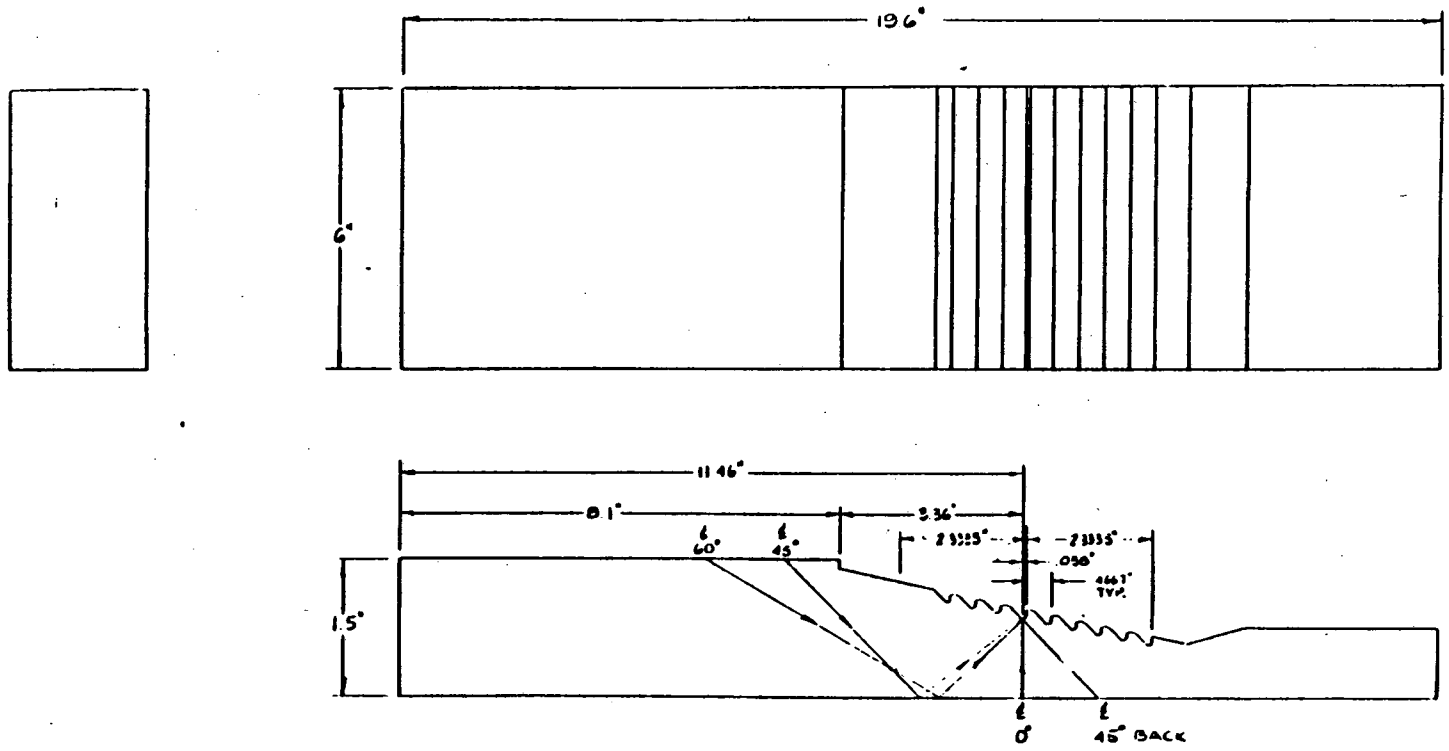

NOTCH SPECIFICATIONS:

1- SEE 64002 FOR EDM NOTCH DIMENSIONS.

2- SPECIMEN SA-A IS A MODIFICATION OF SPECIMEN SA, THREAD PATTERN IS UNCHANGED.

BEAM TRAVEL LENGTHS:

V 45° = 3.41" + 2.54" = 5.81" (147.57 mm)

VI 60° = 4.95" + 2.1" = 7.05" (179.07 mm)

VII 0° = 1.4" (35.56 mm)

VIII 45° BACK = 1.98" (50.29 mm)

OFFSHORE TECHNOLOGY CORP.

SCALE: 1/2	APPROVED BY:	DRAWN BY RD
DATE: 2-11-87		REVISED 2-11-87

SPECIMEN SA-A

DRAWING NUMBER 377 SK013

FIGURE 3

Figure F-7

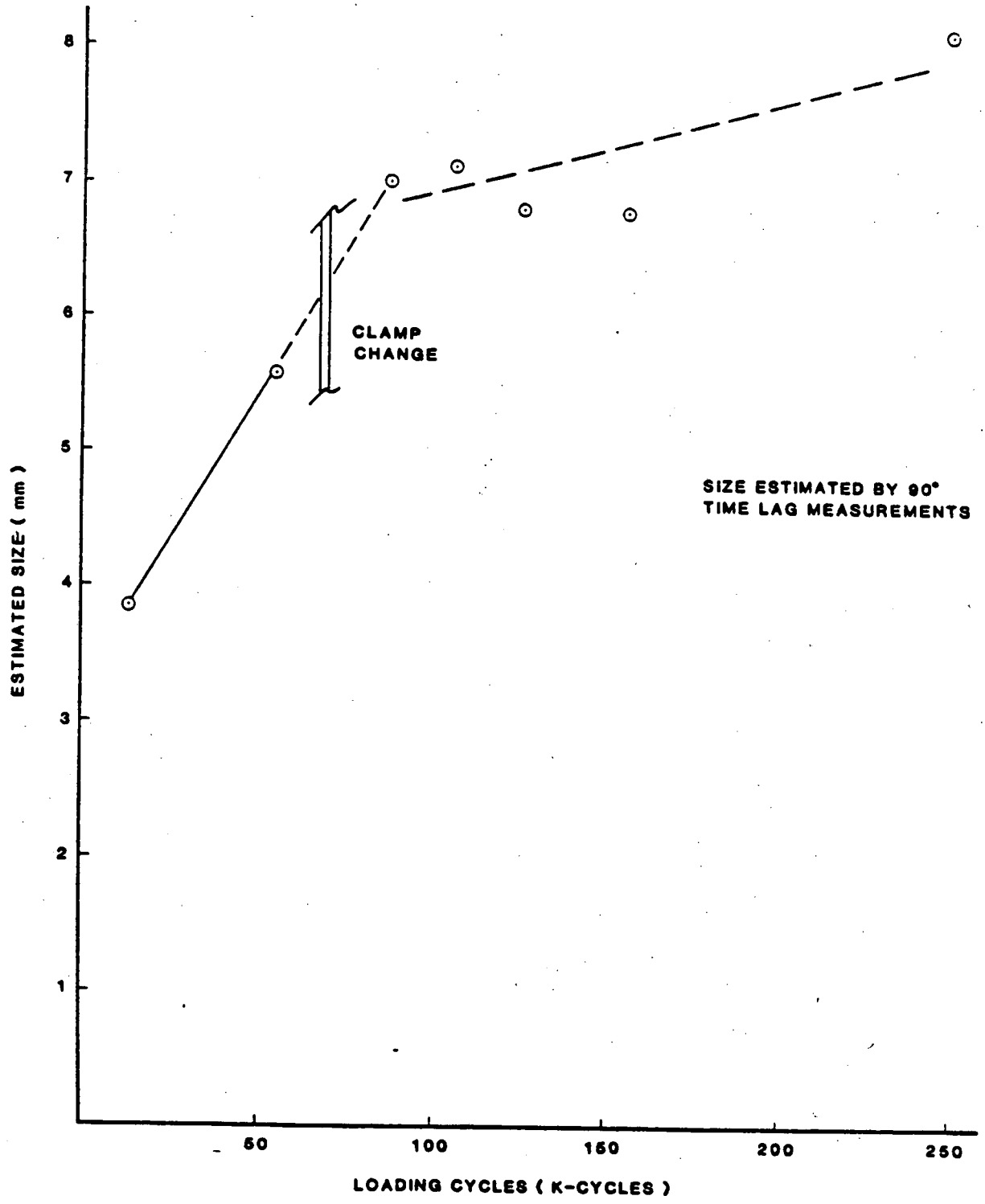

FIGURE F-8. Specimen 5A-A Crack Growth

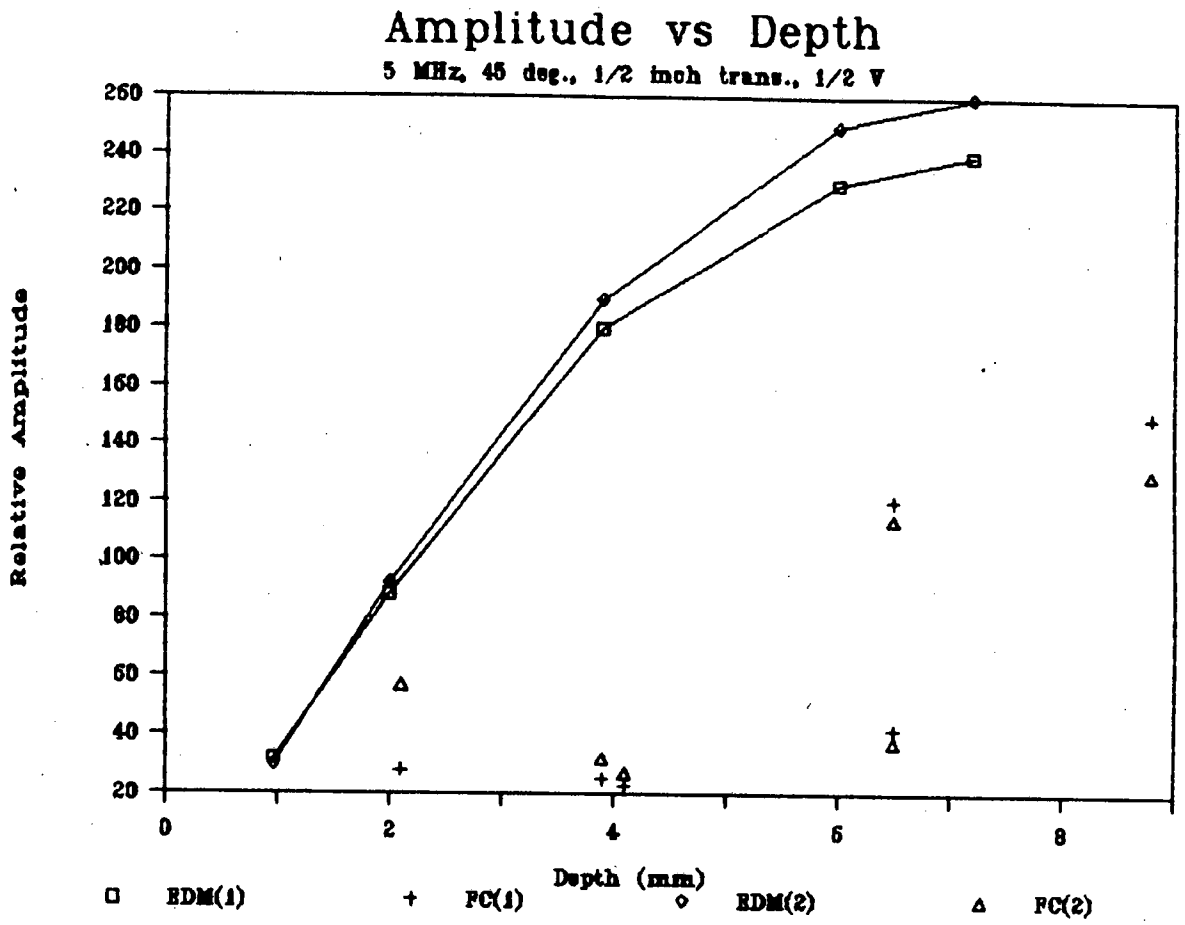
Amplitude vs Depth
5 MHz, 45 deg., 1/2 inch trans., 1/2 V
Relative Amplitude
260
240
220
200
180
160
140
120
100
80
60
40
20
0
2
4
6
8
Depth (mm)
EDM(1)
FC(1)
EDM(2)
FC(2)

Figure F-9

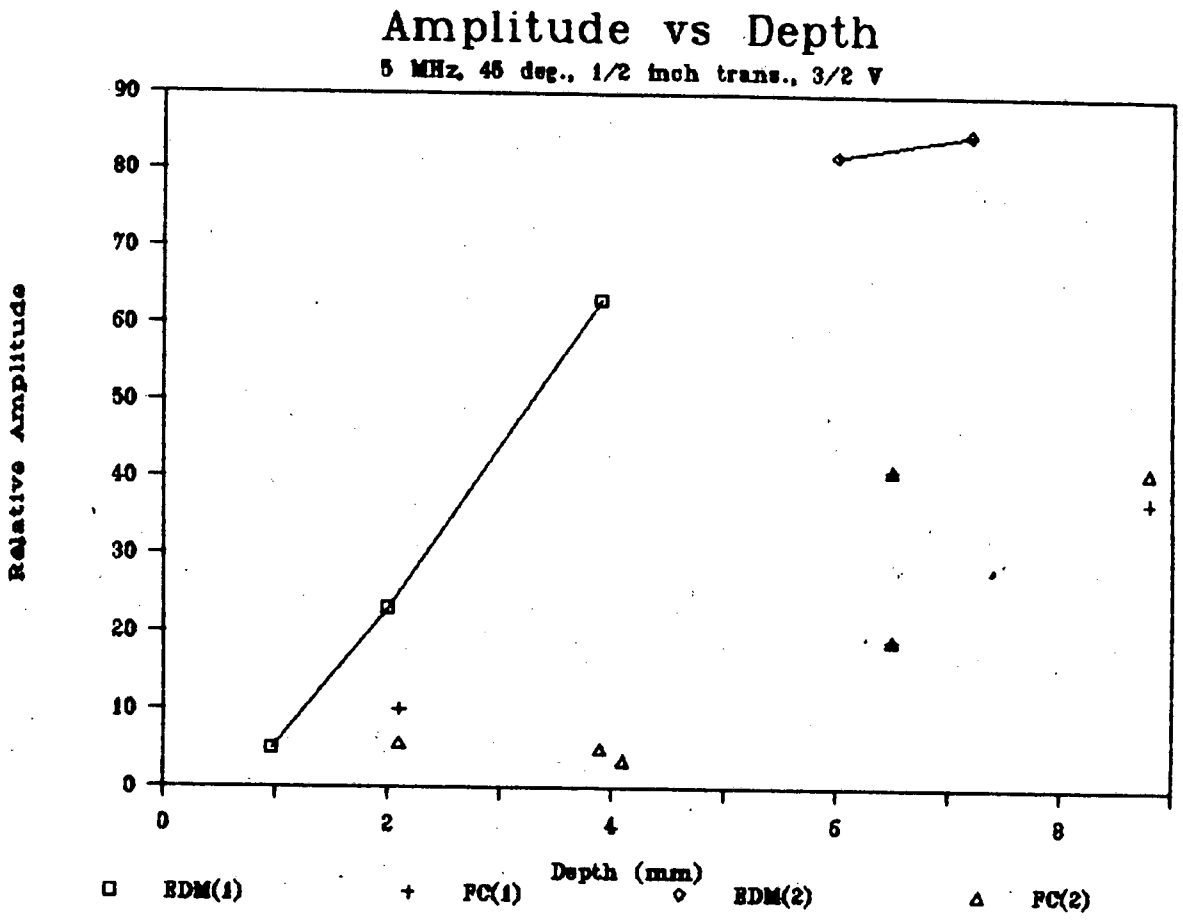
Amplitude vs Depth
5 MHz, 45 deg., 1/2 inch trans., 3/2 V
Relative Amplitude
90
80
70
60
50
40
30
20
10
0
0
2
4
6
8
Depth (mm)
EDM(1)
FC(1)
EDM(2)
FC(2)

Figure F-10

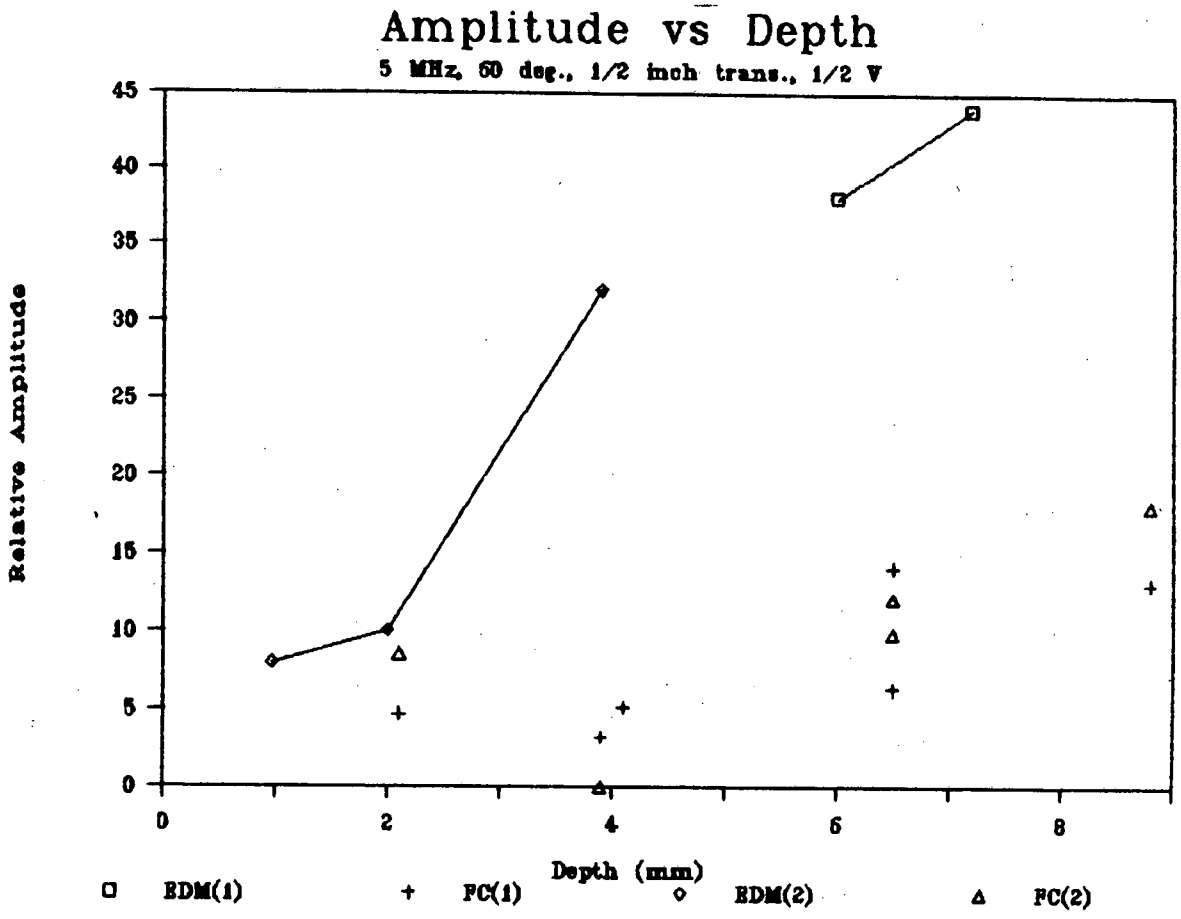
Amplitude vs Depth
5 MHz, 60 deg., 1/2 inch trans., 1/2 V
Relative Amplitude
45
40
35
30
25
20
15
10
5
0
0
2
4
6
8
Depth (mm)
EDM(1)
FC(1)
EDM(2)
FC(2)

Figure F-11

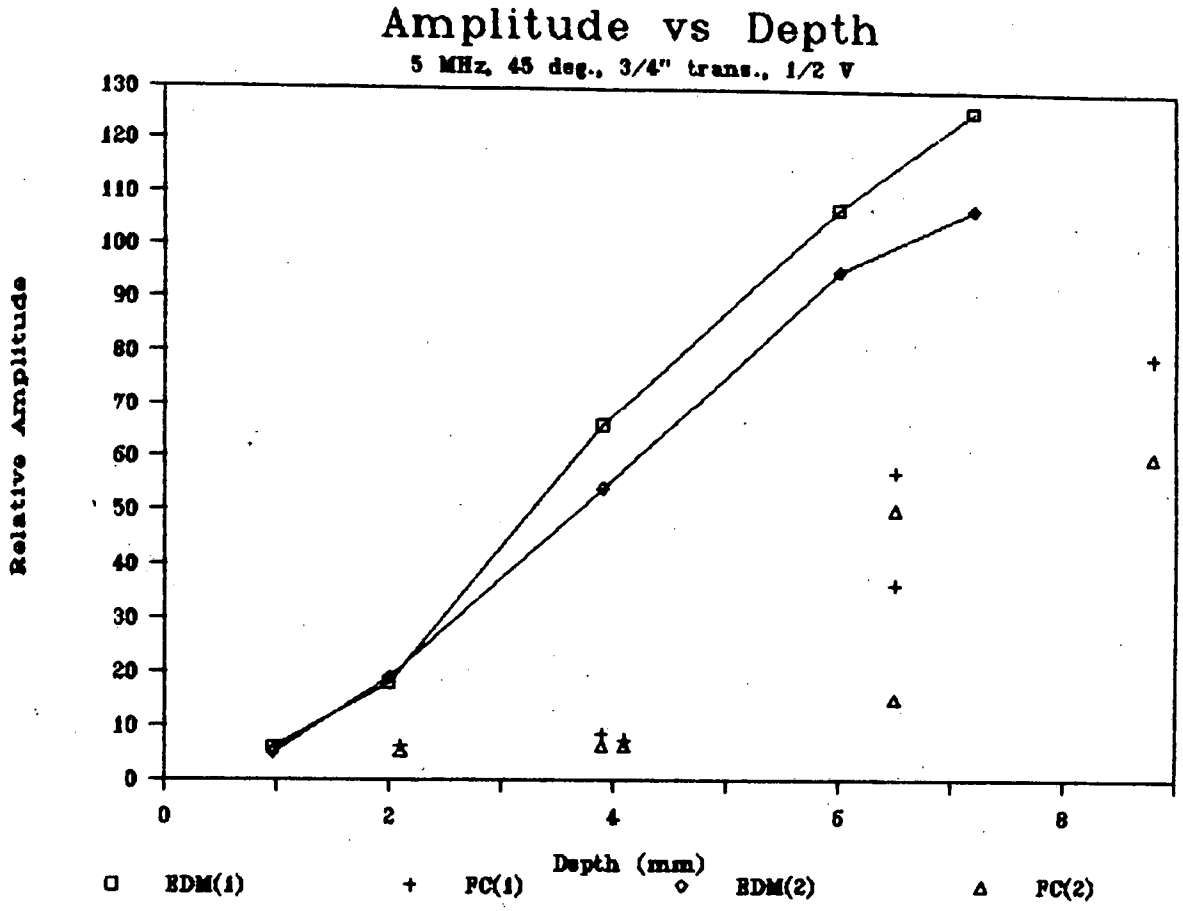
Amplitude vs Depth
5 MHz, 45 deg., 3/4" trans., 1/2 V
Relative Amplitude
130
120
110
100
90
80
70
60
50
40
30
20
10
0
0
2
4
6
8
Depth (mm)
EDM(1)
FC(1)
EDM(2)
FC(2)

Figure F-12

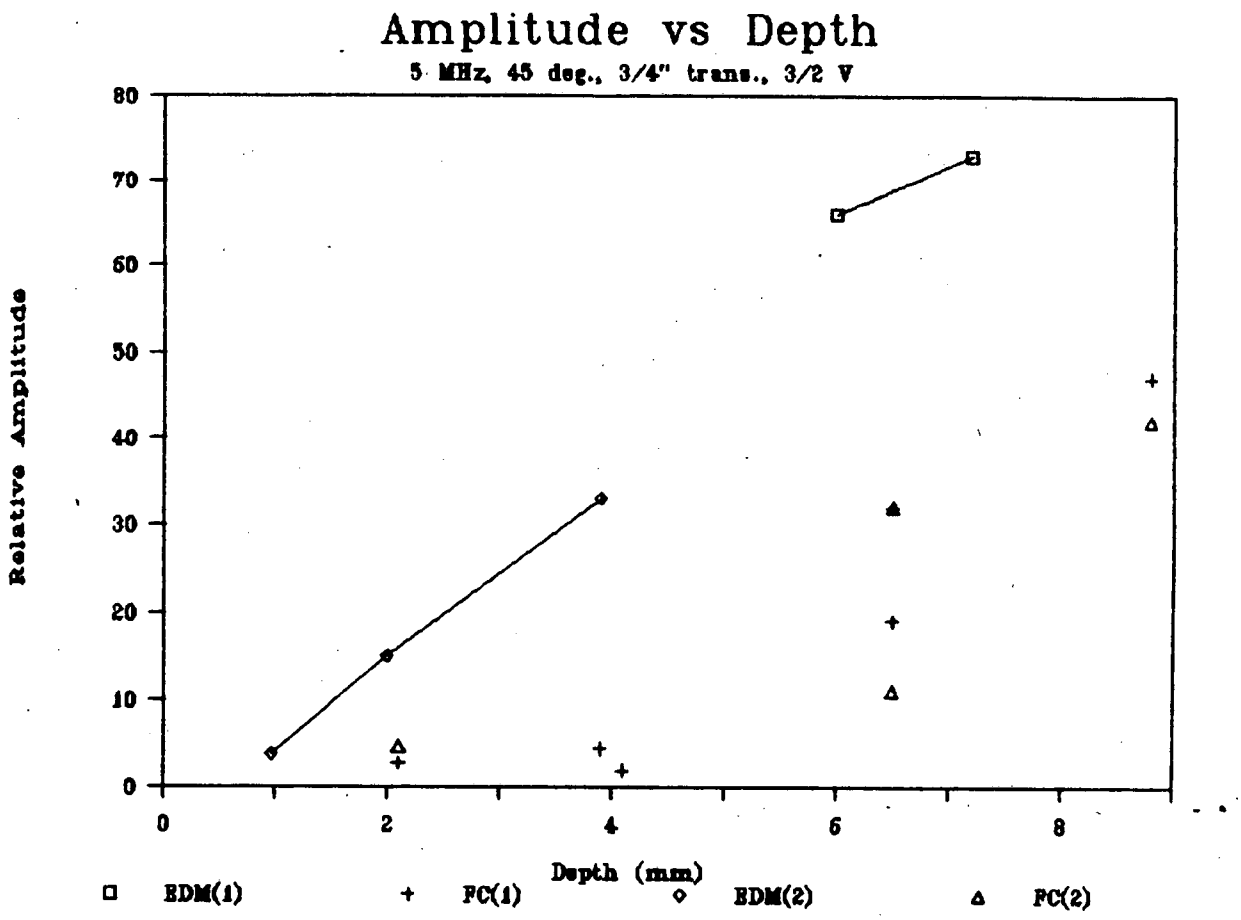
Amplitude vs Depth
5 MHz, 45 deg., 3/4" trans., 3/2 V
Relative Amplitude
80
70
60
50
40
30
20
10
0
0
2
4
6
8
Depth (mm)
EDM(1)
FC(1)
EDM(2)
FC(2)

Figure F-13

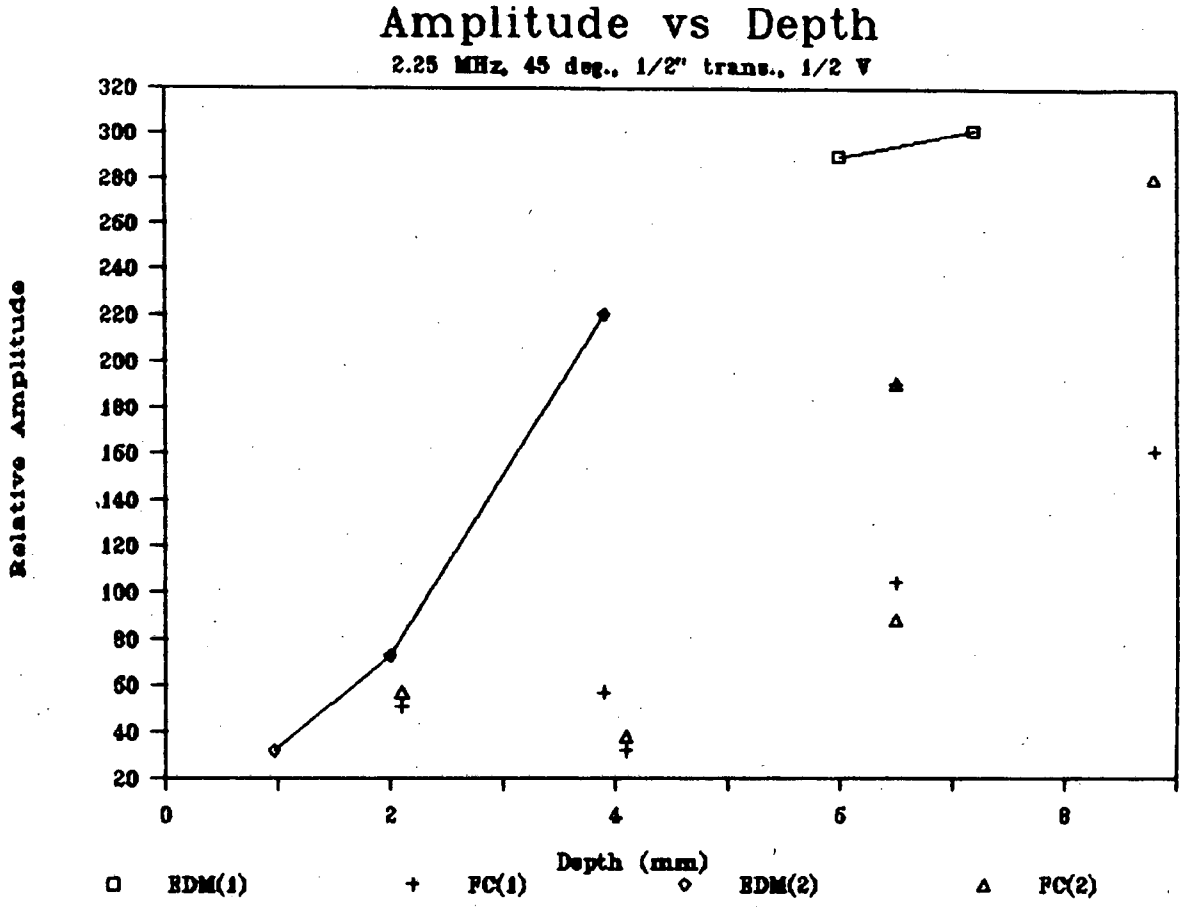
Amplitude vs Depth
2.25 MHz, 45 deg., 1/2" trans., 1/2 V
Relative Amplitude
320
300
280
260
240
220
200
180
160
140
120
100
80
60
40
20
0
2
4
6
8
Depth (mm)
EDM(1)
FC(1)
EDM(2)
FC(2)

Figure F-14

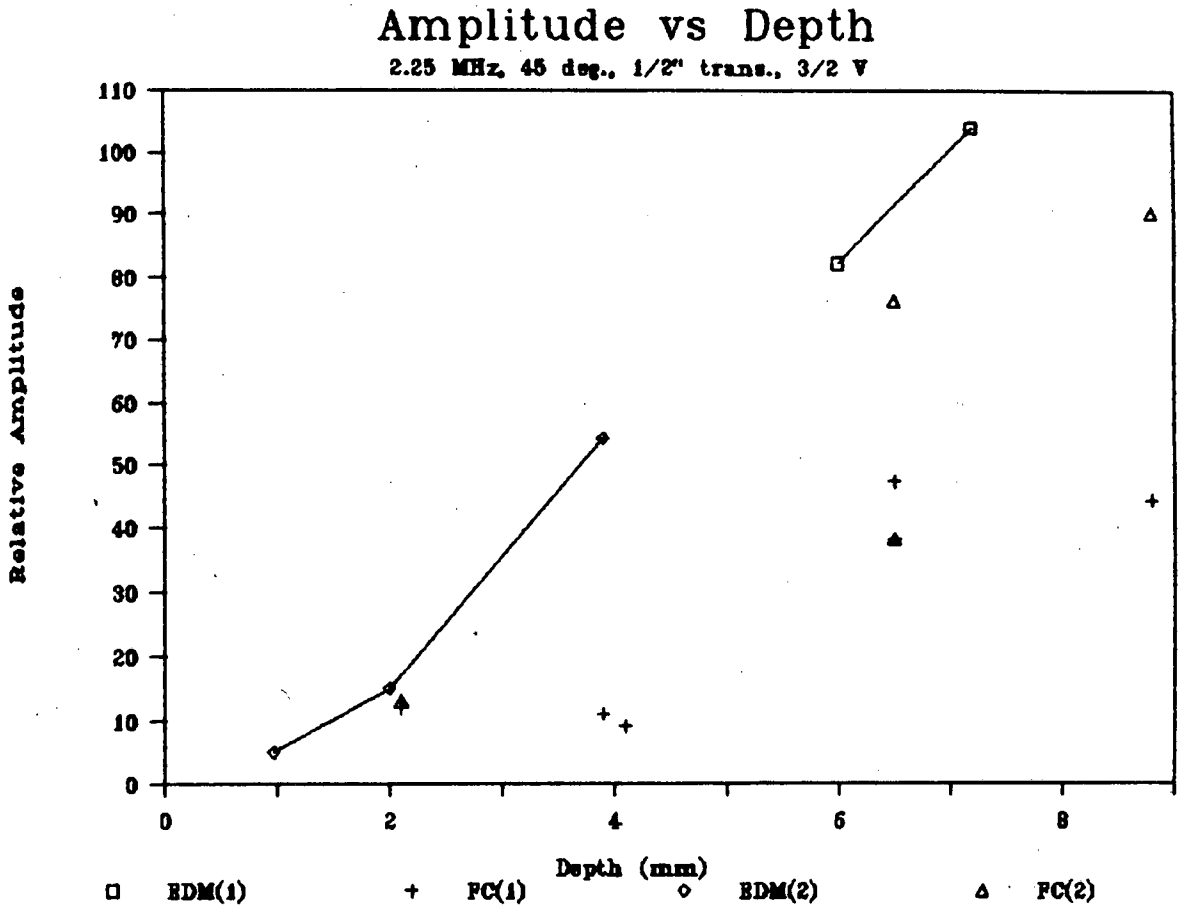
Amplitude vs Depth
2.25 MHz, 45 deg., 1/2" trans., 3/2 V
Relative Amplitude
110
100
90
80
70
60
50
40
30
20
10
0
0
2
4
6
8
Depth (mm)
EDM(1)
FC(1)
EDM(2)
FC(2)

Figure F-15

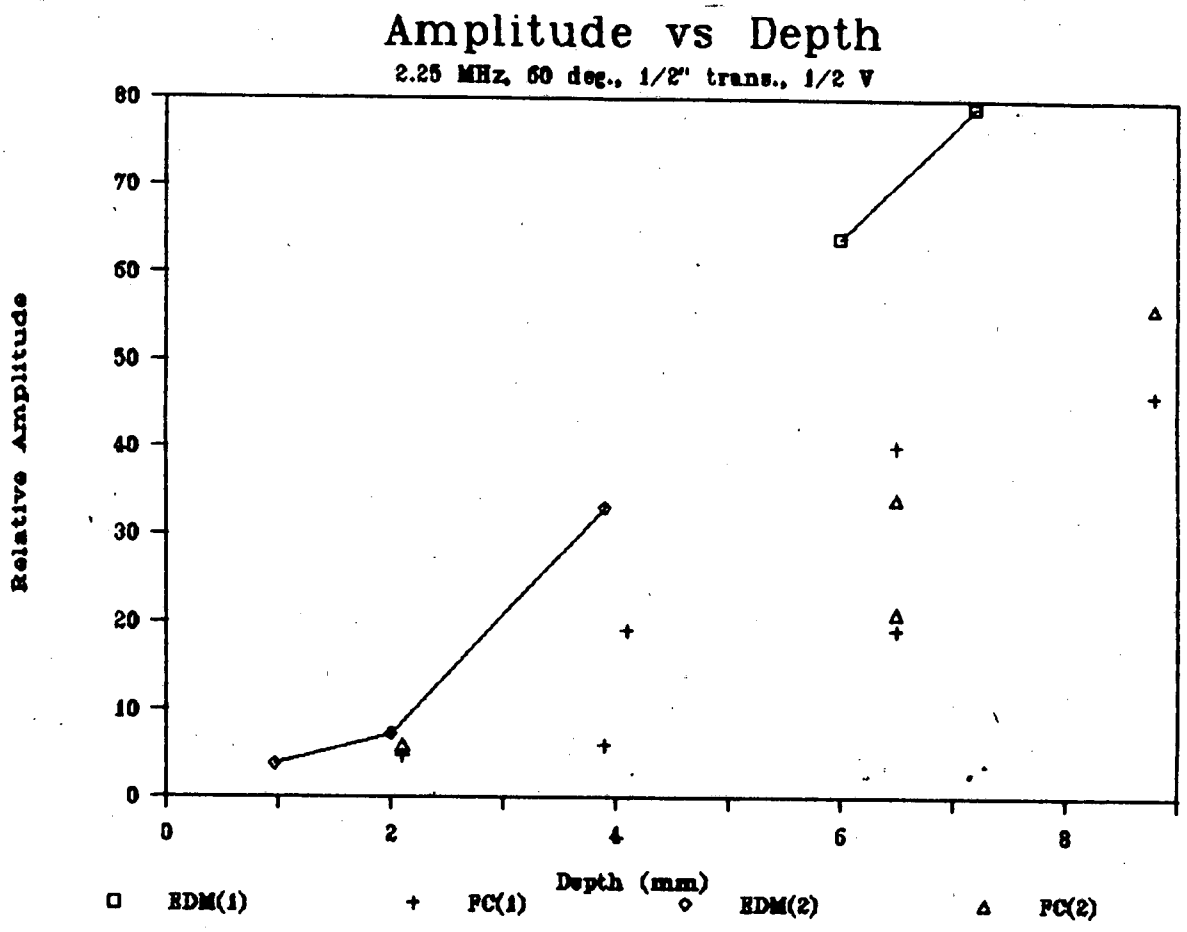
Amplitude vs Depth
2.25 MHz, 60 deg., 1/2" trans., 1/2 V
Relative Amplitude
80
70
60
50
40
30
20
10
0
0
2
4
6
8
Depth (mm)
EDM(1)
FC(1)
EDM(2)
FC(2)

Figure F-16

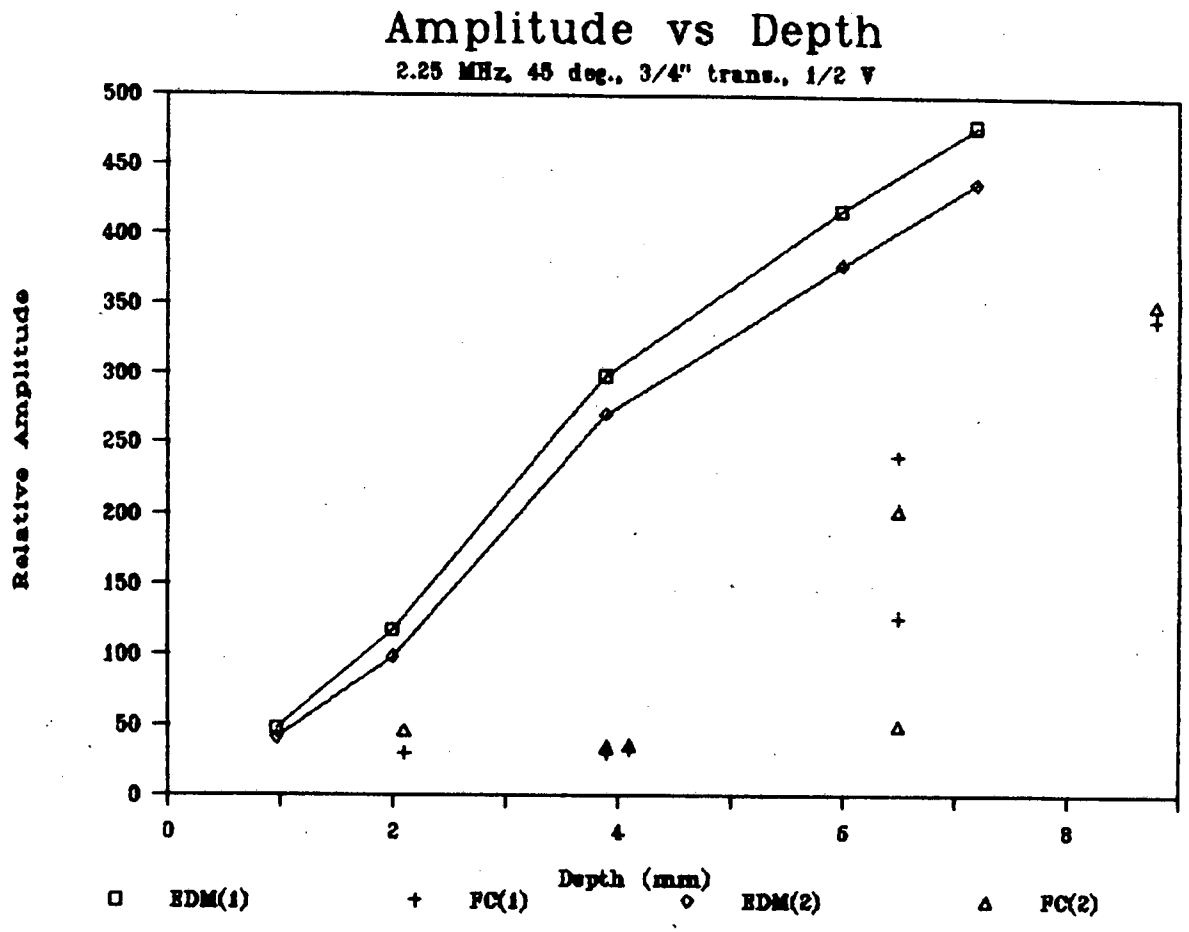
Amplitude vs Depth
2.25 MHz, 45 deg., 3/4" trans., 1/2 V
Relative Amplitude
500
450
400
350
300
250
200
150
100
50
0
0
2
4
6
8
Depth (mm)
EDM(1)
FC(1)
EDM(2)
FC(2)

Figure F-17

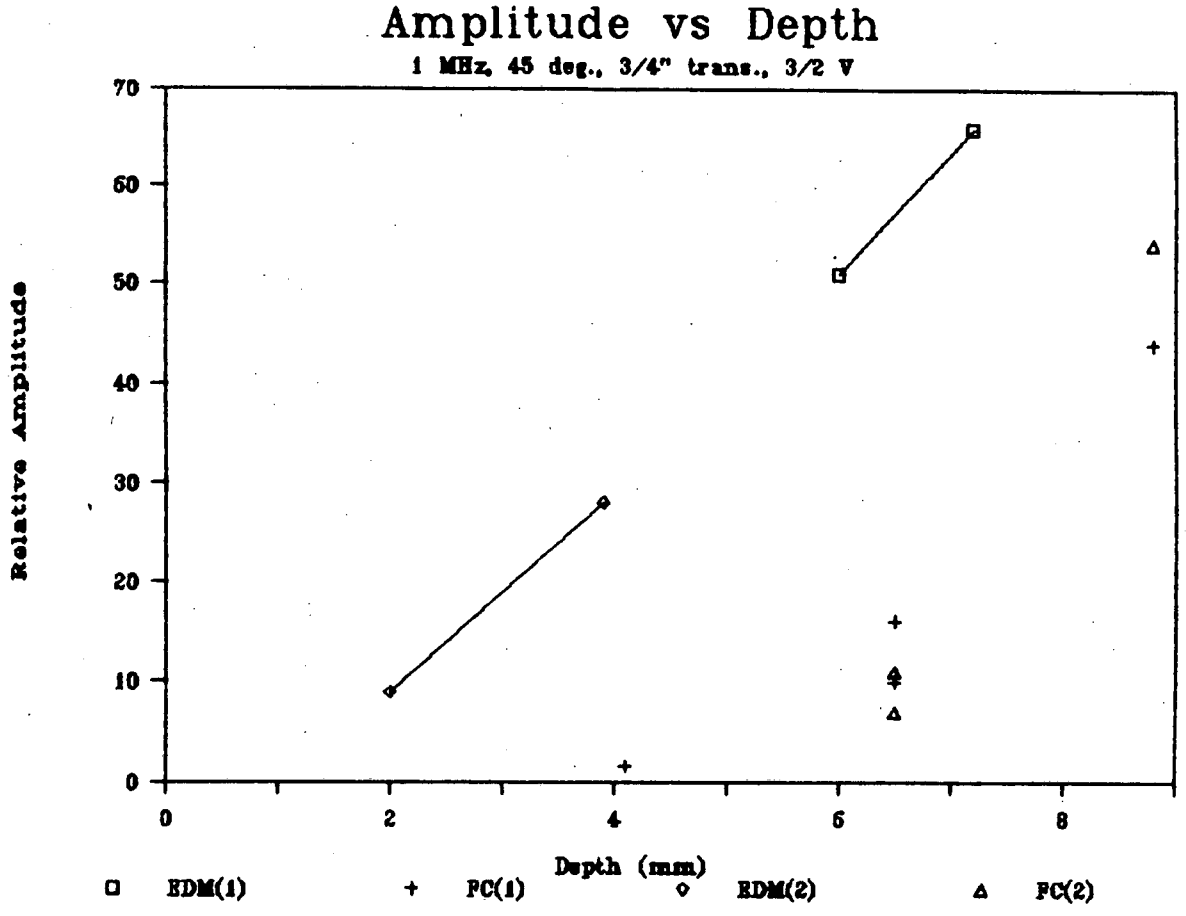
Amplitude vs Depth
1 MHz, 45 deg., 3/4" trans., 3/2 V
Relative Amplitude
70
60
50
40
30
20
10
0
0
2
4
6
8
Depth (mm)
EDM(1)
FC(1)
EDM(2)
FC(2)

Figure F-18

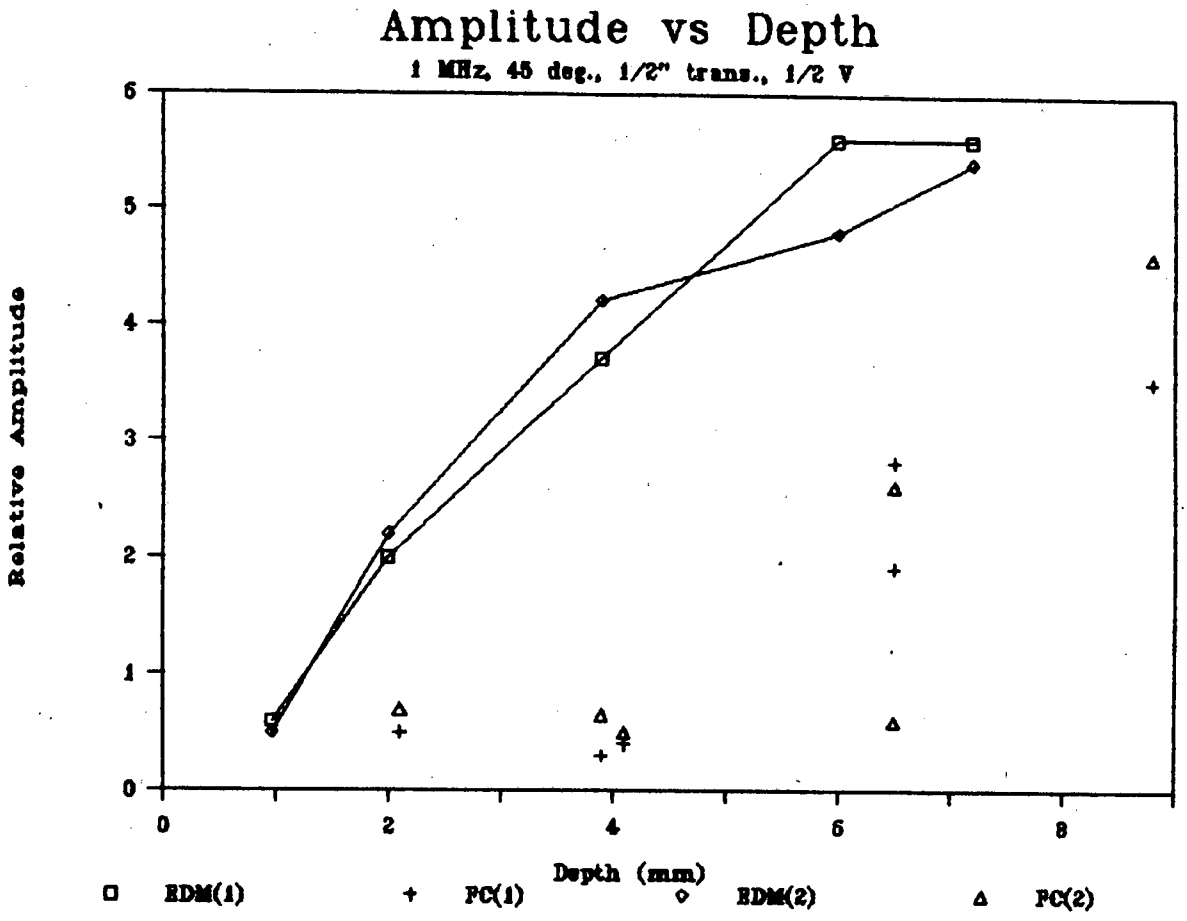
Amplitude vs Depth
1 MHz, 45 deg., 1/2" trans., 1/2 V
Relative Amplitude
0
1
2
3
4
5
6
0
2
4
6
8
Depth (mm)
EDM(1)
PC(1)
EDM(2)
PC(2)

Figure F-19

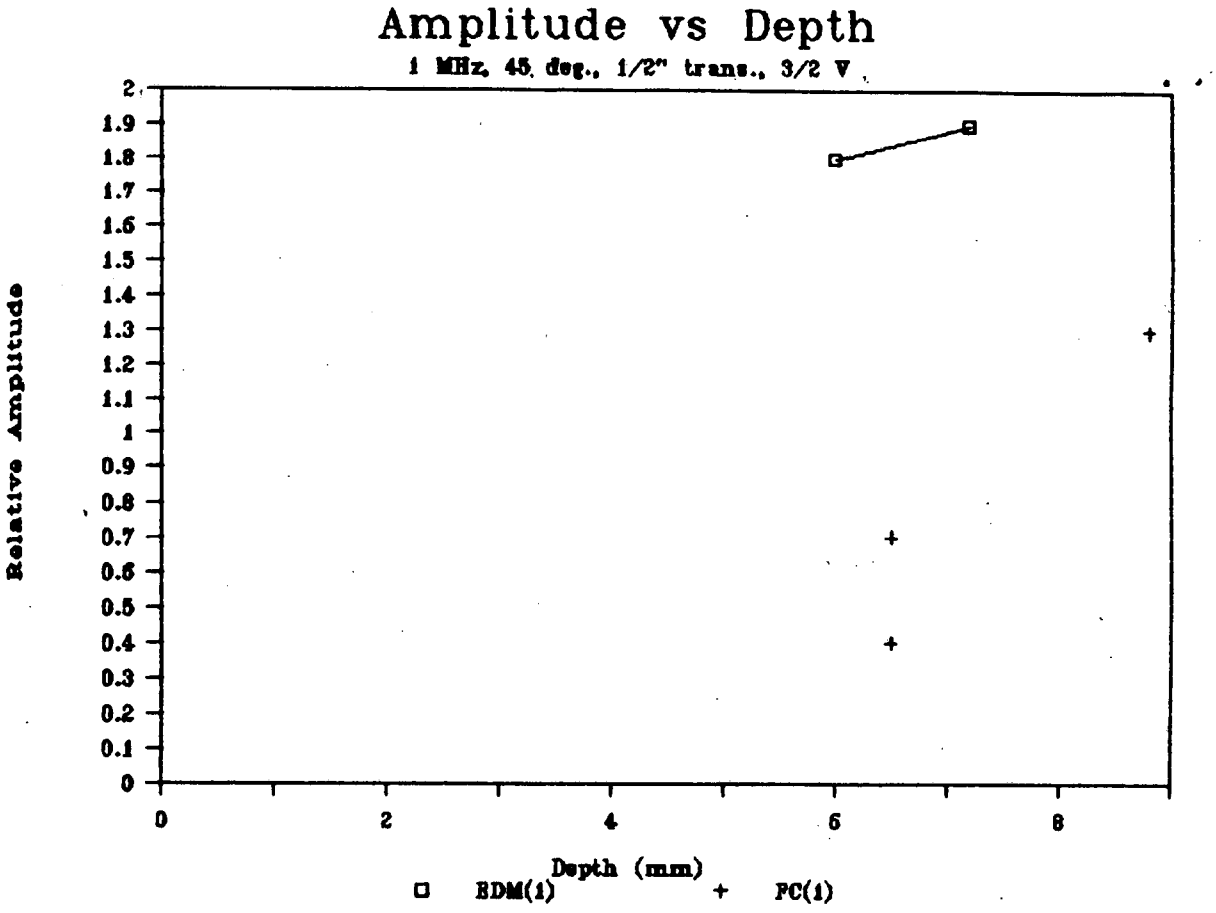
Amplitude vs Depth
1 MHz, 45 deg., 1/2" trans., 3/2 V
Relative Amplitude
2
1.9
1.8
1.7
1.6
1.5
1.4
1.3
1.2
1.1
1
0.9
0.8
0.7
0.6
0.5
0.4
0.3
0.2
0.1
0
0
2
4
6
8
Depth (mm)
EDM(1)
PC(1)

Figure F-20

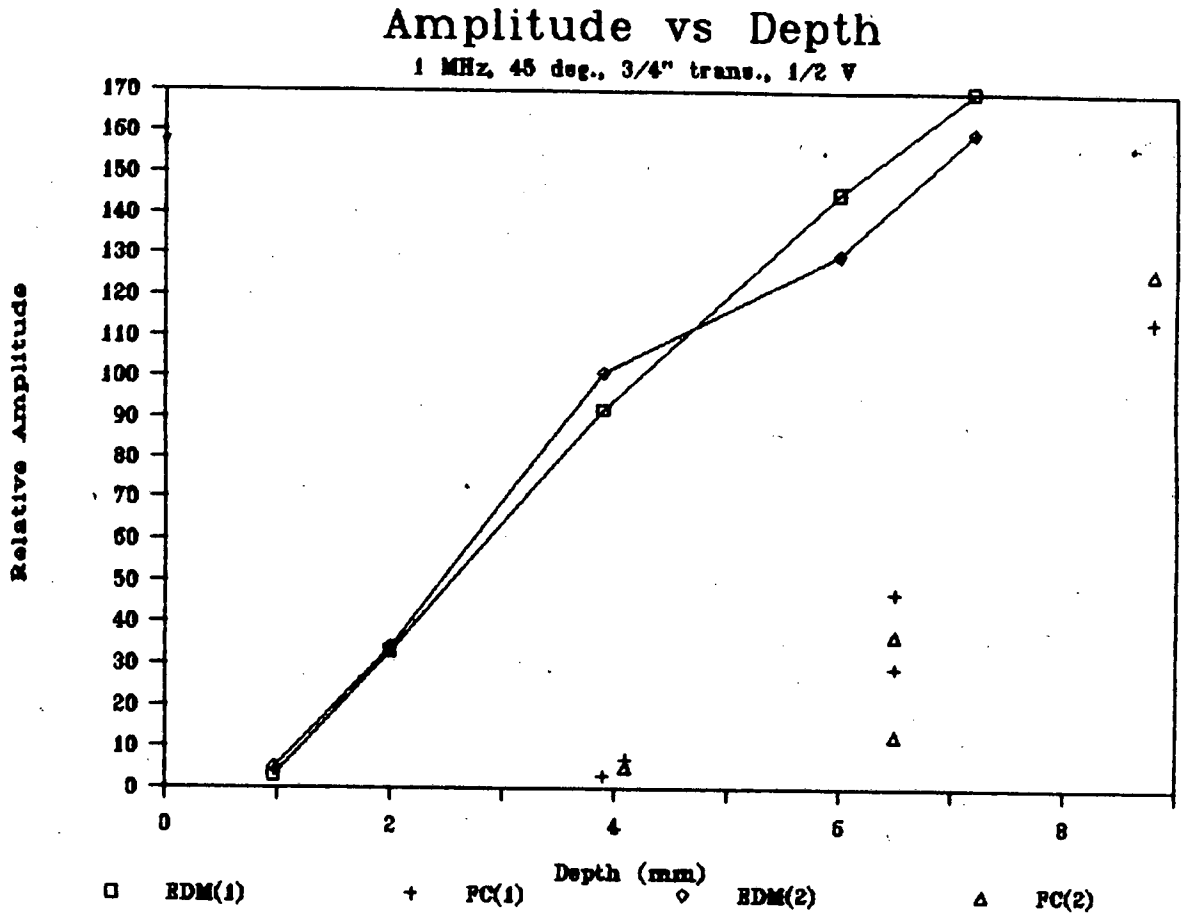
Amplitude vs Depth
1 MHz, 45 deg., 3/4" trans., 1/2 V
Relative Amplitude
170
160
150
140
130
120
110
100
90
80
70
60
50
40
30
20
10
0
0
2
4
6
8
Depth (mm)
EDM(1)
PC(1)
EDM(2)
PC(2)

Figure F-21(a)

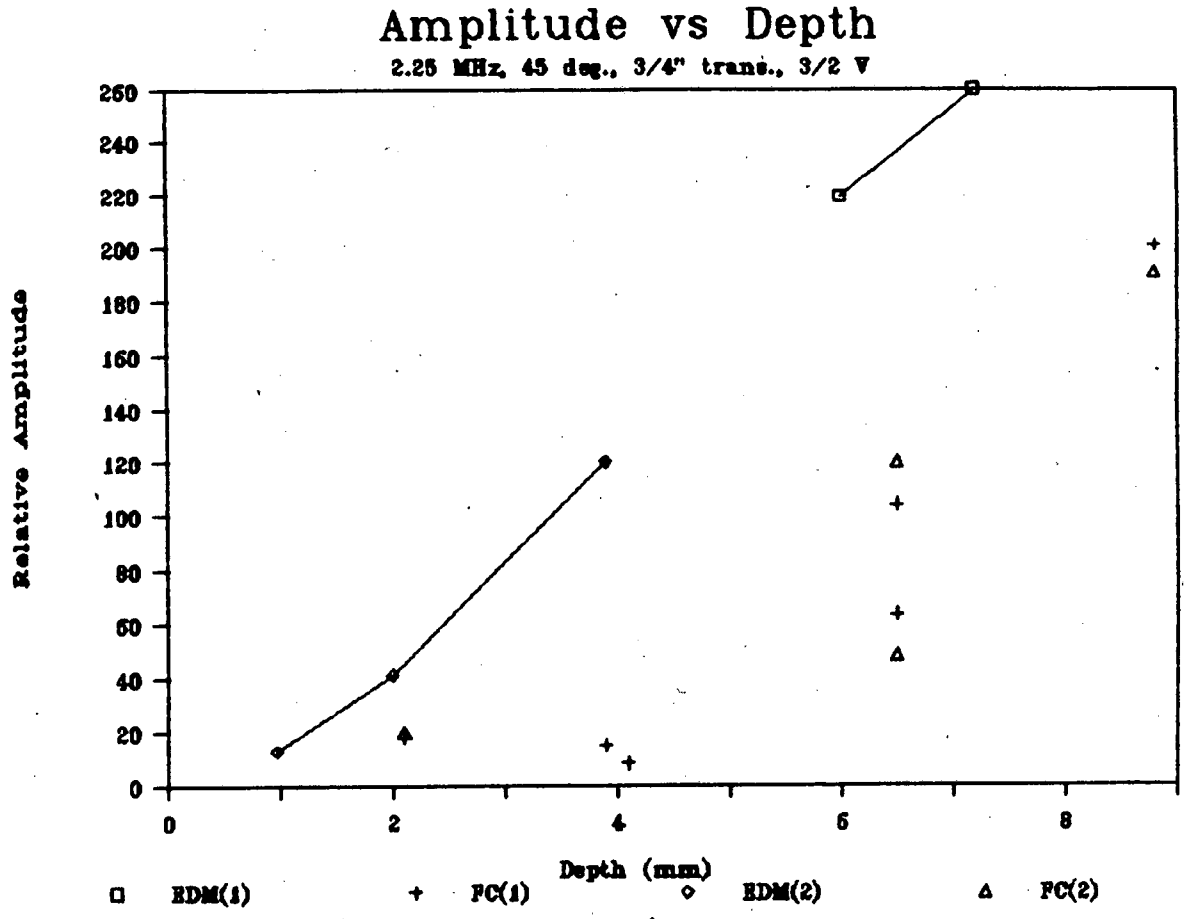
Amplitude vs Depth
2.25 MHz, 45 deg., 3/4" trans., 3/2 V
Relative Amplitude
260
240
220
200
180
160
140
120
100
80
60
40
20
0
0
2
4
6
8
Depth (mm)
EDM(1)
FC(1)
EDM(2)
FC(2)

Figure F-21(b)

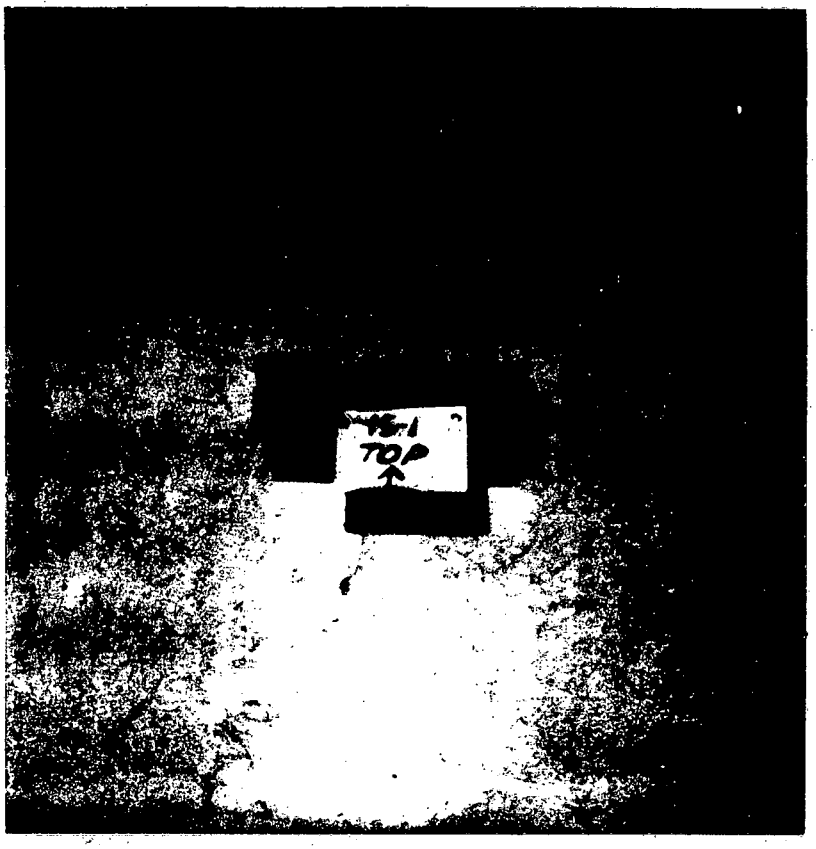

Figure F-22 Specimen 15-1

Figure F-23 Specimen 15-2

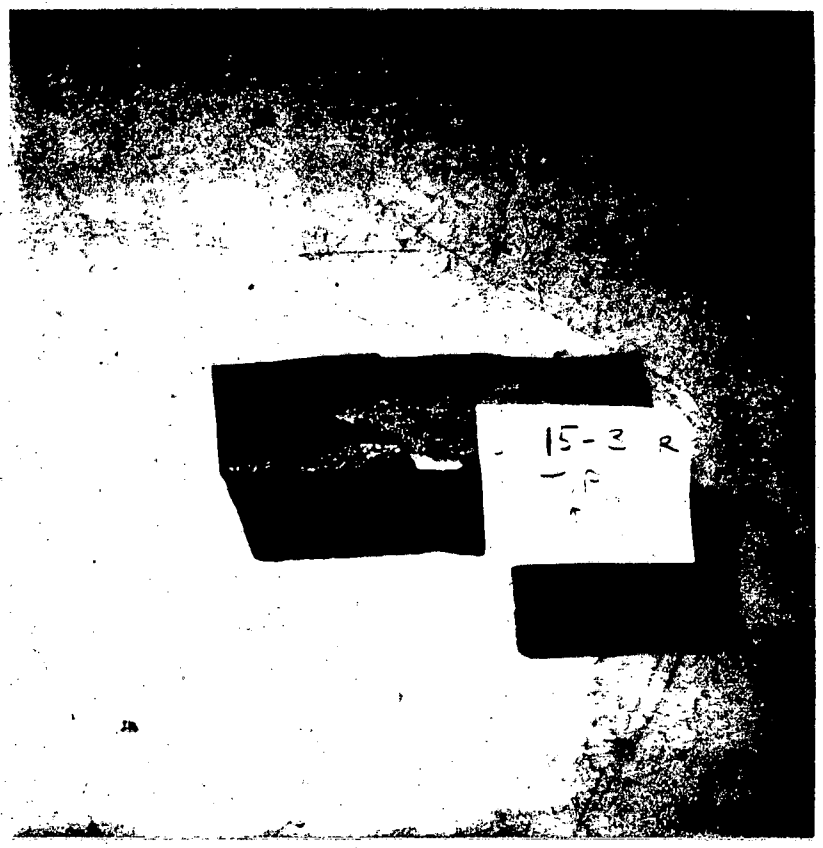

Figure F-24 Specimen 15-3

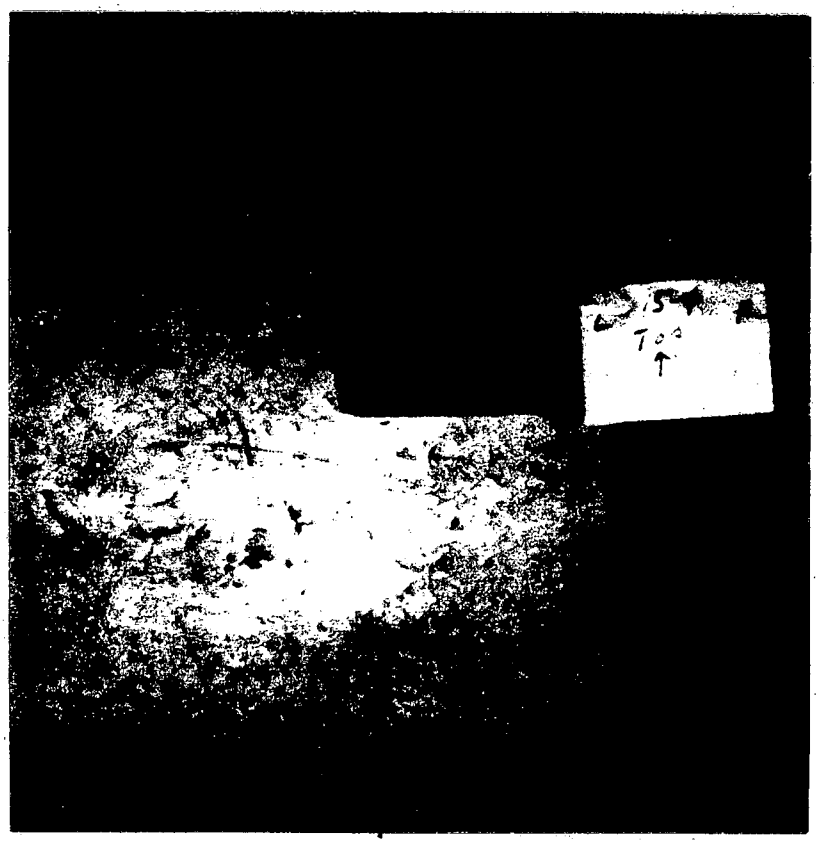

Figure F-25 Specimen 15-4

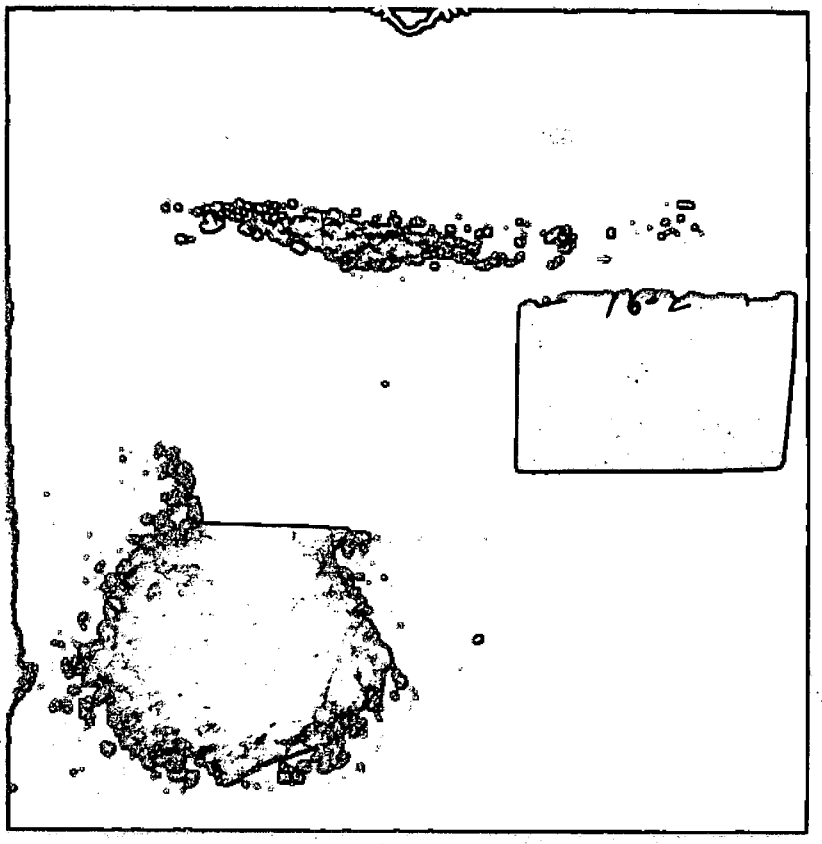

Figure F-26 Specimen 16-2

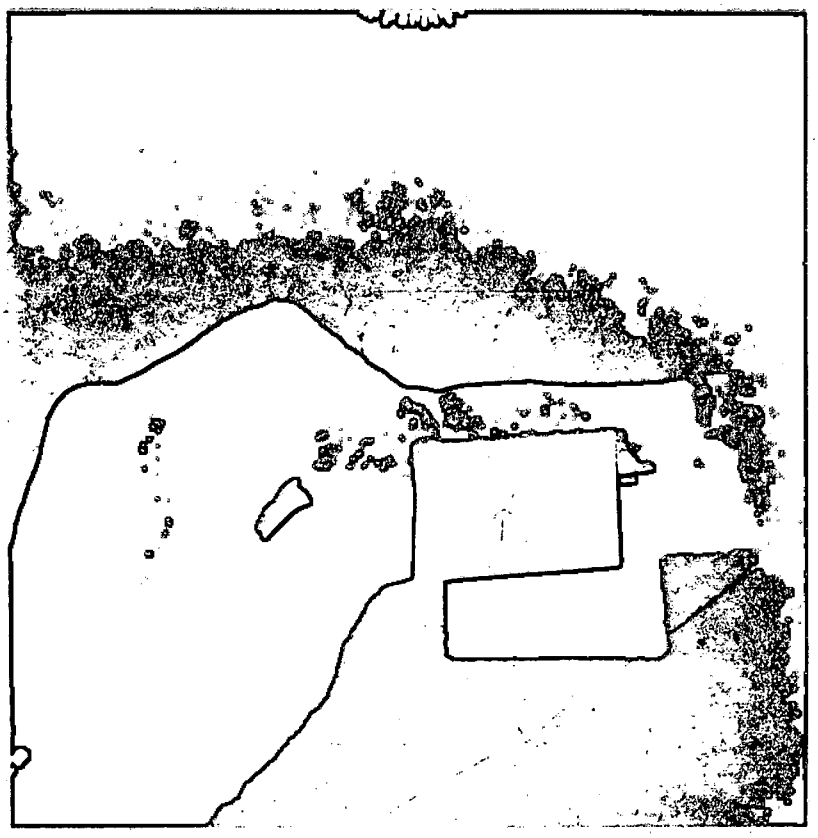

Figure F-27 Specimen 16-3

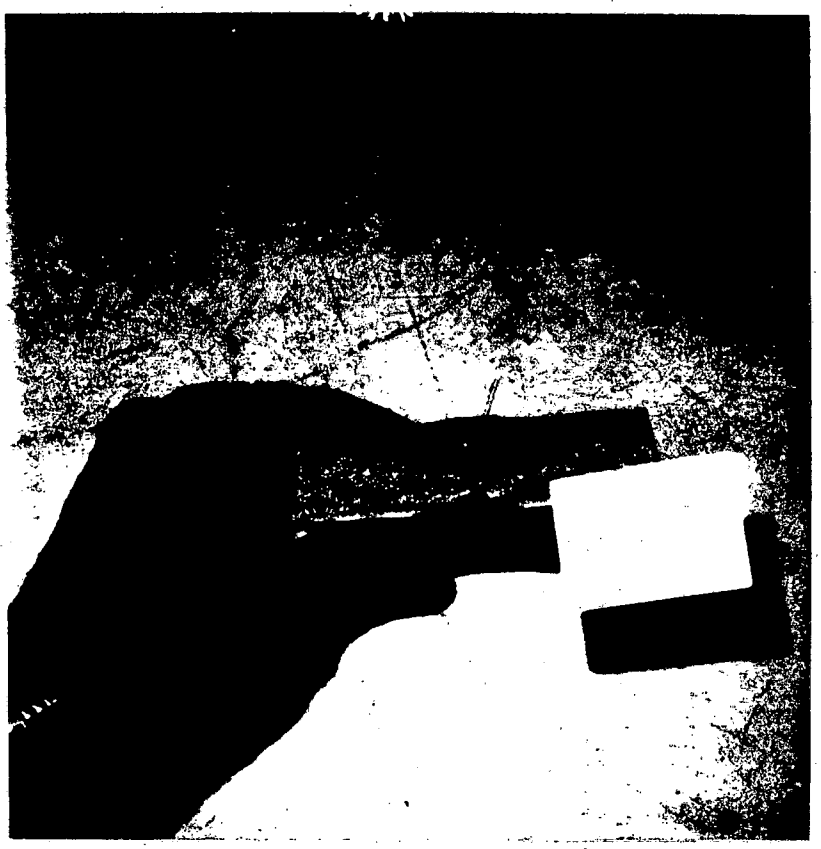

Figure F-28 Specimen 16-4

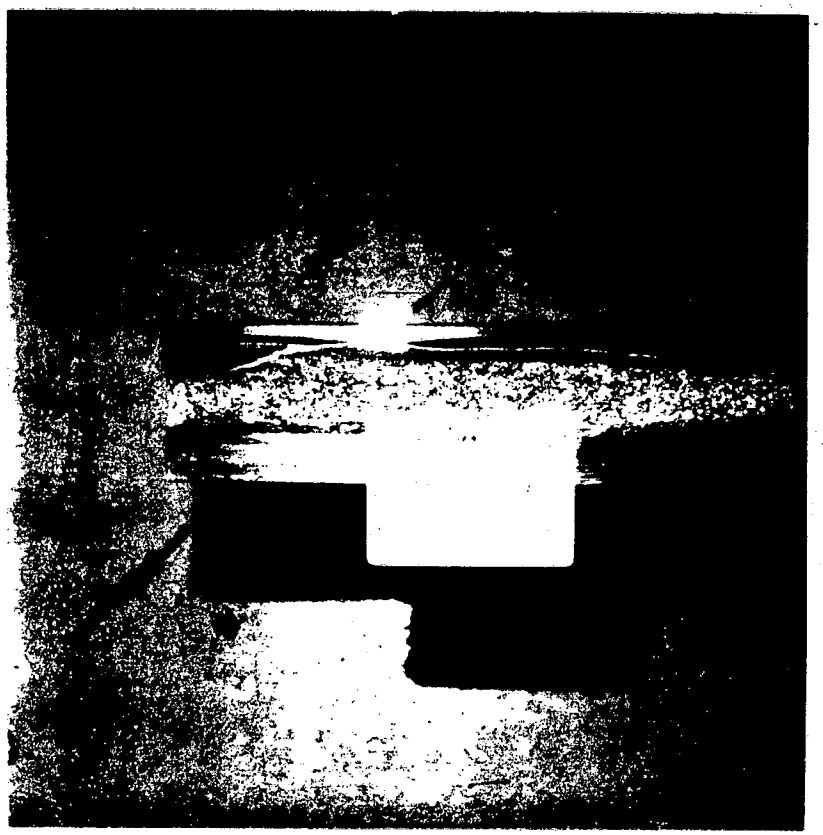

Figure F-29 Speciment 5-AA

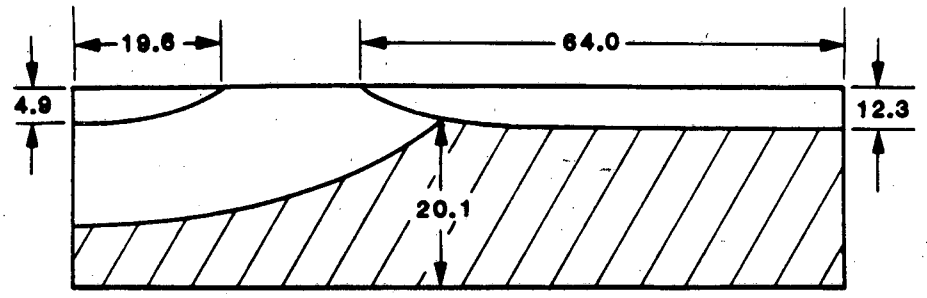

Specimen 15-1

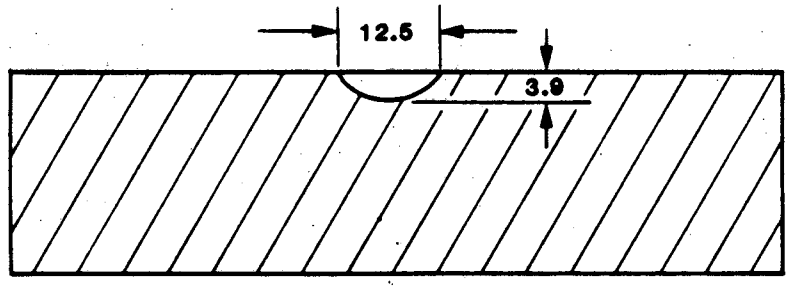

Specimen 15-2

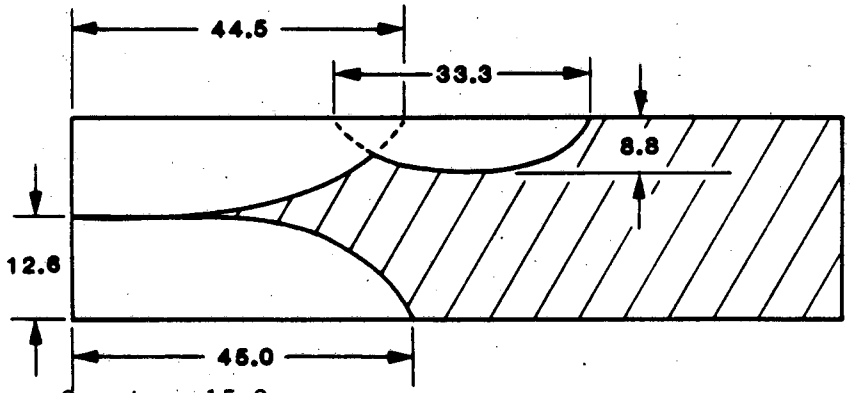

Specimen 15-3

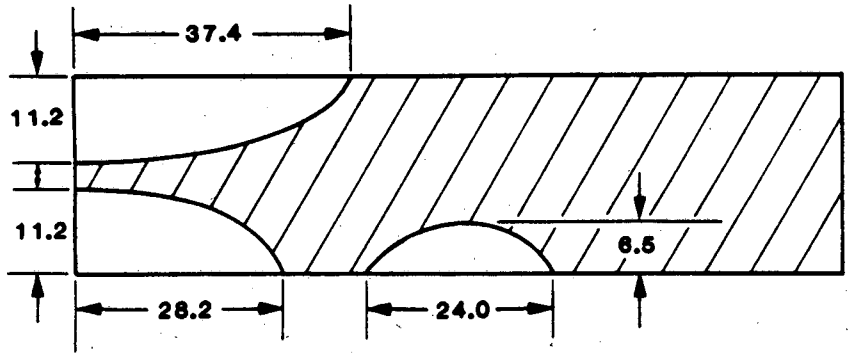

Specimen 15-4

Figure F-30 Actual Crack Sizes for Specimen 15 (mm) Shown Full Size

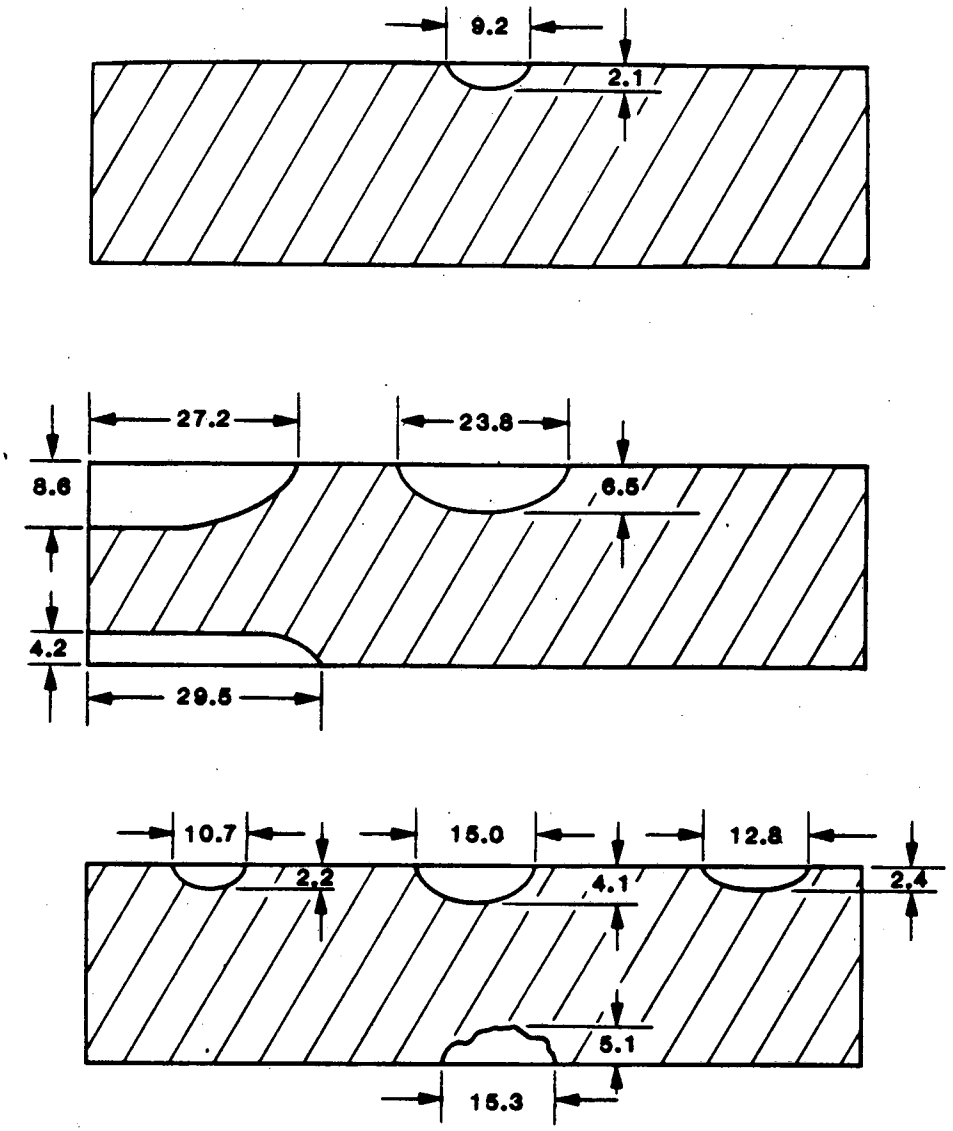

Figure F-31 Actual Crack Sizes for Specimen 16 (mm) Shown Full Size

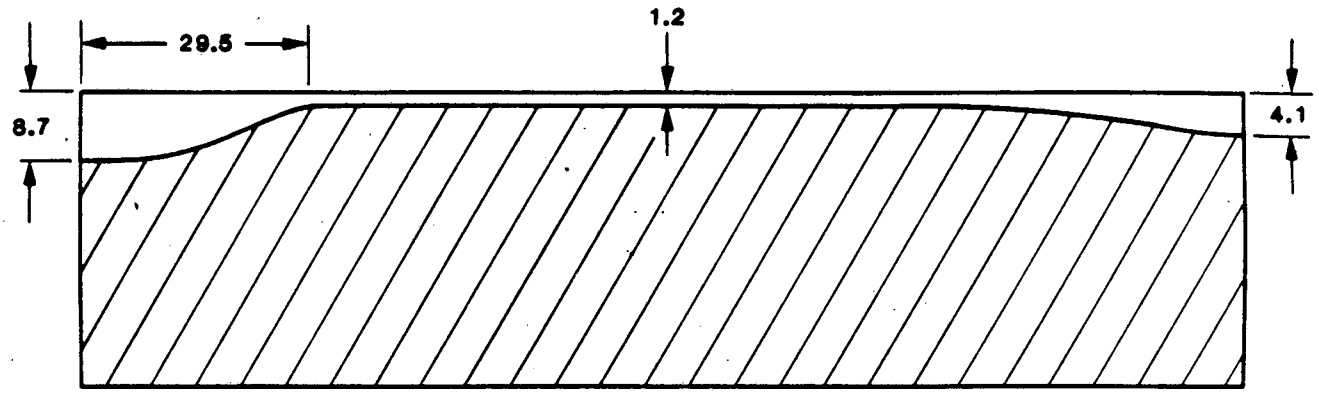

Figure F-32 Actual Crack Size for Specimen 5A-A
(Shown Full Size Looking Toward Connector Tang)

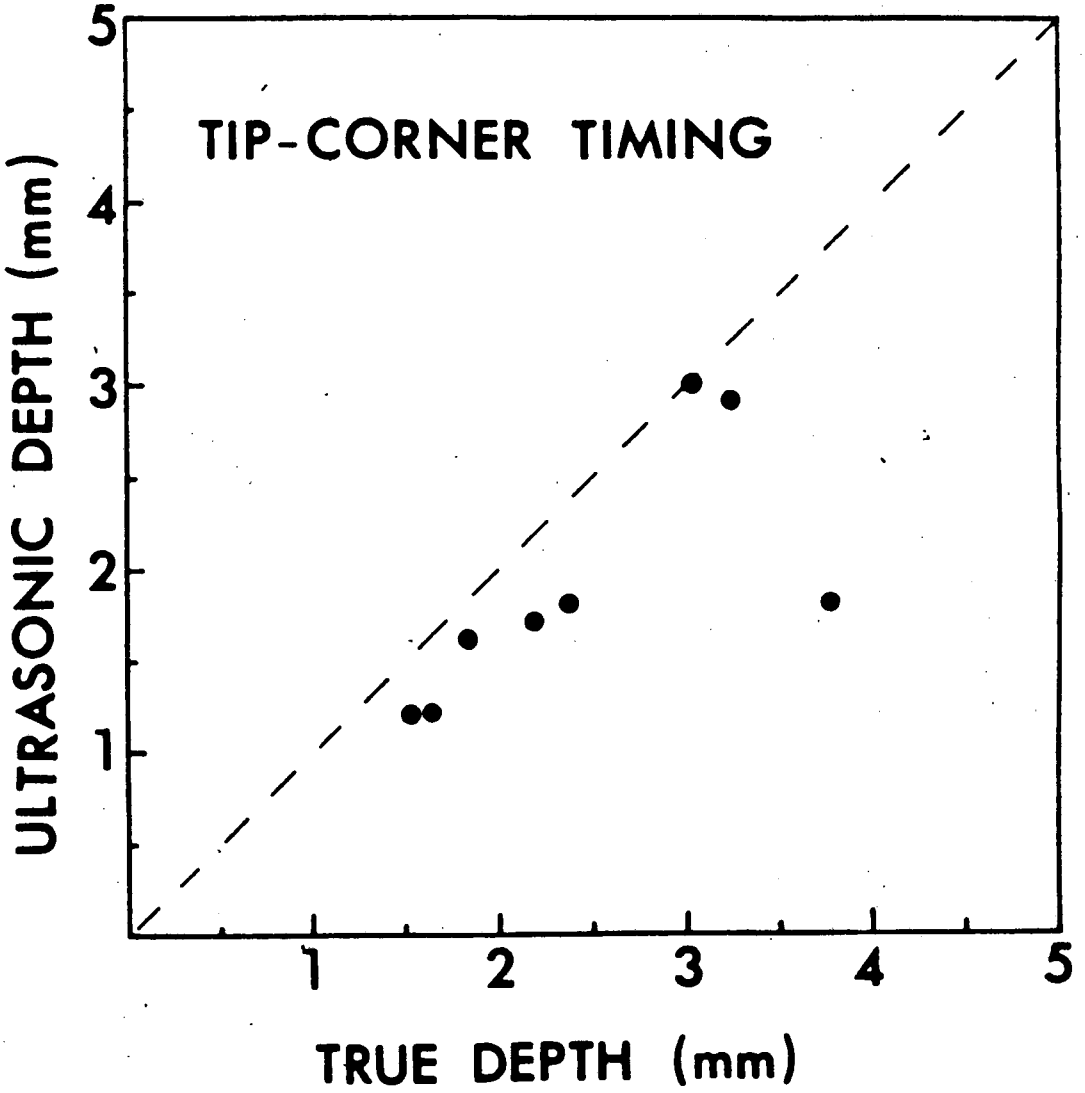

Figure F-33 Results of Defect Depth Measurement by the Tip-Corner Timing Method Using a Focussed Probe [Hayman, 1985]

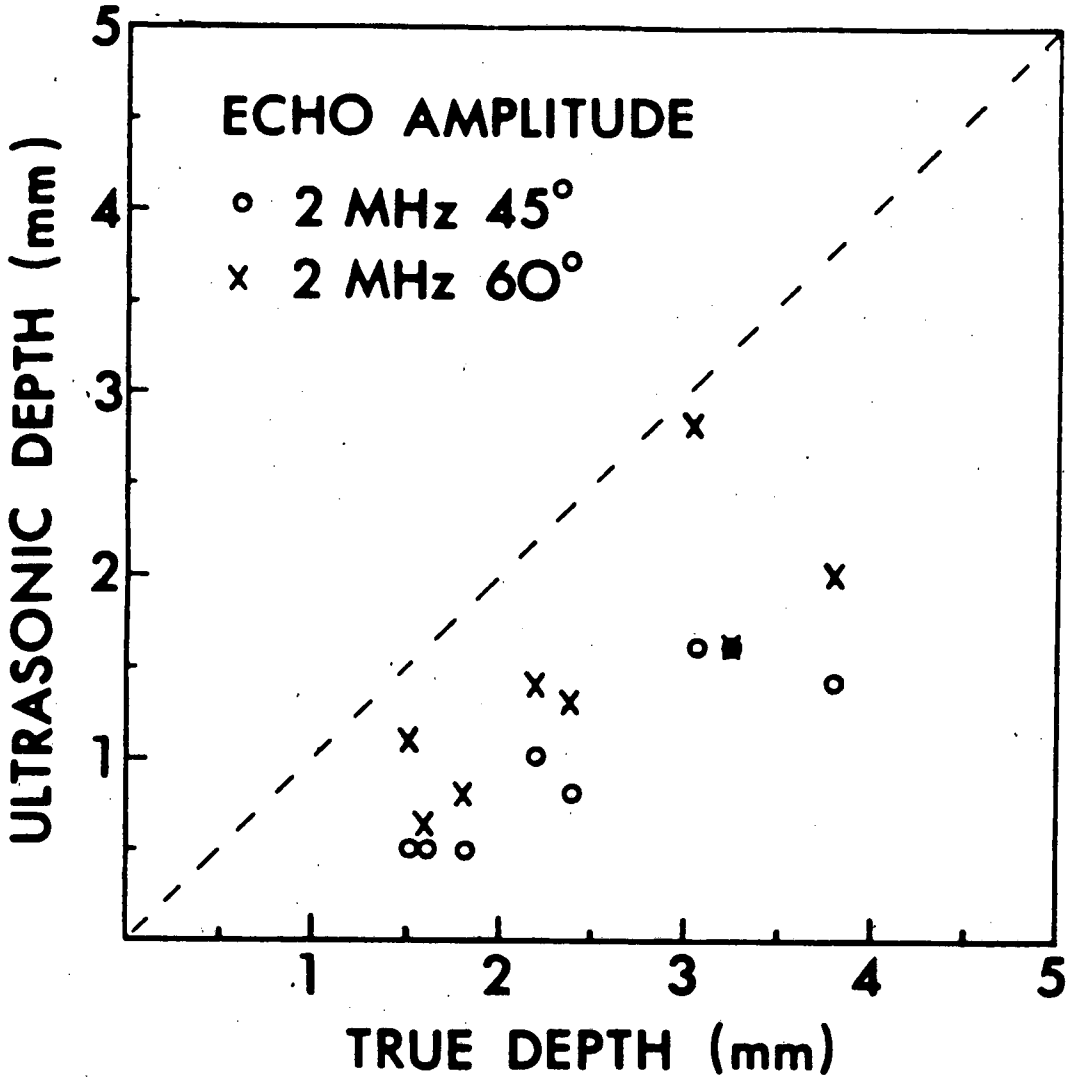

Figure F-34 Results of Defect Depth Estimation by Echo Amplitude with Contact Probes, [Hayman, 1985]

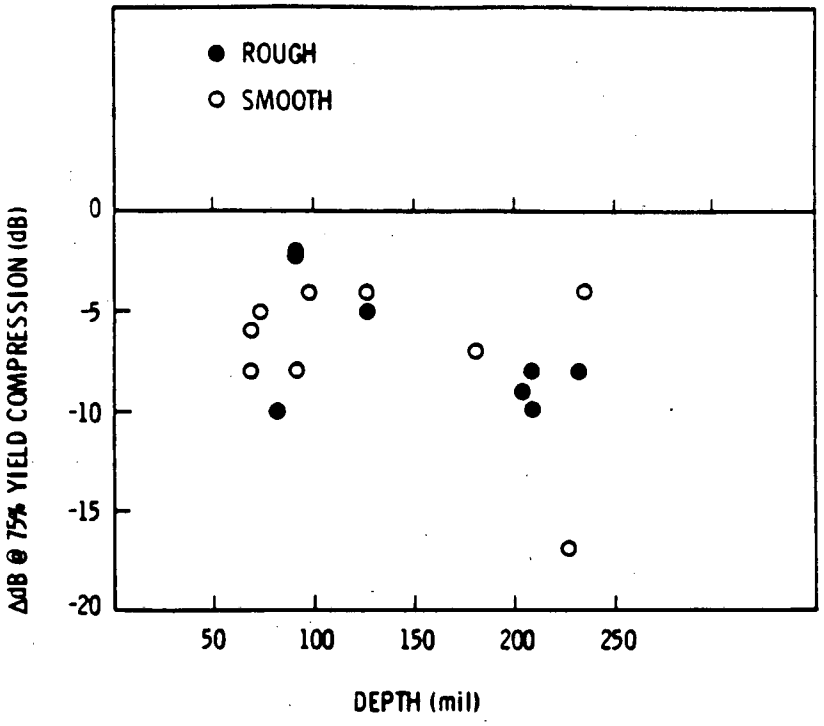

Figure F-35(a) Change in Ultrasonic Response of Bending Fatigue Cracks Upon Compression to 75% of Yeild Stress

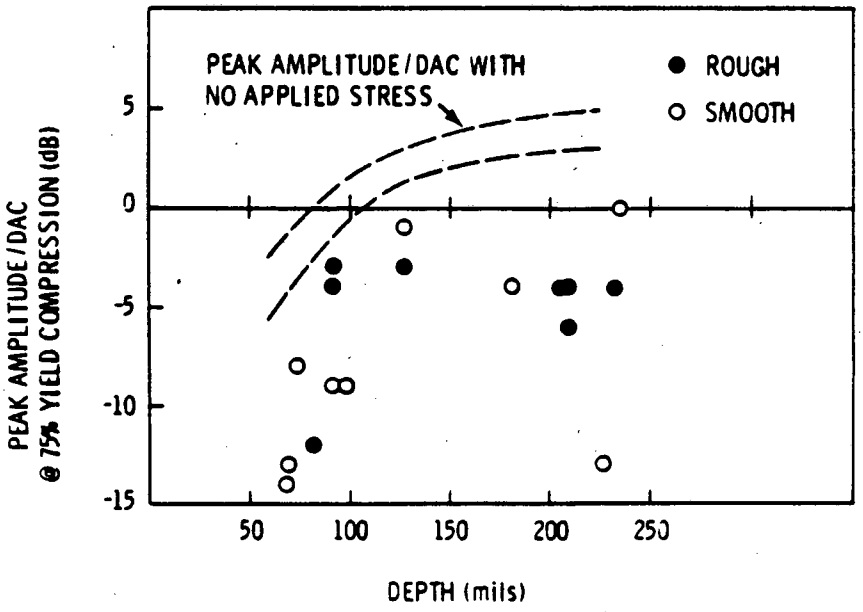

Figure F-35(b) Ultrasonic Response of Bending Fatigue Cracks Compressed to 75% of Yield Stress [Becker et al, 1981]

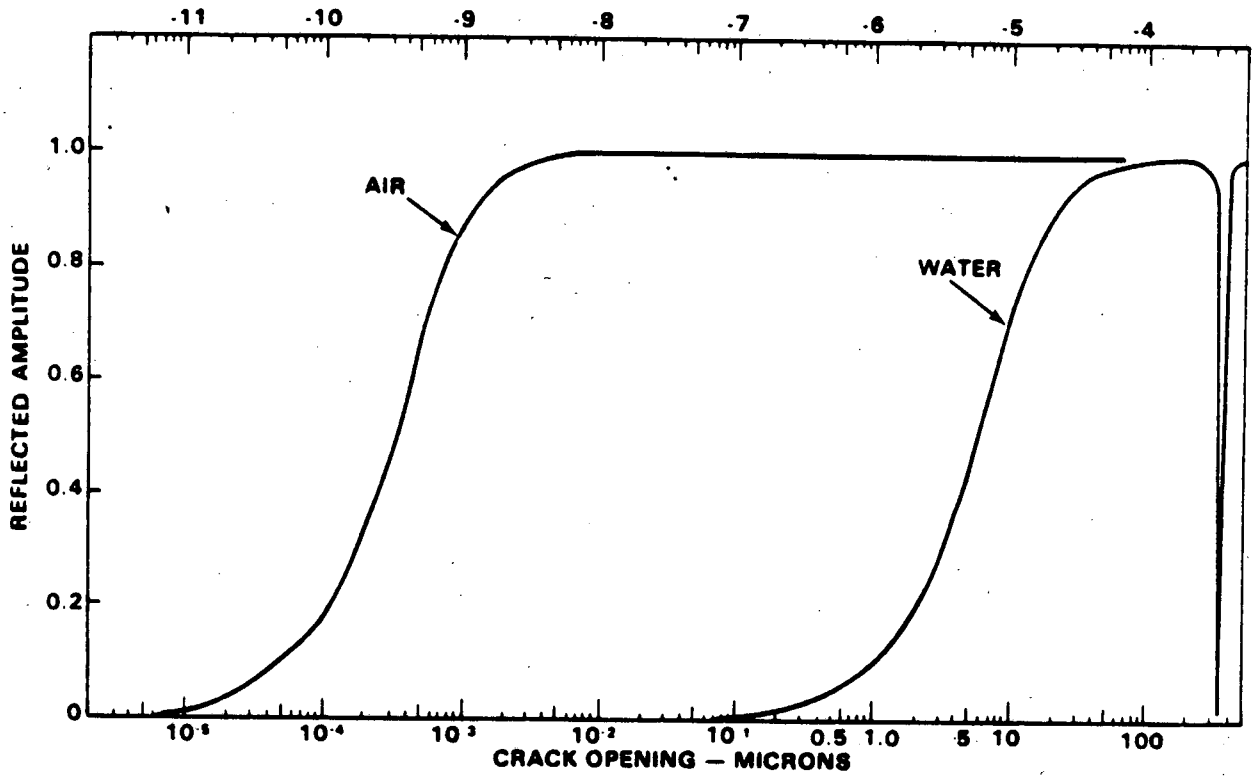

Figure F-36 Theoretical Ultrasonic Reflection Coefficient from Plane Parallel Stainless Steel Plates Separated by Air and Water, for 2.25 MHz Shear Wave at 45° [Becker, et al, 1985]

APPENDIX G

Description of Fatigue Tests and Photographic Record

G.1 Introduction

The tests using specimen 13 through 16 were designed to determine if the EDM notch calibration procedure was valid for fatigue crack size measurements using ultrasonic non-destructive testing. All specimens were 20 by 4 by 1 inch thick steel plates with a composition specified by ASME SA 387-22 Class 1 (2 1/4 Cr, 1 Mo). All pieces were heat treated (quenched and tempered) to a minimum 50 Rc as quenched condition, and a maximum 30 Rc as tempered.

A variety of EDM notches was machined in specimen 13. Each individual notch was scanned using a 5 MHz, 45 degree transducer at four differenc scanning paths. The notch signal strength as well as the time delay between its tip and root were recorded.

Four different fatigue cracks were then generated in each of the other specimens. Crack growth was estimated with ultrasonic scans along different scanning paths and each crack was grwon until it reached an estimated 6 mn in depth. The final crack depth and shape was verified by breaking the specimen at each crack location and measuring the crack characteristics (see Appendix F).

G.2 EDM Notch Calibration, Speciment 13

A total of five different EDM notches were machined in Specimen 13. Four different scanning paths were used. A 5 MHz, 45 degree transducer measured notch signal strength as well as tip to root time of flight delay.

G.3 Fatigue Crack Generation, Specimens 14, 15 and 16

G.3.1 Test Setup and Instrumentation Description

G.3.1.1 Test Fixture Description

The test fixture used to generate fatigue cracks in Specimen 14 through 16 is shown in Figure F-2. A heavy steel bench with a clamping mechanism mounted on its top was used for the stationary specimen side while a set of long "T" beams was used as lever arm and clamping mechanism for the oscillatory speciment side. The fixed steel test bench weighed close to 3000 pounds in order to insure that the fixed speciment side remained stationary.

The stationary claming device was made of two inch thick steel mating plates which sandwiched the specimen. The entire assembly was bolted down to the bench using six half-inch diameter bolts. The bolts were torqued evenly in order to maintain equal clamping pressures across the specimen.

The oscillatory clamping beams were 3/8 inch thick "T" beams clamped around the specimen on one side and supporting the oscillatory load generation mechanism on the other. High clamping pressures are required to apply the full load to the specimen and avoid any clamping mechanism movement which would modify the strain measurement calibration. Three evenly torqued half-inch diameter bolts were used on each side to distribute the clamping pressures as evenly as possible. Twenty pounds were attached to the beams underneath the cyclic load generation mechanism in order to increase the load generation capability.

G.3.1.2 Cyclic Load Generation

A D.C. current motor was mounted at the end of the oscillatory clamping beams with its rotating axis parallel to the notch centerline. A six inch diamter plate was mounted on the shaft with one 1.5 pound weight located on its perimeter. An SCR speed controller was used to adjust the rotation speed. As the plate rotates, it creates a vertical load perpendicular to the specimen centerline. The generated cyclic load is a pure bending load. The system weight was set such that the SCR control range of zero to 1500 rpm would allow the system to operate below and above the resonance frequency. The system resonance frequency was found to be around 850 rpm or 14 Hz.

The clamping setup weight, including the motor weight and the additional twenty pounds, caused an inequality in the load cycle amplitudes during the mostly used sub-resonance regimes. The measured load cycles were close to symetric when operating at the resonance frequency. The measured load peaks were averaged to compute the load acting on the specimen. This assumption underestimates the actual fatigue crack generating load since the slightly larger downward load performs the crack growth while the upward load, or crack lip closure, has a reduced impact on crack growth.

G.3.1.3 Cycle Count

The cycle count was performed using a digital stroboscope to accurately measure the rotations per minute and a stopwatch to measure the elapsed time.

G.3.1.4 Strain Level Measurement

Strain was measured during the experiments along the estimated crack propagation centerline. One strain gage was installed during most tests on the opposite side of the neutral axis and as far away from it as possible to increase the amplification. The strain gage was also installed for a few tests aligned with the crack but on the specimen top side. This caused wrong strain readings due to gage slippage as soon as the fatigue crack propagated. The strain gage type used were 350 ohn gages with a gage factor equal to 2.125. The quarter bridge gage was inserted in a bridge completion circuit and the output signal amplified for an oscilloscope reading.

G.3.1.5 Stress Calibration

The strain gage was claibrated after the complete clamping setup was assembled and tight. Using 100 pounds calibrated weight increments, a total of 500 pounds was suspended straight underneath the motor. The strain gage output voltage was recorded. During the actual cycling tests, the strain measurments were converted in equivalent pounds acting with a known lever arm. The stress could therefore be computed at the strain gage location.

G.3.1.6 Ultrasonic Non-Destructive Testing Equipment

Generated fatigue crack size was determined using the combination of an ultrasonic pulser and receiver. The pulse was set for a 125 volt spike to the transducer with a 50 ohm damping. A one quarter inch diameter Aerotech 5 MHz transducer was used with a 45 degree contact wedge. Ultrasonic coupling gel was used between the transducer and the specimen. The fatigue crack ultrasonic echo on an oscilloscope determined the crack size. Ultrasonic signal strength as well as time of flight computations were used to estimate the crack size. Ultrasonic paths are shown in Figure F-3.

G.4 Results from Specimens 13-16

Table G-1 through G-5 present the results of the UT inspection for specimens 13-16. Table G-6 documents the actual UT records photographed in 119 photos, attached. These results were summarized and discussed in Appendix F.

G.5 Test Setup for Specimen 5A-A

G.5.1 Test Fixture Description

The test fixture used to generate fatigue cracks in Specimen 5A-A is shown in Figure G-1. This setup was identical to that used for Specimens 13-16 discussed above. Ultrasonic paths are shown in SK-013 (see Appendix H).

G.5.2 Test Results

G.5.2.1 Stress Computation

The stress at the notch bottom was generated using cyclic bending loads. The test specimen was clamped on one side of the notch while the other side was cycled up and down generating pure bending loads at the notch. Strain gages were used to measure strain levels underneath the notch as described in Figure SK-014 (see Appendix H). The strain level has to be measured a little lower than the notch bottom due to the possible crack propagation and with sufficient amplification to optimize the measurement accuracy. The strain gages were therefore installed on the opposite side of the neutral axis and as far away from it as possible to increase the measurement amplitude. The measured strain levels were calibrated by handing known weights straight underneath the load generating motor. The measured strain levels during the experiment were then converted to an equivalent weight hanging with a known lever arm from the notch to compute the bending moment acting at the notch.

Two strain gages were installed in order to be able to verify the linear stress distribution in the specimen section below the notch and on the opposite side from the neutral axis. If the stress pattern is found to be linear in that area, the stress can be computed at the notch bottom knowing the bending moment, the cross-sectional moment of inertia, the distance from the neutral axis to the notch bottom and the stress intensity factor for a notched specimen.

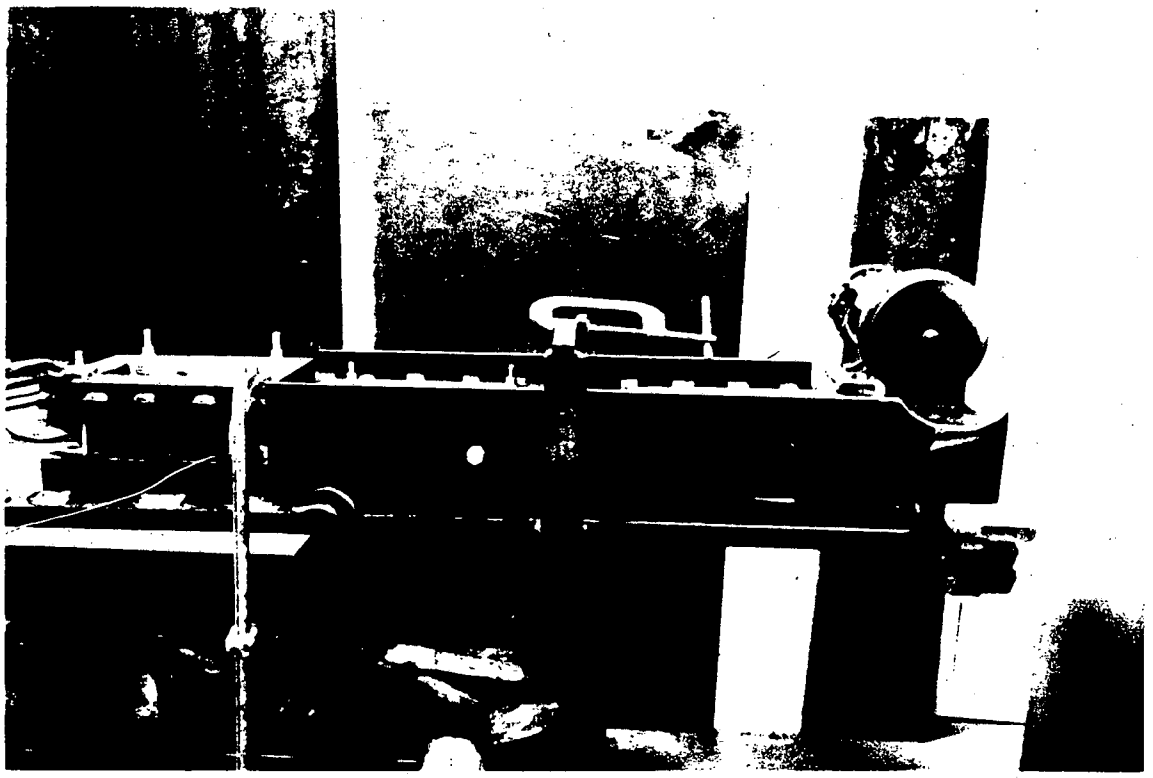

Figure G-1 Fatigue Test Fixture for Specimen 5A-A

TABLE G-1

#13 EDM CALIBRATION SPECIMEN

E.D.M. Size	(Probe Reading) Notch Width	Bounce Path	Root Reflection Maximum Voltage	Tip-Root Delay
1 mm	1.5	Front-1	1.6 V	---
2 mm	1.6	Front-1	5 V	.50µs
4 mm	2.2	Front-1	8 V	1.50µs
6 mm	2.7	Front-1	8 V	2.10)s
8 mm	3.2	Front-1	8 V	2.90µs

TABLE G-2

Test Specimens 14, 15 and 16 By Crack Size

Part - Crack#	Total K-Cycles	Crack Location	(Probe Reading) Crack Width	Bounce Path	Root Reflection Maximum Voltage	Root Postion	Tip-Root Delay	Estimated Size
14-3	23.4	C	1.5	Front-1	.4-1.4	C	---	Small Crack
16-2	31.8	C	3.1	Front-1	4.0	C	.25 μs	Hard to see tip
16-4	31.25	C	2.5	Front-1	5.0	C	.50 μs	2 mm
15-2	28.5	C	2.8	Front-1	5.6	C	1.00 μs	2-4 mm
16-3	30.1	C	3.7	Front-1	8.0	C	2.00 μs	6 mm
15-4	34.8	C	3	Front-1	8.0	C	3.00 μs	8 mm
14-1	35.9	A-D	6.1	Front-1	7.5-9.0	C	5.50 - 5.75 μs	8 mm+

ARCTEC OFFSHORE CORPORATION

TABLE G-3

Part Crack # 14-1

Total K-Cycles	Crack Location	Crack Width	Bounce Path	Root Reflec. Maximum Volts	Root Position	Tip-Root Delay in μs	Comments
Date: 8 Sept. '86							
35.9	A - D	6.1 cm	Front-1	7.5 V	C	5.50-5.75	Possibly 8+mm Crack
Part Crack # 14-2 Date: 16 Sept. '86							
22.65	D - E	1.5 cm	Front-1	1.6 V	E	?	Not a good specimen. Cracked only on edge where clamped.
Part Crack # 14-3 Date: 26 Sept. '86							
23.4	C	1.5 cm	Front-1	1.4 V	C	.25 - .30	Could not get 1.4 V response on 15 Oct. to

TABLE G-4

Part Crack # 15-1

Total K-Cycles	Crack Location	Crack Width	Bounce Path	Root Reflec. Maximum Volts	Root Position	Tip-Root Delay in μs	Comments
Date: 30 Sept. '86							
73.4	-A - E+	Full width of part	Front-1	2.3 V	C	5.00	Root reflection never grew at "C". Not a good specimen.
Part Crack #15-2 Date: 14 Oct. '86							
29.5	C	2.8 cm	Front-1	5.6	C	1.00	Well behaved crack, 3-4 mm
Part Crack # 15-3 Date:16 Oct. '86							
26.9	C,D, & E	3.5 cm @ C 3.9 @ D&E	Front-1	8 V @ C 8.5 @ D	C	3.00	C is a perfect match to 8mm EDM calibration photos. D&E started from clamp pressure.

TABLE G-5

Part Crack # 15-4

Total K-Cycles	Crack Location	Crack Width	Bounce Path	Root Reflec. Maximum Volts	Root Position	Tip-Root Delay in μs	Comments
Date: 17 Oct. '86							
34.8	C & E	3 cm & 1 cm	Front-1	8 V	C	2.00	C is well behaved & perfect match to 6mm EDM. E is from clamp press.
Part Crack 16-2 Date: 21 Oct. '86							
31.8	C	3.1 cm	Front-1	4 V	C	.25	Difficult to identify tip and root.
Part Crack # 16-3 Date: 21 Oct. '86							
30.1	C	3.7 cm	Front-1	8 V	C	2.00	Possibly another EDM 6mm match
Part Crack #16-4 Date: 21 Oct. '86							
31.25	C	2.5 cm	Front-1	5 V	C	.50	Approx. 2mm crack

TABLE G-6

Photo Log Specimens 13, 14, 15, and 16

45 Degree 5 Mhz Probe

Photo #	Specimen #	Notch/ Crack #	Bounce Path	Description				
1	13	1mm EDM	I	Front-1	1. V	0dB	10us	
2	13	1mm EDM	I	Front-1	1. V	0dB	1us	
3	13	1mm EDM	I	Front-1	.1V	0dB	1us	tip & root
4	13	1mm EDM	II	2-Bounce	.2V	0dB	10us	
5	13	1mm EDM	II	2-Bounce	.2V	0dB	1us	
6	13	1mm EDM	II	2-Bounce	50 mV	0dB	1us	tip & root
7	13	1mm EDM	III	Back	2. V	0dB	10us	
8	13	1mm EDM	III	Back	2. V	0dB	1us	
9	13	1mm EDM	III	Back	.5V	0dB	1us	tip & root
10	13	1mm EDM	IV	Back-1	.2V	0dB	10us	
11	13	1mm EDM	IV	Back-1	.2V	0dB	1us	
12	13	1mm EDM	IV	Back-1	50 mV	0dB	1us	tip & root
13	13	2mm EDM	I	Front-1	2. V	0dB	10us	
14	13	2mm EDM	I	Front-1	1. V	0dB	1us	
15	13	2mm EDM	I	Front-1	.1V	0dB	1us	tip & root
16	13	2mm EDM	II	2-Bounce	.5V	0dB	10us	
17	13	2mm EDM	II	2-Bounce	.5V	0dB	1us	
18	13	2mm EDM	II	2-Bounce	50 mV	0dB	1us	tip & root
19	13	2mm EDM	III	Back	5. V	0dB	10us	
20	13	2mm EDM	III	Back	5. V	0dB	1us	
21	13	2mm EDM	III	Back	.5V	0dB	1us	tip & root
22	13	2mm EDM	IV	Back-1	1. V	0dB	10us	
23	13	2mm EDM	IV	Back-1	1. V	0dB	1us	
24	13	2mm EDM	IV	Back-1	.1V	0dB	1us	tip & root
25	13	4mm EDM	I	Front-1	5. V	0dB	10us	
26	13	4mm EDM	I	Front-1	5. V	0dB	1us	
27	13	4mm EDM	I	Front-1	.2V	0dB	1us	tip & root
28	13	4mm EDM	II	2-Bounce	2. V	0dB	10us	
29	13	4mm EDM	II	2-Bounce	2. V	0dB	1us	
30	13	4mm EDM	II	2-Bounce	50.mV	0dB	1us	tip & root
31	13	4mm EDM	III	Back	5. V	0dB	10us	
32	13	4mm EDM	III	Back	5. V	0dB	1us	
33	13	4mm EDM	III	Back	.5V	0dB	1us	tip & root
34	13	4mm EDM	IV	Back-1	2. V	0dB	10us	
35	13	4mm EDM	IV	Back-1	2. V	0dB	1us	
36	13	4mm EDM	IV	Back-1	.1V	0dB	1us	tip & root
37	13	6mm EDM	I	Front-1	5. V	0dB	10us	
38	13	6mm EDM	I	Front-1	5. V	0dB	1us	
39	13	6mm EDM	I	Front-1	.1V	0dB	1us	tip & root
40	13	6mm EDM	II	2-Bounce	2. V	0dB	10us	
41	13	6mm EDM	II	2-Bounce	2. V	0dB	1us	
42	13	6mm EDM	II	2-Bounce	50.mV	0dB	1us	tip & root
43	13	6mm EDM	III	Back	5. V	0dB	10us	
44	13	6mm EDM	III	Back	5. V	0dB	1us	
45	13	6mm EDM	III	Back	2. V	0dB	1us	tip & root

TABLE G-6 (cont'd.)

Photo Log Speciments 13, 14, 15, and 16

45 Degree 5 Mhz Probe

Photo #	Specimen #	Notch/ Crack #	Bounce Path	Description
46	13	6mm EDM	III	Back-1 5. V 0db 10us
47	13	6mm EDM	IV	Back-1 5. V 0dB 1us
48	13	6mm EDM	IV	Back-1 .1V 0dB 1us tip & root
49	13	8mm EDM	I	Front-1 5. V 0dB 10us
50	13	8mm EDM	I	Front-1 5. V 0dB 1us
51	13	8mm EDM	I	Front-1 .2V 0dB 1us tip & root
52	13	8mm EDM	II	2-Bounce 2. V 0dB 10us
53	13	8mm EDM	II	2-Bounce 2. V 0dB 1us
54	13	8mm EDM	II	2-Bounce .1V 0dB 1us tip & root
55	13	8mm EDM	III	Back 5. V 0dB 10us
56	13	8mm EDM	III	Back 5. V 0dB 1us
57	13	8mm EDM	III	Back .5V 0dB 1us tip & root
58	13	8mm EDM	IV	Back-1 5. V 0dB 10us
59	13	8mm EDM	IV	Back-1 5. V 0dB 1us
60	13	8mm EDM	IV	Back-1 .1V 0dB 1us tip & root
61	14	14-1	I	Clean bar at start, positions A - C 1. V 0dB 10us
62	14	14-1	I	Scribe, position 'C' at start 1. V 0dB 10us
63	14	14-1	I	Scribe, position 'C' at start 1. V 0dB 1us
64	14	14-1	I	After set-up and acid drop pos.'C' 1. V 0dB 10us
65	14	14-1	I	After set-up and acid drop pos.'C' 1. V 0dB 1us
66	14	14-1	I	Crack, position 'C' 35.9 K-cycles 1. V 0dB 10us
67	14	14-1	I	Crack, position 'C' 35.9 K-cyc. 1. V 0dB 1us
68	14	14-1	I	Crack, position 'C' 35.9 K-cyc. 5. V 0dB 10us
69	14	14-1	I	Crack, position 'C' 35.9 K-cyc. 5. V 0dB 1us
70	14	14-1	I	Crack, position 'C' 35.9 K-cyc. .5V 0dB 1us tip & root.
71	14	14-1	I	Crack, position 'A' 35.9 K-cyc. 5. V 0dB 1us
72	14	14-1	I	Crack, position 'B' 35.9 K-cyc. 5. V 0dB 1us
73	14	14-1	I	Crack, position 'D' 35.9 K-cyc. 5. V 0dB 1us
74	14	14-1	I	End of crack, position 'E' 35.9 K-cyc. 5. V 0dB 1us
75	14	14-2	I	At start, positions 'A-E' (same) 1. V 0dB 10us
76	14	14-2	I	At start, position 'C' .2V 0dB 1us
77	14	14-2	I	Crack, position 'E' 22.65 K-cyc. 1. V 0dB 10us

TABLE G-6 (cont'd.)

Photo Log Speciments 13, 14, 15, and 16

45 Degree 5 Mhz Probe

Photo #	Specimen #	Notch/ Crack #	Bounce Path	Description
78	14	14-2	I	Crack, position 'E' 22.65 K-cyc. 1. V 0dB 1us
79	14	14-2	I	Crack, position 'E' 22.65 K-cyc. .1V 0dB 1us tip & root
80	14	14-2	I	Crack, position 'D' 22.65 K-cyc. 1. V 0dB 10us
81	14	14-2	I	Crack, position 'D' 22.65 K-cyc. 1. V 0dB 1us
82	14	14-2	I	Crack, position 'D' 22.65 K-cyc. .1V 0dB 1us
83	14	14-3	I	Scribe at start, position 'C' .2V 0dB 10us
84	14	14-3	I	Scribe at start, position 'C' .2V 0dB 1us
85	14	14-3	I	Crack, position 'C' 23.4 K-cyc. 1. V 0dB 10us
86	14	14-3	I	Crack, position 'C' 23.4 K-cyc. 1. V 0dB 1us
87	14	14-3	I	Crack, position 'C' 23.4 K-cyc. .2V 0dB 1us tip & root
88	14	14-3	I	Crack, back center, 23.4 K-cyc. 2. V 0dB 10us
89	14	14-3	I	Crack, back center, 23.4 K-cyc. 2. V 0dB 1us
90	14	14-3	I	Crack, back center, 23.4 K-cyc. .5V 0dB 1us tip & root
91	15	15-1	I	Crack, position 'C' 73.4 K-cyc. 2. V 0dB 10us
92	15	15-1	I	Crack, position 'C' 73.4 K-cyc. 2. V 0dB 1us
93	15	15-1	I	Crack, position 'C' 73.4 K-cyc. 1. V 0dB 10us
94	15	15-1	I	Crack, position 'C' 73.4 K-cyc. 1. V 0dB 1us
95	15	15-1	I	Crack, position 'C' 73.4 K-cyc. 1. V 0dB 1us tip & root
96	15	15-2	I	Crack-starting, position 'C' 13.1 K-cyc. .5V 0dB 10us
97	15	15-2	I	Crack, position 'C' 28.5 K-cyc. 2. V 0dB 10us
98	15	15-2	I	Crack, position 'C' 28.5 K-cyc. 2. V 0dB 1us
99	15	15-2	I	Crack, position 'C' 28.5 K-cyc. .2V 0dB 1us tip & root
100	15	15-3	I	Scribe at start, position 'C' .2V 0dB 10us
101	15	15-3	I	Crack-starting, position 'C' 12.6 K-cyc. 1. V 0dB 10us
102	15	15-3	I	Crack, position 'C' 26.9 K-cyc. 5. V 0dB 10us

TABLE G-6 (cont'd.)

Photo Log Speciments 13, 14, 15, and 16

45 Degree 5 Mhz Probe

Photo #	Specimen #	Notch/ Crack #	Bounce Path	Description
103	15	15-3	I	Crack, position 'C' 26.9 K-cyc. 5. V 0dB 1us
104	15	15-3	I	Crack, position 'C' 26.9 K-cyc. .2V 0dB 1us tip & root
105	15	15-4	I	Scribe at start, position 'C' .2V 0dB 10us
106	15	15-4	I	Crack, position 'C' 34.8 K-cyc. 5. V 0dB 10us
107	15	15-4	I	Crack, position 'C' 34.8 K-cyc. 5. V 0dB 1us
108	15	15-4	I	Crack, position 'C' 34.8 K-cyc. .2V 0dB 1us tip & root
109	16	16-2	I	Crack, position 'C' 31.8 K-cyc. 2. V 0dB 10us
110	16	16-2	I	Crack, position 'C' 31.8 K-cyc. 2. V 0dB 1us
111	16	16-2	I	Crack, position 'C' 31.8 K-cyc. .2V 0dB 1us tip & root
112	16	16-3	I	Scribe at start, position 'C' .2V 0dB 10us
113	16	16-3	I	Crack, position 'C' 30.1 K-cyc. 5. V 0dB 10us
114	16	16-3	I	Crack, position 'C' 30.1 K-cyc. 5. V 0dB 1us
115	16	16-3	I	Crack, position 'C' 30.1 K-cyc. .2V 0dB 1us tip & root
116	16	16-4	I	Scribe at start, position 'C' .2V 0dB 10us
117	16	16-4	I	Crack, position 'C' 31.25 K-cyc. 2. V 0dB 10us
118	16	16-4	I	Crack, position 'C' 31.25 K-cyc. 2. V 0dB 1us
119	16	16-4	I	Crack, position 'C' 31.25 K-cyc. .1V 0dB 1us tip & root

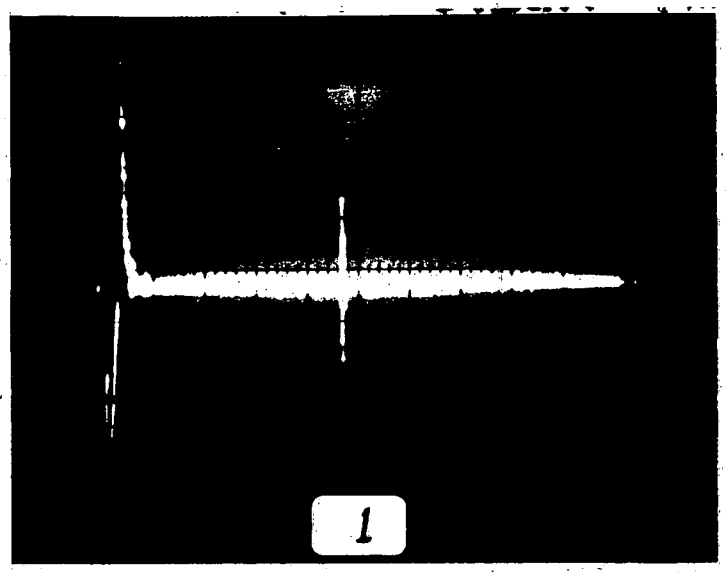
1

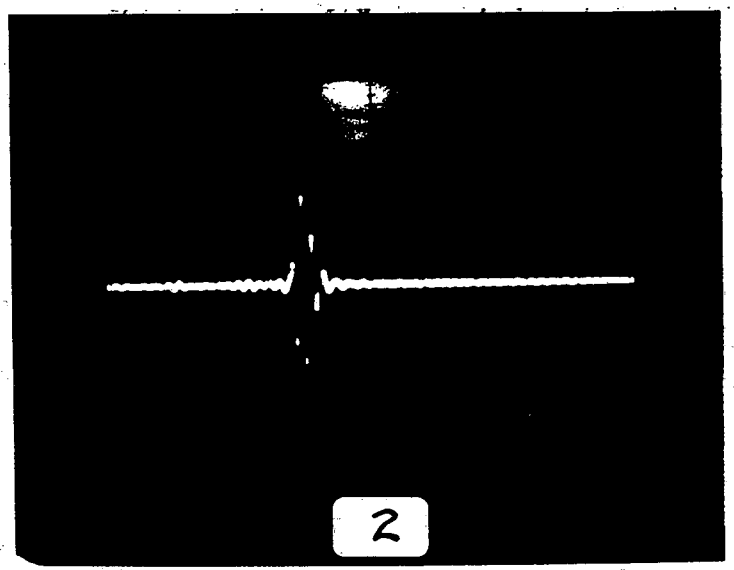
2

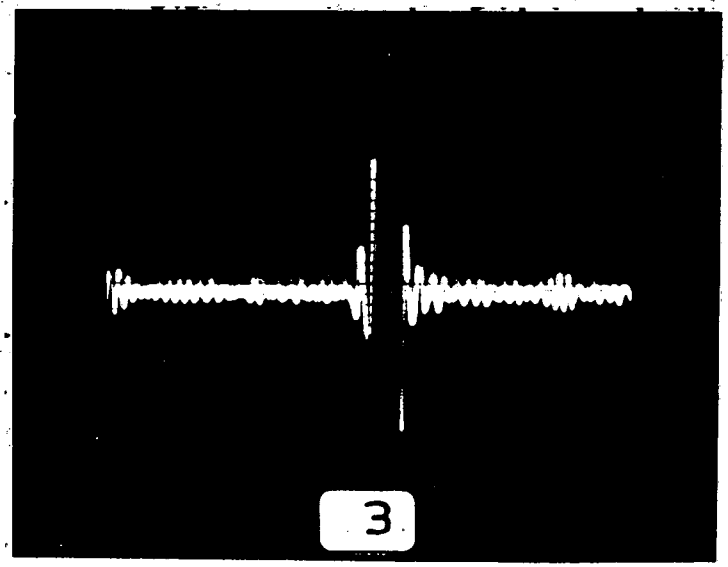
3

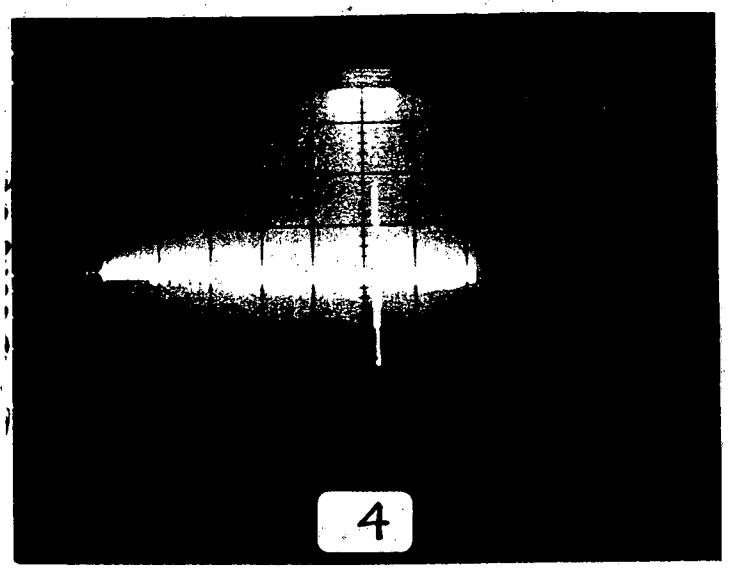
4

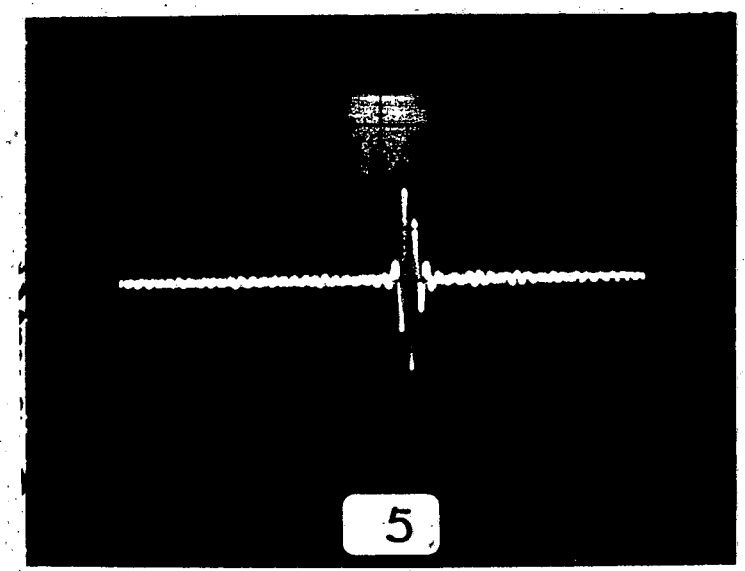
5

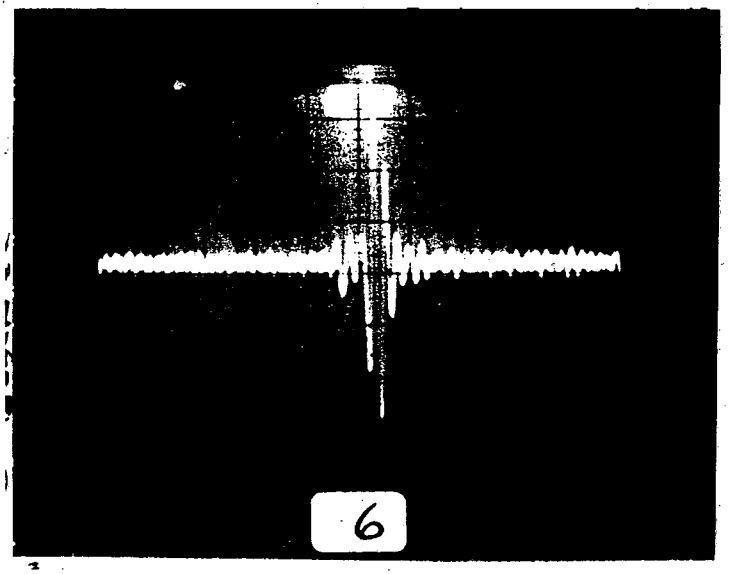
6

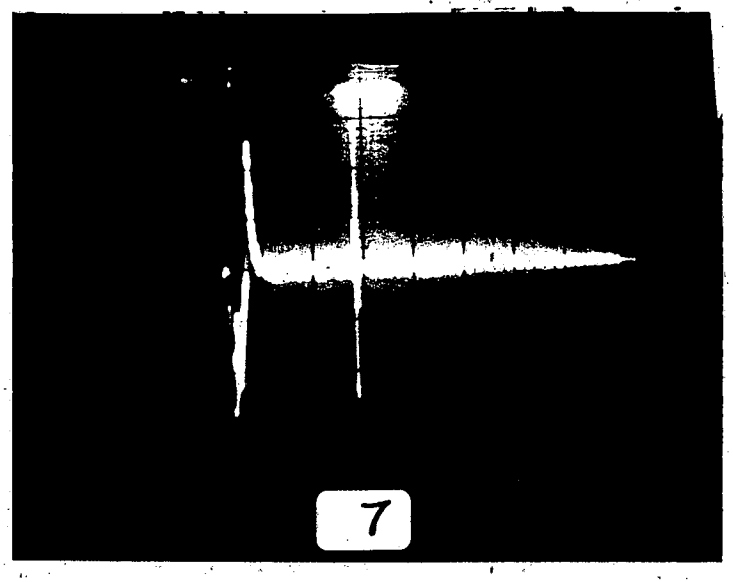
7

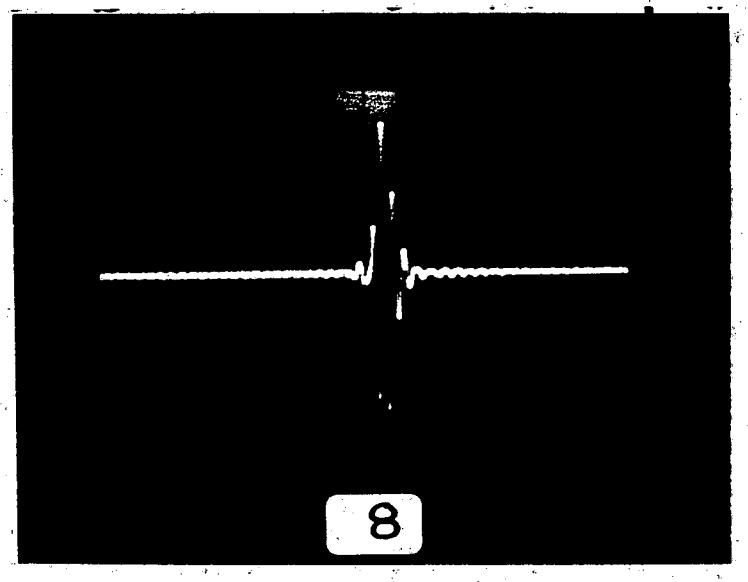
8

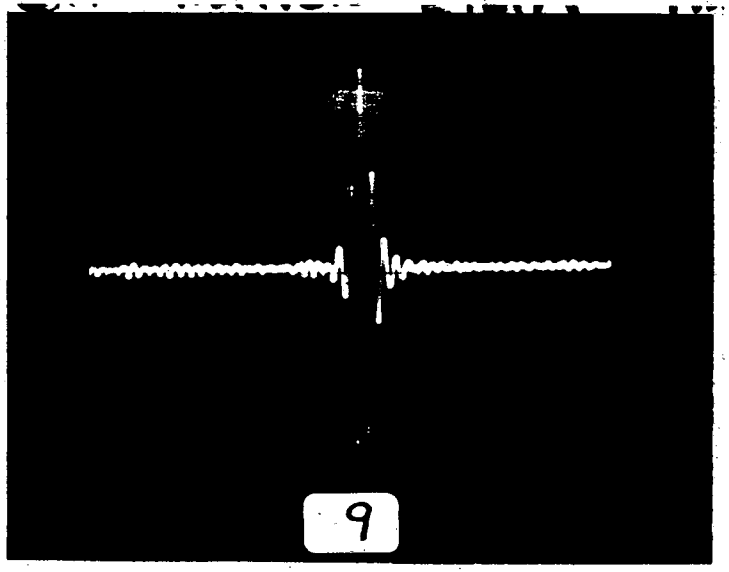
9

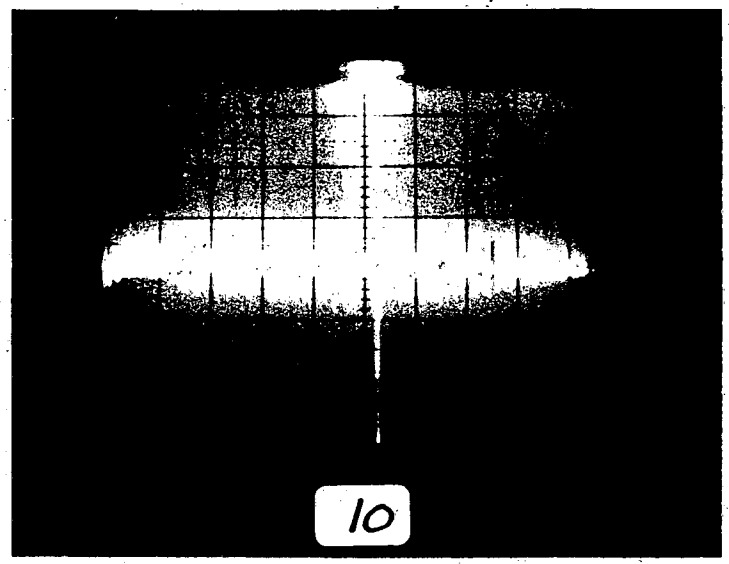
10

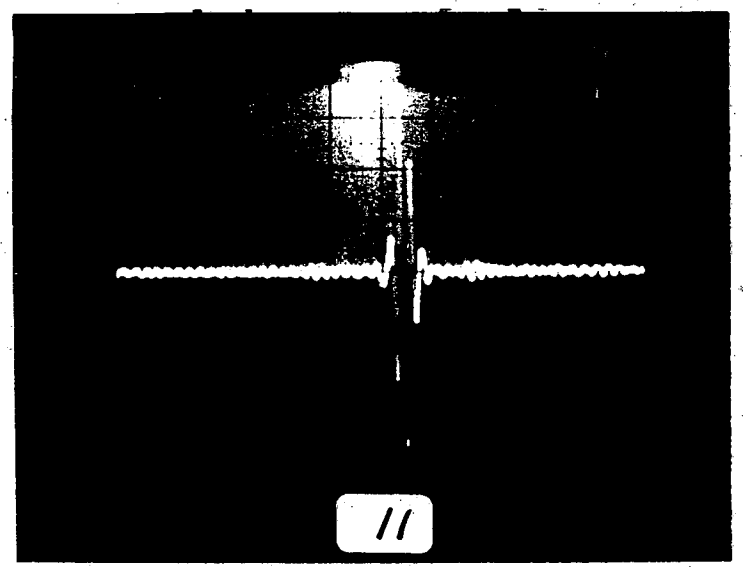
11

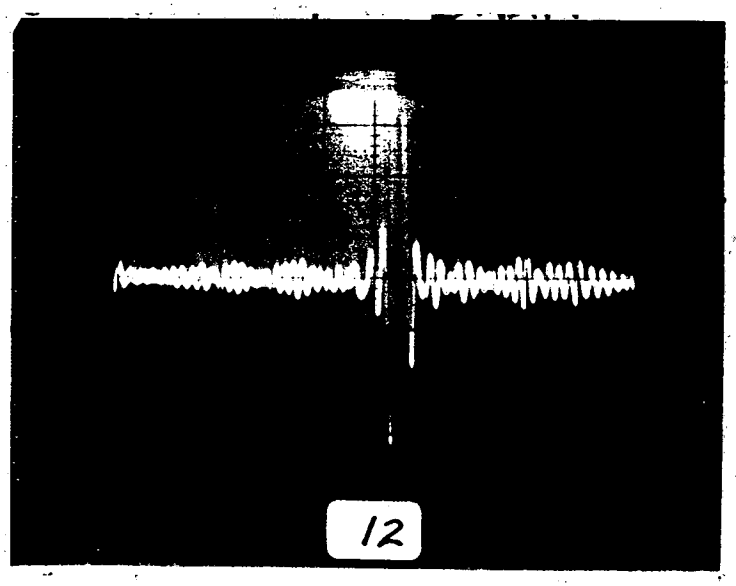
12

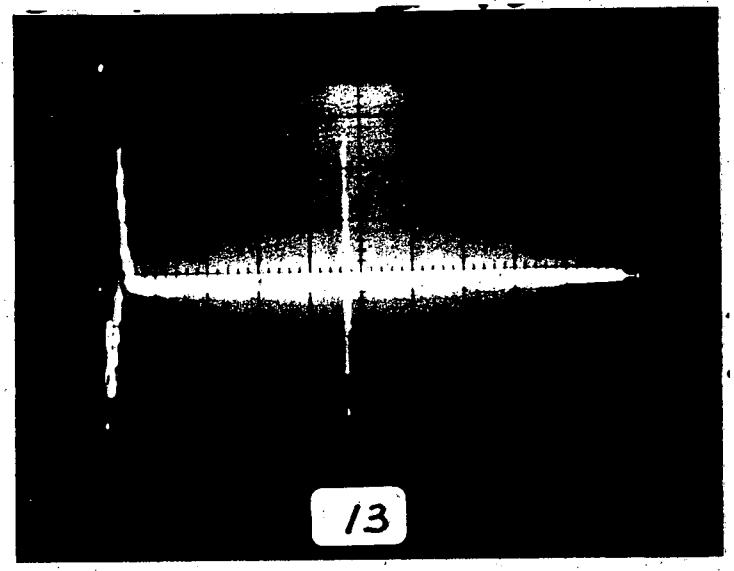
13

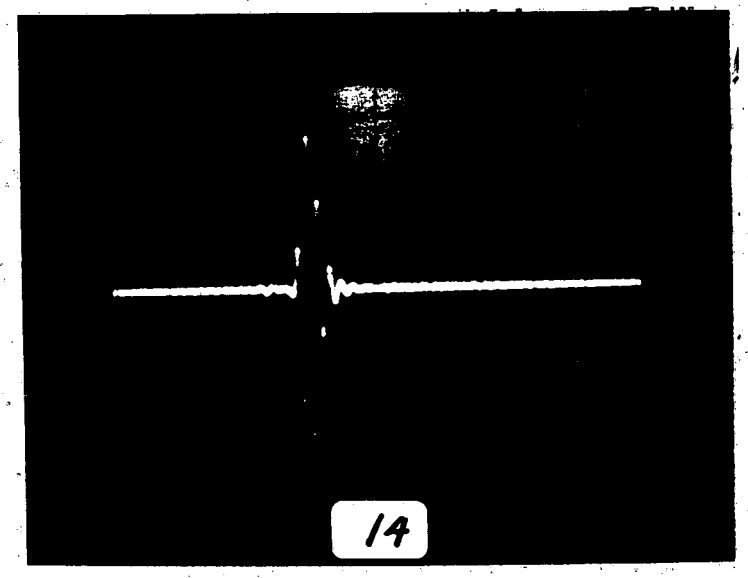
14

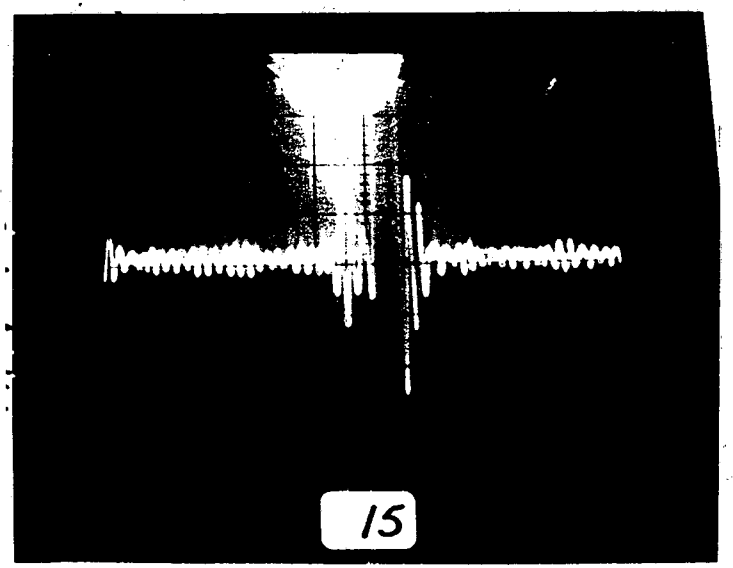
15

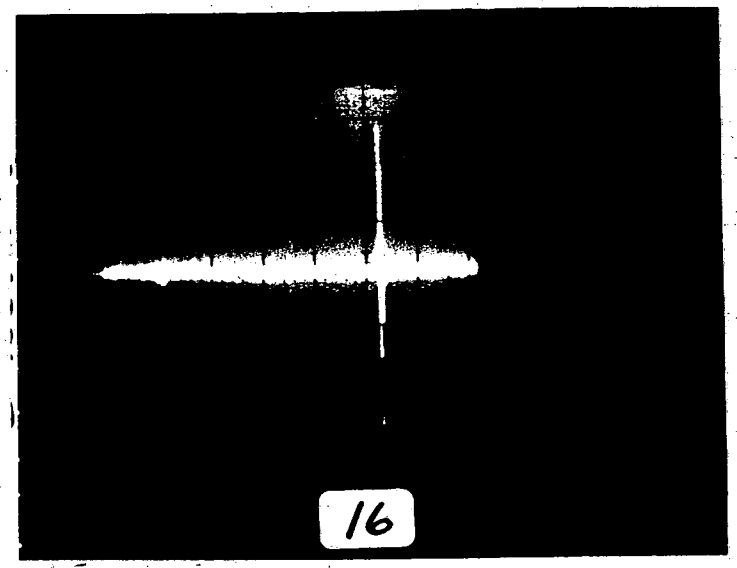
16

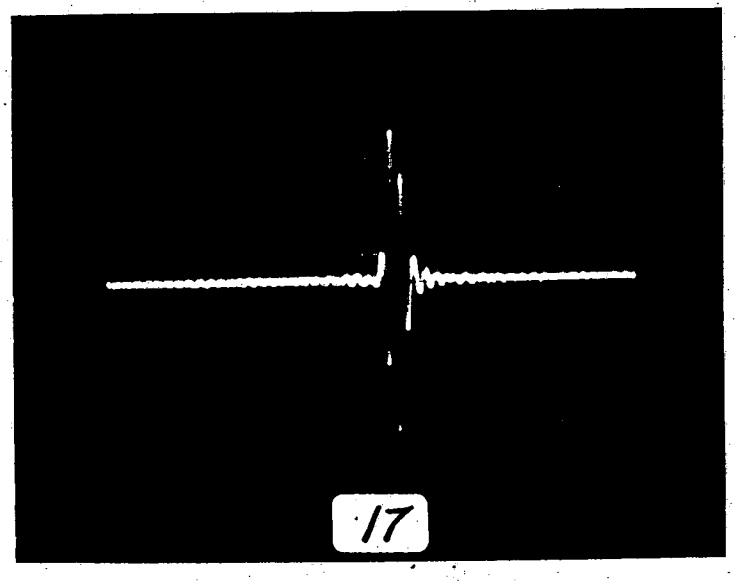
17

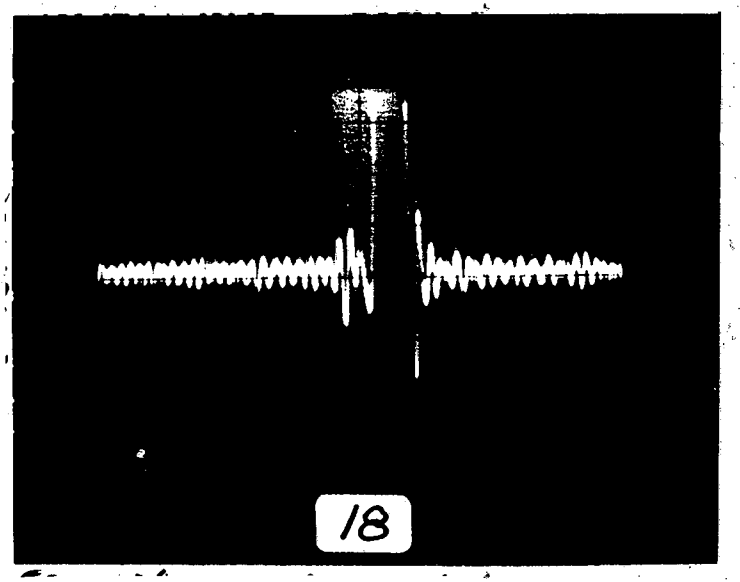
18

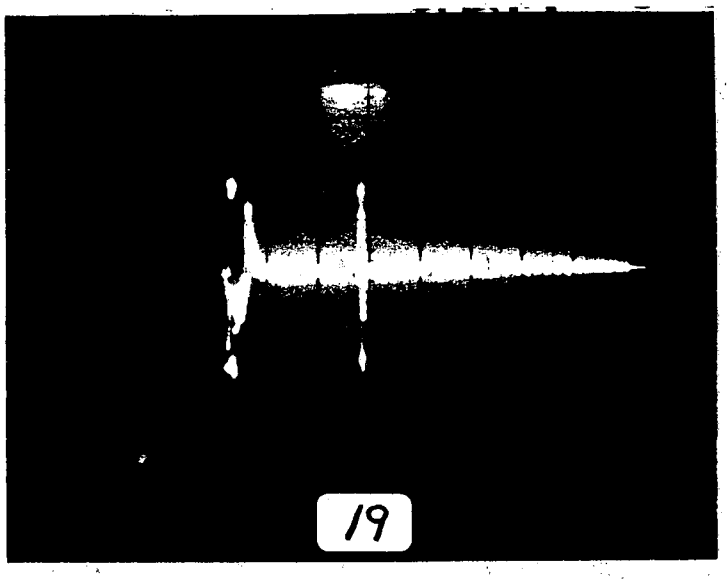
19

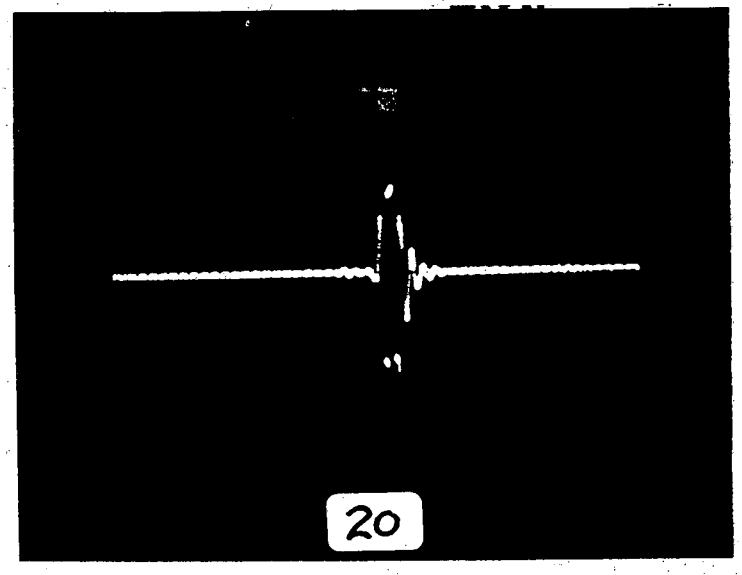
20

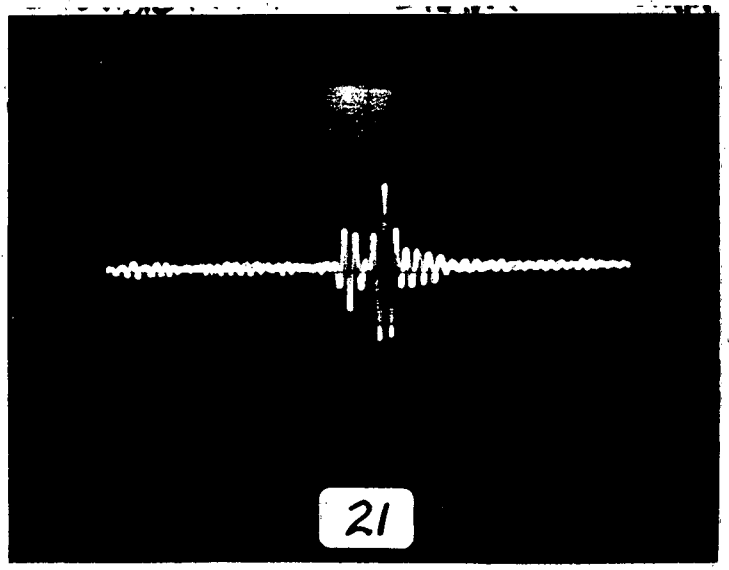
21

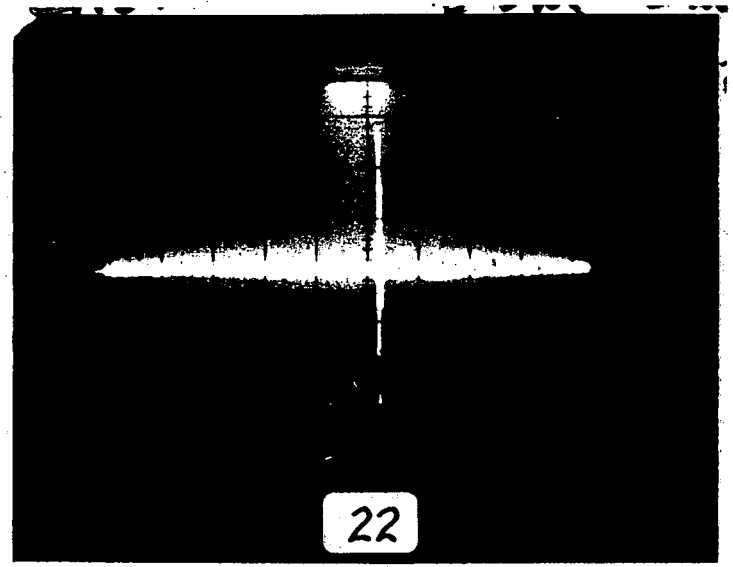
22

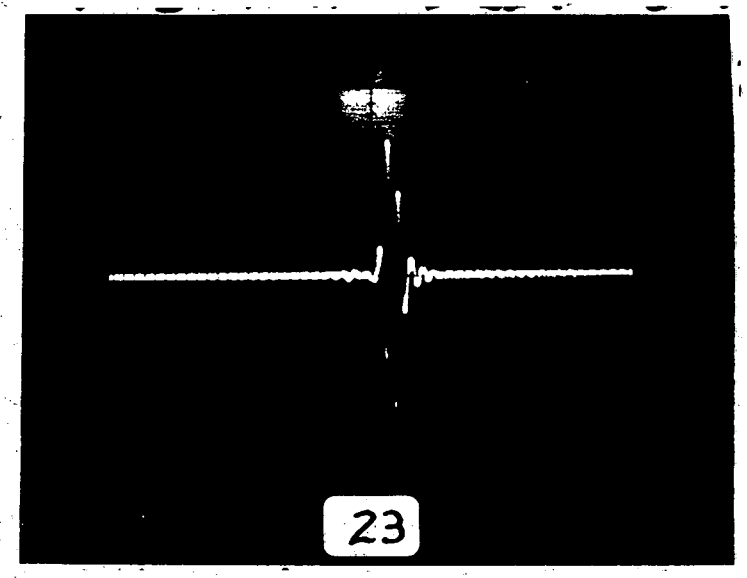
23

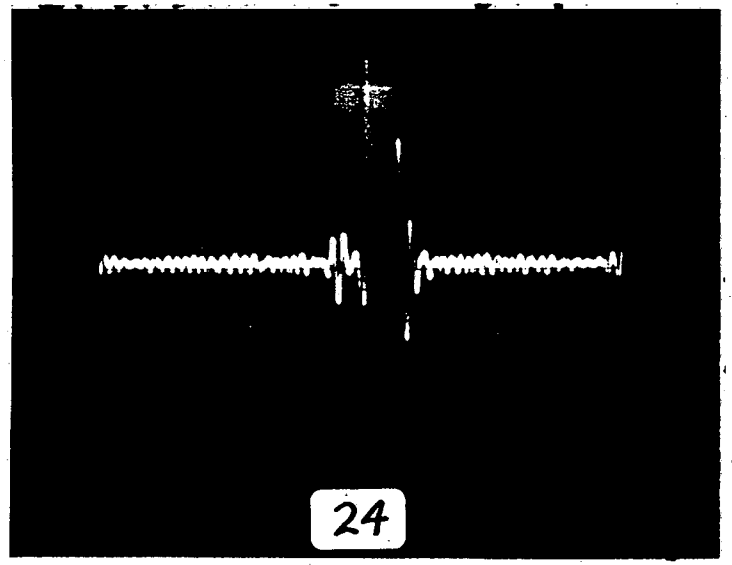
24

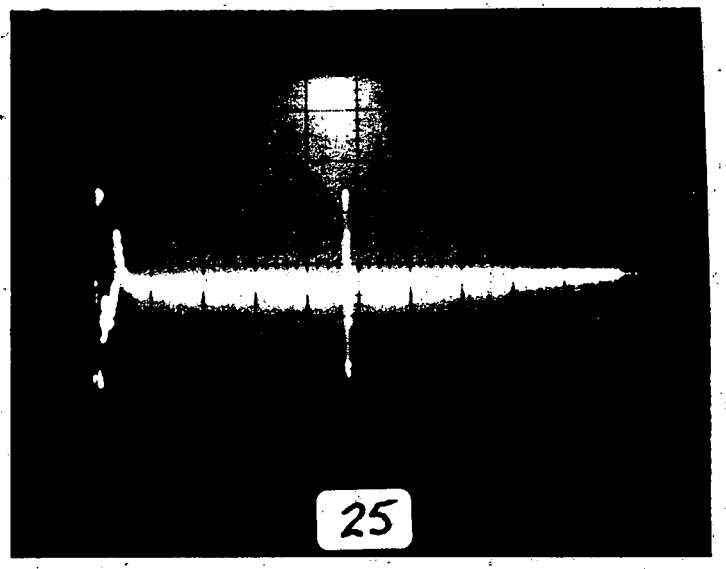
25

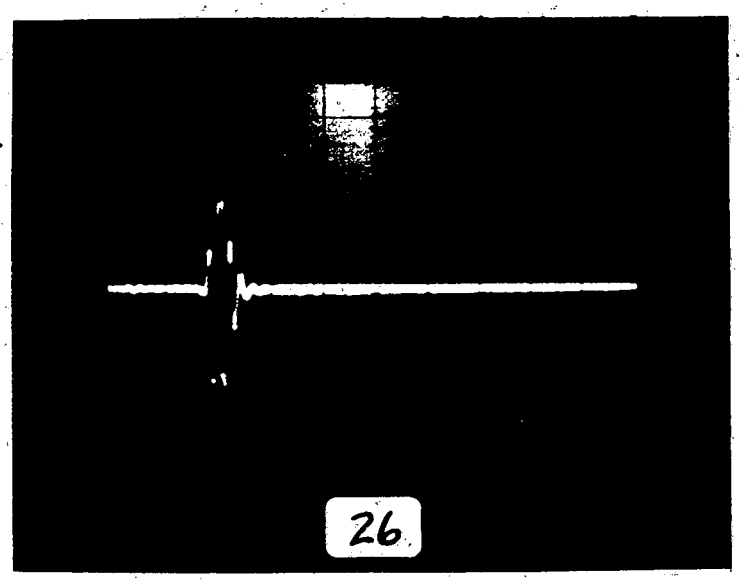
26

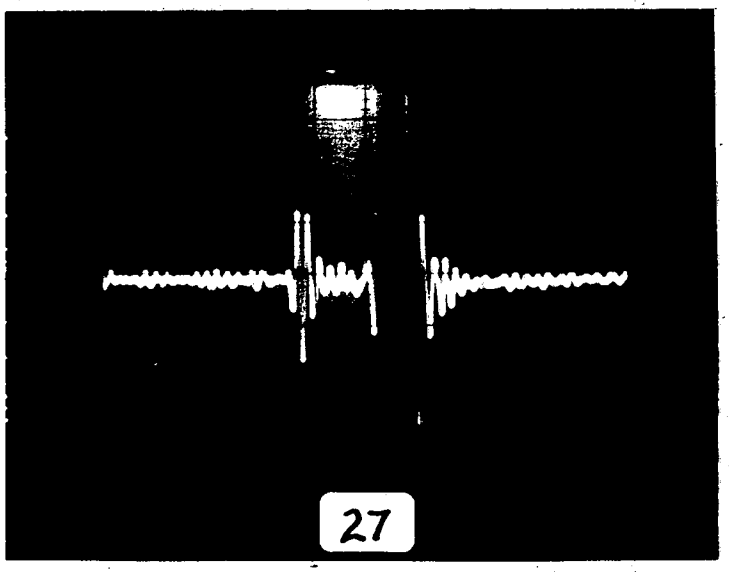
27

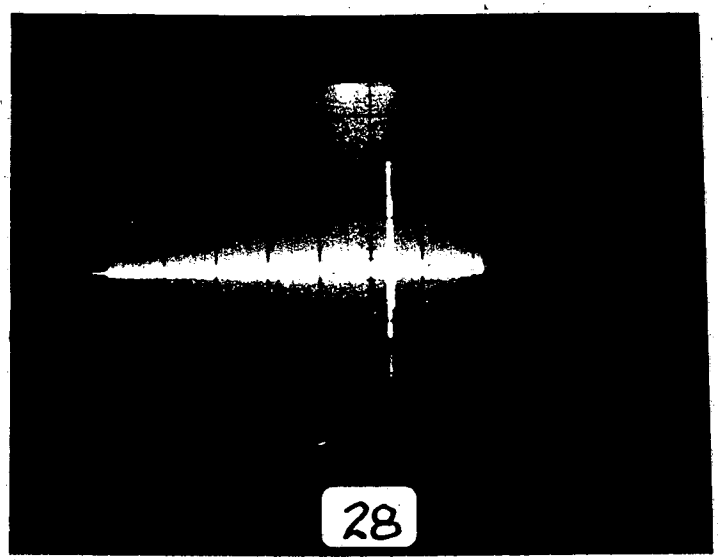
28

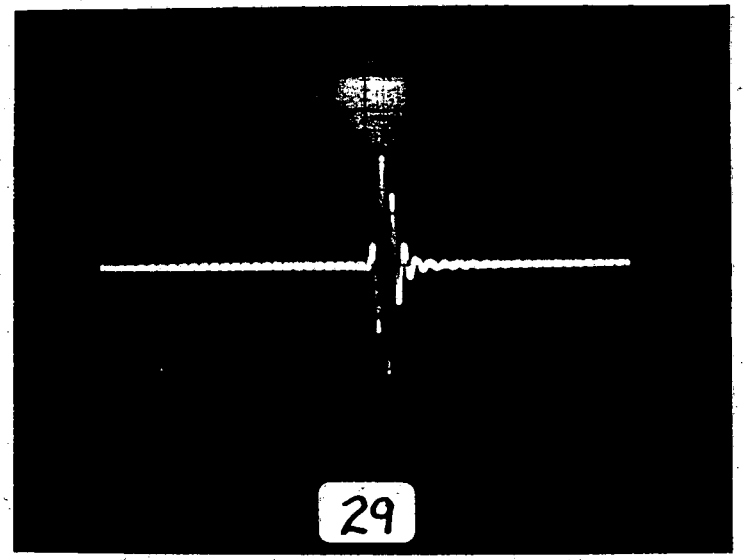
29

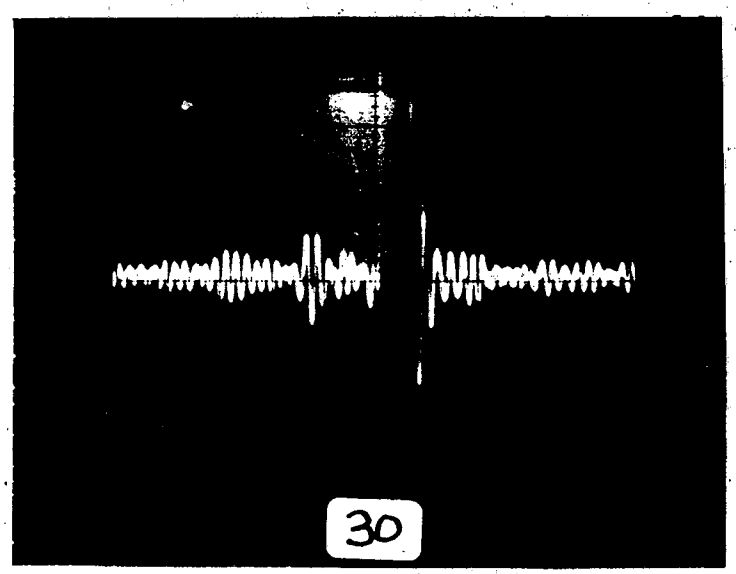
30

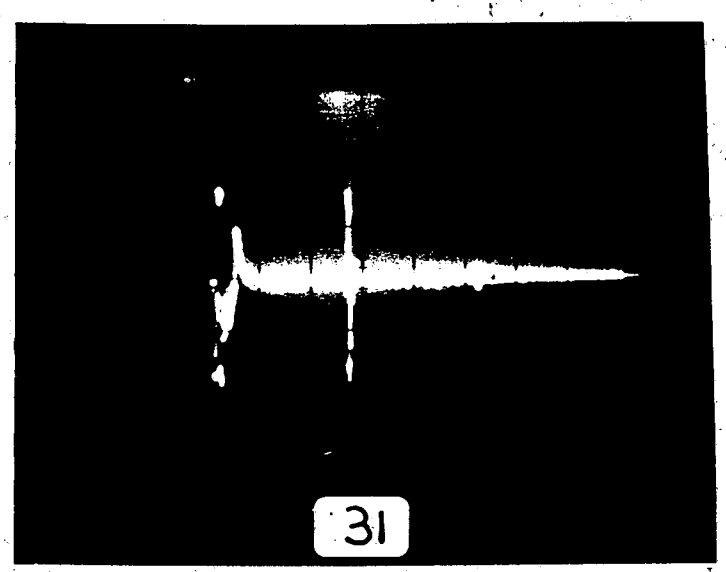

31

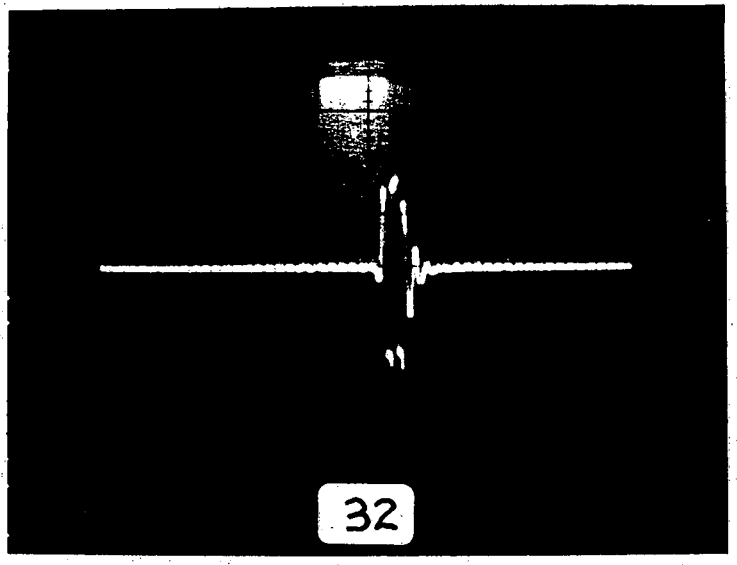

32

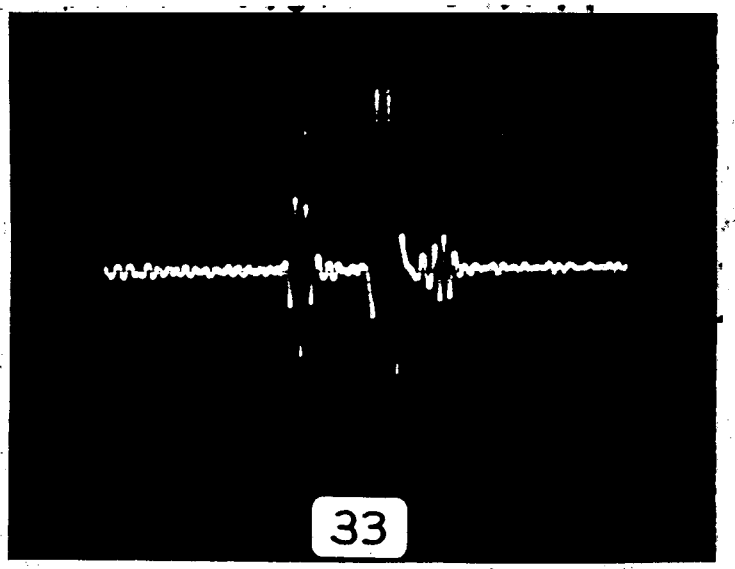

33

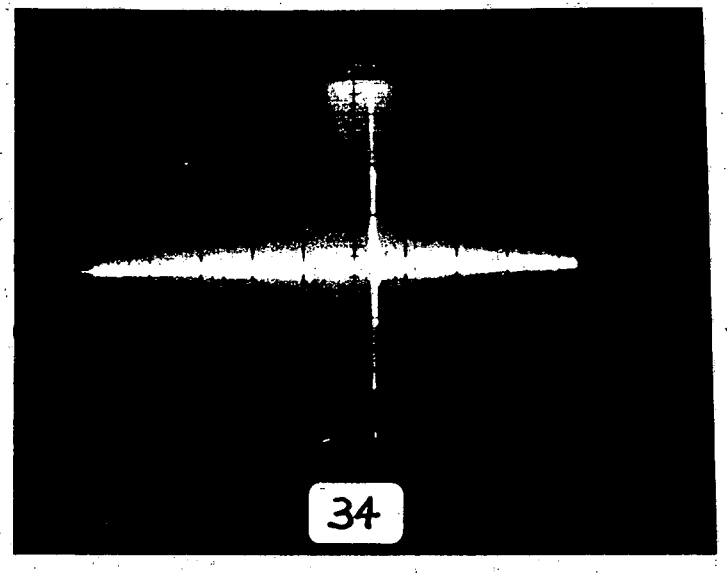
34

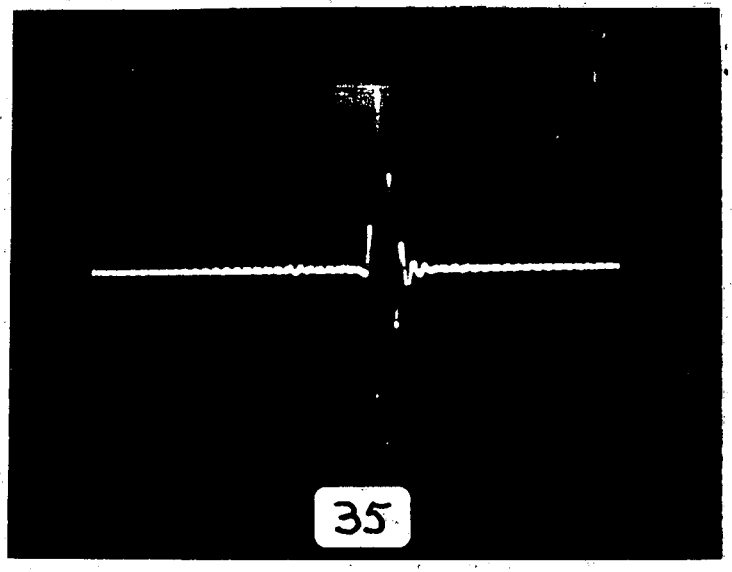
35

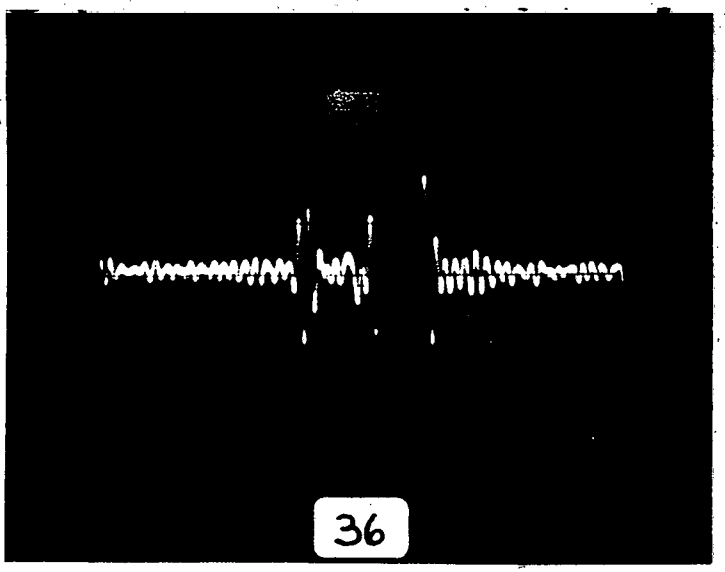
36

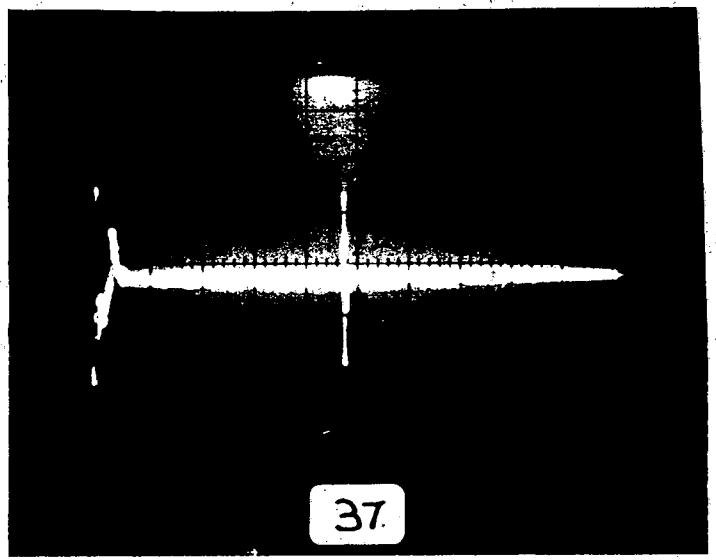
37

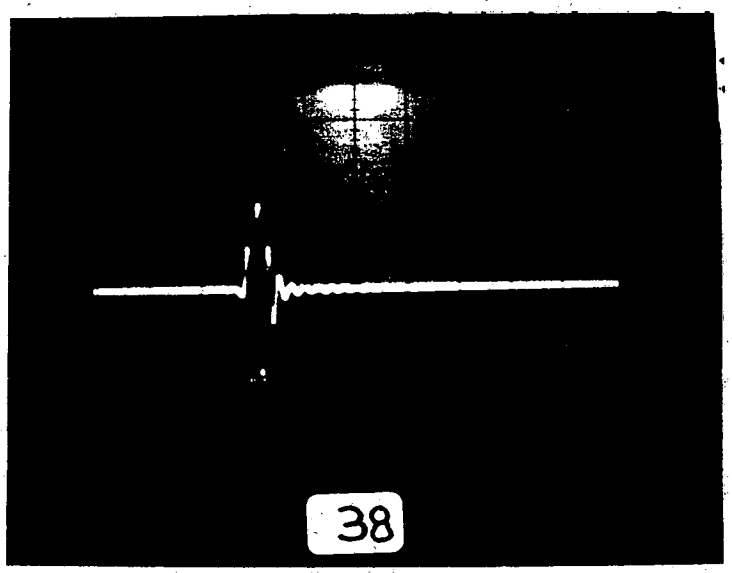
38

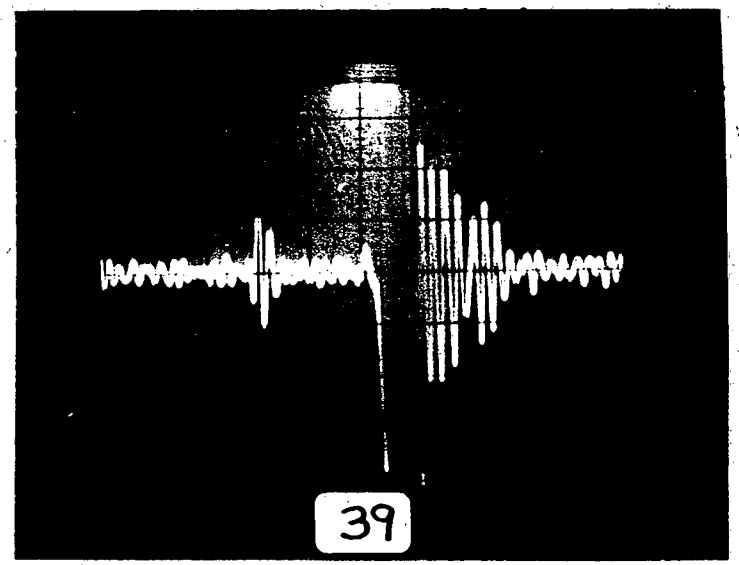
39

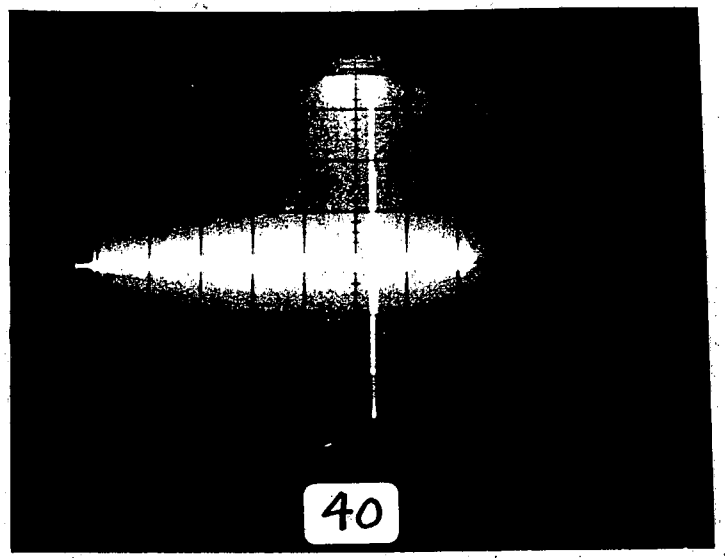
40

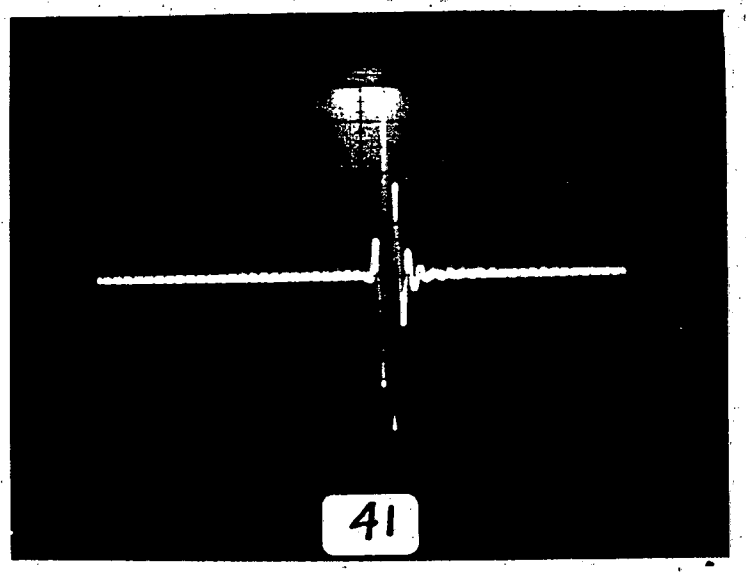
41

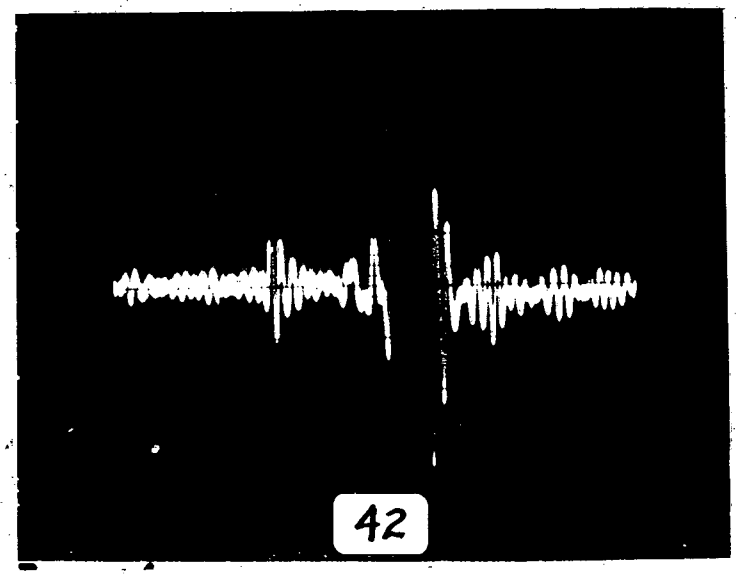
42

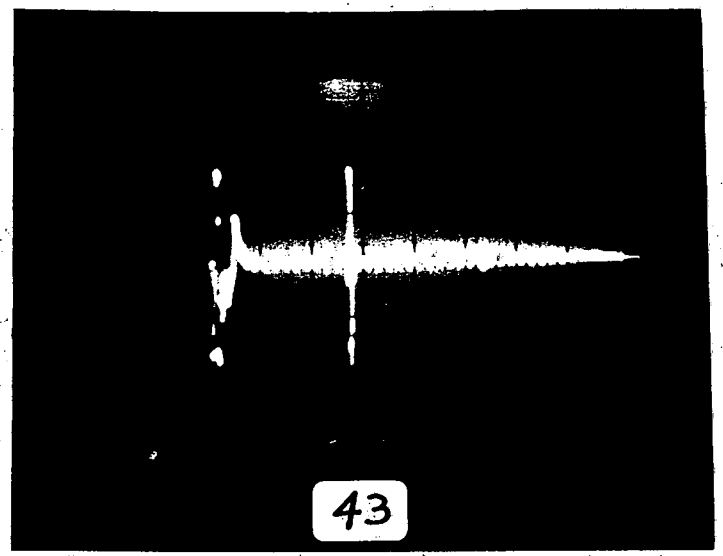
43

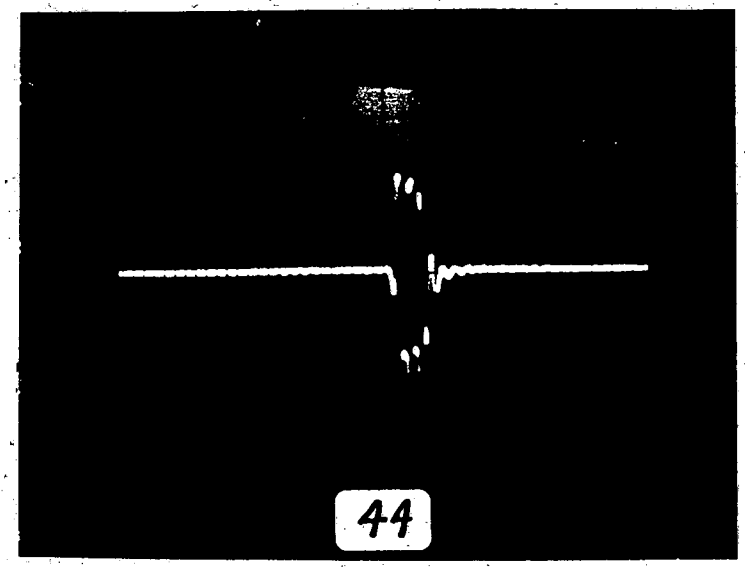
44

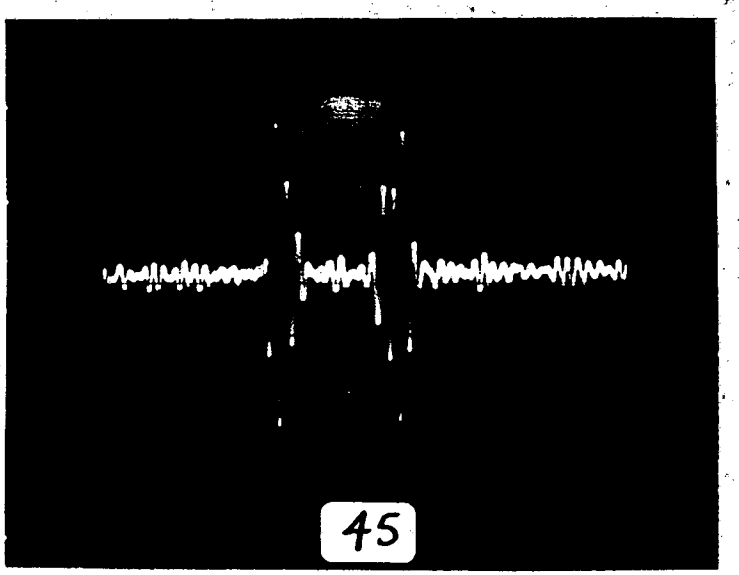
45

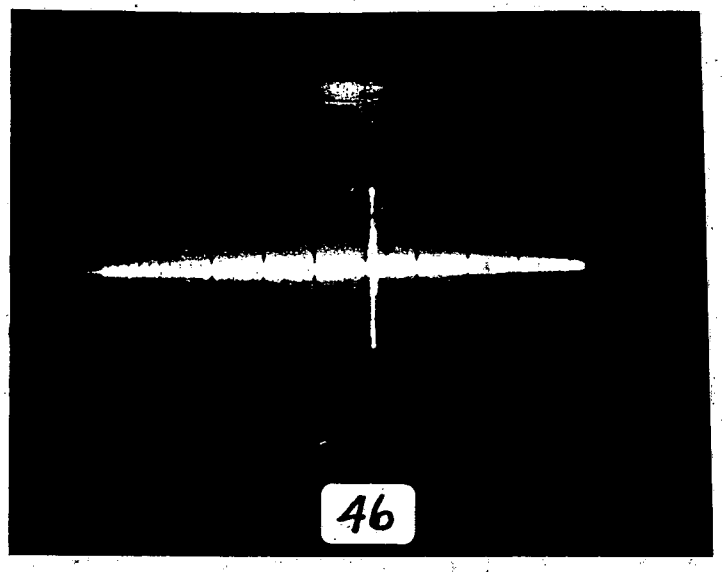
46

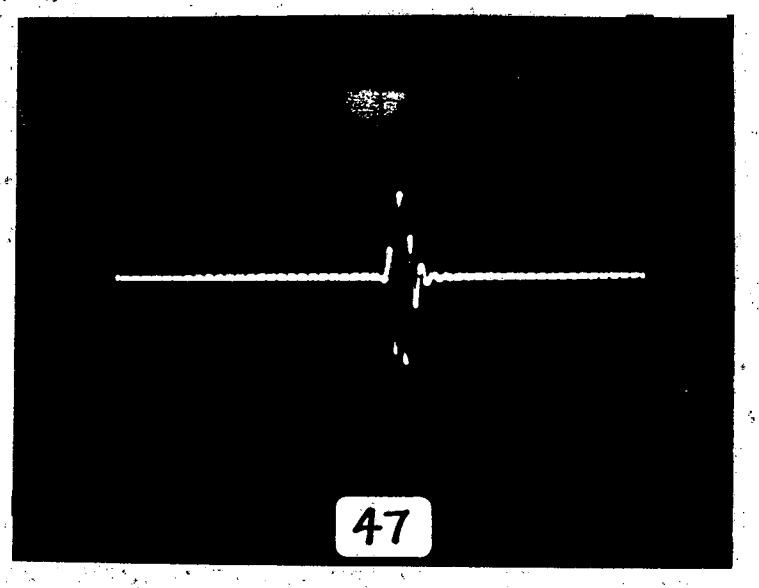
47

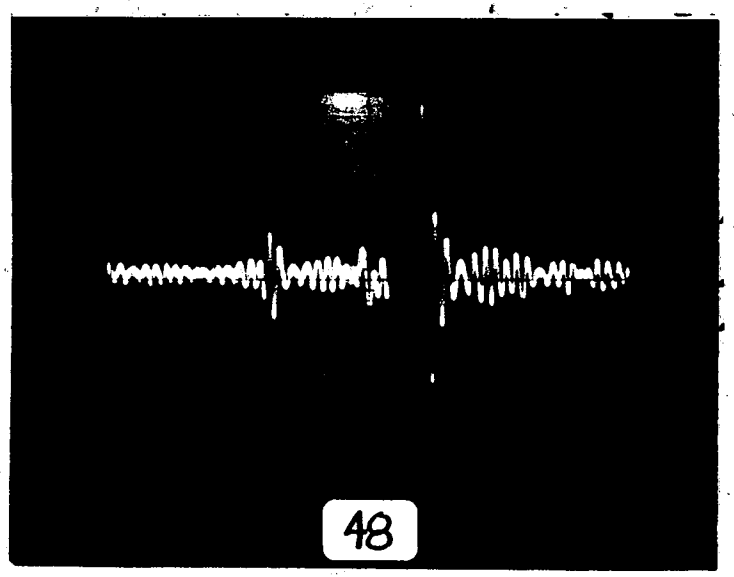
48

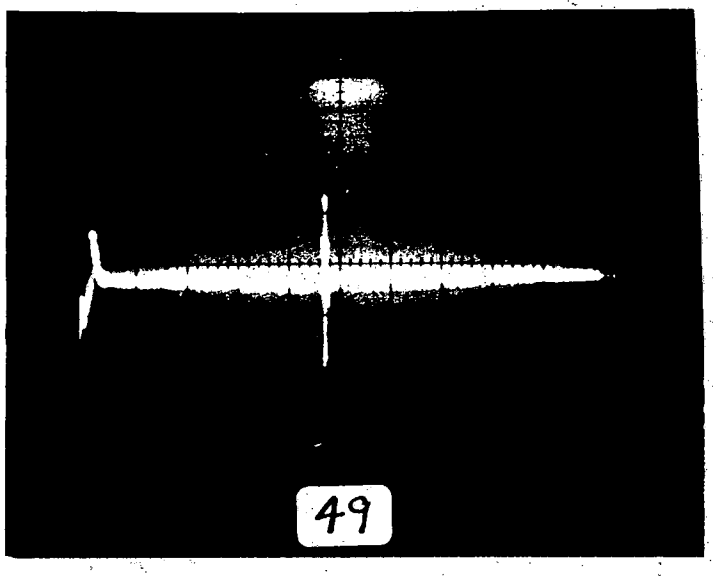
49

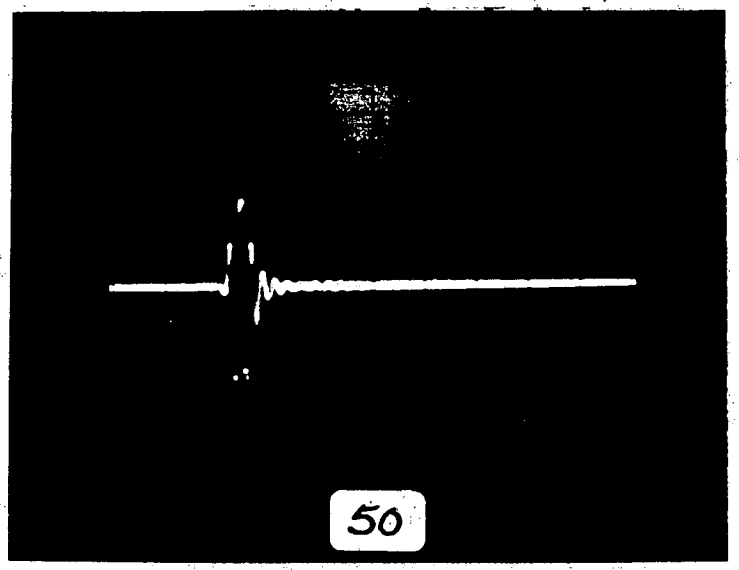
50

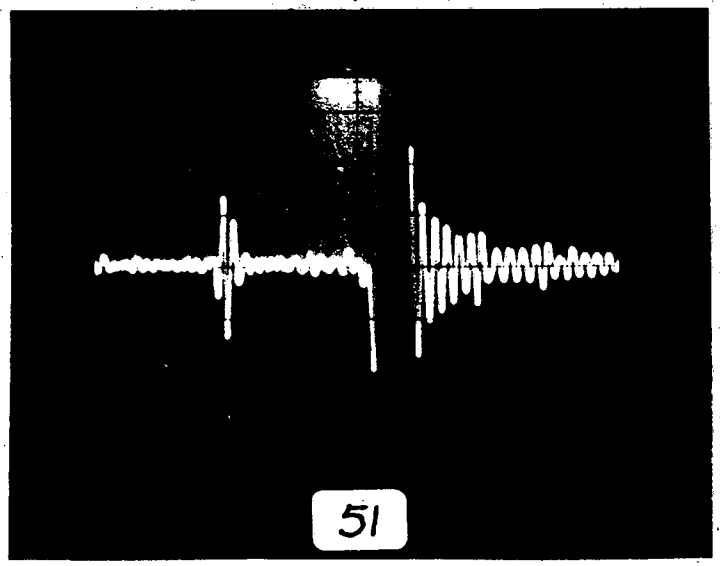
51

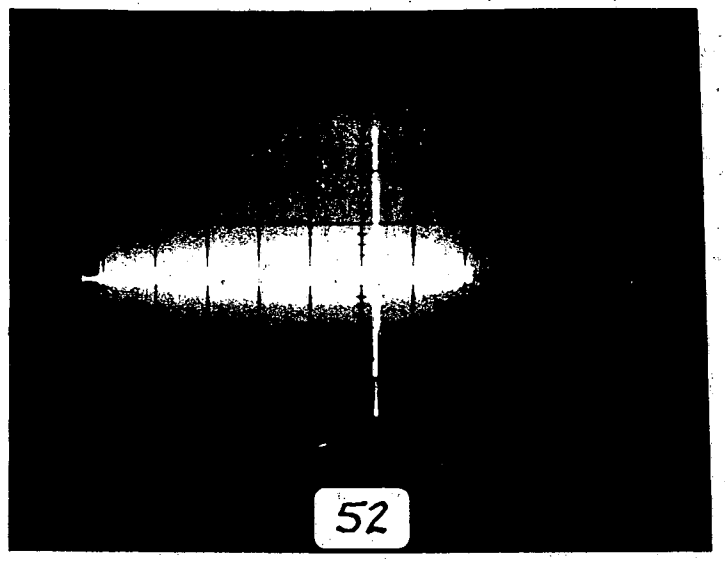

52

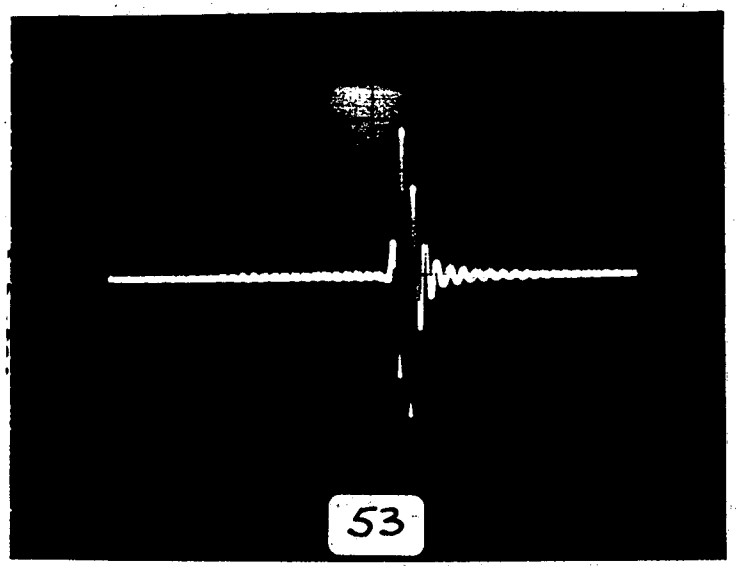

53

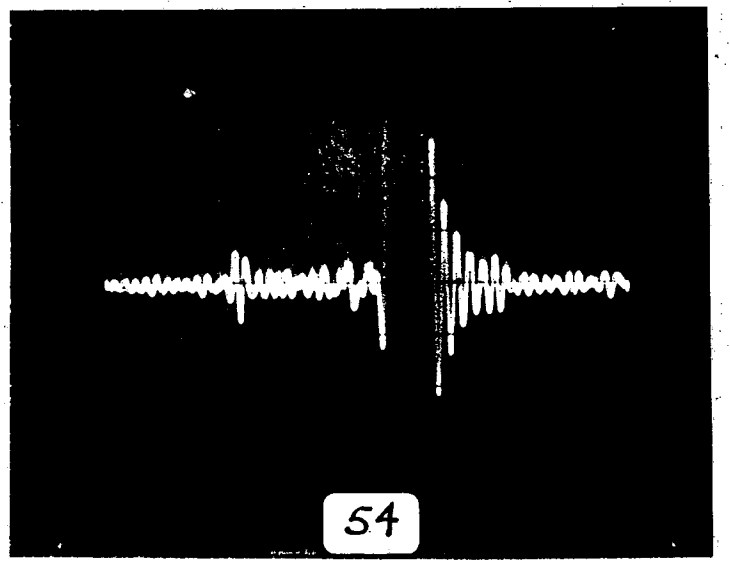

54

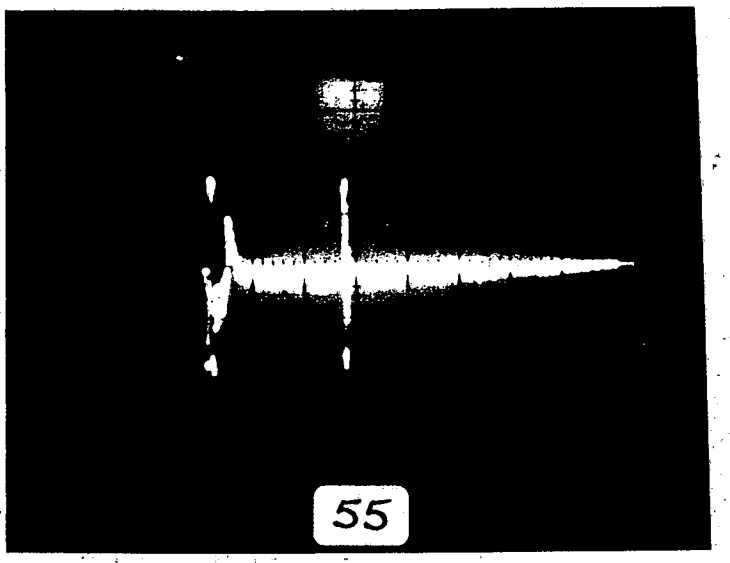
55

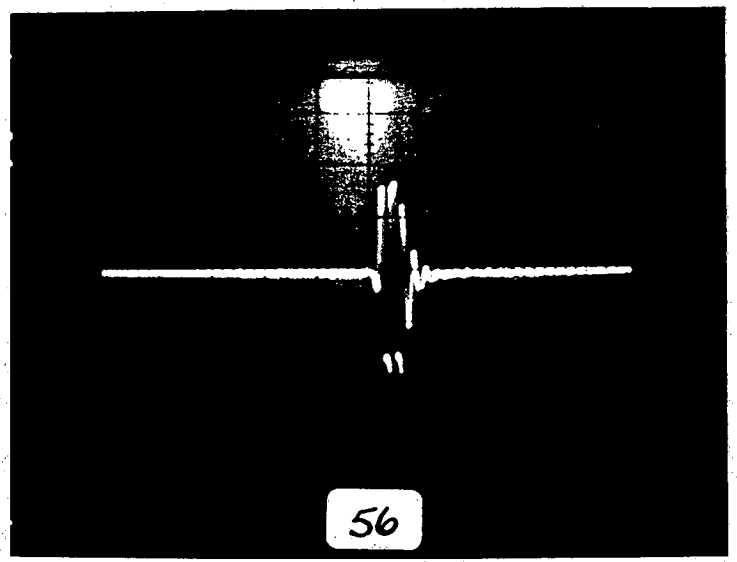
56

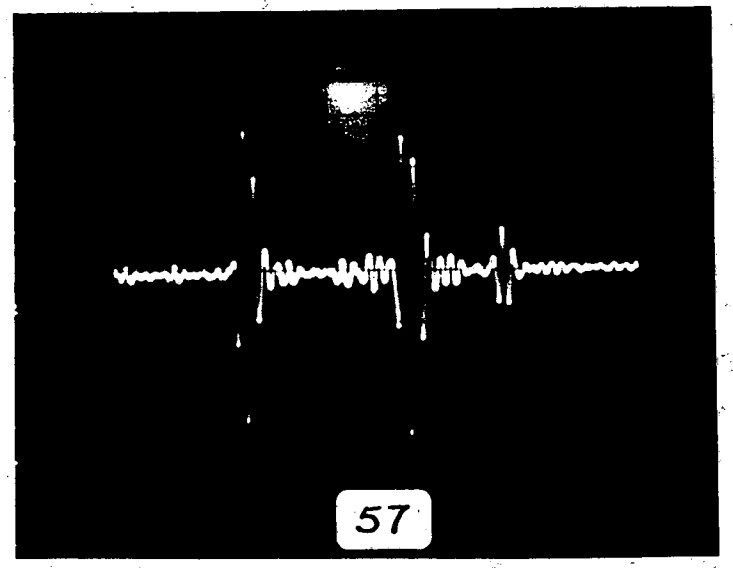
57

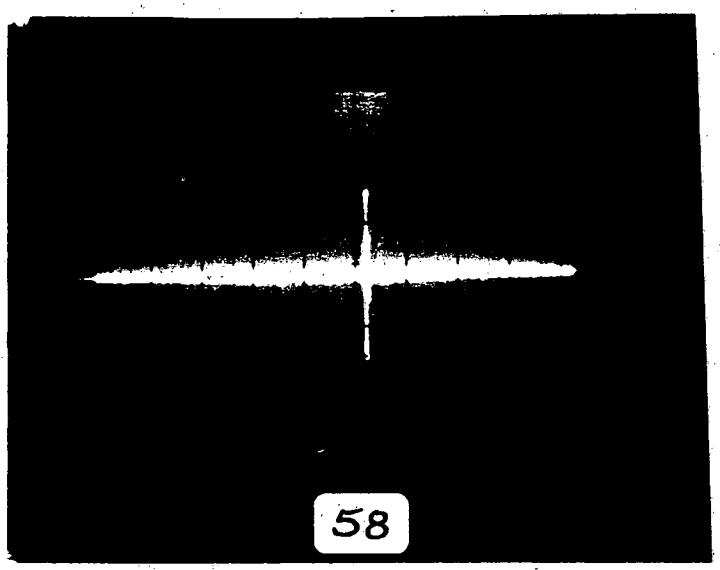

58

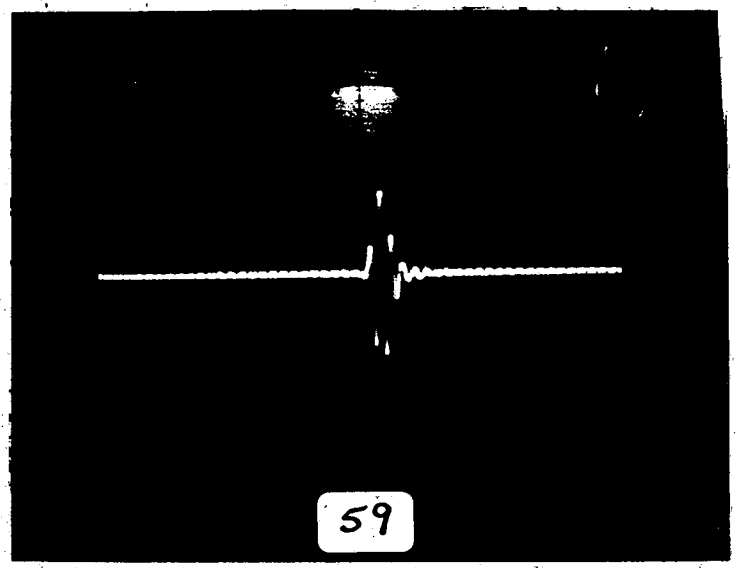

59

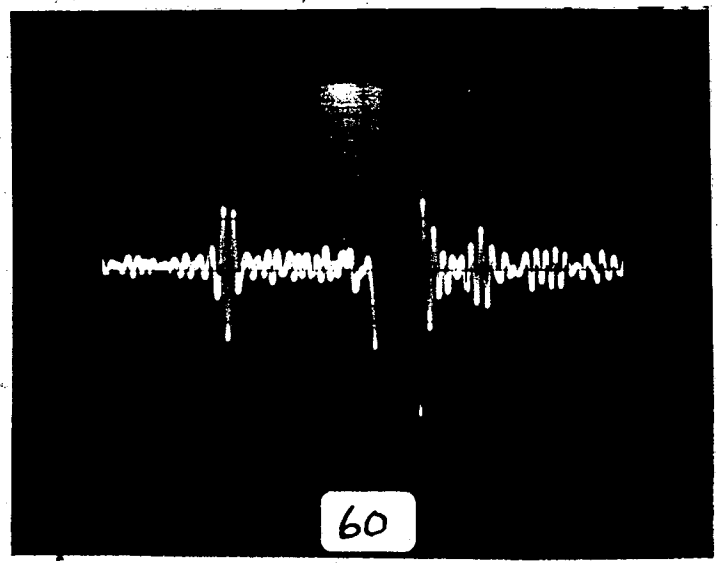

60

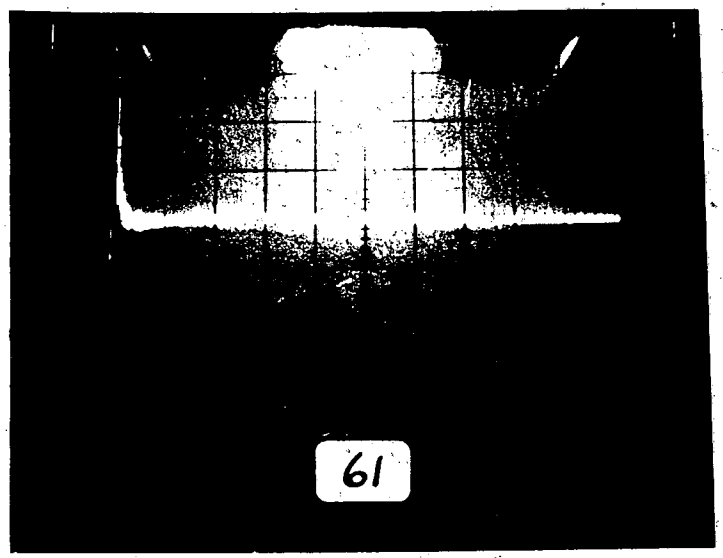
61

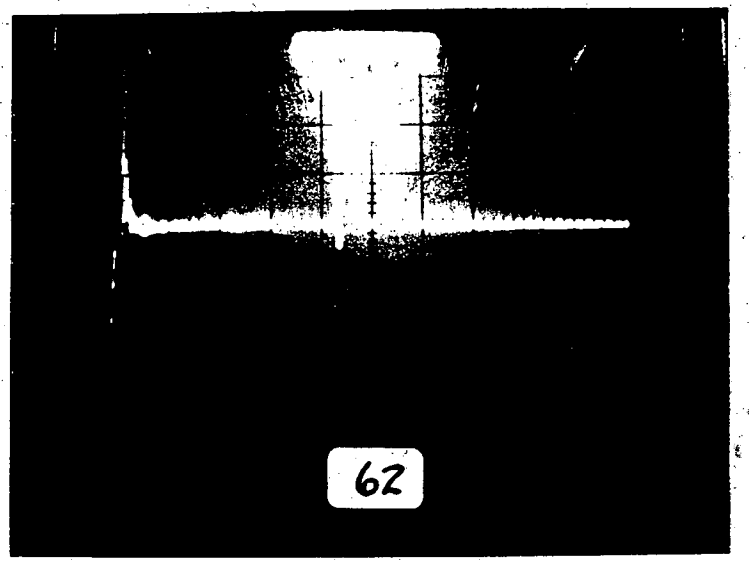
62

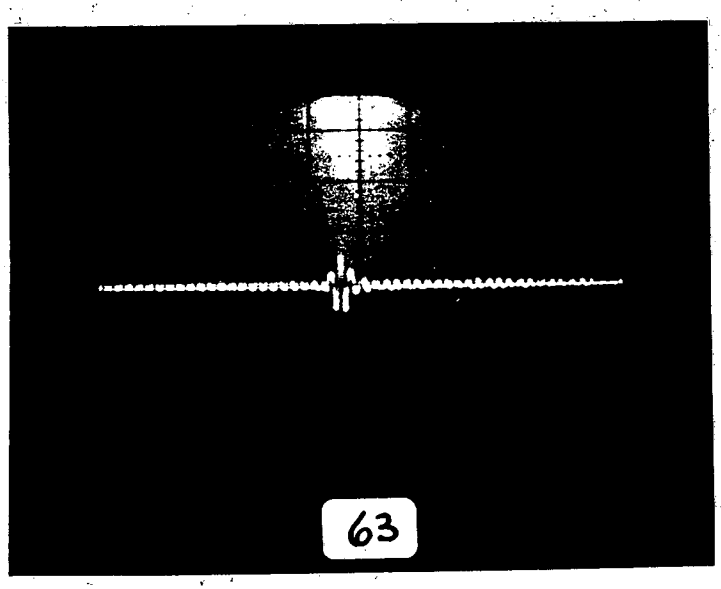
63

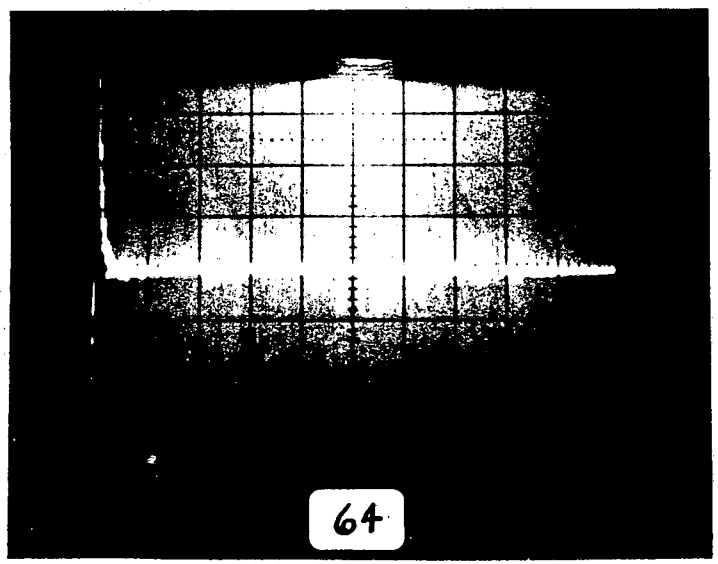
64

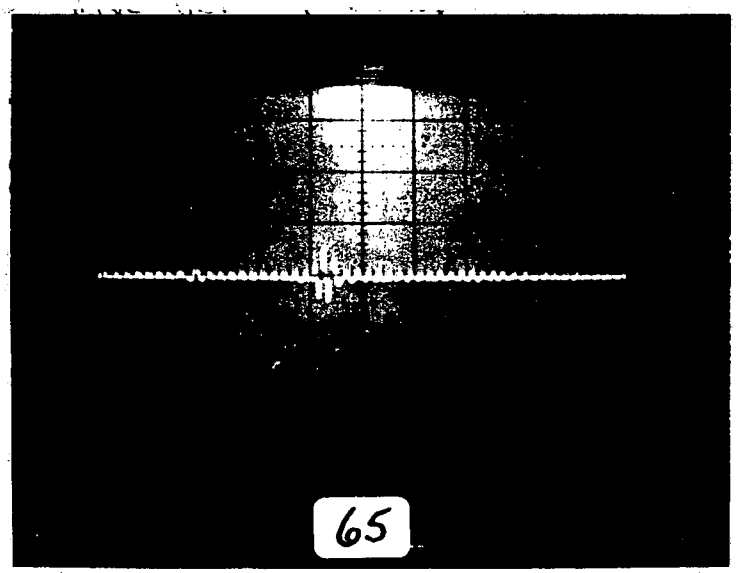
65

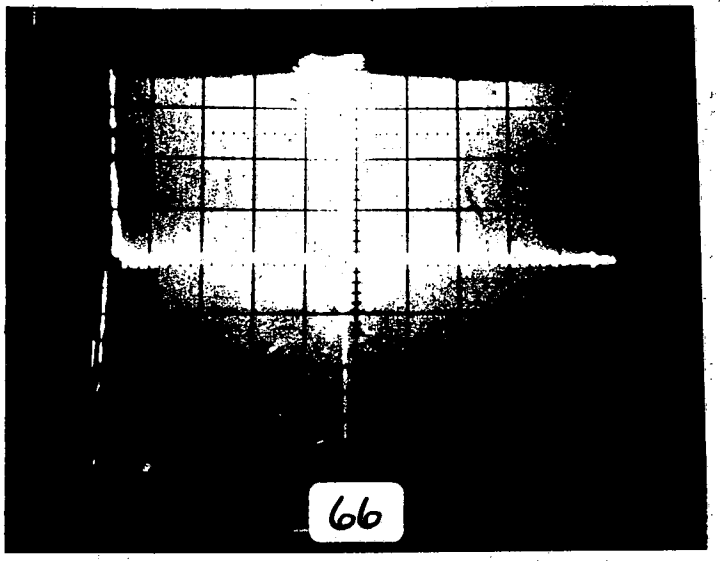
66

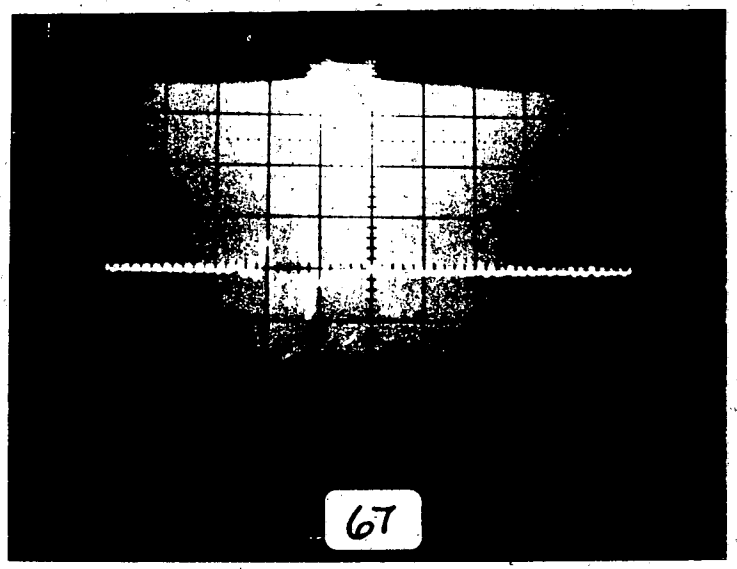
67

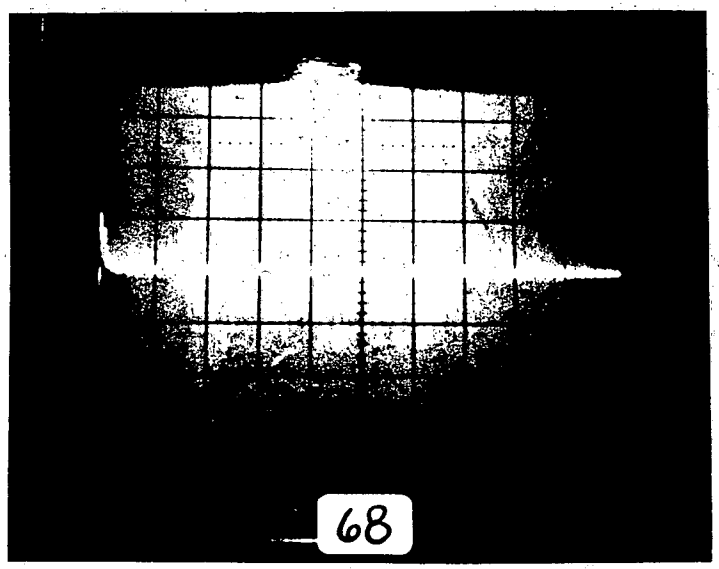
68

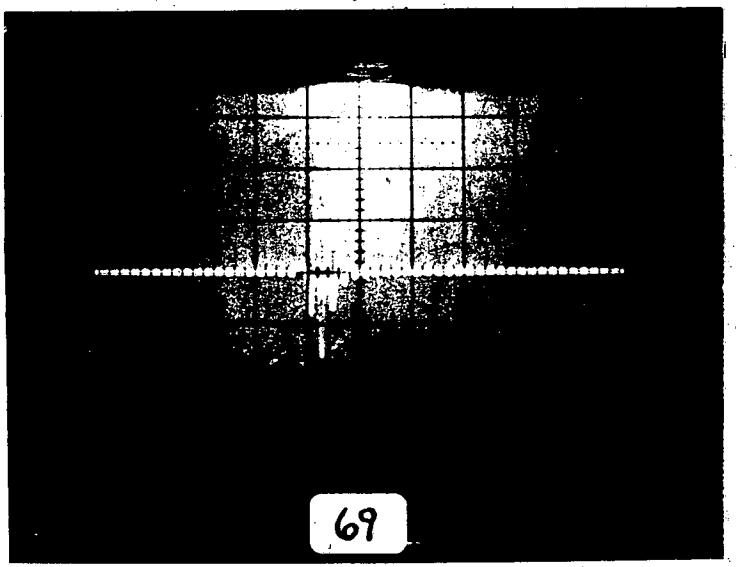
69

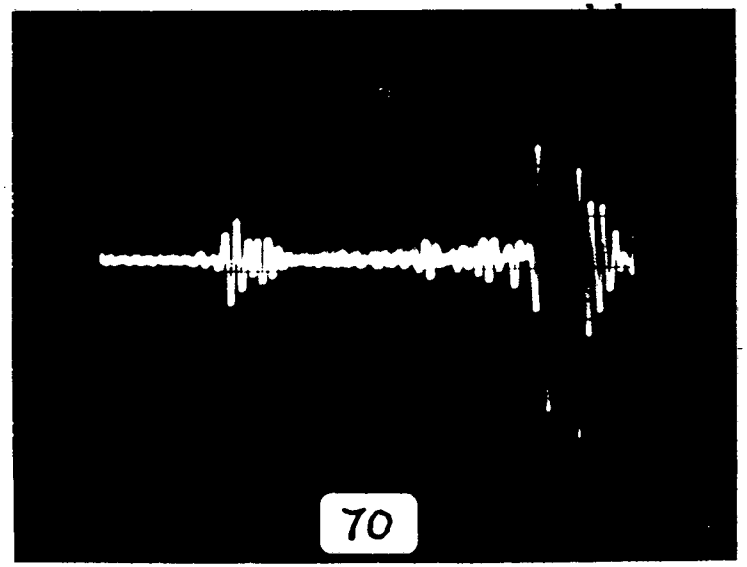
70

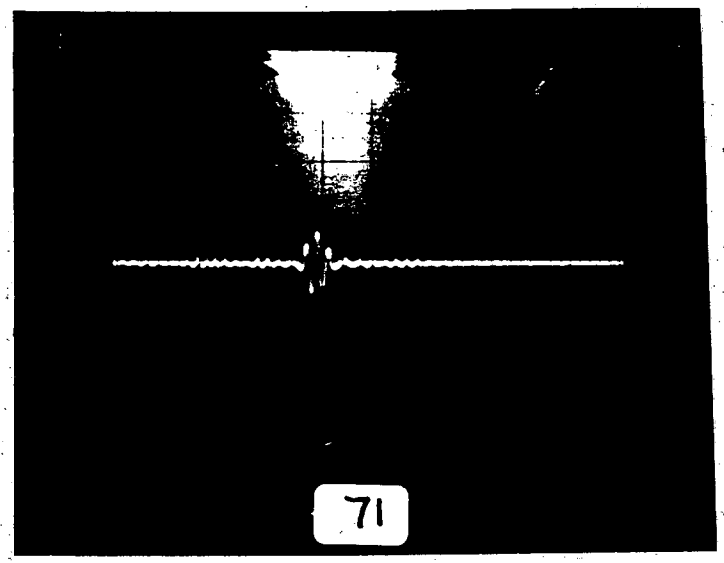
71

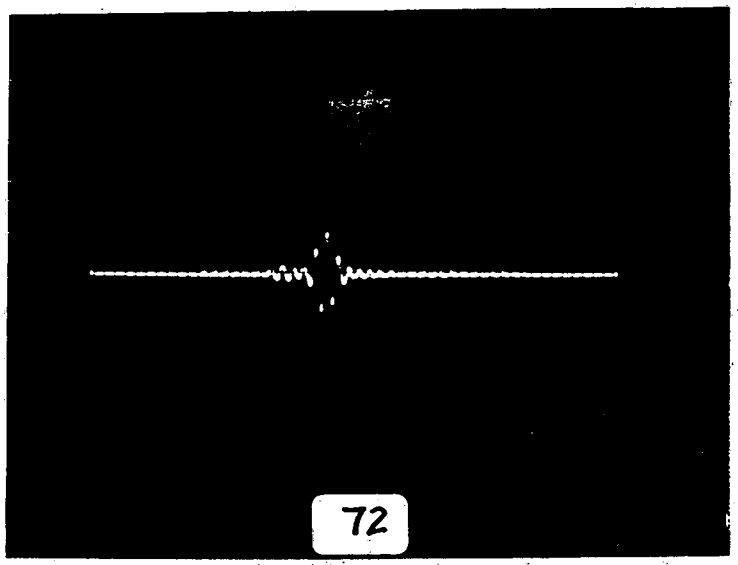
72

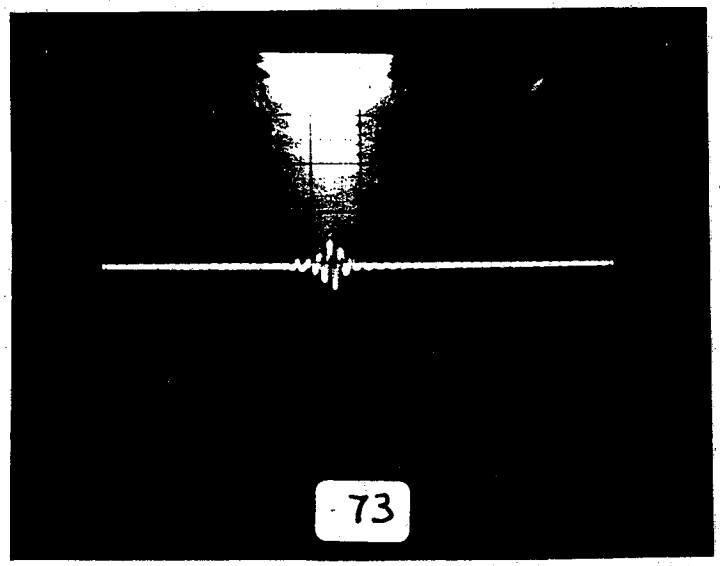
73

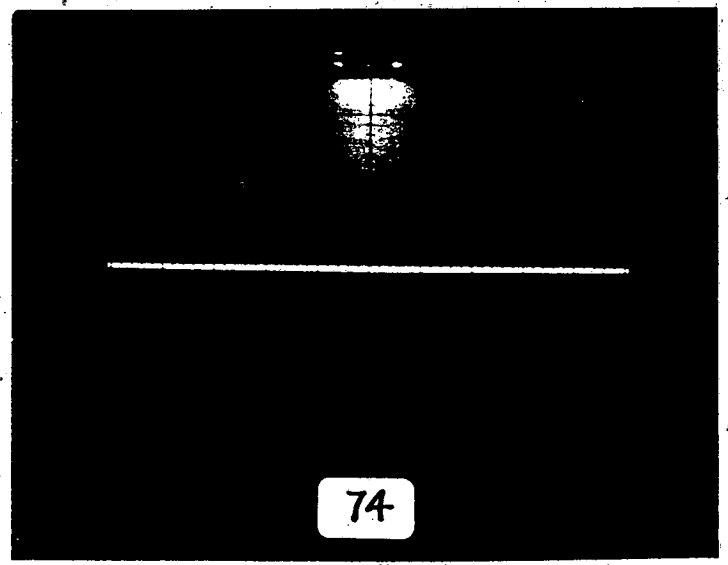
74

76

78

75

77

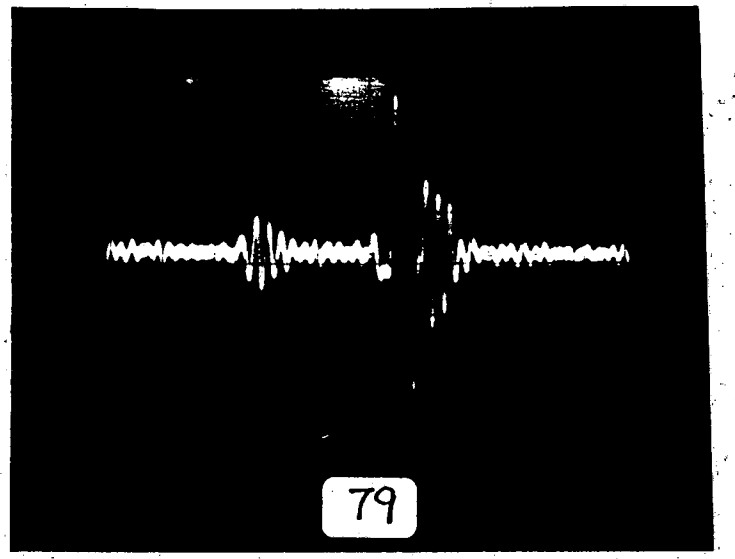
79

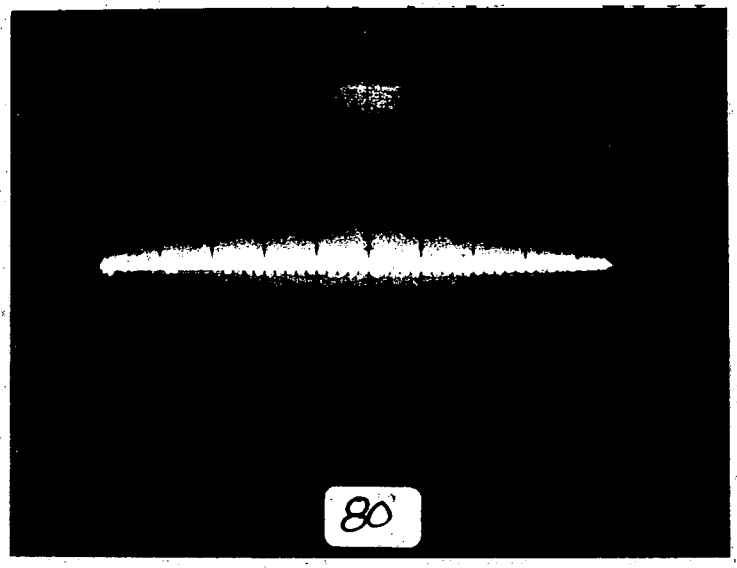
80

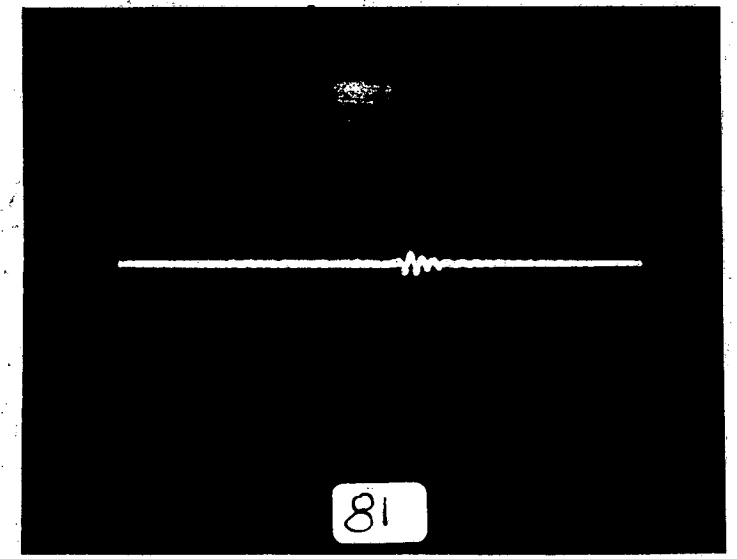
81

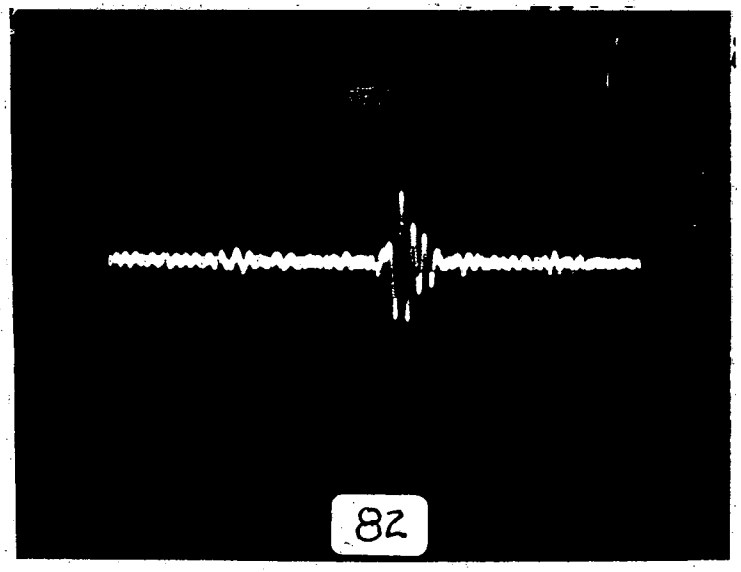
82

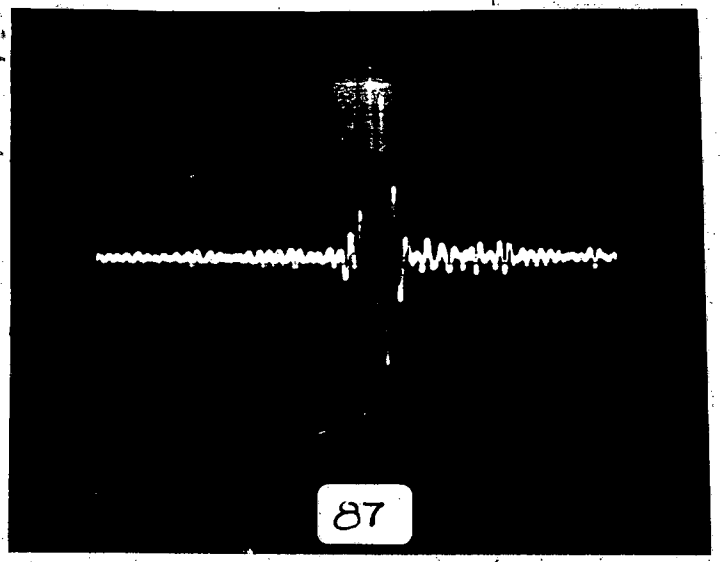
87

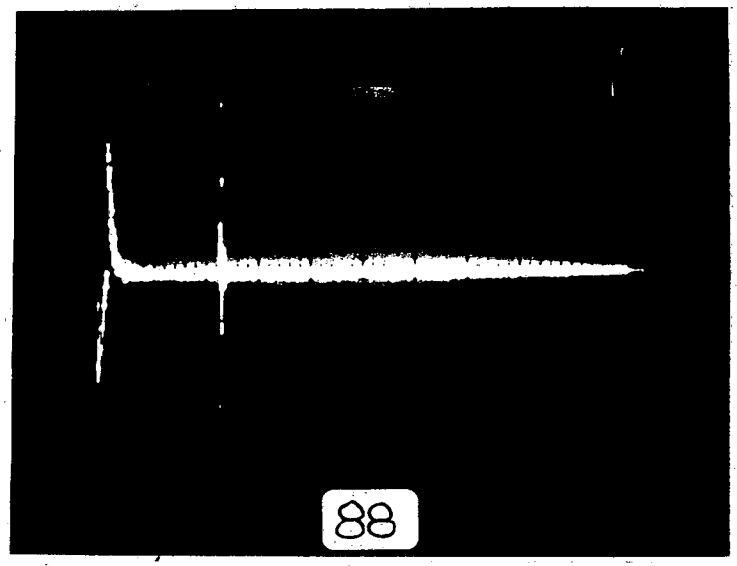
88

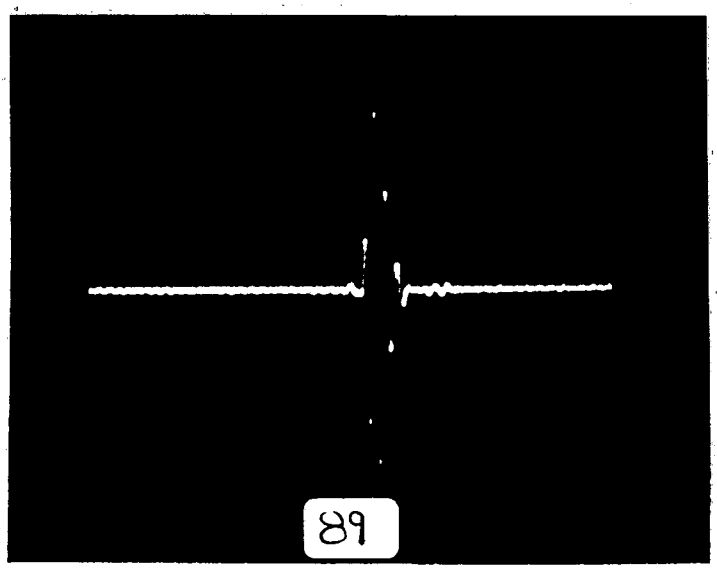
89

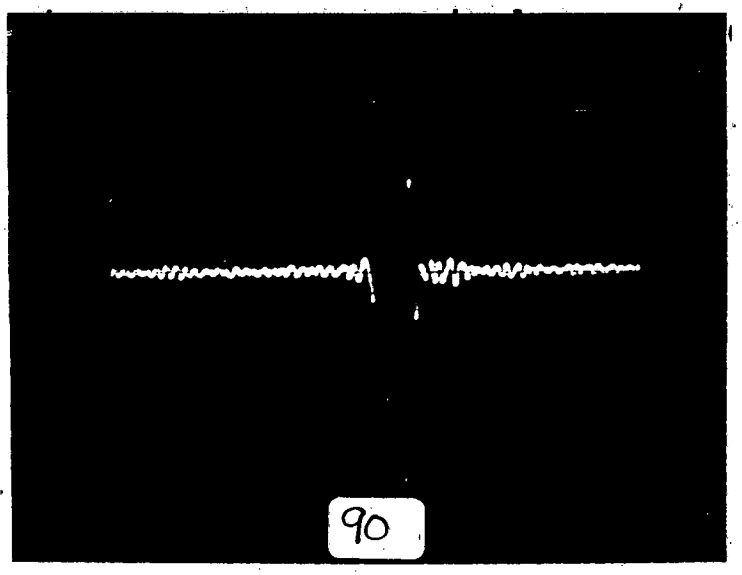
90

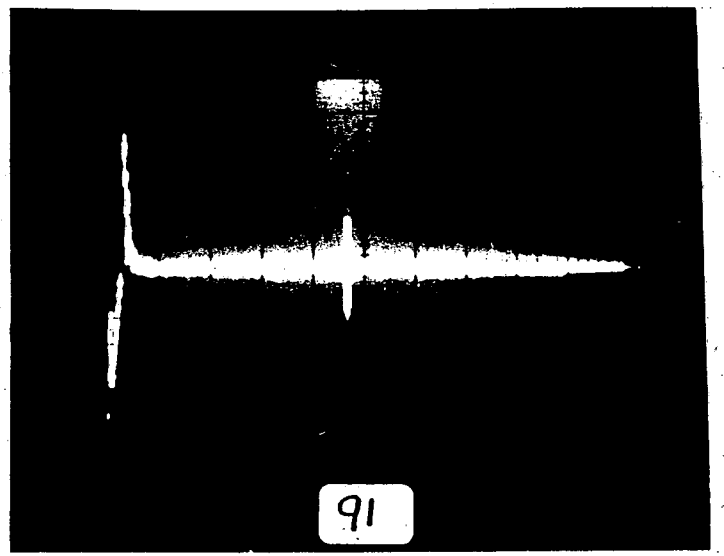
91

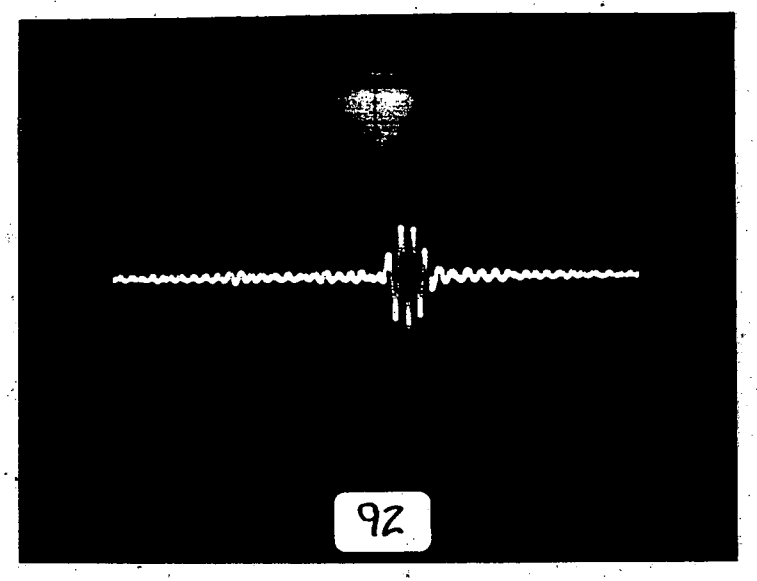
92

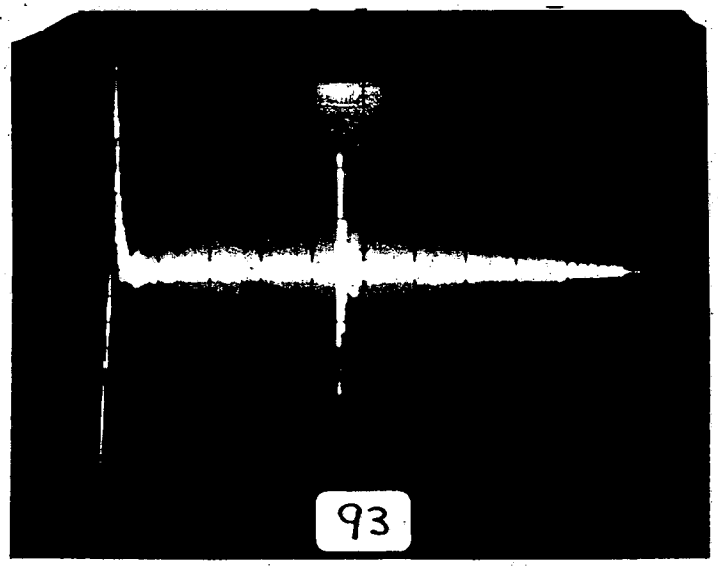
93

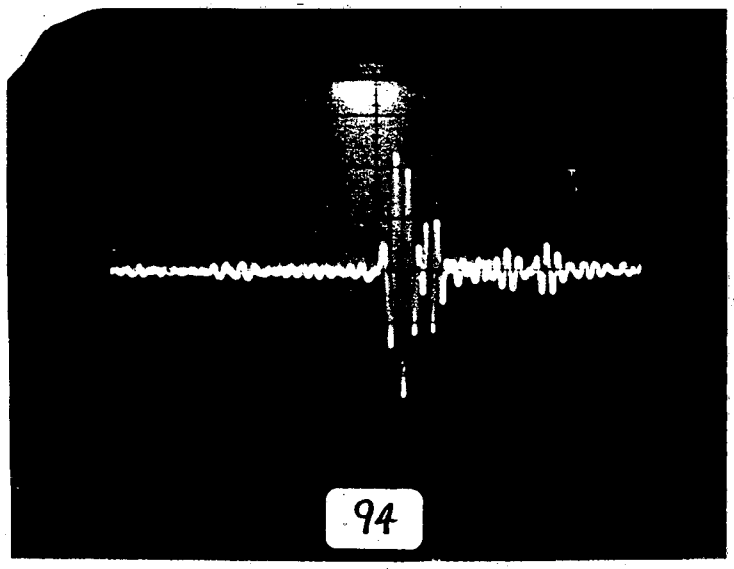
94

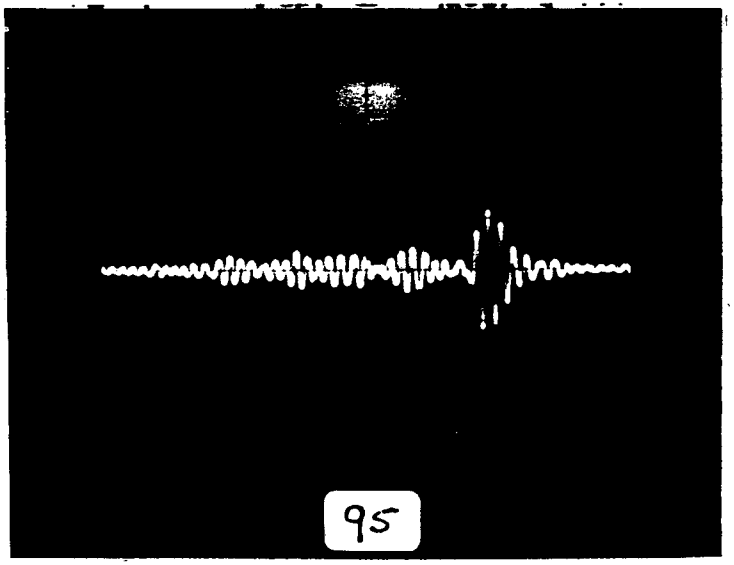
95

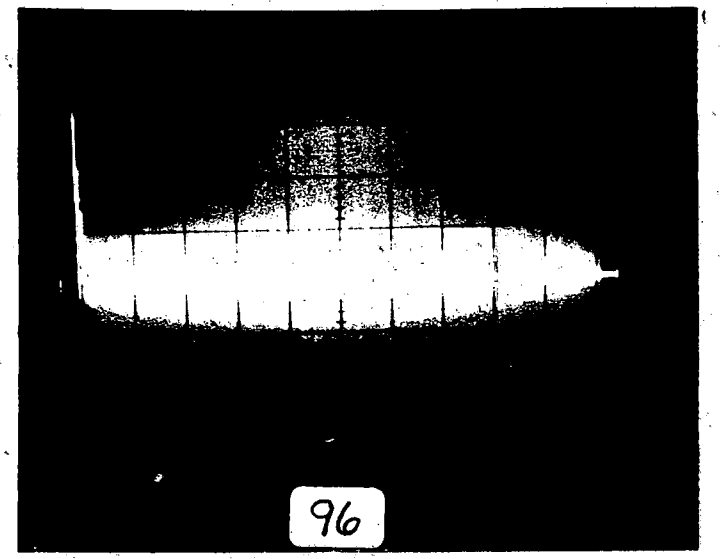
96

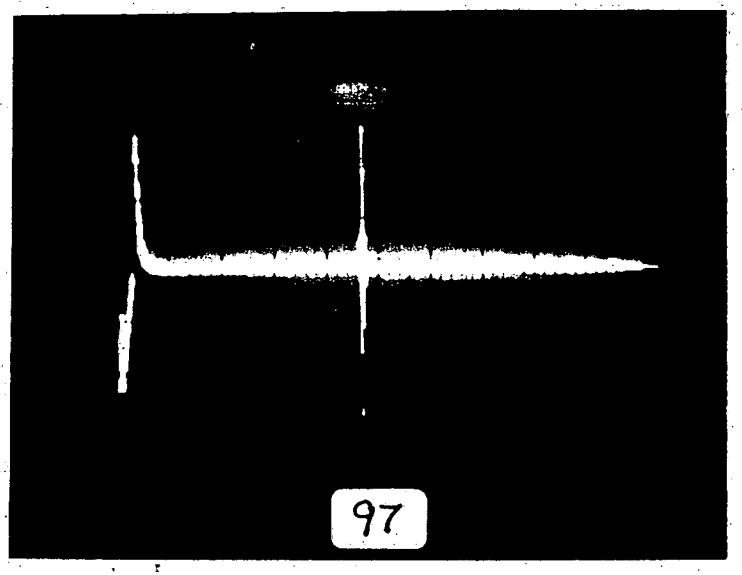
97

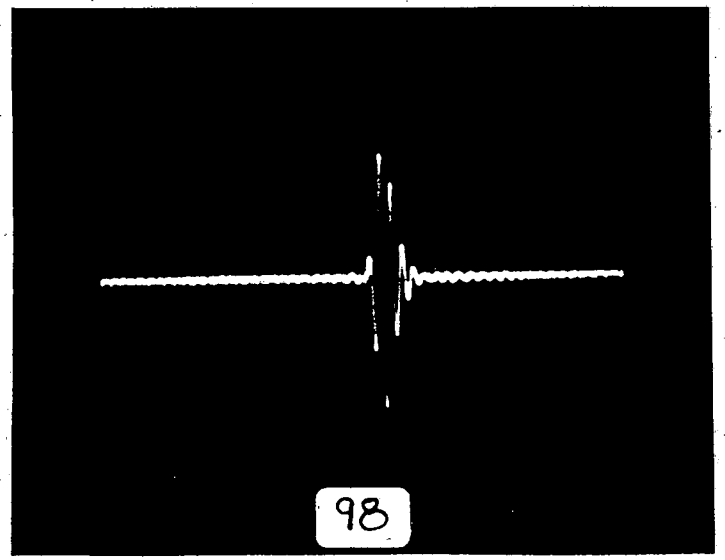
98

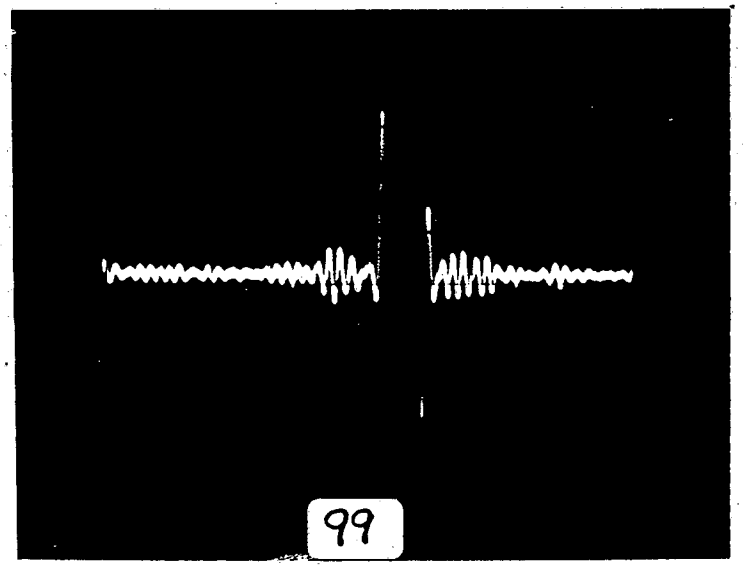
99

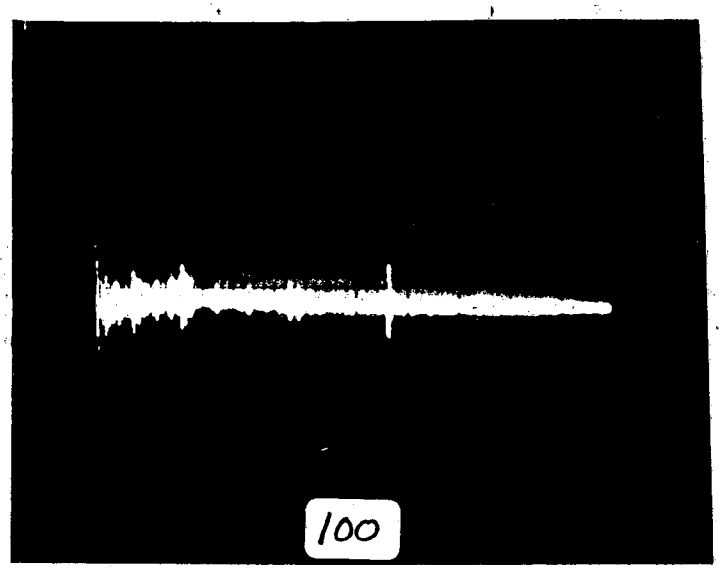
100

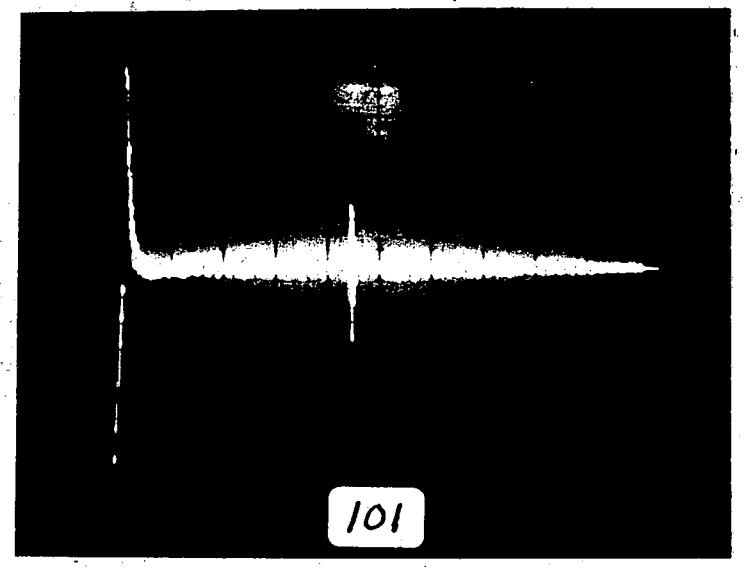
101

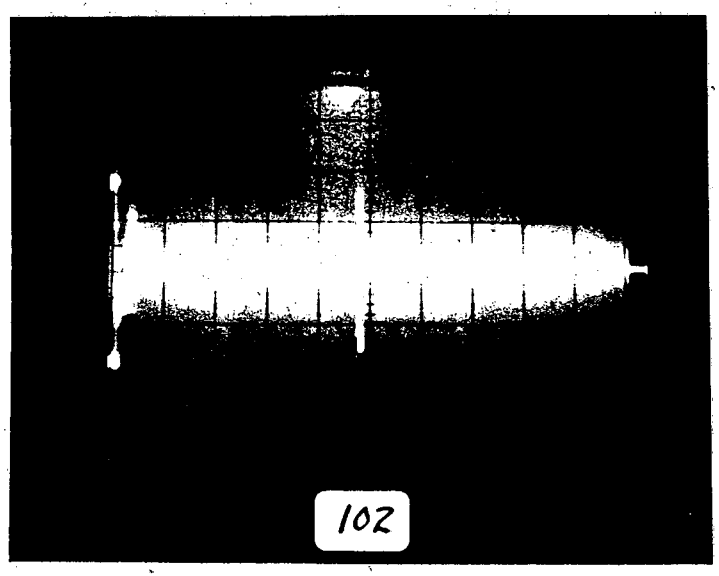
102

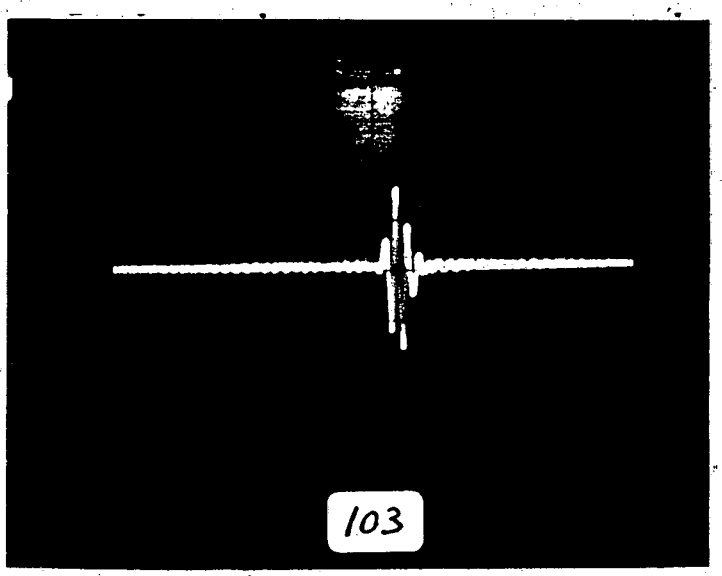
103

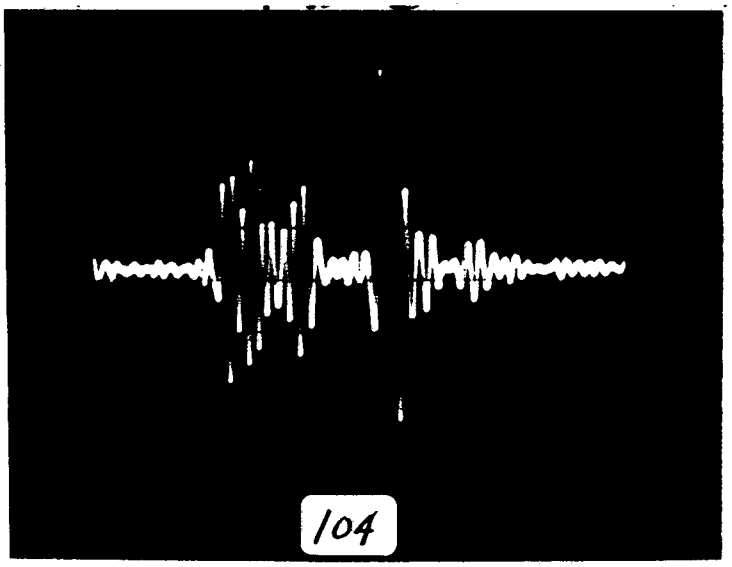
104

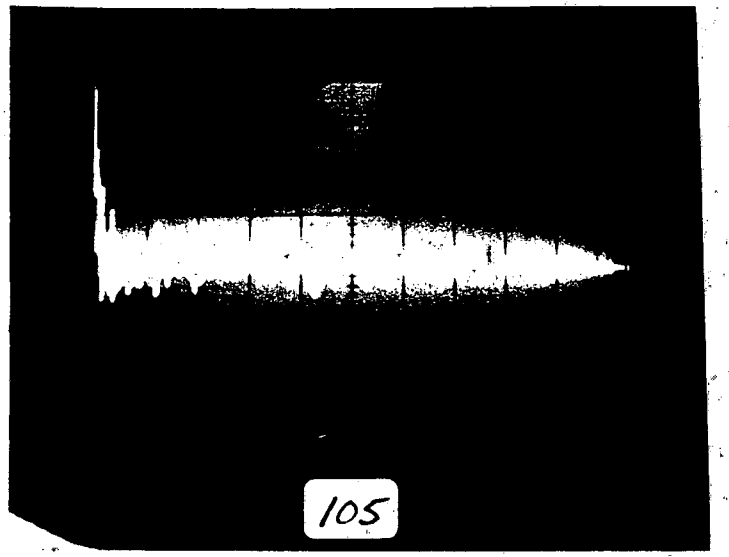
105

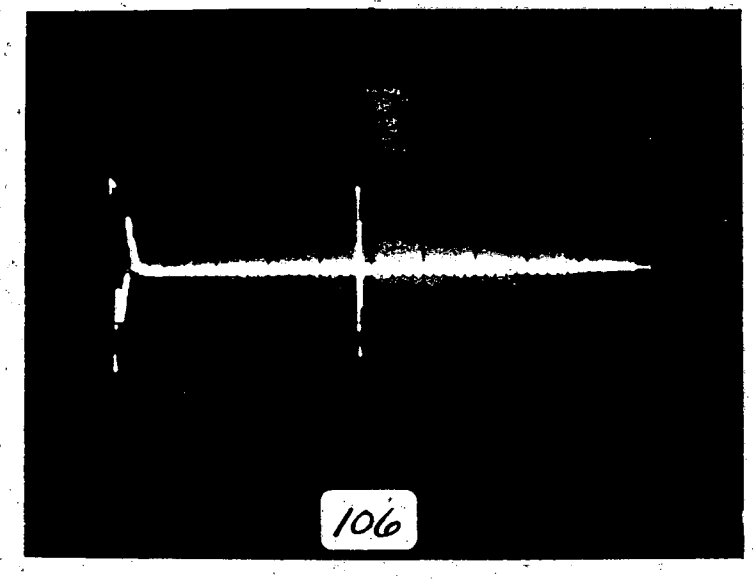
106

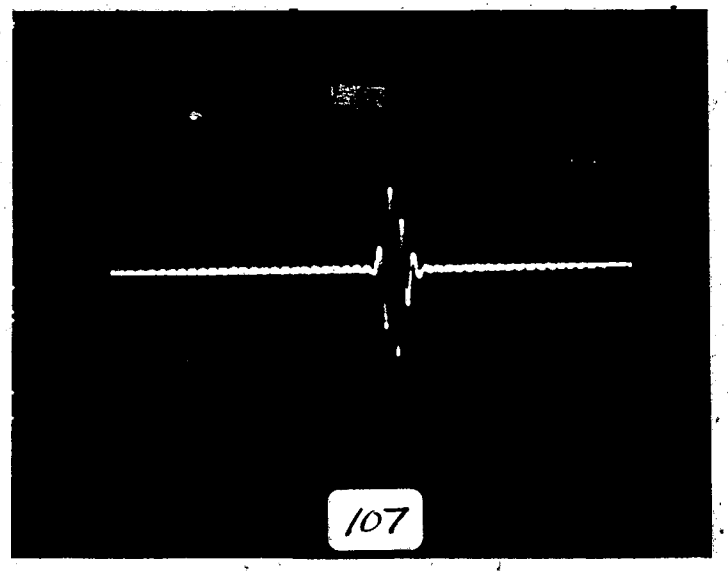
107

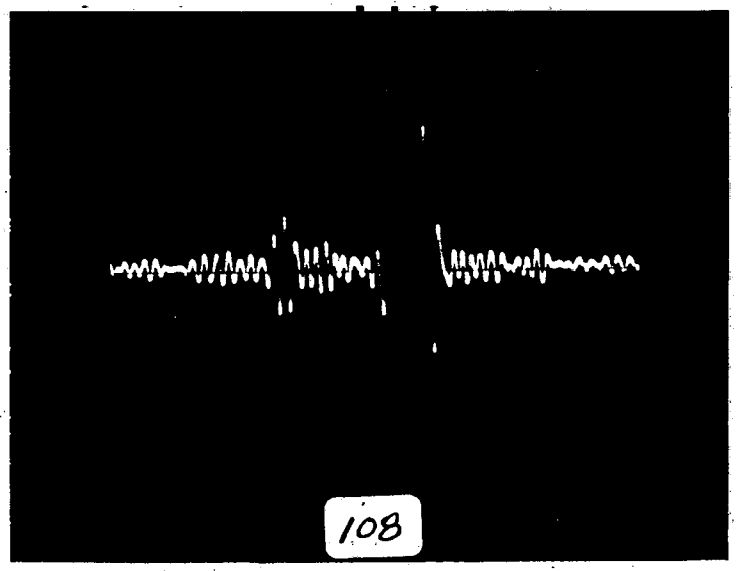
108

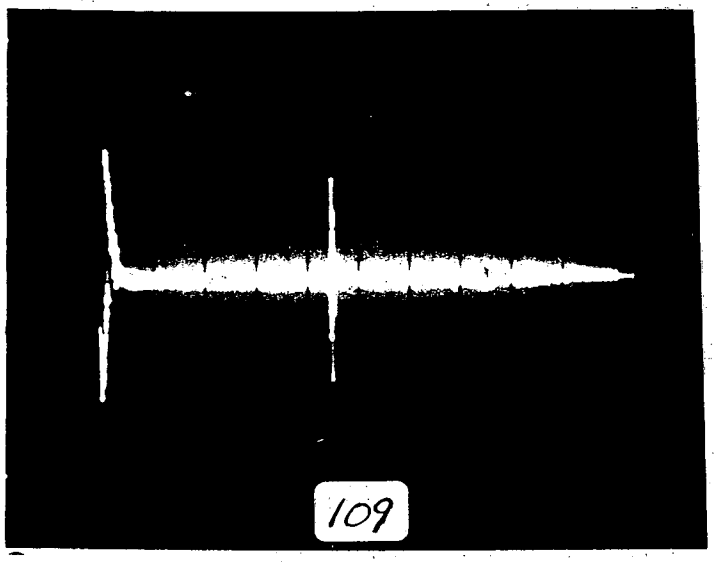
109

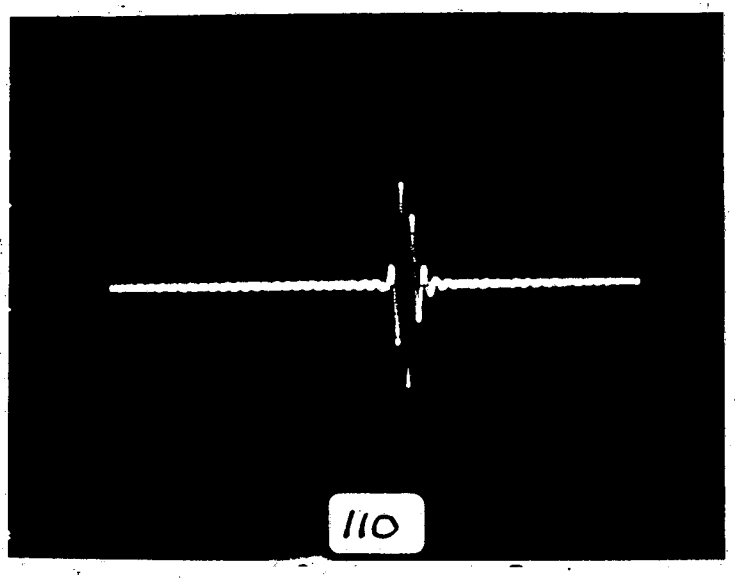
110

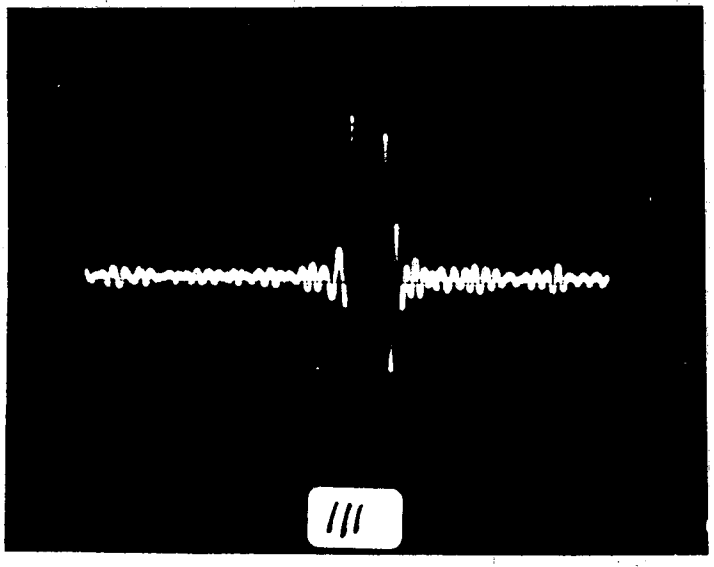
111

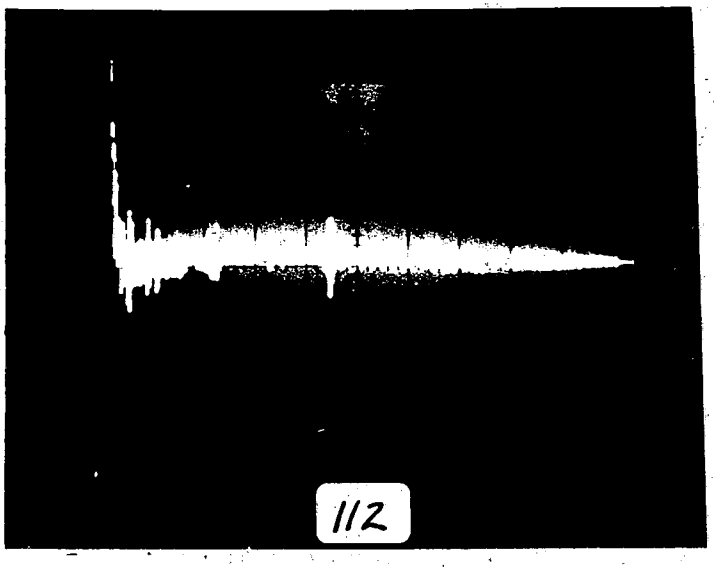

112

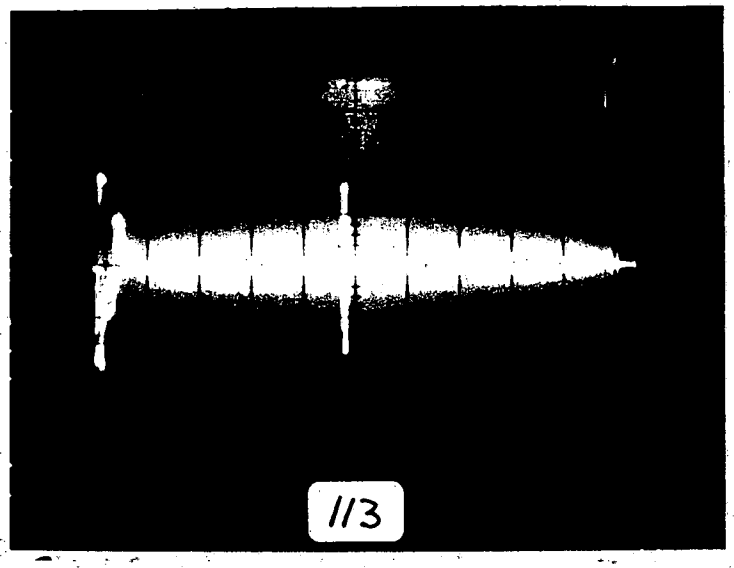

113

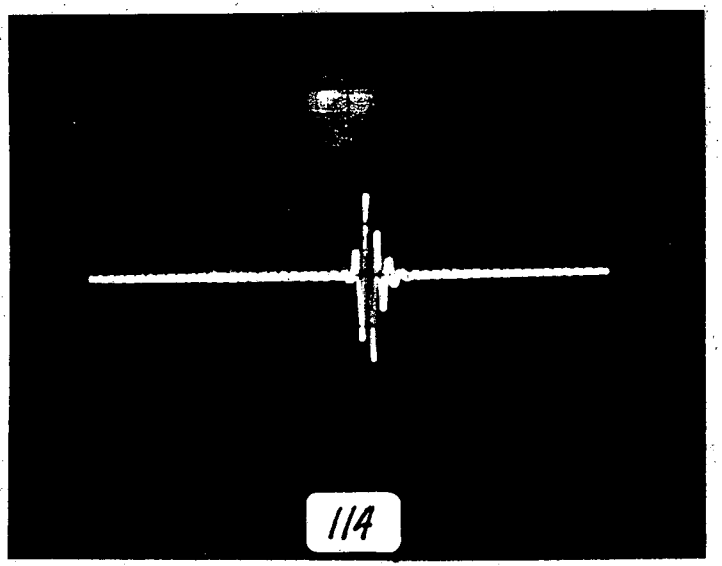

114

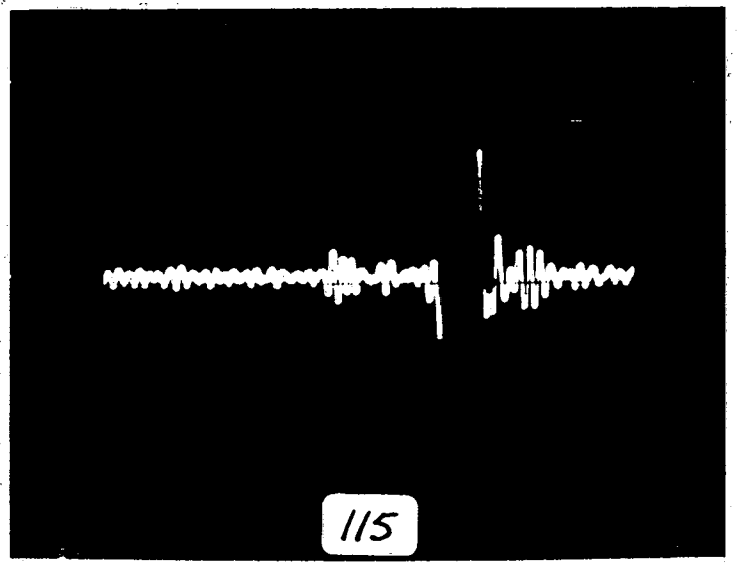

115

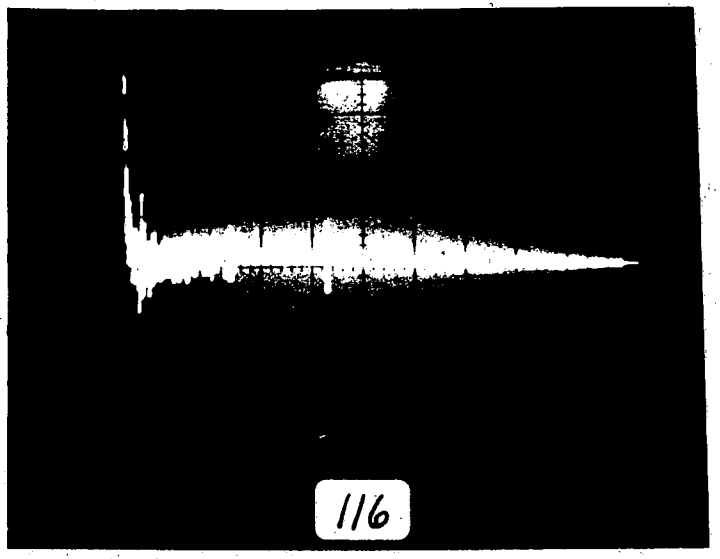

116

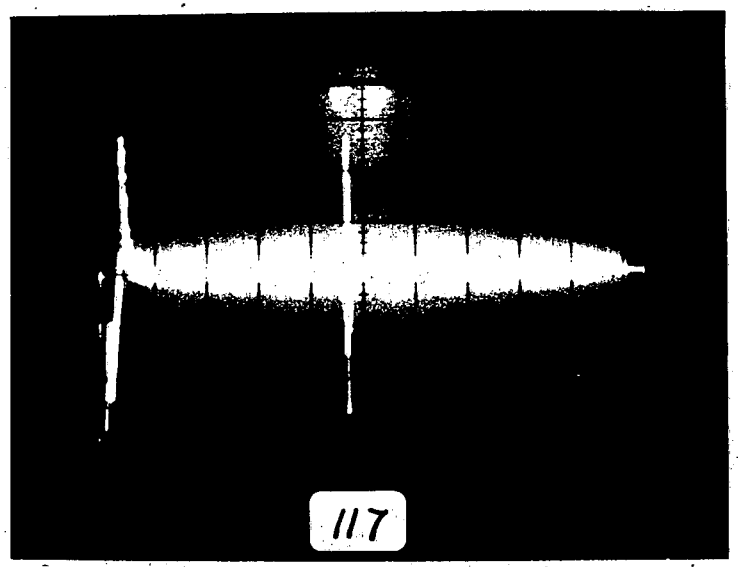

117

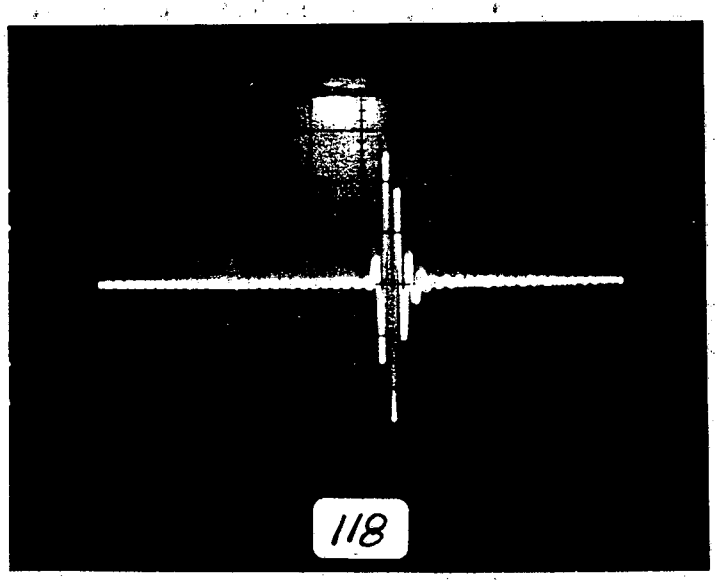

118

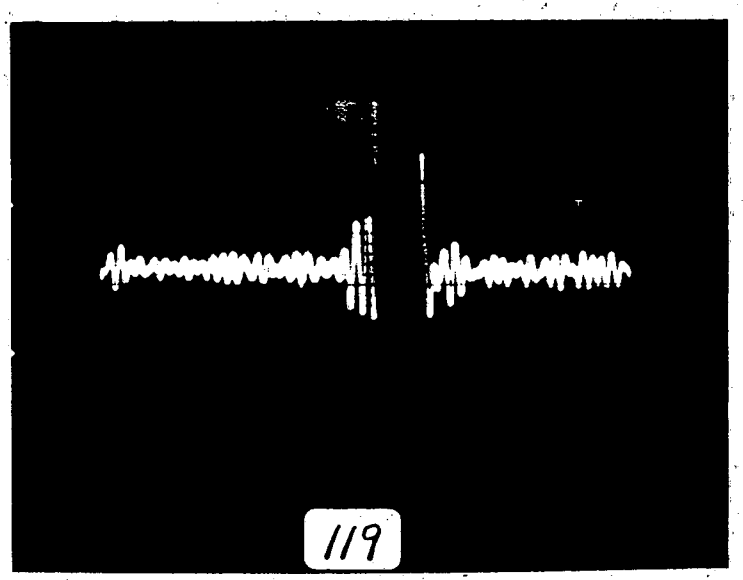

119

The measured strain levels were re-calibrated each time the specimen was taken out of its mount for ultra-sonic inspection. This was performed a total of nine times over the experiment. The strain level difference between the two locations and the known distance between strin-gage centerlines provide the estimated strain distribution slope in the material. The strain distribution slope was also computed during the actual cycling tests. Assuming that the stress distribution is linear below the neutral axis, the neutral axis location computation, using the static and dynamic strain distribution estimates, indicates that the neutral axis is located exactly midway between the specimen's lower edge and the notch bottom. The stress distribution can therefore be assumed to be linear on the specimen lower side, within the accuracy of the strain level measurement, and the stress level at the notch bottom before crack initiation can be computed.

The theoretical stress intensity factor due to this particular notch geometry is equal to 3.46 in the case of pure bending loads. The notch bottom stress level is therefore being computed using the equivalent weight strain level measurement with a 32.25 inches lever arm, a moment of inertia equal to 1.37 inches^4 and a distance to the neutral axis of 0.7 inch. The stresses given in the test result tables (Table G-7) are computed as described above and do not include the stress intensity factor due to the crack initiation and propagation.

Strain gages were only installed on one side assuming that the stress distribution across the specimen would be close to uniform because of its width and thickness. This assumption appeared not to be true because of the clamping mechanism procedure. The specimen was being clamped along its sides and a high torque was applied to the clamping bolts to avoid any possible play and movement during testing. Although the clamping beams were welded together and reinforced at the notch, the stress level on the sides was much higher than in the center. This was confirmed by the wear marks on the specimen side surfaces and the crack propagation data. Two large cracks were generated on the edges while the crack initiation scribed in the center remained the same as longa as the same test setup was maintained. Two large cracks were therefore generated in the edges first before the test setup was modified to increase the stress in the center. This was done by slightly raising the clamp level in the speciment center. The crack growth estimation data has therefore to be divided into two distinctive sections, before and after the clamping setup modification. A crack growth analysis can be performed for the right edge crack during the first test setup and the analysis can be performed for the center crack during the second test setup. In the case of the center crack, it will be assumed that the stress measurements on the specimen are valid for the center crack stress intensity factor computation within the accurach of the stress measurement and its intensity factor analysis assumptions.

G.5.2.2 Crack Size Estimation

Specimen 13 was used to calibrate the ultra-sonic echo due to a crack using EDM notches of a known depth. Four different scanning paths were used individually defined by their path length and number of reflections off the speciment steel-air interface. Specimen 13 was one inch thick and the different path lengths were as follows:

- Top, one bounce, 45 deg, 5 Mhz: 71.83 mm
- Top, two bounces, 45 deg, 5 Mhz: 143.77 mm
- Bottom, no bounce, 45 deg, 5 Mhz: 35.92 mm
- Bottom, one bounce, 45 deg, 5 Mhz: 107.75 mm

In the case of the 5A-A specimen, the scanning path lengths were as follows:

- Top, one bounce, 45 deg, 5 Mhz: 147.57 mm
- Top, one bounce, 60 deg, 5 Mhz: 179.07 mm
- Bottom, no bounce, 0 deg, 5 Mhz: 35.56 mm
- Bottom, no bounce, 45 deg, 5 Mhz: 50.29 mm

There is therefore, no calibration data which applies directly to the specimen 5A-A scanning procedures as far as number of bounces and path length. The number of reflections and path length influence the return echo attenuation and the measured crack signal strength can therefore, not be used for crack size estimation. However, the "time of flight" between crack tip and root can be used for identical incident angles between the calibration specient and speciment 5A-A. Because of the clamping setup, it was not possible to measure a crack top to root signal delay in the case of the top 45 degree scan. The clamping fixture layout made it impossible to approach the crack sufficiently on the top flat surface area in order to be able to measure a clear tip to root signal delay.

The only remaining method to accurately estimate the crack depth was using the zero degree scanning method and assume a longitudinal velocity of ultrasound in this specific steel equal to 5900 m/sec. The crack estimate computation will therefore only be rigorously possible when a type VII scan was performed. The crack tip to root time delay represents the necessary time for the ultrasonic wave to travel twice the crack depth distance at 5900 m/sec. The longitudinal ultrasonic velocity in the test specimen steel could not be verified because all calibration procedures were performed with the transducer at an angle and therefore generating shear waves with a different velocity.

G.6 Results

Table G-7 gives the results for the fatigue tests on specimen 5A-A. Results are tabulated for each transverse location of the sensor.

Table G-8 includes a log of all the UT photos.

TABLE G-7A

SPECIMEN 5A-A TEST RESULTS
EXTREME RIGHT LOCATION

K-CYCLES TOTAL	K-CYCLES INCREMENT	NOTCH BOTTOM STRESS LEVEL [MPa]	BEAM PATH	ECHO AMPLITUDE [VOLTS]	TIP & ROOT TIME LAG [us]	ESTIMATED SIZE [mm]	PHOTO #
12.16	12.16	541.5	–	–	–	–	–
14.21	2.05	402.5	VII	–	1.3	3.8	28
15.21	1.0	353.7	–	–	–	–	–
55.0	39.79	195.2	–	–	–	–	–
55.9	.9	329.9	VII	–	1.9	5.6	50
		CLAMP CHANGED FOR CENTER STRESS POINT					
86.0	30.1	198.3	–	–	–	–	–
87.0	1.0	415.7	VII	–	2.37	7.0	74
105.8	18.8	197.8	–	–	–	–	–
106.84	1.04	445.4	VII	–	2.42	7.14	91
111.0	4.61	192.1	–	–	–	–	–
116.0	5.0	280.5	–	–	–	–	–
126.0	10.0	192.1	VII	–	2.3	6.78	104
127.0	1.0	385.7	–	–	–	–	–
157.0	30.0	280.5	–	–	–	–	–
158.0	1.0	395.2	VII	–	2.3	6.78	108
188.0	30.0	280.5	–	–	–	–	–
189.0	1.0	406.2	–	–	–	–	–
229.3	40.3	280.5	–	–	–	–	–
249.3	20.0	333.2	VII	–	2.75	8.11	112

TABLE G-7B

SPECIMEN 5A-A TEST RESULTS
1" FROM EXTREME LEFT LOCATION

K-CYCLES TOTAL	K-CYCLES INCREMENT	NOTCH BOTTOM STRESS LEVEL [MPa]	BEAM PATH	ECHO AMPLITUDE [VOLTS]	TIP & ROOT TIME LAG [us]	ESTIMATED SIZE [mm]	PHOTO #
12.16	12.16	541.5	V	4.0	-	-	14
14.21	2.05	402.5	V	4.2	-	-	26
15.21	1.0	353.7	-	-	-	-	-
55.0	39.79	195.2	-	-	-	-	-
55.9	.9	329.9	VII	-	.9	2.65	51/52
		CLAMP CHANGED FOR CENTER STRESS POINT					
86.0	30.1	198.3	V	4.5	-	-	70
87.0	1.0	415.7	VII	-	1.2	3.54	75
105.8	18.8	197.8	V	4.0	-	-	86
106.84	1.04	445.4	VII	-	1.3	3.8	95
111.0	4.16	192.1	-	-	-	-	-
116.0	5.0	280.5	-	-	-	-	-
121.0	5.0	192.1	V	3.8	-	-	98
126.0	5.0	192.1	-	-	-	-	-
127.0	1.0	385.7	-	-	-	-	-
157.0	30.0	280.5	-	-	-	-	-
158.0	1.0	395.2	-	-	-	-	-
188.0	30.0	280.5	-	-	-	-	-
189.0	1.0	406.2	-	-	-	-	-
229.3	40.3	280.5	-	-	-	-	-
249.3	20.0	333.2	VII	-	1.0	2.95	113

TABLE G-7C

SPECIMEN 5A-A TEST RESULTS
CENTER LOCATION

K-CYCLES TOTAL	K-CYCLES INCREMENT	NOTCH BOTTOM STRESS LEVEL [MPa]	BEAM PATH	ECHO AMPLITUDE [VOLTS]	TIP & ROOT TIME LAG [us]	ESTIMATED SIZE [mm]	PHOTO #
12.16	12.16	541.5	V	2.0	-	-	12
14.21	2.05	402.5	VII	-	N/A	-	21
" "	-	-	V	3.0	-	-	27
15.21	1.0	353.7	-	-	-	-	-
55.0	39.79	195.2	-	-	-	-	-
55.9	.9	329.9	V	2.8	-	-	46
" "	-	-	VII	-	-	-	49
CLAMP CHANGED FOR CENTER STRESS POINT							
86.0	30.1	198.3	V	2.0	-	-	69
87.0	1.0	415.7	VII	-	.25	.74	72
95.8	8.8	197.8	V	3.0	-	-	79
105.8	10.0	197.8	-	-	-	-	-
106.84	1.04	445.4	VII	-	.3	.88	92
111.0	4.16	192.1	-	-	-	-	-
116.0	5.0	280.5	-	-	-	-	-
121.0	5.0	192.1	V	4.0	-	-	97
126.0	5.0	192.1	VII	-	.3	.88	103
127.0	1.0	385.7	-	-	-	-	-
157.0	30.0	280.5	-	-	-	-	-
158.0	1.0	395.2	VII	-	.45	1.33	106
188,0	30.0	280.5	-	-	-	-	-
189.0	1.0	406.2	-	-	-	-	-
229.3	40.3	280.5	-	-	-	-	-
249.3	20.0	333.2	V	4.0	-	-	109
" "	-	-	VII	-	.85	2.5	115

TABLE G-7D

SPECIMEN 5A-A TEST RESULTS
1" FROM EXTREME RIGHT LOCATION

K-CYCLES TOTAL	K-CYCLES INCREMENT	NOTCH BOTTOM STRESS LEVEL [MPa]	BEAM PATH	ECHO AMPLITUDE [VOLTS]	TIP & ROOT TIME LAG [us]	ESTIMATED SIZE [mm]	PHOTO #
12.16	12.16	541.5	V	2.0	-	-	13
14.21	2.05	402.5	V	2.0	-	-	25
15.21	1.0	353.7	-	-	-	-	-
55.0	39.79	195.2	-	-	-	-	-
55.9	.9	329.9	VII	-	1.2	3.54	47
		CLAMP CHANGED FOR CENTER STRESS POINT					
76.0	20.1	198.3	V	2.0	-	-	61
86.0	10.0	198.3	V	2.0	-	-	71
87.0	1.0	415.7	VII	-	1.4	4.13	76
95.8	8.8	197.8	V	2.5	-	-	81
105.8	10.0	197.8	V	2.2	-	-	87
106.84	1.04	445.4	VII	-	1.0	2.95	94
111.0	4.16	192.1	-	-	-	-	-
116.0	5.0	280.5	-	-	-	-	-
121.0	5.0	192.1	V	2.0	-	-	99
126.0	5.0	192.1	-	-	-	-	-
127.0	1.0	385.7	-	-	-	-	-
157.0	30.0	280.5	-	-	-	-	-
158.0	1.0	395.2	-	-	-	-	-
188.0	30.0	280.5	-	-	-	-	-
189.0	1.0	406.2	-	-	-	-	-
229.3	40.3	280.5	-	-	-	-	-
249.3	20.0	333.2	V	2.0	-	-	111
"	"	-	VII	-	1.3	3.83	116

TABLE G-7E

SPECIMEN SA-A TEST RESULTS
EXTREME RIGHT LOCATION

K-CYCLES TOTAL	K-CYCLES INCREMENT	NOTCH BOTTOM STRESS LEVEL [MPa]	BEAM PATH	ECHO AMPLITUDE [VOLTS]	TIP & ROOT TIME LAG [us]	ESTIMATED SIZE [mm]	PHOTO #
12.16	12.16	541.5	-	-	-	-	-
14.21	2.05	402.5	VII	-	.9	2.65	39
15.21	1.0	353.7	-	-	-	-	-
55.0	39.79	195.2	-	-	-	-	-
55.9	.9	329.9	VII	-	1.6	4.72	48
		CLAMP CHANGED FOR CENTER STRESS POINT					
86.0	30.1	198.3	-	-	-	-	-
87.0	1.0	415.7	VII	-	1.7	5.01	77
105.8	18.8	197.8	-	-	-	-	-
106.84	1.04	445.4	VII	-	1.4	4.13	93
111.0	4.61	192.1	-	-	-	-	-
116.0	5.0	280.5	-	-	-	-	-
126.0	10.0	192.1	VII	-	1.7	5.01	105
127.0	1.0	385.7	-	-	-	-	-
157.0	30.0	280.5	-	-	-	-	-
158.0	1.0	395.2	VII	-	1.5	4.42	107
188.0	30.0	280.5	-	-	-	-	-
189.0	1.0	406.2	-	-	-	-	-
229.3	40.3	280.5	-	-	-	-	-
249.3	20.0	333.2	VII	-	1.7	5.01	117

TABLE G-8

Photo Log Specimen 5A-A

Photo #	Beam Path	Probe degree / MHz	Description
120	V	45 / 5	Scan L - R before and after scribe 5. V 10us 0dB
121	V	45 / 5	Scan L - R before and after scribe 5. V 1us 0dB
122	VI	60 / 2.25	Scan L - R before scribe .2V 20us 6dB
123	VI	60 / 2.25	Scan L - R before scribe .2V 2us 6dB
124	VI	60 / 5	Scan L - R before scribe .2V 20us 6dB
125	VI	60 / 5	Scan L - R before scribe .2V 2us 6dB
126	VI	60 / 2.25	Scribe at start .2V 2us 6dB
127	VI	60 / 5	Scribe at start .2V 2us 6dB
128	VI	60 / 5	12.16 K-cyc. center .2V 2us 6dB
129	VI	60 / 5	12.16 K-cyc. left side .2V 2us 6dB
130	VI	60 / 5	12.16 K-cyc. right side .2V 2us 6dB
131	VI	60 / 2.25	12.16 K-cyc. center .2V 20us 6dB
132	VI	60 / 2.25	12.16 K-cyc. center .2V 2us 6dB
133	VI	60 / 2.25	12.16 K-cyc. right side .2V 2us 6dB
134	VI	60 / 2.25	12.16 K-cyc. left side .2V 2us 6dB
135	V	45 / 5	12.16 K-cyc. center 5. V 10us 0dB
136	V	45 / 5	12.16 K-cyc. center 5. V 1us 0dB
137	V	45 / 5	12.16 K-cyc. right side 5. V 1us 0dB
138	V	45 / 5	12.16 " left side 5. V 1us 0dB
139	VI	60 / 2.25	14.21 K-cyc. center .2V 2us 6dB
140	VI	60 / 2.25	" " left side .2V 2us 6dB
141	VI	60 / 2.25	" " right side .2V 2us 6dB
142	VI	60 / 5	" " center .2V 2us 6dB
143	VI	60 / 5	" " left side .2V 2us 6dB
144	VI	60 / 5	" " right side .2V 2us 6dB
145	V	45 / 5	" " right side 5. V 1us 0dB
146	V	45 / 5	" " left side 5. V 1us 0dB
147	V	45 / 5	" " center 5. V 1us 0dB
148	VII	0 / 5	" " center .5V .5us 20dB
149	VII	0 / 5	" " extreme left .2V .5us 0dB
150	VII	0 / 5	" " extreme right .2V .5us 0dB
151	V	45 / 5	14.21 K-cyc. Maximum third signal, at center 5. V 1us 0dB
152	V	45 / 5	" " 1/8 inch away from max., at center 5. V 1us 0dB
153	V	45 / 5	" " 1/4 inch away from max., at center 5. V 1us 0dB
154	VIII	45 / 5	" " back-center at maximum amplitude 5. V 1us 0dB
155	VIII	45 / 5	" " back-center, moving away from crack 5. V 1us 0dB
156	VIII	45 / 5	14.21 K-cyc. back-center, moving away from crack 5. V 1us 0dB
157	VIII	45 / 5	" " Maximum third signal, from back far-left 5. V 1us 0dB
158	VIII	45 / 5	14.21 K-cyc. 1/8 inch away from max., from back far-left 5. V 1us 0dB

TABLE G-8 (cont'd.)

Photo Log Specimen 5A-A

Photo #	Beam Path	Probe degree / MHz	Description
159	VIII	45 / 5	14.21 K-cyc. 1/4 inch away from max., from back far-left 5. V 1us 0dB
160	VIII	45 / 5	14.21 K-cyc. 3/8 inch away from max., from back far-left 5. V 1us 0dB
161	VIII	45 / 5	14.21 K-cyc. one inch away from max., from back far-left 5. V 1us 0dB
162	VI	60 / 2.25	17.21 K-cyc. center .2V 2us 6dB
163	VI	60 / 2.25	" " right side .2V 2us 6dB
164	VI	60 / 5	25.21 K-cyc. center 5. V 1us 6dB
165	V	45 / 5	" " center 5. V 1us 0dB
166	VI	60 / 5	35.21 K-cyc. center .2V 2us 6dB
167	VI	60 / 5	" " left side .2V 2us 6dB
168	VI	60 / 2.25	" " center .2V 2us 6dB
169	V	45 / 5	55.9 K-cyc. center 5. V 1us 0dB
170	VII	0 / 5	" " right side .2V .5us 20dB
171	VII	0 / 5	" " extreme right .2V .5us 20dB
172	VII	0 / 5	" " center .2V .5us 20dB
173	VII	0 / 5	" " extreme left .2V .5us 20dB
174	VII	0 / 5	" " 3/4 inch from extreme-left. .2V .5us 20dB
175	VII	0 / 5	55.9 K-cyc. one inch from extreme-left. .2V .5us 20dB
176	V	45 / 5	" " left side from back 5. V 2us 20dB
177	V	45 / 5	" " left side from back 5. V 1us 20dB
178	V	45 / 5	" " right side from back 5. V 1us 0dB
179	V	45 / 5	" " right side from back moving away 5. V 1us 0dB
180	V	45 / 5	55.9 K-cyc. center from back 5. V 1us 0dB
181	V	45 / 5	71.0 K-cyc. one inch right of center 5. V 1us 0dB
182	V	45 / 5	" " 1/2 inch right of center 5. V 1us 0dB
183	V	45 / 5	76.0 K-cyc. center 5. V 1us 0dB
184	V	45 / 5	" " right side 5. V 1us 0dB
185	V	45 / 5	" " left side 5. V 1us 0dB
186	VI	60 / 5	" " left side .2V 2us 6dB
187	VI	60 / 5	" " center .2V 2us 6dB
188	VI	60 / 5	" " right side .2V 2us 6dB
189	VI	60 / 5	86.0 K-cyc. center .2V 2us 6dB
190	VI	60 / 5	" " right side .2V 2us 6dB
191	VI	60 / 5	" " left side .2V 2us 6dB
192	V	45 / 5	" " center 5. V 1us 0dB
193	V	45 / 5	" " left side 5. V 1us 0dB
194	V	45 / 5	" " right side 5. V 1us 0dB
195	VII	0 / 5	87.0 K-cyc. center .2V .5us 20dB
196	VII	0 / 5	" " 1/4" right of center .2V .5us 20dB
197	VII	0 / 5	" " extreme left .2V .5us 20dB

TABLE G-8 (cont'd.)

Photo Log Specimen 5A-A

Photo #	Beam Path	Probe degree / MHz	Description
198	VII	0 / 5	" " 1" from extreme left .2V .5us 20dB
199	VII	0 / 5	" " 1" from extreme right .2V .5us 20dB
200	VII	0 / 5	" " extreme right .2V .5us 20dB
201	V	45 / 5	87.0 K-cyc. 1/2" right of center 5. V 1us 0dB
202	V	45 / 5	95.8 K-cyc. center 5. V 1us 0dB
203	V	45 / 5	" " left side 5. V 1us 0dB
204	V	45 / 5	" " right side 5. V 1us 0dB
205	VI	60 / 5	95.8 K-cyc. center .2V 2us 6dB
206	VI	60 / 5	" " left side .2V 2us 6dB
207	VI	60 / 5	" " right side .2V 2us 6dB
208	V	45 / 5	105.8 K-cyc. center 5. V 1us 0dB
209	V	45 / 5	" " left side 5. V 1us 0dB
210	V	45 / 5	" " right side 5. V 1us 0dB
211	VI	60 / 5	105.8 K-cyc. center .2V 2us 6dB
212	VI	60 / 5	" " left side .2V 2us 6dB
213	VI	60 / 5	" " right side .2V 2us 6dB
214	VII	0 / 5	106.84 K-cyc. extreme left .2V .5us 20dB
215	VII	0 / 5	" " 1" from extreme left .2V .5us 20dB
216	VII	0 / 5	" " center .2V .5us 20dB
217	VII	0 / 5	" " 1" from extreme right .2V .5us 20dB
218	VII	0 / 5	" " extreme right .2V .5us 20dB
219	V	45 / 5	116.0 K-cyc. center 5. V 1us 0dB
220	V	45 / 5	121.0 K-cyc. center 5. V 1us 0dB
221	V	45 / 5	" " left side 5. V 1us 0dB
222	V	45 / 5	" " right side 5. V 1us 6dB
223	VI	60 / 5	121.0 Kcyc. center .2V 2us 6dB
224	VI	60 / 5	" " left side .2V 2us 6dB
225	VI	60 / 5	" " right side .2V 2us 6dB
226	VII	0 / 5	126.0 K-cyc. center .2V .5us 20dB
227	VII	0 / 5	" " extreme left .2V .5us 20dB
228	VII	0 / 5	" " extreme right .2V .5us 20dB
229	VII	0 / 5	158.0 K-cyc. center .2V .5us 20dB
230	VII	0 / 5	" " extreme right .2V .5us 20dB
231	VII	0 / 5	" " extreme left .2V .5us 20dB
232	V	45 / 5	249.3 K-cyc. center 5. V 1us 0dB
233	V	45 / 5	" " left side 5. V 1us 0dB
234	V	45 / 5	" " right side 5. V 1us 0dB
235	VII	0 / 5	" " extreme left .2V .5us 20dB
236	VII	0 / 5	" " 1" from extreme left .2V .5us 20dB
237	VII	0 / 5	" " center .2V .5us 20dB
238	VII	0 / 5	" " center .2V .5us 20dB
239	VII	0 / 5	" " 1" from extreme right .2V .5us 20dB
240	VII	0 / 5	" " extreme right .2V .5us 20dB

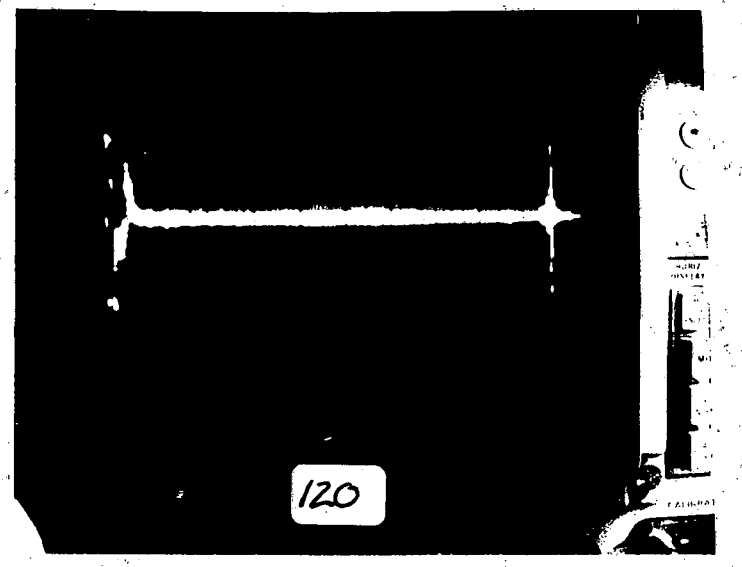
120

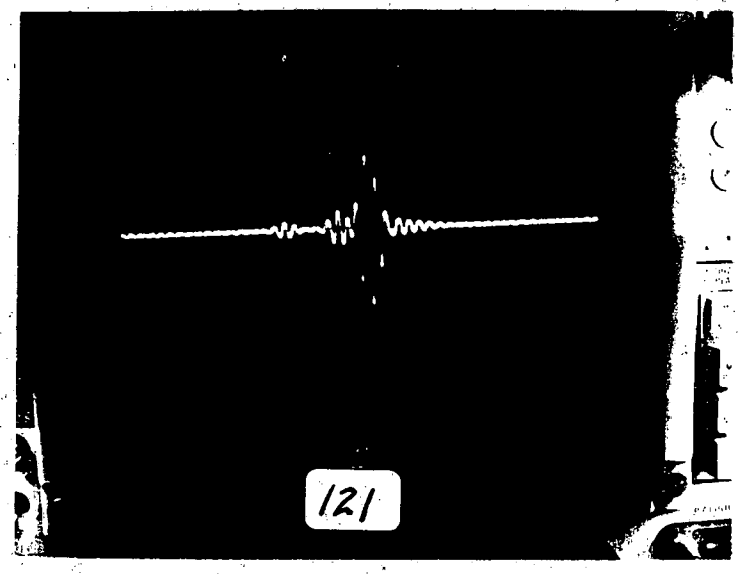
121

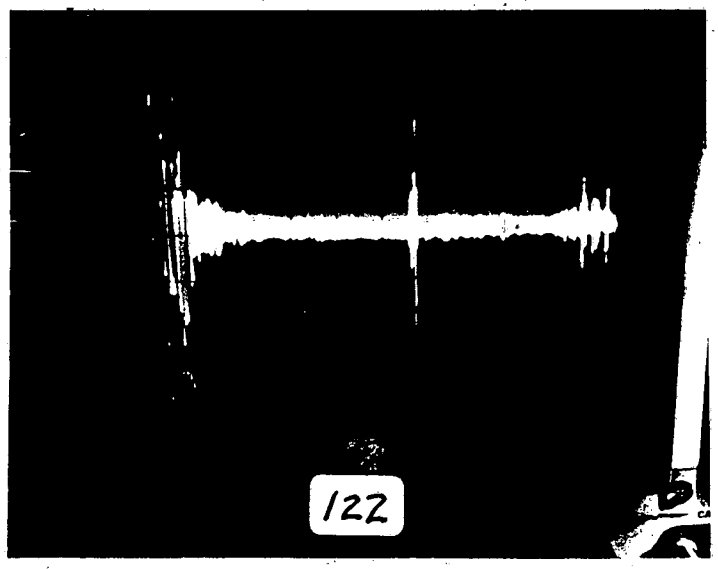
122

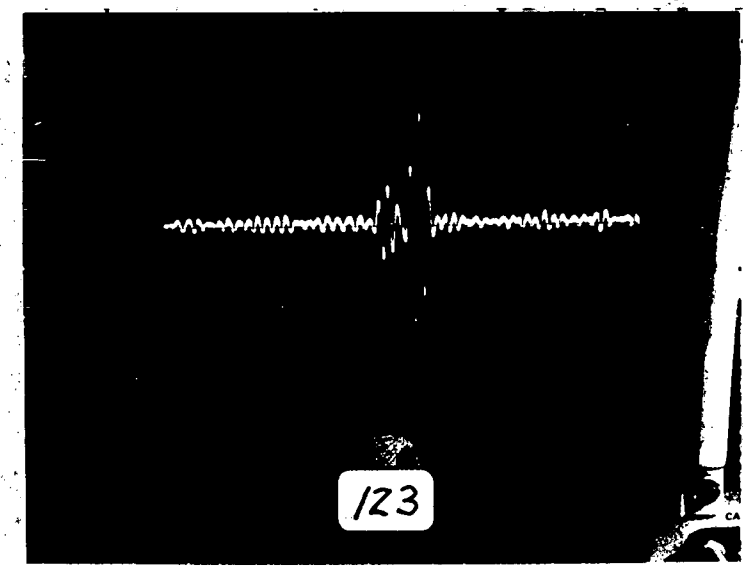
123

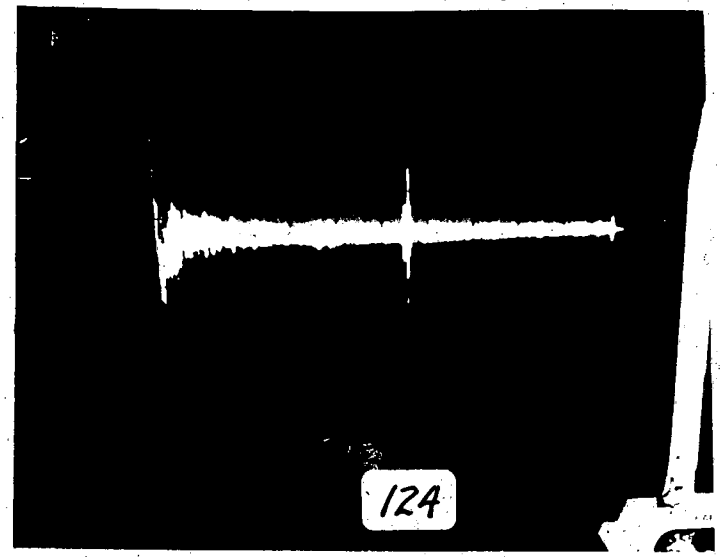
124

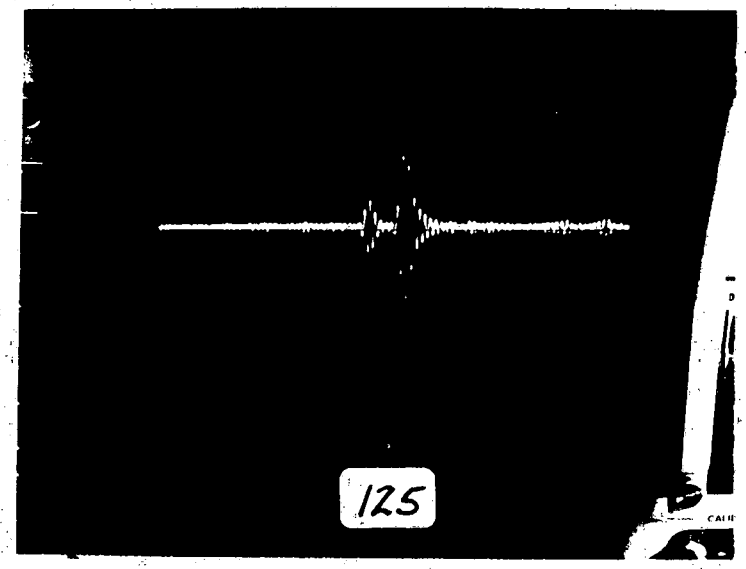
125

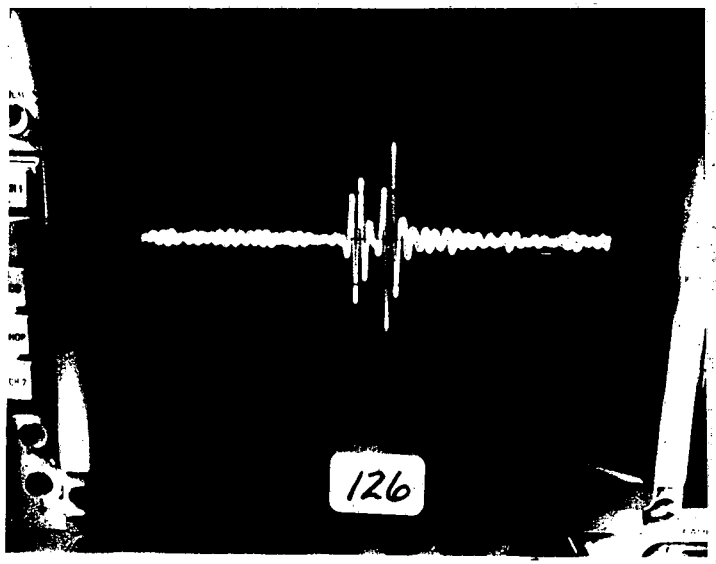
126

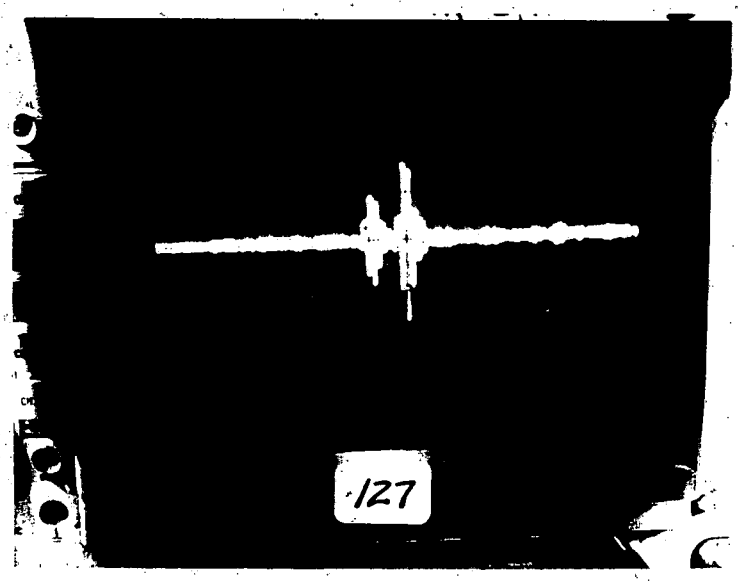
127

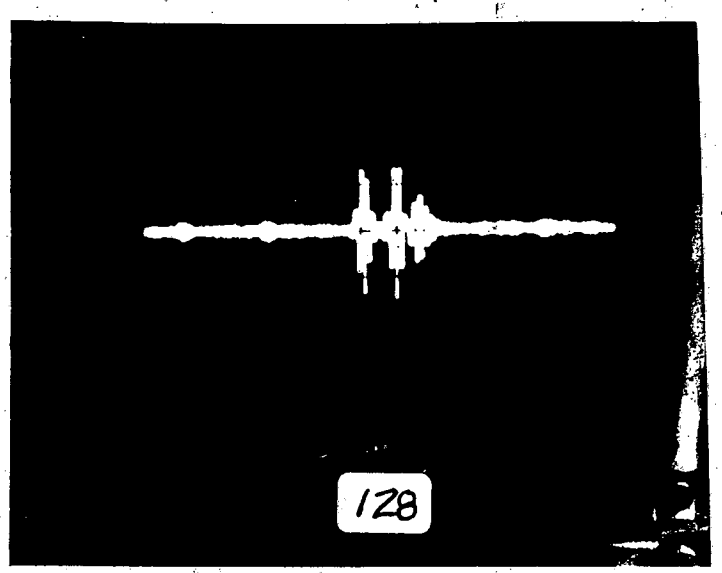
128

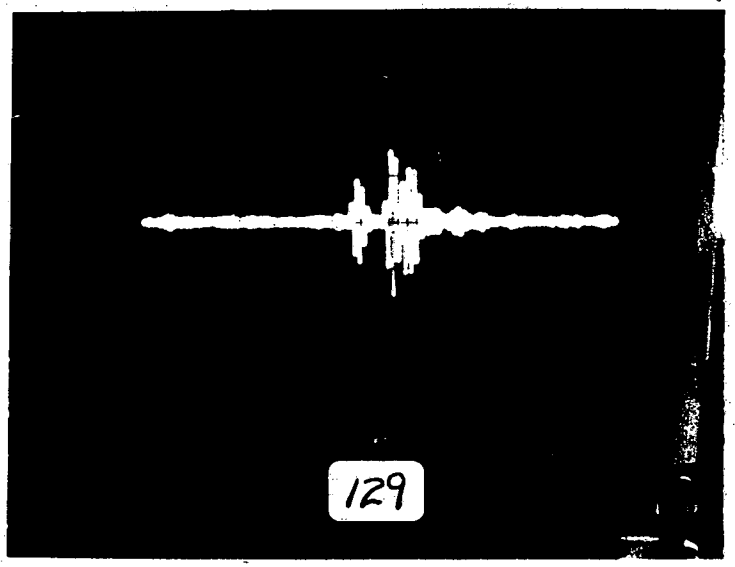
129

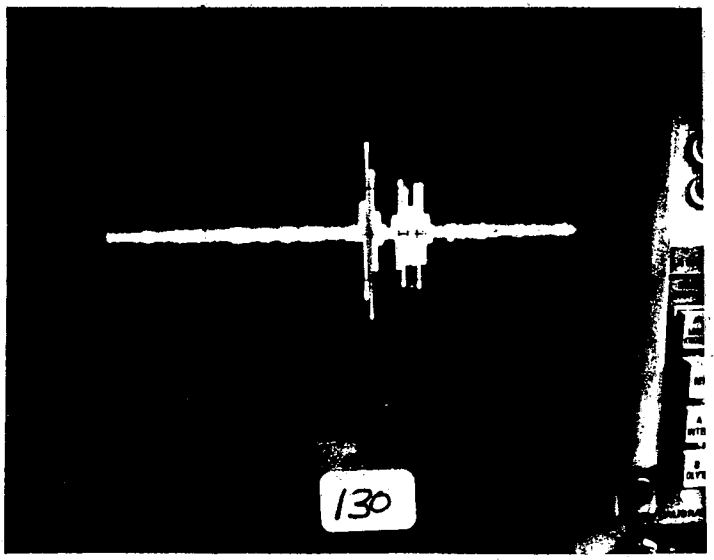
130

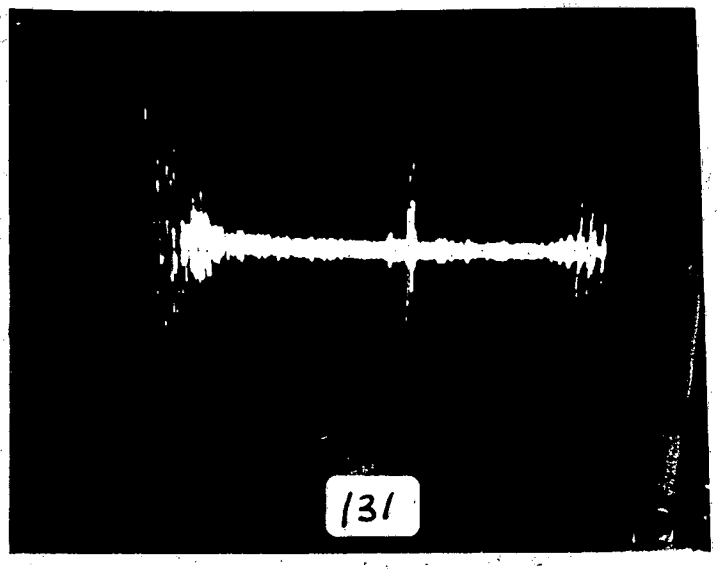
131

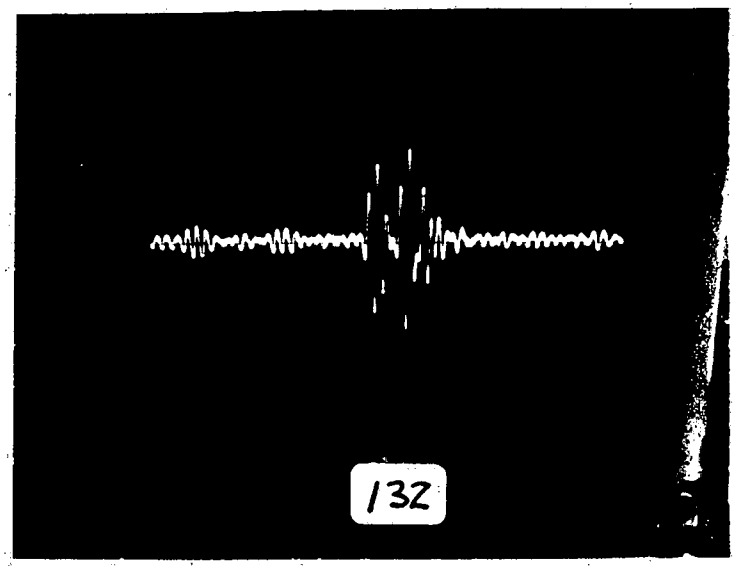
132

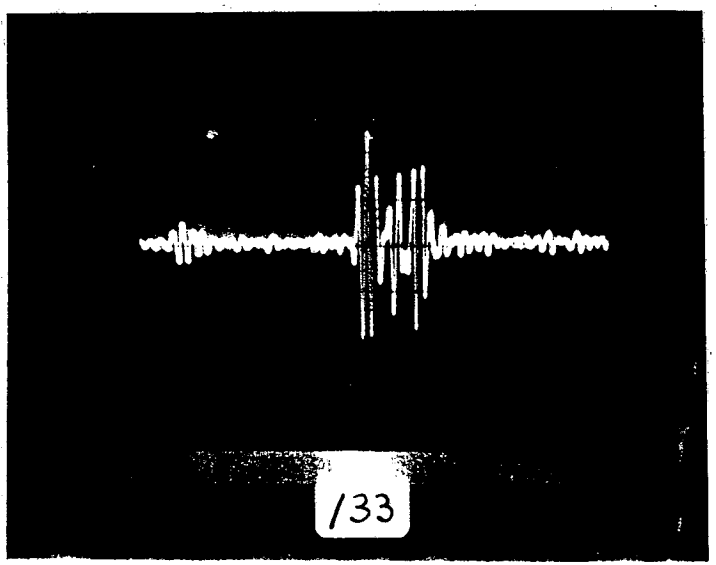
133

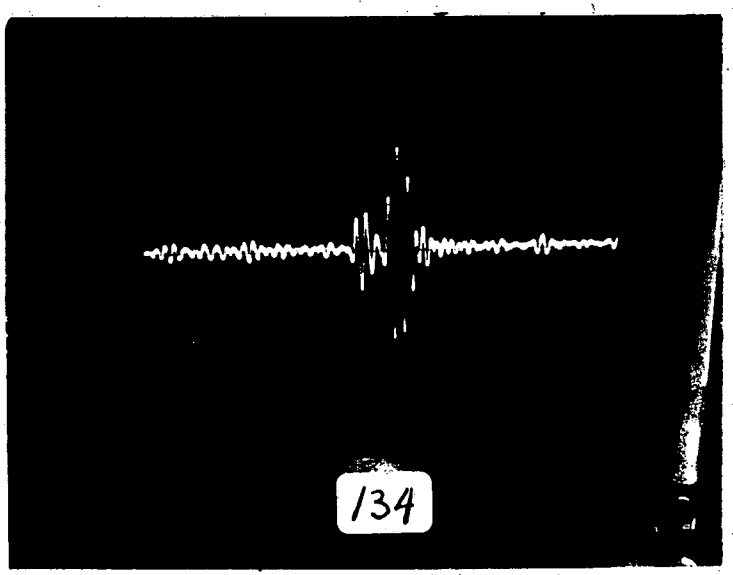
134

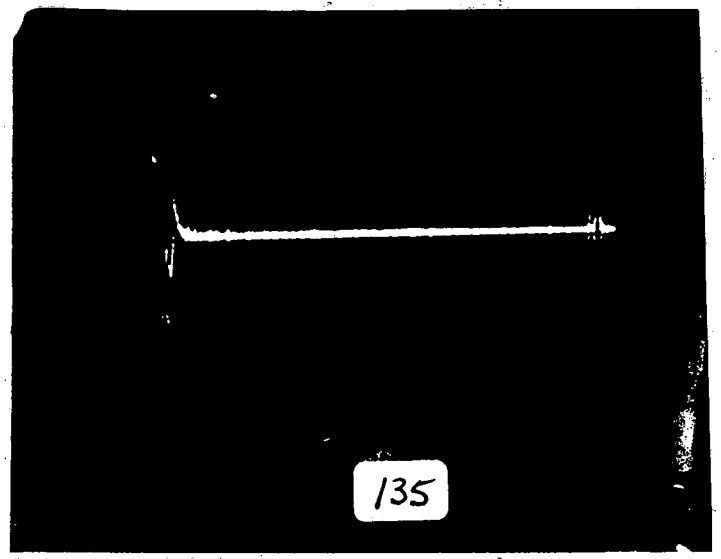
135

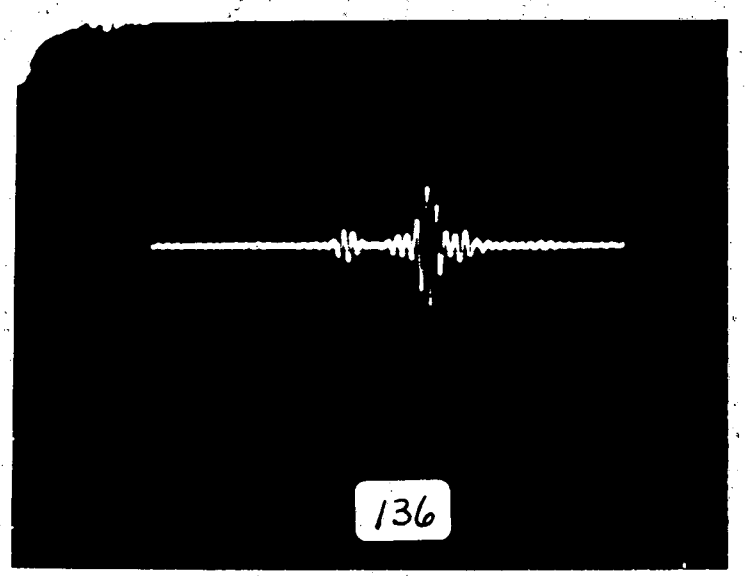
136

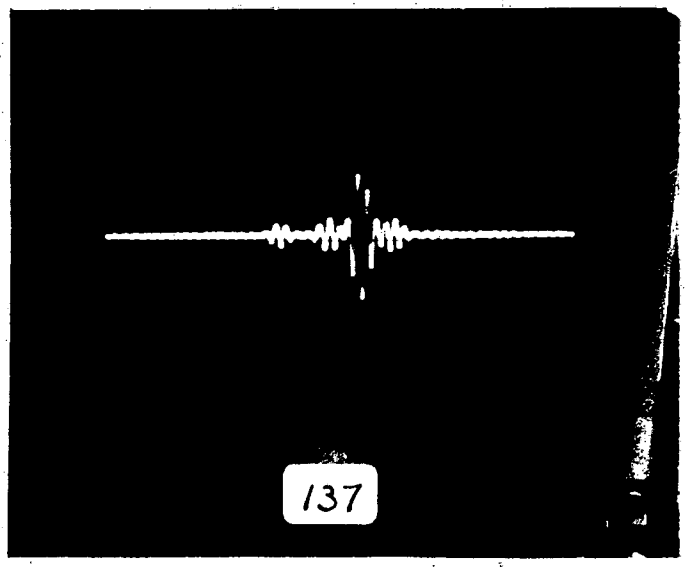
137

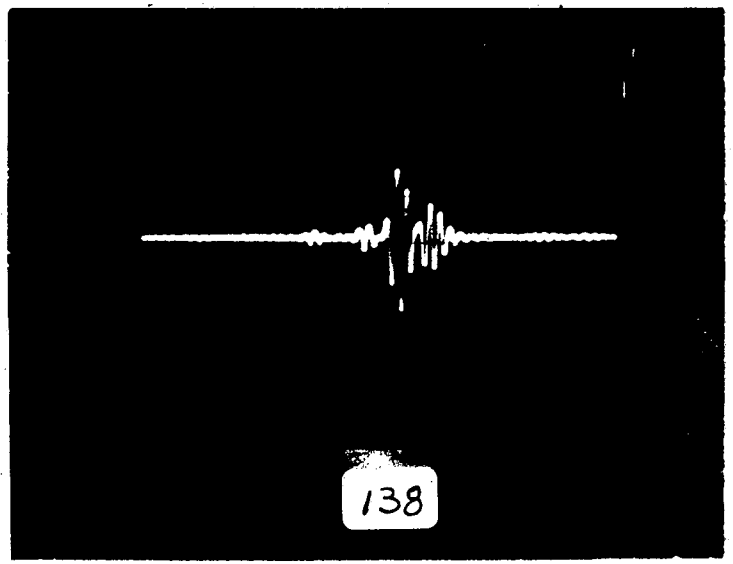
138

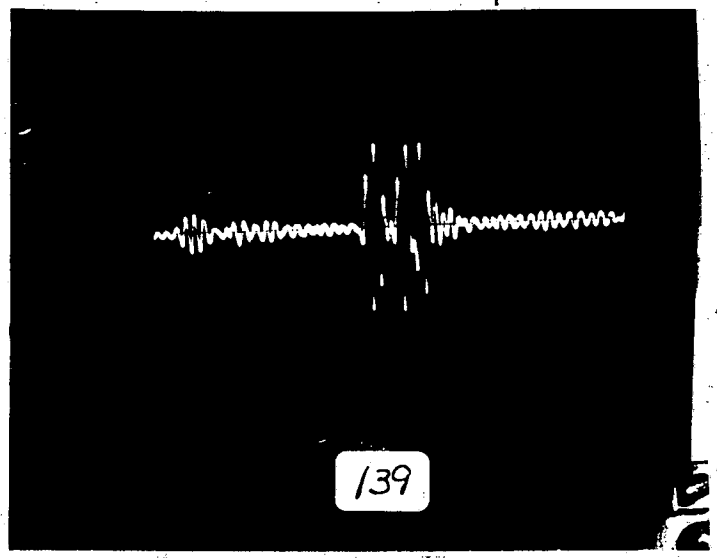
139

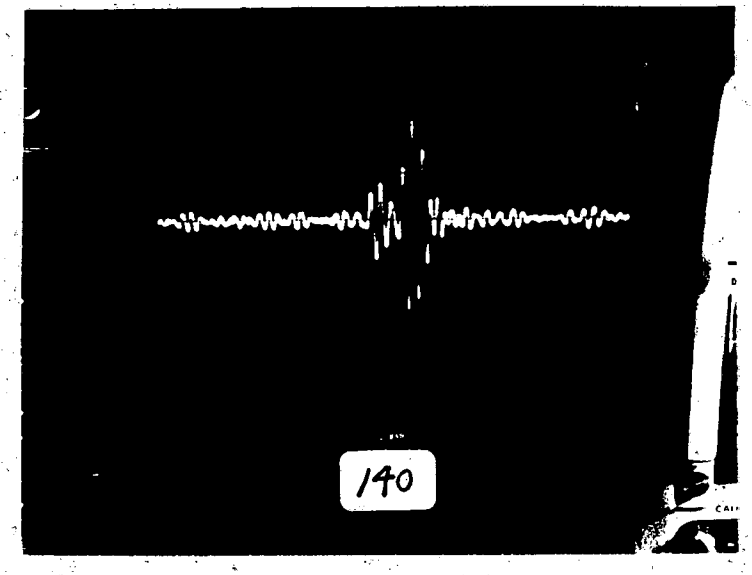
140

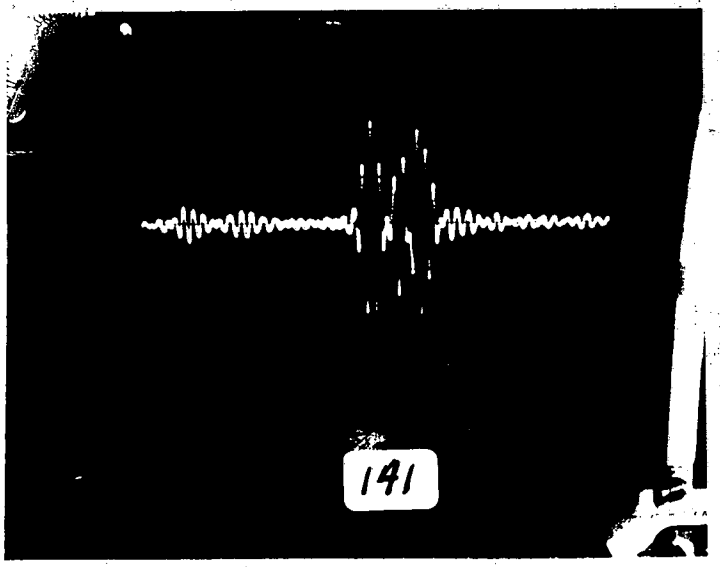
141

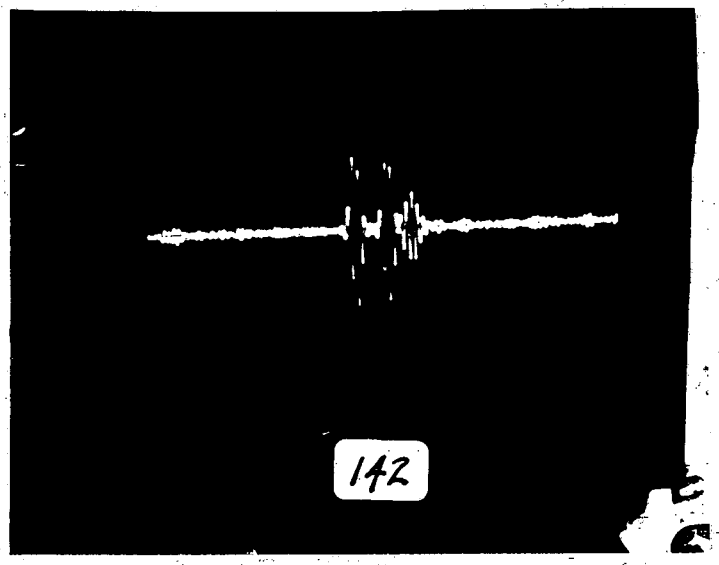
142

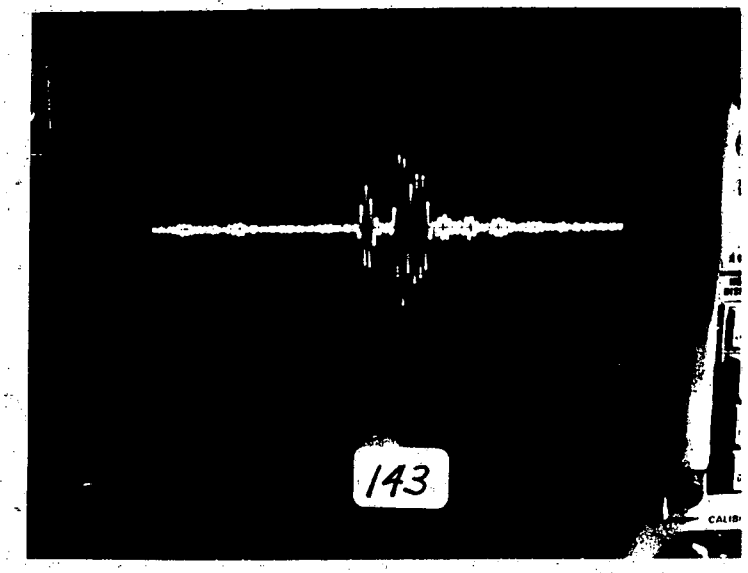
143

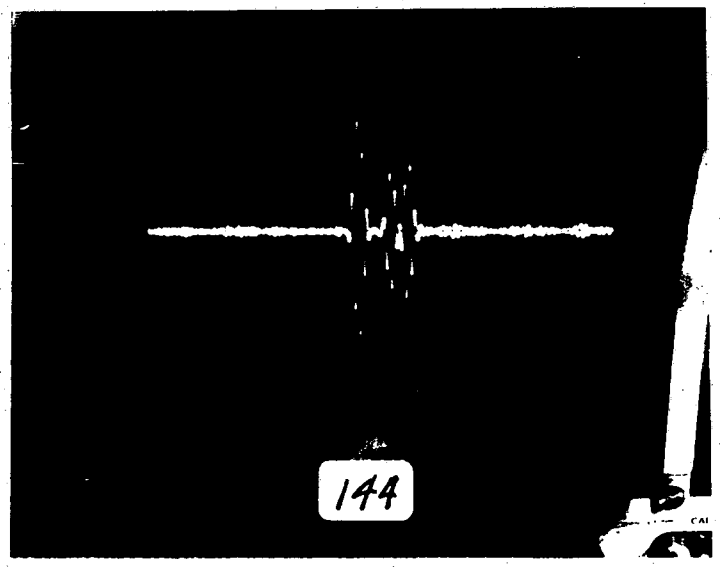
144

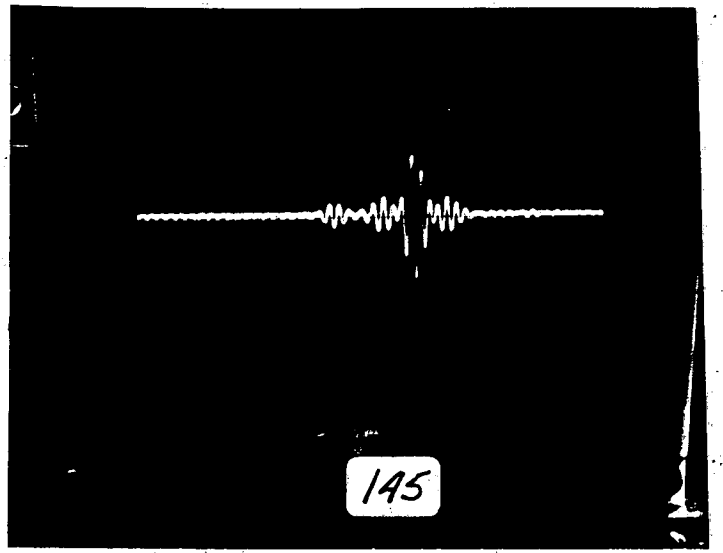
145

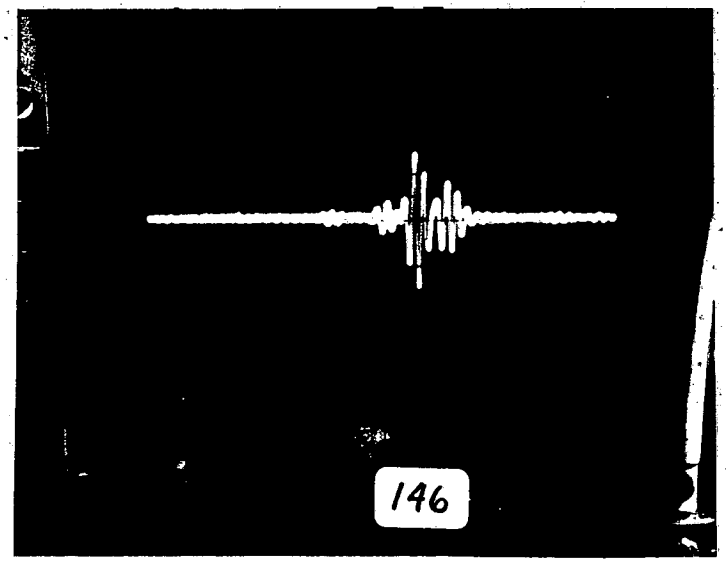
146

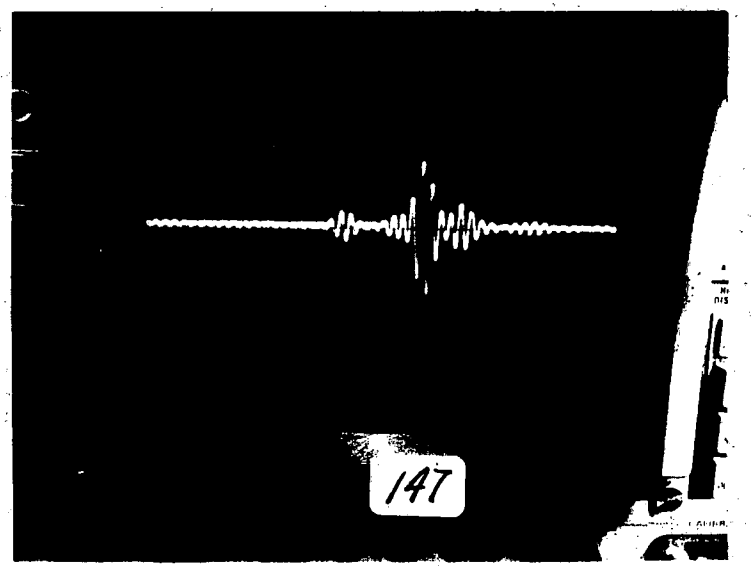
147

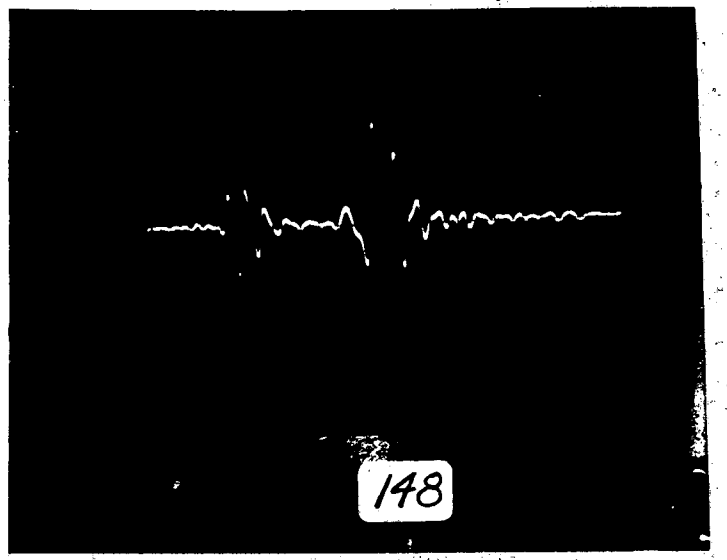
148

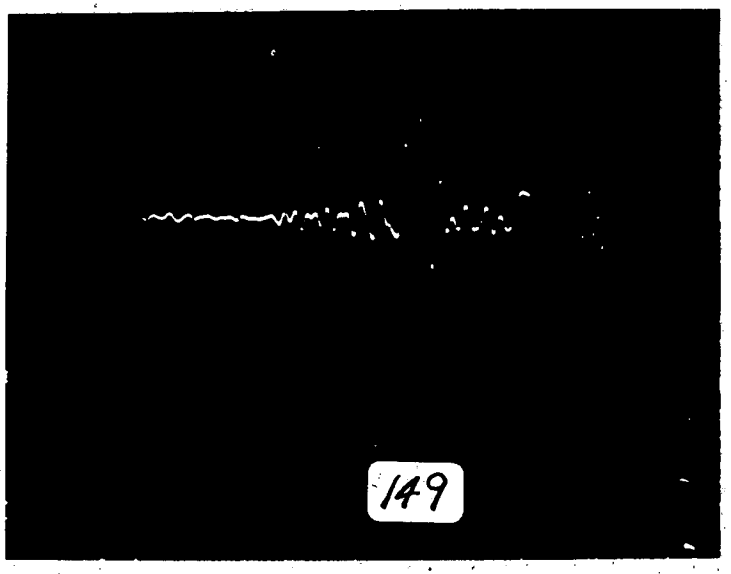
149

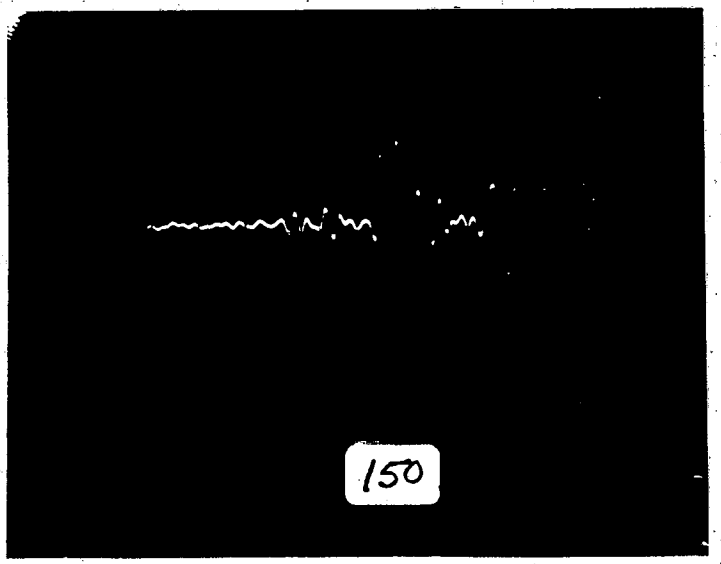
150

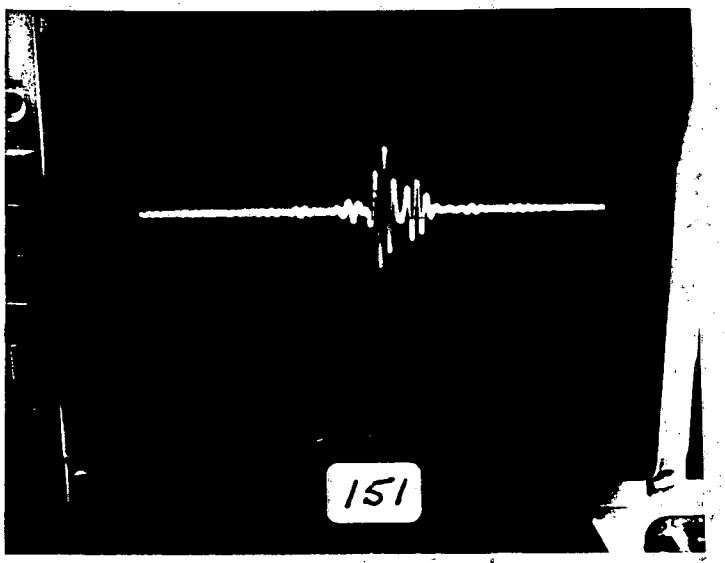
151

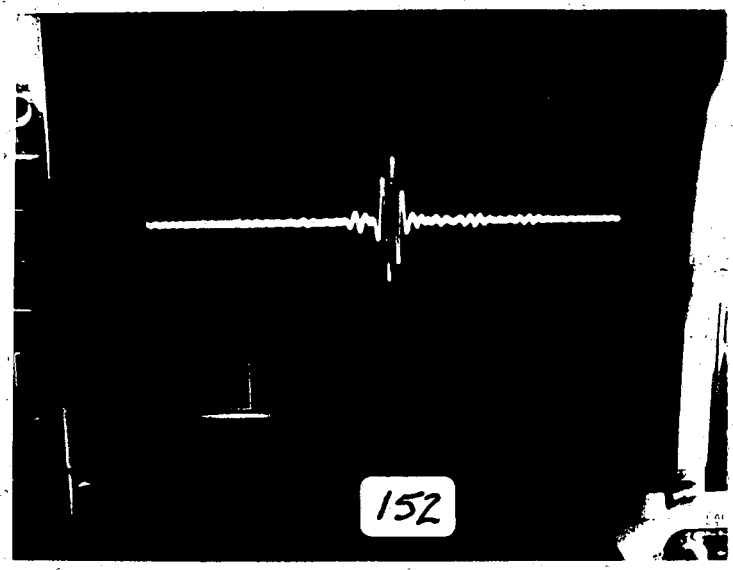
152

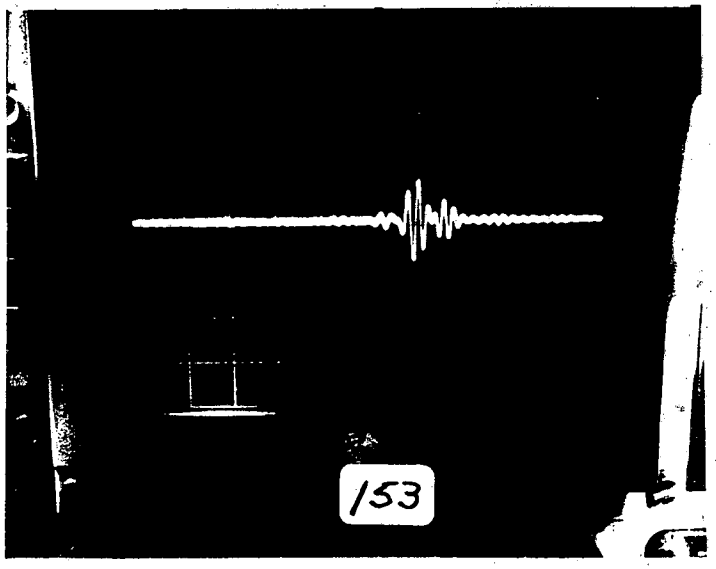
153

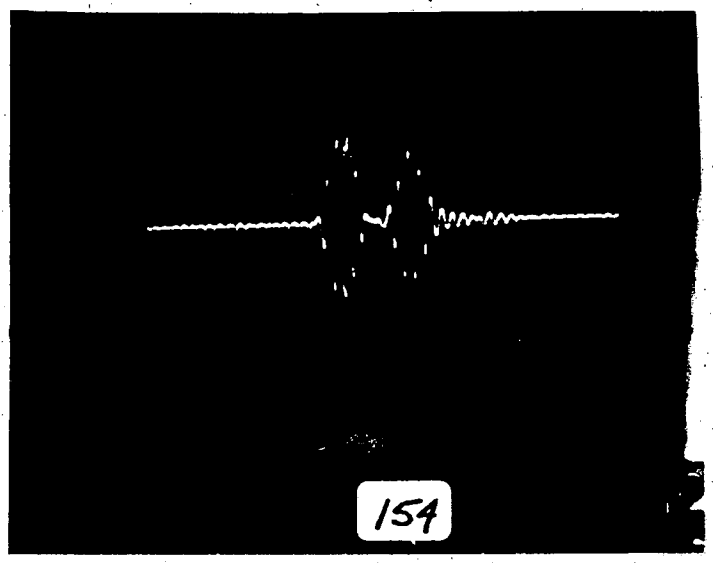
154

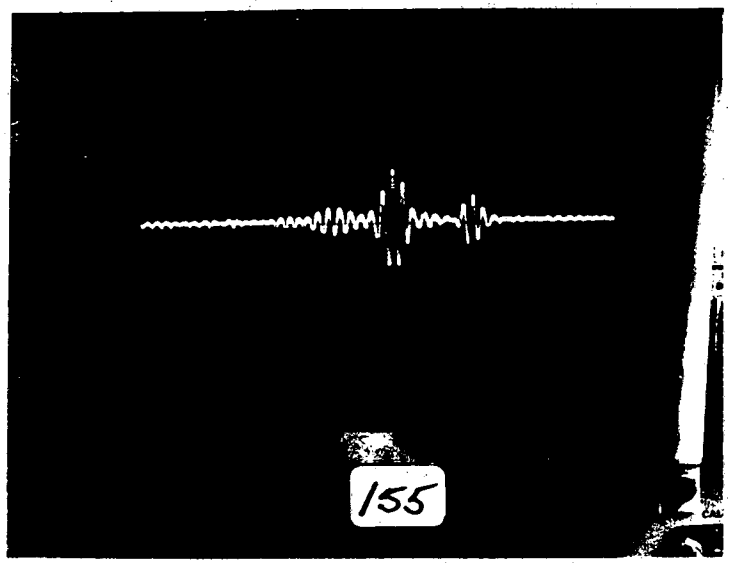
155

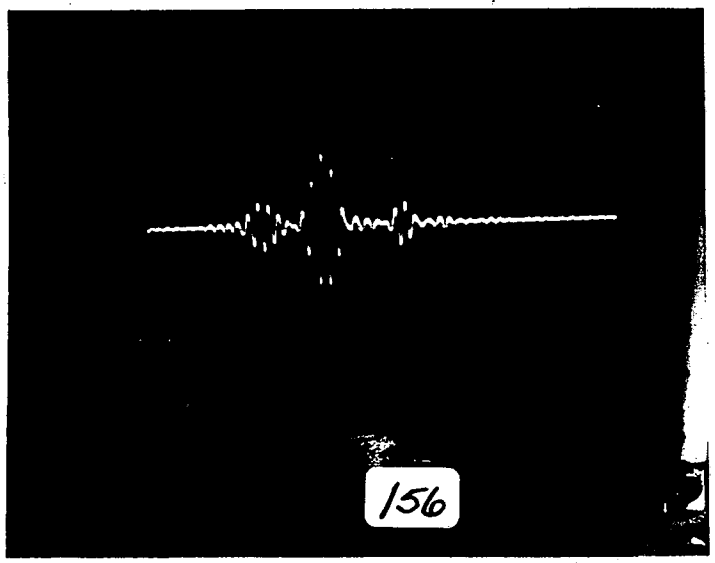
156

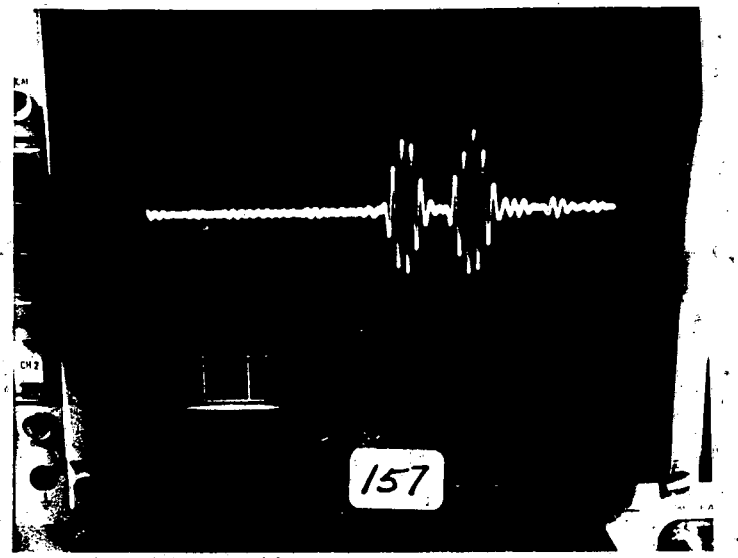
157

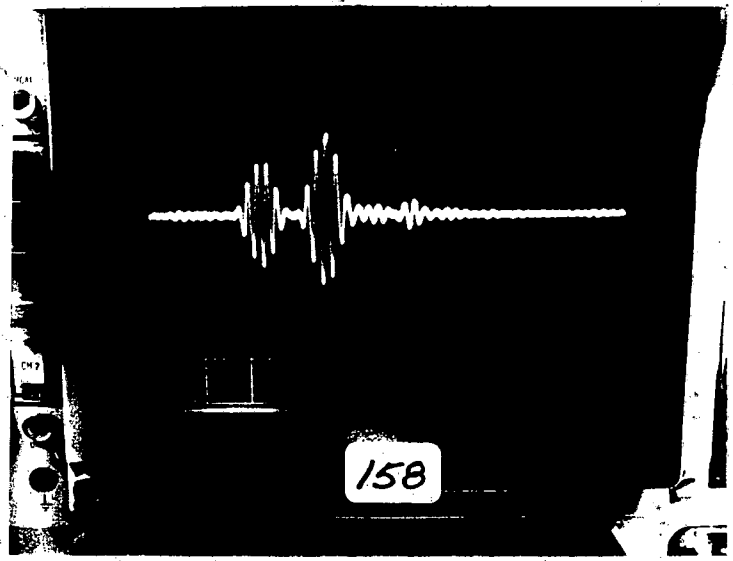
158

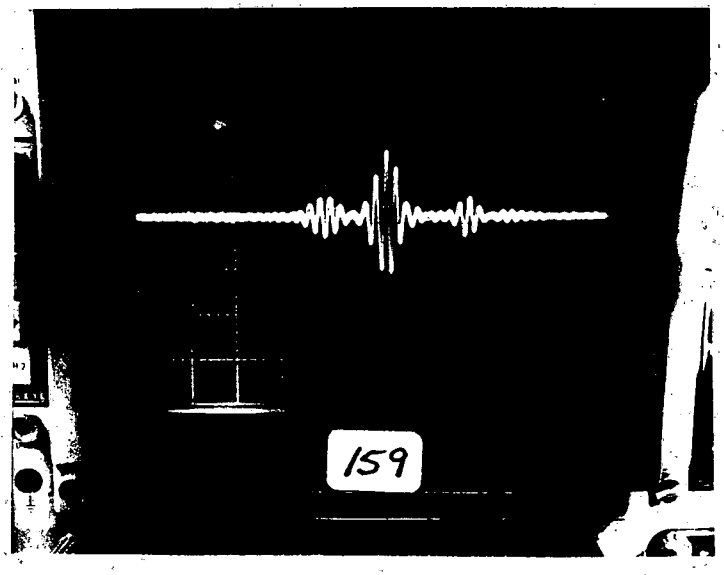
159

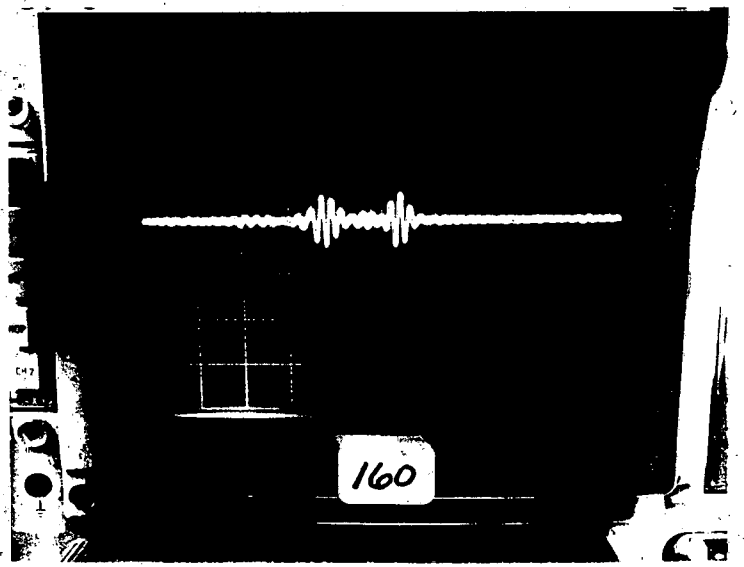
160

191

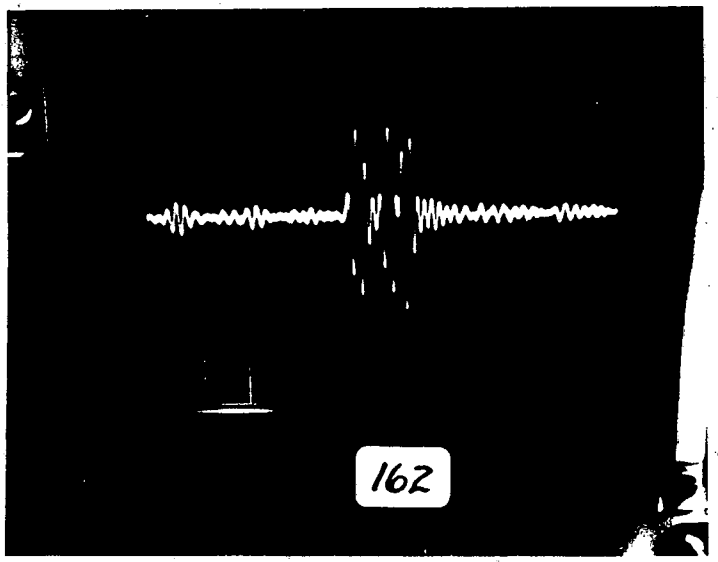
162

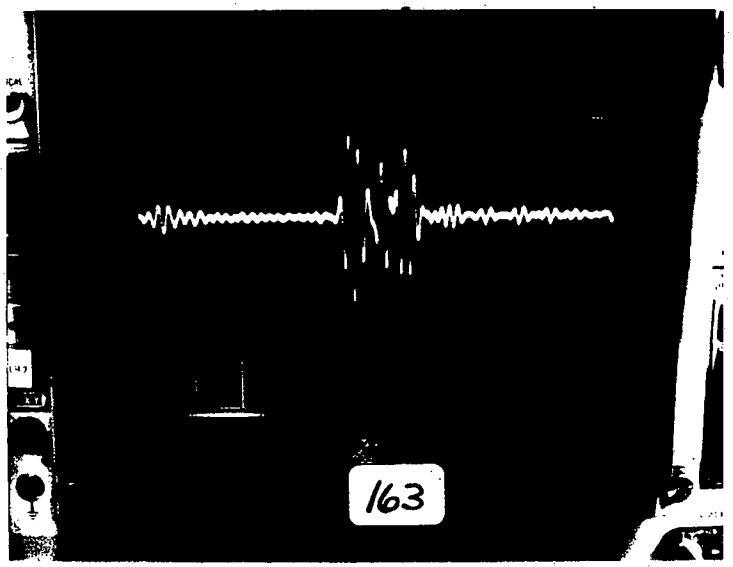
163

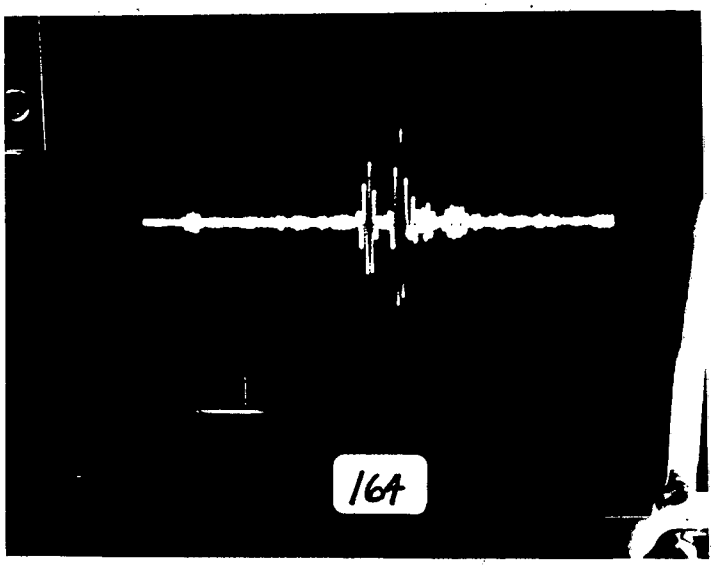
164

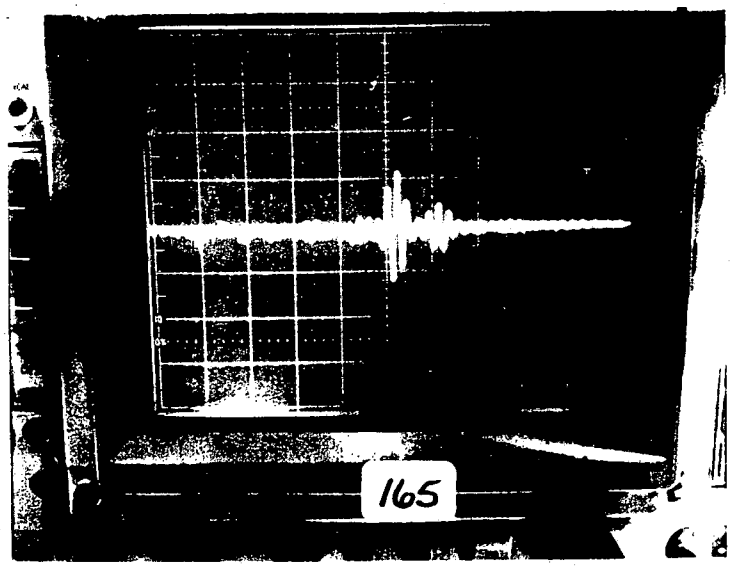
165

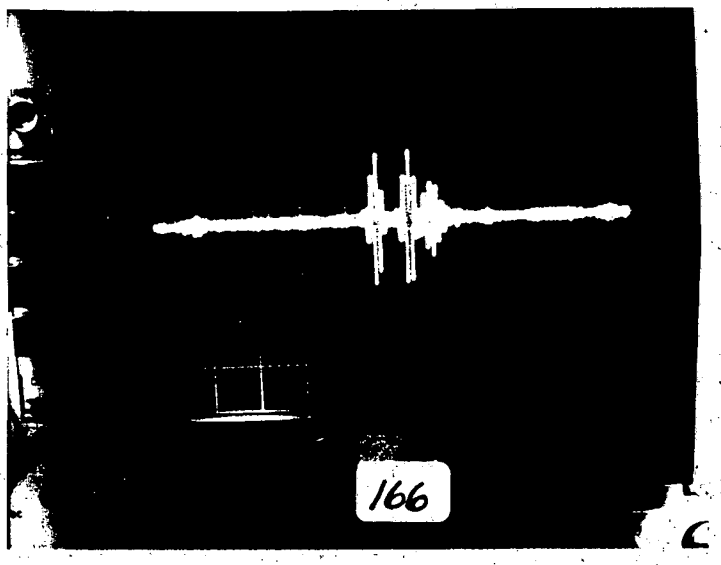
166

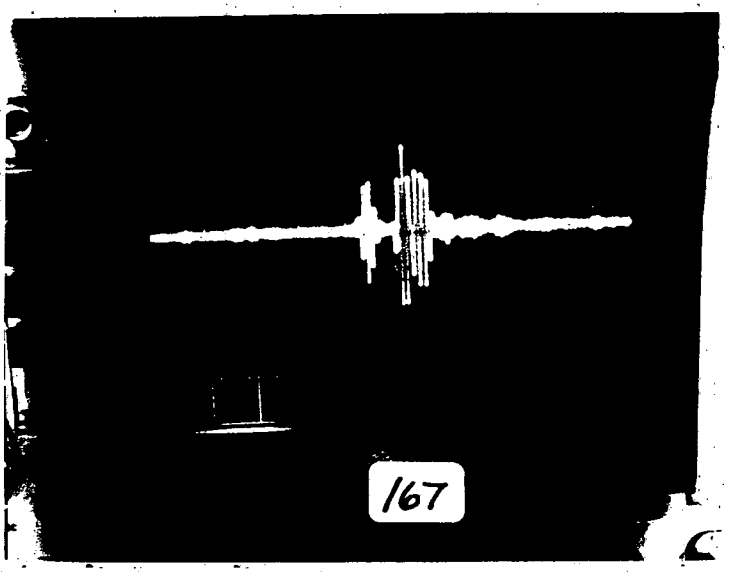
167

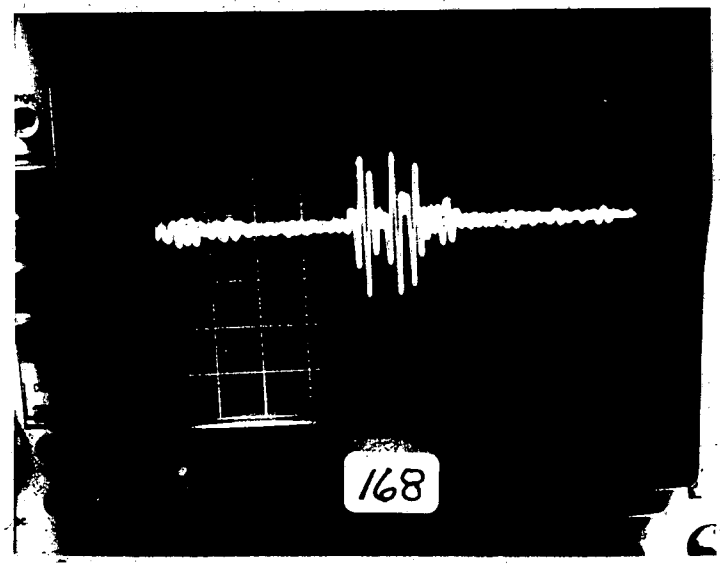
168

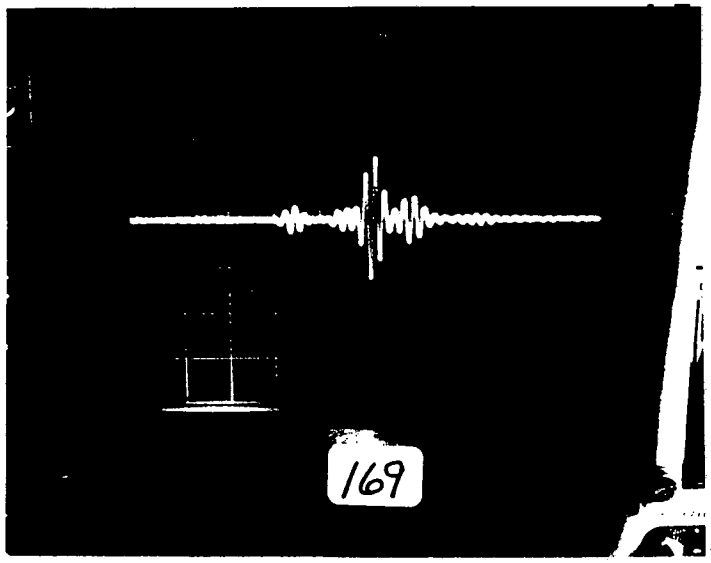
169

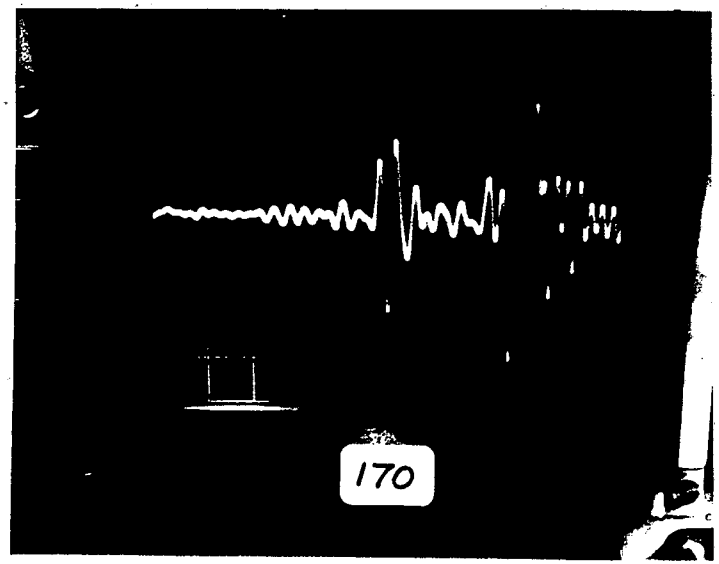
170

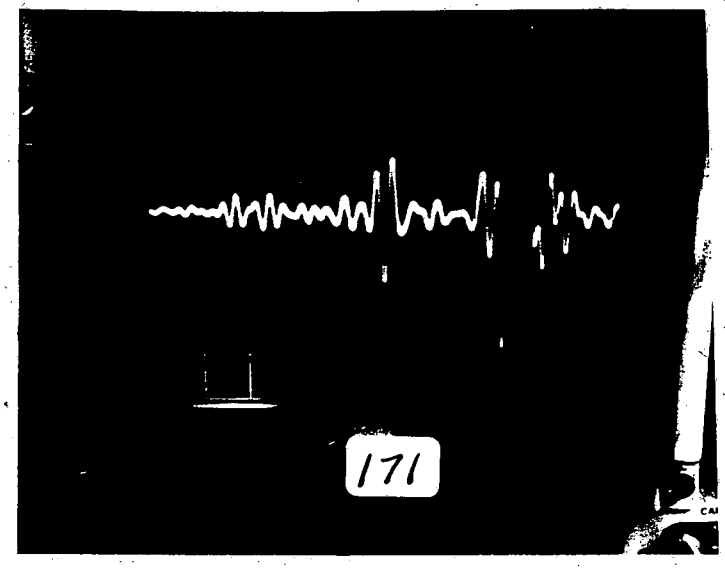
171

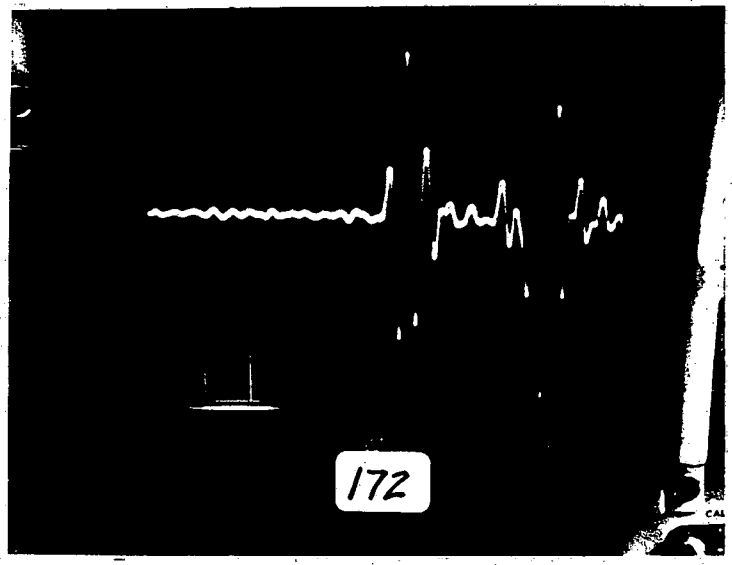
172

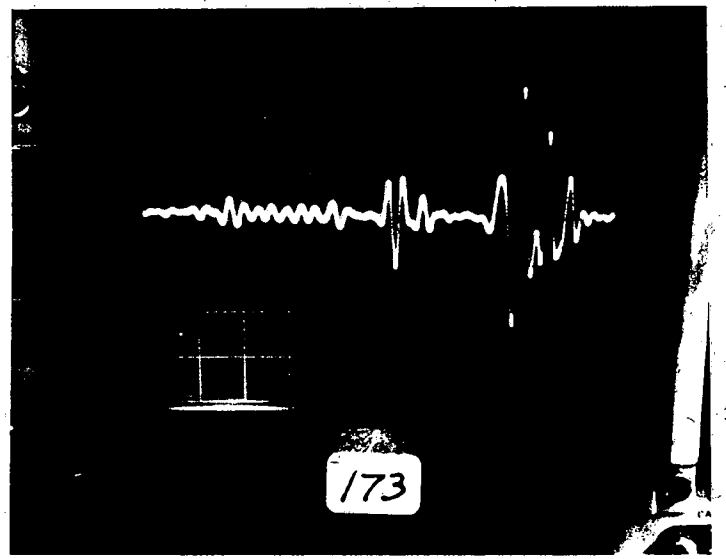
173

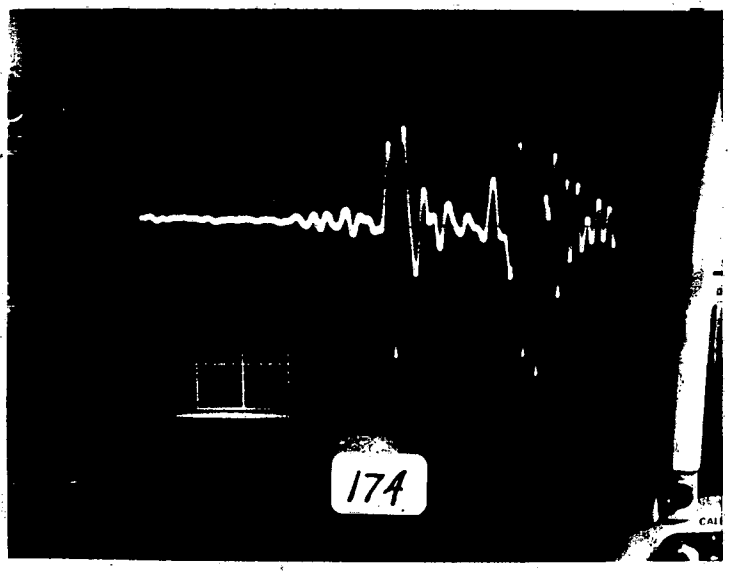
174

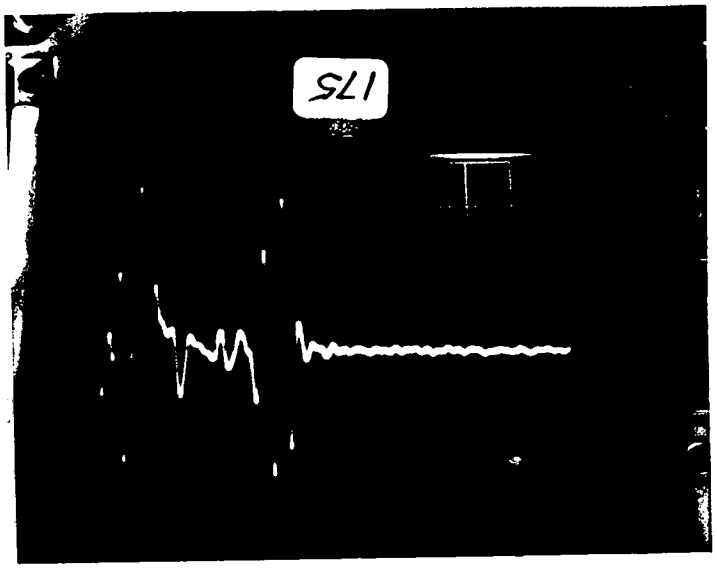
SL1

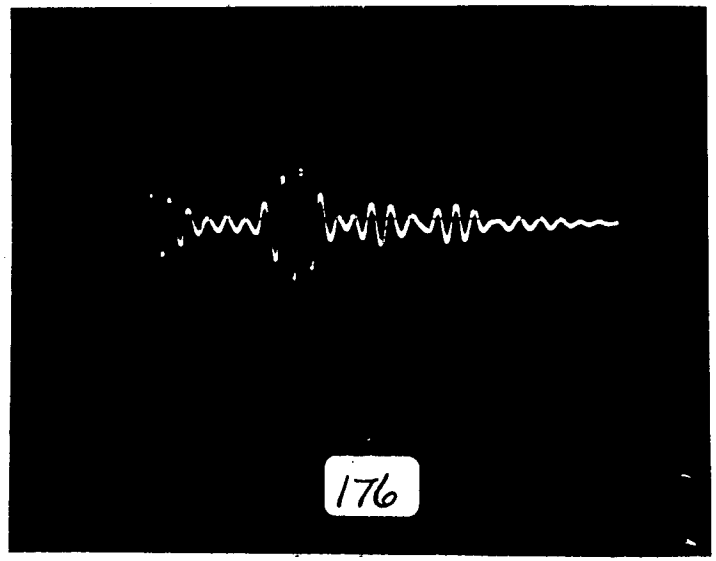
176

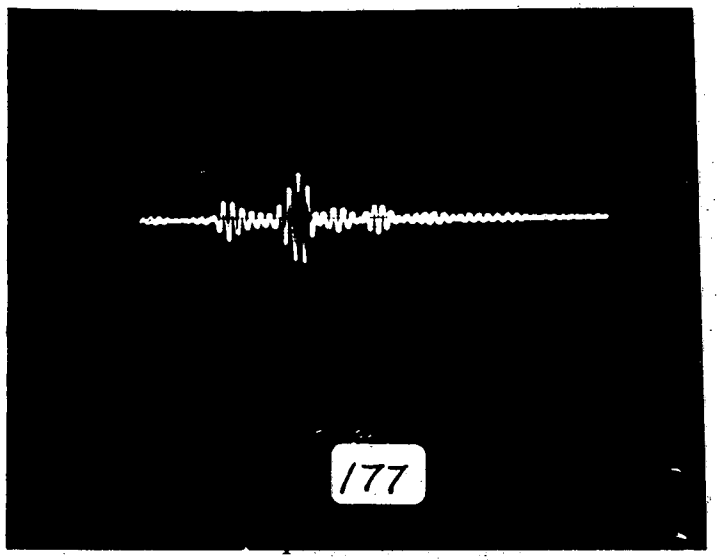
177

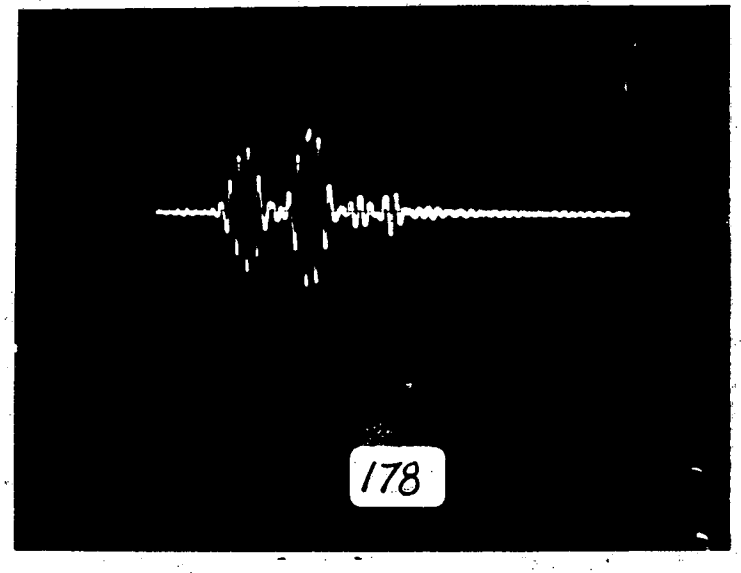
178

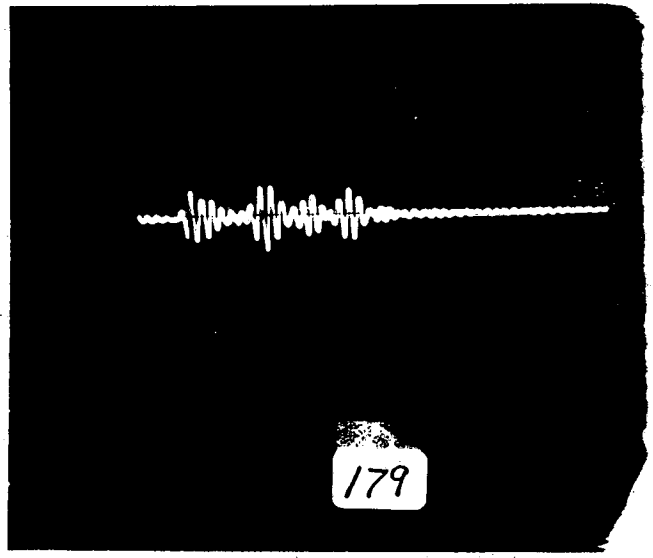
179

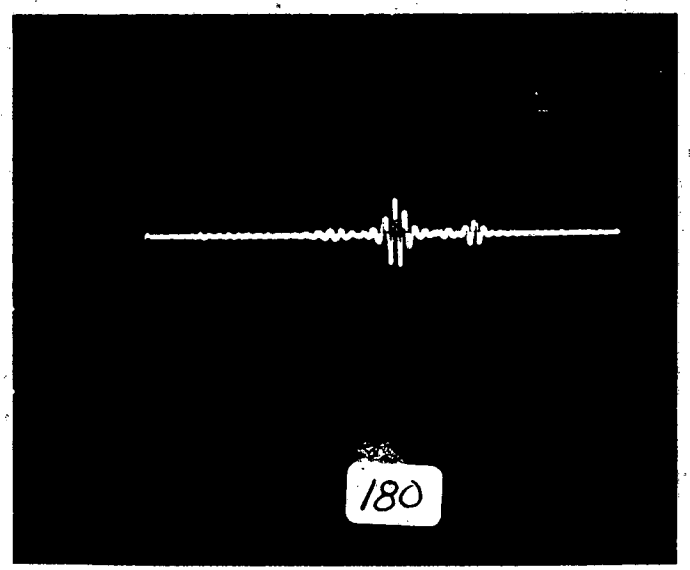
180

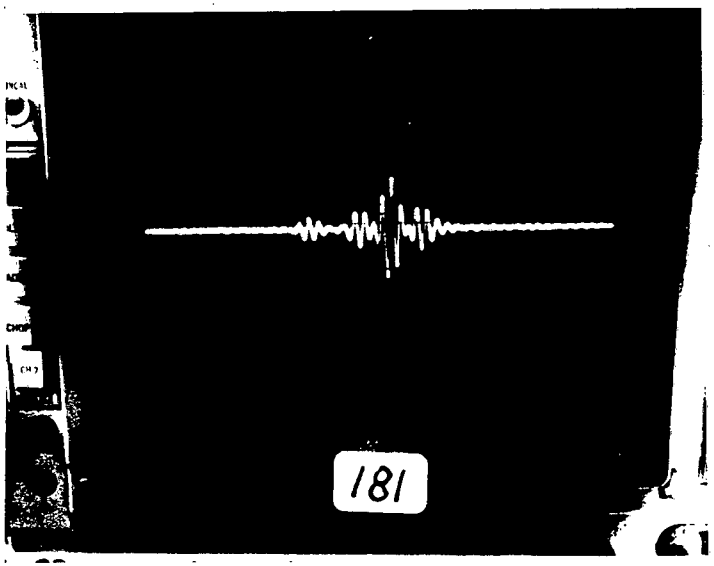
181

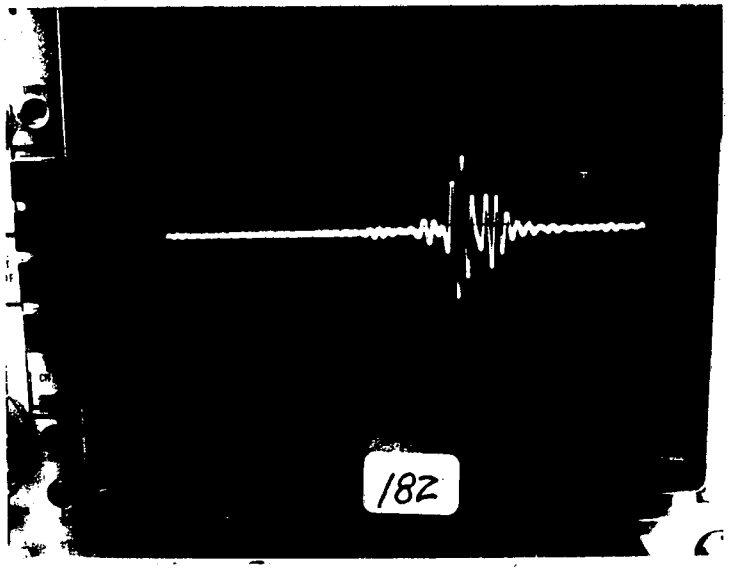
182

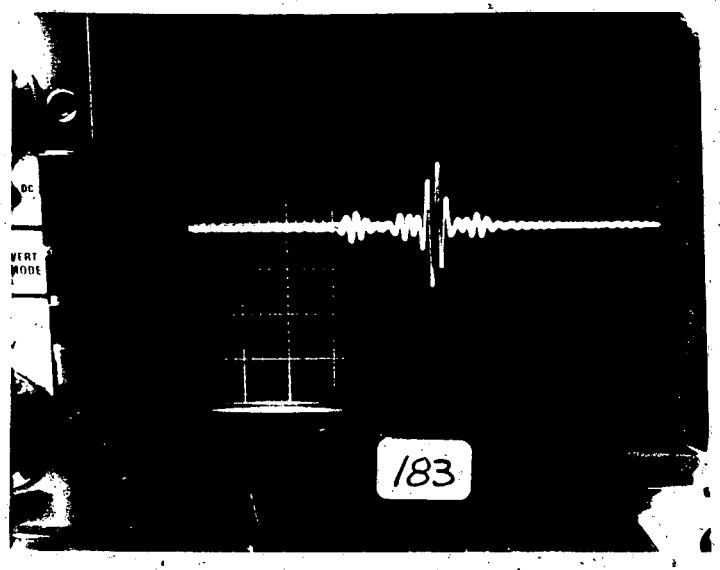
183

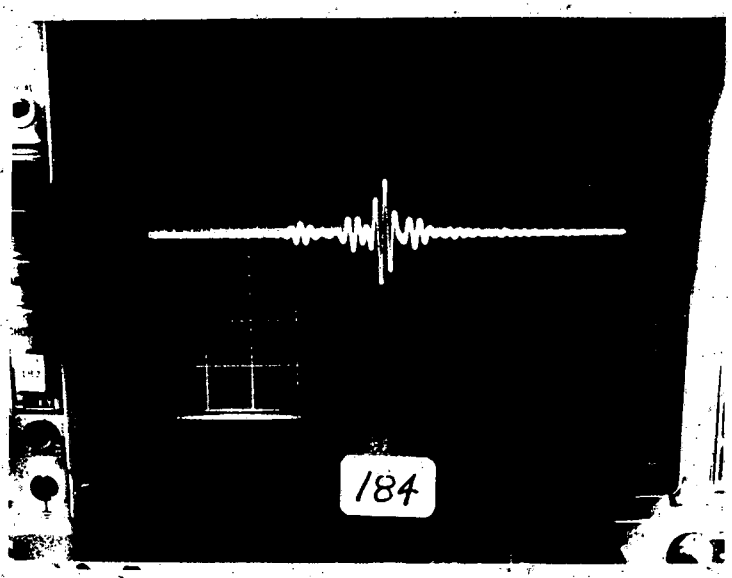
184

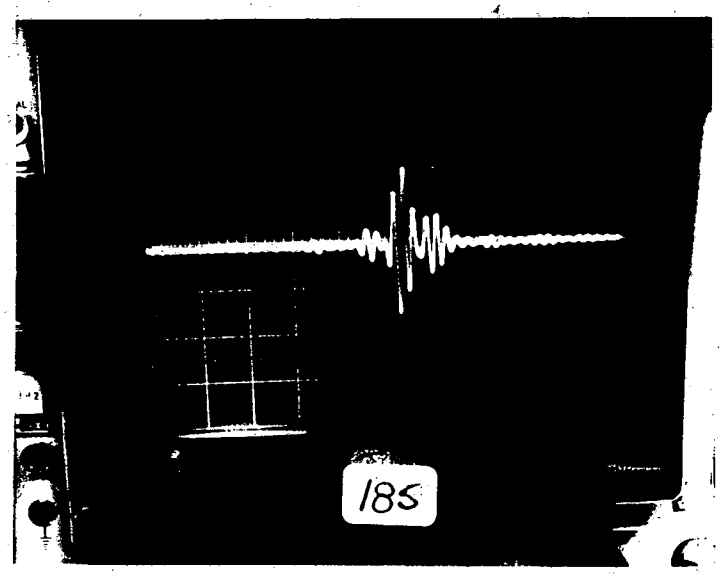
185

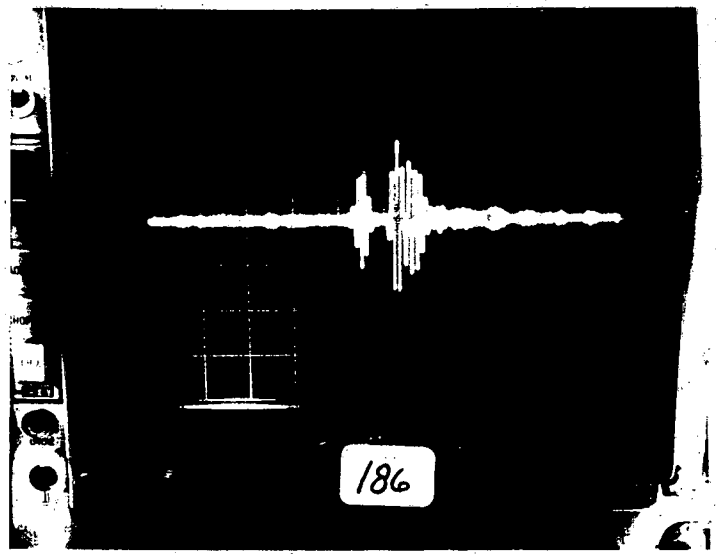
186

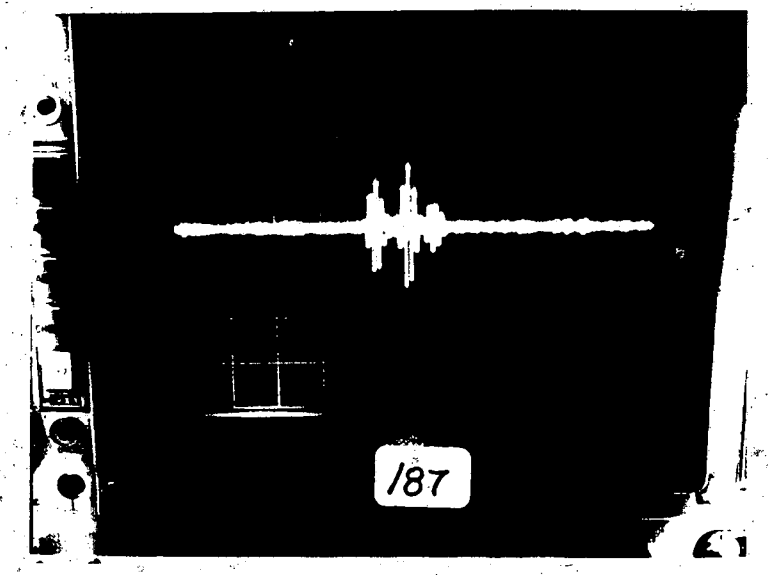
187

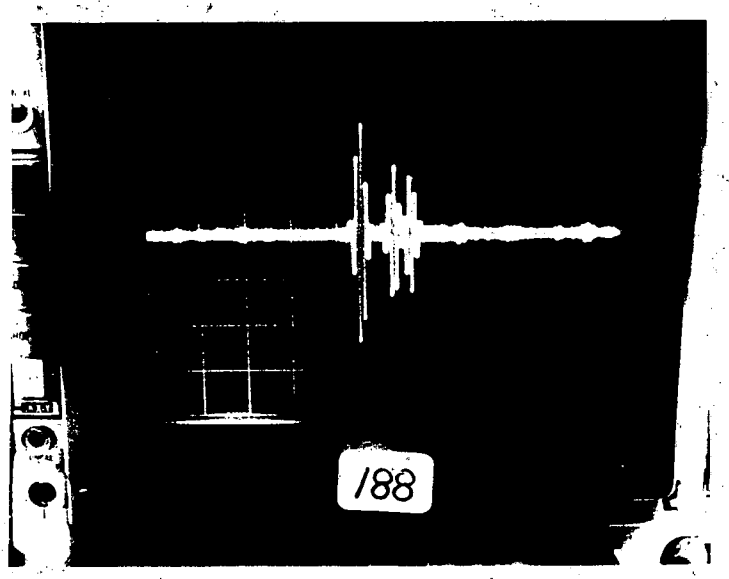
188

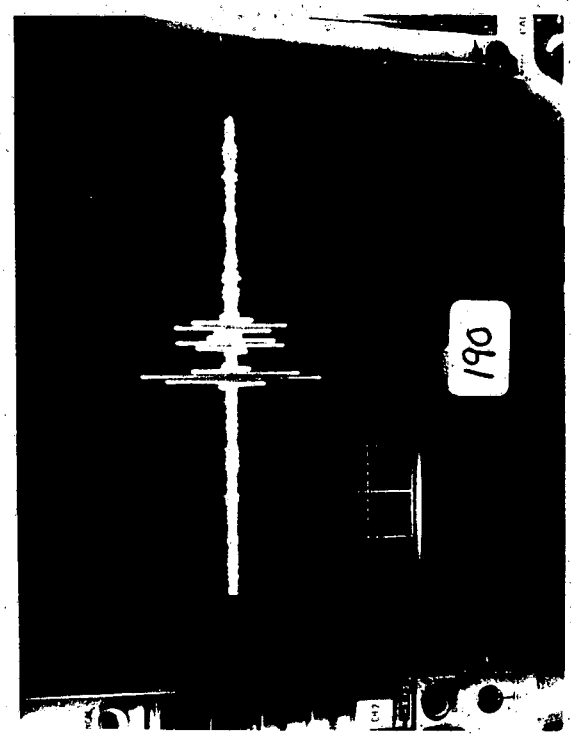
190

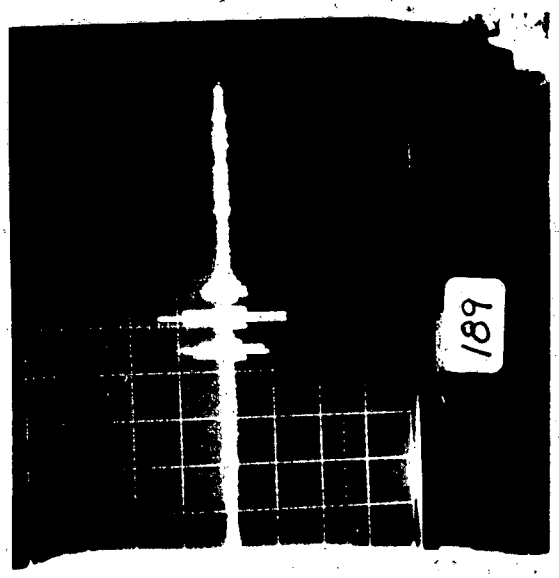
189

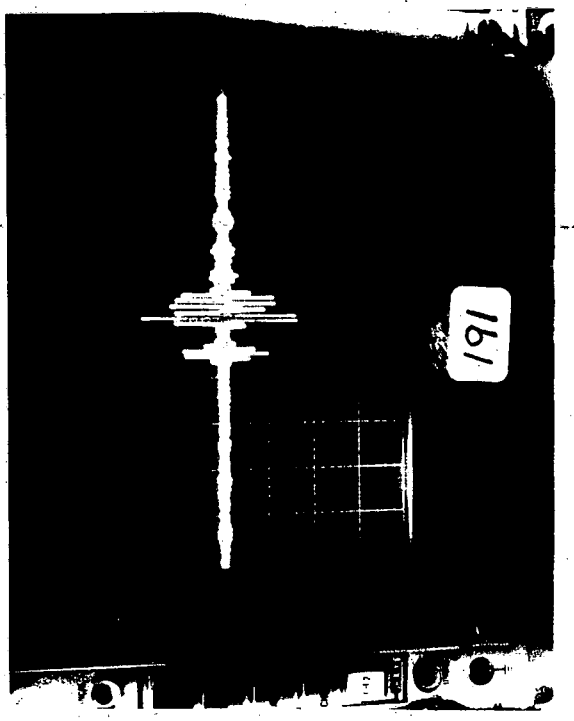
191

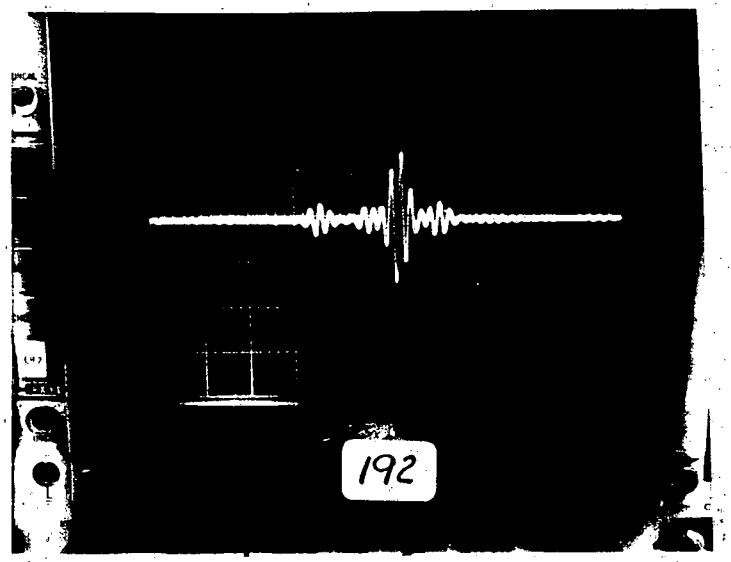
192

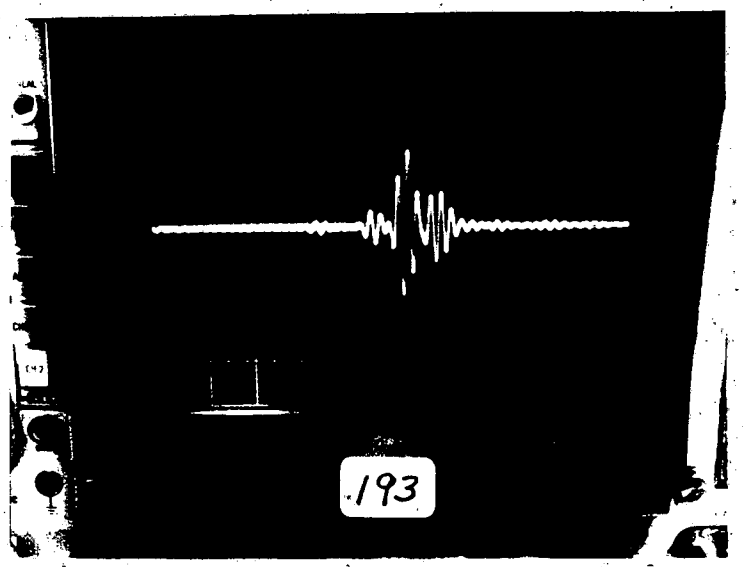
193

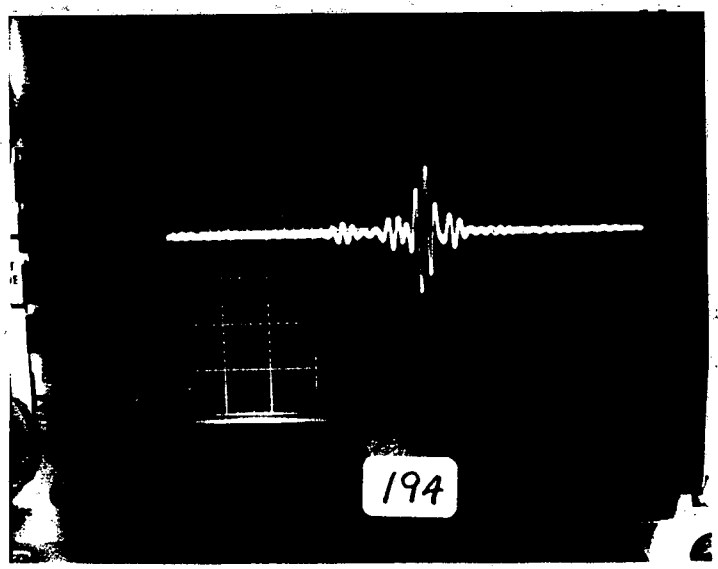
194

196

198

195

197

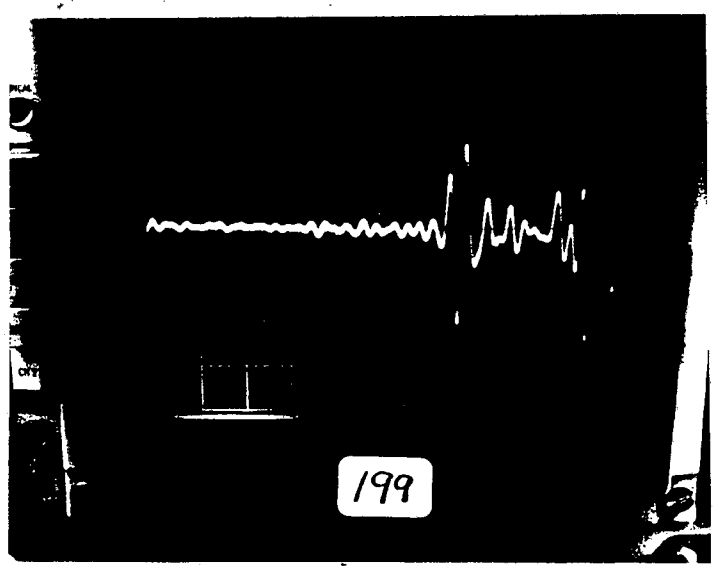
199

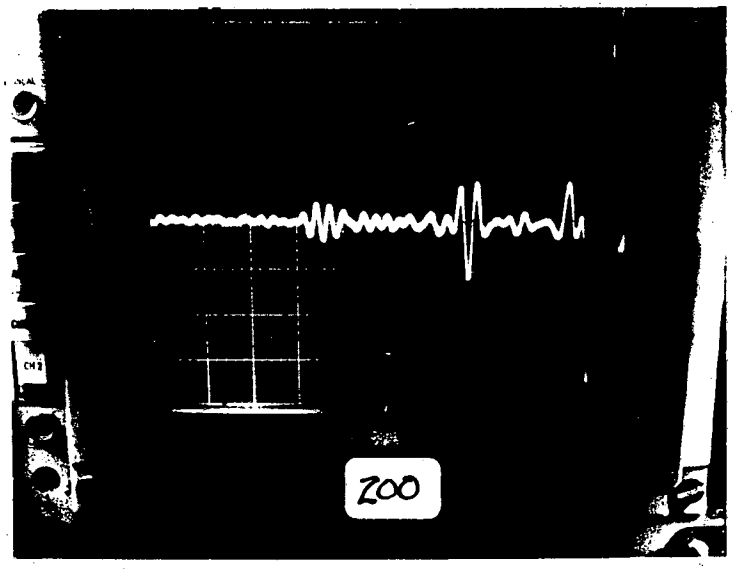
200

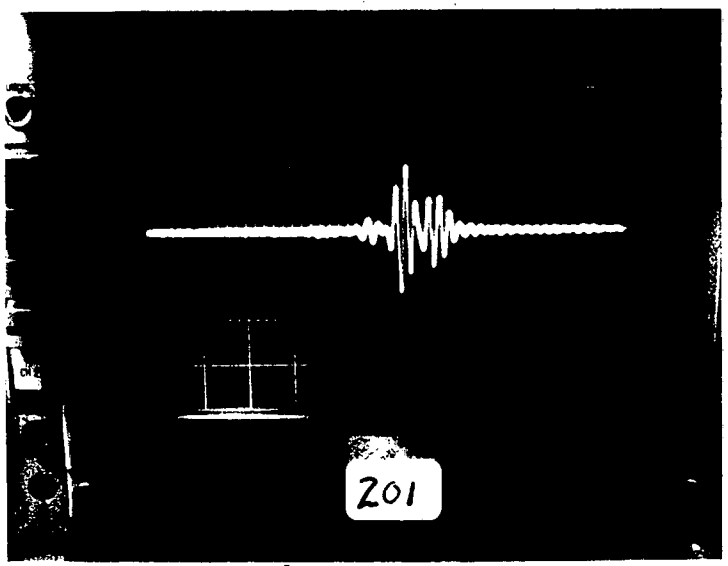
201

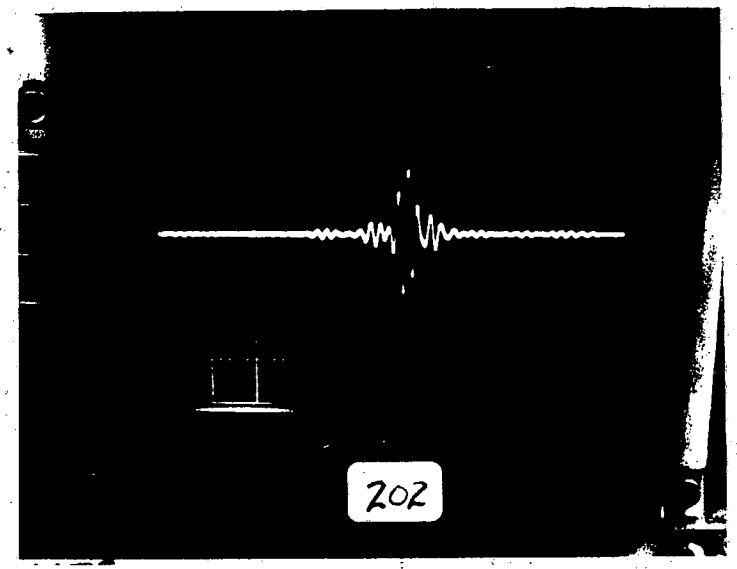
202

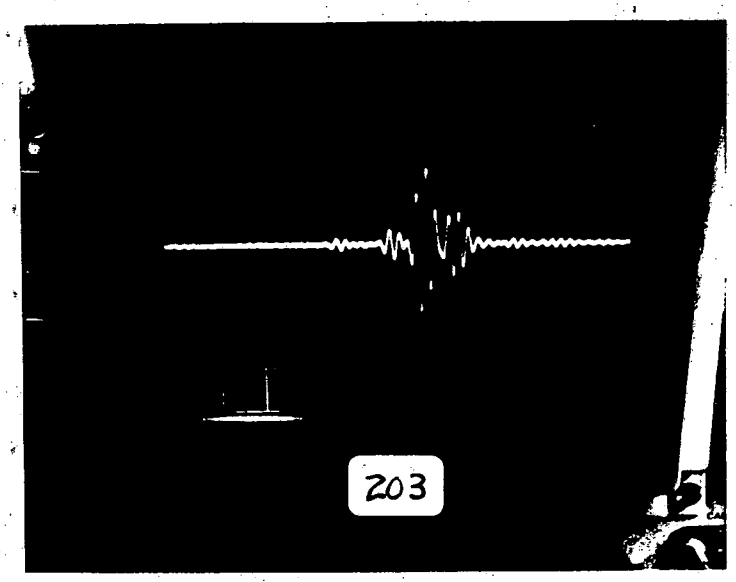
203

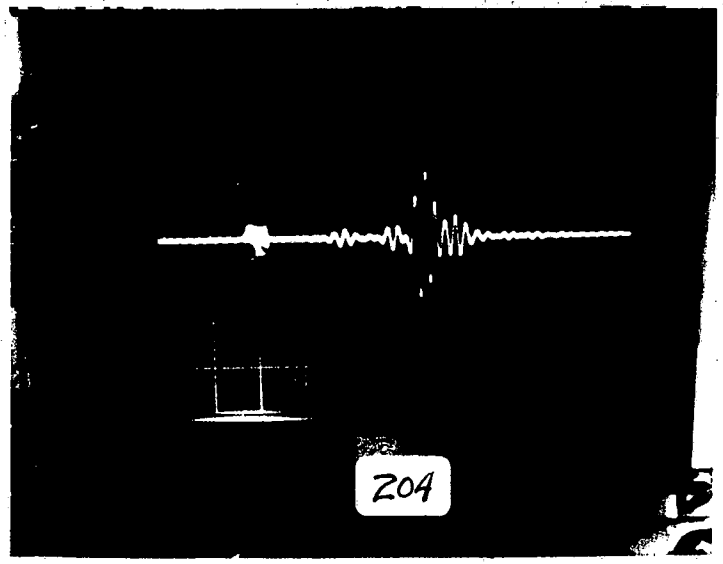
204

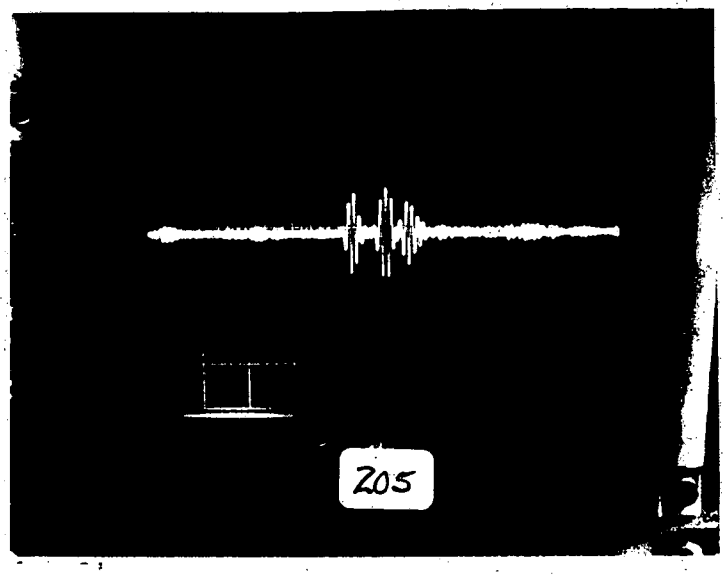
205

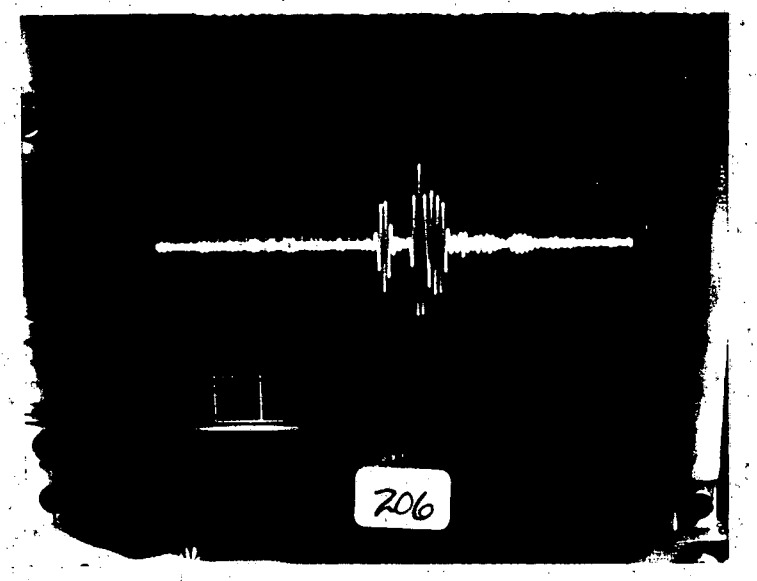
206

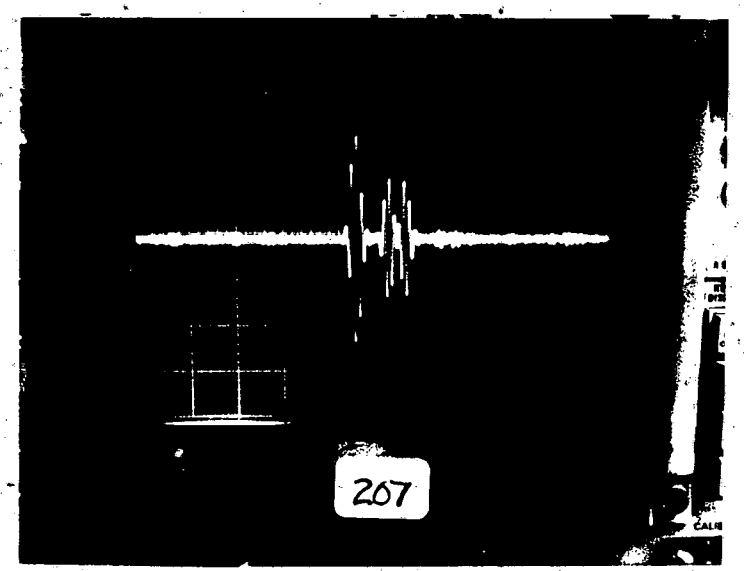
207

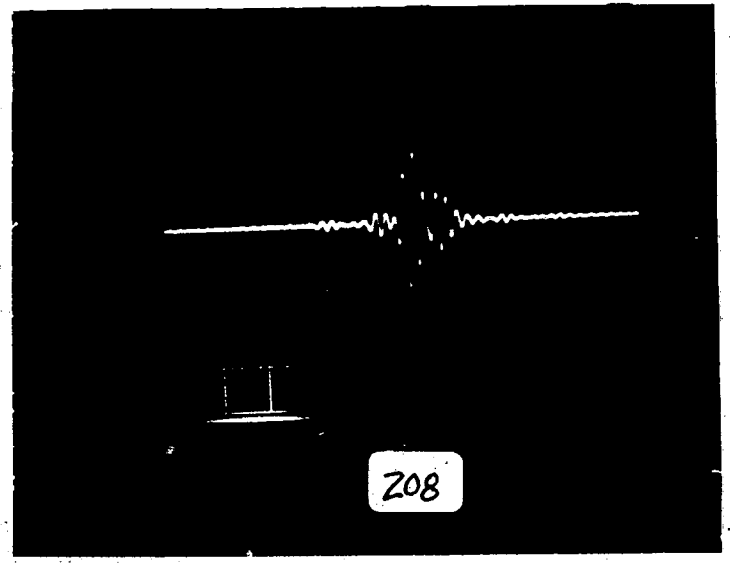
208

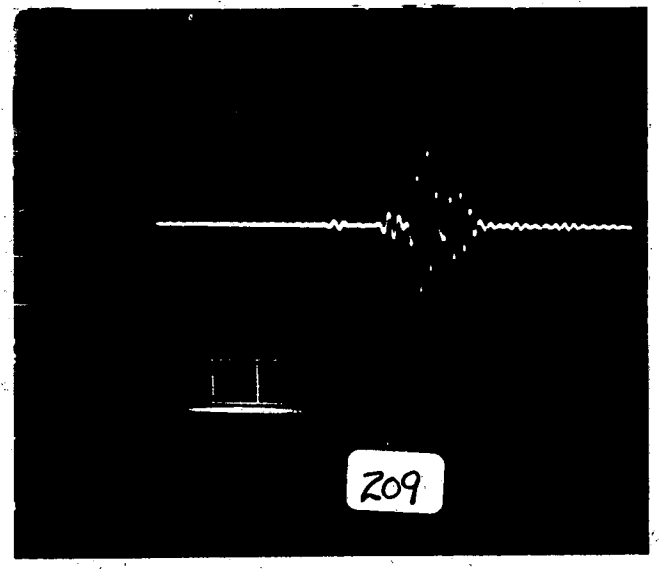
209

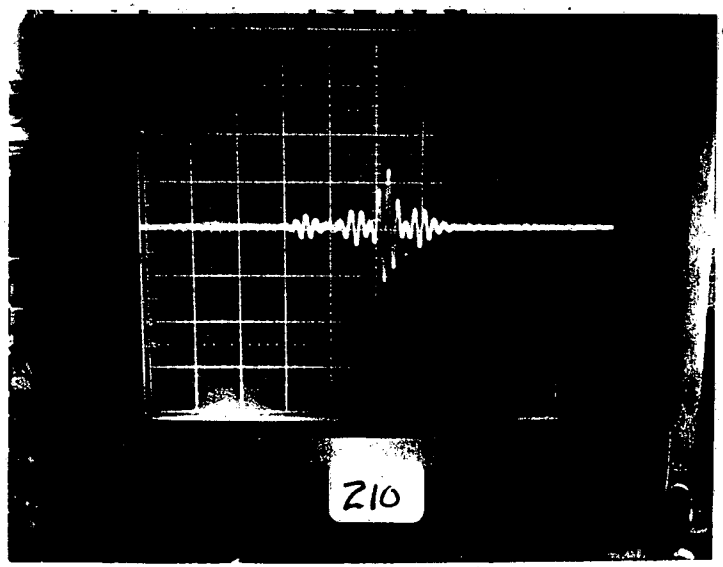
210

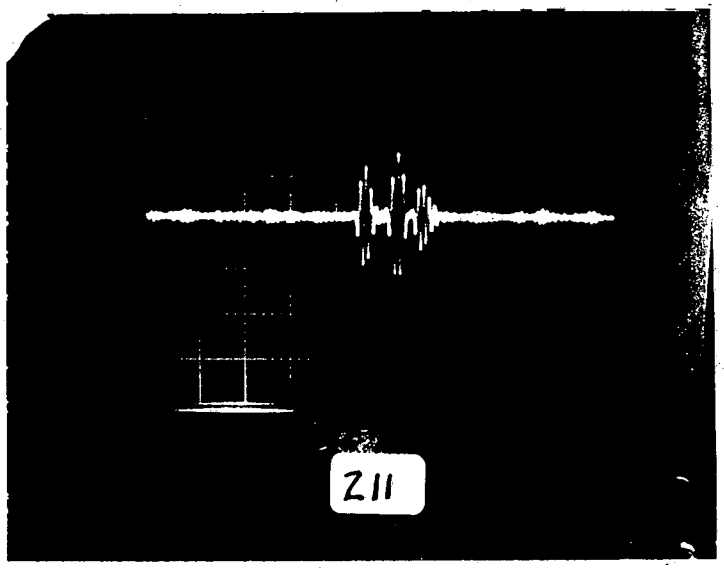
211

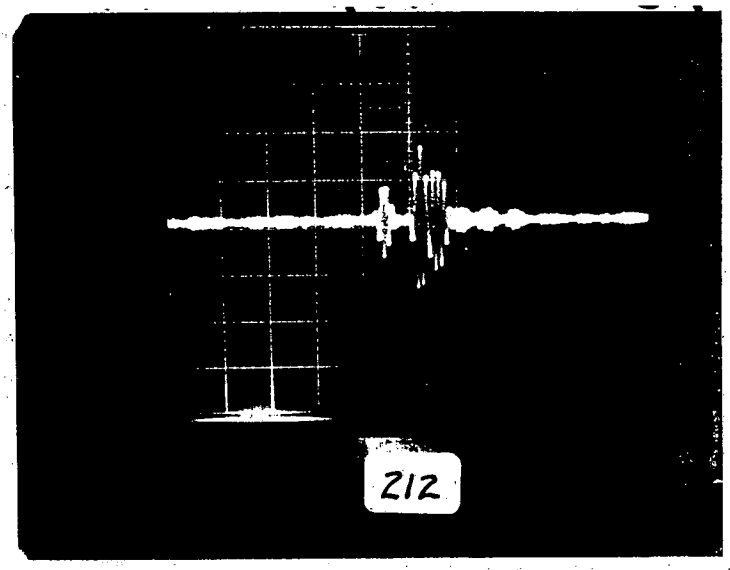
212

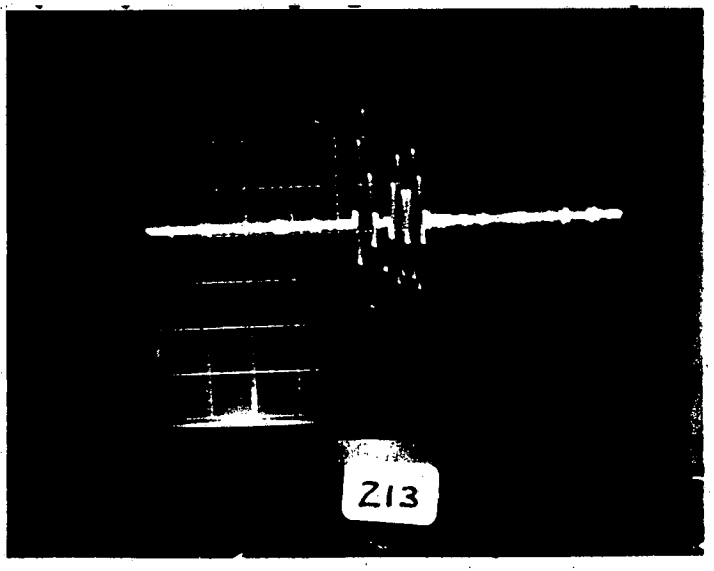
213

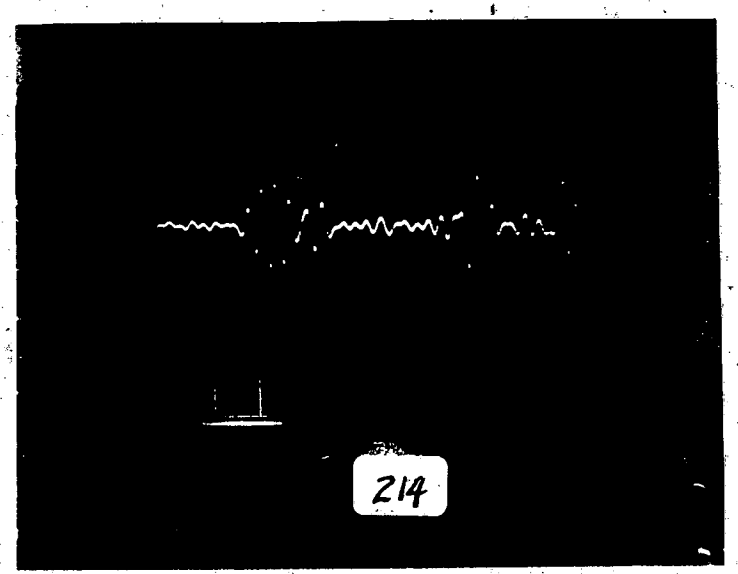
214

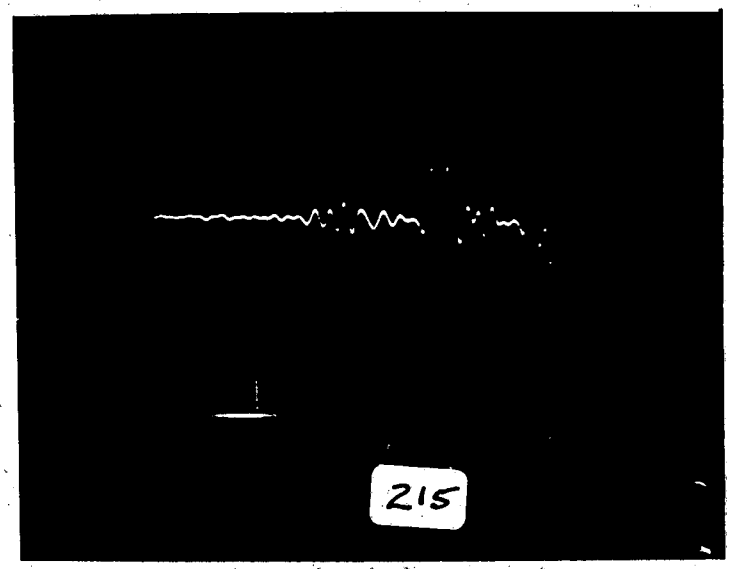
215

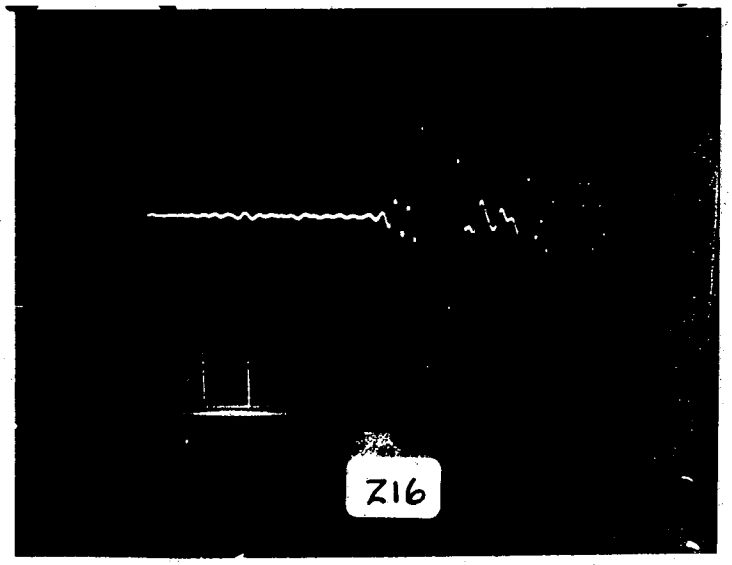
216

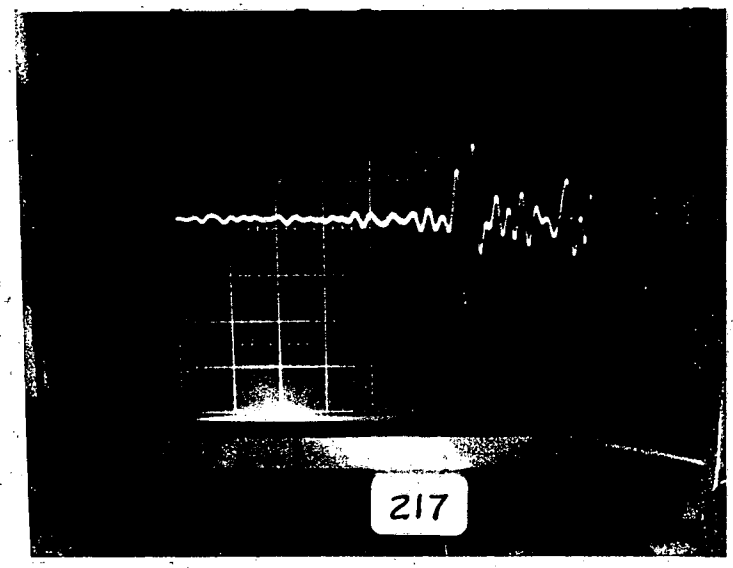
217

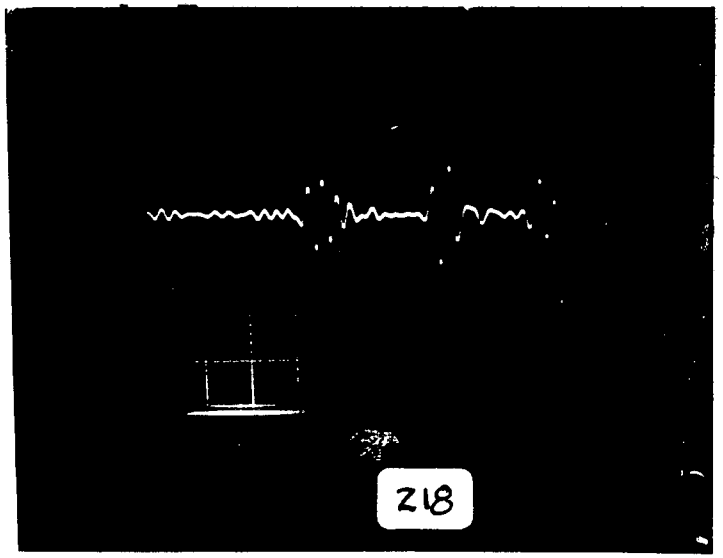
218

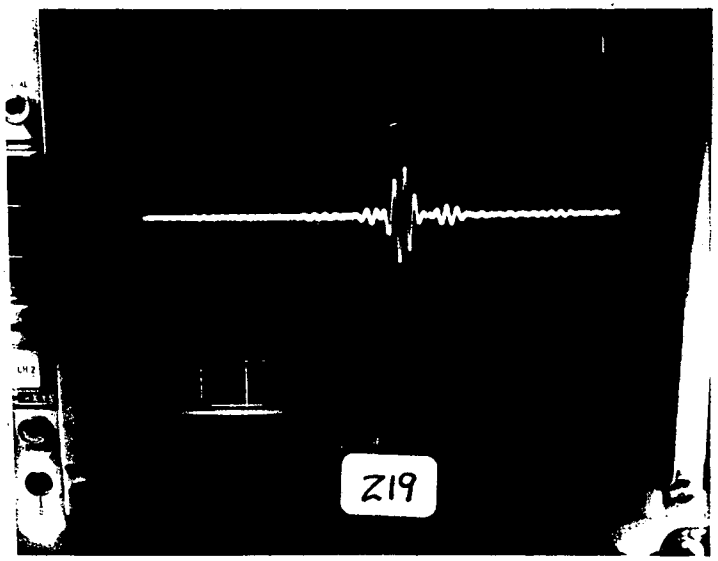
Z19

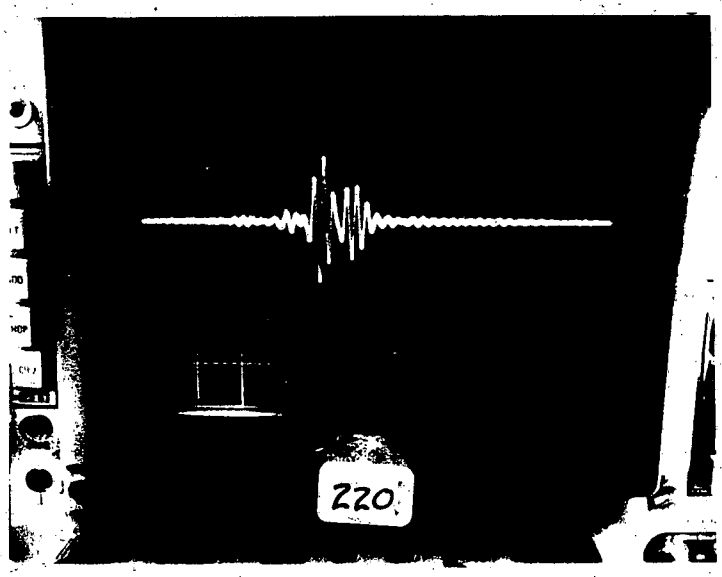
220

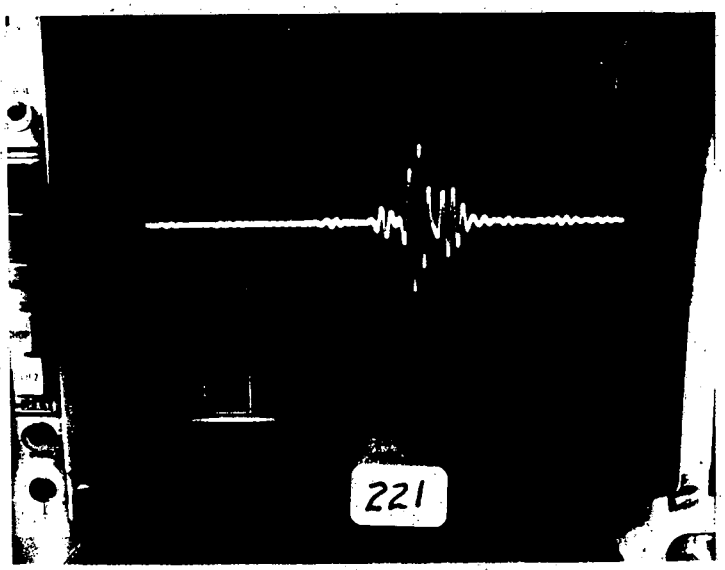
221

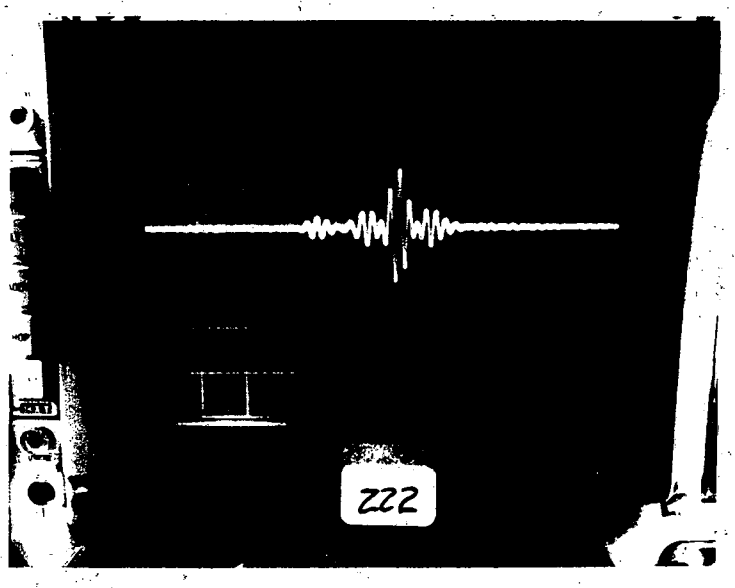
222

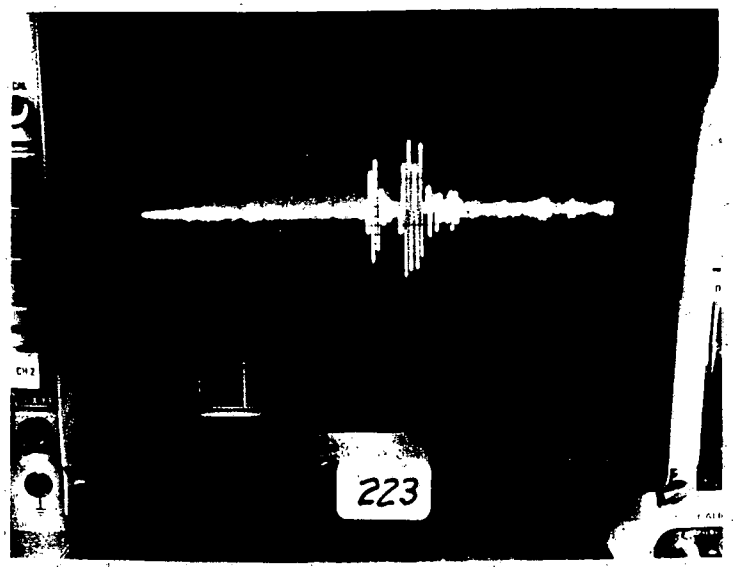
223

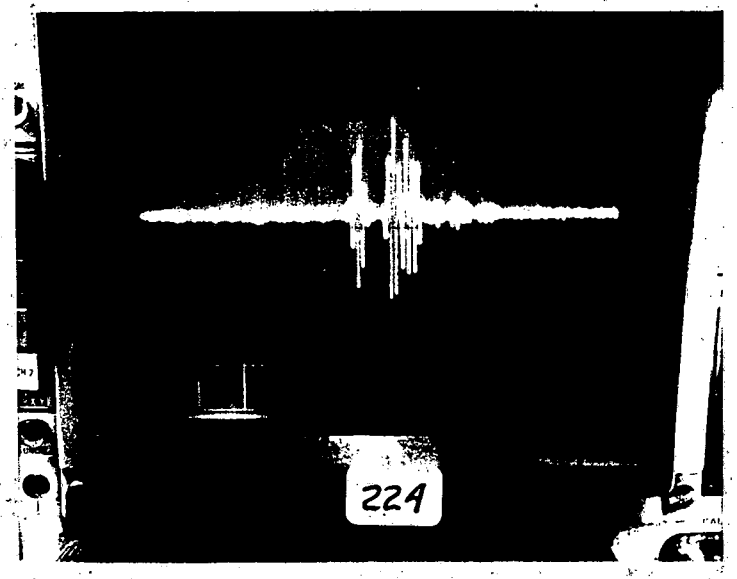
224

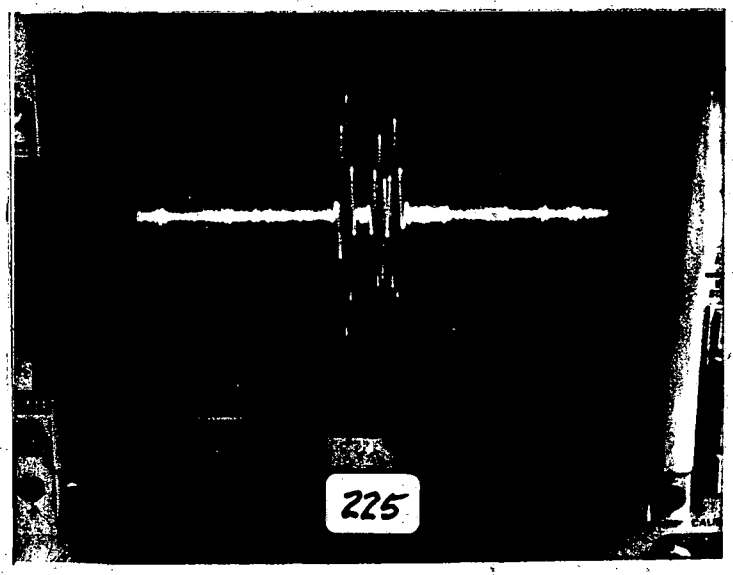
225

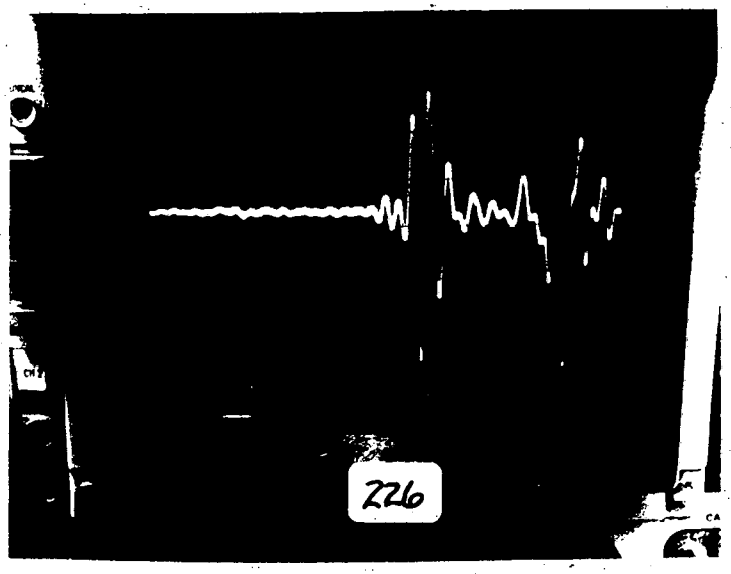
226

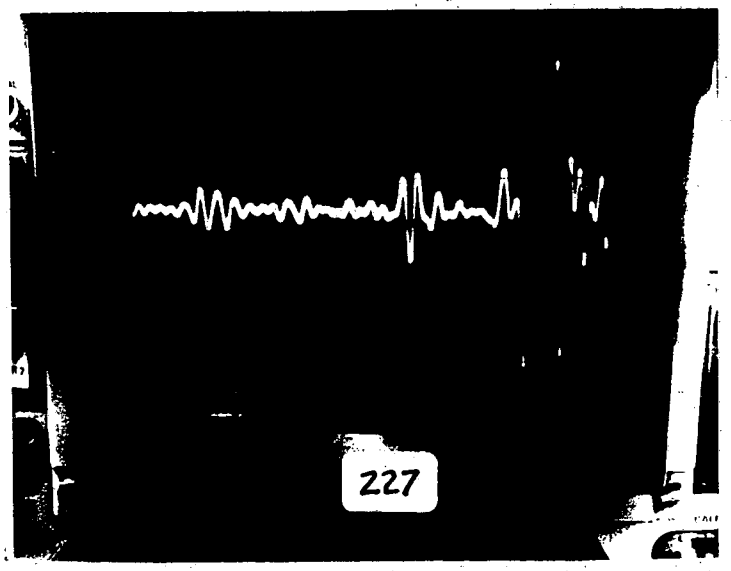
227

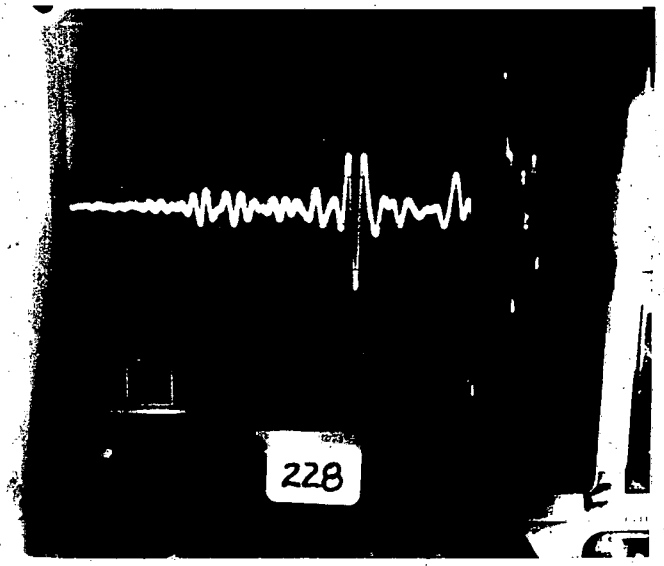
228

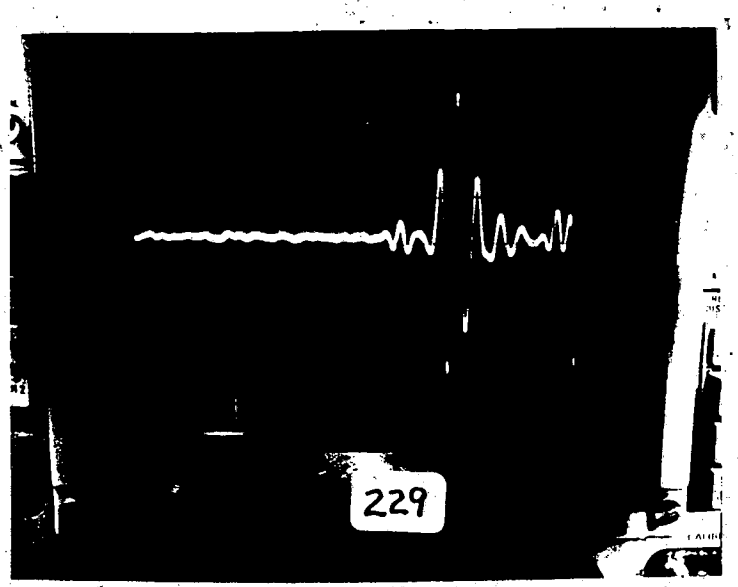
229

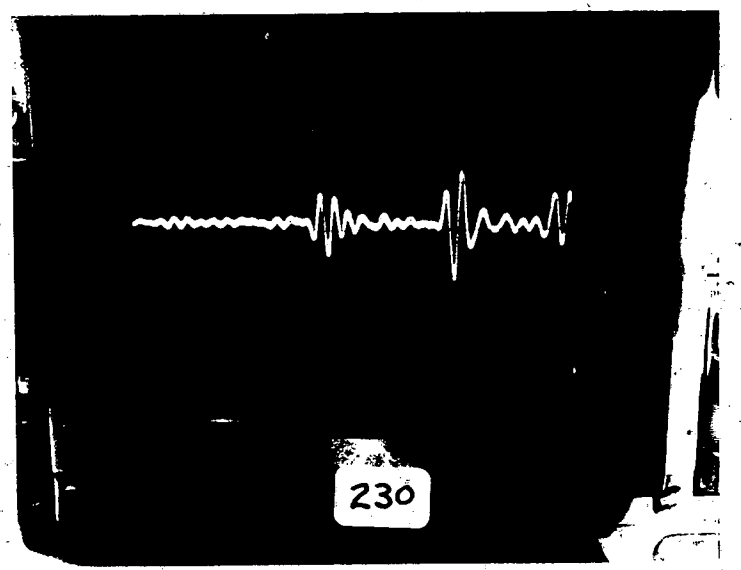
230

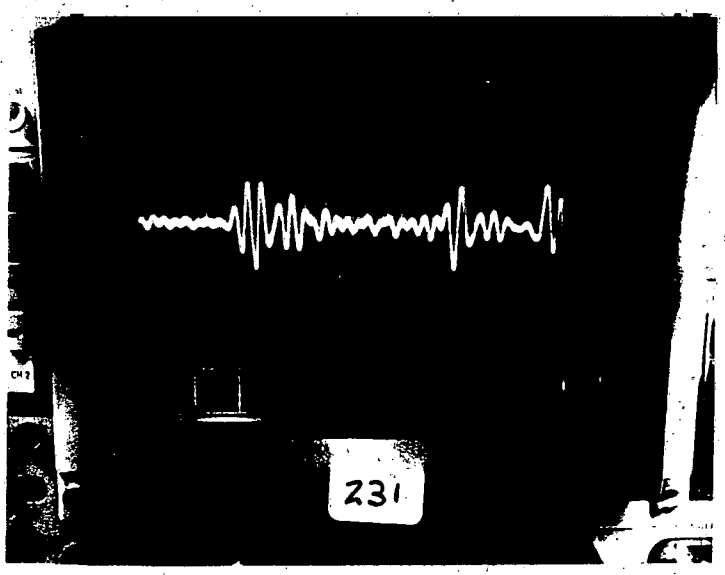
231

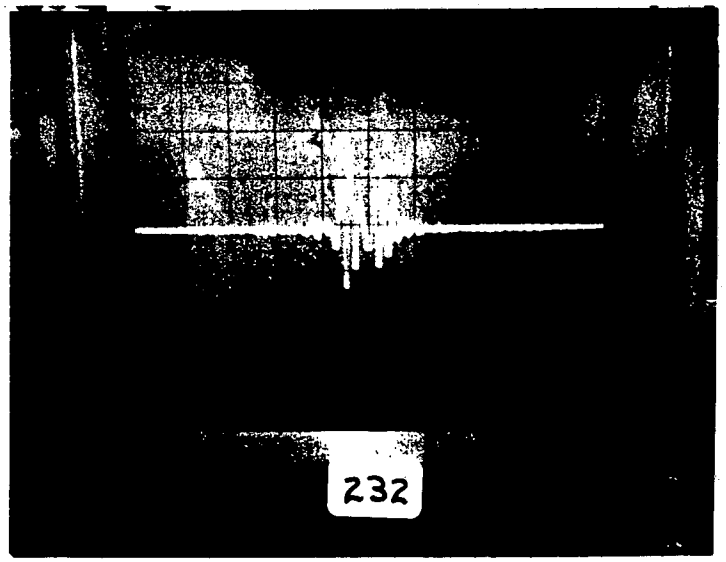
232

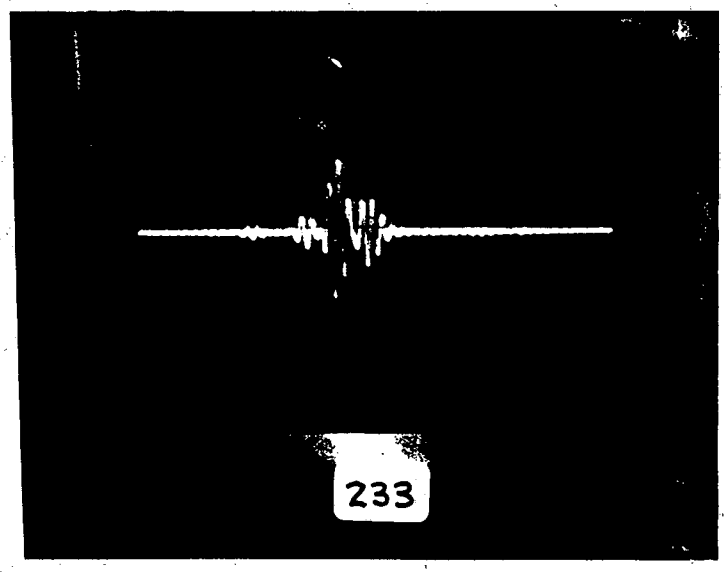
233

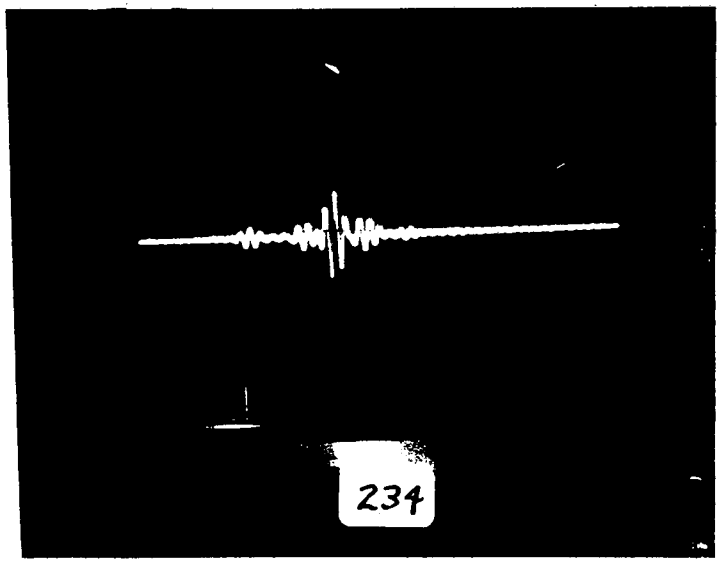
234

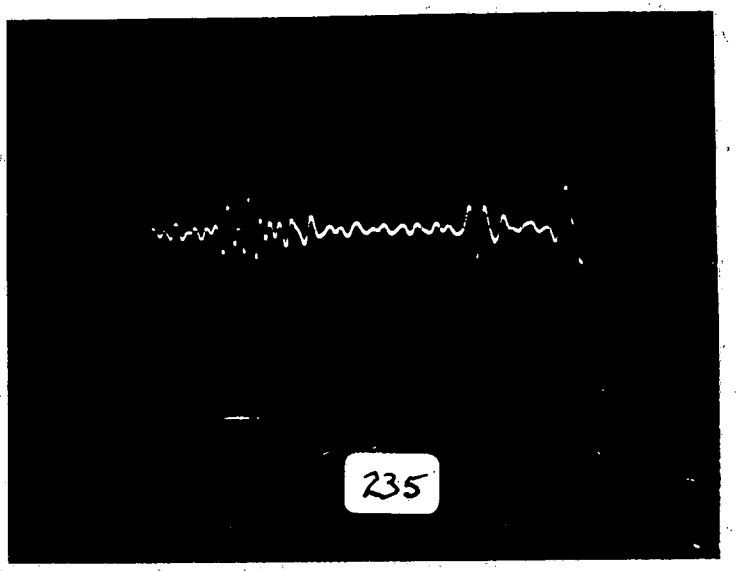
235

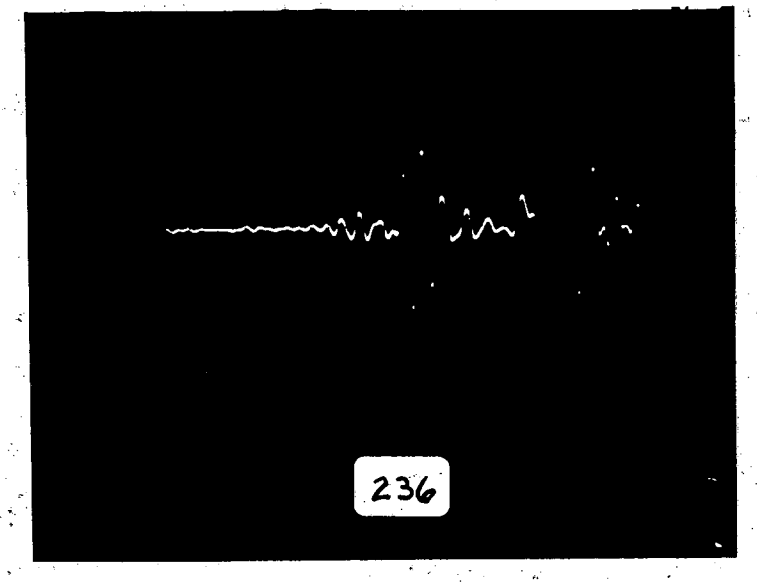
236

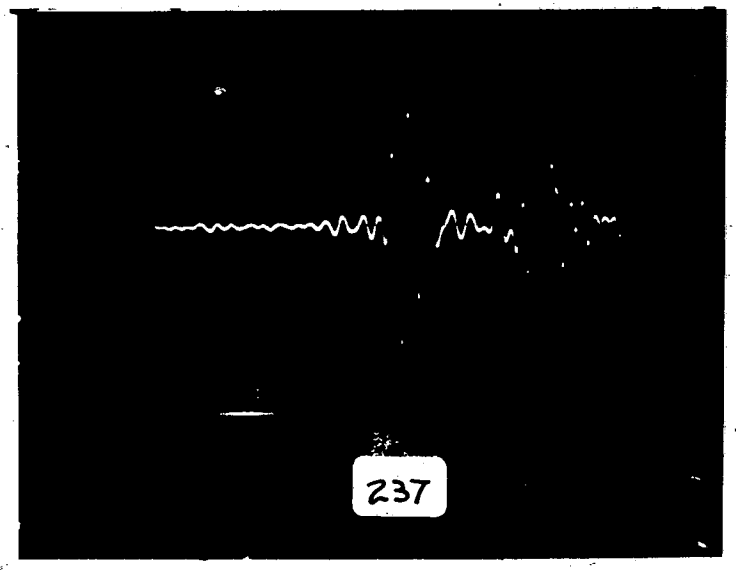
237

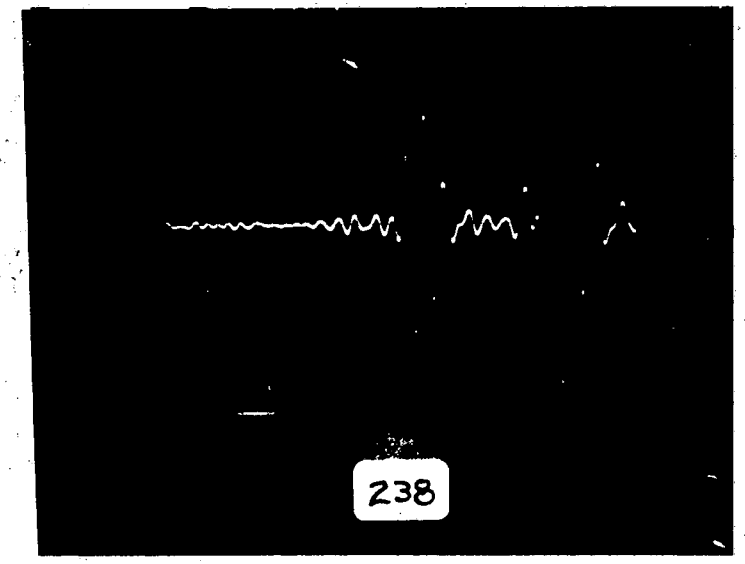
238


239

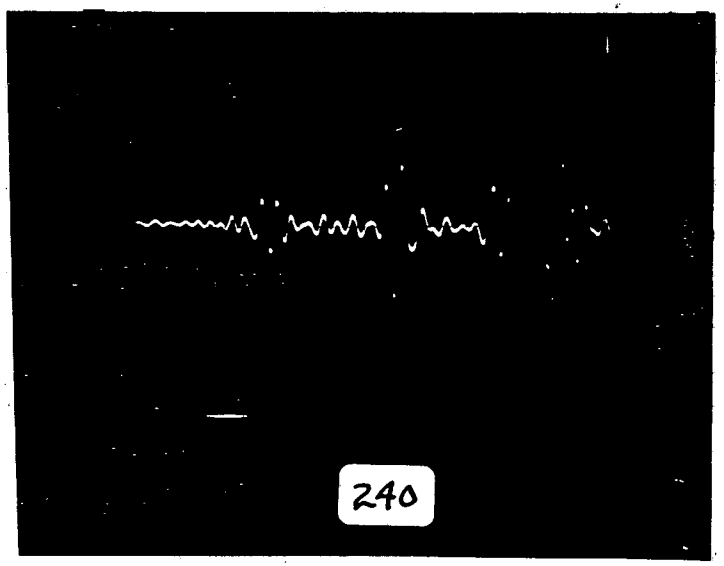
240

APPENDIX H

Drawings of Test Specimens and Fixtures

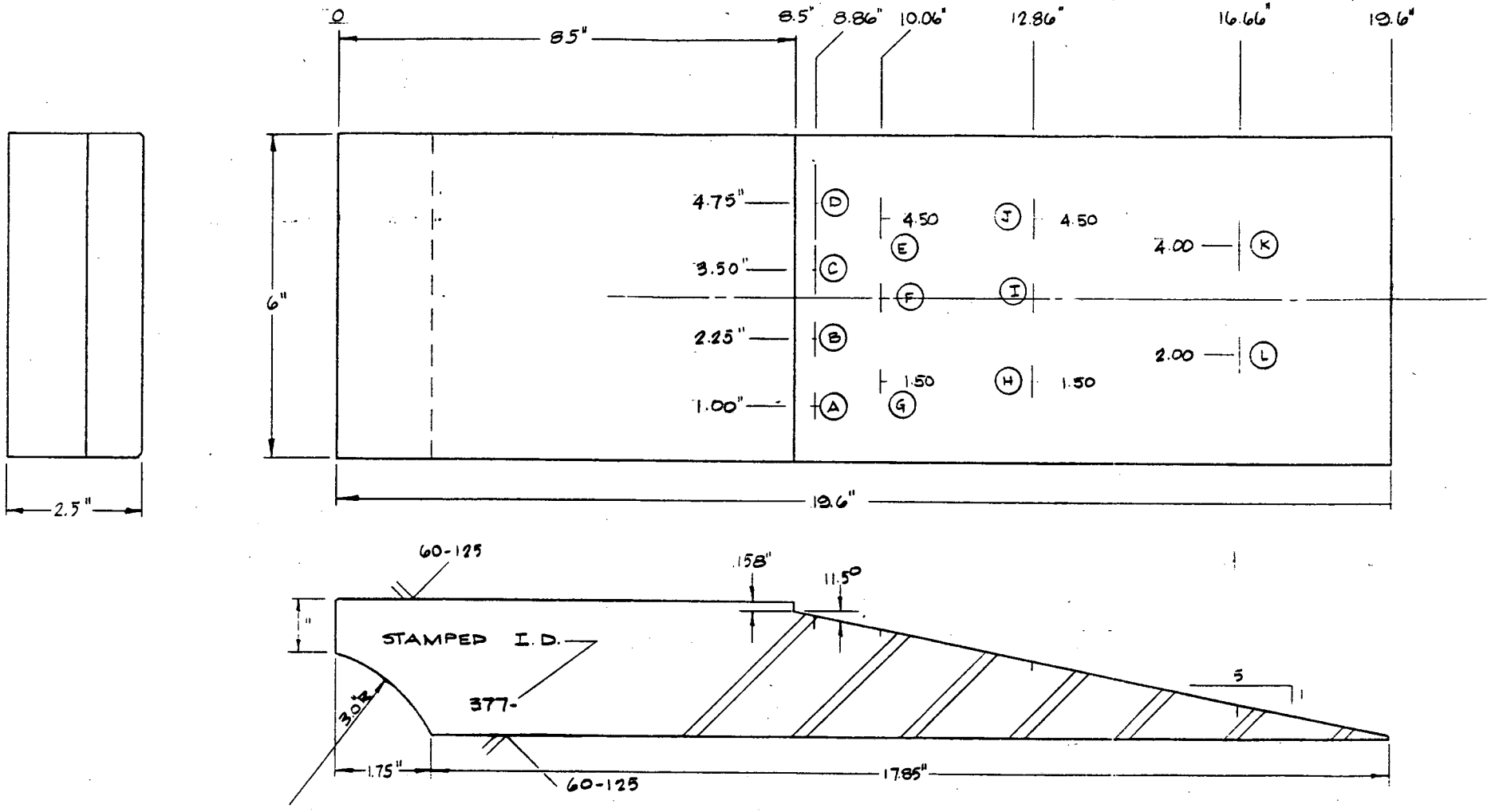

OFFSHORE TECHNOLOGY CORP.		
SCALE: 1/2	APPROVED BY:	DRAWN BY RB
DATE: 12-8-86		REVISED
SPECIMEN 4 & 5		
		DRAWING NUMBER 377-SK00

X 17 PRINTED ON NO. 1000H CLEARPRINT ●

EDM NOTCH DIMENSIONS

NOTCHES	mm			INCHES			TOLERANCES (INCHES)		
	a	c	R	a	c	R	a	c	R
A	2.0	6.0	3.3	0.079	0.236	0.128	0.001	0.002	0.001
B	3.0	9.0	4.8	0.118	0.354	0.192	0.001	0.004	0.002
C	4.0	12.0	6.5	0.157	0.472	0.256	0.002	0.005	0.003
D	6.0	18.0	9.8	0.236	0.709	0.384	0.002	0.007	0.004
E	6.0	18.0	9.8	0.236	0.709	0.384	0.002	0.007	0.004
F	2.0	6.0	3.3	0.079	0.235	0.128	0.001	0.002	0.001
G	4.0	12.0	6.5	0.157	0.472	0.256	0.002	0.005	0.003
H	5.0	15.0	8.1	0.197	0.591	0.320	0.002	0.006	0.003
I	4.0	12.0	6.5	0.157	0.472	0.256	0.002	0.005	0.003
J	6.0	18.0	9.8	0.236	0.709	0.384	0.002	0.007	0.004
K	8.0	24.0	13.0	0.315	0.945	0.512	0.003	0.009	0.005
L	6.0	18.0	9.8	0.236	0.709	0.384	0.002	0.007	0.004
M	1.0	3.0	1.6	.	.	.			

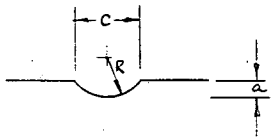

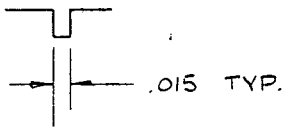

$A = R^2(\theta - \frac{1}{2} \sin 2\theta)$

$\theta = \sin^{-1}(c/2R)$

OFFSHORE TECHNOLOGY CORP.		
SCALE: —	APPROVED BY:	DRAWN BY RB
DATE: 12-8-86		REVISED
EDM NOTCH DIMENSIONS		
		DRAWING NUMBER 377-SK002

7 PRINTED ON NO. 1000H CLEARPRINT ●

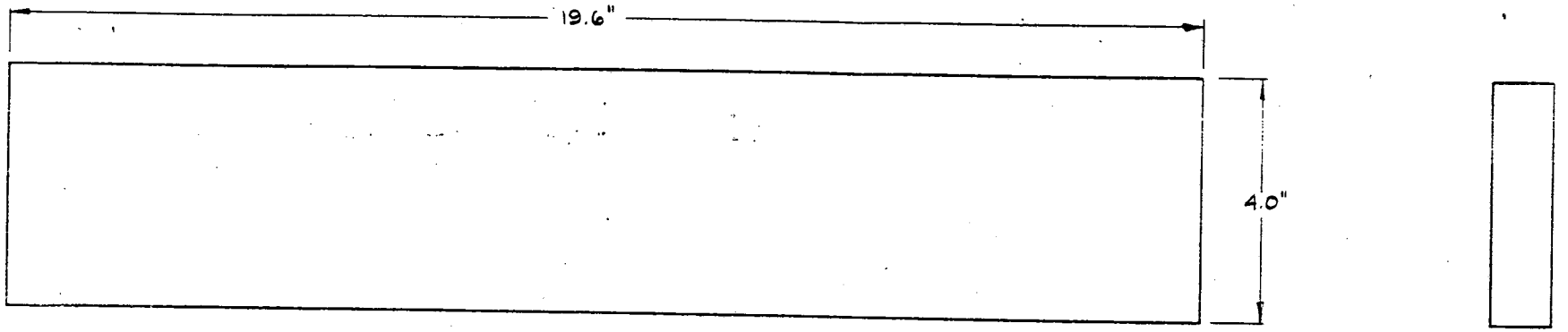

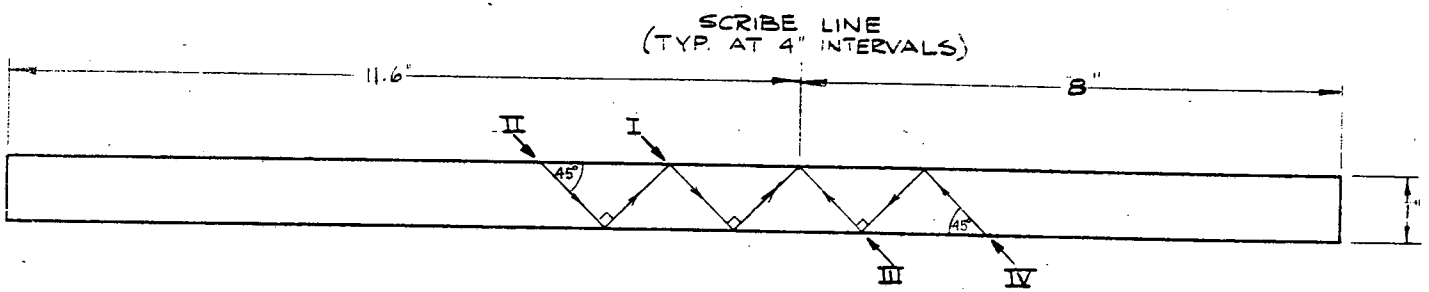

45° BEAM TRAVEL LENGTHS:

I	2.828"	71.83 mm
II	5.656"	143.66 mm
III	1.414"	35.92 mm
IV	4.242"	107.75 mm

OFFSHORE TECHNOLOGY CORP.

SCALE: 1/2	APPROVED BY:	DRAWN BY: RB
DATE: 12-4-83		REVISED

SPECIMEN 14, 15, 16

ACCOUSTIC COUPON EE3 & EE4

DRAWING NUMBER 377-SK00

17 PRINTED ON NO. 1000H CLEARPRINT ●

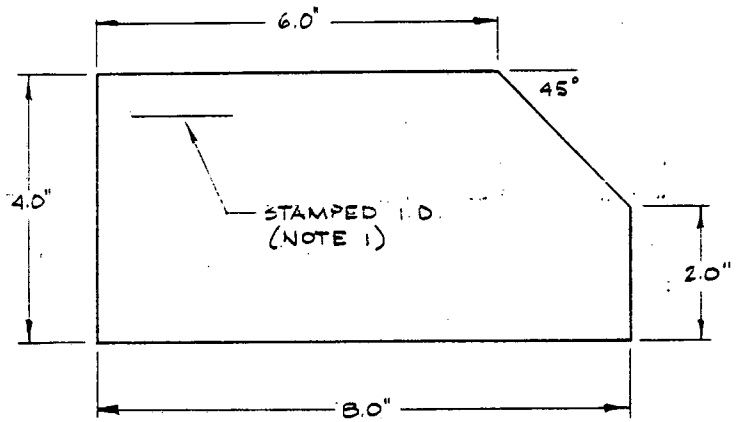

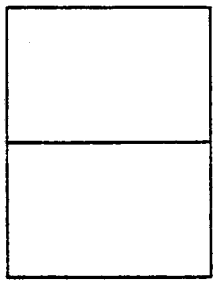

NOTES: 1- I.D. AS FOLLOWS:

377-1	2¼ Cr - 1Mo
377-2	HY-80
377-3	4340

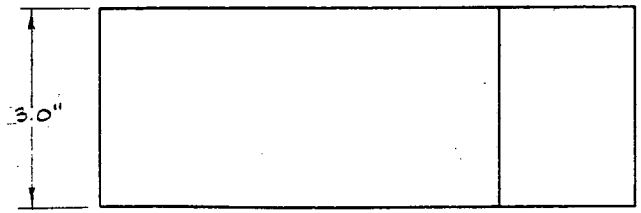

OFFSHORE TECHNOLOGY CORP.		
SCALE: ½	APPROVED BY:	DRAWN BY RB
DATE: 12-4-86		REVISED
SPECIMEN 1		
(ACOUSTIC COUPON EE-5)		DRAWING NUMBER 377-SK004

X 17 PRINTED ON NO. 1000H CLEARPRINT ●

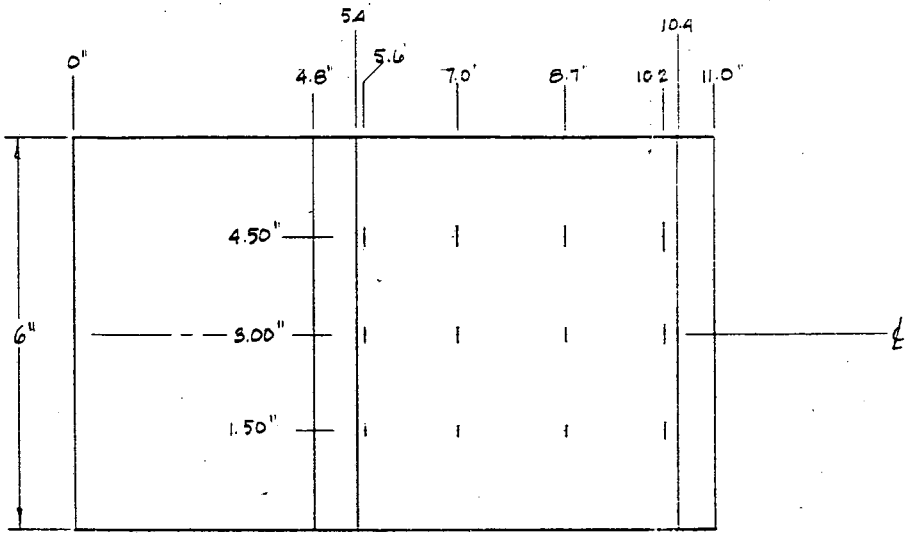

EDM NOTCH DIMENSIONS

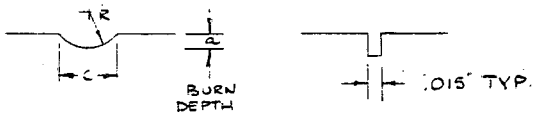

NOTCH	a	c	R
A	.12	.36	.19
B	.08	.24	.13
C	.04	.12	.07
D	.16	.48	.26

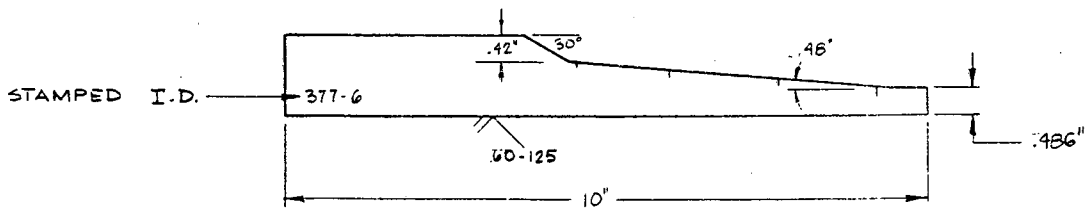

OFFSHORE TECHNOLOGY CORP.

SCALE: 1/2	APPROVED BY:	DRAWN BY RB
DATE: 12-8-86		REVISED

SPECIMEN 6

DRAWING NUMBER 377-SK005

11 X 17 PRINTED ON NO. 1000H CLEARPRINT ●

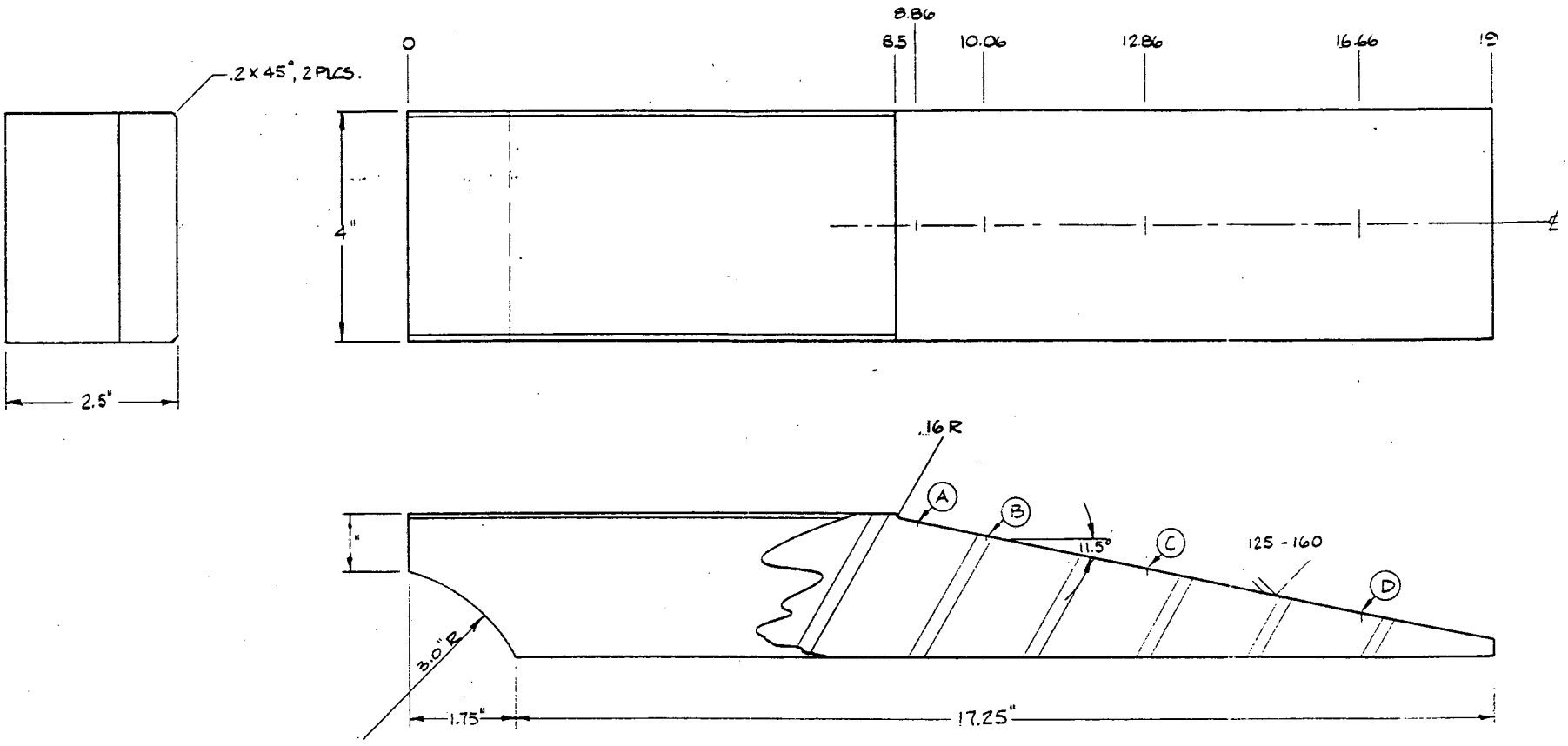

OFFSHORE TECHNOLOGY CORP.,

SCALE: 1/2	APPROVED BY:	DRAWN BY RB
DATE: 12-3-86		REVISED

SPECIMEN 7 & 8

DRAWING NUMBER
377 - SK006

11 X 17 PRINTED ON NO. 1000H CLEARPRINT ●

BASIC TEST BLOCKS,

WELDED TEST BLOCKS: TWO SAMPLES ① 15X16Xt (t IS THICKNESS OF MATERIAL)
② 4X4Xt

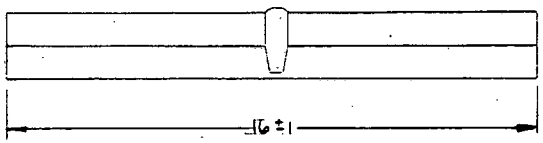

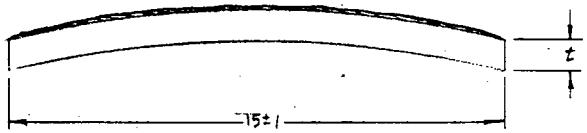

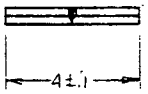

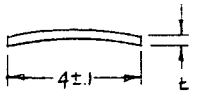

OFFSHORE TECHNOLOGY CORP.,		
SCALE: 1/4	APPROVED BY:	DRAWN BY RB
DATE: 12-8-86		REVISED
SPECIMEN 17, 18, 19		
		DRAWING NUMBER 377-SK007

11 X 17 PRINTED ON NO. 1000H CLEARPRINT ●

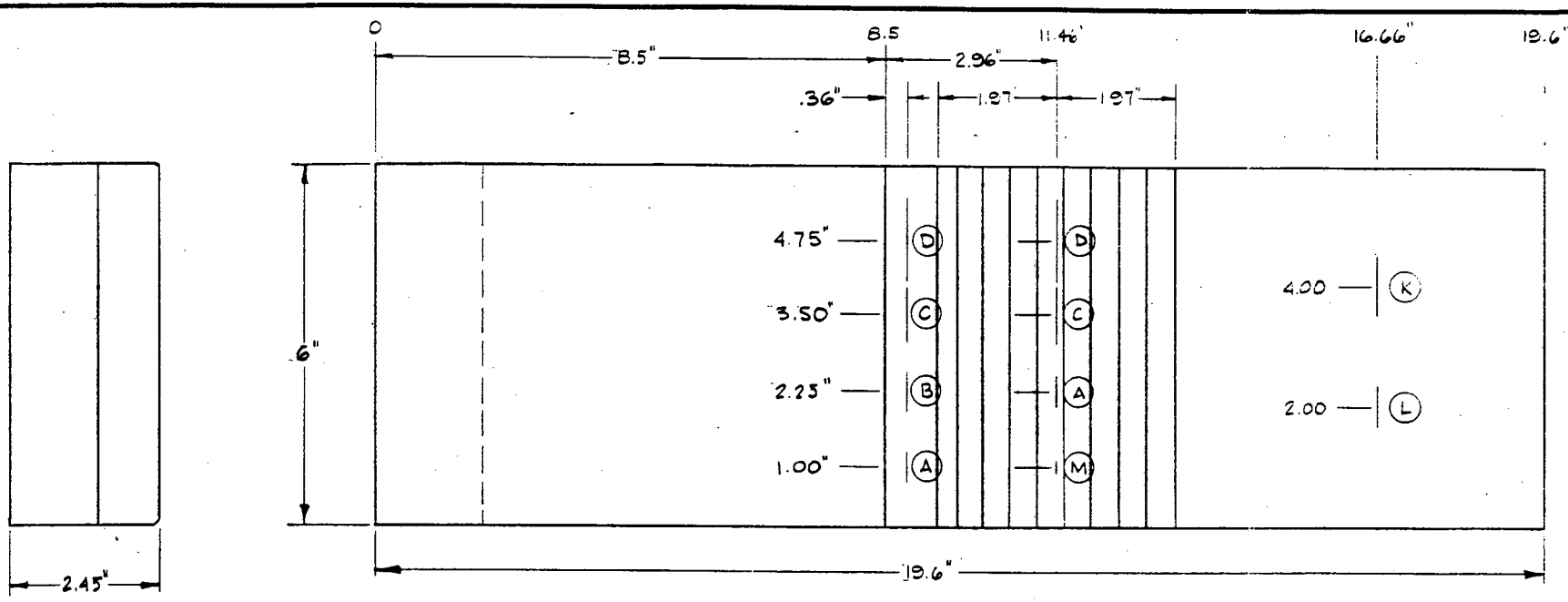

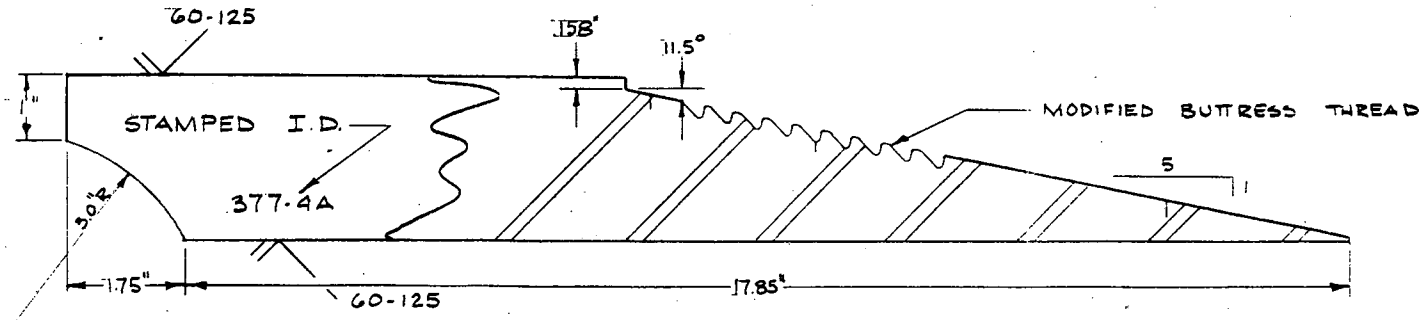

NOTES

1- SEE SK002 FOR EDM NOTCH DIMENSIONS.

2- SPECIMEN 4A IS A MODIFICATION OF SPECIMEN 5.

OFFSHORE TECHNOLOGY CORP.

SCALE: 1/2	APPROVED BY:	DRAWN BY RB
DATE: 12-3-86		REVISED

SPECIMEN 4A

DRAWING NUMBER 377-SK008

11 X 17 PRINTED ON NO. 1000H CLEARPRINT ●

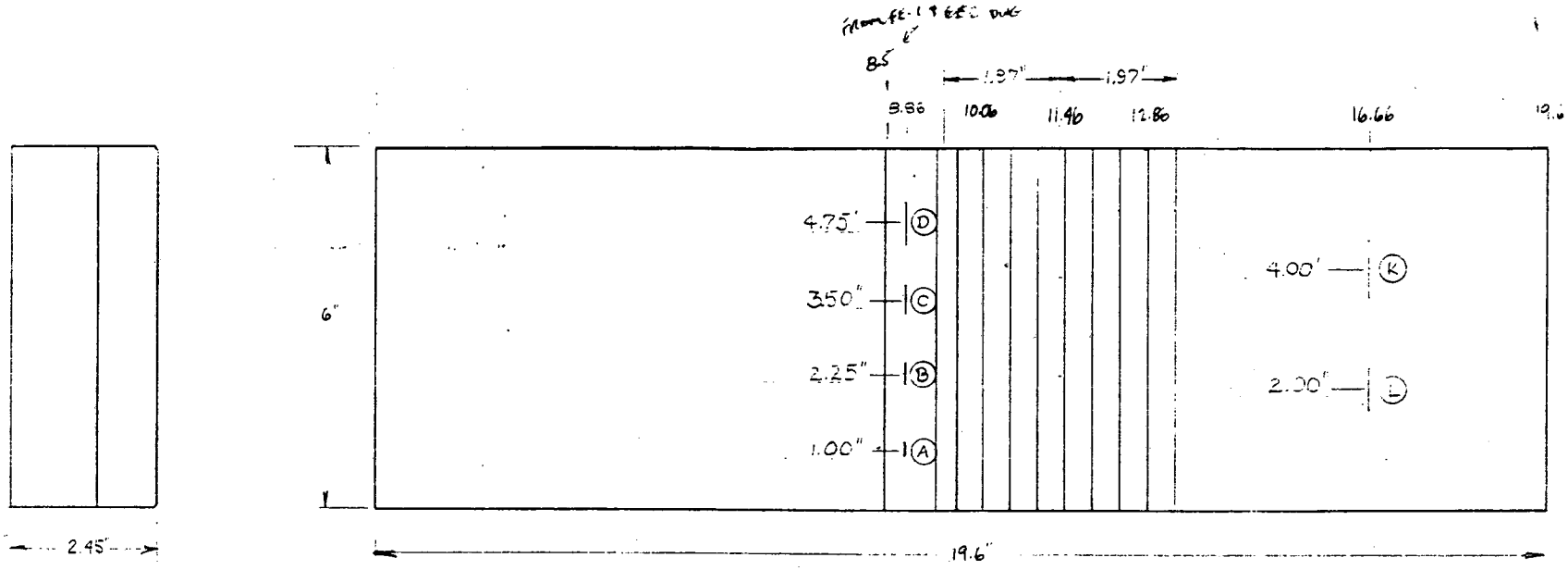

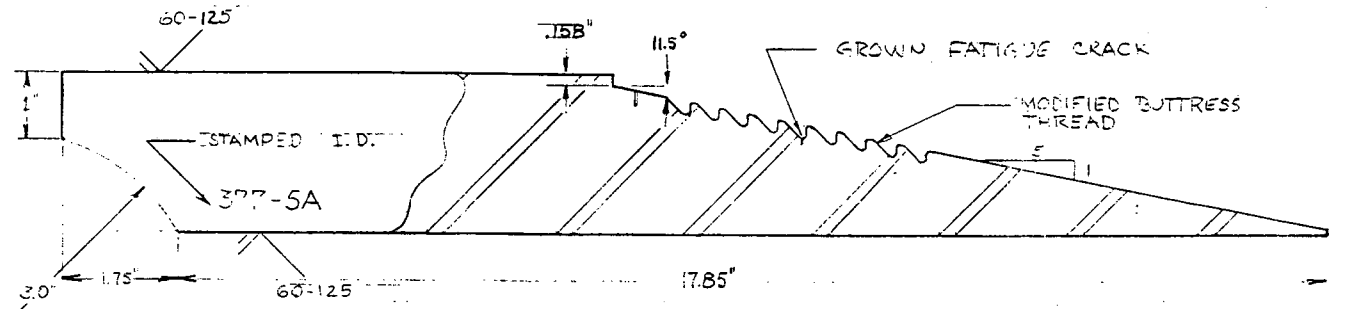

NOTE: SEE SK002 FOR EDM NOTCH DIMENSIONS

NOTE SPECIMEN 5A IS A MODIFICATION OF SPECIMEN 5

OFFSHORE TECHNOLOGY CORP., - MECHANICAL RESEARCH DIV.,		
SCALE: ½" = 1"	APPROVED BY:	DRAWN BY R.A.B.
DATE: 6/26/86		REVISED
SPECIMEN 5A		
		DRAWING NUMBER 377-SK009

11 X 17 PRINTED ON NO. 1000H CLEARPRINT

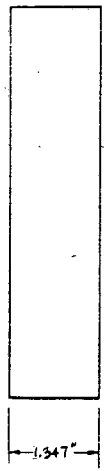

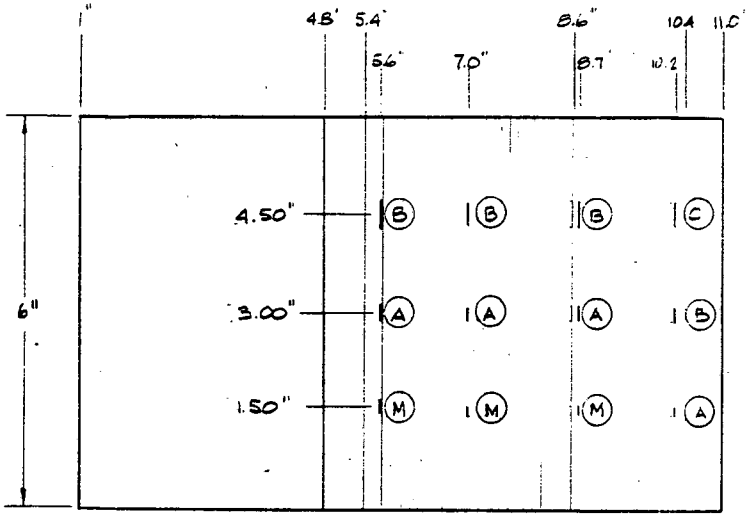

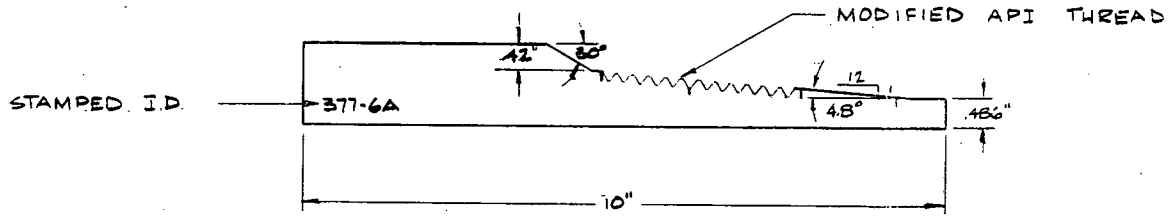

SEE SK002 FOR
EDM NOTCH DIMENSIONS

OTE: SPECIMEN 6A IS A MODIFICATION
OF SPECIMEN 6 - SK005

OFFSHORE TECHNOLOGY CORP.

SCALE: 1/2	APPROVED BY:	DRAWN BY RB
DATE: 6/26/86		REVISED 2-12-87

SPECIMEN 6A

DRAWING NUMBER
377-SK010

11 X 17 PRINTED ON NO. 1000H CLEARPRINT ●

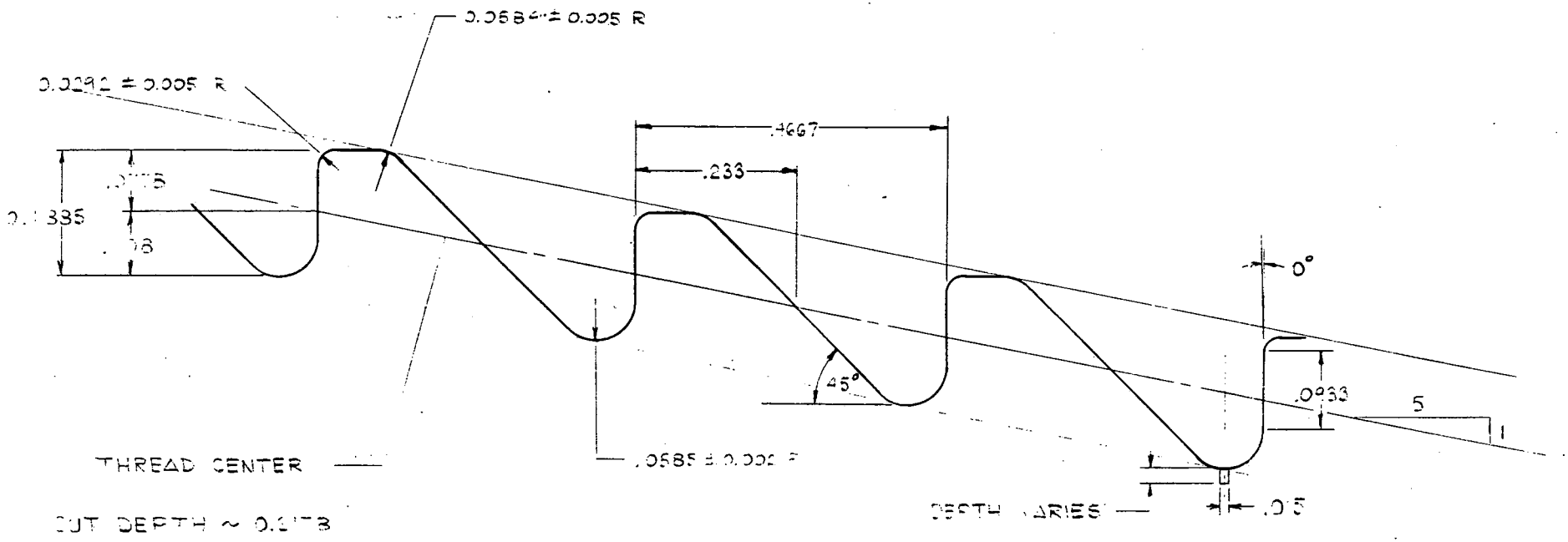

OFFSHORE TECHNOLOGY CORP. MECHANICAL RESEARCH DIV.		
SCALE: .222	APPROVED BY:	DRAWN BY RAB
DATE: 7-14-86		REVISED
THREAD DETAIL - 5A		
MODIFIED BUTTRESS THREAD		DRAWING NUMBER 277-SK011

11 X 17 PRINTED ON NO. 1000H CLEARPRINT ®

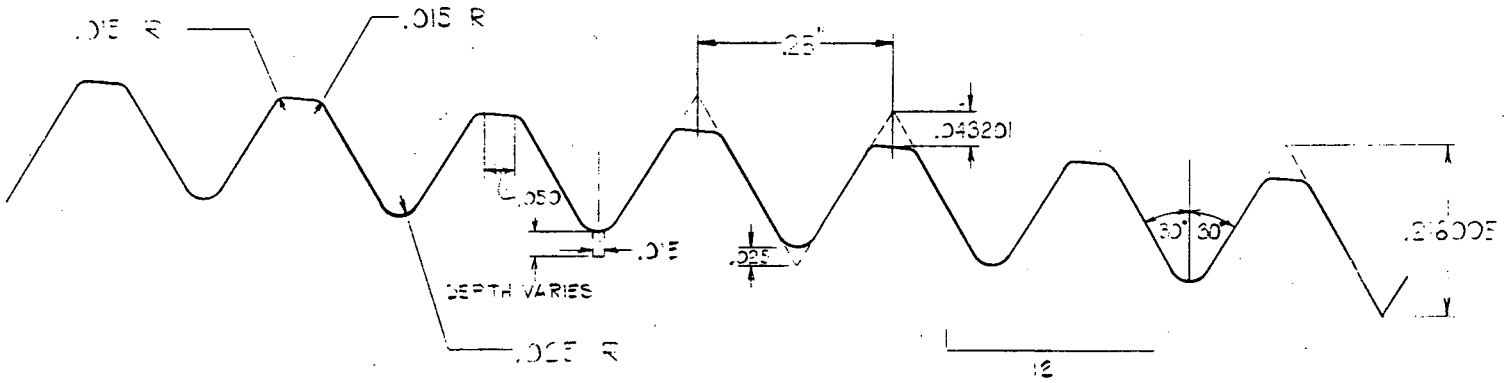

OFFSHORE TECHNOLOGY CORP. MECHANICAL RESEARCH DIV.		
SCALE: 1:6.22	APPROVED BY:	DRAWN BY RAB
DATE: 7-14-86		REVISED
THREAD DETAIL SPECIMEN 5A		
MODIFIED API THREAD		DRAWING NUMBER OTT-5A012

11 X 17 PRINTED ON NO. 1000H CLEARPRINT ●

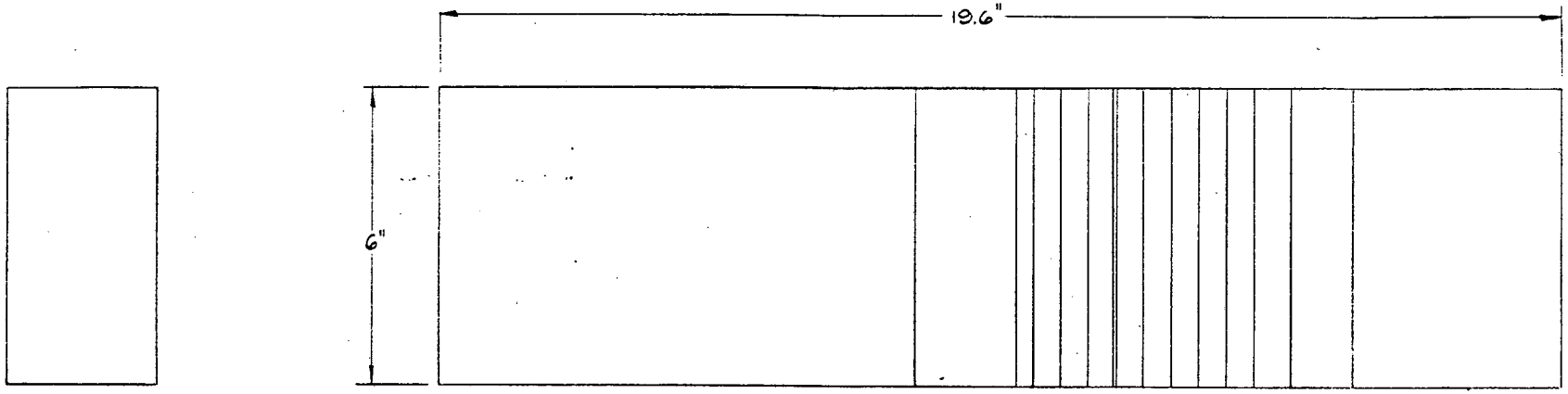

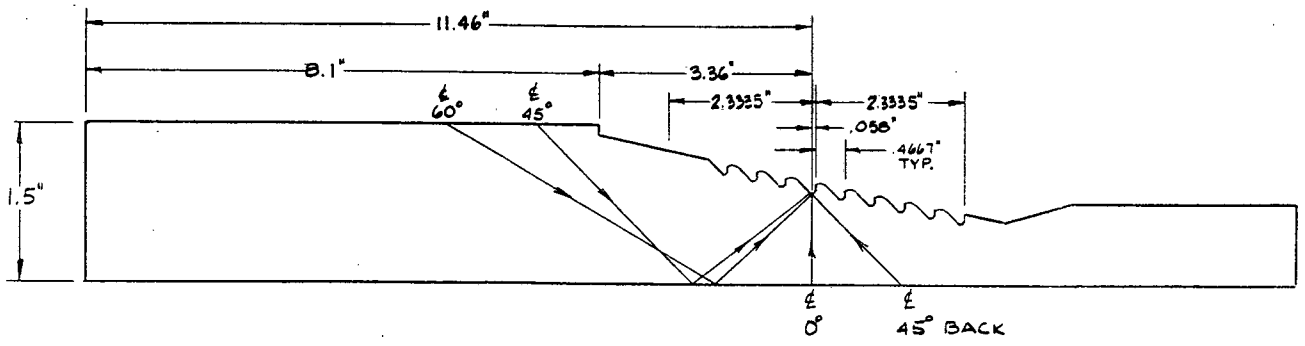

NOTCH SPECIFICATIONS:

1- SEE SK002 FOR EDM NOTCH DIMENSIONS.

2- SPECIMEN 5A-A IS A MODIFICATION OF SPECIMEN 5A; THREAD PATTERN IS UNCHANGED.

BEAM TRAVEL LENGTHS:

V 45° = 3.47" + 2.34" = 5.81" (147.57 mm)

VI 60° = 4.95" + 2.1" = 7.05" (179.07 mm)

VII 0° = 1.4" (35.56 mm)

VIII 45° BACK = 1.98" (50.29 mm)

OFFSHORE TECHNOLOGY CORP.,

SCALE: ½ | APPROVED BY: | DRAWN BY RB

DATE: 2-11-87 | REVISED 2-11-87 Ⓐ

SPECIMEN 5A-A

DRAWING NUMBER 377 SK013

11 X 17 PRINTED ON NO. 1000H CLEARPRINT ●

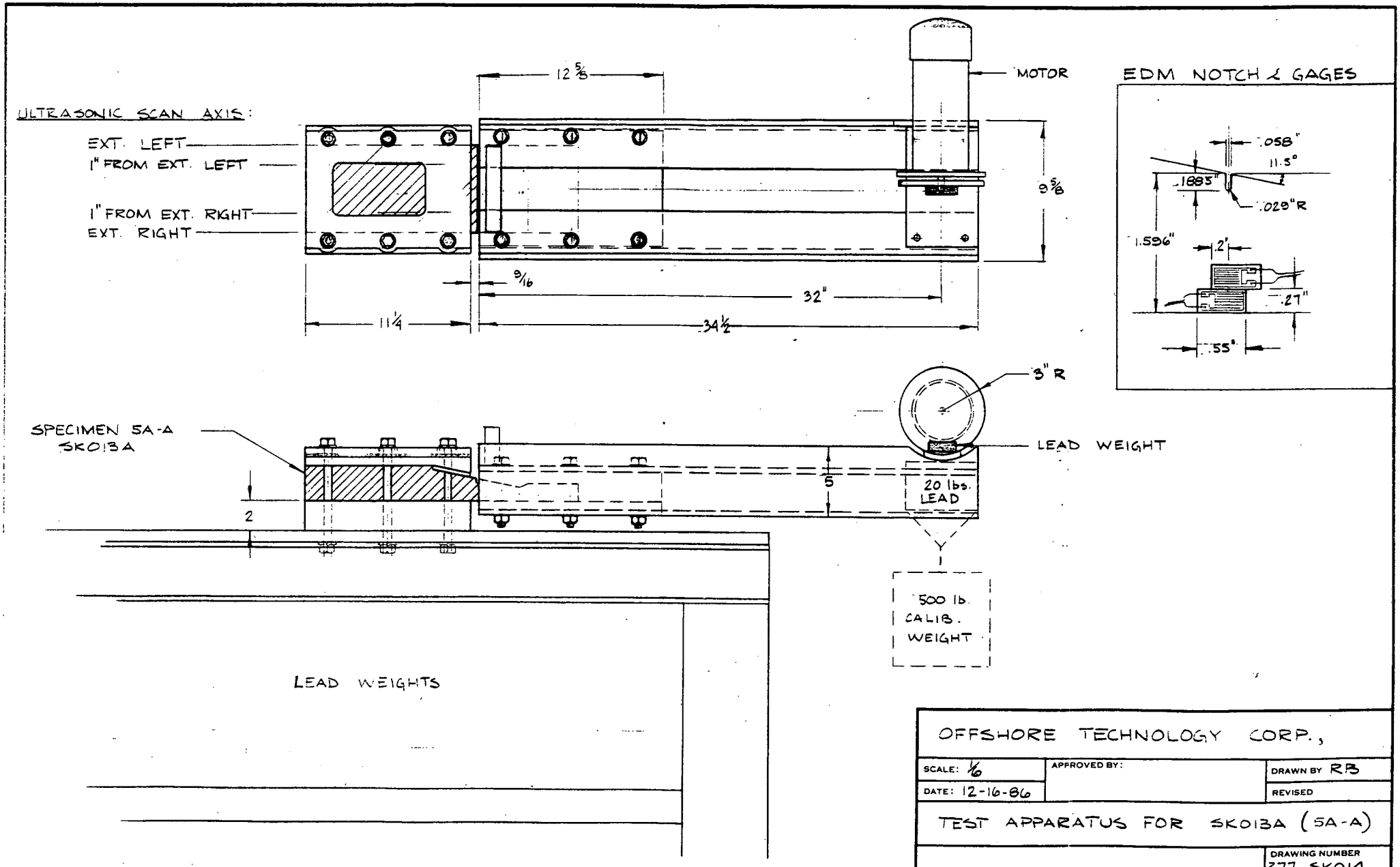

OFFSHORE TECHNOLOGY CORP.,		
SCALE: 1/6	APPROVED BY:	DRAWN BY RB
DATE: 12-16-86		REVISED
TEST APPARATUS FOR SK013A (5A-A)		
		DRAWING NUMBER 377-SK014

11 X 17 PRINTED ON NO. 1000H CLEARPRINT ®

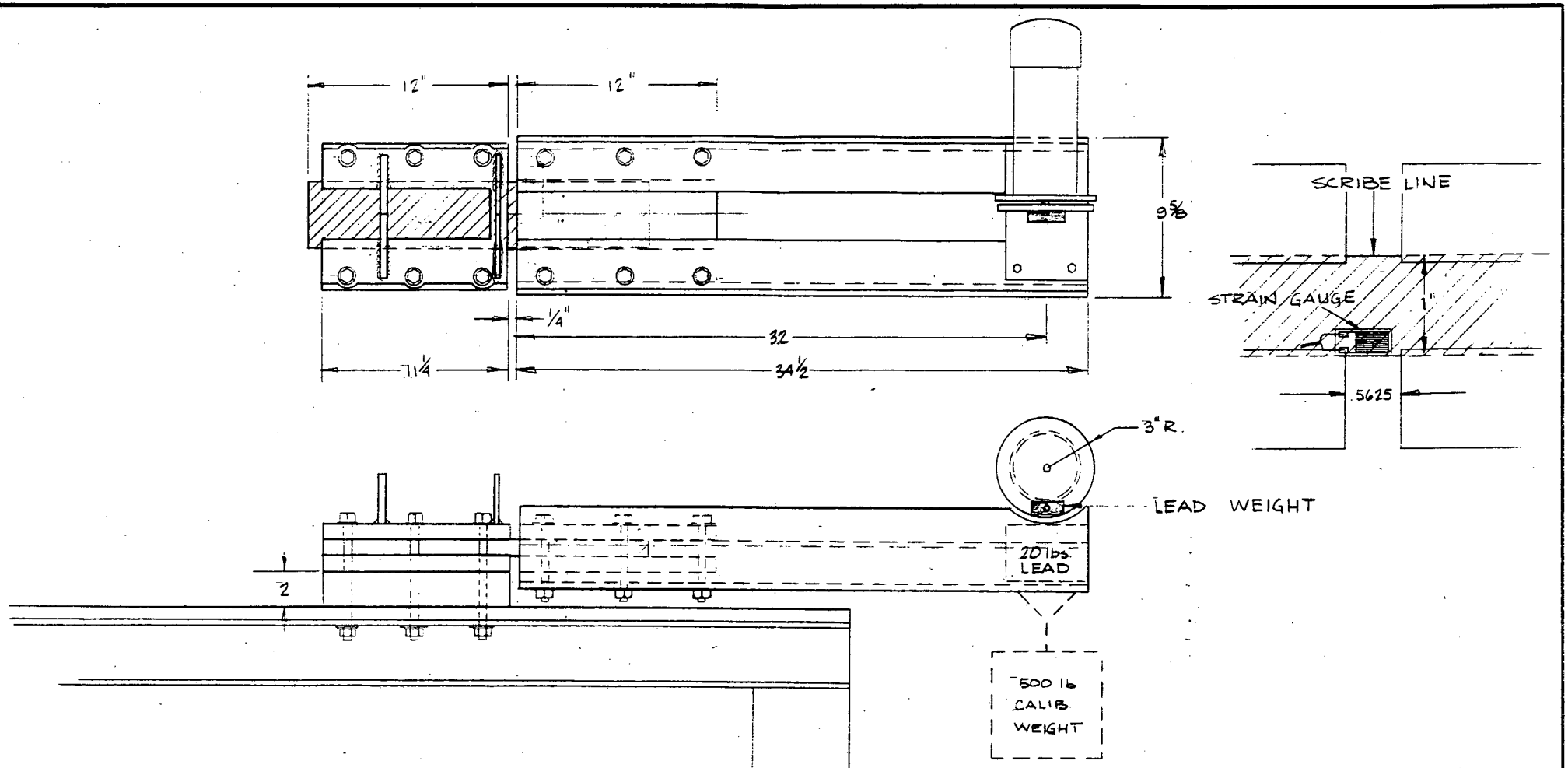

OFFSHORE TECHNOLOGY CORP.

SCALE: 1/6	APPROVED BY:	DRAWN BY RB
DATE: 12-16-66		REVISED

TEST APPARATUS FOR PART # 14,15,16

DRAWING NUMBER
377-SK015

11 X 17 PRINTED ON NO. 1000H CLEARPRINT ®

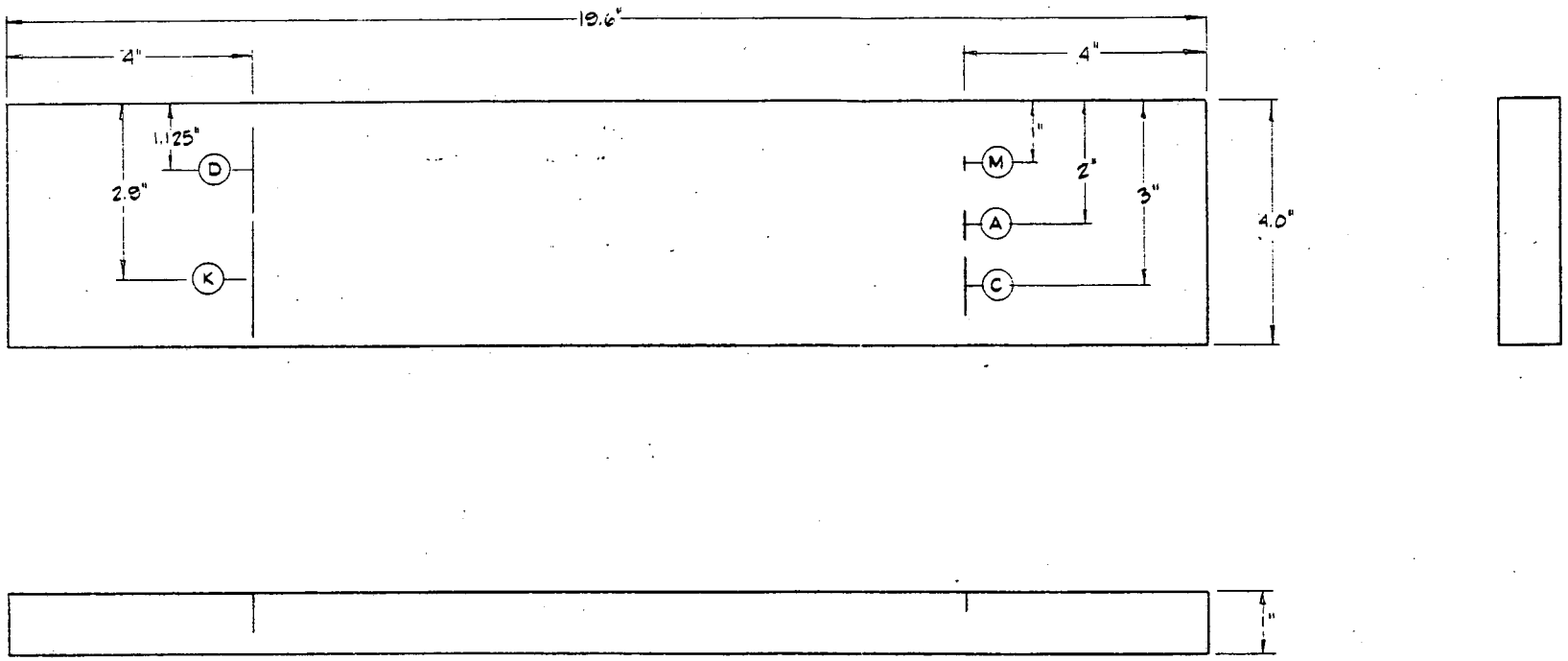

NOTCH DIMENSIONS		
NOTCH	DEPTH (mm)	LENGTH (mm)
A	2	6
C	4	12
D	6	18
K	8	24
M	1	3

OFFSHORE TECHNOLOGY CORP.,

SCALE: 1/2	APPROVED BY:	DRAWN BY RB
DATE: 2-12-87		REVISED

SPECIMEN 13

DRAWING NUMBER 377-SK0016

11 X 17 PRINTED ON NO. 1000H CLEARPRINT ®

APPENDIX I

Steel Specifications

HIGH STRENGTH QA STEEL, INC.

Specimen 2

HY-80

PACKING LIST

SOLD TO
Offshore Technology Corp
578 Enterprise St.
Escondido, CA 92025

SHIP TO
same

CUSTOMER ORDER NUMBER	DATE SHIPPED	SHIPPED VIA	OUR ORDER NUMBER
2426	12-19-85	UPS	QH1387

ITEM	QUANTITY ORDERED	QUANTITY SHIPPED	DESCRIPTION/IDENTIFICATION	WEIGHT
1	1	1	3 x 4 x 8 MIl-S-16216J HY80 Ty II	27

HIGH STRENGTH QA STEEL, INC.

INSPECTION REPORT

CUSTOMER: Offshore Technology Corp S/O # QH1387

SPECIFICATION: MIL-I-16216J HY80 Ty II

ADDITIONAL REQUIREMENTS:

Low stress stamp with heat, grade, mfg & spec.

ITEM 1 QTY 1 SIZE 3 x 4 x 8

PLATE NO. 200022-6 HEAT NO. 49205

PRODUCER Armco SLAB NO. _____

INSPECTED BY: S Beckman (X) ACCEPTED

DATE: 12-18-85 ( ) REJECTED

COMMENTS: _____

ITEM ___ QTY _____ SIZE _____

PLATE NO. _____ HEAT NO. _____

PRODUCER _____ SLAB NO. _____

INSPECTED BY: _____ ( ) ACCEPTED

DATE: _____ ( ) REJECTED

COMMENTS: _____

ITEM QTY _____ SIZE _____

PLATE NO. _____ HEAT NO. _____

PRODUCER _____ SLAB NO. _____

INSPECTED BY: _____ ( ) ACCEPTED

DATE: _____ ( ) REJECTED

COMMENTS: _____

P.O. Box 40606 • 12247 FM 529 • Houston, Texas 77240-0606 • (713) 937-7720 • 1-800-231-4574 • Telex 79-4402

Weste[illegible]teel Division
Houston, Texas 77015

[illegible]ST REPORT

317-1302-10-13-83

"ACCEPTANCE OF THIS REPORT TO A THIRD PAR[illegible] UNDER THE NAME OF SUCH CONSIGNEE." MUST BE RECEIVED

28 CONTRACT NO.

HIGH STRENGTH STEEL, INC.

P O BOX 40606

HOUSTON TX 77040

HIGH STRENGTH STEEL, INC.

12247 FM 529

HOUSTON TX 77040

PURCHASE ORDER DATE	PURCHASE ORDER NUMBER
07/11/83	H9278

SHIPPERS NO.	MILL ORDER NO	DATE SHIPPED
7153893	TAH93768	10/13/83

C. T. VEHICLE IDENTIFICATION 1 TRUCK

MAIL TO

HIGH STRENGTH STEEL, INC.

P O BOX 40606

HOUSTON TX 77040

093970408-6042 SP 16

THE CHEMICAL, PHYSICAL OR MECHANICAL TESTS REPORTED ARE CORRECT AS CONTAINED IN THE RECORDS OF THE COMP

D. D. REED PHYS. MET

SIGNED METALLURGICAL DEPT.

PL# 200022

MILL TEST REPORTS FURNISHED BY HIGH STRENGTH STEEL

DATE 12-18-85

CUSTOMER [illegible]

CUSTOMER P.O. 2426

OUR W.O. NO. QH1387

900HY-80 PLATES ALLOY QUENCH TEMP * MIL-S-16216J TYPE II VAC DEQAB UT, UQ D & . QUALITY SYSTEMS PER MIL-I-45208A.

ITEM	MATERIAL DESCRIPTION	QNTY.	WEIGHT	HEAT NO.	PIECE NUMBER	YIELD P.S.I.	TENSILE P.S.I.	% ELONG	% REDUCT	BEND	1	2	3	AV
01	3 96 X 240													

ARMCO, INC. HEREBY CERTIFIES THAT IN THE PRODUCTION OR TESTING OF THIS MATERIAL BY ARMCO, INC. NO ALPH EMITTING RADIATION DEVICES, DIRECT CONNECTED MERCURY MANOMETER, MERCURY VACUUM PUMPS, MERCURY SEALS OR MERCURY-IN-GLASS THERMOMETERS HAVE BEEN USED, NOR IN SUCH PRODUCTION OR TESTING HAS (A)MERCURY BEEN HANDLED IN THE IMMEDIATE VICINITY OF SUCH MATERIAL OR (B)RADIOACTIVE MATERIAL BEEN APPLIED TO ITS SURF THE MATERIAL COVERED BY THIS CERTIFICATION WAS MANUFACTURED IN ACCORDANCE WITH MIL-S-SPECIFICATION 16216J WE CERTIFY THAT SAMPLES REPRESENTATIVE OF THE LISTED MATERIAL HAVE BEEN TESTED AND THE RESULTS CONFORM TO THE REQUIREMENTS OUTLINED IN THE MIL-S-SPECIFICATION 16216J

RECORDS ARE AVAILABLE COVERING HEAT NUMBER OF THE MATERIAL USED, PROCESSING OF PLATE, DIMENSIONAL CONTROL EMPLOYED, ULTRASONIC TESTING, QAQING AND HEAT TREATMENT.

THIS MATERIAL HAS BEEN MANUFACTURED IN ACCORDANCE WITH ARMCO'S QAP REV. 4 DATED 06/15/81 WHICH CONFO TO THE REQUIREMENTS OF MIL-I-45208A

CERTIFIED A TRUE COPY OF THE ORIGINAL RETAINED IN OUR FILE HIGH STRENGTH STEEL, INC.

S Beckmann
Q.A. DEPARTMENT

QA APPROVED
3-5-85
S Beckmann

NUMBER	TYPE	G.S.	C	Mn	P	S	Si	Cr	Ni	Mo	Cu	Ti	V	B	Cb	Co	Al	N
7205	LDL	7	.16	.25	.010	.015	.22	1.64	3.02	.43	.19	.002	.002					

1485 REV. 5-72

ARMCO STEEL CORPORATION
HOUSTON WORKS
METALLURGICAL DEPARTMENT

NON-DESTRUCTIVE TESTING REPORT

CUSTOMER:	CUSTOMER ORDER OR CONTRACT NO.:	CUST. ITEM NO.:	MILL ORDER NO.:	DATE:
gh STRENGTH	HS278	1	TAHS 5768	9-30-83

MATERIAL TESTED:	SPECIFICATION:	SIZE:	HEAT & SEQ. NO.:	DWG. NO.:	TOP SURFACE
PLATE HY80	MIL-S-16216J TYPE II	3.000 x 96" x 240"	49205	P90708	PAINTED

TEST R4 INSTRUMENT USED:	TYPE TRANSDUCER:	AMPLITUDE:	COUPLANT:	GRID SIZE:	BOTTOM SURFACE
AH 80-2-012 KB DM2	5MHZ - ½" DIA.	—	WATER	24"	PAINTED

TEST R4 INSTRUMENT USED:	TYPE TRANSDUCER	AMPLITUDE:	COUPLANT:	GRID SIZE:	TYPE PAINT
AH 80-2-012 KB USM2	2.25MHZ - 1⅛" DIA	100%	WATER	24" DIAG	"B"

NESS	EAST	WEST	MARK NO.	INSPECTORS NAME & LEVEL: ASNT-TC-1A	WITNESSED BY
	235	235		Brown II Phillips II	

E

U.T. THICKNESS MICROMETER	6" R.P.	30	54	78	102	126	150	6"	
	3.081			3.083					
6"	3.079	3.090	3.090	3.064				3.072	6"
30" 3.080	3.079	3.085	3.075	3.078				3.065	3.073 30"
54	3.071	3.084	3.085	3.080				3.069	54
78	3.071	3.083	3.088	3.074				3.073	78
102	3.072	3.084	3.091	3.082				3.067	102
126	3.077	3.098	3.094	3.085				3.070	3.077 126
150 3.045	3.086	3.095	3.096	3.089				3.070	150
174	3.085	3.098	3.102	3.090				3.076	174
198	3.085	3.098	3.092	3.088				3.080	198
222 3.065	3.091	3.099	3.095	3.089				3.084	3.064 222
246									246
270									270
294									294
318									318
342									342
366									366
390									390
414									414
438									438
462									462
486									486
510									510
534									534
6"	3.094	3.094	3.095	3.080				3.073	6"
	3.064			3.065					
	6"	30	54	78	102	126	150	6"	

THICKNESS	SPEC.	MICROMETER	ULTRASONIC
MINIMUM	2.990		3.064
MAXIMUM	3.125		3.102
AVERAGE	—		3.084

U. T. DEFECTS - CLASS & LOCATION ON PLATE

CLASS	SIZE	LOCATION FROM REF. PT.
		Satisfactory

VISUAL INSPECTION

	1ST	2ND
SURFACE	OK	OK
EDGES	OK	
DIMENSIONAL	OK	
FLATNESS	OK	
CAMBER	OK	

THE N.D.T. TESTS REPORTED HEREWITH ARE CORRECT AS CONTAINED IN THE RECORDS OF THE CORPORATION:

AHMCO [illegible] INC.
[illegible]n Steel Division
Houston, Texas 77015

TEST REPORT

317-1302-10-13-83

PURCHASED FROM AHMCO INC. TO AVOID [illegible] REDELIVERY OF THIS REPORT TO A THIRD PARTY IT MUST BE RECERTI UNDER THE NAME OF SUCH CONSIGNEE."

JOB CONTRACT NO.

HIGH STRENGTH STEEL, INC.

P O BOX 40606

HOUSTON TX 77040

HIGH STRENGTH STEEL, INC.

12247 FM 529

HOUSTON TX 77040

PURCHASE ORDER DATE	PURCHASE ORDER NUMBER	
07/11/83	H6278	
SHIPPERS NO.	MILL ORDER NO	DATE SHIPPED
7153893	TAH85768	10/13/83
C T VEHICLE IDENTIFICATION	1	TRUCK

MAIL TO: HIGH STRENGTH STEEL, INC.

P O BOX 40606

HOUSTON TX 77040

093970408-6042 8P 16

THE CHEMICAL, PHYSICAL OR MECHANICAL TESTS REPORT ARE CORRECT AS CONTAINED IN THE RECORDS OF THE C

D. D. REED PHYS. MET

SIGNED _____ METALLURGICAL DEPT.

3900HY-80 PLATES ALLOY QUENCH TEMP * MIL-S-16216J TYPE II VAC DEGAS UT, UQ D & C. QUALITY SYSTEMS PER MIL-I-45208A.

ITEM	MATERIAL DESCRIPTION	ONTY.	WEIGHT	HEAT NO.	PIECE NUMBER	YIELD P.S.I.	TENSILE P.S.I.	% ELONG	% REDUCT	BEND	1	2	3
001	3 96 X 240 (CONT'D)												
	BOTH THE FOLLOWING PLATES AND TEST COUPONS WERE AUSTENITIZED AT 1650 DEGS F FOR 30 MINUTES AND WATER QUENCHED TEMPERED AT 1260 DEGS F FOR 30 MINUTES AND AIR COOLED												
		1		49205	P90708	90800	108800	22.0-2"	66.3				
						88900	107400	23.0-2"	63.3				
						TYPE A IMPACT T @ -120 DEGS F FULL SIZE EQY.					52	57	59
						TYPE A IMPACT T @ 0 DEGS F FULL SIZE EQY.					59	62	63
					P90708-	1 UT OK/LEV 2 TECH #7214-33 NO RECORDABLES PAINTED SURFACE				SEE	NOTE 1		
	NOTE 1: USM2-M 2.25 MHZ 1-1/8"D TRANSDUCER WATER COUPLANT					TYPE A IMPACT T @ -120 DEGS F FULL SIZE EQY.					56	56	62
						TYPE A IMPACT T @ 0 DEGS F FULL SIZE EQY					58	62	64

T NUMBER	TYPE	G.S.	C	Mn	P	S	Si	Cr	Ni	Mo	Cu	Ti	V	B	Cb	Co	Al	N
9205	LDL	7	.16	.25	.010	.015	.22	1.64	3.02	.43	.19	.002	.002					
9205	FHA		.16	.27	.010	.015	.22	1.64	3.02	.43	.20	.002	.002					
9205	FHA		.16	.27	.010	.015	.22	1.63	3.01	.43	.20	.002	.002					

PURCHASER:

3 • AMERICAN ALLOY STEEL, INC
P. O. BOX 40469
HOUSTON, TEXAS
77040

COATESVILLE, PA. 19320

TEST CERTIFICATE

DATE 7/17/80 FILE NO. 284-01-01
CONSIGNEE:

MILL ORDER NO.	CUSTOMER P.O.	
37862 B	5341	S71180 L71480 RL

ORIGINAL FILE COPY. DO NOT REMOVE

A15643

THIS MATERIAL HAS BEEN MANUFACTURED AND TESTED IN ACCORDANCE WITH PURCHASE ORDER REQUIREMENTS AND SPECIFICATION(S)

SA-387 GR 22 CL 1 SUM 79 PVQ

BEND TEST HOMOGENEITY TEST

CHEMICAL ANALYSIS

MELT NO.	C	MN	P	S	CU	SI	NI	CR	MO	V	TI	AL	B		BASIC PROCESS
D9870	.14	.44	.008	.020		.25		2.30	1.00						ELEC.

PHYSICAL PROPERTIES

MELT NO.	SLAB NO.	YIELD PSI X100	TENSILE PSI X100	% ELONG IN 2"	% R.A.	BHN	IMPACTS				DESCRIPTION
D9870	4	573	759	30	62.9						1- 2-1/2 X 96 X 240

PLATE AND TEST ANNEALED 1475/1525/ F HELD 1 HR. PER INCH MIN., AND FURNACE COOLED WITHIN A RATE OF 100 F PER HR. TO 1200 F HELD 2 HRS. AND FURNACE COOLED TO 800 F, AND AIR COOLED.

We hereby certify the above information is correct.

SUPERVISOR-TESTING F. H. Kline

CUSTOMER OFFSHORE TECHNOLOGY CORP
CUST P.O.# P 2425
A.A.S. S/O# 54513 PLATE# 2 HEATS
DATE MAILED 12-16-80
DESCRIPTION 1 PC - 2 PCS - 2½" x 24" x 6'

Certified a true copy of the original, retained in our file.
AMERICAN ALLOY STEEL, INC
Charles E. Schu...

Specimens 4 & 5

A15419

CERTIFICATE OF TESTS

Armco Steel Corporation
P. O. Box 96120, Houston, Texas 77015

OUR ORDER NO.	CUST. ORDER NO.	SHIPPED VIA	CAR INITIAL AND NO.	DATE SHIPPED	SHIP REF. NO.	DATE MTR.	BY
DUNS 8069	5451	truck				3/29/77	SC

DESCRIPTION	BAR OR PLATE No.	No. PCS.	YIELD PSI	TENSILE PSI	% ELONG.	% REDUCT.	BEND TEST	FRACT. TEST	BHN	IMPACT: TYPE ORIEN	TEMP.	NOTCH SIZE 1	2	3	AVG.
STL PLT ALLOY ASME SA387 GR 22 CLASS 1 PVQ ANNEALED					2"										
HEAT 56086 1 3/8 x 100 x 430"	RG9203	1	43200	72400	27.0	53.2									

BOTH PLTS & TEST CPNS WERE AUSTENITIZED @ 1650°F, TIME @ TEMP: 101 MINS. & FURNACE COOLED TO 1325°F, (TRANSFORMATION TEMP.), TIME @ TEMP: 118 MINS. & AIR COOLED.

HEAT	C	Mn	P	S	Si	Cr	Ni	Mo	Cu	Ti	V	B	Cb	Al	N				GRAIN
56086	.13	.51	.010	.019	.29	2.30		.94											8
																			1

THE CHEMICAL, PHYSICAL OR MECHANICAL TESTS REPORTED HEREWITH ARE CORRECT AS CONTAINED IN THE RECORDS OF THE CORPORATION.

SIGNED _____ METALLURGICAL DEPT.

AMERICAN ALLOY STEEL INC
P O BOX 40469
HOUSTON, TEXAS 77040
ATTN: VELVET HILTON

"THIS CERTIFIED TEST REPORT HAS BEEN DELIVERED TO A CONSIGNEE OF MATERIAL PURCHASED FROM ARMCO STEEL CORPORATION. TO AVOID THE POSSIBILITY OF ITS MISUSE, ON THE REDELIVERY OF THIS REPORT TO A THIRD PARTY IT MUST BE RECERTIFIED BY AND UNDER THE NAME OF SUCH CONSIGNEE."

CUSTOMER Offshore Technology Corp
CUST P.O.# P2425
A.A.S. S/O# 59813 PLATE# A15419
DATE MAILED 12-16-77
DESCRIPTION 1st 4 - 1PC - 1 3/8 x 11" x 11"

Certified a true copy of the original, retained in our file.
AMERICAN ALLOY STEEL, INC.

Charles E. Schultz

9 samples

Specifications for Acoustic Coupon

Procurable material designation: 4340 steel (SAE or AISI)

Composition Limits (%) of 4340

Carbon	0.38-0.43
Manganese	0.60-0.80
Silicon	0.20-0.35
Nickel	1.65-2.00
Chromium	0.70-0.90
Molybdenum	0.20-0.30
Phosphorus	0.040 max.
Sulphur	0.040 max.

Properties of 4340 utilized in this application.

Hardenability band at 1.25 inches from quench: 46-57 Rockwell C
Normalizing Temperature: 1600°F
Austinitizing Temperature: 1550°F

Fabrication Requirements:

Overall dimensions of the coupon shall be torch cut from 2.5" TK plate followed by stress relief.

Machining to tolerances per print.

After machining, heat treatment shall require a minimum as quenched hardness of 50 Rc tempered to a maximum hardness of 30 Rc and a minimum of 90% martensitic structure.

APPENDIX A

HEAT TREAT SPECIFICATION FOR 2 1/4 Cr - 1 Mo STEEL

1. All temperatures shall be monitored using a thermocouple attached to the specimen.
2. Austenitize at 1650-1800° F. (max) for at least 1 hour for each 1" of wall thickness.
3. Water quench.
4. Temper at 1200° ± 25° F. for at least 1 hour for each 1" of wall thickness.
5. Air Cool.

APPENDIX B

MATERIAL SPECIFICATIONS

LeTourneau
marathon longview division
Testing Laboratory

ORIGINAL FILE COPY.
DO NOT REMOVE

Report of CHEMICAL and PHYSICAL TESTS of ....Steel Plate.....

Shipped To ....American Alloy.....

Customer's Order No. .....9388.....

Date: ....March 23, ... 19 ..84.....

Mill Order No. ....L-133980.....

2" Gage

AMERICAN ALLOY
PLATE # A15924

Melt No.	Slab No.	Specs.	CHEMICAL ANALYSIS C	Mn	S	P	Si	Cr	Ni	Mo				Yield Point P.S.I.	Ten Strength P.S.I.	Elongation %	Reduction %	Charpy ft/lbs	Bend Test	SIZE OF PLATE	Qty
D18874	B665	SA387-22 CL 1	.08	.36	.027	.017	.26	2.00		.90				43,500	68,500	29.0	75.0			3 x 96 x 190	1

Normalized @ 1700°F for 3 hours
Tempered @ 1250°F for 5 hours

CUSTOMER OFFSHORE TECHNOLOGY CORP
CUST P. O.# P 2425
A.A.S. S/O# 59513 PLATE# A15924
DATE MAILED 12-16-85
DESCRIPTION IT #3 - 1 PC - 3" x 8" x 4"

TEST REPORT APPROVED DATE 3/27/84
AMERICAN ALLOY STEEL BY R Dugan

Certified a true copy of the original, retained in our file.
AMERICAN ALLOY STEEL, INC.

I Hereby Certify that the Above Tests Are Correct to the best of My Knowledge and Belief.

MARATHON LeTOURNEAU COMPANY
K. E. Wright
Asst. of Tests

Specimen 1
2¼Cr 1Mo

ORIGINAL COPY
DO NOT MOVE

AMERICAN ALLOY
PLATE # A15960

PURCHASER
3 •
AMERICAN ALLOY STEEL, INC.
P.O BOX 40669
7721 PINEMONT
HOUSTON, TEXAS 77040

LUKENS STEEL COMPANY
COATESVILLE PA 19320
TEST CERTIFICATE

MILL ORDER NO	CUSTOMER P.O		DATE 9/10/80	INT NO/USS 01-01
42696 1	2205	S7080 1 9910 0 RL	CONSIGNEE 191294	

1-387 QR 22 CL 1 MIN 79

MHO TEST HOMOGENEITY TEST

CHEMICAL ANALYSIS

MELT NO	C	MN	P	S	CU	SI	NI	CR	MO	V	TI	AL	B	BASIC PROCESS
C2271	.13	.44	.011	.005		.21		2.00	1.00					ELEC.

PHYSICAL PROPERTIES

MELT NO	STAR NO	YIELD PSI 1000	TENSILE PSI 1000	% ELONG IN 2"	% R A	BHN	IMPACTS	DESCRIPTION
C2271	20	405	766	26	51.1			1- 1 X 96 X 480

PLATE AND TEST ANNEALED 1475/1525 F HELD 1 HR. PER INCH MIN., AND FURNACE COOLED WITHIN A RATE OF 100 F PER HR. TO 1200 F HELD 2 HRS. AND FURNACE COOLED TO 800 F. AND AIR COOLED.

We hereby certify the above information is correct.

C. F. Fr. Kline

TEST REPORT APPROVED DATE 10/15/80
AMERICAN ALLOY STEEL BY C. Snyder

CUSTOMER Offshore Technology Corp.
CUST P. O.# P 24-25
A.A.S. S/O# 59513 PLATE# A15960
DATE MAILED 12-16-85
DESCRIPTION IT#2 - 2 Pcs - 1" x 20" x 4"

Certified a true copy of the original, retained in our file.
AMERICAN ALLOY STEEL, INC.

Specimens
13 #14